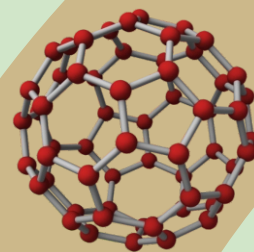# International Journal of Modern Engineering Research (IJMER)

International Journal of Modern Engineering Research (IJMER)

Contents :

Noise Removal with Morphological Operations Opening and Closing Using Erosion and Dilation

ALKA BISHNOI[1]

[1] Mtech. Ece, Suraj College Of Engg. & Technology, Distt. Mahendergarh, University-Mdu Rohtak, State-Haryana.

Abstract: *The mathematical operations are proposed in this paper. By using two mathematical operations erosion and dilation we can add and remove pixels. We can remove the noise or interference in power system. Opening and closing operations also discussed with erosion and dilation. These four morphological operations are also helpful in developing a morphological filter.*

I. Introduction

Erosion and dilation

Two fundamental mathematical morphological operations are: dilation and erosion. In fact, many of the morphological algorithms are based on these two primitive operations. In gray scale images, we develop algorithms for boundary extraction via a morphological gradient operation, and for region partitioning based on texture content. We operation are also useful in smoothing and sharpening, which often are useful as per- or post processing steps.

The morphological operators may be classified as

(1) Binary morphological operators
(2) Grayscale morphological operators
   Binary morphological operations deal with set of points of the domain D and the gray scale morphological operators deal with functions.

Opening and Closing

The combination of erosion followed by dilation is called an opening, referring to the ability of this combination to open up gaps between just-touching features,It is one of the most commonly used sequences for removing pixel noise from binary images. Performing the same operations in the opposite order (dilation followed by erosion) produces a different result. This sequence is called a closing because it can close breaks in features. There are several parameters that can be used to adjust erosion and dilation operations, particularly the neighbor pattern or rules for adding or removing pixels and the number of iterations, as discussed below. In most opening or closing operations, these are kept the same for both the erosion and the dilation.

1.1 Erosion

Erosion removes pixels from features in an image or, equivalently, turns pixels OFF that were originally ON. The purpose is to remove pixels that should not be there. The simplest example is pixels that have been selected by thresholding because they fell into the brightness range of interest, but that do not lie within large regions with that brightness. Instead, they may have that brightness value either accidentally, because of finite noise in the image, or because they happen to straddle a boundary between a lighter and darker region and thus have an averaged brightness that happens to lie within the range selected by thresholding. These pixels cannot be distinguished by simple thresholding because their brightness value is the same as that of the desired regions. It may be possible to remove them by using Boolean logic, for instance using the gray level as one criterion and the gradient as a second one, and requiring that the pixels to be kept have the desired gray level and a low gradient.

The simplest kind of erosion is to remove (set to OFF) any pixel touching another pixel that is part of the background (is already OFF). This removes a layer of pixels from around the periphery of all features and regions, which will cause some shrinking of dimensions and may create other problems if it causes a feature to break up into parts. We will deal with these difficulties below. Erosion can entirely remove extraneous pixels representing point noise or line defects (e.g., scratches) because these defects are frequently only 1 or 2 pixels wide.

1.2 Dilation

Instead of removing pixels from features, a complementary operation known as dilation (or sometimes dilatation) can be used to add pixels. The classical dilation rule, analogous to that for erosion, is to add (set to ON) any background pixel that touches another pixel that is already part of a foreground region (is already ON). This will add a layer of pixels around the periphery of all features and regions, which will cause some increase in dimensions and may cause features to merge. It also fills in small holes within features.

Because erosion and dilation cause a reduction or increase in the size of regions, respectively, they are sometimes known as etching and plating or shrinking and growing. There are a variety of rules for deciding which pixels to add or remove and for forming combinations of erosion and dilation.

In the rather simple example described above and illustrated in Figure, erosion to remove the extraneous lines of pixels between light and dark phases causes a shrinking of the features. Following the erosion with dilation will more or less restore the pixels around the feature periphery, so that the dimensions are (approximately) restored. However, isolated pixels and lines that have been completely removed do not cause any new pixels to be added. They have been permanently erased from the image.

II. Mathematical Representation of Erosion and Dilation

Let $f(x)$ denote a one-dimensional original signal whose definition domain is $\{0,1,\ldots,N\}$. Let $g(x)$ denote structuring element whose definition domain is $\{0,1,\ldots,M\}$. It is further assumed that $M < N$ and the origin of $g(x)$ is defined in 0. The formula of dilation operation is:

$$(f \oplus g)(n) = \max_{\substack{m=0,1,\ldots,M-1 \\ n=0,1,\ldots,N+M-2}} \{f(n-m)+g(m)\}$$

The formula of erosion operation is:

$$(f \ominus g)(n) = \min_{\substack{m=0,1,\ldots,M-1 \\ n=0,1,\ldots,N-M}} \{f(n+m)-g(m)\}$$

The calculations of dilation and erosion are very simple, which contain only addition and subtraction, not involving multiplication and division. So the processing speed corresponding to real-time signal is fast and the delay is small. Compared with traditional digital filtering algorithm, their calculations are greatly simple.
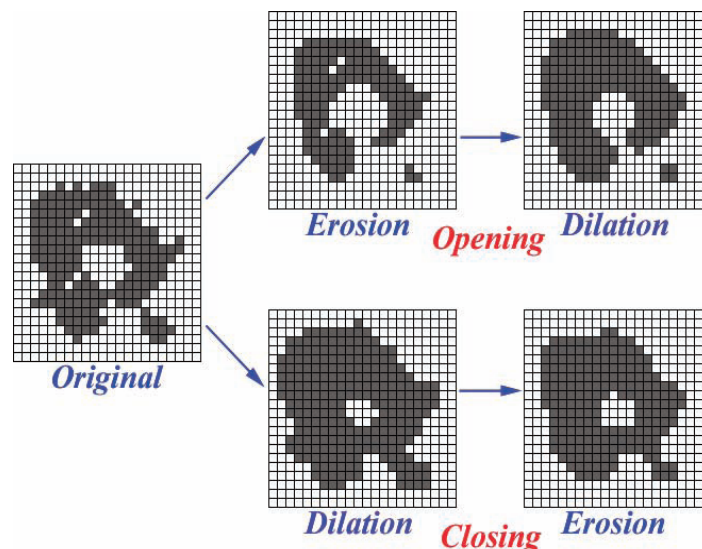

Fig 1.1 Combining erosion and dilation to produce an opening or a closing.

The result is different depending on the order of application of the two operations. Since the original image is ambiguous, it is necessary to use a priori *knowledge to select the proper combination.*

2.1 Opening

Openings can be used in some cases to separate touching features. In the example shown in Figure 2.1, the features are all similar in size. This fact makes it possible to continue the erosion until all features have separated but none have been completely erased. After the separation is complete, dilation grows the features back toward their original size. They would merge again unless logic is used to prevent it. A rule that prevents turning a pixel ON if its neighbors belong to different features maintains the separation shown in the figure. This requires performing feature identification for the pixels, so the logic discussed above is required at each step of the dilation. An additional rule prevents turning on any pixel that was not on in the original image, so that the features are restricted to their original sizes. If the features had different original sizes, the separation lines would not be positioned correctly at the junctions, and some features might disappear completely before others separated.

The formula for Opening operation is,
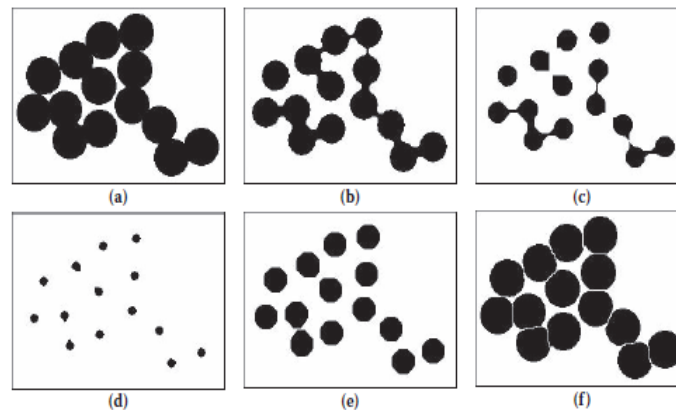
$$(f \circ g)(x) = ((f \ominus g) \oplus g)(x)$$

Fig 2.1 Separation of touching features by erosion/dilation: (a) original test image; (b) after two cycles of erosion; (c) after four cycles; (d) after seven cycles (features are now all fully separated); (e) four cycles of dilation applied to image d (features will merge on next cycle); (f) additional cycles of non-merging dilation restricted to the original pixel locations, which restores the feature boundaries.

2.2 Closing

As shown in Figure 1.1, the closing sequence is performed in the other order, a dilation followed by erosion, and the result is not the same. Instead of removing isolated pixels that are ON, the result is to fill in places where isolated pixels are OFF, missing pixels within features, or narrow gaps between portions of a feature. Figure 2.2 shows an example of a closing used to connect the parts of the cracked fibers shown in cross section. The cracks are all narrow, so dilation causes the pixels from either side to spread across the gap. The increase in fiber diameter is then corrected by erosion, but the cracks do not reappear.
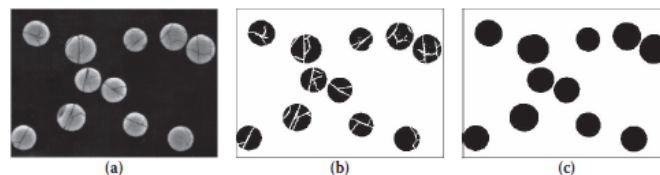
Fig 2.2 Joining parts of features with a closing: (a) original image, cross section of cracked glass fibers; (b) brightness thresholding, showing divisions within the fibers; (c) after application of a closing.

The classical erosion and dilation operations illustrated above turn a pixel ON or OFF if it touches any pixel in the opposite state. Usually, touching in this context includes any of the adjacent 8 pixels, although some systems deal only with the 4 edge-sharing neighbors. These operations would be much simpler and more isotropic on a hexagonal pixel array, because the pixel neighbor distances are all the same, but practical considerations lead to the general use of a grid of square pixels.

The formula for Closing operation is ,

$$(f \bullet g)(x) = ((f \oplus g) \ominus g)(x)$$

III. Conclusion

By using morphological operations erosion and dilation in opening and closing operations are very helpful in filters. They can add and remove pixels. Morphological filters developed on the basis of combination of closing and opening operations are discussed. This is a future aspect.

REFERENCES

[1.] Rafael C. Gonzalez and Richard E. Woods "Digital Image Processing" , Third Edition
[2.] WANG Jing, LIU Pan, LIU Di-chen "The design and analysis of improved adaptive generalized morphological filter(2008),(School of Electrical Engineering of Wuhan University, Wuhan 430072, China)
[3.] Rafael C. Gonzalez and Richard E. Woods "Digital Image Processing using Matlab" , Third Edition
[4.] MATLAB 7.0.4 (help)
[5.] John C.Russ "The image Processing Handbook" Fifth edition
[6.] Image Processing Toolbox For Use with MATLAB User's Guide ,Version 2 ,The mathswok.inc
[7.] http://www.mathworks.com/access/helpdesk/help/toolbox/images/index.html

Diffusion Bonding of Semi-Solid (SSM 356) Cast Aluminum Alloy

Chaiyoot Meengam[1], Prapas Muangjunburee[2], Jessada Wannasin[3]

[1, 2, 3]*Department of Mining and Materials Engineering, Faculty of Engineering, Prince of Songkla University, Hat Yai, Songkhla, Thailand, 90112*

Abstract: *A new technique to achieve the globular weld structure of SSM 356 aluminum alloy was conducted. The effect of joining parameters on the microstructure and mechanical properties of diffusion bonding butt joints of semi-solid SSM 356 aluminum alloy was investigated by conditions as follows: compressive pressure at 0.4, 0.9, 1.8, 2.4 and 2.7 MPa, with holding time 3 hours and temperature at 495ºC under argon atmosphere at 4 liters per minute. The results showed that the compressive pressure 1.8 MPa, with holding time 3 hours and temperature 495ºC, under argon atmosphere provided the highest joint strength to 124.48 MPa. In addition, the results of the investigation have shown that the joint efficiency was 72 percent compared with base metal and microstructure in weld zone (WZ) after welding becomes globular structure. This microstructure, similar to the original structure of the base material, is a globular structure but the grain size can grow at a higher temperature.*
Keywords: *SSM 356 Aluminium alloy, Diffusion Bonding, Bond line, Semi-Solid Metal*

I. INTRODUCTION

Semi-solid metals (SSM) have been receiving considerable attention due to its advantages for application in automotive and aircraft industries. SSM processing exhibits distinctive advantages such as components are near net shape, the temperature of SSM processing is lower than conventional casting and its globular microstructure is shown in Fig 1 [1]. It was clear that the joint of SSM aluminum alloys have expanded in the usage of casting components. Joining of SSM aluminum alloys has been carried out with a variety of fusion and solid state welding processes. Conventional welding processes lead to the formation of porosities in weld as well as change in weld microstructure [2]. Therefore, a suitable joining technique is required to overcome these problems. These difficulties have led to joining in solid state by diffusion bonding. In this study, SSM 356 aluminum alloy was obtained from a new rheocasting technique, named gas induced semi solid (GISS) process.

Diffusion bonding is a solid state joining process, which consists of three main parameters such as time, temperature and pressure. In this method, mating materials are brought into contact under a pressure far below the yield strengths of the base materials, and generally the bonding temperature is chosen between $0:5-0:8Tm$, where Tm is the melting point of the base materials [3]. Diffusion bonding of aluminum alloys faces some problems due to its protective oxide film (Al_2O_3). This oxide has great stability and tenacity at high temperatures and to hinder diffusion of atom [4]. However, problems from oxide film can be avoided by joining in a vacuum or under atmospheric shielding gas [5].
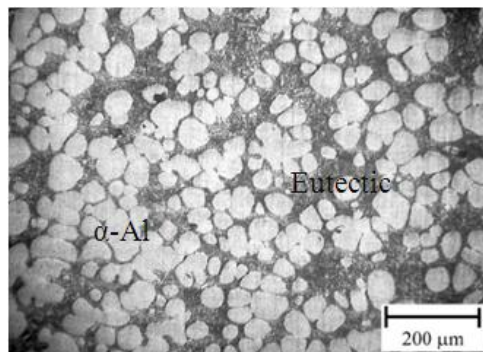

Fig: 1 Microstructure of base materials SSM 356 [6]

In this research, systematic study on the effect of joining parameters on the microstructure and mechanical properties of diffusion bonding butt-welded joints of SSM 356 aluminum alloy was investigated and the results were reported and discussed.

II. MATERIALS AND METHODS

The material used in this study was aluminum semi-solid metal SSM 356 with chemical composition shown in table 1. The mechanical properties of SSM 356 are as follows; ultimate tensile strength (UTS) is 168 MPa, yield strength (YS) 137 MPa and elongation (E) 9.7 percent

Table 1: The chemical compositions of SSM 356 (% weight) [7].

Materials	Si	Fe	Cu	Mn	Mg	Zn	Ti	Cr	Ni	Al
SSM 356	7.74	0.57	0.05	0.06	0.32	0.01	0.05	0.02	0.01	Bal.

The base material for diffusion bonding was supplied in the form of cylindrical shape of dimensions 11 mm. in diameter and 40 mm in length. The specimen preparation was carried out by grinding surfaces with P180 grit SiC paper and cleaning in acetone for 30 s. just before diffusion bonding. Bonding was performed in argon atmosphere at 4 liters per minute in a high temperature chamber attached to a testomatic tensile testing/compression testing machine. The temperature of the chamber was set at 495°C. Bonding pressure were 0.4, 0.9, 1.8, 2.4 and 2.7 MPa and heating holding time of 3 hours. The variables used in this experiment are summarized below:

1. Diffusion bonding temperature: 495 °C
2. Applied pressure: 0.4, 0.9, 1.8, 2.4 and 2.7 MPa
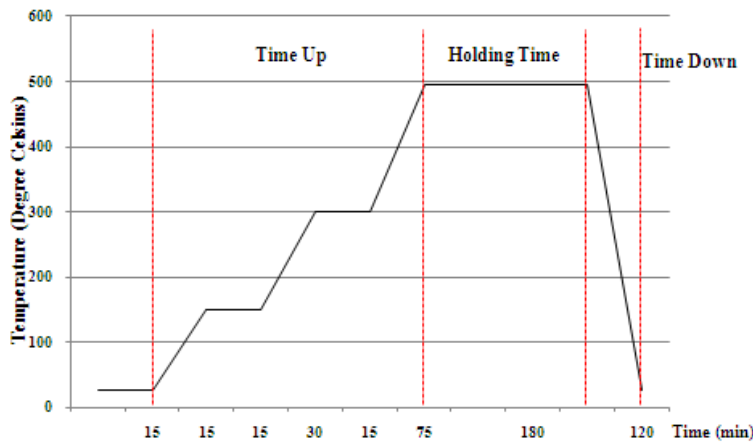3. Heating holding time of 3 hours.

Fig: 2 temperature cycle time

Total time of heating cycle is 7 hours 45 minutes as shown in Fig 2. Finally desired compression force and all of which are controlled under the oven shown in Fig 3.
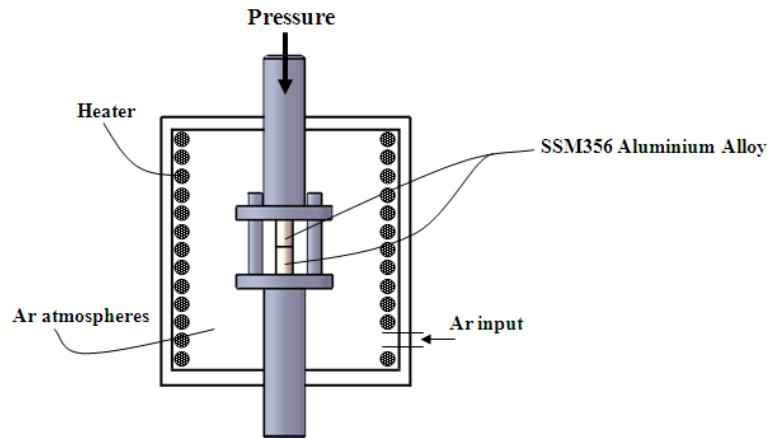

Fig: 3 Set-up used for bonding.

III.   RESULTS AND DISCUSSION

3.1 Metallography

Fig 4(a) shows the cross section macrograph of the diffusion bond line. It can be seen that no macro defects were observed, in addition, two base materials were sound bonded. Fig 4(b), 4(c), 4(d), 4(e), and 4(f) show the microstructure along the bond line from top to bottom. The results have indicated that only one void was observed in the bond interface obtained from Fig 4(d). This elongated void located at the center of the bond line to this is due to the elimination of the interfacial voids was nearly completed. It is generally considered that a sound bond was achieved despite little evidence of the bond line. Bond line was part of the specimens where microstructure is not changed due to heating cycles, and microstructure in bond line zone has globular structure which is similar to base structure SSM 356 but different in sizes – the size of bond line grain is about 12-15 µm but the size of base structure grown about 19-22 µm. Fig 4(b)-4(f) also reveals smaller grain size at the interface compared with base materials away from the interface. Microstructure at and near the interface was influenced by temperature, time and pressure resulting in changes to the shape and size of grains. [8] Fig 4(a) and 4(b) suggest a small misalignment at the top and bottom during bonding process.
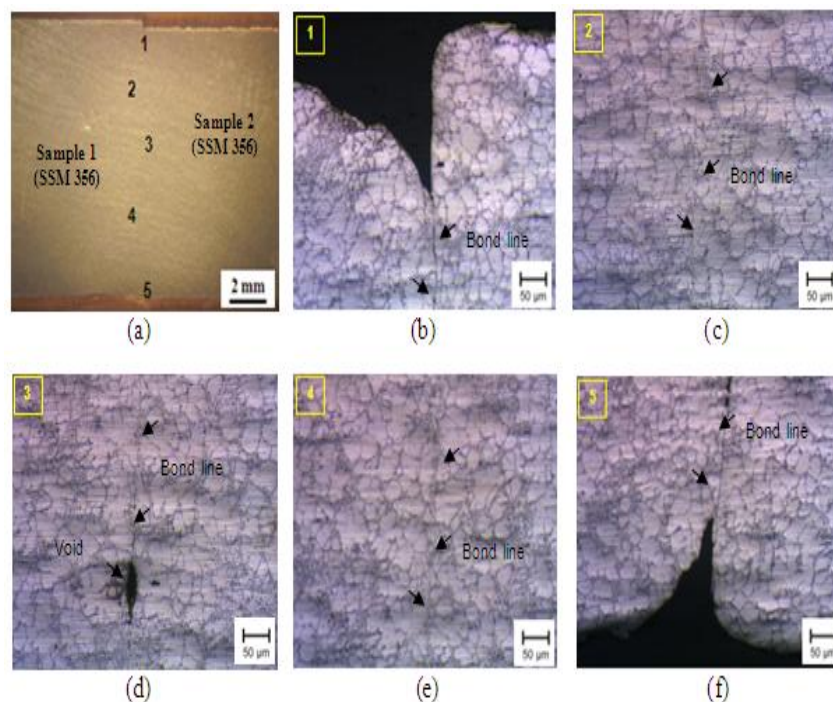

Fig: 4 Macro-Microstructure of interface for SSM 356. After diffusion bonding method (a) macrostructure at the interface, (b) on the top edge, (c) top, (d) medium, (e) bottom and (f) on the bottom edge.

Fig 5 shows microstructure revealed by scanning electron microscopy (SEM) with joining parameters at temperature 495 °C, pressure 1.8 MPa and time 3 hours. Fig 5 (a) reveals aluminums matrix phase (α-Al) and void. A small voids was obtained in the bond interface. In addition, broken silicon particles were also obtained at and near the bond interface. The void along the top to the bottom is very small. Silicon particles were broken by pressure and the influence of heat; then, the silicon and magnesium as combination of Mg_2Si have formed as shapes of the plates and rods [9]. Mg_2Si from shaped plate is grown about 4 µm and about 10-15 µm long, and Mg_2Si from rods-like-shape particle is about 1.5 µm wide and about 10-30 µm in length. Based materials on silicon from rods-like-shape particle is about 1.5 µm wide and plates-like-shape particle is 2.5 µm in length. For both rods-like-shape particle and plates-like-shape particle is about 15-20 µm wide. It is obvious that Mg_2si phase are arrangement parallel along the bond lines show in Fig 5 (b). Heating the silicon particles diffusion into bond line at the right time result in complete diffusion show in Fig 5 (c, d) and Mg_2Si are distributed throughout the aluminum matrix. Although Mg_2Si particle is smaller in size, this promotes material strength. Small voids were observed in the bond interface. In addition, some broken silicon were also observed at and near the bond line.
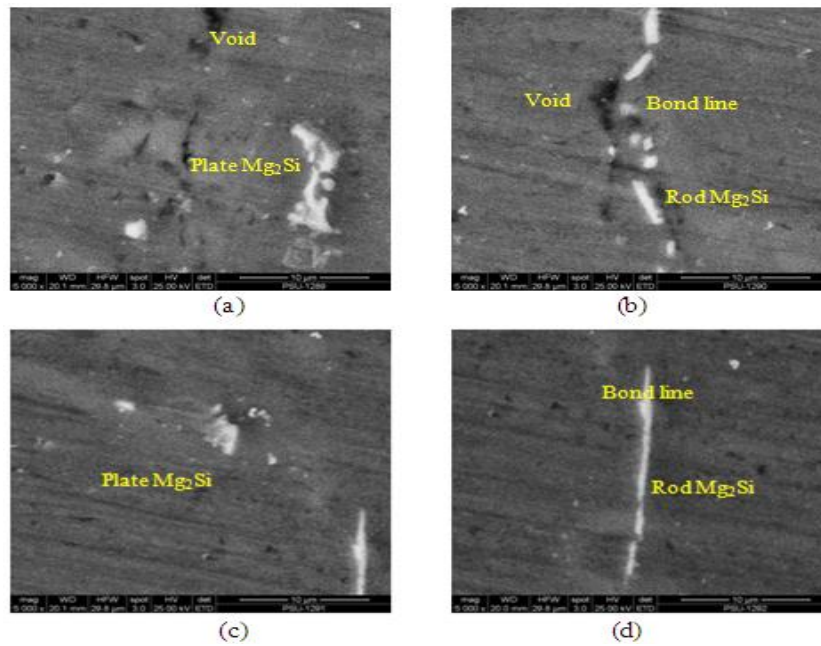
Fig: 5 Scanning Electron Microscopy of interface for SSM 356

Table 2: Chemical compositions of each zone in the bond line for 1.8 MPa at 495 $^{\circ}$C (at.%)

Zone	Al	Si	Mg	Fe
A$_1$	72.55	25.74	1.27	0.44
A$_2$	79.80	16.57	2.65	0.98
A$_3$	59.12	38.71	1.26	0.91
A$_4$	75.52	22.51	1.38	0.61
A$_5$	83.82	14.11	1.61	0.46

Fig 6 shows an inspection of line scan and point analysis by energy-dispersive x-ray (EDX) analyze diffusion elements to bond line. It is found that the microstructures along bond line have silicon particle (Si) distributing throughout the aluminum matrix which forms a combination of magnesium and silicon into solid solution Mg$_2$Si where is nearby bond line. In addition, the maximums amount of silicon is located at the center because the interface zone has the same behavior as grain boundary which assists atoms to diffuse easily on interface grain. The chemical compositions of each zone in the bond line for 495 $^{\circ}$C, pressure 1.8 MPa and time 3 hours by EDX shown in Table 2. According to the table, the silicon phase maximum diagram and the morphologies of A$_3$ have 38.71 percent.
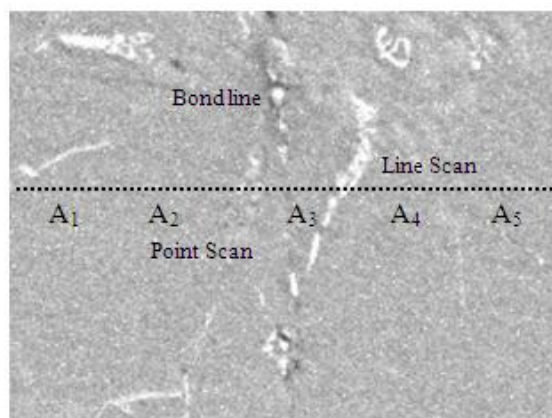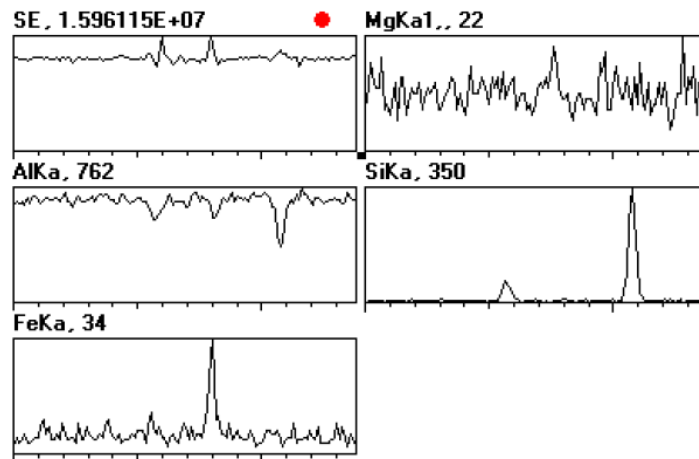
Fig: 6 Energy-Dispersive X-ray of interface for SSM 356

3.2 Tensile Strength of Joints

The tensile properties and fracture locations of joints welded at different welding condition are show in Fig 7. From investigation, the increase in the contact pressure leads to increase in the tensile strength, a maximum average value tensile strength of 129.3 MPa was achieved by the joint parameter at contact pressure 1.8 MPa, holding time 3 hours. temperature 495°C, under argon atmosphere flow 4 l/min. Compared with the base material is around 76.96 percent of efficiency joints by base material aluminums SSM 356 is 168 MPa. Joint efficiency can be measured by the percentage of bonded area [4]. The equation used to calculate the joint efficiency is given as:

$$\text{Joint efficiency} = \frac{\text{UTS of bonded specimen}}{\text{UTS of SSM 356 specimen}} \times 100$$

From Fig 7, it shows that if the contact pressure is too low, the tensile strength and the bonding surface is small too. In contrast, the more pressure increase, the more tensile strength increases, respectively. But if the pressure is too high, the tensile strength will be decreased and the specimen will be deformed. The pressure variables 0.4 MPa for tensile strength is very low 51.1 MPa because contact the surface of the sample is very little to diffusion of atoms together is difficult. Increasing pressure is 0.9 MPa, the tensile strength was increased to 101.5 MPa. Likewise, the pressure is 1.8 MPa while contributing to the higher tensile strength to value of 129.3 MPa this phenomenon as a result of right pressure. Recovery time is the compression of the grain in compression at high or too low.

Fig: 7 Tensile properties of SSM 356 diffusion bonding

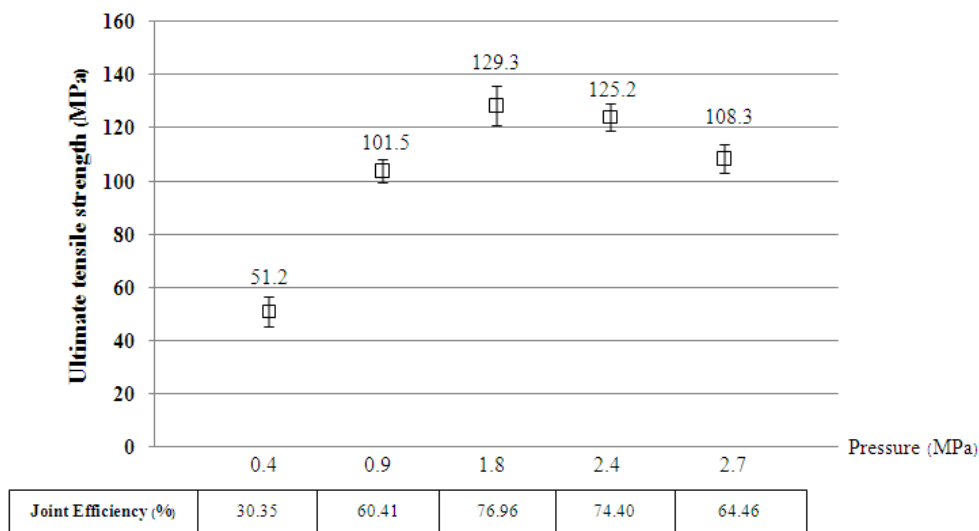Increasing pressure is too high resulting in a decrease in tensile strength as a result of grain surface area is compressed by the massive force stress at the interface lead to use of energy higher in the release of stress [4]. The high pressure causes the recovery longer described by variable pressure 2.4 and 2.7 MPa is 125.2 and 108.3 MPa respectively. In experiments, the pressure that directly affect the tensile strength and the deformation of the sample after welding. The variable temperature and time it is also important could result in a change in metallurgy. Therefore, the variables right is important for the diffusion bonding. Another reason for the high strength specimen of the bonded as well due to the amount of void is interface zone has minimal.

3.3 Hardness Test

The microhardness distributions on the transverses cross-section of joints welded at all welding condition the data is summarized in Fig.8 It is observed that the bond lines with a hardness higher than other areas descriptive by bond line have Mg_2Si phase, The influence of temperature resulting in particles together and specimen by diffusion bonding through all regions were slightly decreased in comparison with the base materials [10]. Base materials have average hardness in the range 67 HV but after the experimental specimen average hardness increases is 93 HV which comes from the heat in due movement of the atoms from Mg_2Si phase. The average hardness is 35.48 percent. Heat during welding support to specimen with the hardness increases. Finally, diffusion bonding processes help increase of the hardness of the specimen after welding.
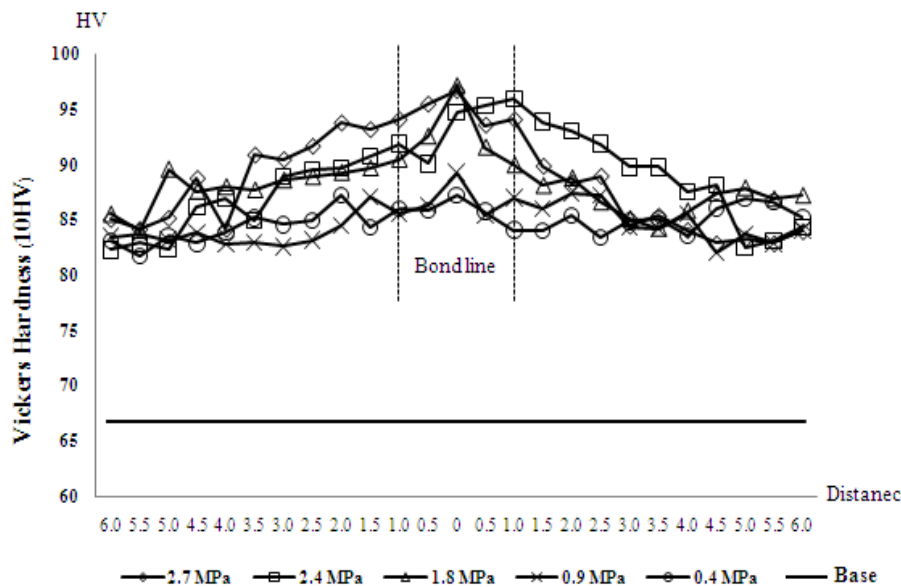
Fig: 8 Microhardness results for diffusion bonding.

IV. CONCLUSION

In the present study SSM 356 aluminum alloys were joined by diffusion bonding under contact pressure and holding time were investigated. Summarizing the mean features of the results, the following conclusions may be drawn:

1. The highest joint strength reaches 129.8 MPa when the specimen is bonded at pressure 1.8 MPa, holding time 3 hours. temperature 495°C, under argon flow 4l/min.
2. Microstructure after welding is globular structure is the same as the original texture of the material but the grain size to grow at a higher temperature.
3. Silicon particles in formed fracture of the increasing pressure and at the influence of heat is diffusion to the bone line combined with magnesium form solid solution Mg_2si
4. Solid solution Mg_2si shaped plate is grown about 12 μm and a length of about 15-25 μm and shaped rods is about 3 μm in length and about 10-40 μm.

Acknowledgements

REFERENCES

[1]   R.F. Tylecote, Diffusion bonding (Welding and Metal Fabrication, 1967).

[2]   D.V. Dunford and P. G. Partridge, Proc. CIT Grandfield Con. on Super plasticity in Aerospace-Aluminum, UK, 1985, 252.

[3]   N. Masahashi, Effect of Pressure Application by HIP on Microstructure Evolution during Diffusion Bonding, Materials Transactions, 46)7(, 2005, 1651-1655.

[4]   C.S. Lee, H. Li and R.S. Chandel, Vacuum-free diffusion bonding of aluminium metal matrix composite, Journal of Materials Processing Technology, 89-90, 1999, 326-330.

[5]   X-P. Zhang, L. Ye, and Y.W Mai, Investigation on diffusion bonding characteristics of SiC particulate reinforced aluminium metal matrix composites (Al/SiCp-MMC), International Journal of Composites: Part A, 30, 1999, 1415–1421.

[6]   J. Wannasin, S. Junudom, T. Rattanochaikul, and M.C. Flemings, Development of the Gas Induced Semi-Solid Metal Process for Aluminum Die Casting Applications" Solid State Phenom, 141, 2008, 97-102.

[7]   J. Wannasin, and S. Thanabumrungkul, Development of a semi-solid metal processing technique for aluminium casting applications, Songklanakarin Journal Science Technology, 30(2), 2008, 215-220.

[8]   H. Moller, G. Govender and W.E. Stumpf, The T6 heat treatment of Semi-solid Metal Processed Alloy A356, The Open Materials Science Journal, 2, 2008, 6-10.

[9]   A. Urena and J.M. Gomezde Salazar, Bonding of aluminium matrix composites for application in the transport industry, Journal de Physique Archives, 3, 1993, 1037-1042.

[10] S. Kuntongkam, S. Wisutmethangoon, T. Plookphol and J. Wannasin, Influence of Heat Treatment Processing Parameters on the Hardness and the Microstructure of Semi-Solid Aluminum Alloy A356, Journal of Metals, Materials and Minerals, 18)2(, 2008, 93-97.

Evaluation of the Glucuronic Acid Production and Other Biological Activities of Fermented Sweeten-Black Tea by Kombucha Layer and the Co-Culture with Different Lactobacillus *Sp.* Strains

Nguyen K. Nguyen[1], Ngan T.N. Dong[2], Phu H. Le[3], Huong T. Nguyen[4]

[1, 2, 3] *(School of Biotechnology, International University, Vietnam National University HCMC, Vietnam)*
[4] *(Department of Biotechnology, University of Technology, Vietnam National University HCMC, Vietnam)*

Abstract: *The interactions between lactic acid bacteria (LAB) and acetic acid bacteria (AAB) from Kefir and Kombucha (KBC) have been concerned during the last decade since their positive stimulation on growth rate, biomass, and secondary metabolites. However, more study needs to be conducted to ascertain whether those enhancement can bring out actual benefits for human consumption. In this study, evaluation of three main healthy properties of KBC, which were glucuronic acid (GlcUA) concentration, antibacterial and antioxidant activities and under co-culture of LAB from Kefir is our main target. The combination of high-performance liquid chromatography (HPLC) and mass spectrophotometer (MS) detector was used to determine the GlcUA concentration. The agar-well diffusion method was used to test the antibacterial activities against three serious food borne pathogenic bacteria which were Escherichia coli ATCC 8739, Salmonella typhimurium ATCC 14028; Bacillus cereus ATCC 11778. 1, 1-Diphenyl-2picrylhydrazyl (DPPH) was applied to measure the radicals scavenging activity of KBC. The result shows that Lactobacillus casei can improve the GlcUA up to 39.6% while Lactobacillus platarum can enhance the antibacterial and antioxidant activities as a higher level comparing to the normal fermented tea and mixed culture with other LAB strains.*
Keywords: *Antibacterial activities, DPPH, fermented tea, glucuronic acid, KBC.*

I. INTRODUCTION

Kombucha (KBC) known as "tea fungus" is a sour, tasty, and healthy drink obtained by the fermentation of sucrose-sweetened black tea. It has been consumed at least two thousand years in China BC and then spread out to Korea, Japan, Russia and now on over the world [1]. Many studies have shown that the microbial composition in KBC tea is symbiosis between acetic acid bacteria (AAB) and yeast[2]. They can be *Acetobacter* sp., *Gluconobacter* sp., *Bacterium* sp., *Saccharomyces* sp., *Zygosaccharomyces* sp., and *Pichia* sp., etc [3,4].

This fermented tea was considered as a healthy drink for human due to its detoxifying properties of glucuronic acid (GlcUA), inhibiting growth of pathogenic bacteria and antioxidant ability. The metabolites in KBC that mainly contribute to its value properties were identified as acetic, lactic, ethanol, glycerol, vitamin B complex, folic acid, D-saccharic acid 1,4 lactone (DSL), gluconic and GlcUA [5]. The GlcUA is the important key component found in KBC beverage which normally produces by a healthy liver [6]. It is well-known in an important process for detoxification and excretion of exogenous chemicals called glucuronidation [1] which was responsible for biotransformation of endogenous reactive metabolites, such as bilirubin, oxidized fatty acids and excess of steroid hormones. The conjugation of GlcUA with undesirable compounds, results in the decreased toxicity due to an increased solubility of them that further facilitates transport and elimination from the body. On the other hand, GlcUA can be converted in to glucosamine and associated with cartilage, collagen and the fluid which lubricate the joints [6]. GlcUA has many benefits to human health but its concentration level in KBC is not well documented and various from every culture since microbial symbiosis is depended on the different geographic and climatic conditions [7].

LAB presents a large amount in Kefir, a health benefit fermented milk produced by the symbiosis association mainly between LAB and yeast in Kefir grains [8]. On the other hand, Lactic acid bacteria (LAB) were also found in some certain KBC but in small amount and were not considered as the essential role in the symbiosis of tea fungus. Therefore it were not drawn much attentions in the past [9]. In recent years, the interest on bacterial co-operation between LAB from Kefir and AAB from KBC to improve the growth rate, biomass and their secondary metabolites has been concerned. In 2010, the symbiosis between LAB from Kefir and AAB

from KBC was investigated in improving D-saccharic acid 1,4 lactone (DSL) productions. The author has pointed out that the LAB can improve the survival of AAB and this combination would be an optimal mixed culture to enhance KBC function [9]. In 2011, LAB was applied as a core factor in a optimal conditions for KBC fermentation with AAB and yeast [10]. In 2013, Analy mentioned about the vitamin B complex which was secreted by AAB (*Acetobacter sp.*) may support a favorable environment for other growth of LAB and yeast in Kefir grains [8].

Although much works has been done to date to evaluate positive stimulation in growth rate, biomass, and secondary metabolites which were provided by the cooperation of *Lactobacillus sp.* from Kefir and *Acetobacter sp.* form KBC, actually human health benefiting properties form this combination remains unclear. Therefore, more studies need to be conducted to ascertain the significant role of LAB in mixed culture of KBC tea to enhance its three important functions for human consumption which were GlcUA concentration, antibacterial and antioxidant ability.

In this study, LAB strains were isolated form Kefir and cultured with KBC layer in the sweeten-black tea medium. The GlcUA production was determined by HPLC-MS, the antibacterial and antioxidant activities were also evaluated by agar-well diffusion method and DPPH radical scavenging capacity, respectively. Therefore, enhancement of three main functions of KBC tea by mixed culture of LAB and KBC layer is our main target. Moreover, this purpose is identified as being significance of the research in producing healthy and valuable fermented tea for the beverage industry since this kind of drink is so popular on over the world.

II. MATERIALS AND METHODS

2.1 Reagents, apparatus and medium preparation

Kefir grain, KBC layer was kindly provided by Biotechnology lab of University of Technology, Vietnam National University, HCMC and Food Technology lab of International University, Vietnam National University, HCMC. Black tea used in this study was Lipton black tea, a product of Unilever Company. Glucuronic acid (G5269-10G, Sigma), was used as standard in performance of HPLC-MS. The 1,1-diphenyl-2picrylhydrazyl (DPPH) (Sigma) was used in the antioxidant test. *Escherichia coli* ATCC 8739, *Salmonella typhimurium* ATCC 14028, and *Bacillus cereus* ATCC 11778 were used as the testing microorganism provided by Microbiologist USA Company. *Lactobacillus* de Man, Rogosa and Sharpe (MRS) medium culture and Trypton Soybean Agar (TSA) were provided by Himedia Company (India). The HPLC system (Agilent 1200) equipped with a MS detector (micrOTOF-Qll, Bruker) and ACE3 C-18 column (4.6 x 150 mm) was applied to determine the GlcUA concentration.

2.2 Prepare sweeten-black tea.

1000 mL of sweeten-black tea was prepared by adding Lipton black tea and sugar to fresh boiled water to the final concentration as 1 g/L and 100g/L, respectively. The mixture was autoclaved at 121 °C for 15 min.

2.3 Culture of KBC layer.

The KBC layers were weekly maintained in sweeten-black tea culture by adding 5g of wet layer in 100 mL of the total medium.

2.4 Fermented tea by single KBC layer and the mix culture with different LAB.

Pellet of 1 mL MRS broth culture of 8 x 10^8 different *Lactobacillus* strains were centrifuged at 10,000 rpm for 5 min at 4^{0}C, and then were added in sweeten-black tea. The mixed culture contained KBC layer and *Lactobacillus* pellet, the single culture contained only KBC layer. The fermentation was carried out in the following conditions: initial pH 5, 5 days, 30^0 C and the culture medium was 40% of the total volume vessel [10]. The unfermented sweeten-black tea was used as the negative control.

2.5 Isolation of *Lactobacillus spp.* strains from Kefir grain.

Kefir grain from Vietnam was maintained by serial subculture in defatted milk at 25^{0}C for 3 days and the bacterial strains were selected from the homogenous milk based on the growth habits and morphology. The single colony was exhibited on MRS after incubated at 37^{0}C, 72 hours under anaerobic condition.

The pure cultures were maintained and weekly transferred in MRS broth culture medium. Molecular sequences were identified by Nam Khoa Bioteck Company in HCMC. The nucleotide sequencing was analyzed by free BLAST soft -ware.

2.6 Quantification of glucuronic acid by HPLC-MS

The process was performed at Central Laboratory for Analysis in University of Science, Vietnam National University, HCMC. Tea sample was loaded through SPE C18 column then passed through Millipore filter (0.45 μm) before injected to HPLC vials. 20 μl of the filtrate was injected to a HPLC system equipped

with a MS detector and ACE3 C-18 column for the analysis. A mobile phase was 0.1% acid formic in deionized water, the stationary phase was 0.1% formic acid in methanol. The flow rate was maintained as 0.5 mL/min at room temperature (23-25^{0}C) of 210 nm wave-length. The resolution peaks were recorded on the HPLC chart according to the retention time of GlcUA as standards. The concentrations were quantified from standard curves and multiplied dilution factor.

2.7 Antibacterial activities by agar-well diffusion
Escherichia coli ATCC 8739, *Salmonella typhimurium* ATCC 14028, *Bacillus cereus* ATCC 11778 were used as the testing microorganism in agar diffusion method described [11]. 30 mL of TSA medium was poured in to 90mm diameter-Petri dish. A 5 day- fermented tea broth was obtained by 10,000 rpm centrifugation at 4^{0}C for 10 min, then the suspension was passed through 0,22 μm spore size filter papers. 100 μl of the sterilized tea samples were added into 9 mm diameter wells. The negative control well contained unfermented tea and the agar plate was incubated at 37^{0}C and the inhibited zone was observed at 18 hours for *E.coli* and *Bacillus*, 24 hours for *Salmonella*.

2.8 Determination antioxidant activities by DPPH
The antioxidant assay using DPPH were determined spectrophotometrically, according to the method described by [12] with slightly modification. 100 μM of concentration of Vitamin C solution was used as the positive control. The reaction contained of 0.5 mL sample was mixed with 1.5 mL of 250 μM ethanolic DPPH solution. The mixture of absolute ethanol 1.5 mL and sample 0.5 mL serve as blank. The absorbance was measured at 517 nm wave-length. The percentage of inhibition was calculated by following equations (1):

$$x\% = 100 - [\frac{(Abs_{sample} - Abs_{blank})x\,100}{Abs_{control}}$$

The experiment was performed in triplicate for each substance. The results were generated as percentage decrease with resp.ect to control values and compared by one-way ANOVA. A difference was considered statistically significant if p≤0.05.

III.   RESULTS AND DISCUSSION
The symbiosis between yeast and AAB has long been known. The AAB support yeast to produce ethanol and then ethanol may sever as the substrate for the acetic acid production[5]. The combination of ethanol and acetic acid prevents competition from other pathogenic bacteria [3]. However, LAB does not draw much attention in KBC, and its roles in this kind of fermented tea have not been shown [9].

3.1 Isolation and identification of *Lactobacillus sp.* from Kefir grains.
The isolated bacterial strains showed morphology of rod shape, non-spore forming, gram positive under microscope, round and milky colonies on MRS agar. The results of nucleotide sequencing compared by BLAST software showed the three different bacterial strains was identified *Lactobacillus acidophilus*, *Lactobacillus casei*, and *Lactobacillus plantarum*.

3.2 Evaluation the glucuronic acid production
The interest of GlcUA producing for food application has increased strongly during the last decade. Many studies have tried different methods to enhance the GlcUA producing by changing fermentation conditions and the culture medium as well, but this is the first report of using *Lactobacillus sp.* as the compositions of symbiosis in KBC.
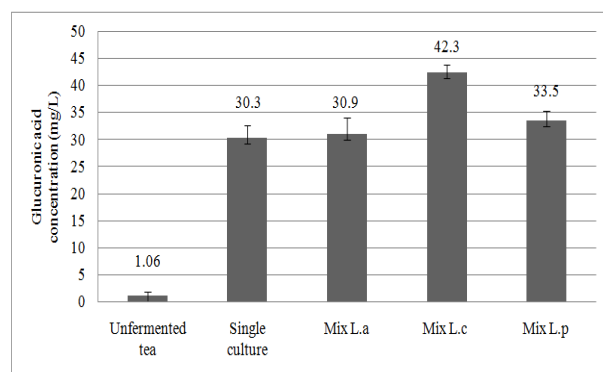
Fig. 1: The glucuronic acid production of KBC under the co-culture with each *Lactobacillus spp.* strain. Mix L.a: Mixed culture with *Lactobacillus acidophilus*, Mix L.c: Mixed culture with *Lactobacillus casei*, Mix L.p: Mixed culture with *Lactobacillus plantarum*, Single culture: The fermentation of sweeten black tea only by KBC layer. Unfermented tea: the sweeten-black tea.

At the 5th day of fermentation, the combination of *Lactobacillus casei* and KBC layer produced much more GlcUA about 39.6% than the single culture, which were 42.3 mg/L compared with 30.3 mg/L. In addition, *L.casei* can stimulate for the GlcUA production than the other LAB strains did.

According to Zhiwei, the co-culture of LAB with AAB in KBC tea can also stimulate the D-saccharic acid 1,4 lacton (DSL) a compound related to indirect anticancer activities, from 4,86% up to 86.7%. Being parts of glucuronate pathway, the presence of DSL can determine the existence of GlcUA and allow it to repel toxicant easier include carcinogen, some tumor promoters, and hepatotoxin [9]. So LAB in Kefir can promote the DSL production in KBC, they may also improve the GlcUA production.

The amount of GlcUA produced by the single culture and by the mixed culture with *L. casei* in this study were 30.3 mg/L and 42.3 mg/L, higher than those reported by Blanc [13] and Loncar [14] were only 10 mg/L and 3,39 mg/L, respectively. In those researches, there are very similar fermented conditions such as: black tea, concentration of sucrose, temperature and even longer duration (days) so, the GlcUA concentration may different since the various symbiotic culture [7].

The more study needs to be conducted to ascertain *L. casei,* a potential LAB, that can be applied for KBC tea to improve many other health benefits for human.
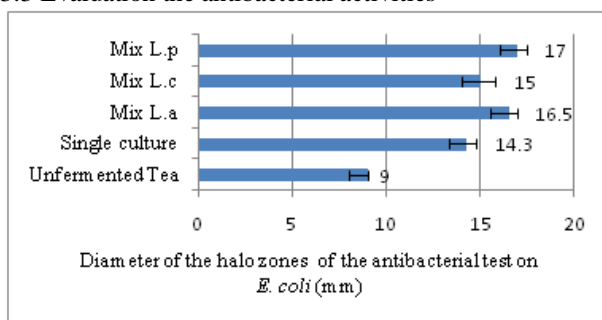
3.3 Evaluation the antibacterial activities

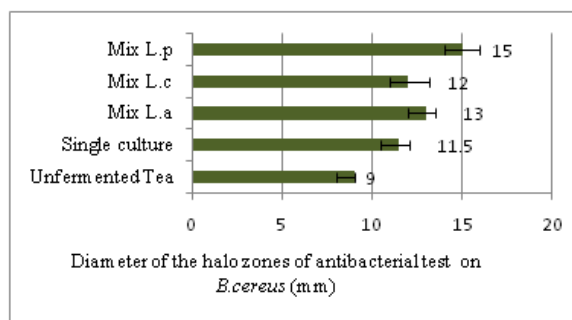Fig. 2a**:** The antibacterial activities of KBC tea on *E. coli B. cereus*

Fig. 2b: The antibacterial activities of KBC tea on
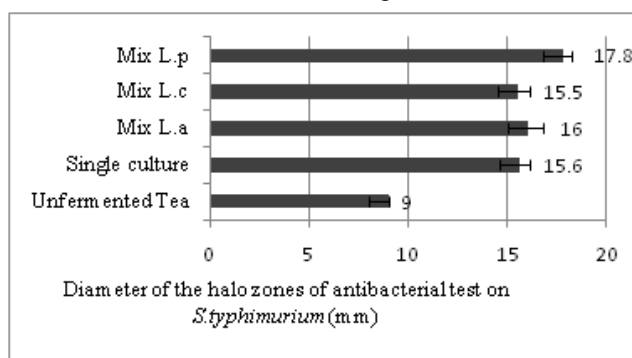
Fig. 2c**:** The antibacterial activities of KBC tea on *S. typhimurium*

Fig2a, 2b, 2c: The antibacterial test of KBC tea under the co-culture of different *Lactobacillus sp.* Mix L.a: Mixed culture with *Lactobacillus acidophilus*, Mix L.c: Mixed culture with *Lactobacillus casei*, Mix L.p: Mixed culture with *Lactobacillus plantarum*, Single culture: The fermentation of sweeten black tea only by KBC layer. Unfermented tea: the sweeten-black tea. The diameter of the well: 9 mm.

The observation on antibacterial activities of KBC tea shows the clear inhibition on three pathogenic bacteria. The longest diameter of the halo zones recorded on *E. coli, B. cereus, S. typhimurium* were 17, 15, 17.8 (mm) respectively, by the fermented tea of KBC layer and *L. plantarum*. The halo zone of the unfermented tea sample was not recognized, so the data were presented in 9 mm- diameter of the well. In some reports, the tea extract or unfermented tea can against *S. tiphimurium* but does not effect on *E. coli* [15]. It is different from our study the unfermented tea sample inhibits none of these strains. However, this results contributed to the significant antibacterial abilities of fermented tea in control the growth of *E. coli, B. cereus* and *S .tiphimurium* because these microorganisms are responsible for diarrheal disease, food-borne illness, gastroenteritis and enteric fever, which are still the most serious and important public health problems in many developing countries [16,17]. Findings more about the effect of fermented tea are so helpful because KBC is popular drinks

on over the world. The results can use for producing an oriented valuable drink that improve the gastrointestinal systems. Moreover, the combination of *Lactobacillus* in this research also provides a healthy, functional and potential probiotic property for human consumption [18].

3.4 Evaluation the antioxidant activities

This systematic study determines the direct antioxidant potential of KBC tea, fermented by single culture and mix culture with different *Lactobacillus spp.*, against a spectrum of oxidant 1,1-diphenyl-2picrylhydrazyl (DPPH). The mechanism of antioxidant properties on DPPH radical scavenging may because of their hydrogen-donating ability. DPPH scavenger capacity of tea sample was compared with the known antioxidant substance as vitamin C.

As the results, the level of DPPH decolonization of KBC sample shows no significant differences between the mixed culture of KBC layer with *lactobacillus spp.*, and the single KBC layer, which were 80.28% to 88.56%. The mix culture of *L. platarum* and KBC layer shows the higher antioxidant activities compared to other combinations. The positive control, vitamin C showed the highest percentage of 91.15 % and the lowest 63.63% belong to the unfermented tea. The antioxidant properties of KBC tea may high because of vitamin C, Vitamin B, DSL synthesized during the fermentation. This result is lower than those reported in lemon-blam KBC, which the antioxidant percentage was about 95.5% [19]. The reason may because of the difference in amount used and antioxidant compounds of black and lemon-blam tea.
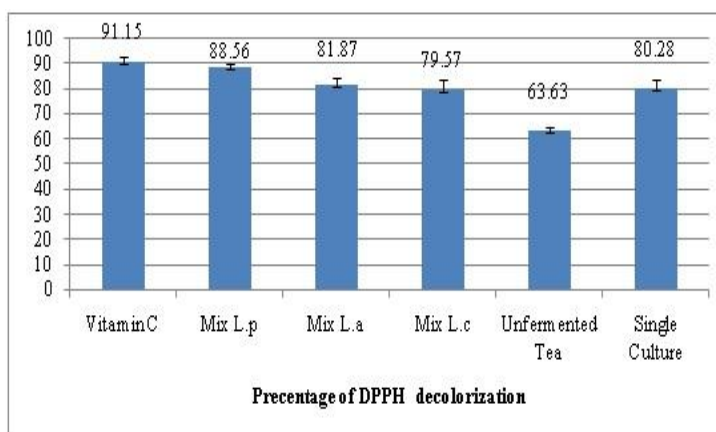

Fig 3: The DPPH antioxidant test of KBC tea under the co-culture of *Lactobacillus* sp. Mix L.a: Mixed culture with *Lactobacillus acidophilus*, Mix L.c: Mixed culture with *Lactobacillus casei*, Mix L.p: Mixed culture with *Lactobacillus plantarum, v*itamin C: a standard vitamin C served as the positive concentration. Single culture: The fermentation of sweeten black tea only by KBC layer. Unfermented tea: the sweeten-black tea.

IV. CONCLUSION

In this study, *Lactobacillus casei* and *Lactobacillus plantarum* have advantages in improving the glucuronic acid concentration and antibacterial, antioxidant activities in the original KBC tea. These enhancements of biological functions of KBC tea may contribute to the orientation of fermented drink production for human. However, more study need to be investigated about the customer's taste, order, and overall appearance of the mixed culture compared to the original KBC tea. On the other hand, this study is identified as being significance of the research in producing healthy and valuable fermented tea for the beverage industry since this kind of drink is well-known through many countries on over the world.

REFERENCES

Journal Papers
[1]   V. Ilmara , Raimonds.L, P. Arturs, and S. Pavels, Glucuronic acid from fermented beverages: biomedical function in humans and its role in health protection, International journal of research and reviews in applied science, 14(2), 2013, 218-230.
[2]   Goh, W.N., Rosma A., Kaur, B., Fazilah, A., Karim A.A. and Rajeev Bhat. Fermentation of black tea broth (KBC): I. Effects of sucrose concentration and fermentation time on the yield of microbial cellulose. International Food Research Journal, 19(1),2012, 109-117.
[3]   C.H. Liu, W.H. Hsu, F.L. Lee and C.C. Liao, The isolation and identification of microbes from a fermented tea beverage, Haipao, and their interactions during Haipao fermentation. Food Microbiology ,13(6), 1996, 407-415.
[4]   A.L Teoh, G. Heard and J.Cox, Yeast ecology of KBC fermentation. International Journal of Food Microbiology, 95(2),2004, 119-126.

[5]   Dufresne, C. and E. Farnworth,. Tea, KBC and health: a review. Food Research International, 33(6), 2000, 409-421.

[6]   Y. Nafiseh, M.A Mahnaz, B.M Mohammad and L. Kambiz. Resp.onse Surface Methodology for Optimization of Glucuronic Acid Production using KBC Layer on Sour Chaerry Juice. Australian Journal of Basic and Applied Sciences, 5(11), 2010, 3250-3256.

[7]   P. Mayser , C. Stephanie and K. Grunder, The yeast spectrum of the tea fungus KBC. Mycoses, 38(5), 1995, 289-295.

[8]   M.O. L Analy, A. L M Marco, S.P Raquel, S. R Alexandre, T. S Joab and M. F. P Vania, Microbiological, technological and therapeutic properties of kefir: a natural probiotic beverage, Brazilian Journal of Microbiology 44(2), 2013, 341-349.

[9]   Y.Zhiwei, Z.Feng, J. Baoping, L.Bao, L.Yangchao, Y.Li and L.Tao, Symbiosis between microorganism from Kombucha and Kefir: Potential significance to the enhancement of Kombucha function. Applied biochemical Biotechnology, 160(2), 2000, 446-455.

[10]   **Y.** Zuo, and B.Ming-hong, Optimization of fermentation conditions for Kombucha Tea**,** Food science, 11, 2011.

[11]   I. Saba, M. Maryum and P. Farzana , In-vitro Antibacterial activities of three medicinal plant using agar well diffusion method, Research Journal of Biology, 2(1), 2012, 1-8.

[12]   K. Nurgun, G. Aysegul, T.N. Nilufer, A. Ahmet, Antioxidant activity and total phenolic content of aqueous extract from Raohanus Rapphanistrum L. Turkish Journal of Pharmaceutical Sciences, 9(1), 2012, 93-100.

[13]   Ph.J Blanc, Characterization of the tea fungus metabolites. Biotechnology Letter, 18, 1996, 139-142.

[14]   Loncar E.,Petrovic S., Malbasa R., Verac R. Biosynthesis of glucuronic acid by means of tea fungus. Nahrung, 44(2), 2000, 138-139.

[15]   M. Toda, S. Okubo, R. Hiyoshi, and Tadakatsu,S. The bactericidal activity of tea and coffee. Letters in Applied Microbiology, 8, 1989, 123-125.

[16]   J.S.J Rodrigo, A.B Rejane, A.R Sheyla, X.F Lauro, and S.L. Alvaro, Antimicrobial activity of broth fermented with KBC colonies, Journal of Microbial & Biochemical Technology, 1(1), 2009, 72-78.

[17]   Michael E. O and Samuel I.M, Salmonella: A model for bacterial pathogenesis, Annual review of Medicine. 52, 2001, 259-274 (2001).

[18]   C.V Maaike, E.V Elain, K. Michiel, and M.V. Willem, Lactobacillus plantarum-survial, functional and probiotic properties in the human intestinal tract. International Dairy Journal 16, 2006, 1018-1028.

[19]   S.V Aleksandra, D.C Dragoljub, L.M Sinisa, T.T Vesna, and M.S Sladana, Antimicrobial and antioxidant activity of lemon Blam KBC., Acta Periodica Technologica, 38, 2007, 165-172.

Dynamic Spectrum Allocation in Wireless sensor Networks

Santosh Subedi[1], Saubhagya Das[2], N. Shekar V. Shet[3]

[1, 2, 3] *(Department of E&C, NITK, Surathkal, India)*

Abstract: *Radio frequency spectrum is considered the most expensive and scarce resource among all wireless network resources, and it is closely followed by the energy consumption, especially in low energy, battery powered wireless sensor network devices. These days, there is a tremendous growth in the applications of wireless sensor networks (WSNs) operating in unlicensed spectrum bands (ISM). Moreover, due to the rapid growth of wireless devices that are designed to be operated in unlicensed spectrum bands, these spectrum bands have been overcrowded. The problem with overcrowded spectrum or scarcity of spectrum can be solved by Dynamic Allocation of Spectrum. In this paper we have presented the implementation and analysis of dynamic spectrum allocation in Wireless Sensors Networks using the concept of Cognitive Radio Ad Hoc Network.*

Keywords: *Cognitive Radio Ad Hoc Network (CRAHN), Dynamic Spectrum Access (DSA), Primary Users (PU), Secondary Users (SU), Wireless Sensor Networks (WSN).*

I. Introduction

Wireless Sensor Network (WSN) refers to a group of spatially dispersed and dedicated sensors for monitoring and recording the physical conditions of the environment and organizing the collected data at a central location [1]. WSNs measure environmental conditions like temperature, sound, pollution levels, humidity, wind speed and direction, pressure etc. WSNs were initially designed to facilitate military operations but its application has since been extended to health, traffic, and many other consumer and industrial areas. A WSN consists of anywhere from a few hundreds to thousands of sensor nodes. The sensor node equipment includes a radio transceiver along with an antenna, a micro-controller, an interfacing electronic circuit, and an energy source, usually a battery. Multi-hop routing is a critical service required for WSN. WSNs are often deployed in an ad hoc fashion, routing typically begins with neighbor discovery [2]. Nodes send rounds of messages (packets) and build local neighbor tables. These tables include the minimum information of each neighbor's ID and location. This means that nodes must know their geographic location prior to neighbor discovery.

The leading areas of research and development in wireless communications are techniques and mechanisms to implement the most cost effective and efficient utilization of the radio frequency spectrum and energy. WSNs operate in the unlicensed band (ISM) of 2.4 GHz. Meanwhile, same spectrum band is shared by the other rapidly growing wireless devices with wireless applications like Wi-Fi and Bluetooth [3]. Due to which, the unlicensed spectrum band has become overcrowded. This yields interference among the WSNs nodes, which degrades the performance of WSNs. According to [4], the portions of the spectrums in 30MHz to 30GHz are underutilized. This huge imbalance in the use of different portions of spectrums can be minimized by the dynamic allocation of spectrum. This technique of dynamic spectrum allocation where licensed spectrum is accessed opportunistically is called the Cognitive Radio Technology. Including this section on introduction, the paper is organized on six sections. Brief description of CR technology is given in section 2; Sub-sections 2.1 & 2.2 gives the overview about routing protocol and MAC protocols for CR technology. A model for Cognitive Radio Ad Hoc Network is explained in Section 3. Section 4 will present simulation scenarios, results and analysis. The conclusion of the paper will be in Section 5.

Fig 1: Licensed Spectrum Usage [16]

II. Cognitive Radio Technology

Cognitive Radio (CR) is an adaptive, intelligent radio and network technology that can automatically detect available channels in a wireless spectrum and change transmission parameters enabling more communications to run concurrently and also improve radio operating behavior. CR technology aims at making use of the network resources currently used in wireless communication systems more efficiently. CR allows opportunistic use of the licensed spectrum band by an unlicensed user with minimum allowable interference to the licensed user, and without compromising on the desired quality of service required by the unlicensed user. The CR technology is well explained by the cognitive cycle (Fig. 2). Normally, cognitive cycle contains three major steps namely; Spectrum sensing, Spectrum Analysis and Spectrum Decision Making [15].
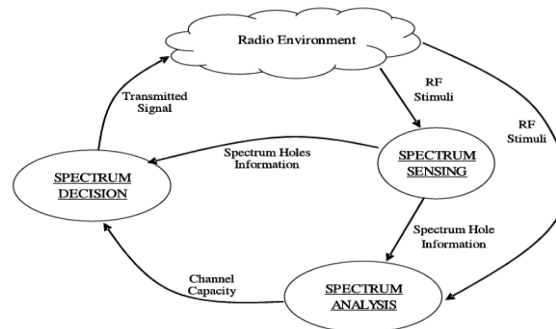

Fig.2: Cognitive Cycle [15]

Spectrum sensing is the first step which determines the presence/absence of primary user on the band. After sensing the spectrum, the cognitive radio can share the result of its detection with other cognitive radios. Spectrum sensing is the ability to measure, sense and be aware of the parameters related to the radio channel characteristics, availability of spectrum and transmit power, interference and noise, radio's operating environment, user requirements and applications, available network (infrastructures) and nodes, local policies and other operating restrictions. It is done across Frequency, Time, Geographical Space, Code and Phase. There are various ways of spectrum sensing. Hypothesis testing, Likelihood ratio test, use of Detectors etc are few candidates.

Spectrum Analysis is based on spectrum sensing which is analyzing the situation of several factors in the external and internal radio environment (such as radio frequency spectrum use by neighboring devices, user behavior and network state) and finding the optimal communication protocol and changing frequency or channel accordingly. It is also known as channel estimation.

Spectrum Decision Making calls for reconfiguration for the channel and protocol required for constantly adapting to mobile changing environments and adjustment of output power or even alteration of transmission parameters (such as modulation formats (e.g. low to high order QAM), variable symbol rates, different channel coding .

Development of cognitive radio technology involves extensive areas of research from physical to network layer. The studies on physical layer focus on various topics including development of Software-Defined Radio (SDR), modulation scheme based on Orthogonal Frequency- Division Multiple Access (OFDMA), spectrum sensing, channel characteristics and power control etc. Most of the research and published papers are focused on the layer above the physical layer namely Medium Access Control (MAC protocol) and Routing Protocol.

2.1 Routing Protocol for CR Technology

Mobile Ad hoc network is network where nodes communicate without any central administration or network infrastructure. They are connected via wireless channels and can use multiple hops to exchange data. Routing protocols are needed for communication in such Ad hoc networks, where it targets for efficient and timely delivery of message. A Cross Layer Routing Protocol has been proposed in [6] which operate with CHARN. This routing protocol exploits the passage of CR performance information from the physical/MAC layers up to Network layer as contributing factors within the route selection algorithms. The proposed routing protocol takes suitable sub-channel information of each hop into account. With the sensing capability of each node, the condition of all sub-channels between two neighbours will be fully captured and the information will be forwarded from the Physical layer to MAC and Network layers via the cross layer mechanism in each node. Location- Aided Routing Protocol [7] is a routing protocol for Cognitive Radio Networks that uses a common

control channel to convey the message among the secondary users. This routing protocol has a minimal route setup delay, prefers stable routes, handles primary user's heterogeneity, and handles secondary user's mobility.

2.2 MAC Protocol for CR Technology

In Cognitive radio networks, the spectrum can be divided into several channels, either non-overlapping or partially overlapping. When we say a channel is available for a secondary user to use, it means either no primary user works on that channel or the interference from this secondary user to the active primary users is tolerable. MAC protocols are used to utilize these available channels. The cognitive radio MAC acts as a bridge between the cognitive radio physical layer and the cognitive radio network layer. On the one hand, it can utilize the spectrum-sensing results from the cognitive radio physical layer, characterize the channels, and decide which channel to use and when to access. On the other hand, it can help the cognitive radio network layer to decide the routing path by reporting the characteristic information and the list of available channels. Also, the cognitive radio network layer can tell the cognitive radio MAC to choose a suitable channel for a dedicated quality-of-service (QoS) requirement.

A Simple Greedy MAC for Cognitive Radio Networks [8] has been proposed for CR networks. This Greedy MAC is the combination of Simple Sequential MAC [9] and Greedy algorithm where the secondary users excess the channel in greedy manner. The network works on Simple Sequential MAC for certain time and later it works on Greedy MAC. The channel with maximum received packets is recorded and the secondary users try to access the channel which has received more packets. Packet Reservation Multiple Access (PRMA) based MAC protocol [10] for cognitive machine-to-machine communications uses cognitive radio technology at the physical layer. PRMA is a combination of slotted ALOHA, TDMA and a reservation scheme. This MAC protocol tries to access the vacant TV channels for audio transmission.

III. A Model for Cognitive Radio Ad Hoc Networks

A Cognitive Radio Ad Hoc Network model [5] has been proposed which doesn't use any specially designed Routing Protocol or MAC protocol for CR technology. It uses 802.11 MAC (wireless LAN) protocol and Ad Hoc on- Demand Distance Vector (AODV) protocol. This CR Ad Hoc network takes the information about channels and number of Primary users, their arrival and departure time and the range of primary users from two different files namely' map.txt and channel.txt. In order to describe the dynamic nature of CR networks, a new metric that captures the statistical behaviour of primary networks called primary user (PU) activity is introduced. In this model, the PU traffic can be modelled as a two state birth–death process with death rate ά (Alpha) and birth rate β (Beta). An ON (Busy) state represents the period used by PUs and an OFF (Idle) state represents the unused period. Since each user arrival is independent, each transition follows the Poisson arrival process. According to [5],

The changing spectrum environment and the importance of protecting the transmission of the licensed users of the spectrum mainly differentiate classical ad hoc networks from CRAHNs. In CRAHNs, the available spectrum bands are distributed over a wide frequency range, which vary over time and space. Thus, each user shows different spectrum availability according to the PU activity. As opposed to this, classical ad hoc networks generally operate on a pre-decided channel that remains unchanged with time. Also, classical Ad hoc Network sends periodic beacon message in the channel for topology control, whereas in CRAHNs, as the licensed spectrum opportunity exists over large range of frequencies, sending beacons over all the possible channels is not feasible.

This model of Cognitive Radio Ad Hoc network uses Cross- Layer Repository to enable channel information sharing between MAC and routing protocols. The receiver channel for each node is set randomly. Each sending channel is initialized as NOT active for each node. When a PU is detected, a pre-defined threshold is used to decide whether to stay or leave the current channel. Spectrums are decided based on allocation policy namely Random Switch and Round Robin Switch. Frequent handoff of spectrum is performed as per requirements. We have followed this model of Cognitive Radio Ad Hoc Network in order to implement the dynamic Spectrum Allocation in Wireless Sensor Networks. For the analysis of dynamic spectrum allocation in WSNs, we have used three different parameters namely Throughput, Packet Drop Rate and Average Packet End to End delay.

IV.   Simulation Results and Analysis

For implementation of dynamic spectrum allocation in WSN, we've used Network Simulator-2(ns-2.31) as a Simulator. We've modified the network simulator for the implementation of dynamic spectrum allocation in WSN. During the simulation, primary users may vary from one to ten in numbers. The arrival and departure of PUs are set in a manner that we can see the effect of primary users on the communication of secondary users. For e.g.: In a case of 10 primary users, 5 of them arrive at the beginning of the simulation and departure after 70secs. Similarly, next 5 primary users arrive at 30secs and remain till end. Hence in the simulation time of 30-70secs there are maximum numbers of primary users. The effect due to the presence of maximum number of primary users can be seen in the throughput plot.

We have taken three different cases for analysis, first case contains ten primary users, second case contains eight primary users and the third case contains four primary users in the network. The resulting throughput, average end-to-end delay and packet drop rate plot depicts primary user activity behavior on secondary users.The simulation specifications are as follows:

Total no. of channels	11
Number of PUs	Varies from 1 to 10
Number of SUs	10
Transport Protocol	UDP
Packet Rate	300Kbps
Packet Size	512
Node speed	10, 15 m/s
Simulation Time	100 s
Height of Antenna	1.5m
Tx /Rx Gain	1
Bandwidth	2.4 GHz
Propagation Loss	0.5

Table.1: Simulation Specifications

4.1 Ten Primary Users

In this case, for the first 30secs, there are only five PUs; during 30 to 70secs there are ten PUs and after 70secs five PUs departure from the network. So there is heavy PU traffic activity at 30 to 70secs of Simulation time.
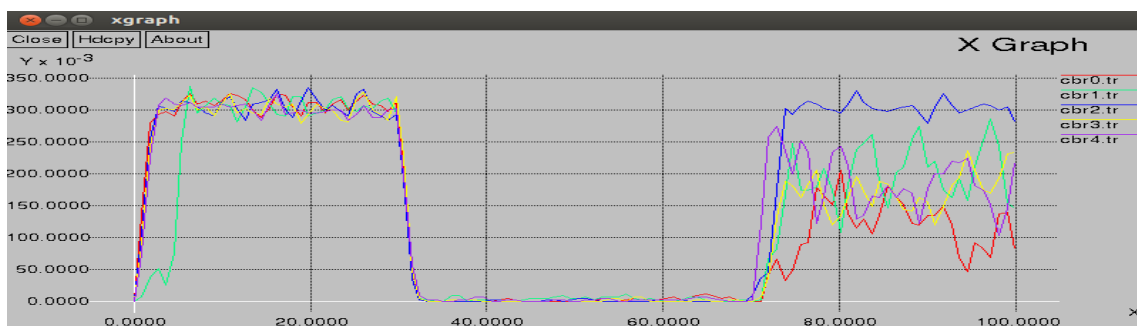

Fig.3: Throughput Plot (X: simulation time/ Y: Throughput)

As shown in Fig.3, in the first and last 30secs of simulation time, only five PUs exist, so throughput of SUs is high. But during 30 to 70secs of simulation time there exist ten PUs, only one channel is left for secondary users, so throughput of the SUs has reduced to almost zero.
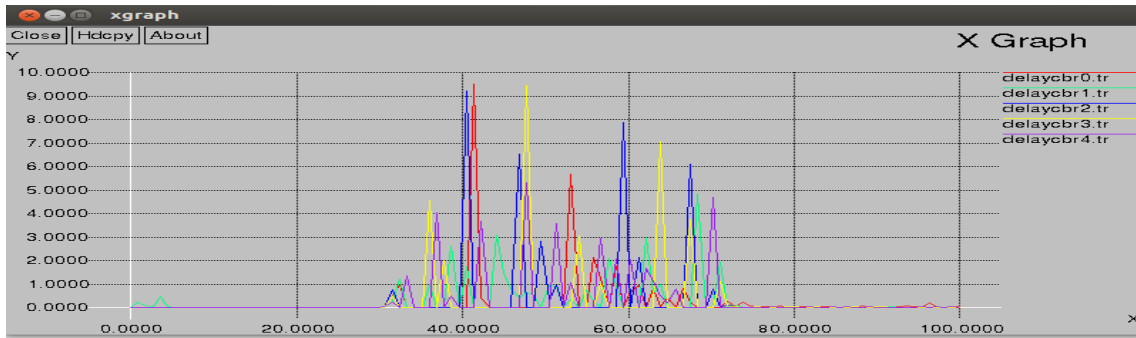
Fig.4: Average Packet End-to-End delay(X: Simulation time/Y: Delayed packets)

As shown in Fig.4, when there is enough channels for secondary users, there is no packet end-to-end delay. But when only one channel is available for all the SUs, all the SUs try to access it resulting into high packet end-to-end delay.
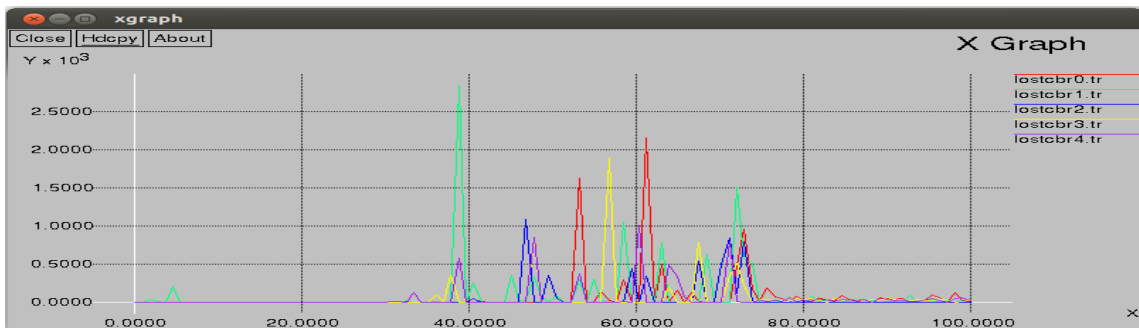

Fig.5: Packet Drop Rate.

In fig.5, since throughput of SUs at simulation time 30-70secs is almost zero, increasing average end to-end delay boosts up the Packet Drop Rate.

4.2 Case II. Eight Primary Users
Similar to case I, four PUs exist in first 30secs; eight PUs in between 30-70secs and among eight PUs four PUs departure after 70secs.
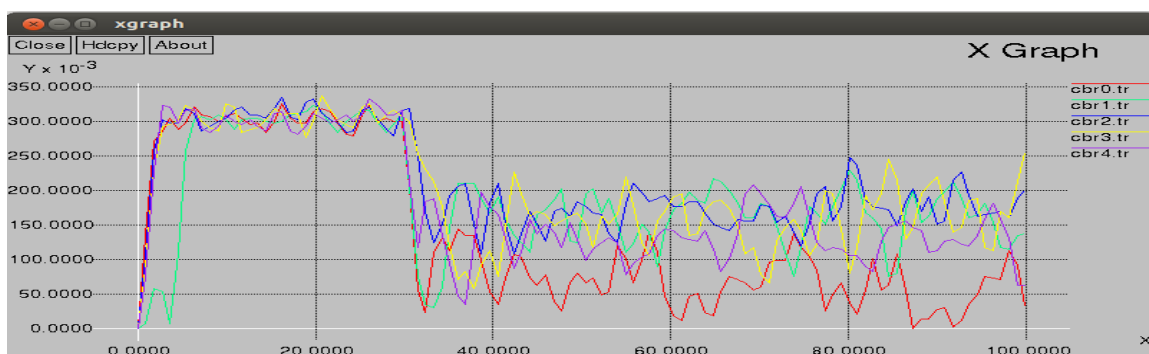

Fig.6: Throughput Plot.

In Fig.6, after the first 30secs of simulation time, SUs still can transfer their data because total no. of channels is not fully utilized by the PUs. The fluctuation in throughput of SUs is due to the several handoffs of channels. After the departure of four PUs (after 70secs), the throughput of SUs does not raise significantly due to the movement of SUs nodes.
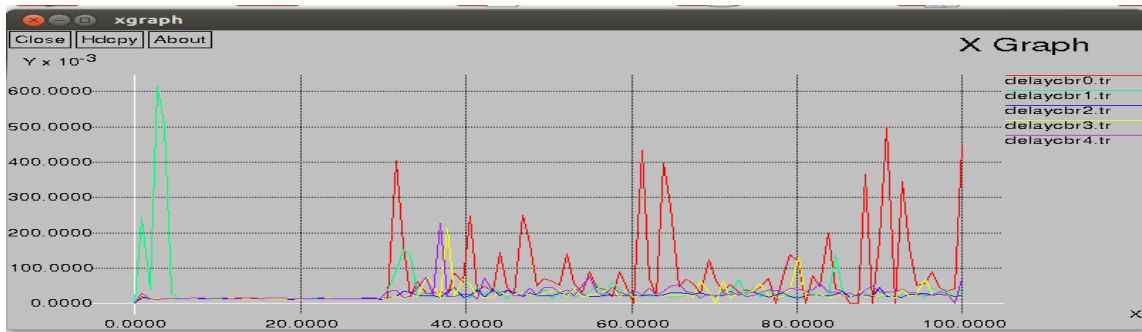
Fig.7: Average Packet End-to-End delay

Here, due to the several handoff operations and movement of WSNs nodes, few packets are delayed after 30secs of run time.
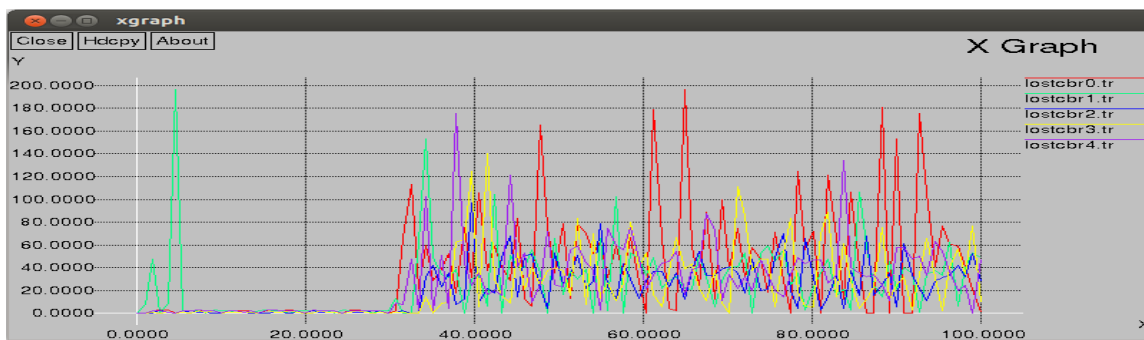
Fig.8: Packet Drop Rate

Fig.8 shows the packet drop rate due to the packet end-to-end delay in run time.

4.3 Case III. Four Primary Users
In case III, we reduced the number of PUs to half of Case II. The arrival and departure of PUs is in the same fashion as earlier cases.
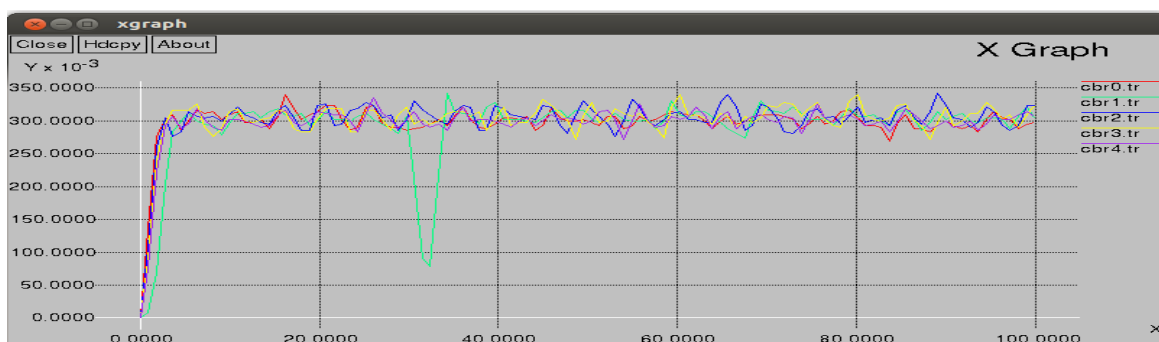
Fig.9: Throughput Plot.

Here, after the simulations starts, there is always surplus amount of channels in the network for the SUs, hence throughput of SUs does not decrease gradually, but fluctuates due to handoffs.
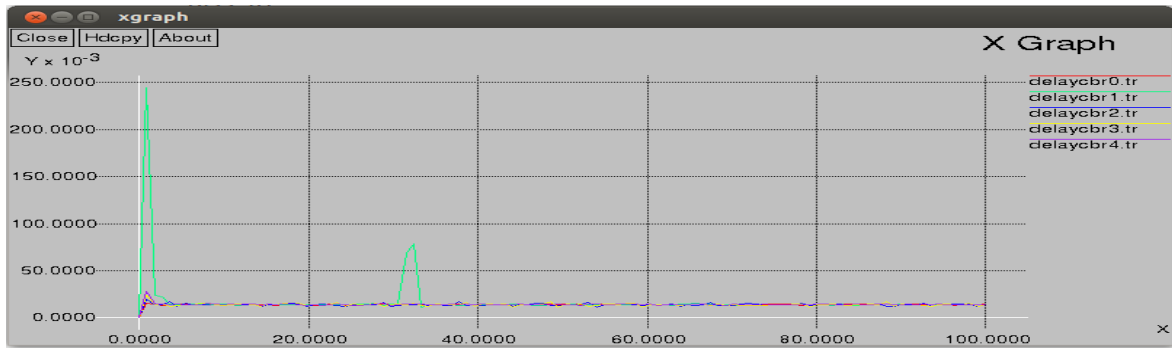
Fig.10: Average Packet End-to-End delay.

In fig.10, Packet end-to-end delay has been reduced drastically due to the availability of enough channels for data transmission.
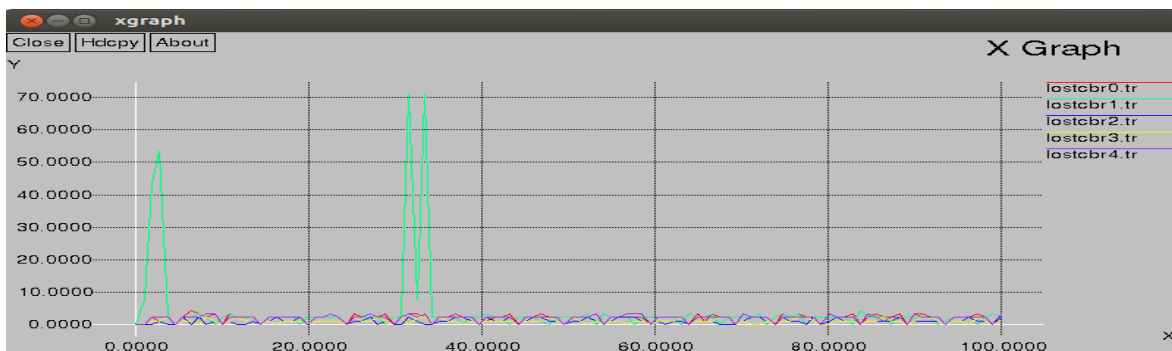
Fig.11: Packet Drop Rate.

Since there is no significant Packet end-to-end delay, no significant packet drop rate is present. The packet drop in cbr1 (green) is due to the movement of nodes.

These three cases are the cases where we can see the effect of available channels on the throughput of secondary users distinctly. Moreover we calculated the throughput due to secondary users in the presence of various numbers of primary users. Here, arrival and departure of PUs is in similar fashion, with same transmission range (of PUs) throughout the simulation. The location of PUs may slightly vary.
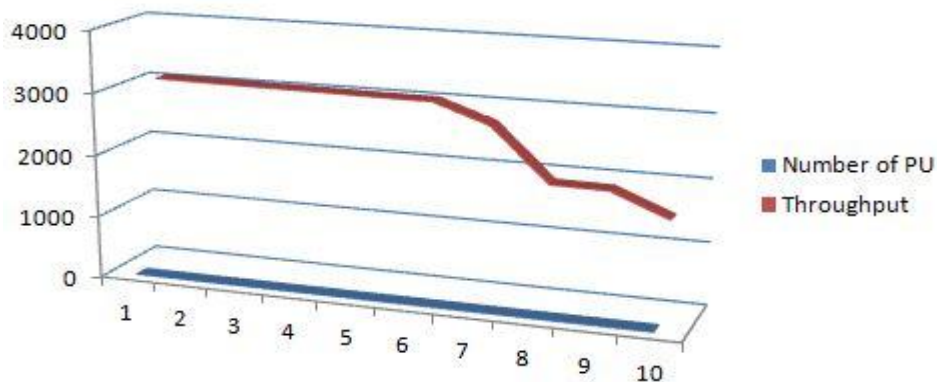
Fig.12: Average throughput by SUs in the presence of different no. of PUs.

Here, we can see the drastic change is average amount of throughput by SUs when the number of PUs increases from six to ten. It is so because, in our simulation, all the WSN nodes transfer data in pairs. So for a pair of five WSN nodes, five channels are enough to transfer data.

V. Conclusion

We would like to conclude our experiment on two aspects namely; throughput and energy. Since Wireless Sensor Nodes are deployed in environment in huge numbers, it's not pragmatic to change the energy source (battery) of the WSN nodes frequently. Hence, along with spectrum, energy source is also precious in case of WSNs. In our experiment we got a good throughput even in the presence of lots of Primary users. Spectrum sensing, spectrum analysis, spectrum decision and handoff operations require a lot of computations which results in the consumption of heavy energy source. Therefore, only throughput cannot be the major parameter in the dynamic spectrum allocation of WSNs. Future work will be focused on the design of a good MAC protocol for dynamic spectrum allocation in Wireless Sensor Networks which can access the licensed spectrum opportunistically with fewer computations and less consumption of energy source.

REFERENCES

[1]   Neha Singh et al, "Network Simulator NS2-2.35 ", International Journal of Advanced Research in Computer Science and Software Engineering , Volume 2, Issue 5, May 2012.
[2]   John A. Stankovic "Wireless Sensor Networks", Department of Computer Science, University of VirginiaCharlottesville, Virginia 22904.
[3]   Dave Cavalcanti et al, "Cognitive Radio based Wireless Sensor Networks", Wireless Communications and Networking Department, Philips Research North America Briarcliff Manor, NY, 10510.
[4]   C. Liu., "Spectrum sharing in dynamic spectrum access networks: WPE-ii written report", Technical Reports (CIS), 2009.
[5]   Ian F. Akyildiz et al, "CRAHNs: Cognitive radio ad hoc networks ", Broadband Wireless Networking Laboratory, School of Electrical and Computer Engineering, Georgia Institute of Technology, Atlanta, GA 30332, United States .
[6]   Yan Sun et al, "A Cross Layer Routing Protocol in CRMANET", Queen Mary University of London, School of Electronics Engineering and Computer Science, Mile End Road, London, UK.
[7]   Karim Habak et al, "A Location-Aided Routing Protocol for Cognitive Radio Networks ", Department of Computer Science and Engineering, Egypt-Japan Univ. of Sc. and Tech. (E-JUST),Alexandria, Egypt
[8]   Humaira Afzal et al, "A Simple Greedy Algorithm for Cognitive Radio Networks", School of Computing, Information and Media, University of Bradford, UK.
[9]   Usman Shahid Khan et al, "CRN Survey and A Simple Sequential MAC Protocol for CRN Learning", Computer Science Department , COMSATS Institute of Information Technology , Abbottabad, Pakistan.
[10]   Adnan Aijaz et al," A PRMA based MAC Protocol   for Cognitive Machine-to-Machine Communications", Institute of Telecommunications, King's College London, and London WC2R 2LS, UK.
[11]   Yan Zhang et al, "Cognitive Radio Networks: Architecture, Networks and Standars", Simula Research Laboratory, Norway.
[12]   Gyanendra Prasad Joshi et al, "Cognitive Radio Wireless Sensor Networks: Applications, Challenges and Research Trends", Department of Information and Communication Engineering, Yeungnam University, 214-1 Dae-dong, Gyeongsan-si, Kyongsan 712-749, Gyeongsangbuk-do, Korea .
[13]   Abolarinwa J.A et al, "Cognitive Radio-based Wireless Sensor Networks as Next Generation Sensor Network: Concept, Problems and Prospects", Department of Telecommunication Engineering, Federal University of Technology Minna, Nigeria.
[14]   Pingnan Lee et al, "NS2 Model for Cognitive Radio Networks Routing ", School of Computer Science and Technology, Beijing University of Posts and Telecommunications, Beijing 100876, China .
[15]   Abolarinwa J.A et al, "Cognitive Radio-based Wireless Sensor Networks As Next Generation Sensor Network: Concept, Problems and Prospects", Department of Telecommunication Engineering, Federal University of Technology Minna, Nigeria.
[16]   B. Wang and K. J. Ray Liu,"Advances in Cognitive Radio Networks: A Survey", IEEE Journal of Selected topics in signal processing, vol. 5, no. 1, PP. 5-23, 2011
[17]   Antônio Dâmaso et al, " Evaluating the Power Consumption of Wireless Sensor Network Applications Using Models", Centre of Informatics, Federal University of Pernambuco, 50740-540, Recife, PE, Brazil.
[18]   Amir Ghasemi," Spectrum Sensing in Cognitive Radio",Networks: Requirements, Challenges and Design Trade-offs", Communications Research Centre Canada and University of Toronto Elvino S. Sousa, University of Toronto.
[19]   Ozgur B. Akan et al, "Cognitive Radio Sensor Networks", Next generation Wireless Communications Laboratory (NWCL), Department of Electrical and Electronics Engineering, Middle East Technical University, Ankara, Turkey.
[20]   Zhe Chen, "Demonstration of Real-time Spectrum Sensing for Cognitive Radio", Department of Electrical and Computer Engineering Center for Manufacturing Research Tennessee Technological University Cookville, TN 38505, USA.
[21]   Geoffrey Sampson, "Perl for Beginners", © 2010 Geoffrey Sampson & Ventus Publishing ApS ISBN 978-87-7681-623-0.

Modeling and Structural Analysis of Ladder Type Heavy Vehicle Frame

V. Vamsi Krishnam Raju[1], B. Durga Prasad[2], M. Balaramakrishna[3], Y. Srinivas[4]

[1, 2, 3, 4] *(Department of Mechanical Engineering, Vishnu Institute of Technology, India)*

Abstract: *The automobile is divided into two parts body and chassis. The chassis is basic structure of a vehicle. It contain all the engine parts and power systems but the frame is the main portion of chassis which do not contain any other assemblies like engine parts. Its principle function is to safely carry the maximum load for all designed operating conditions. This paper describes modeling and structural analysis of conventional type heavy vehicle frame. Weight reduction is now the main issue in automobile industries. In the present work, the dimensions of an existing heavy vehicle frame of a TATA 1109 EX2 vehicle is taken for modeling and analysis. The vehicle frame is initially modeled by considering 'C' cross section in SOLID WORKS 2011 and then it is imported to ANSYS 13.0. The analysis is done with three different composite materials namely Carbon/Epoxy, E-glass/Epoxy and S-glass/Epoxy subjected to the same pressure as that of a steel frame. The design constraints are stresses and deformations. The results are then compared to finalize the best among all the four frames.*

Keywords: *frame, Auto CAD 2012, SOLID WORKS 2011, ANSYS 13.0, TATA 1109 EX2.*

I. Introduction

Automotive chassis is a French word that was initially used to represent the basic structure. It is a skeletal frame on which various mechanical parts like engine, tires, axle assemblies, brakes, steering etc. are bolted. It gives strength and stability to the vehicle under different conditions.

At the time of manufacturing, the body of a vehicle is flexibly molded according to the structure of chassis. Automobile chassis is usually made of light sheet metal or composite plastics. It provides strength needed for supporting vehicular components and payload placed upon it. Automotive chassis or automobile chassis helps keep an automobile rigid, stiff and unbending. It ensures low levels of noise, vibrations and harshness throughout the automobile.

Automobile chassis without the wheels and other engine parts is called frame. Automobile frames provide strength and flexibility to the automobile. The backbone of any automobile, it is the supporting frame to which the body of an engine, axle assemblies are affixed. Tie bars that are essential parts of automotive frames are fasteners that bind different auto parts together. Automotive frames are basically manufactured from steel. Aluminum is another raw material that has increasingly become popular for manufacturing these auto frames. In an automobile, front frame is a set of metal parts that forms the framework which also supports the front wheels.

1.1 Types of frames

There are three types of frames
1. Conventional frame
2. Integral frame
3. Semi-integral frame

1.1.1 Conventional frame

It has two long side members and 5 to 6 cross members joined together with the help of rivets and bolts. The frame sections are used generally.
   a. Channel Section – Good resistance to bending
   b. Tabular Section – Good resistance to Torsion
   c. Box Section – Good resistance to both bending and Torsion

1.1.2 Integral frame

This frame is used now in most of the cars. There is no frame and all the assembly units are attached to the body. All the functions of the frame carried out by the body itself. Due to elimination of long frame it is cheaper and due to less weight most economical also. Only disadvantage is repairing is difficult.

1.1.3 Semi – Integral frame
In some vehicles half frame is fixed in the front end on which engine gear box and front suspension is mounted. It has an advantage when the vehicle is met with an accident the front frame can be taken easily to replace the damaged chassis frame. This type of frame is used in American and European cars.

1.2 Functions of the frame
1. To carry load of the passengers or goods carried in the body.
2. To support the load of the body, engine, gear box etc.,
3. To with stand the forces caused due to the sudden braking or acceleration.
4. To with stand the stresses caused due to the bad road condition.
5. To with stand centrifugal force while cornering.

1.3 Various loads acting on the frame
1. Short duration Load – While crossing a broken patch.
2. Momentary duration Load – While taking a curve.
3. Impact Loads – Due to the collision of the vehicle.
4. Inertia Load – While applying brakes.
5. Static Loads – Loads due to chassis parts.
6. Over Loads – Beyond Design capacity.

II.   Problem Specification

Weight reduction is now the main issue in automobile industries. Because if the weight of the vehicle increases the fuel consumption increases. At the same time as the weight of the vehicle increases the cost also increases which becomes a major issue while purchasing an automobile. For example if we take frame of TATA 1109 EX 2 heavy vehicle frame. It is manufactured with Structural Steel. Steel structures exposed to air and water, such as bridges are susceptible to corrosion. In conditions of repeated stress and more temperatures it can suffer fatigue and cracks. These are the main problems of steel and these are compensated by inducing composite materials.

2.1 Composite Materials
A composite material is defined as a material composed of two or more materials combined on a macroscopic scale by mechanical and chemical bonds. Unique characteristic of many fiber reinforced composites is their high internal damping capacity. This leads to better vibration energy absorption within the material and results in reduced noise transmission to neighboring structures. Many composite materials offer a combination of strength and modulus that are either comparable to or better than any traditional metallic metals. Because of their low specific gravities, the strength to weight-ratio and modulus to weight-ratios of these composite materials are markedly superior to those of metallic materials. The fatigue strength to weight ratios as well as fatigue damage tolerances of many composite laminates are excellent. For these reasons, fiber composites have emerged as a major class of structural material and are either used or being considered as substitutions for metals in many weight-critical components in aerospace, automotive and other industries.

High damping capacity of composite materials can be beneficial in many automotive applications in which noise, vibration, and hardness is a critical issue for passenger comfort.

2.2 Specifications of Existing Heavy Vehicle TATA 1109 EX2 Frame

Sl. No.	Description	Dimension (mm)
1	Wheel base	3600
2	Front track	1800
3	Rear track	1690
4	Overall length of vehicle with load body	6600
5	Max. width	2270
6	Frame length	5620

Sl. No.	Description	Weight (kg)
1	Max. permissible FAW	7950
2	Max. permissible RAW	3950
3	Max. permissible GVW	11900
4	Passing payload for cab load body	8315

III. Design

Design may be done in two ways one way is the component design which is done by improving the existing ones. The other is conceptual design where there is no reference and creation of new machines. A new or better machine is one which is more economical in the overall cost of production and operation. The process of design is a long and time consuming one. From the study of existing ideas, a new idea has to be conceived. The idea is then studied keeping in mind its commercial success and given shape and form in the form of drawings. In the preparation of these drawings, care must be taken about the availability of resources like money, man power and materials required for the successful completion of the new idea into an actual reality. In designing a machine component, it is necessary to have a good knowledge of many subjects such as Mathematics, Engineering Mechanics, Strength of Materials, Theory of Machines, Workshop Processes and Engineering Drawing.

Generally the design of a component involves various steps in it. Initially, the drawings must be drawn in user friendly software and they must be converted into a 3D model. This 3D model must be imported into an analyzing medium where it is structurally or thermally analyzed to sustain the need.

Different steps involved in designing a component are
1. Part drawing
2. Modeling
3. Structural analysis

The present frame is divided in to individual components and each component is drawn, modeled and structurally analyzed by using software and its procedure is explained as below.

3.1 Part Drawing

It is a document that includes the specifications for a part's production. Generally the part drawings are drawn to have a clear idea of the model to be produced. The part drawing of the entire frame is drawn with all the views in AUTO CAD 2012.
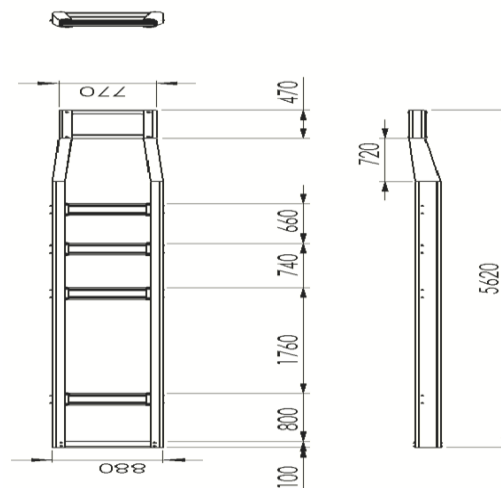

Fig. 3.1 Part drawing of assembly in AUTO CAD 2012

3.2 Modeling

It is the process of developing a mathematical representation of any three-dimensional surface of object via specialized software. The product is called a 3D model.

There are three basic types of three dimensional computer geometric modeling methods
1. Wire frame modeling
2. Surface modeling
3. Solid modeling

3.2.1 Wire Frame Modeling
A wire frame model is visual presentation of a 3 dimensional or physical object used in 3D computer graphics. It is created by specifying each edge of the physical object where two mathematically continuous smooth surfaces meet, or by connecting an object's constituent vertices using straight lines or curves. The object is projected on to a display screen by drawing lines at the location of each edge.
The wire frame format is well suited and widely used in programming tool paths for DNC (Direct Numerical Control) machine tools.
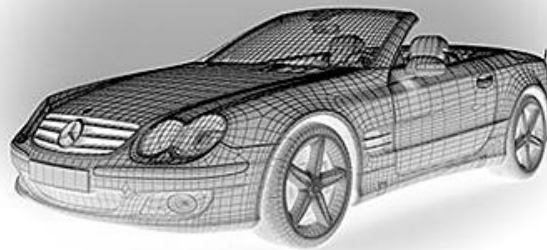

Fig. 3.2 Wire Frame Modeling

3.2.2 Surface Modeling
These models are with no thickness. These models are widely used in industries like automobiles, aerospace, plastic, medical and so on. Surface models should not be confused with thick models that are models having mass properties. The only difference between the soli model and the surface model is solid model will have mass properties.

Fig. 3.3 Surface Modeling

The present frame is modeled by solid modeling because of its ease in construction and realistic profile.

3.2.3 Solid Modeling
A solid model of an object is a more complete representation than its surface (wireframe) model. It provides more topological information in addition to the geometrical information which helps to represent the solid unambiguously. There are different software that are used for generating these solid models like Solid works and Pro.E. In this project the frame is modeled by using SOLID WORKS 2011. All the parts that are required for constructing the frame are modeled in part module by using different commands like extrude, rotate, loft, fillet, extrude cut etc..,

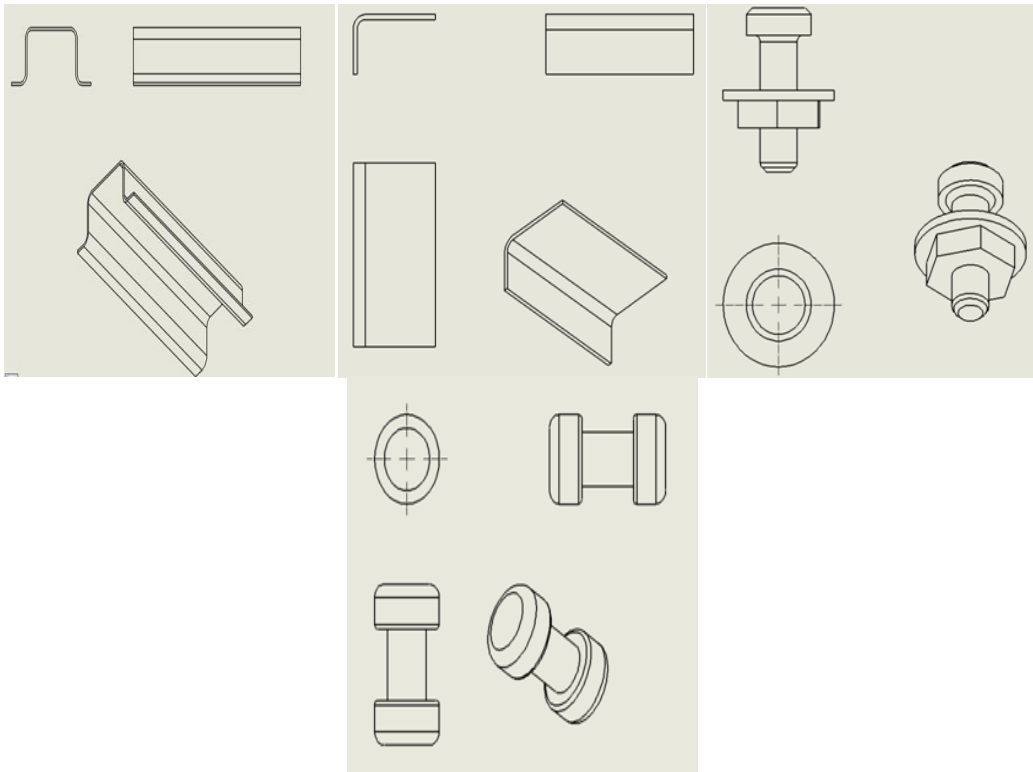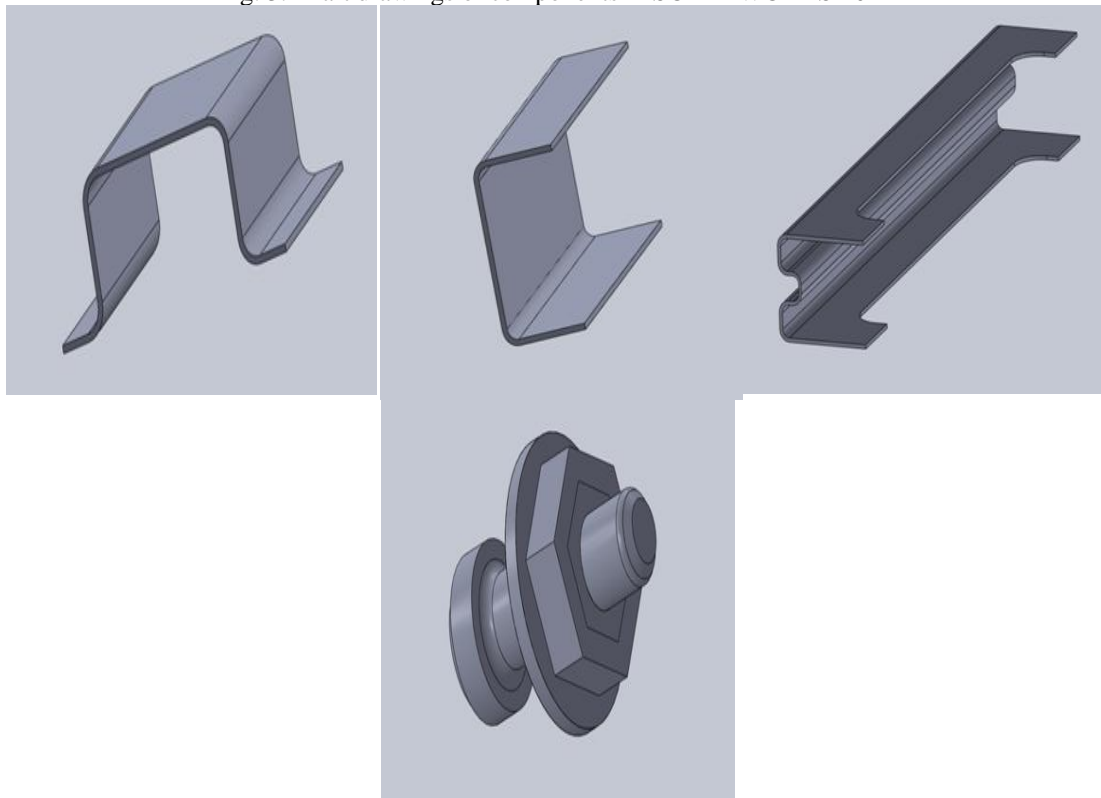Fig. 3.4 Part drawings of components in SOLID WORKS 2011

Fig. 3.5 Modeled components in SOLID WORKS 2011

3.3 Assembly

The components that are generated in part module are imported to assembly module and by using 'insert components' command and all these components are mated together to form the required assembly. The different views of assembly and the drawing generated in SOLID WORKS 2011 are as shown below.
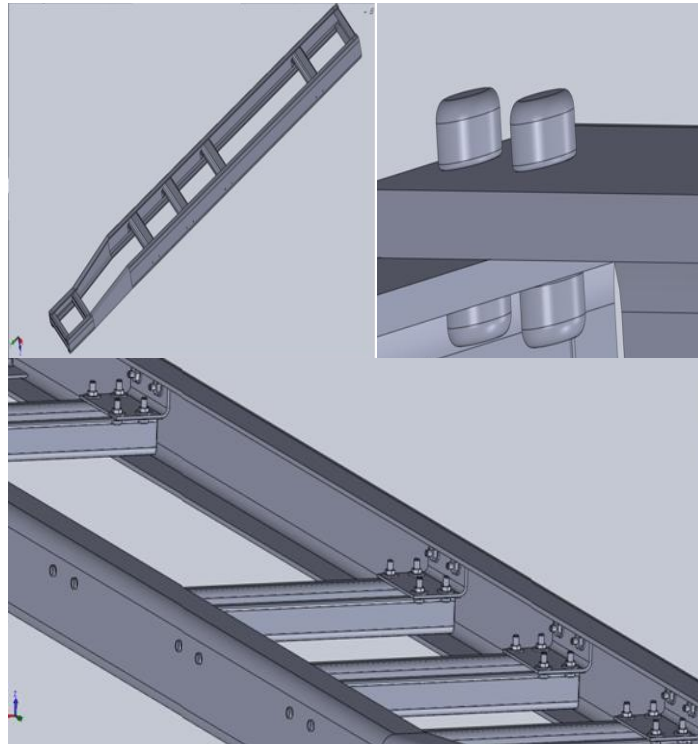
Fig. 3.6 Different views of the frame assembly in SOLID WORKS 2011

3.4 Structural Analysis

It is the methodology of determining the effects of loads on physical structures and their components. Structures subject to this type of analysis include buildings, bridges, vehicles, machinery, furniture, attire, soil strata, prostheses and biological tissue. Structural analysis incorporates the fields of applied mechanics, materials science and applied mathematics to compute a structure's deformations, internal forces, stresses, support reactions, accelerations, and stability. The results of the analysis are used to verify a structure's fitness for use, often saving physical tests. Structural Analysis is thus a key part of the engineering design of structures.

The present frame model is converted into IGES format and it is then imported to ANSYS Workbench 13.0.There are various steps that are to be followed in analyzing a component structurally. They are

1. Mesh generation
2. Fixed supports
3. Application of loads
4. Evaluating result

3.4.1 Mesh Generation

The process for generating a mesh consists of three general steps

1. Set the element attributes
2. Set mesh controls (optional)
3. Meshing the model

It is not always necessary to set mesh controls because the default mesh controls are appropriate for many models. If no controls are specified, the program will use the default settings (DESIZE) to produce a free mesh. Alternatively, you can use the Smart Size feature to produce a better quality free mesh.

ANSYS Meshing technology provides multiple methods to generate a pure hex or hex- dominant mesh. Depending on the model complexity, desired mesh quality and type, and the time available to perform meshing, ANSYS Meshing provides a scalable solution. Quick automatic hex or hex-dominant mesh can be generated for optimal solution efficiency and accuracy.
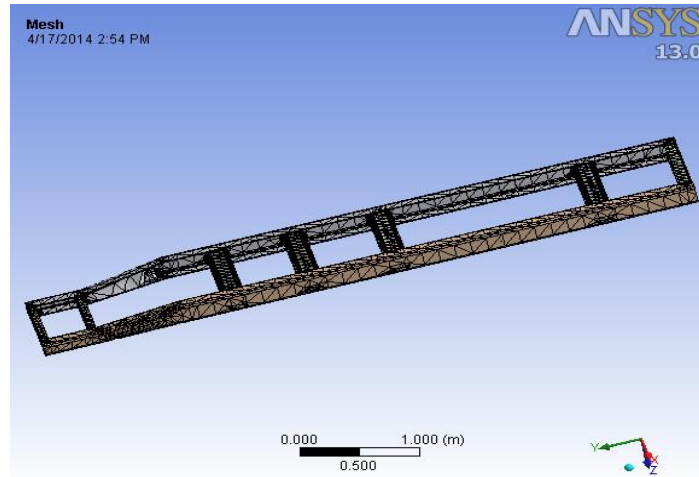
Fig. 3.7 Isometric View of Frame after Meshing

3.4.2 Fixed Supports
The fixed supports for the frame are placed at the wheel positions. The total number of supports is four. The first support is placed at 470 mm from the front end the second support is placed at 1680 mm from the rear side. The other two supports are placed at same positions on the other side.
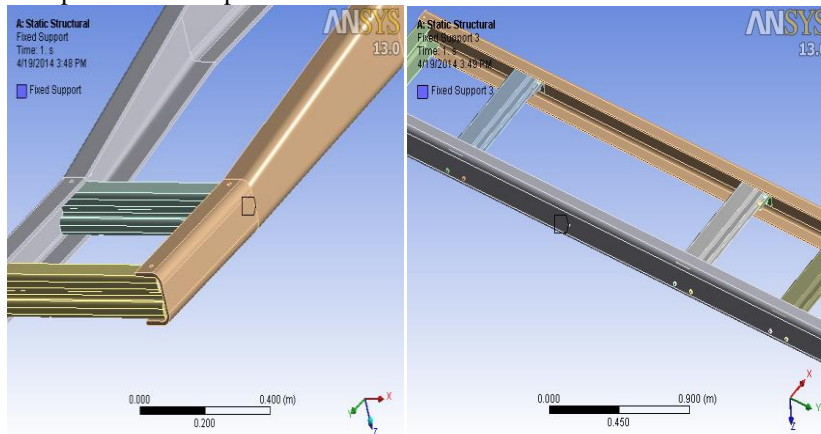
Fig. 3.8 Fixed supports at Front and Rear wheel positions

3.4.3 Application of Loads
The load application is the major part in the analysis of a component. There may be different types of loads like Uniformly Distributed Load, Uniformly Varying Load and Point Load.

The present frame carries the UDL through out its length.

From the vehicle specifications

$$FAW = 7950 \ Kg$$
$$RAW = 3950 \ Kg$$
$$Total \ GVW = 11900 \ Kg$$

As the frame supports the bodt by its two side frames, the load on each side member

$$= 11900/2 = 5950 \ kg$$

The total area on which the UDL is placed $= 5620 \times 100 = 562000 \ mm^2$

Total pressure applied $= $ Total load /Total area $= 5950/562000$

$$= 0.01058 \ kg/mm^2 = 0.1038 \ N/mm^2 = 0.1038 \ MPa$$

The pressure is applied on the two side members of the frame as shown in Fig. 3.9

Fig. 3.9 Area on which Pressure is applied

3.5 Structural Steel

It is steel construction material, a profile, formed with a specific shape or cross section and certain standards of chemical composition and mechanical properties. Structural steel shape, size, composition, strength, storage, etc., is regulated in most industrialized countries. Composition 0.565%C, 1.8% Si, 0.7%Mn, 0.045%P and 0.045% S
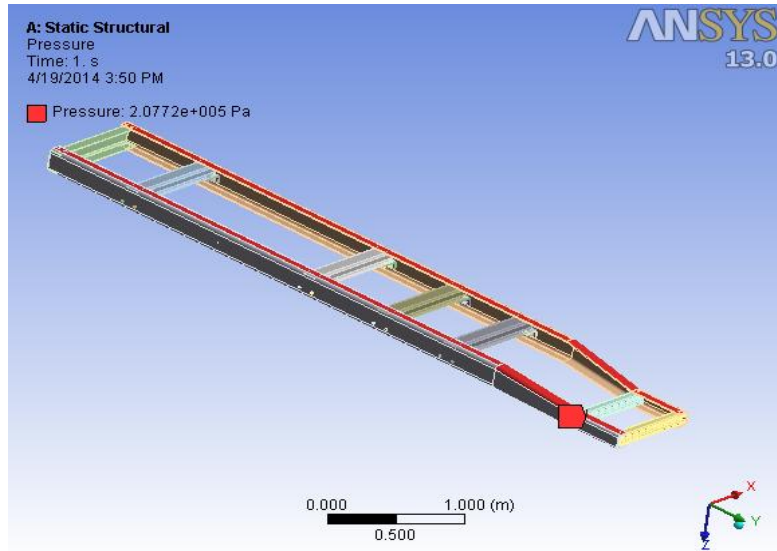
3.5.1 Mass of Frame

The mass of an object is a fundamental property of the object, a numerical measure of its inertia, a fundamental measure of the amount of matter in the object.
Mathematical equation for mass is

$$\text{Mass} = \text{Volume} \times \text{Density}$$

We know, Density of steel = 7850kg/m^3

Volume of frame = 4.9104×10^{-2} m³

Total mass of frame = 7850×0.049104

= 385.46 kg

3.5.2 Stresses developed in Frame

It is a physical quantity that expresses the internal forces that neighboring particles of a continuous material exert on each other. For example, when a solid vertical bar is supporting a weight, each particle in the bar pulls on the particles immediately above and below it. These macroscopic forces are actually the average of a very large number of intermolecular forces and collisions between the particles in those molecules. There are many types of stresses developed in a component. The frame is analyzed by considering Equivalent stress and normal stress.

Normal stress

The component of stress which is perpendicular to the plane on which the force is applied is called Normal stress. This stress is also called as principle stress. Its value should not exceed the yield strength of the material. In some of the situations design is considered to be safe if its value is less than the yield strength of the material. The normal stress distribution in the frame for structural steel is as shown in Fig. 3.10. From the Fig. 3.10 it can be inferred that

Maximum normal stress = 3359 Mpa
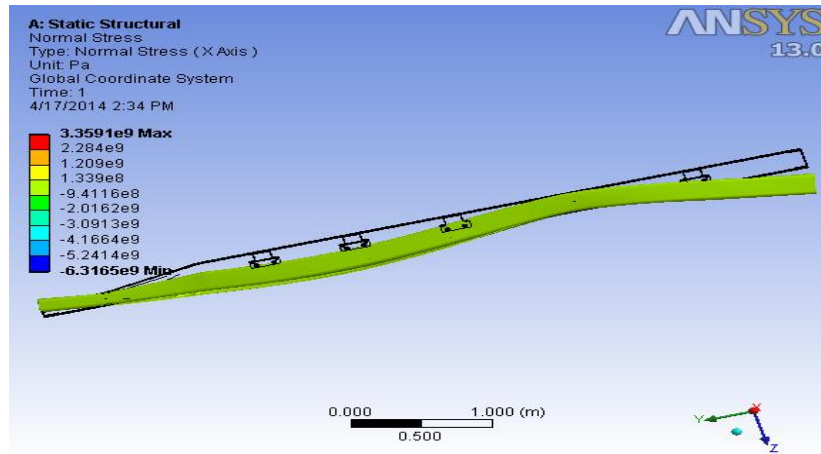
Minimum normal stress = - 6317 Mpa

Fig. 3.10 Normal Stress Distribution in Frame (Structural Steel)

Equivalent stress

When an elastic body is subjected to loads in its three dimensions, the stresses will get developed along the principle axis of the bodystresses. These stresses should not exceed the yield stress of the material. VonMises postulated that, even though none of the principal stresses exceeds the yield stress of the material, it is possible for yielding of the same from the combination of stresses. So all these stresses in three dimensions are together called as Equivalent stress. Von Mises stress is considered to be a safe haven for design engineers. Using this information an engineer can say his design will fail, if the maximum value of Von Mises stress induced in the material is more than strength of the material. It works well for most of the cases, especially when the material is ductile in nature.

The Equivalent stress distribution in the frame for structural steel is as shown in Fig. 3.11. From Fig. 3.11 it can be inferred that

Maximum Equivalent stress   = 17686 MPa (Approx.)
Minimum Equivalent stress   = 0 MPa
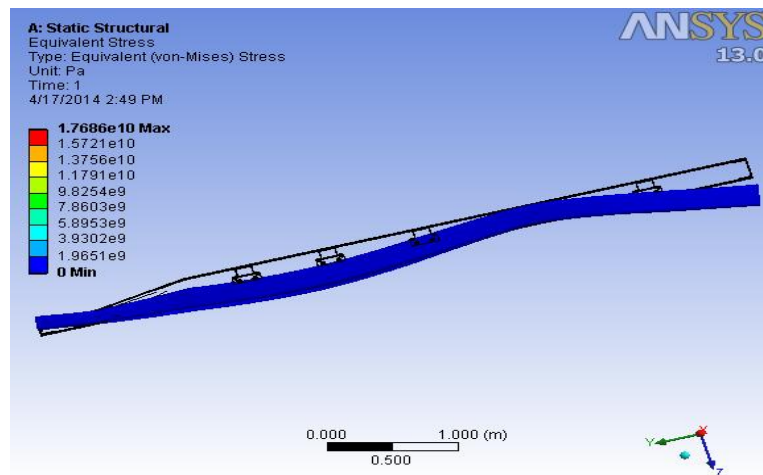
Fig. 3.11 Equivalent Stress Distribution in Frame (Structural Steel)

3.5.3 Deformation

When an object is subjected to loading its shape may be changed temporarily or permanently due to applied force. This change in shape is called deformation. If the object deforms permanently it is called plastic deformation or failure. If it deforms temporarily it is called elastic deformation. While analyzing a frame the frame should deform elastically within the maximum loading limit so that the design is safe. The values of deformation obtained in ANSYS 13.0 for structural steel are as shown in Fig. 3.12

Maximum deformation = 5.7 mm (Approx.)
Minimum deformation = 0 mm
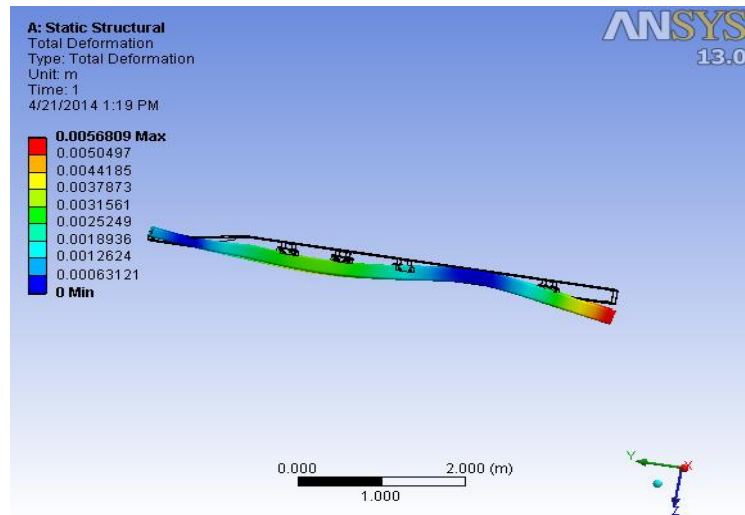
Fig. 3.12 Total deformation in frame (Structural steel)

3.6 Carbon/ Epoxy

Carbon-Fiber-Reinforced Polymer, Carbon-Fiber-Reinforced Plastic or Carbon-Fiber- Reinforced Thermo Plastic (CFRP, CRP, CFRTP or often simply carbon fiber, or even carbon) is an extremely strong and light Fiber-Reinforced Polymer which contains carbon fibers.

The binding polymer is often a thermo set resin such as epoxy, but other thermoset or thermoplastic polymers, such as polyester, vinyl ester or nylon, are sometimes used. The composite may contain other fibers, such as aramid e.g. Kevlar, Twaron, Aluminium or Glass fibers as well as Carbon fiber. The properties of the final CFRP product can also be affected by the type of additives introduced to the binding matrix (the resin). The most frequent additive is silica, but other additives such as rubber and carbon nanotubes can be used. CFRPs are commonly used in the transportation industry; normally in cars, boats and trains, and in sporting goods industry for manufacture of bicycles, bicycle components, golfing equipment and fishing rods.

Although carbon fiber can be relatively expensive, it has many applications in aerospace and automotive fields, such as Formula One racing and wherever high strength-to-weight ratio and rigidity are required such as sailing boats and rowing shell hulls, top-end bicycles and motorcycles, As manufacturing techniques improve and costs reduce it is becoming increasingly common in small consumer goods that require strength, lightness and stiffness such as laptop bodies, tripod legs, tent poles, fishing rods, hockey sticks, bows and arrows, racquet frames, stringed instrument bodies, drum shells, golf clubs, crash helmets and billiards cues.

Composition: Bisphenol-based epoxy 60-90%, Amine-based curing agent 1-30%, Imidazole-based curing catalyst 0.1-3% and Carbon Black 1-10%.

3.6.1 Mass of Frame

Mathematical equation for mass is

$$\text{Mass} = \text{Volume} \times \text{Density}$$

We know Density of Carbon/Epoxy $= 1600 \text{ kg/m}^3$

Volume of frame $= 4.9104 \times 10^{-2} \text{ m}^3$

Total mass of frame $= 1600 \times 0.049104 \qquad = 79 \text{ kg (Approx.)}$

3,6,2 Stresses Developed in Frame

The two types of stresses are considered for analyzing the frame and their respective stress distributions are as shown below
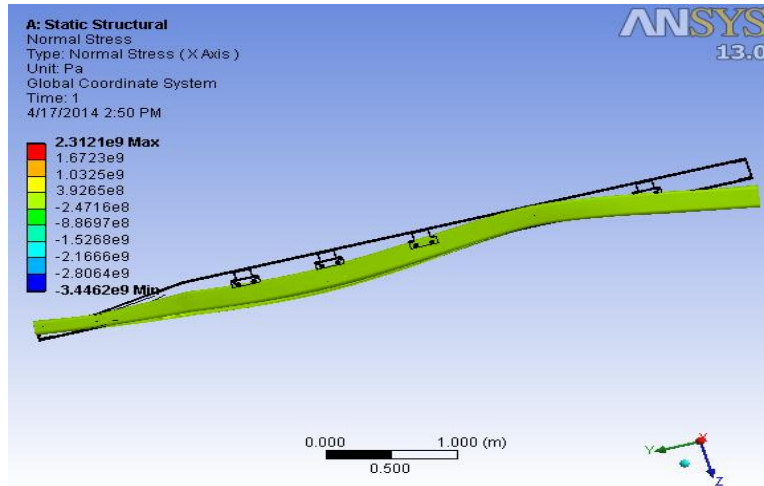
Fig. 3.13 Normal Stress Distribution in Frame (Carbon/ Epoxy)

Maximum normal stress   = 2312 MPa
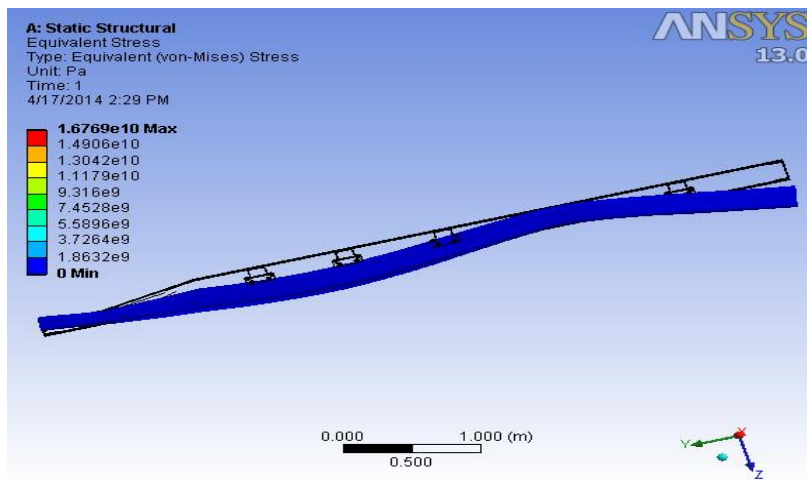Minimum normal stress   = -3446 MPa

Fig. 3.14 Equivalent stress distribution in frame (Carbon/ Epoxy)
Maximum Equivalent stress   = 16769 MPa
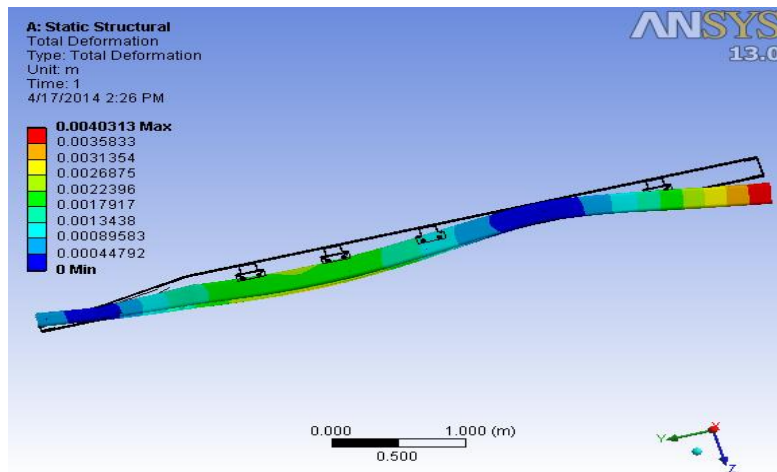Minimum Equivalent stress   = 0 MPa

3.6.3 Deformation

Fig. 3.15 Total Deformation in Frame (Carbon/ Epoxy)

Maximum deformation   = 4.03 mm
Minimum deformation   = 0 mm

3.7 E-glass/ Epoxy

An individual structural glass fiber is both stiff and strong in tension and compression that is, along its axis. Although it might be assumed that the fiber is weak in compression, it is actually only the long aspect ratio of the fiber which makes it seem so i.e., because a typical fiber is long and narrow, it buckles easily. On the other hand, the glass fiber is weak in shear that is, across its axis. Therefore if a collection of fibers can be arranged permanently in a preferred direction within a material, and if the fibers can be prevented from buckling in compression, then that material will become preferentially strong in that direction. Furthermore, by laying multiple layers of fiber on top of one another, with each layer oriented in various preferred directions, the stiffness and strength properties of the overall material can be controlled in an efficient manner. In the case of fiberglass, it is the plastic matrix which permanently constrains the structural glass fibers to directions chosen by the designer. With chopped strand mat, this directionality is essentially an entire two dimensional plane; with woven fabrics or unidirectional layers, directionality of stiffness and strength can be more precisely controlled within the plane.

E-Glass / Epoxy Resin Composites are extremely strong materials used in roofing, pipes and automobiles.
Composition: 54% SiO_2 - 15% Al_2O_3 - 12% CaO

3.7.1 Mass of frame

Mathematical equation for mass is
                    Mass   = Volume × Density
We know Density of E-glass/Epoxy= 2600 kg/m^3
                    Volume of Frame= 4.9104×10^{-2} m³
                    Total mass of Frame   = 2600 × 0.049104   = 127.67 kg

3.7.2 Stresses Developed in Frame

The two types of stresses are considered for analyzing the frame and their respective stress distributions are as shown
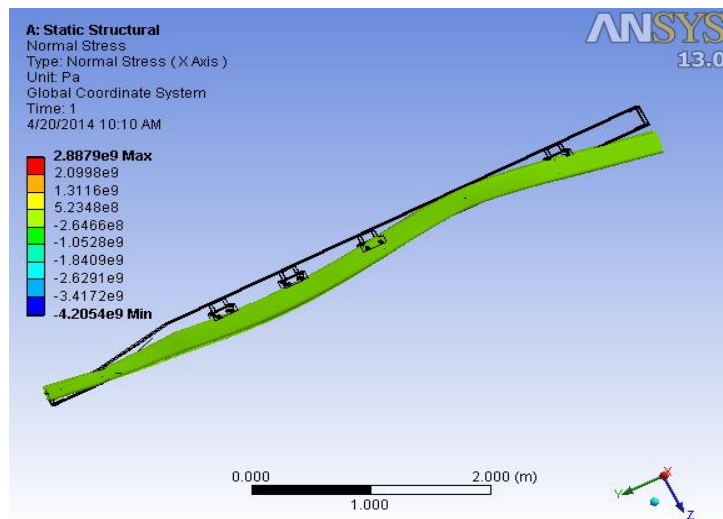
Fig. 3.16 Normal Stress Distribution in Frame (E-glass/ Epoxy)
Maximum normal stress = 2887.9 = 2888 Mpa (Approx.)
Minimum normal stress = -4205.4 = -4205 Mpa (Approx.)

Fig. 3.17 Equivalent Stress Distribution in Frame (E-glass/ Epoxy)
Maximum Equivalent stress = 17055 Mpa
Minimum Equivalent stress = 0 MPa

3.7.3 Deformation
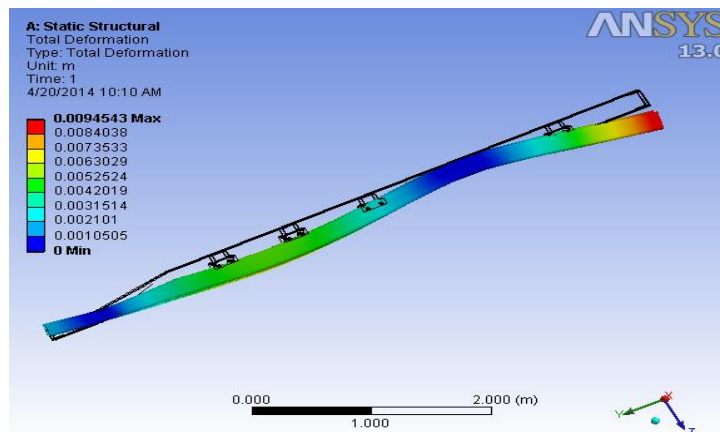
Fig. 3.18 Total Deformation in Frame (E-glass/ Epoxy)
Maximum deformation = 9.45 mm
Minimum deformation = 0 mm

3.8 S-glass/ Epoxy
The manufacturing process for glass fibers suitable for reinforcement uses large furnaces to gradually melt the silica sand, limestone, kaolin clay, fluorspar, colemanite, dolomite and other minerals to liquid form. Then it is extruded through bushings, which are bundles of very small orifices (typically 5–25 micrometers in diameter for E-Glass, 9 micrometers for S-Glass). These filaments are then sized (coated) with a chemical solution. The individual filaments are now bundled together in large numbers to provide a roving. The diameter of the filaments, as well as the number of filaments in the roving determines its weight.

Common uses of S-glass include high performance aircraft (gliders), boats, automobiles, baths, hot tubs, septic tanks, water tanks, roofing, pipes, cladding, casts, surfboards and external door skins.

Composition: 64% SiO_2- 24% Al_2O_3- 10% MgO

3.8.1 Mass of Frame
Mathematical equation for mass is

Mass $\quad$ = Volume × Density

We know Density of S-glass/ epoxy $\quad$ = 2495 kg/m^3

Volume of frame $\quad$ = 4.9104×10^{-2} m³

Total mass of frame $\quad$ = 2495×0.049104 $\quad$ = 123 kg (Approx.)

3.8.2 Stresses developed in Frame

The two types of stresses are considered for analyzing the frame and their respective stress distributions are as shown below
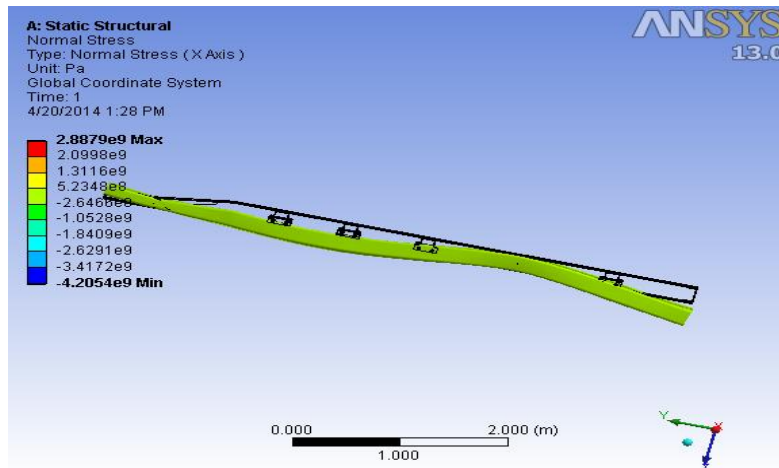
Fig. 3.19 Normal Stress Distribution in Frame (S-glass/ Epoxy)
Maximum normal stress = 2888 MPa (Approx.)
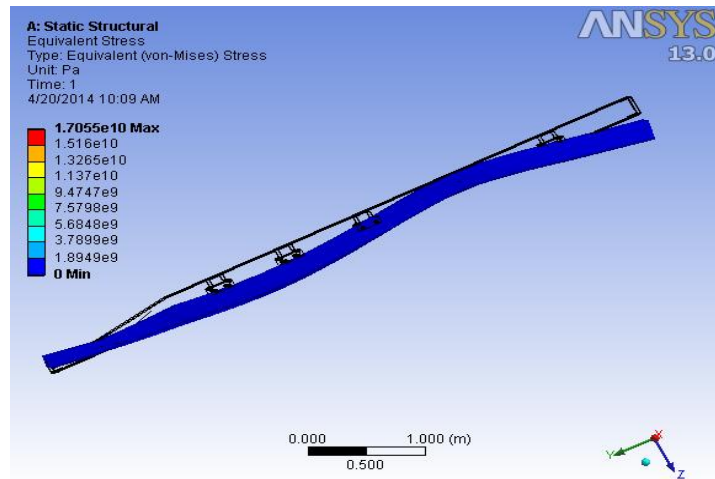Minimum normal stress = -4205 MPa (Approx.)
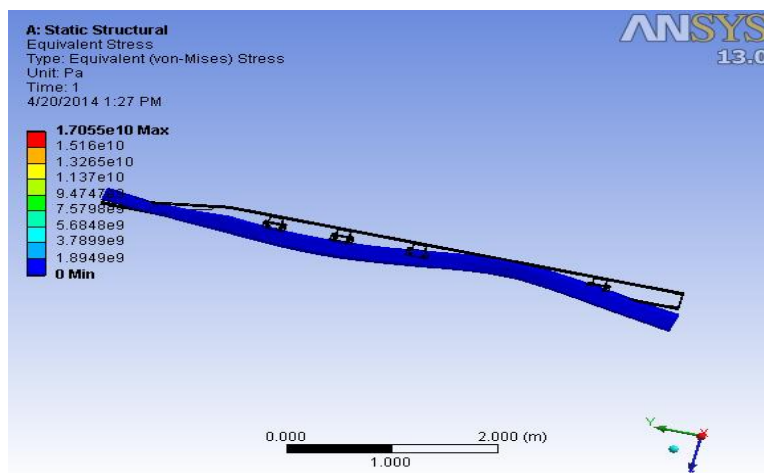
Fig. 3.20 Equivalent Stress Distribution in Frame (S-glass/ Epoxy)
Maximum Equivalent stress = 17055 MPa
Minimum Equivalent stress = 0 Mpa

3.8.3 Deformation
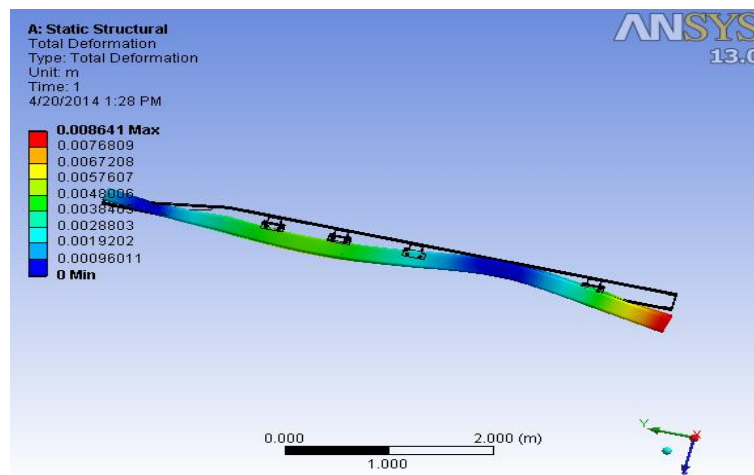
Fig. 3.21 Total Deformation in Frame (S-glass/ Epoxy)

Maximum deformation = 8.64 mm
Minimum deformation = 0 mm

IV. Results

From the above analysis using different materials, the results obtained for stresses and deformations are tabulated below.

Table 4.1 Comparison of Results

Material	Mass (kg)	Max.Normal stress (MPa)	Max.Equivalent stress (MPa)	Max.Deformation (mm)
Structural steel	385	3359	17686	5.68
Carbon/ Epoxy	79	2312	16769	4.03
E-glass/ Epoxy	128	2888	17055	9.45
S-glass/ Epoxy	123	2888	17055	8.64

From the above table it can be inferred that Carbon/ Epoxy is having the least values when compared to remaining three materials. For less mass the Carbon/ Epoxy gives more strength. It can be explained by following calculations

For Structural Steel,

$$\text{Density} = 7850 \text{ kg/m}^3$$
$$\text{Ultimate tensile strength} = 900 \text{ MPa}$$
$$\text{Strength to weight ratio} = 900/7850 = 0.1146 \text{ MNm/kg}$$
$$= 115 \text{ Nm/g (Approx.)}$$

For Carbon/Epoxy,

$$\text{Density} = 1600 \text{ kg/m}^3$$
$$\text{Ultimate tensile strength} = 600 \text{ MPa}$$
$$\text{Strength to weight ratio} = 600/1600 = 0.375 \text{ MNm/kg}$$
$$= 375 \text{ Nm/g}$$

The results obtained are represented graphically as shown below.
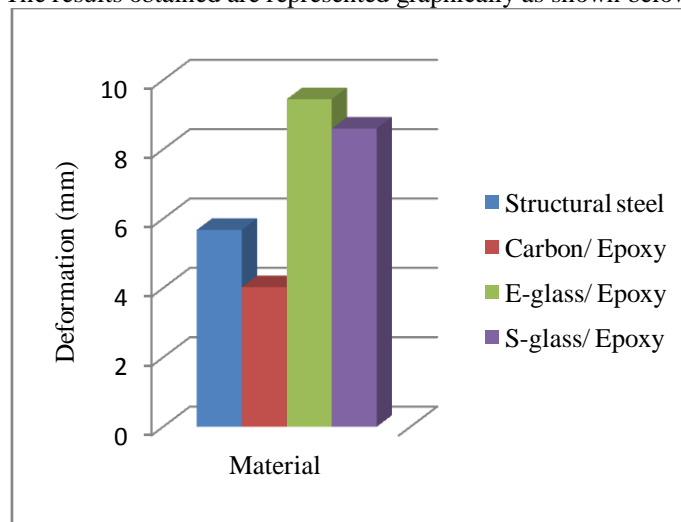
Fig. 4.1 Graphical Representation of Deformation
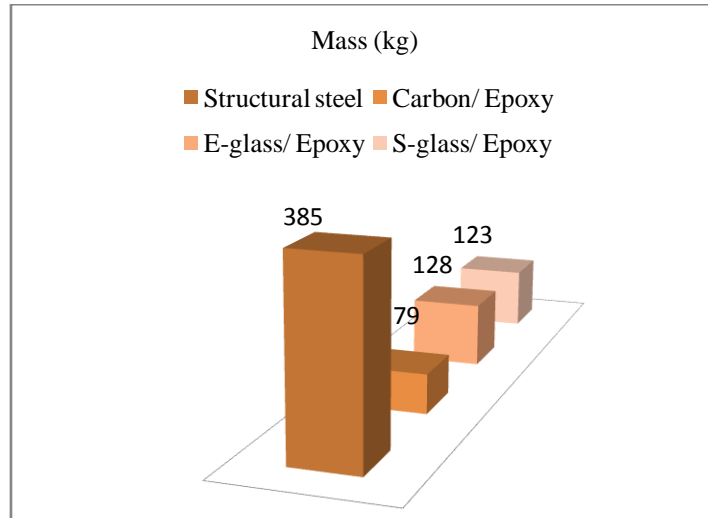
Fig. 4.2 Graphical Representation of Mass
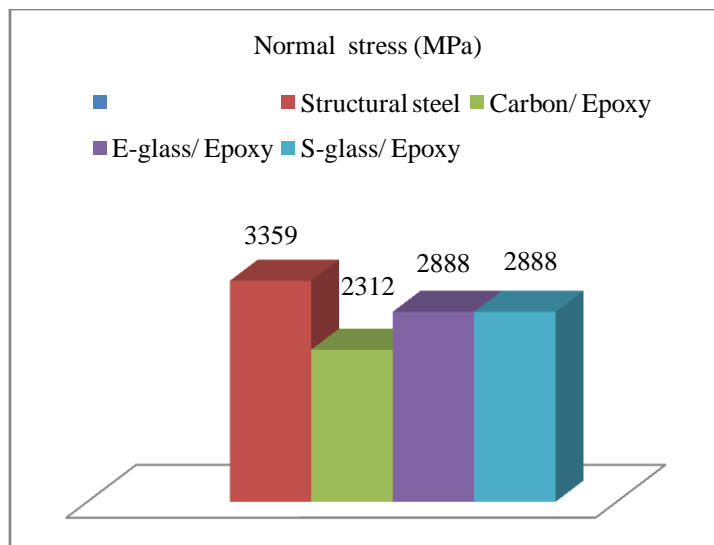
Fig. 4.3 Graphical representation of Normal stress
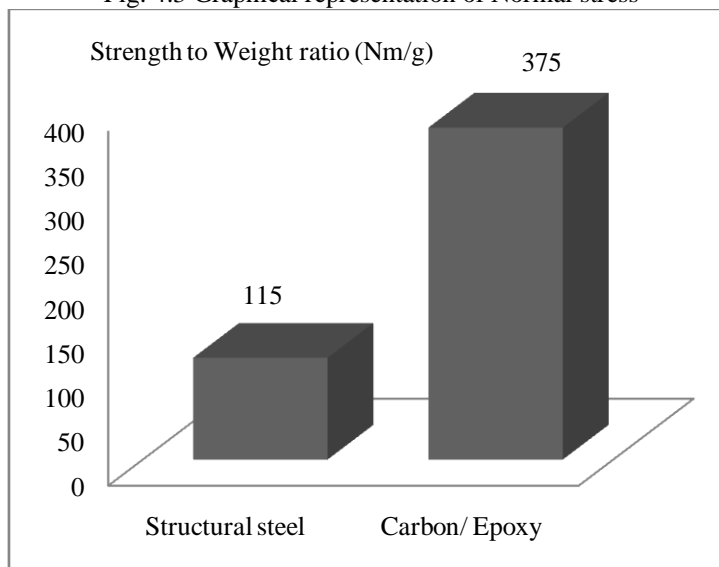
Fig. 4.4 Graphical Representation of Strength to Weight Ratio
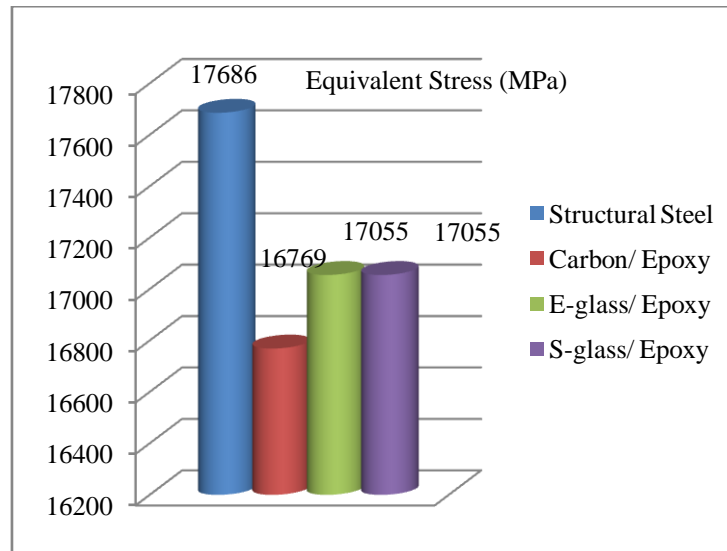
Fig. 4.5 Graphical representation of Equivalent stress

V. Conclusion

Present used material for chassis is steel. We have considered polymeric composites like Carbon/Epoxy, E-glass/Epoxy and S- glass /Epoxy for chassis material. By employing a polymeric composite heavy vehicle chassis for the same load carrying capacity, there is a reduction in weight of 70% to 80%. Based on the results it was inferred that Carbon/Epoxy polymeric composite heavy vehicle chassis has superior strength, less deformation, less normal stress and less weight compared to steel, E-glass/Epoxy and S- glass /Epoxy.

So we conclude that it is better to use Carbon/ Epoxy as a material for frames of heavy vehicle chassis. So that the fuel consumption decreases for the vehicles.

REFERENCES

[1]   Vijaykumar V. Patel, "Structural analysis of a ladder chassis frame," World Journal of Science and Technology 2012, 2(4)05-08
[2]   Cicek Karao a journal on analysis of a chassis frame with joints was performed by using software
[3]   M. Ravi Chandra, S. Sreenivasulu & Syed Altaf Hussain, "Modeling And Structural Analysis Of Heavy Vehicle Chassis Made Of Polymeric Composite Material By Three Different Cross Sections", Journal of Mechanical and Production Engineering Research and Development (IJMPERD), ISSN 2249-6890, Vol.2, Issue 2,Sep 2012 45-60.
[4]   C. Karaoglu, N. S. Kuralay, Stress analysis of a truck chassis with riveted joints, Finite Elements in Analysis and Design, 38, (2002), 1115-1130.
[5]   N.V.Dhandapani, Dr. G Mohan Kumar, Dr K.K.Debnath, Static Analysis of Off-High Way Vehicle Chassis supporting Structure for the effect of various Stress distributions IJART, Vol.2 Issue 1, 2012, 1-8.
[6]   Sairam Kotari, V.Gopinath,**"**Static and dynamic analysis on Tatra chassis**"** International Journal of Modern Engineering Research (IJMER), Vol.2, Issue.1, pp-086-094.
[7]   K.W. Poh, P.H. Dayawansa, A.W. Dickerson, I.R. Thomas, Steel membrane floors for bodies of large rear-dump mining trucks, Finite Elements in Analysis and Design 32, (1999), 141-161.
[8]   H J Beermann, English translation by Guy Tidbury, The Analysis of Commercial Vehicle Structures, Verlag TUV Rheinland GmbH Koln-1989.
[9]   Mohd Husaini Bin Abd Wahab, "Stress Analysis of Truck Chassis", Project Report University Malaysia Pahang, 2009
[10]   Machine Tool Design hand book by Central Machine Tool Institute Edition 1 – 2004 Mc Graw Hill Publications
[11]   http://ansys.com/Industries/Academics/Tools/Curriculum+Resources

OPEN ACCESS

Effect of Imperfection on Shear Behaviour of Hybrid Plate Girder

Ajeesh S S[1], Sreekumar S.[2]

[1,2] *(Ajeesh S.S, M.Tech student, Professor, Department of Civil Engineering, College of Engineering Trivandrum, Kerala)*

Abstract: *The influence of initial imperfection of plates on the shear resistance of hybrid plate girder fabricated using slender plate elements is studied. Nonlinear finite element analysis was performed to compute the ultimate shear strength of hybrid girder. Imperfection analysis was performed by varying the magnitude of imperfection on web panel of hybrid plate girder to compare the variation in ultimate shear strength. The study was also done by varying the yield strength and slenderness ratio of web panel. The result of the study indicates that the ultimate shear strength of hybrid plate girder decreases with increase in the magnitude of initial imperfection. The effect of imperfection on shear strength was significantly high for plate girder with low web slenderness ratio and high yield strength of web panel. The maximum lateral as well as the vertical deflection at ultimate strength state of the model increases with increase in magnitude of imperfection.*

Keywords: *buckling, finite element analysis, hybrid, imperfection, nonlinear, steel plate girder, ultimate shear strength, web panel.*

I. Introduction

Usage of high strength steel is now prominent in the steel design and construction industry, which necessitate making of hybrid structures with thin walled slender sections. The low strength-weight ratio is one of the main advantages of such structures, consequently considerable economy and material savings can be achieved. On the other hand, these structures are more susceptible to deformations due to instability related issues. Buckling of slender members is the main kind of stability loss affecting the shear resistance of thin walled steel structures. In the process of fabrication, particularly welding, initial imperfections may occur to some extent in thin plate components of steel structural members. Hybrid plate girders have different grades of steel for flanges and web panel. Usually the flanges of the girder are fabricated using high strength steel and comparatively low strength steel is used for the web panel.

Lee and Yoo[1] conducted finite element analysis to study the effect of imperfections on shear strength of plate girder. The effect of web slenderness ratio on imperfection was also discussed. Hassanein[2] compared the effect of imperfection on shear strength by varying flange width to web depth ratio, flange to web thickness ratio, and web slenderness ratio of stainless steel plate girders. Chacon et al.[3] performed finite element analysis on the patch load resistance of hybrid plate girder by incorporating the effect of initial imperfection. Kala et al.[4] conducted finite element analysis to study the effect of initial imperfections on the load carrying capacity of plate girder. The effect of the shape of initial curvature and the magnitude of initial curvature were considered in the analytical study. Alinia et al.[5] analysed a number of full scale plate girders to determine their shear failure mechanism characteristics. Gheitasi and Alina[6] studied the post bucking behaviour of slender unstiffened shear plates of stainless steel and aluminium girders. Numerical investigation was conducted by Zhou et al.[7] on the shear behaviour of aluminium alloy pate girders. Studies related to the effect of imperfection on shear resistance of hybrid plate girder are scarce.

The effect of initial imperfection in the web panel of hybrid plate girder is analysed in the present study. The analytical work presented here is mainly concentrated on the variation in magnitude of imperfection of web panel (d/100000 to d/10) on shear strength of hybrid plate girder where 'd' is the depth of plate girder Although the design codes limit the maximum imperfection to d/100, sufficient data was not available on imperfection analysis for plate girders fabricated using high strength steel and hence the imperfection magnitude was increased upto d/10. The study was extended by varying the web slenderness ratio as well as the yield strength of web panel. Nonlinear buckling analysis was performed to compare the effect of imperfection on ultimate shear strength of hybrid plate girder.

II. Shear resistance of hybrid girder

The web panel of plate girder is usually slender in cross section and susceptible to buckling phenomenon. There are two important contributions to the shear resistance of transversely stiffened plate girders:

- Shear buckling resistance of web panel
- Shear postbuckling resistance of web panel.

Web buckling due to shear is essentially a local buckling phenomenon. The elastic buckling stress (τ_{cr}) of a rectangular web plate (width c, depth d and thickness t_w) was given by Timoshenko and Gere[8] as

$$\tau_{cr} = k\frac{\pi^2 E}{12\left(1-\mu^2\right)\left(\dfrac{d}{t_w}\right)^2} \tag{1}$$

Where E=Young's modulus of elasticity, μ=Poisson's ratio and k=web shear buckling coefficient.

The web shear buckling coefficient 'k' is a key factor influencing the shear strength of plate girder. The real boundary condition of the web–flange juncture is still unknown. The boundary of web panel is assumed to be simply supported in order to find the value of shear buckling coefficient in theoretical formulations. The shear buckling coefficient for simply supported edge condition is given by

$$k = 4 + \frac{5.35}{\left(\dfrac{c}{d}\right)^2} \qquad \text{for c/d<1} \tag{2}$$

$$k = 5.35 + \frac{4}{\left(\dfrac{c}{d}\right)^2} \qquad \text{for c/d≥1} \tag{3}$$

The nominal shear resistance of a plate girder can be calculated using any of the two methods proposed in IS 800:2007[9]- simple post critical method or tension field method. Both these methods consider the buckling of web panel as the governing failure criterion of the plate girder under shear load. The simple post critical method can be applied to both stiffened and unstiffened girders, provided that the web has transverse stiffeners at the supports. The nominal shear strength by this method is given by

$$V_n = A_v\tau_b \tag{4}$$

Where A_v is the shear area and τ_b is the shear stress corresponding to web buckling.

The nonlinear shear stress and normal stress interaction that takes place from the onset of elastic shear buckling to the ultimate strength state contributes to postbuckling shear strength. For transversely stiffened girders, where the stiffener spacing lies within the range 1.0 ≤ c/d ≤ 3.0, the tension field method utilizes the post buckling shear resistance of the girder. This reserve strength arises from the development of "tension field action" within the girder. Once the web panel of plate girder has buckled in shear, it loses its resistance to carry additional compressive stresses.

In the post buckling range, a new load carrying mechanism is developed, where by any additional shear load is carried by an inclined tensile membrane stress field. This tension field anchors against the top and bottom flanges and against the transverse stiffeners on either side of the web panel. The resistance offered by the web plate is analogous to that of the diagonal tie bars in a truss. The shear strength of plate girder (V_{tf}) according to tension field method is given by

$$V_{tf} = \left[A_v\tau_b + 0.9w_{tf}t_w f_v \sin\phi\right] \le V_p \tag{5}$$

$$V_p = \frac{A_v f_{yw}}{\sqrt{3}} \tag{6}$$

Where V_p = plastic shear resistance of girder, w_{tf} = width of tension field, t_w = thickness of web panel, f_v = yield strength of tension field, φ = inclination of tension field and f_{yw} = yield strength of web panel.

In order to study the variation of yield strength of web panel on shear strength, a hybrid factor (HF) was introduced in the analytical study as given by

$$HF = f_{yf}/f_{yw} \tag{7}$$

Where f_{yf} is the yield strength of flange plate and f_{yw} is the yield strength of web panel.

III. Imperfection analysis

Nonlinear finite element analysis was performed using the program ANSYS to study the effect of imperfection on hybrid plate girder. Structural steel conforming to the Indian Standard IS 2062[10] was chosen for modelling the girder by incorporating both geometrical and material nonlinearities. Thickness of the flange (t_f = 30 mm), depth of the web (t_w = 700 mm), and breadth of flange (b_f = 200 mm) were maintained constant for all finite element models. Modelling was done by adopting high strength steel for flanges (f_{yf}= 450 N/mm^2) and varying the material properties of web panel (f_{yw}= 250, 300, 350, 410 and 450 N/mm^2). The material nonlinearity was modelled using ideal elasto-plastic assumption. The material relationship was modelled as von Mises material with isotropic hardening law. Young's modulus of $2x10^5$ N/mm2 and Poisson's ratio 0.3 were used for the analysis.

Finite element modelling of plate girder was performed using shell element having six degrees of freedom: translations in the x, y, and z directions, and rotations about the x, y, and z axes. Simply supported end condition was adopted for the model and concentrated force was applied on the mid span of the girder to calculate the shear strength of girder. The imperfections were introduced in one of the web panel using scaled first eigen buckling mode (Chacon et al.[3]). The finite element model used to study the effect of imperfection is shown in Fig.1.
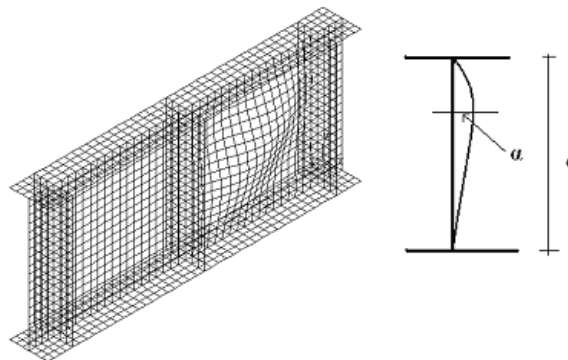
Fig.1 Finite element model with initial imperfection

The validation of the analytical procedure was done by analyzing a stainless steel plate girder problem reported in literature (Estrada et al [11]). Both critical shear buckling strength (V_{cr}) and ultimate shear strength (V_u) were computed using finite element method. The results of finite element analysis were comparable with the analytical and experimental results available (Table 1.). The error in the estimation of results using finite element method was less than 5%.

Table 1 Comparison of FEM results with experimental results

Girder	Present study		Analytical study by Estrada et al.[11]		Experimental study by Estrada et al.[11]	
	V_{cr} (kN)	V_u (kN)	V_{cr} (kN)	V_u (kN)	V_{cr} (kN)	V_u (kN)
nr700ad15	145	307	148.39	319.22	150	309.21
nr500ad25	177.5	232.8	178.62	231.37	175	228.05

In the present study, the ultimate shear strengths of 75 models were compared by varying the magnitude of imperfection (α), web slenderness ratio (d/t_w) and hybrid factor (HF) of the girder.

IV. Results and discussion

The results of finite element analysis used for comparison of ultimate shear strength are summarised in Table 2. The effect of imperfection on ultimate shear strength was compared by varying the magnitude of imperfection and thickness of web panel. Three web slenderness ratios were incorporated in the analysis by setting the thickness of web panel t_w=6, 7 and 8 mm. The variation in hybrid factor was achieved by increasing the yield strength of web panel. Nonlinear buckling analysis was performed by incorporating material and geometric nonlinearity to compute the ultimate shear resistance of hybrid girder.

Table 2 Effect of imperfection on ultimate shear strength

Finite Element Model	d/t_w	t_f/t_w	b_f/t_w	Magnitude of imperfection (α)	Ultimate shear strength (kN)				
					$V_{u,FEM}$ (HF=1.8)	$V_{u,FEM}$ (HF=1.5)	$V_{u,FEM}$ (HF=1.29)	$V_{u,FEM}$ (HF=1.1)	$V_{u,FEM}$ (HF=1)
1	117	5	33	d/100000	599.89	676.31	751.56	842.43	901.63
2	117	5	33	d/10000	588.47	669.67	749.77	841.58	900.93
3	117	5	33	d/1000	568.21	655.73	738.96	834.03	894.77
4	117	5	33	d/100	576.87	659.23	742.58	842.15	907.69
5	117	5	33	d/10	562.8	634.07	703.06	783.69	836.52
6	100	4.2	28	d/100000	730.44	855.62	963.14	1058.78	1117.48
7	100	4.2	28	d/10000	717.06	843.04	946.1	1056.26	1127.46
8	100	4.2	28	d/1000	694.68	811.6	918	1037.1	1113.06
9	100	4.2	28	d/100	662.22	764.92	867.44	989.16	1068.9
10	100	4.2	28	d/10	638.32	723.86	807.54	905.94	970.48
11	88	3.8	25	d/100000	858.92	1007.28	1153.74	1321.1	1415.78
12	88	3.8	25	d/10000	837.94	988.48	1135.78	1301.64	1386.54
13	88	3.8	25	d/1000	810.66	959.24	1100.46	1250.54	1342.48
14	88	3.8	25	d/100	742.2	873.94	1001.18	1148.66	1243.76
15	88	3.8	25	d/10	714.56	816.9	917.92	1037.18	1115.4

As the magnitude of imperfection (α) increases from d/100000 to d/10, the ultimate shear strength of hybrid plate girder decreases. The maximum variation in ultimate shear strength with increase in imperfection magnitude was 7% for low values of web slenderness ratio ($d/t_w = 117$). The percentage decrease in ultimate shear strength becomes 21% for $d/t_w = 88$. Also the imperfection of web panel significantly reduces the load carrying capacity of plate girder with high web yield strength. The effect of imperfection becomes significant for low values of web slenderness ratio ($d/t_w = 88$) and hybrid factor (HF = 1).

The maximum lateral deflection of the web panel due to increase in load for various imperfection values is shown in Fig.2. An increase in lateral deflection of web panel is observed with increment in imperfection magnitude for all the hybrid plate girder models considered in the present study. For imperfection magnitude (α) less than d/1000, the percentage variation in maximum lateral deflection of web panel is less than 40%. A variation of 90% is observed in maximum lateral deflection, as the imperfection magnitude increases from d/1000 to d/100. For the model with α=d/10, the load-deflection graph loses its linearity at low load values compared to other imperfection magnitudes. The lateral deflection of the web panel gives a clear indication of the strength reduction in web panel with increase in imperfection magnitude.
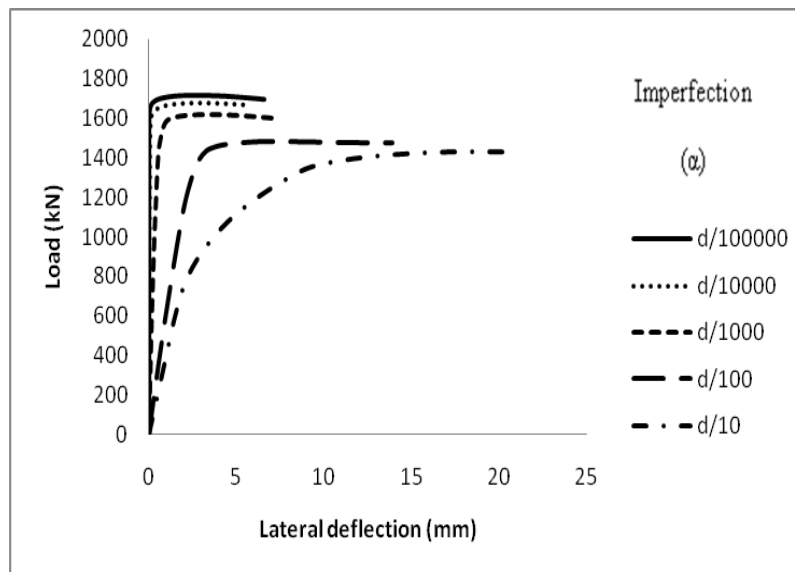
Fig.2 Plot of load versus maximum lateral deflection

(d/t$_w$=88, HF=1.8)

The vertical deflection of the plate girder model with increase in loading is compared for various imperfection magnitudes as shown in Fig.3. The load-deflection plots of the models were almost similar with increase in imperfection α upto d/100. The load deflection curve was linear for almost 80% of the maximum load for imperfection magnitude α≤d/100. The variation in magnitude of maximum vertical deflection of the girder was less than 70% with increase in α upto d/100. The vertical deflection of girder with α=d/10 was 110% greater than other imperfection magnitudes for highest load level. The highest imperfection factor suggested in most of the international welding standards is d/100.
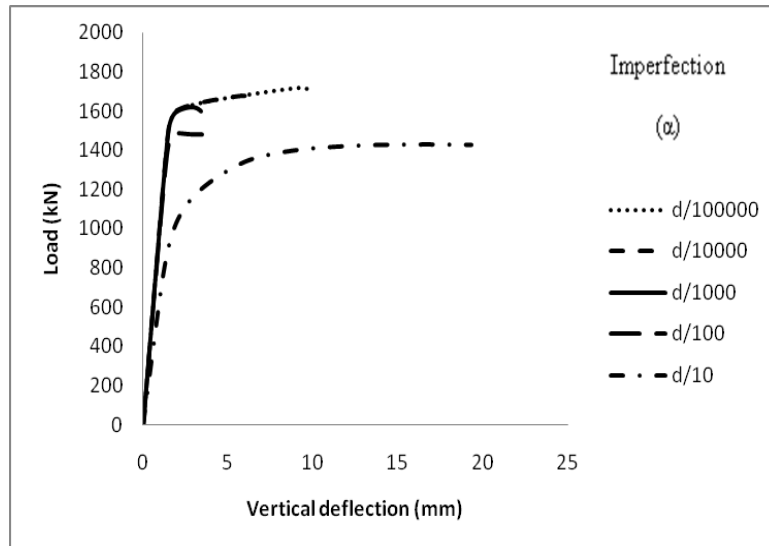
Fig.3 Plot of load versus vertical deflection (d/t$_w$=88, HF=1.8)

The von Mises stress distribution of the model (d/t$_w$=88, HF=1.8) for various imperfection values are compared in Fig.4. For all imperfections, the maximum von Mises stress values is observed in the flanges and this gives a clear indication of the contribution of flange plate in ultimate shear strength of the model. The von Mises stress in web panel also reaches the yield strength of web (250 MPa) at ultimate strength state for all imperfections. For imperfection magnitude d/100000, the von Mises stress in flanges reaches the yield strength of flange plate (450 MPa) at the point of loading in flange plate. For α=d/10, wide spreading of the maximum von Mises stress is observed in compression flange near the loading point. In the stress distributions, there is a clear indication of gradual development of tension yield band in the web panel at higher values of imperfections. Similar stress distributions were also obtained for other values of d/t$_w$ (100 and 117) with various hybrid factors considered. As depth of girder and width and thickness of flange are taken as constant for all models considered, it is clear that the ratio of thickness of flange to web does not affect the mechanism of failure for all imperfections.

V. Conclusion

The main conclusions of the imperfection analysis of hybrid plate girder are listed below:
1. The imperfection on web panel significantly affects the shear load carrying capacity of hybrid plate girder and as the magnitude of imperfection increases, the ultimate shear strength of girder decreases.
2. The web slenderness ratio and yield strength of web panel are the two main factors which influences the ultimate shear strength of girder with imperfections in web panel. The percentage reduction in shear strength was 21% for low values of web slenderness ratio and hybrid factor of girder (d/t$_w$=88, HF=1).
3. The maximum lateral deflection as well as the vertical deflection of plate girder model increases with increase in imperfection magnitude from d/100000 to d/10.
4. As the magnitude of initial imperfection increases, the von Mises stress distribution in the web panel reaches the yield strength at relatively low value of applied loading.
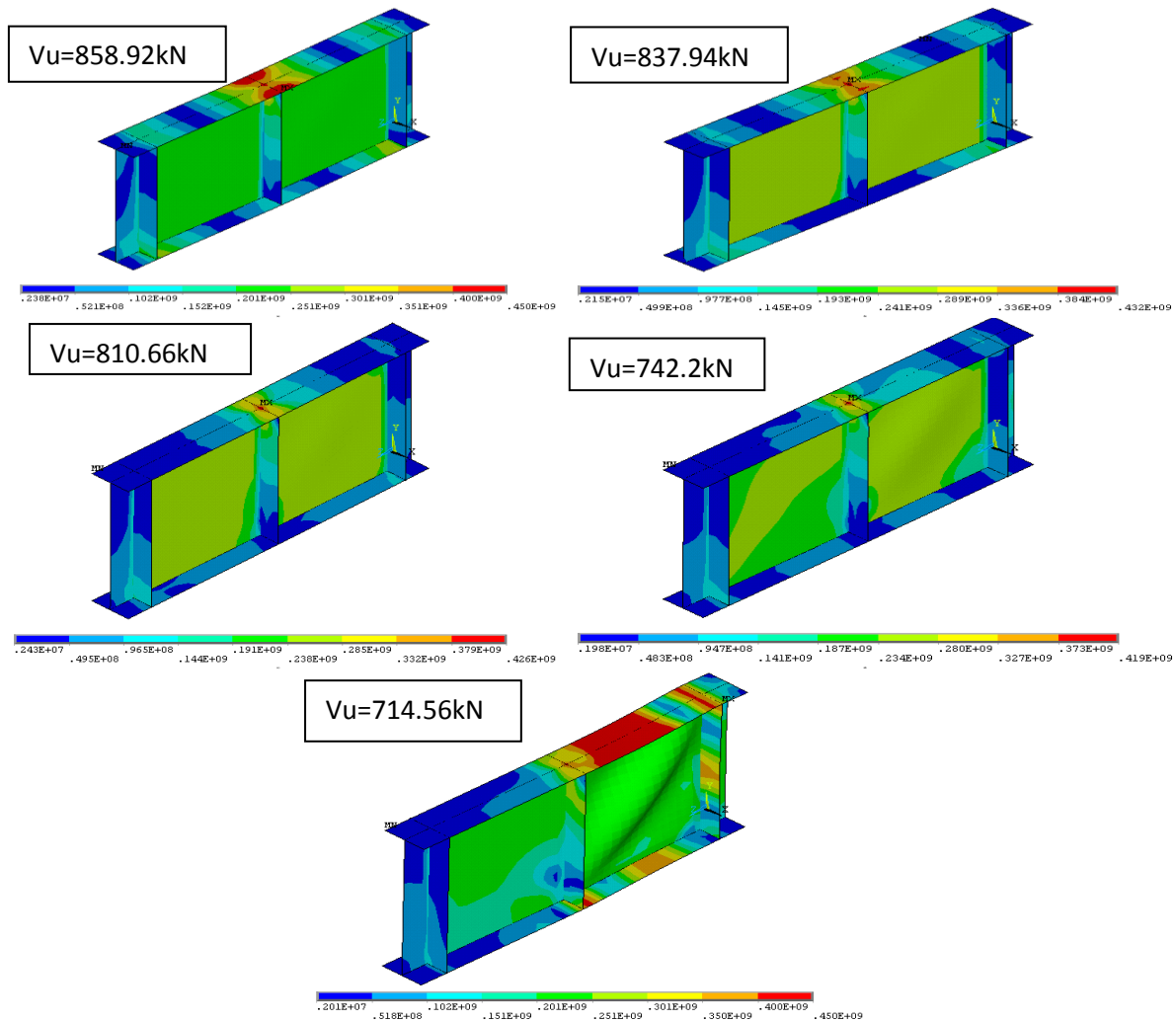
Fig.4 Von Mises stress distribution at ultimate stage for various imperfections (d/t_w=88, HF=1.8); (a) d/100000, (b) d/10000, (c) d/1000, (d) d/100, (e) d/10

REFERENCES

[1.]   Lee, S. C., and Yoo, C. H. (1998), 'Strength of plate girder web panels under pure shear', Journal of Structural Engineering, 124, pp. 184–194.
[2.]   Hassanein, M. F. (2010), 'Imperfection analysis of austenitic stainless steel plate girders failing by shear', Engineering Structures, 32, pp. 704–713.
[3.]   Chacon, R., Mirambell, E., and Real, E. (2010), 'Hybrid steel plate girders subjected to patch loading, Part 1: Numerical study', Journal of Constructional Steel Research, 66, pp. 695–708.
[4.]   Kala, Z., Kala, J., Melcher, J., Skaloud, M., and Omishore, A. (2009), 'Imperfections in steel plated structures – should we straighten their plate elements?', NSCC-2009, pp.552-555.
[5.]   Alinia, M.M, Marvam Shakiba, and Habashi, H.R. (2009), 'Shear failure characteristics of steel plate girders', Thin-Walled Structures, 47,12, pp.1498-1506.
[6.]   Gheitase, A., and Alinia, M.M. (2010), 'Slenderness classification of unstiffened metal plates under shear loading', Thin-Walled Structures, 48,7, pp.508-518.
[7.]   Zhou, F., Young, B., and Lam, H.C. (2012), 'Welded aluminum alloy plate girders subjected to shear force', Advanced Steel Construction, 8, 1, pp.71-94.
[8.]   Timoshenko, S. P., and Gere, J. M. (1961), Theory of elastic stability (2nd ed), Newyork: McGraw-Hill.
[9.]   IS 800:2007, 'Code of practice for general construction in steel', BIS, New Delhi-110002.
[10.] IS 2062:2006, 'Indian Standard hot rolled low, medium and high tensile structural steel', BIS, New Delhi-110002.
[11.] Estrada, I., Real, E., and Mirambell, E. (2007), 'General behavior and effect of rigid and non-rigid end post in stainless steel plate girders loaded in shear. Part I: Experimental study', Journal of Constructional Steel Research, 63, pp. 970–984.

A Study of Wind Turbine Blade Power Enhancement Using Aerodynamic Properties

S. Senthilkumar[1], M. Gokulraj[2], G. Sivaraj[3], P. Maniiarasan[4]

[1, 2, 4] *(Department of Aeronautical Engineering ,Nehru Institute of Engineering Technology, India)*
[3] *(Department of Aeronautical Engineering , Bannari Amman Institute of Technology, India)*

Abstract: *Technological advancements have improvised them over time. In this paper we shall glance at the features. Wind energy is the most popular renewable energy. In order to increase the use of wind energy, it is important to develop wind turbine rotor models with high rotation rates and power coefficients. These elemental forces are summed along the span of the blade to calculate the total forces and moments exerted on the turbine. This study aimed at manufacturing highly efficient wind turbine rotor models using NACA profiles.*
Keywords: *Blade, NACA profiles, Power coefficients, Wind turbine, Wind energy.*

I. INTRODUCTION

A wind turbine is a kind of turbo machine that operates externally (without casing) and wind is generally considered to be incompressible, but sometimes the blade velocity at the tip may exceed 0.3 Mach and at such high blade speeds, wind may be considered as compressible at that region. Therefore the air density in the compressible region should be calculated separately from the incompressible region. In the incompressible region one should consider the free stream density of the air.

The abbreviation "HAWT" is used to indicate "Horizontal Axis Wind Turbine" and the term "VAWT" is used for its vertical case. We will focus on HAWT systems in this study rather than VAWTs. The axis "horizontal" implies that the rotor main shaft of the machine is parallel to the ground; on the contrary "vertical" implies the rotor main shaft is perpendicular to the ground. HAWT rotors decelerate the air rather than accelerating, and their tip speeds are much lower than those of aircraft propellers. Rotor blades aerodynamic features are very important. It is necessary to put forward the power value that can be obtained from rotor blades, real rotor blades have to be produced. And this means cost. For this reason, first miniature blades can be produced and the test can be conducted on these miniature rotor blades. This, along with theoretic studies, will help us to have a good opinion.

II. MODEL DIMENSIONS

As the technology developed, wind turbines were also improved just like the other technologies until recent times and they are continuously evolving. As it was mentioned earlier there are also VAWTs which geometrically differ from HAWTs. The world's largest horizontal axis wind turbine built on Hawaii Island, manufactured by Boeing Aerospace Industry. This turbine has a rotor diameter of 97.5m and has a rotor swept area of 7,470m2. Its rated power is 3.2 MW .

HAWTs are most preferable wind power machines due to their effectiveness when compared with VAWTs, but VAWTs have some superiorities upon HAWTs. One of them is they do not need any yaw mechanism and their installation is more easy and so their maintenance as well.
Scale model of this project is NTK/41 wind turbine.

- Scale ratio 1:120
- Model dimensions
  Rotor Diameter : 340 mm
  Hub Diameter   : 60 mm
  Blade length   : 140 mm
   No. of blades   :

III. WIND TURBINE DESIGN

Blade element theory assumes that blades can be divided into small elements that act independently of surrounding elements and operate aerodynamically as two-dimensional airfoils whose aerodynamic forces can be calculated based on the local flow conditions.

These elemental forces are summed along the span of the blade to calculate the total forces and moments exerted on the turbine. The other half of BEM, the momentum theory, assumes that the loss of pressure or momentum in the rotor plane is caused by the work done by the airflow passing through the rotor plane on the blade elements. This coupling of two theories ties together blade element momentum theory and sets up an iterative process to determine the aerodynamic forces and also the induced velocities near the rotor.

We have two equations derived from a consideration of blade forces which express the axial force and torque in terms of the lift and drag coefficients of the aerofoil (**Equations 1 & 2**)

$$\frac{a}{1-a} = \frac{\sigma'[C_L \sin\beta + C_D \cos\beta]}{4Q\cos^2\beta} \tag{1}$$

$$\frac{a'}{1-a'} = \frac{\sigma'[C_L \sin\beta - C_D \cos\beta]}{4Q\lambda_r \cos^2\beta} \tag{2}$$

IV. TORQUE & THRUST EXERTED ON A HAWT BLADE

When the incoming flow interacts with a HAWT blade, it tries to turn the blade around its axis of rotation, and tries to push the blade in the axial direction. These two main forces are called "lift" and "drag" do so. The forces acting on a (2D airfoil) HAWT blade.The torque exerted on the shaft axis a blade section comes from both lift and drag, and they are opposite in direction, but thrust components from both forces are same in direction (towards the axial direction). Higher the torque the wind turbine will be able to deliver more power. Higher the thrust the captured wind power would be lower and the cost of supporting tower will be higher.

V. COMPUTATION ANALYSIS

There are many CFD packages available in the market today. Auto desk CFD simulator and Auto desk CFD simulator packages improve the capability of analyzing a flow and meshing the element respectively. Auto desk CFD simulator is one of the most popular flow analysis packages in use today.

GEOMETRY NOMENCLATURE
The blade has a length (x L), a depth (y L), and a height (z L).The blade length is aligned with the x axis, the depth with the *y* axis, and the height with the *z* axis. The flow is assumed to be symmetric about a plane that bisects the blade in the y-direction and therefore only half the blade is modeled.

MESH
A model that has already been meshed and it has only 130'000 polyhedral cells. Note that at least 5 million cells, with hexagonal in the near-wall regions, would be necessary to obtain reliable and detailed results in such a case.

SPECIFY MATERIAL PROPERTIES
Define the materials is air And it is properties of
Density = 1.225 kg·m-3
Viscosity = 1.464e-5 kg·m-1·s-1

Those values correspond to the ICAO norm. Auto desk CFD simulator means dynamic viscosity as we consider air as incompressible and are not looking for heat transfer problematic, we don't need to specify properties.

BOUNDARY CONDITIONS
Blade model is "wall" with "blade" (in the field "Zone Name").We considers our model as a wind-tunnel model. So the blade is a stationary wall, the viscosity makes the air stick at the blade coachwork, so no slip the coachwork is very smooth, so a roughness of zero. Ceiling of the wind-tunnel and Side wall of the wind-tunnel are specified shear for this will allow the air to slip on the ceiling wall. This is not realistic, but so, we can use a very coarse mesh without boundary layer problems. Velocity is 25 m·s-1 in the Speed field. Correspond to 90km/h. and 0.05m in the "Roughness Height" field.
Inlet is 25 m·s-1 in the "Velocity Magnitude" field as the blade doesn't move, the air has to in the positive x-direction. Outlet is Zero Pa in the "Gauge pressure" field means we have atmospheric pressure at the outlet.

INITIALIZE THE FLOW FIELD
Initialize the "Compute From"-inlet. This will attribute to all cells of the model, the velocity, pressure and turbulences values that we defined for the inlet

OPERATING CONDITIONS
Let the 101325 Pa which corresponds to the ICAO-Norm. Auto desk CFD simulator works with relative pressure.
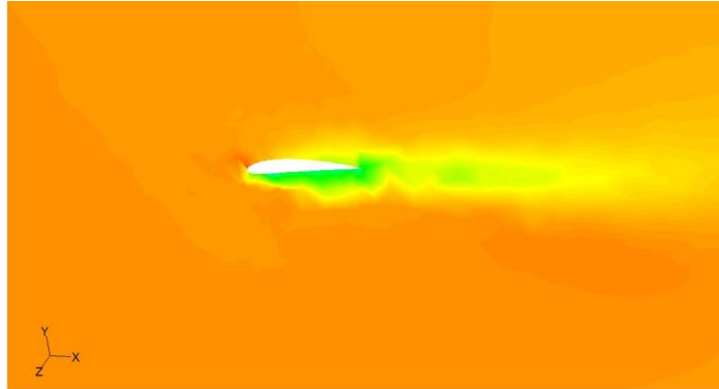
Figure 1: computational analysis of NACA 4420
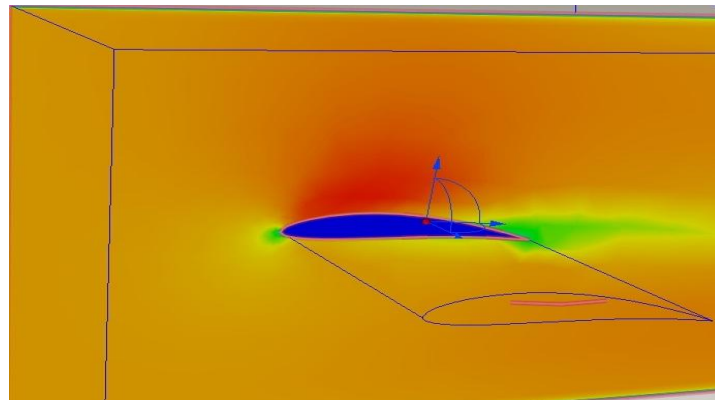
Figure 2: computation Analysis of NACA 65420

VI. CONCLUSION

The Lift/Drag ratio is calculated for different angle of attack ranges from 0° to4 ^{o} for the velocity ranges from 3 to 12 m/sec. The lift/drag ratio for different angle of attack is shown in Table.1.

Angle of attack	NACA 4420	NACA 65410
0	50.7	61.3
1	59.7	73.80
2	67.2	82.3
3	70	80.23

Table 1: Lift/drag ratio comparison of NACA 4420 and NACA 65420

For comparison NACA 4420 and NACA 65420 a rectangular blade was designed with the same platform area. This NACA 65410 blade does produce more power compared to the NACA 4420 blade but not as much as the twisted blades. All four upwind pointing NACA 65420 do result in lower thrust compared the rectangular blade tip, while the downwind pointing NACA 65420 results in comparable or even higher thrust.

Based on the present investigation it is seen that NACA 65420 has the best overall power performance of the upwind pointing, but the increase in power of around 0.8% for wind speeds larger than 6 m/s is relatively low and must be compared to the increase in thrust of around 1.3%. But pointing the NACA 65420 downstream seems to increase the power production even further. The effect of sweep and cant angles is not accounted for in the present investigation and could improve the performance of the NACA 65420s even more.

Acknowledgements

We first thank our 'GOD', the supreme power for giving us a good knowledge and our parents for making us study in a renowned college We owe a great many thanks to my colleagues and friends for their help and encouragement.

REFERENCES

[1]   Manwell J. F. et.al "Wind Energy Explained", John Wiley & Sons Ltd., England, 2002
[2]   Spera, D. "Wind Turbine Technology", ASME Press, 1994
[3]   Buhl, M. L., Jr. "WT_PERF User's Guide", NREL, Colorado, 2004
[4]   Scheck, S. "HAWT Aerodynamics and Models from Wind Tunnel   Measurements, NREL, Colorado, 2002
[5]   Glauert, H. "The Elements of Aerofoil and Airscrew Theory", University   Press, Cambrige, 1959
[6]   Bertin, J. J. and Smith, M. L. "Aerodynamics for Engineers", Third Edition, Prentice Hall, New Jersey, 1998
[7]   Katz J, Plotkin J. "Low Speed Aerodynamics", McGraw- Hill Inc., New York,   1991
[8]   Jureczko.M, Pawlak.M, Mezyk.A Optimisation of wind turbine blades, journal of materials processing technology 167(2005).
[9]   Sohn.Y.U, Chun.H, Kim.Y.C, Chung.C.W, Kim.Y.H, Han.K.S. Blade design of a 750Kw direct- drive wind turbine generator system.
[10]   Kong C, Kim H, Kim J. A study on structural and aerodynamic design of composite blade for large scale HAWT system. Final report, Hankuk Fiber Ltd; 2000.

Remote Access and Dual Authentication for Cloud Storage

Balaiah Gari Venkat Ranga Reddy[1], Kavya.A[2]

[1, 2] *(Department of Computer Science and Engineering/VIT-Chennai/ INDIA)*

Abstract: *Cloud computing is an emerging technology, which provides services over internet such as software, hardware, network and storage. The key role for cloud computing is virtualization which reduces the total cost and gives reliable, flexible and secured services. However compute service are chosen between the providers located in multiple data centres. One of the major security concerns related to the virtualization and the Storage where the outside attackers can use the files in the storage and the data owners are not capable of knowing attacks. In this paper we proposed a high level authentication for the cloud user and remote monitor controlled of your cloud storage. Here our model provides the dual authentication for the cloud and to get the runtime record of the logs and the secured application controls, the logs are remotely accessed and controlled by the owner of the data.*

Keywords: *Attackers, Authentication, Storage, Cloud*.

I. Introduction

Among the cloud services IaaS (Infrastructure as a service) is highly used in the large enterprises where the physical hardware is virtualized and serves to industrial and personal world. Cloud services are cost saving in real business world, and are successful Instead going to traditional cost in purchasing expensive and generation outdated hardware resources.

In virtualization approach several physical servers are connected by switches. The traffic between the servers from switch can't get detailed flow information this impacts some security information. As cloud is an internet based computing model that gives convenient on demand services like Storage as a service in which many business, company and educational societies are moving their services to cloud to store their data remotely located large data centres. The client can authorized to get his data modify, delete and can access remotely anywhere.As the data stored in large volume of data where the malicious attacks can occur at the VM level or at the hypervisor, if a kernel is compromised with rootkits they can easily access or delete the confidential data.

The Hypervisor layer is above the Hardware resources and resides operating system on the hypervisor, it is advantageous to us it gives the natural privilege where traditional security system is built, and the hypervisor acts as the master level in the access to hardware resources and more security levels can be built in hypervisors this paper gives you the dual authentication and the remote access will give the user end of the logs of his cloud storage.

As the cloud clients are need of having the high level authentication check. In the present generation authentication is done in many ways such as, textual, graphical, bio-metric, 3D password and third party authentication [2].In this paper high level authentication is taken care for the cloud clients by introducing the dual authentication technique which generates/authenticates the password in multiple levels to access the cloud services. In this paper, details of proposed dual authentication technique are presented along with the architecture, activities, algorithms and probability in success of breaking authentication is low.

II. Related Work

Most of the work done on the cloud storage security Dexian Chang and Xiaobo Chu has proposed the Flexible root of trust for the cloud[1] specified the attacker model and implemented the lightweight TSD (Trusted Service Domain), root of trust in the virtualization platform which shows the better security and efficiency. Data security in cloud computing based on Virtualization in this study case different type of virtualizations are given where the attacks in the hypervisor and VM level are to be noted, different security attention are given in transferring the data mainly to another cloud.

Thiyagarajan M, Dinesh Kumar K has given the model for authenticating cloud using the QR codes as in this process they use the captured images, the images are decoded with the encoder function() [7] and the data is sent by SMS to the cloud central server to authenticate the user. QR model describes the whole authentication needs an external personal device and also the server will not compromise if any delay in the provider of the mobile.

Authentication of different methodologies were implemented as of digital signature, 3D authentication as there are all at the entry level authorization. Hypervisor is an superior place in the place of authentication as this with the inspection and interposition here the system states are of CPU registers, BIOS, storage are managed the interface of the Operation system the boot loader of the system is loaded in the bios which interfaces the hypervisors, we can say that hardware is the root nodes of the servers.

III.   Problem Statement

In the virtual cloud storage the attackers at the VM level is controlled by the authentication where if the Hypervisor is compromised with any of the boot loader it will erase all the security level and turns firewalls off and other security tools. The attackers like DDoS attack in which layering security across the multivendor networks, client to client attacks where One client has malicious and it can infect to other users of all VM's that relay on the physical hardware on the same hypervisor. Mainly authentication is taken at the application or entry level where the attackers can easily attack the user passwords, but in the hypervisor level we can seal the hardware resources with TPM seal as we can modify the security levels at this state which can increase the security levels of the user data stored in cloud.When the data storage is used by others and attackers the owner will not get to known instead confidential data may be modified or deleted in his virtual storage.

IV.   Proposed Model

Authentication:

In the cloud services the users need the authentication to access his services. The user can access the cloud services if his authentication was successful, the basic and used model for security in any services is authentication. Authentication is used in two types i) Cloud service provider gets to check the privilege user not any attackers ii) Cloud provider to confirm the SLA's and allocates the specified resources to the client as of formal procedure. This authentication is verified at the internet based of entity logging to the services.

The authentication of user in this model is dual authentication, we add some security levels into the grub which is the boot loader for every physical machine, TPM will seal storage of the users in which the data of the user will be encrypted with encryption tools and the data in the storage can be accessed until the dual authentication is successes. Due to this the malicious attackers will be prevented, TPM seal will be decrypted and the storage will be accessed and system will be start up at this stage.Here in this cloud virtualization first VM level attacks are the main causes for security of data where the data of a user is accessed, and cloud provider can use the data of the user some provider vulnerabilities like SQL-injection and core site scripting which cause insecure of the data. Secondly Hypervisor level attacks when an attack is on hypervisor this an highly security issue he can take control of the whole data centre, issuing this problems we had the dual authentication in which the hypervisor will have and second level authentication between hardware and Virtual machines or hypervisor which holds TPM seal on the hardware.In this real time analysis the probability of attack will be low the TPM will not compromise until the password you entered is permitted, this will not support any reverse engineers (password generator) in this grub level loader the authentication is not saved in a plain texts.
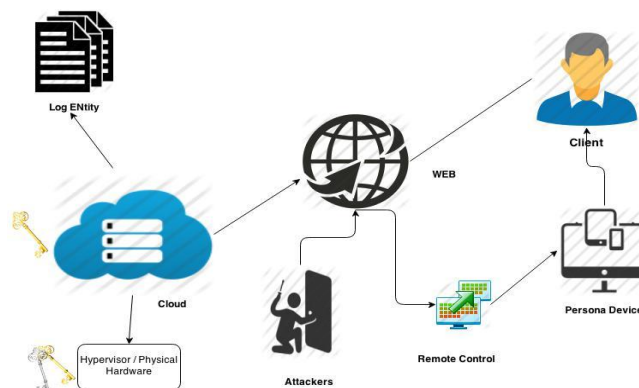

Figure 1: Model of dual authentication and remote assistance of logs

Algorithm for authentication and remote model:
Cloud server
{
if (authentication at entry level=succeed)
    {
    Enter the security key for hypervisor level
    if (security=succeed)

```
        {
else
            {
return authentication failure;
            }
        }
    Decrypt the TPM seal and give privilege to user;
        {
        MalGen records the logs data;
if (user requests the logs)
proxy is authenticated to remote access;
        }
    }
}
```

Remote Compute of logs in cloud:

In the site entity logs that are compromised with authentication and the data used by the user, time had been recorded in the monitoring tools as MalGen is an open source code owned by Google which gives the logs of the large data sets handled by Hadoop. In this log entity if the entry of the user is compromised by the server then the Flag is set to '1', if it gets incorrect password set to '0'.The data format of MalGen is "Event ID|Timestamp|Site ID|Flag|Entity ID"as in our logs the compromised logs areshownas "00799999996007385002449543293305|2014-04-1210:50:41.606070|0445544244954369755|0|0000000000001032397" and the Volatility is the other tool which generates the same logs as they are in the shows GUI of the Hacker when accessed and the directory of access are shown, with this site entity logs the client get over the attack or malicious entry into his cloud.In TheRemote control to the client the server will provide the attestation proxy where the trusted remote access to client, remote login can be accessed by the given proxy he can set to his any personal devices and can be accessed to the logs entity of his cloud storage

V. Conclusion And Future Work

The cloud computing is an emerging technology which reduces the burden of the users and also cost effective resources and used over internet remotely, due to this security issues are also arising where the malicious attackers we can make sure of our data safe by having remote access of our entity logs and we also proposed a model to dual authentication where the user can have his secured cloud.

Dual authentication is where authorised at both the entity of cloud and also the grub level in which takes more time for authentication than the normal authentication we can try to decrease the time for the execution of the whole system in authenticate.

REFERENCES

[1]   Hamdi, M., "Security of cloud computing, storage, and networking," Collaboration Technologies and Systems (CTS), 2012 International Conference on , vol., no., pp.1,5, 21-25 May 2012 doi: 10.1109/CTS.2012.6261019

[2]   Dinesha, H.A.; Agrawal, V.K., "Multi-level authentication technique for accessing cloud services," Computing, Communication and Applications (ICCCA), 2012 International Conference on , vol., no., pp.1,4, 22-24 Feb. 2012 doi: 10.1109/ICCCA.2012.

[3]   Baliga, J.; Ayre, R.W.A.; Hinton, K.; Tucker, RodneyS., "Green Cloud Computing: Balancing Energy in Processing, Storage, and Transport," Proceedings of the IEEE , vol.99, no.1, pp.149,167, Jan. 2011 doi:10.1109/JPROC.2010.2060451

[4]   Kumar, A.; Byung Gook Lee; HoonJae Lee; Kumari, A., "Secure storage and access of data in cloud computing," ICT Convergence (ICTC), 2012 International Conference on , vol., no., pp.336,339, 15-17 Oct. 2012 doi: 10.1109/ICTC.2012.6386854

[5]   IEEE - The Application of Cloud Computing in Education Informatization, Modern Educational Tech... center Bo Wang, HongYu Xing.

[6]   NISTDefinition http://www.au.af.mil/au/awc/awcgate/nist/cloud-def-v15.doc

[7]   CA Technologies cloud authentication system http://www.ca.com/us/authentication-system.aspx

[8]   X. Suo, Y. Zhu, G. S. Owen, "Graphical passwords: A survey," in Proc. 21st Annual Computer Security Application. Conf. Dec. 5–9, 2005, pp. 463–472.

[9]   S. Wiedenbeck, J. Waters, J.-C. Birget, A. Brodskiy, and N. Memon, "Authentication using graphical passwords: Basic results," in Proc.   Human-Comput. Interaction Int., Las Vegas, NV, Jul. 25–27, 2005.

[10]   Barsoum, A.; Hasan, A.,"Enabling Dynamic Data and Indirect Mutual Trust for Cloud Computing Storage Systems," Parallel   and   Distributed   Systems,   IEEE   Transactions   on ,   vol.24, no.12,pp.2375,2385,Dec.2013doi:10.1109/TPDS.2012.337.

Analysis of MOS Capacitor Loaded Annular Ring MICROSTRIP Antenna

Mohit Kumar[1], Surendra Kumar[2], Devendra Kumar[3], Ravi Kumar[4]

[1, 2, 3, 4] *(Assistant Professor, Shri Ram Murti Smarak Womens College of Engineering and Technology Bareilly (U.P.)*

Abstract: *In this paper a new technique is proposed for achieving increased frequency agility by loading the patch antenna with a MOS capacitor. Theoretical investigations have been carried out for the MOS capacitor loaded Annular Ring microstrip antenna, for oxide thicknesses from 100 A to 500 A, to predict the achievable range of operational bandwidth. In spite of numerous advantages, the simple patch antenna has a low operational bandwidth, which limits its applicability. Hence this technique of MOS capacitor loaded Annular Ring microstrip patch antenna is to improve the operating frequency range.*

I.   Introduction

The concept of microstrip radiator was first proposed by Deschamps as 1953. As shown in Fig 1 a microstrip antenna in its simplest configuration consists of a radiating patch on one side of a dielectric substrate ($\varepsilon_r \leq 10$), which has a ground plane on the other side. The patch conductor's steps are generally used to simplify analysis and performance prediction. Ideally the dielectric constant εr of the substrate should be low ($\varepsilon_r \approx 2.5$), so as to enhance the fringing fields which account for the radiation. However, other performance requirements may dictate the use of substrate materials whose dielectric constants may be greater than 5. Various types of substrates having a large of dielectric constants and loss tangents have been developed. Flexible substrates are also available which make it possible to fabricate simple conformal antennas.
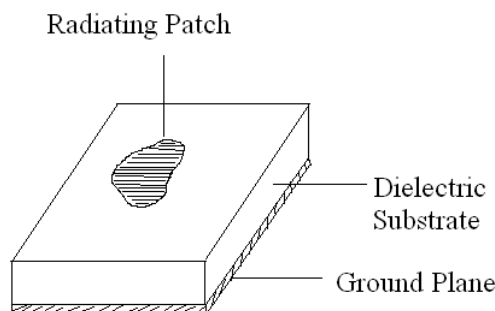
Fig 1 Rectangular Microstrip Antenna

II.   Analysis of Annular Ring Microstrip Antenna

A Microstrip patch antenna (MPA) consist of a conducting patch of any planner geometry of one side of a dielectric substrate backed by a ground plane on other side. The cavity model for the annular microstrip analysis is based on E walls and H walls boundary conditions. Cavity model for the annular ring microstrip antenna is shown and its analysis for the annular microstrip antenna is based on the following observations. The close proximity between the annular patch and ground plane suggests that E has only z component and H only x-y components in the region bounded by the microstrip and the ground plane. The fields in the above mentioned region are independent of the z co-ordinates for all frequencies of interest. The electric current in the microstrip must have no component normal to the edge at point on the edge.

2.1 Fields and Current:

With no current sources the wave equation may be written as,

$$\left(\nabla^2 + K^2\right)\bar{E} = 0$$

Where, k is a wave number given by,

$$k = \omega\sqrt{\mu\varepsilon}$$

The field must be solved by the wave equation and the magnetic wall boundary conditions. Since,

$$E = Z \overline{E}_z \; , \quad \frac{\partial E}{\partial \rho} \mid \rho = a = 0 \qquad \text{and}$$

$$\frac{\partial E}{\partial \rho} \mid \rho = b = 0$$

Thus the solution of the wave equation in the cylindrical; co-ordinates is

$$E_z = E_0 \left| j_n(k\rho) Y'_n(ka) - j'_n(k\rho) Y_n(k\rho) \right| \cos n\phi$$

$$E_\rho = E_\phi = 0$$

2.2 Resonant Frequency:

The resonant frequency can be calculated by taking account the effect of fringing field

$$f_{nm} = c k_{nm} / 2\pi \sqrt{\varepsilon_r}$$

Here c is the velocity of light and ε**r** the relative dielectric constant

2.3 Effective Inner and Outer Radii & Effective Dielectric Constant:

To account the fringing field effects along the curved edges of the ring it is necessary to replace the radius 'a' and 'b' by their effective values, a**eff**, b**eff** and ε**eff** can be calculate as follows

$$\varepsilon_{eff} = \frac{1}{2}(\varepsilon_r + 1) + \frac{1}{2}(\varepsilon_r - 1)\left(1 + \frac{10h}{w}\right)^{-1/2}$$

Now the resonant wave number k**nm** is the m zero of the transcendental equation

$$j'_n(a_e k_{nm}) Y'_n(b_e k_{nm}) - j'_n(b_e k_{nm}) Y'_n(a_e k_{nm}) = 0$$

for the TM**12** mode the solution of the above equation is given by

$$k_{12} = \frac{51.975 \, a_e}{(b_e - a_e)(17.8 a_e - b_e)}$$

After solving the characteristic equation for k**nm**, the resonant frequency can be determined from

$$f_{nm} = \frac{c k_{nm}}{2\pi \sqrt{\varepsilon_{eff}}}$$

It should be pointed out that the correction to the resonant frequency formula involves both the effective permittivity and the effective radii.

2.4 Input Impedance:

Equivalent circuit is effective to design for this type of antenna because of its simplicity and ease of understanding the physical phenomenon. It is a G-L-G lumped element resonator circuit. Using the mode expansion theory, the input impedance of the AR-MSA can be obtained. The input impedance from the feed line can be expressed as a parallel resonator,

$$Z_{in} = \sum_n \sum_m \frac{1}{j\omega c_{nm} - j\frac{1}{\omega L_{nm}} + G_{nm}} + j\omega L_t$$

Where C**nm**, L**nm**, and G**nm** are equivalent circuit parameters including losses corresponding to each mode.

III. Analysis of Annular Micro strip Antenna with MOS Capacitor Loaded

3.1 Mos Capacitor:

A MOS capacitor of MIS (metal± insulator± semiconductor) diode is a voltage variable capacitor. A typical MOS capacitor structure for the proposed analysis is Au± Si3N4± Si, shown in The capacitance is dependent on the oxide thickness, which is evidently clear from

$$C = \frac{\varepsilon . a}{d}$$

Mos capacitance

$$C_{mos} = \left[\left\{ \frac{C_0}{\left(1 + \frac{2VgC_0{}^2}{\varepsilon q Na} \right)^{1/2}} \right\} A \right]$$
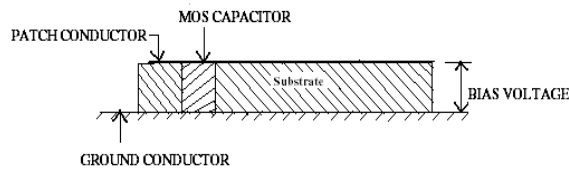
The capacitance of the depletion Cd per unit area

$$\frac{C}{C_0} = \frac{1}{\sqrt{1 + \frac{2VgC_0{}^2}{\varepsilon.qNa}}}$$

The ratio of C/Co decreases with the gate potential accordance with the above expression, and reaches a minimum value when inversion layer is formed.

3.2 Mos Capacitor Loaded Annular Ring Microstrip Antenna

Equivalent circuit for MOS loaded annular ring microstrip antenna is shown below

PRESENTATION OF MOS CAPACITOR LOADED MICROSTRIP ANTENNA

Fig 2 Equivalent circuit for MOS Loaded annular ring microstrip antenna

The patch performance will be affected due to its radiating edge capacitance in addition to the capacitance provided due to the MOS capacitor Under such conditions the total capacitance will be

$$C_{total} = C_{MOS} + C_{SA} + C_{SB} + C_{EQ}$$

Where

$$C_{SA} = 2a \varepsilon_0 \left[\ln\left(\frac{a}{2h} \right) + (1.41 \varepsilon_r + 1.77) + \frac{t_2}{a}(0.268 \varepsilon_r + 1.65) \right]$$

$$C_{SB} = 2b \varepsilon_0 \left[\ln\left(\frac{b}{2h} \right) + (1.41 \varepsilon_r + 1.77) + \frac{t_2}{b}(0.268 \varepsilon_r + 1.65) \right]$$

Thus the **resonance frequency** for the modified mode will be

$$f_r = \frac{1}{2\pi (L_{EQ}C_{total})^{1/2}}$$

IV. Computation of Various Parameters

4.1 Reflection coefficient:

It is defined as the ratio of the reflected voltage or current to the incident voltage or current and is usually denoted by ρ. Reflection coefficient is a vector quantity having magnitude and direction as well. In terms of impedance it can be expressed as

$$\rho = \frac{Z_0 - Z_{in}}{Z_0 + Z_{in}}$$

4.2 Voltage standing wave ratio:

It is defined as ratio of maximum to minimum voltage on a line having standing waves and this ratio is observed as

$$\text{VSWR} = \frac{1 + \rho}{1 - \rho}$$

4.3 Input impedance of the patch:
When we consider only the annular ring patch, than the input impedance will be

$$Z_{in} = R + iX$$

4.4 Quality factor:

It is a measure of any selectivity of a resonant or anti resonant current and is expressed as

$$Q=\omega W/P$$

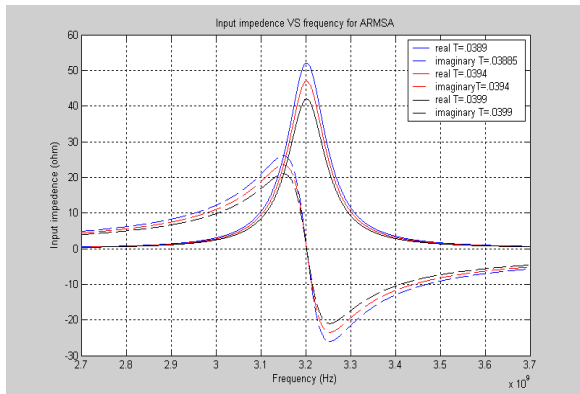W=Maximum stored energy
P=average power loss

Fig 3 Input Impedance vs Frequency for different feed points
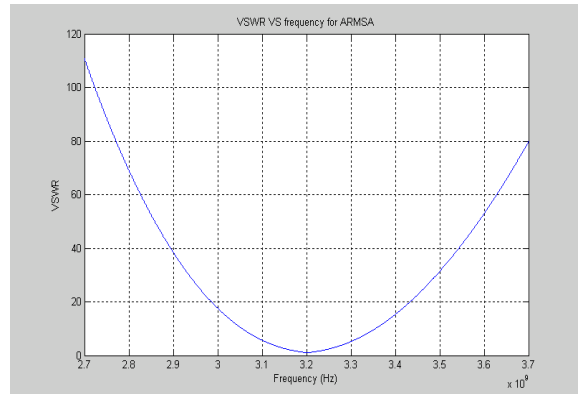
Fig 4 VSWR vs Frequency
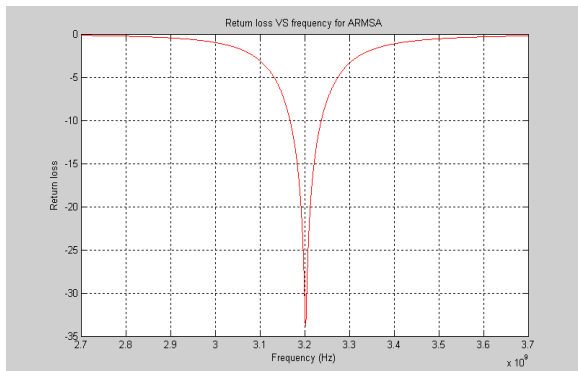
Fig 5 Return Loss vs Frequency Voltage
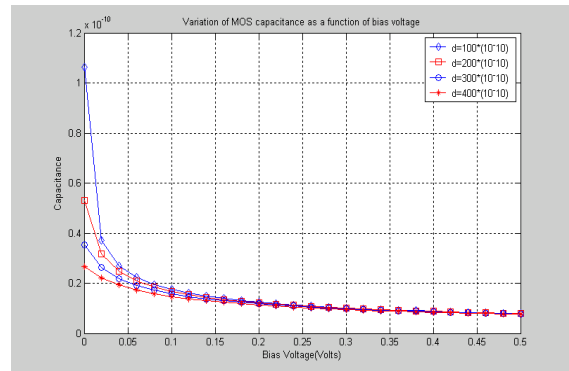
Fig 6 MOS Capacitance vs Bias
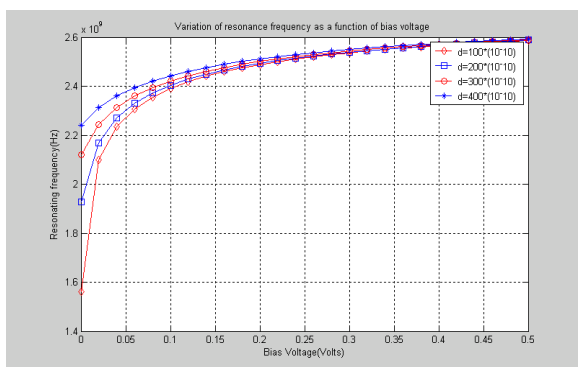
Fig 7 Resonating Frequency vs Bias Voltage
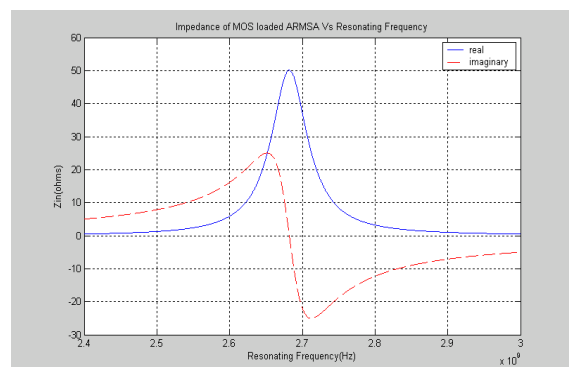
Fig 8 Input Impedance vs Frequency for
MOS Loaded ARMSA

V. Conclusion

This paper has described an analysis of the behavior of Mos capacitor loaded annular ring microstrip antenna. Results have been presented for resonant frequencies and radiation patterns. After loading MOS capacitor on the antenna the operating frequency can be easily controlled.
From above graphical analysis it is observed that-

1. The variation of MOS capacitance is similar for all the five oxide thickness. A larger variation in capacitance is observed with bias voltage near zero bias, but it is very small at higher bias.
2. The maximum frequency agility of 57.08% is obtained for minimum oxide thickness (100A˚). However for maximum value of oxide thickness (500 A˚), the frequency agility is around 38.48% (0.962 GHz),

which is the lowest value. The frequency agility obtained with the MOS capacitor loaded antenna (57.08 %) is higher than the varactor loaded patch (47.24 %).

REFRENCES

[1]   I .J. Bhal and P. Bhartia , Microstrip Antenna , Dedham , MA : Arteh House , 1980 ,

[2]   Special issue on microstrip antennas, IEEE Trans. Antennas Propagation , vol . AP- 29, Jan. 1981.

[3]   I. J. Bhal , S . S . Stuchly , and M . A .Stuchly , "A new microstrip radiator for   medival application , " IEEE Trans Microwave Theory Tech., vol. MTT-28, pp. 1464-1468, 1980.

[4]   J. W. Mink, "Circular ring microstrip antenna elements, "presented at 1980   Antennas Propagat . Soc. Int. Symp. , P.Q, Canada , June 1980.

[5]   S. Ali, W. C. Chew, and J. A. Kong, "Vector Hankel transform analysis of annular ring microstrip antenna , "IEEE Trans . Antenna Propagat . , vol . AP-30

[6]   W.C. Chew, "A broad – band annular – ring microstrip antenna , " IEEE Trans. Antennas Propagation , vol . AP-30, no. 5, pp. 918-922 , Sept. 1982.

[7]   J. S. Dahele and K. D. Lee, "Characteristics of annular ring microstrip antenna, "Electron . Lett. , vol . 18, pp . 1051-1053, Nov.1982.

[8]   L. C. Shen , "analysis of a circular disc printed circuit antenna , " Proc. Inst . Elec,   Eng., vol , 126,no.12 pp.1220-1222, Dec. 1979.

OPEN ACCESS

An Improvement to Sensor Protocol for Information via Negotiation (SPIN) Protocol

Vidhi S. Patel[1], Prof. Chandresh R. Parekh[2]

[1](Wireless and mobile Computing,GTU-PGSchool (BISAG), Gandhinagar)
[2](Department of Electronics and communication, Government Engineering College, Gandhinagar)

Abstract: *Wireless sensor network is collection of one or more homogeneous or heterogeneous sensor nodes which sense some events and inform sink for that by sending that data towards it to perform some action. Data transmission is the most effective factor in sensor network that directly regret energy of sensor node but though energy of sensor node is very crucial one need to save that energy by means of minimizing redundancy and retransmission of data. Till the day many routing protocols are introduced to route data efficiently in order to improve network life time but all protocols have some deficiency. One of the most popular data centric dissemination protocols is Sensor Protocol for Information via Negotiation (SPIN). It efficiently disseminates data among other nodes in the network. This protocol uses meta-data for negotiation and eliminates the transmission of the outmoded data throughout the network. This paper introduced improved SPIN which is further enhancement of SPIN protocol.*
Keywords: *Wireless Sensor Network, Sensor Protocol via Information Negotiation, Advertisement*

I. INTRODUCTION

Wireless sensor network (WSN) is a group of application specified sensor nodes which monitors and handle conditional values in organization, environment or in any system to collect data and send to centrally located node. WSNs measure environmental conditions like sound, pressure, humidity, temperature, pollution levels, wind speed and direction, etc. Initially main motive to introduce wireless sensor network was for military operations, but day by day its usage was enhanced because of its easy use and fast results in health, security management, traffic management, etc.

The sensor node equip with a radio transceiver, an antenna, a microcontroller, an interfacing electronic circuit, and battery as energy source. The size of the sensor nodes can vary from a little dust particle to shoe box and regarding their prices also vary from a few cents to hundreds of dollars depending on the functionality parameters of a sensor like energy consumption, computational speed rate, bandwidth, and memory affect.

The most challenging part of WSN is to have best routing protocols utilized in terms of less memory consumption and high throughput. This paper is the further extension of the paper "Survey on Sensor Protocol for Information via Negotiation (SPIN) protocol"[1]. This paper shows idea for the improvement in SPIN and here in this paper discussed for algorithms and results of it.

II. SPIN PROTOCOL

(**SPIN**) as name suggest is a negotiation based protocol and is among the early work to pursue a data-centric routing mechanism. The idea behind SPIN is to tag the data using high level descriptors or meta-data. In any transmission, before sending data meta-data are exchanged among sensors via data advertisement mechanism, which is the key feature of SPIN.

Each node which receives new data first advertise it to its neighbor and interested neighbors who have not that data send request message to node who advertised. SPIN's meta-data negotiation solves problems of flooding such as redundant information passing, overlapping of sensing areas and resource blindness thus, achieving a lot of energy efficiency. There are three types of messages in SPIN to exchange data between nodes. These are: ADV message to allow a sensor to advertise a particular meta-data, REQ message to request the specific data and DATA message that carry the actual data. Below figure redrawn from, summarizes the steps of the SPIN protocol.
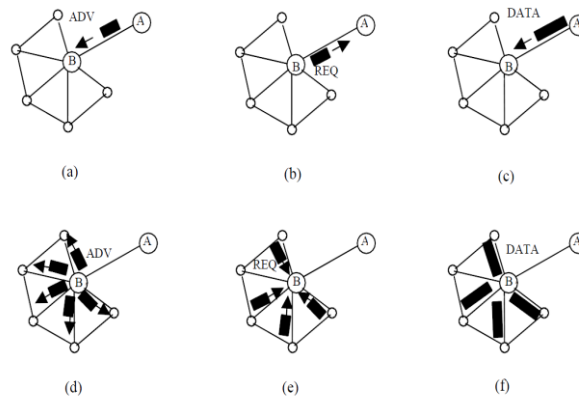
Fig. 1 SPIN Protocol. Node A starts by advertising its data to node B [1]

(a) Node B responds by sending a request to node A
(b) After receiving the requested data
(c) Node B then sends out advertisements to its neighbours
(d) Who in turn send requests back to B (e-f).

Advantage of SPIN is that each node of network need to know about its neighbours only. SPIN gives a factor of 3.5 less than flooding in terms of energy dissipation and meta-data negotiation almost halves the redundant data. However, SPIN's data advertisement mechanism cannot guarantee the delivery of data. For example, if one node need to send data to very far away node so that data would be passed through hops between their both, but if they in between hops are not interested to that transmission then data would never reach to destination sender need to send. Therefore, SPIN is not a good choice for applications such as intrusion detection, which require reliable delivery of data packets over regular intervals.

III. PROBLEM STATEMENT

As survey made on SPIN protocol, by reading different literatures and researches made before, the SPIN protocol still have some loop falls that need to be improve. Papers referred says different modifications made on SPIN protocol but all improvements have some drawback and that need to be solve.

1) One improvement made in SPIN is M-SPIN. That is shown in bellow figure.
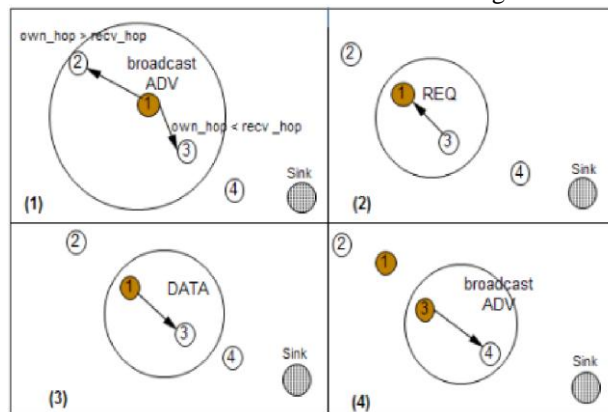
Fig. 2 Transmission in M-SPIN Protocol [6]

(1) Node 1 starts advertising its data to all of its neighbors.
(2) Node 3 responds by sending a request to node 1.
(3) After receiving the request, node 1 sends the data.
(4) Node 3 again sends advertisement out to its neighbors for the data that it received from node-1.[6]

M-SPIN protocol which is more energy efficient rather than traditional SPIN, but problem in that is, this protocol leads to one problem that is nodes nearby sink node dies early, so as per that paper it is one criteria of research to make that nodes power efficient or can make whole network power aware by assuming mobile environment in WSN.

2) Another idea is of SPIN-pi protocol. In traditional SPIN protocol If a node's neighbors are not forwarding data, the data will not continue to be forwarded, so that the user couldn't receive the information. So solution of that is in SPIN-pi that is adding plug-in nodes in the SPIN protocol. They have used nodes which are have AC Power supply, if according to application if there is requirement of having deployments of node in some forest or under water where no continuous power supply can be made, we can use solar cell plugged node, which can takes continuous energy from sun light. Below figure shows an example of SPIN-pi protocol.[7]

Fig. 3 The network communication process in SPIN-Pi[7]

So, by getting idea of such more power efficient nodes and deploying more amount of such much power efficient nodes in network we can improve the life time of our network and make it more reliable and efficient.
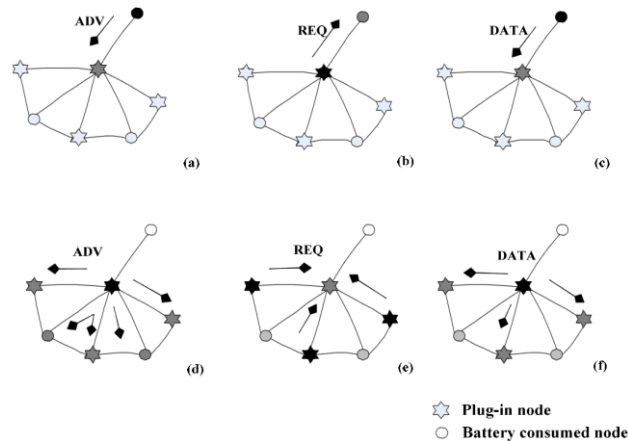
3) In this paper they have introduced new protocol named SPIN- I. In SPIN protocol there are problem of "blind forward" and "data inaccessible". To avoid these problem this protocol using three way handshake mechanism:
1. Data broadcasting stage
2. Data requesting stage
3. Data transmission phase.

In SPIN-I they include timer concept in broadcasting stage means at time of advertisement. And at receiver side means a node who receives ADV message includes flag to determine its energy level. [7]
They simulated SPIN and SPIN-I protocols under certain idealized environment and in that environment SPIN-I performed better than SPIN.
SPIN-I protocol is good solution to solve the "blind forward" and "data unreachable" problem. However, because here the SPIN-I protocol is simulated in a more idealized situation, and its transmission time is longer than SPIN, the solution of these problems needs further research.

IV. PROPOSED SOLUTION
As per literature survey and according to above survey paper[1] defined problem statement as "Reliable data transmission in sensor network using M-SPIN protocol and deploying plug-in nodes in between."
In such case sensor node would be arranged statically in cellular manners. Means at center of each cell there is one plug-in node and around that there are simple sensor nodes. This plug-in node concept is taken from literature discussed 2.6[7], and routing protocol M-SPIN would be used.
There are some pre-assumption considered are as mentioned below.
   1. Assuming that all the nodes used in such network design are homogeneous, but there is difference between nodes in terms of their energy efficiency. That is there are normal sensor nodes which are traditional sensor nodes works on dry battery cells where as other nodes called plug-in nodes are nodes which uses solar energy so they are more energy efficient than that normal sensor nodes.
   2. Energy efficiency of plug-in node is high then normal sensor nodes so their range of the transmission would also high than other normal nodes, and plug-in nodes are high energy efficient so they can route data for long period of time because they are continuously getting power supply and also they never drop any data packet passed through it.

3. Plug-in node always route packet to next destination without failure and if any predecessor node of plug-in node fail to transmit data then plug-in node are capable to retransmit data. So it is reliable to having concept of acknowledgment at plug-in nodes.

By cellular arrangements of nodes, each sensor node is directly connected to minimum 3 plug-in nodes. So in path of routing there are minimum half of the node would be plug-in nodes. So it improves the reliability of path. If we assume that each plug-in node can have more range than other sensor nodes then there might be possibility to send data from one plug-in node to another plug-in node if any in between node would fail or not send data ahead that would improve reliability and save energy too. In below figure it shows the proposed network structure.
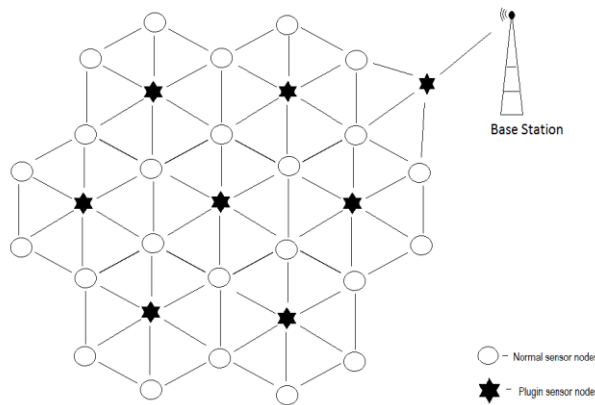
Fig. 4 Proposed solutions' network topology [1]

In proposed scheme routing would be done according to the M-SPIN protocol. In algorithm of the routing scheme of this improved protocol First stage is Distance discovery, then Negotiation and last stage is Data Transmission.

So, it works similarly to M-SPIN mechanism but difference is that, problem in M-SPIN was the node near the Base Station drain out first, so optimizing that problem using plug-in node here. Because plug-in nodes uses solar cells as battery backup so it would charge regularly and other problem in SPIN protocol is reliability, so by adding plug-in nodes in between they improve network efficiency rather than normal nodes because the average failure of network minimized by their installation.

Algorithm: If we consider node A wants to send data to the Base station (sink) node.
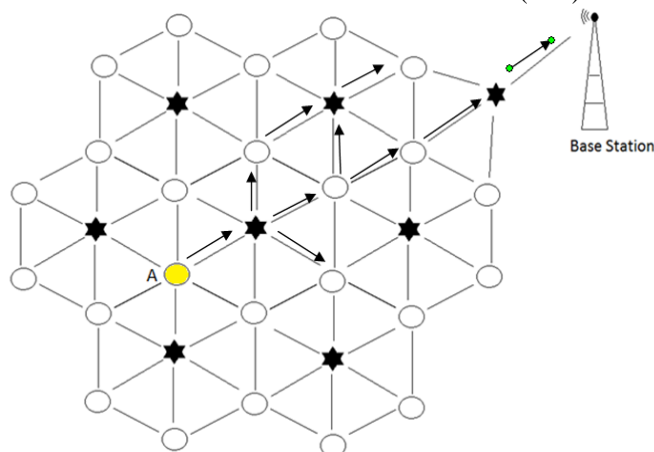
Fig. 5 Network's Work illustration [1]

Step1: Initially Base station (Sink node) sends the Startup packet in the network. Startup packet containing three values, Type, Node ID and Hop. Type means message type, Node ID means ID of sender node and hop means the hop distance of node from sink node.

Step 2: After the distance discovery phase complete, it starts negotiation phase. Same as SPIN-BC protocol it sends ADV message to its neighbor and the neighbor whose hop distance is lesser than sender of ADV only can send REQ message. Here A is the sender node. Who sends ADV message but the neighbor whose hop distance is lesser than hop distance of A only can send REQ message.

Step 3: After sender node get the REQ message it comes to data transmission mode. In which sender sends actual data to that link. This negotiation and Data transmission phase would repeat until it reaches to Base Station.

To increase reliability we can add acknowledgement feature at plug-in node to make confidentiality of data transfer.

V. IMPLEMENTATION OF ALGORITHM

1. Distance Discovery
Step.1: Start Distance Discovery() // Call Function
Step.2: if node_id equals 0 // Node is sink node
          hop<-1
          call startup(1); //sink node calls startup function
Step.3: if node_id not equals 0 && startup type equals 3 // Still its discovering distance
          check for hop counter
          increment in hop
Step.4: else forward hop value to next neighbour
2. Negotiation
Step.1 : Start negotiation function
step.2 : if energy_level is greater than threshold_level
          do
          send ADV message
          wait for specified period of time
          while(not heard REQ from neighbour)
          Send DATA
Step.3 : if own_hop is less than recieved_hop
          if(status equals first receive || nature equals plugin)
          send REQ for DATA
          else
          send Status as second receive
3. Data Transmission
Step.1 : At source node get REQ msg
Step.2 : if get_current REQ_Origin and   REQ_sequance match
          Forward(Stored packet)

Performance Analysis

1. No. of nodes alive
As per problem statement in M-SPIN node resides near to sink node dies earlier and thus it affect to whole network's life time and efficiency.

By applying above algorithm as we used plug in nodes in between it improves network life time by mean of no of node alive after some round iterations. In Figure.6 it shown below.
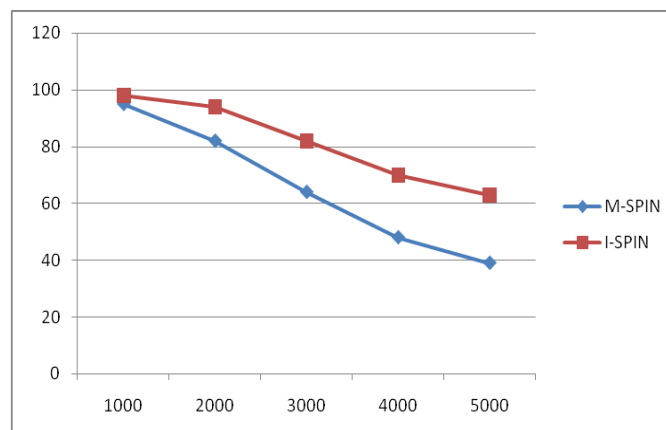

Fig. 6 Number of nodes alive per rounds

2. Packet overhead

In traditional SPIN when ever any new event occure sensor node broadcast Advertisement packet for that event to all of its neighbours in network and among that all neighbours nodes who dont have that data only sends request packets

But in Improved SPIN request packets sent only to the neighbours which are less far from sink than its own distance. So request packets may half of the origional SPIN. Difference is Shown in Figure.7 bellow.
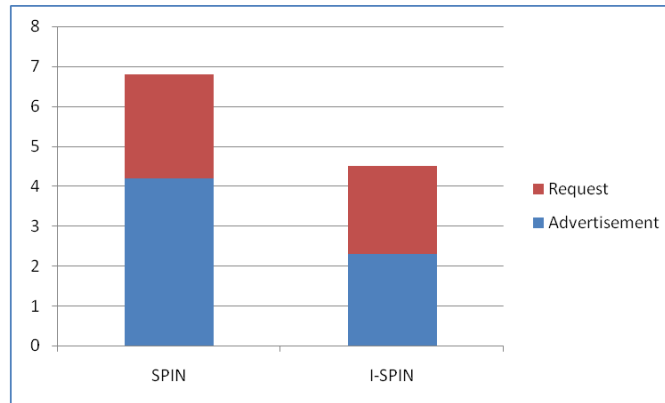
Fig. 7 Differenciate packet overhead

3. Energy consumption based on no. of nodes

In sensor network each transmission would deduct some amount of energy in terms of joules. In M-SPIN energy of each node would be deducted after each transmission but in Improved SPIN as we have used plug in nodes and lifetime of that node are much more than another simple node and energy deduction of that node would be negligible than other nodes so comparatively the total energy usage of network decrease in Improved SPIN than M-SPIN.

Thus bellow Figure.8 shows difference between both protocol's network's total energy consumption as per no. of nodes.
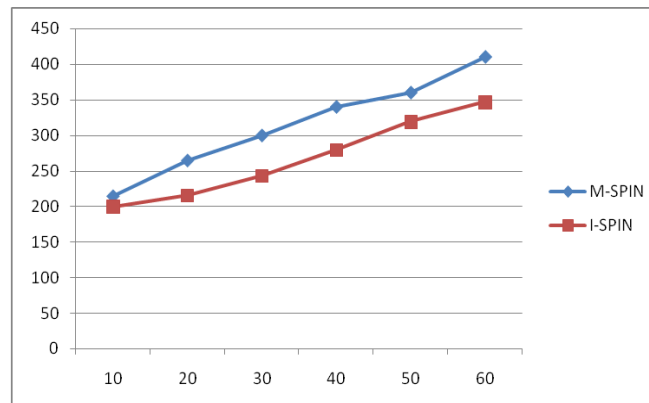
Fig. 8 Energy consumption based on number of nodes

VI. CONCLUSIONS

WSN is very different than other wireless networks. Main crucial issue in WSN is shortage of energy. WSN is made up of hundreds or thousands of nodes which are stand alone and communicate to each other using hope by hope data transmission in network and having minimum amount of energy. Here as discussed in previous researches and survey that is done for new improvement in SPIN is illustrated in algorithm and being implemented in Castalia simulator in this paper. According to network design and algorithm here are some results we get that are shown that using plug in nodes in between the algorithm of M-SPIN it utilize the battery consumption and also improves network lifetime. As plug in nodes are more reliable than normal node it improves network reliability twice. Here we implemented such scenario in some static and greedy format so its need to be implement for mobile environment as further research.

REFERENCE

[1]   Survey On Sensor Protocol For Information Via Negotiation (Spin) Protocol, Vidhi S. Patel, Chandresh R. Parekh. Routing Techniques In Wireless Sensor Networks: A Survey- Jamal N. Al-Karaki, The Hashemite Universityahmed E. Kamal, Iowa State University

[2]   Simulation Study For Routing Protocols In Sensor Networks- AbdelazizAraar, Hakim Khali, and Riyadh A. MehdiFaculty of Computer Sciences, Ajman University, Ajman, UAE

[3]   The Analysis And Research OfWsn's Energy efficient Routing Protocols⁻ Jie XU, Fanglu NING, Dawei JIANG*Eastern Liaoning University, Dandong, China

[4]   Comparison and Analysis Data-Centric Routing protocols in wireless sensor networks- Zahra GhaffariDepartment of ComputerEngineering and InformationTechnology, mirkabir University Tehran, Iran, TaliehJafari,Department of Computer Engineeringand Information Technology,Amirkabir University Tehran, Iran, HosseinEskandariShahraki,Department of Computer Engineeringand Information Technology,Amirkabir University Tehran, Iran

[5]   A Modified SPIN for Wireless Sensor Networks- ZeenatRehenaSchool of Mobile Computing andCommunication, JadavpurUniversityKolkata – 700 098, India, Sarbani Roy Dept of Computer Science &Engineering, JadavpurUniversityKolkata – 700 032, India, NandiniMukherjeeDept of Computer Science &Engineering, JadavpurUniversityKolkata – 700 032, India-2011

[6]   Improving Routing Protocols of WSN in WHSN- Ruochen Tan, Yang Xu, Zheng ChenUniversity of Electronic Science and Technology of ChinaChengdu 611731, P.R.China, Min Zha, Tina TsouHuawei Technologies Co., Ltd.Shenzhen 518129,P.R.China-2010

[7]   Energy Saving Routing Algorithm Based on SPIN Protocol in WSN-Luwei Jing, and FengLiuCollege of Science, Huazhong Agricultural University, Wuhan, 430070, Chin, YulingLiCollege of Information Engineering, Chutian University of Huazhong Agricultural University,Wuhan, 430205, China-2011

[8]   SPIN Implementation in TinyOS Environment usingnesC- Zeenat Rehena1, Krishanu Kumar2, Sarbani Roy2, Nandini Mukherjee21School of Mobile Computing and Communication, Jadavpur University2 Department of Computer Science & Engineering, JadavpurUniversityKolkata – 700 032, India

[9]   Combining SPIN with ns-2 for protocol Optimization-Pedro Merino1 and Alberto Salmeron1 University of Malaga, Campus de Teatinos, 29071, Malaga, Spain fpedro, salmerong@lcc.uma.es

[10]   Negotiation based protocol for Disseminating Information in
Wireless Sensor Networks- Joanna Kulik, Wendi RabinerHeinzelman, and hariBalakrishnanMassachusetta Institute of Technology, Cambridge, MA 02139

[11]   Performance Comparison of SPIN basedPush-Pull Protocols,RavishKhosla, XuanZhong, GunjanKhanna, SaurabhBagchi, and Edward J. CoyleSchool of Electrical and Computer EngineeringPurdue University, West Lafayette, Indiana 47907

International Journal of Modern Engineering Research (IJMER)

Contents :

A New 5 Level Inverter for Grid Connected Application

Nithin P N[1], Stany E George[2]

[1] (PG Scholar, Electrical and Electronics, Federal Institute of Science and Technology, Mahatma Gandhi University, India)
[2] (Assistant Professor, Department of Electrical and Electronics, Federal Institute of Science and Technology, Mahatma Gandhi University, India)

Abstract: *A five-level inverter is developed and applied for injecting the real power in to the grid to reduce the switching power loss, harmonic distortion, and electromagnetic interference caused by the switching operation of power electronic devices. Two dc capacitors, a dual-buck converter, a full-bridge inverter, and a filter configure the five-level inverter. The input of the dual-buck converter is two dc capacitor voltage sources. The dual-buck converter converts two dc capacitor voltage sources to a dc output voltage with three levels and balances these two dc capacitor voltages. The output voltage of the dual-buck converter supplies to the full-bridge inverter. The power electronic switches of the full-bridge inverter are switched in low frequency synchronous with the utility voltage to convert the output voltage of the dual-buck converter to a five-level ac voltage. The output current of the five-level inverter is controlled to generate a sinusoidal current in phase with the utility voltage to inject into the grid.*

Keywords: *Carrier, Filter, Five-level, THD, Voltage balance.*

I. Introduction

Energy scenario is changing. The intensified research on renewable energy has lead to the emergence of a new era where renewable energy resources like solar, wind etc play the lead role. The use of hazardous fossil fuels has become obsolete. The birth of semiconductor technology and its widespread acceptance and applications fuelled the design of various power converter topologies. It has become the key responsibility of these converters to integrate the renewable energy sources in to the grid with required efficiency.

However, there exist a tough competition between classic power converter topology using high voltage semiconductor and new converter topologies like multilevel inverters using medium voltage semiconductors. Nowadays multilevel converters prove to be a good solution to power application due to the fact that they can achieve high power using medium power semiconductor devices.

Multilevel converters present great advantage when compared with two level converters. These advantages are fundamentally focused on improvement in output signal quality. As the number of level increase, the THD in the inverter output remain less when compared to two level inverters. The electromagnetic interference is also minimized.

While bestowing all these advantages, the multilevel converters bear some limitations too. The control of the converter is complex when compared to conventional topologies. Balancing of dc capacitor voltage, high switching losses still remain a serious issue.

The most common multilevel converter topologies are the neutral point clamped (NPC), flying capacitor (FC), cascaded H-bridge(CHB). These converters present widespread applications in ac motor drives such as in conveyors, pumps, fans etc. Cascaded H-bridge has been successfully commercialized for very high power and power quality demanding applications up to range of 31MVA due to its series expansion capabilities.

This paper reveals the working and simulation of a new 5 level inverter topology which proves to overcome some of the limitations of conventional multilevel topologies.

II. Proposed Topology

This five-level inverter is configured by two dc capacitors, a dual buck converter, a full-bridge inverter, and a filter. The dual-buck converter is configured by two buck converters. The two dc capacitors perform as energy buffers between the dc–dc converter and the five-level inverter. The output of the dual-buck

converter is connected to the full-bridge inverter to convert the dc voltage to ac voltage. An inductor is placed at the output of the full bridge inverter to form as a filter inductor for filtering out the high-frequency switching harmonic generated by the dual-buck converter.

The block schematic is shown in Fig 2.1 and circuit is shown in Fig 2.2
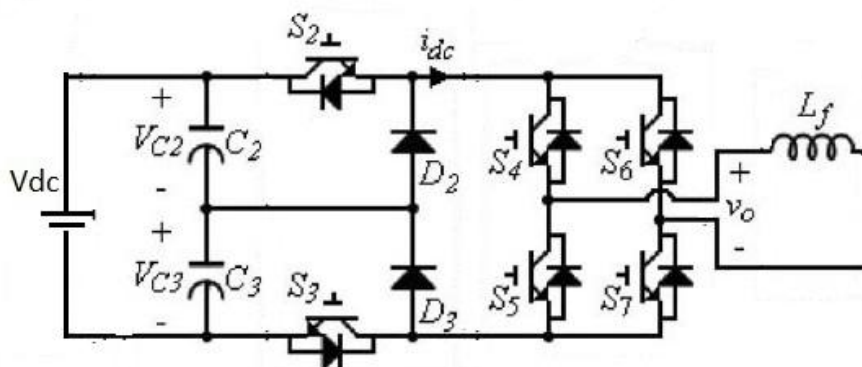
Figure 2.2.Circuit of proposed topology

2.1 Operating Principle

The operation of this five-level inverter can be divided into eight modes. Modes 1–4 are for the positive half-cycle, and modes 5–8 are for the negative half-cycle. The power electronic switches of the full-bridge inverter are switched in low frequency and synchronously with the utility voltage to convert the dc power into ac power for commutating. The power electronic switches S4 and S7 are in the ON state, and the power electronic switches $S5$ and $S6$ are in the OFF state during the positive half-cycle. On the contrary, the power electronic switches S4 and S7 are in the OFF state, and the power electronic switches $S5$ and $S6$ are in the ON state during the negative half-cycle. Since the dc capacitor voltages VC2 and VC3 are balanced by controlling the five-level inverter, the dc capacitor voltages VC2 and VC3 can be represented as shown in equation (1):

VC2 = VC3 =1/2Vdc   (1)

The operation modes of this five-level inverter are stated as follows.

Mode 1: Fig 2.3 shows the operation circuit of mode 1.

The power electronic switch of the dual-buck converter S2 is turned ON and S3 is turned OFF. DC capacitor C2 is discharged through S2, S4 , the filter inductor, the utility, S7 , and D3 to form a loop. Both output voltages of the dual-buck converter and five-level inverter are Vdc/2.
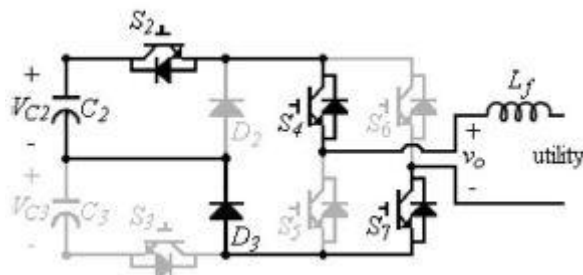
Figure 2.3 Mode 1 operation

Mode 2: Fig 2.4 shows the operation circuit of mode 2.

The power electronic switch of the dual-buck converter $S2$ is turned OFF and $S3$ is turned ON. DC capacitor $C3$ is discharged through D2, $S4$, the filter inductor, the utility, $S7$, and $S3$ to form a loop. Both output voltages of the dual-buck converter and five level inverter are Vdc/2.
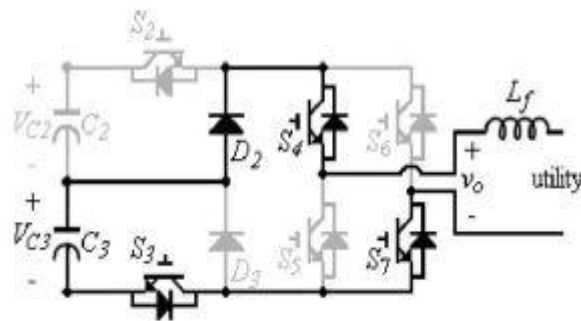
Figure 2.4 Mode 2 operation

Mode 3: Fig 2.5 shows the operation circuit of mode 3.
Both power electronic switches $S2$ and $S3$ of the dual-buck converter are turned OFF. The current of the filter inductor flows through the utility, S7, D3, D2, and S4. Both output voltages of the dual buck converter and five-level inverter are 0.
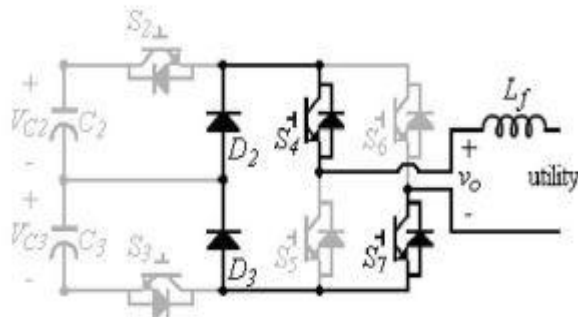
Figure 2.5 Mode 3 operation

Mode 4: Fig 2.6 shows the operation circuit of mode 4. Both power electronic switches S2 and S3 of the dual-buck converter are turned ON. DC capacitors C2 and C3 are discharged together through $S2, S4$, the filter inductor, the utility, S7, and S3 to form a loop. Both output voltages of the dual-buck converter and five-level inverter are Vdc.
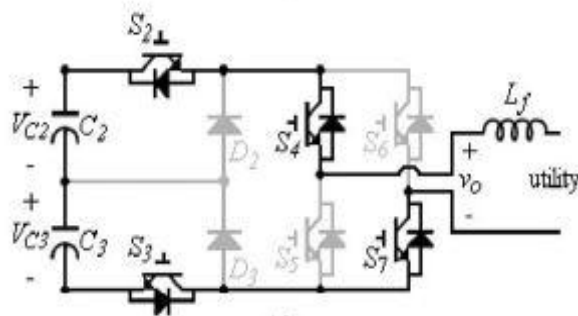
Figure 2.6 Mode 4 operation

Modes 5–8 are the operation modes for the negative half cycle shown in Fig 2.7 to Fig 2.10. The operations of the dual-buck converter under modes 5–8 are similar to that under modes 1–4, and the dual-buck converter can also generate three voltage levels Vdc/2, Vdc/2, 0,and Vdc, respectively. However, the operation of the full-bridge inverter is the opposite. The power electronic switches $S4$ and $S7$ are in the OFF state, and the power electronic switches $S5$ and $S6$ are in the ON state during the negative half-cycle. Therefore, the output voltage of the five-level inverter for modes 5–8 will be −Vdc/2, −Vdc/2, 0, and −Vdc, respectively. Considering operation modes 1–8, the full-bridge inverter converts the dc output voltage of the dual-buck converter with three levels to an ac output voltage with five levels which are Vdc, Vdc/2, 0, −Vdc/2, and −Vdc.
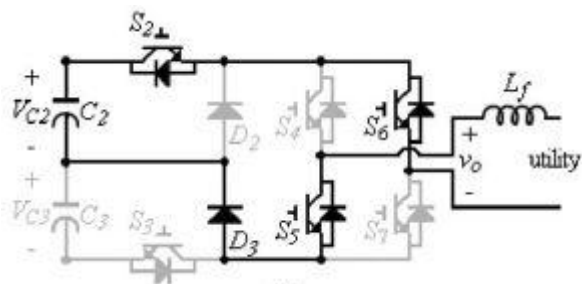
Figure 2.7 Mode 5 operation
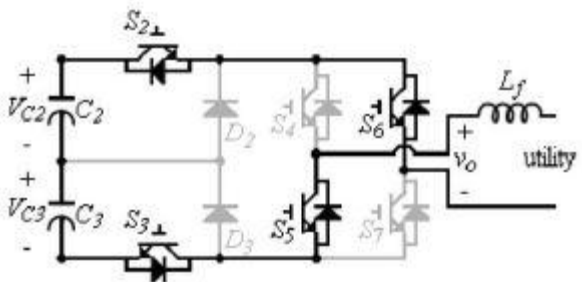
Figure 2.8 Mode 6 operation
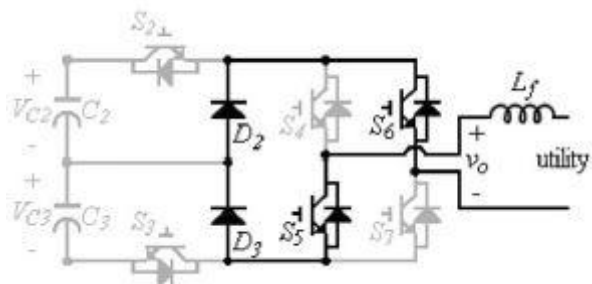
Figure 2.9 Mode 7 operation
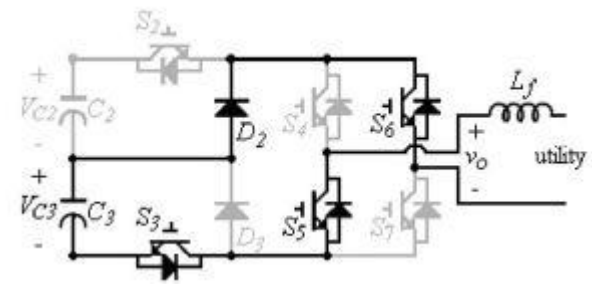
Figure 2.10 Mode 8 operation

The operation of power electronic switches $S2$ and $S3$ should guarantee the output voltage of the dual-buck converter is higher than the absolute of the utility voltage. The waveforms of output voltage of five-level inverter and utility voltage are shown in Fig 2.11.
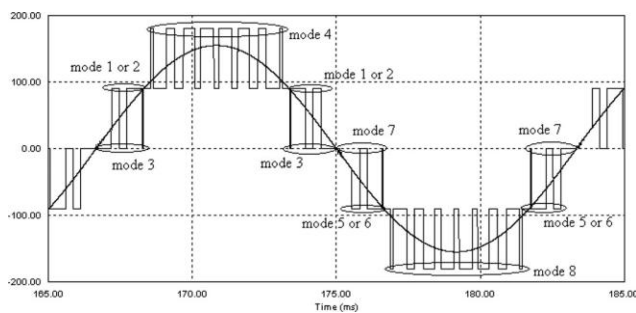
Figure 2.11 Overall operation of 5 level inverter

Due to the operation of full-bridge inverter, the voltage and current in the dc side of full-bridge inverter are their absolute values of the utility voltage and the output current of the five level inverter. When the absolute of the utility voltage is smaller than Vdc/2, the output voltage of the dual-buck converter should change between Vdc/2 and 0. Accordingly, the power electronics of five-level inverter is switched between modes 1 or 2, and mode 3 during the positive half-cycle. On the contrary, the power electronics of five-level inverter is switched between modes 5 or 6, and mode 7 during the negative half-cycle. One of the power electronic switches S2 and S3 is in the OFF state and the other is switched in high frequency during one PWM period.

2.2 Voltage Balance of Five-Level Inverter

Balancing the voltages of dc capacitors is very important in controlling the multilevel inverter. The voltage balance of dc capacitor voltages VC2 and VC3 can be controlled by the power electronic switches S2 and S3 easily. When the absolute of the utility voltage is smaller than Vdc/2, one power electronic switch either *S*2 or *S*3 is switched in high frequency and the other is still in the OFF state. Which power electronic switch is switched in high frequency depends on the dc capacitor voltages VC2 and VC3. If dc capacitor voltage VC2 is higher than dc capacitor voltage VC3, power electronic switch *S*2 is switched in high frequency. In this situation C2 will be discharged.

Thus, the dc capacitor voltages VC2 decreases. On the contrary, power electronic switch *S*3 is switched in high frequency when voltage VC3 is higher than voltage VC2. Thus, the dc capacitor voltages VC3 decreases. In this way, the voltage balance of C2 and C3 can be achieved. When the absolute of the utility voltage is higher than Vdc/2, one power electronic switch either S2 or S3 is switched in high frequency and the other is still in the ON state.

Which power electronic switch is switched in high frequency depends on the dc capacitor voltages VC2 and VC3. If dc capacitor voltage VC2 is higher than dc capacitor voltage VC3, the power electronic switch S3 is switched in high frequency.

When the power electronic switch S3 is turned ON, both C2 and C3 are discharged. However, only C2 supplies the power when the power electronic switch S3 is turned OFF. Thus, C2 will discharge more power than that of C3. On the contrary, the power electronic switch *S*2 is switched in high frequency when dc capacitor voltage VC3 is higher than dc capacitor voltage VC2. When the power electronic switch S2 is turned ON, both C2 and C3 are discharged. However, only C3 supplies the power when the power electronic switch S2 is turned OFF. Thus, C3 will discharge more power than that of C2. In this way, the voltage balance of C2 and C3 can be achieved. The voltages of capacitors C2 and C3 can be easily balanced compared with the conventional multilevel inverter.

2.3 Comparison with Conventional 5 Level Topologies

Table 1: Comparison with Conventional 5 Level Topologies

	Diode clamped	Flying capacitor	Cascaded H-bridge	Developed topology
Power electronics	8	8	8	6
Capacitors	2	4	2	2
Voltage balance of capacitors	hard	hard	hard	easy
High frequency switches	8	8	8	2

III. Inverter Control

The five-level inverter performs the functions of converting the dc power into high-quality ac power and injecting it into the utility, balancing two dc capacitor voltages VC2 and VC3.
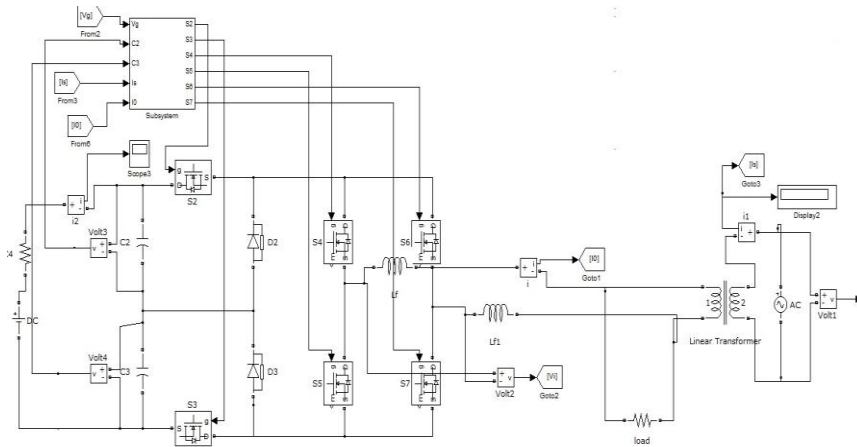
Figure 3.1 Main circuit configuration

Fig 3.2 shows the control block diagram of five-level inverter. In the operation of the five-level inverter, the dc bus voltage must be regulated to be larger than the peak voltage of the utility, and the dc capacitor voltages of C2 and C3 must be controlled to be equal. Besides, the five-level inverter must generate a sinusoidal current in phase with the utility voltage to be injected into the utility.
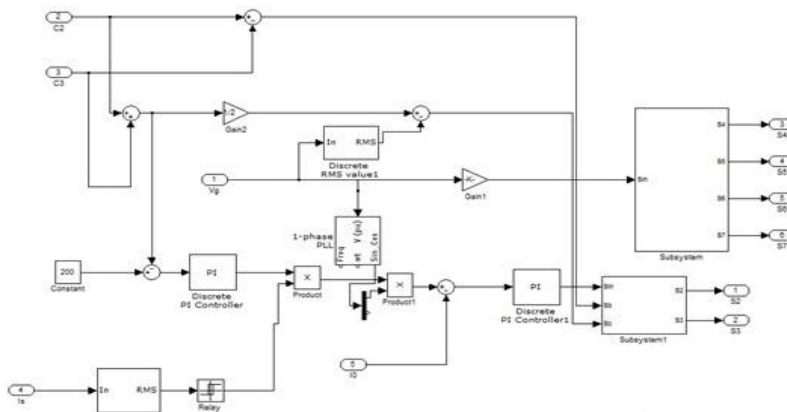
Figure 3.2 Control of 5 level inverter

A multilevel carrier based PWM technique is utilized to generate the switching signal for switches S2 and S3. For an m-level inverter, (m-1) carriers with the same frequency fc and same peak-to-peak amplitude Ac are disposed such that the bands they occupy are contiguous. The reference, or modulation waveform has peak-to-peak amplitude Am and frequency fm, and it is centered in the middle of the carrier set. The reference is continuously compared with each of the carrier signals the switching pulses are generated according to the switching logic. The carrier has a frequency of 20kHz.
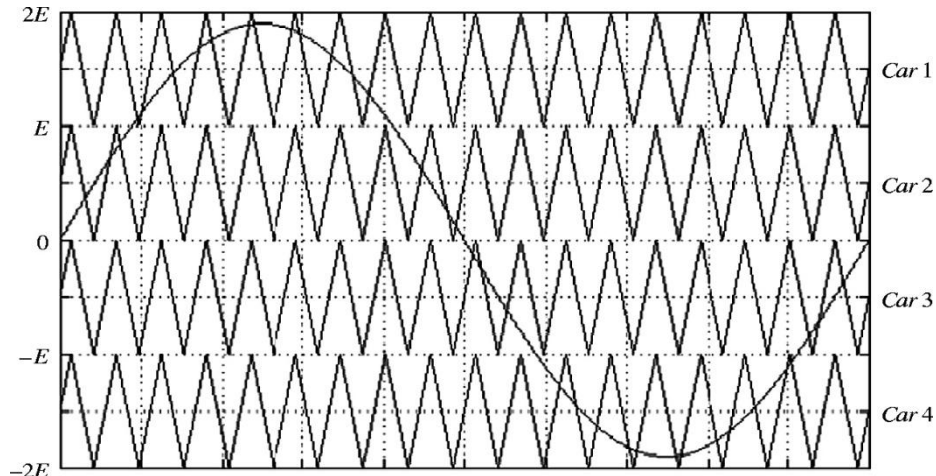
Figure 3.3 Carrier and reference signal comparison

The detected utility voltage is also sent to a comparator to obtain the switching signal for the full bridge inverter switches S4 to S7. These switches are switched in utility frequency. For positive half cycle switches S4 and S7 are turned ON. For negative half cycle switches S5 and S6 are turned ON. As mentioned earlier, only two power electronic switches S2 or S3 in the five-level inverter should be switched in high frequency, and only one of them is switched in high frequency at any time, and the voltage level of every switching is Vdc/2. Therefore, the five-level inverter can reduce the switching loss effectively. Overall switching states of inverter is shown in Table 2.

Table 2.Overall switching states of inverter

S2	S3	S4	S5	S6	S7	Vout
1	1	1	0	0	1	+Vdc
1	0	1	0	0	1	+Vdc/2
0	1	1	0	0	1	+Vdc/2
0	0	1	0	0	1	0
0	0	0	1	1	0	0
1	0	0	1	1	0	-Vdc/2
0	1	0	1	1	0	-Vdc/2
1	1	0	1	1	0	-Vdc

IV. Simulation Results

The proposed model was simulated in MATLAB/Simulink. The grid voltage was chosen to be 110V and the DC voltage was chosen as 165V since it must be greater than peak of grid voltage. Waveforms of grid voltage, inverter output current, inverter output voltage and capacitor voltages were obtained. Fig 4.1 shows the grid voltage waveform. Fig 4.2 shows inverter output current which is obtained with 20 % current ripple by using a filter inductor of 5mH. The THD of inverter current was found to be 3.0%. Fig.4.3 shows waveform of inverter output voltage. THD was found to be 8.83%. Fig.4.4 shows the combined waveform of grid voltage and inverter output voltage. Fig 4.5 shows the combined waveform of inverter current and grid voltage. The voltage of dc link capacitors shown in Fig 4.6 were found to be balanced and each of the two capacitors stores 82.5V with a voltage ripple of 0.13%. The power factor was found to be 0.9903.

Table 3 : Parameters used in simulation

DC bus capacitor (C_2 and C_3)	2,200 μ F
Filter inductor (L_f)	5mH
DC bus setting voltage	170V
Switching frequency(PWM)	20kHz
Utility voltage	110V
Utility frequency	60Hz
Load resistor	100Ω
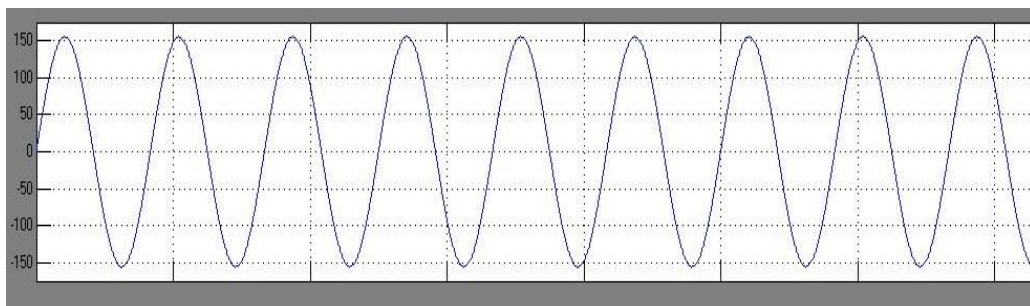
Figure 4.1. Grid voltage waveform
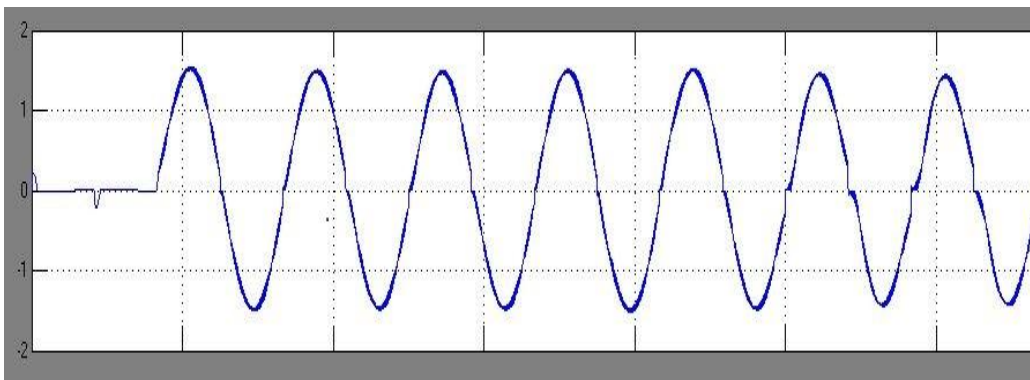
Figure 4.2. Inverter output current waveform
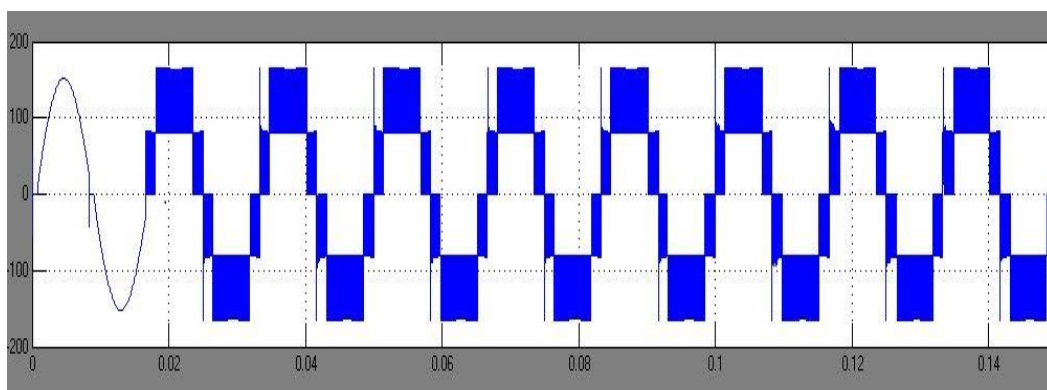
Figure 4.3. Inverter output voltage waveform
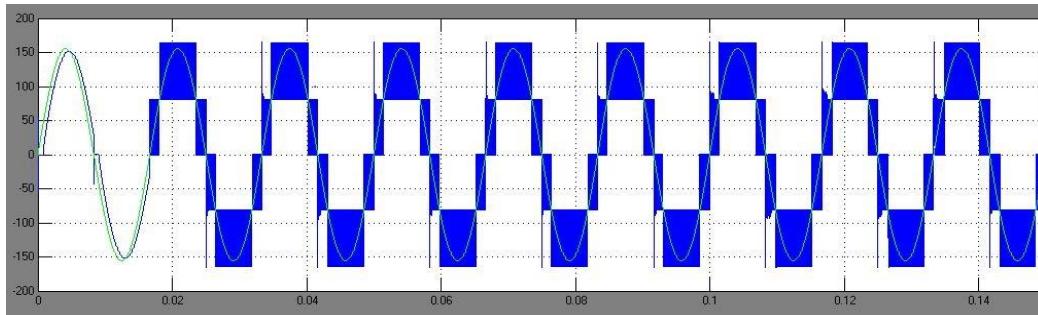
Figure 4.4. Inverter output voltage and grid voltage waveform
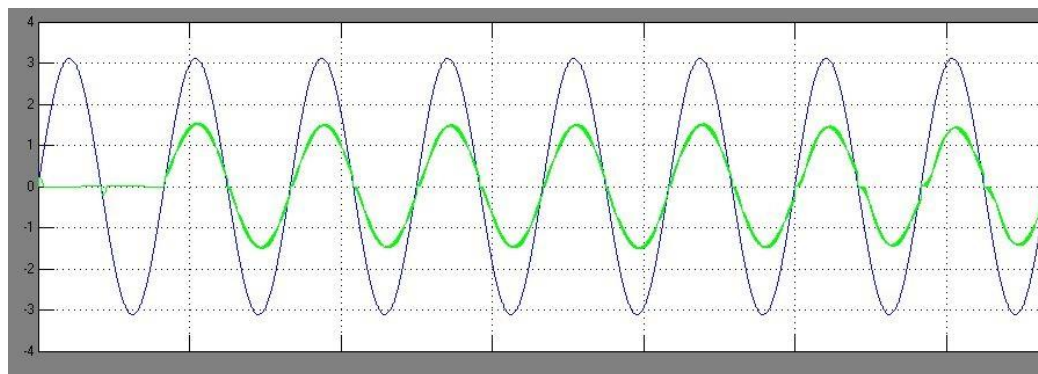
Figure 4.5. Inverter output current and grid voltage waveform
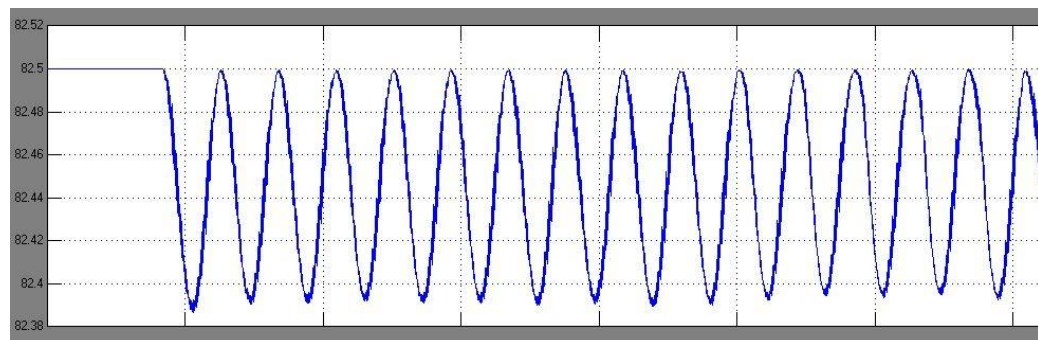
Figure 4.6. DC link capacitor voltage waveform

V. Conclusion

Proposed 5 level inverter was simulated and necessary waveforms were obtained. Waveforms of grid voltage, inverter current, voltage, capacitor voltage etc were obtained. The capacitor voltage was found to be almost balanced. The THD of inverter current and voltage were verified. THD was found to be less than 5%. The power factor of the system was found to be above 0.9. The switching losses will be less when compared to conventional topologies since less number of power electronic switches are used .Thus as a whole the proposed 5 level inverter is found to have good performance under grid connected application.

REFERENCE

[1]   Jia-Min Shen, Hurng-Liahng Jou, Jinn-Chang Wu and Kuen-Der Wu, "Five-Level Inverter for Renewable Power Generation System," IEEE Trans. Energy Conversion, Vol. 28, No. 2, June 2013

[2]   David Velasco de la Fuente, César L. Trujillo Rodríguez, Gabriel Garcerá, Emilio Figueres, "Photovoltaic Power System With Battery Backup With Grid-Connection and Islanded Operation Capabilities," IEEE transactions on industrial electronics, vol. 60, no. 4, April 2013

[3]   Javier Chavarría, Domingo Biel, Francesc Guinjoan, Carlos Meza, Juan J. Negroni," Energy-Balance Control of PV Cascaded Multilevel Grid-Connected Inverters Under Level-Shifted and Phase-Shifted PWMs," IEEE Transactions on industrial electronics, vol. 60, no. 1, January 2013

[4]   Miss. Sangita R Nandurkar , Mrs. Mini Rajeev, "Design and Simulation of three phase Inverter for grid connected Photovoltic systems," Proceedings of Third Biennial National Conference, NCNTE- 2012, Feb 24-25

[5]   Mukhtiar Singh, Vinod Khadkikar, Ambrish Chandra, Ambrish Chandra, "Grid Interconnection of Renewable Energy Sources at the Distribution Level With Power-Quality Improvement Features," IEEE transactions on power delivery, vol. 26, no. 1, January 2011

[6]   J. Rodriguez, S. Bernet, B. Wu, J. Pontt, and S. Kouro, "Multilevel voltage-source-converter topologies for industrial medium-voltage drives," IEEE Trans. Ind. Electron., vol. 54, no. 6, pp. 2930–2945, Dec. 2007

[7]   Mahrous Ahmed, Maha G. Elsheikh, Mahmoud A. Sayed, and Mohamed Orabi, Single-Phase Five-Level Inverter with Less Number of Power Elements for Grid   Connection

[8]   Brendan Peter McGrath, and Donald Grahame Holmes, "Multicarrier PWM strategies for multilevel inverters", IEEE Transactions on Industrial Electronics, Vol. 49, Issue 4, pp. 858- 867, August 2002.

[9]   J. Rodriguez, J.-S. Lai, and F.Z. Peng, "Multilevel inverters: A survey of topologies, controls, and applications," IEEE Trans. Ind. Electron., vol. 49, no. 4, pp. 724–738, Aug. 2002.

[10]   Leon M. Tolbert, Fang Zheng Peng, Thomas G. Habetler, "Multilevel PWM Methods at Low Modulation Indices," IEEE Trans. Power electronics, vol. 15, no. 4, JULY 2000

[11]   Lai, J. S., and Peng, F. Z., "Multilevel converters–a new breed of power converters," IEEE Transactions on Industrial Applications, vol. 32, Issue 3, pp. 509-517, May/June 1996.

[12]   Villanueva, E.; Correa, P.; Rodriguez, J.; Pacas, M., "Control of a Single-Phase Cascaded H-Bridge Multilevel Inverter for Grid- Connected Photovoltaic Systems", IEEE Transactions on Industrial Electronics, Vol. 56 , Issue 11, 2009, pp. 4399-4406.

An Automated Method for Segmentation of the Hand In Sign Language

B. Luna-Benoso[1], R. Flores-Carapia[2], O. Camacho-Nieto [3], A. L. Barrales-López[4], H. Flores-Gutiérrez[5]

[1](*Escuela Superior de Cómputo, Instituto Politécnico Nacional, México*)
[2, 3, 4, 5] (*Centro de Innovación y DesarrolloTecnológico en Cómputo, Instituto Politécnico Nacional, México*)

Abstract: *This paper presents an automated method for hand segmentation in images that make use of signs language. For this, used an images bank that was captured by a webcam to which were applied spatial domain methods for hand segmentation.*
Keywords: *Digital images processing, spatial domain methods, images segmentation.*

I. Introducción

Around of 70 million deaf people in the world use the signs language as their maternal language or main language [1]. The difficulties faced the people deaf-mute in the daily life are quite due to the difficult understanding or total ignorance of signs language meaning that use. The signs language is a communication mean for the people with deficiency hearing, where the words and sentences are represented for hand gestures, and have grammatical structures perfectly defined. Due to the difficult communication that be between a deaf people that use the signs language for take charge of the translation process with the finality of study to deeply the deaf culture with psychotherapeutic purpose[2]. A system capable of carry out the automatic recognition of sign language without the need of an individual translator can eventually provide an excellent tool for deaf people to communicate with people that disown the language, and this way we can achieve a better way to live [3]. This paper proposes a methodology for carry out the automatic segmentation of hand in images that show the Mexican sign language (figure 1). For this, images were captured by a people webcam doing some Mexican sign language, later with digital treatment techniques of images basing in the spatial domain was obtained the sign segmentation doing by the individual.
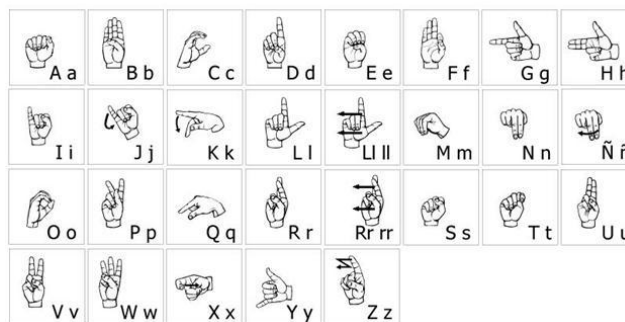
Figure 1: Mexican sign language

II. Basic concepts

In the section three will be shown the proposed method, however for that, make use of the mathematical morphology, and for that reason, in the following lines we show the concerning concepts for the mathematical morphology.

The mathematical morphology is a framework based exclusively in the set theory. The original theory developed by Georges Matheron and Jean Serra, has been used with huge success in the digital processing of binary images. There are two fundamental operations in the mathematical morphology: dilatation and the erosion. The dilatation is a term referred to increase, expand, rise, among other actions, of any object. On the other hand, the erosion is referred to the contraction, reduction, decrease, among other actions, of any object. In the following lines are the accuracy definitions of the fundamental operations of the mathematical morphology.

2.1 Dilation

Started the short dilation operation study. For this, consider in all that follow, discrete sets 2-dimensional, that is, subsets of $\mathbb{Z}^2$.

Definition 2.1.1:BeA $\subseteq \mathbb{Z}^2$. The set A is denoted byA $^-$, is defined by:

$$A^- = \{-x|x \in A\} (1)$$

Definition 2.1.2:BeA $\subseteq \mathbb{Z}^2$ andx $\in \mathbb{Z}^2$. The translation of A by x denoted by $(A)_x$ is defined as:

$$(A)_x = \{a + x|a \in A\} (2)$$

The following definition shows the formal concept of what is dilation operation.

Definition 2.1.3: BeA, B $\subseteq \mathbb{Z}^2$, the dilation of A by B, denoted byA $\oplus$ B, is the sum of Minkowskiof A and B; this is:

$$A \oplus B = \{a + b|a \in A \text{ and } b \in B\} (3)$$

The set B of the previous definition will be called structuring element.
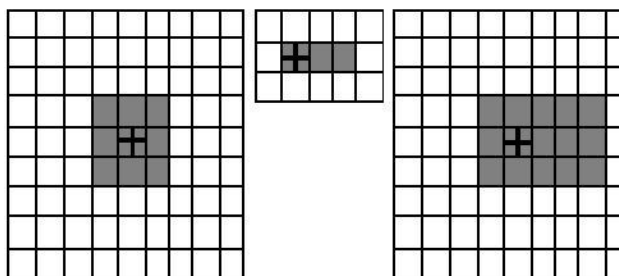
Figure 2: Representing the set A, the structuring element B = $\{(0,0),(1,0),(2,0)\}$ and the dilationA $\oplus$ B

Theorem 2.1.1:Be A, B $\subseteq \mathbb{Z}^2$. It holds that:

$$A \oplus B = \{x|(B^-)_x \cap A \neq \emptyset\} (4)$$

Demonstration:

x $\in$ A $\oplus$ BIfx $=$ a + b for somea $\in$ A and b $\in$ B if x $-$ b = a for some a $\in$ A and b $\in$ B if x $-$ b = a for some a $\in$ A and $-$b $\in$ B$^-$ if a $-$ x = $-$b for some a $\in$ A and $-$b $\in$ B$^-$ if a $\in$ $(B^-)_x$ and a $\in$ A if a $\in$ $(B^-)_x \cap$ A for some a if $(B^-_x \cap A) \neq \emptyset$.■

The previous theorem allows us to define an alternative form, which is the dilation of a set A by the structuring element B.

2.2 Erosion

Then be show the formal concept of what is erosion.

Definition 2.2.1: Be A, B $\subseteq \mathbb{Z}^2$. The erosion of A by B, denoted by A $\ominus$ B, the subtraction of Minkowski of Aby B; this is:

$$A \ominus B = \{x \in \mathbb{Z}^2|x + b \in A \text{ for each } b \in B\} (5)$$
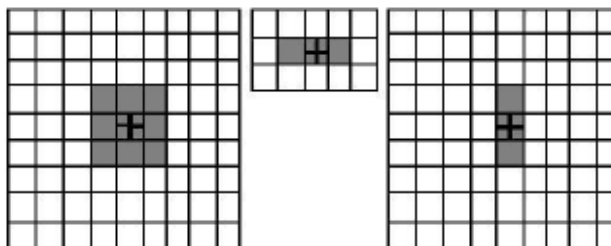
Figure 3: Representación the set A, the structuring element B = $\{(-1,0),(0,0),(1,0)\}$ and the erosion A $\ominus$ B

Theorem 2.2.1: be $A, B \subseteq \mathbb{Z}^2$, it holds that:

$$A \ominus B = \{x | (B)_x \subseteq A\} \quad (6)$$

Demonstration:
$x \in A \ominus B$ If $x + b \in A$ for each $b \in B$ by the definition 2.2.1 if $(B)_x \subseteq A$ by the definition 2.1.2 ∎

The previous theorem allows us to define an alternative form, which is the erosion of a setA by the structuring element B.

III. Proposed method

Before to arrive on detail with proposed method, it's necessary give the definition about a digital image. A digital image is a Two-dimensional function $f(x, y)$, of the light intensity (Sheen/brightness) on a space point, so (x, y), the coordinates for that point [9]. Inasmuch as a digital image is a function $f(x, y)$ discretised on the space coordinates so in the sheen, sometimes could be representative like a two-dimensional matrix $F_{ij} = (f_{ij})_{mxn}$, where m and n are the size of the image and $f_{ij} = f(x_i, x_j)$.

The proposed method is dived in two parts: 1) image acquisition and 2) signal segmentation of the individual done.
1) *Image acquisition*: With webcam help, to get images of persons doing a signal of LSM set. Like in figure 4.

Figure 4: Imageacquisition.

2) *Signal segmentation*: For this part it could be considerate the next stages:

Step 1. The image need to be separate in three components red, green and blue (RGB) and it was considerate the red component because of the human skin is more sharp for this component (figure 5).
Step 2. It was considerate to grayscale from red component, this is, the value of the red component is copied to the green and blue component, thereby obtaining the image in grayscale.
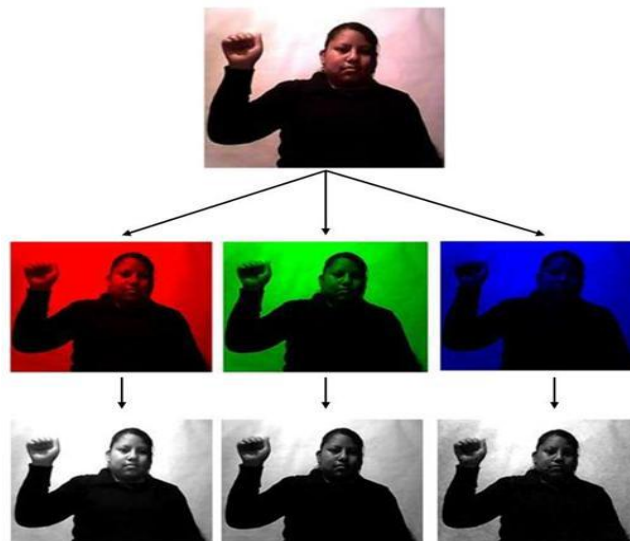
Figure 5: Decomposing an image into its three RGB components, and grayscale.

Step 3. The histogram was obtained of the image with gray levels in the range [0, 255], where the histogram is a discrete function H[k]represents the number of colors of each gray level (k = 0, …, 255) [9].

Step 4. Given an image f (x, y)and two variables u and v, the binarization by thresholding is used defined as follows:

$$bin_{ij} = \begin{cases} 0 & if\ u \leq f_{ij} \leq v \\ 255 & if\ f_{ij} < u\ or\ f_{ij} > v \end{cases}$$

Shown in Figure 6, that the histogram shows two maximum peaks at 0 and 255, to eliminate these peaks, were considered as thresholds u = 20 and v = 185.
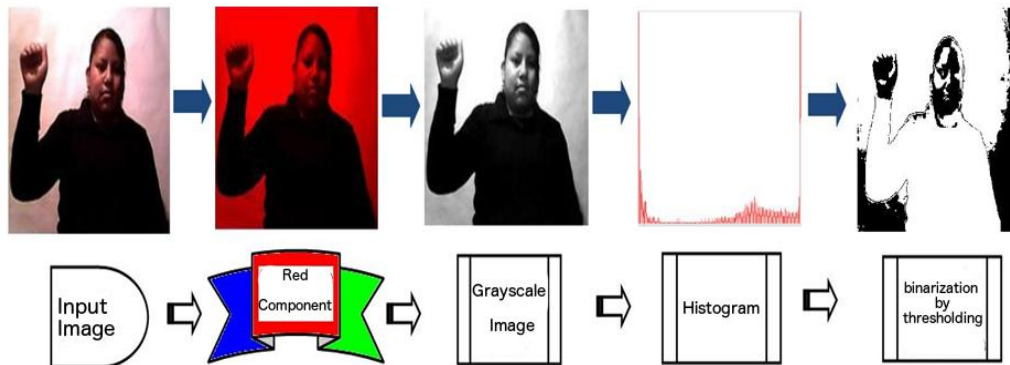
Figure 6: Show the first 4 steps applied to a color image.

Once obtained, the binarized image, we proceeded to locate the corresponding part of the hand, for it is considered that:

Step 5. Consider a mask size x within a mask size y as shown in Figure 7. Variablesu and v be two to locate the area corresponding to the hand image, the following function is implemented for each point (i, j) on the image, it is M_y^{ij} mask size and centered at (i, j), the function $T_{ij}$is defined at each point (i, j)as:

$$T_{ij}: M_y^{ij} \rightarrow [0, 255]$$

Where

$$T_{ij}(r, s) = \begin{cases} f_{rs} & if\ A_x \geq u\ and\ A_y - A_x \leq v \\ 255 & if\ A_x < u\ or\ A_y - A_x > v \end{cases}$$

WithA_x and A_y the areas enclosed by the masks of size x and y respectively.
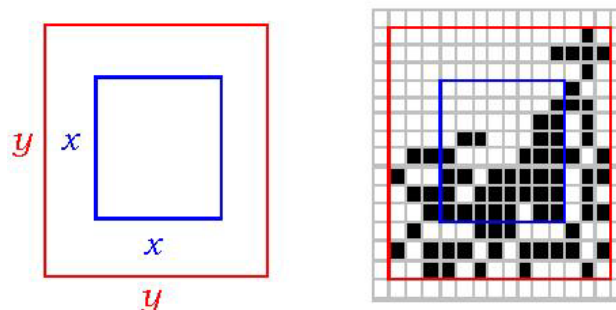
Figure 7: Masks of size x and y.

Step 6.Once located the section of image binary corresponding of the hand, morphological erosion operator was applied.

Step 7. Morphological dilation operator was applied.
The figure 8 shows the process of applying erosion to the image hand segmented with a Moore neighborhood, and subsequently applying dilation 6 times with the same vicinity. Finally, shows the image of the hand segmented to color.
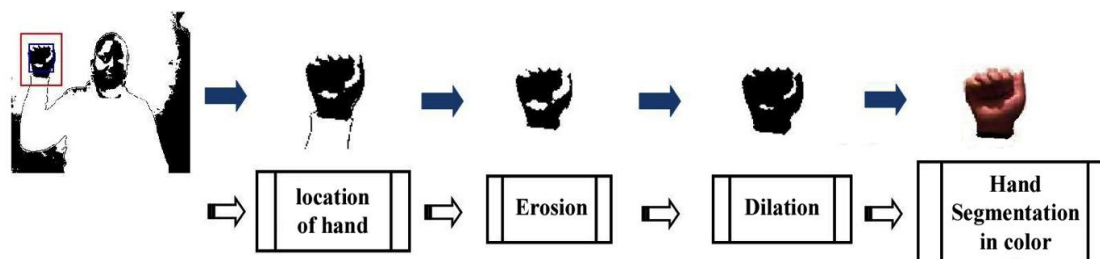
Figure 8: Process segmentation of the hand to locate the sign on.

IV. Conclusión

This paper is presented an automated method for segmentation of abnormalities in digital mammography images. The method was applied an images bank that was captured by a webcam The proposed segmentation method can be a useful to the development of computational systems that address the problem of patterns classification focused on the problem of sign language.

Acknowledgements

REFERENCES

[1]   World Federation of the Deaf. www.wfdeaf.org.
[2]   Porter A, (1999), *Sign-language interpretation in psychotherapy with deaf patients*.American Journal of Psychotherapy;Spring1999, Vol. 53 Issue 2, p163.
[3]   M. Krishnaveni, V. Radha. Classifier fusin base don Bayes aggregation method for Indian sign language datasets. Procedia Engineering, vol 30, 2012, pp 1110-1118.
[4]   Matheron, G. (1975). *Random Sets and Integral Geometry*. Wiley, New York.
[5]   Serra, J. (1982). *Image Analysis and Mathematical Morphology*. Vol. I, Academic Press, London.
[6]   Serra, J. (1988). *Image Analysis and Mathematical Morphology*. Vol. 11: Theoretical Advances, Academic Press, London.
[7]   Dougherty, E. R., Lotufo, R. A. (2003). *Hands-om morphological image processing*. Vol TT59, spie press.
[8]   Aptoula, E., Lefèvre, S. (2007). *A comparative study on multivariate mathematical morphology*. Pattern Recognition.
[9]   Gonzalez, R., Woods, J., *Digital image processing*, 3rd ed., Prentice Hall, New Jersey, 2008.
[10]   J.H. Sossa-Azuela, C. Yáñez-Márquez, J. L. Díaz de León S. *Computing geometric moments using morphological erosion*. Pattern Recognition, Volume 34, Issue 2, February 2001, Pages 271-276.

Steady State Operation And Enhancement Of Transient Stability In Hydel Power Plant Using Statcom

Mohd. Ilyas[1], Hashim Farooq Makhdoomi[2]

[1, 2](Assistance Professor (EEE department),Al-Falah University, Faridabad, India)

Abstract: *In this paper, the effect of STATCOM for improving the stability and steady state operation of the hydel power system is investigated. The STATCOM is used to control power flow of power system by injecting appropriate reactive power during dynamic state. Simulation results show that STATCOM not only considerably improves transient stability but also compensates the reactive power in steady state. Therefore STATCOM can increase reliability and capability of AC transmission system. To illustrate the performance of the FACTS controller (STATCOM), a three machine nine bus, Multi-Machine Power System has been considered.*
Keywords: *FACTS(statcom), hydel power plant ,steady state operation, Transient Stability ,simulation.*

I. Introduction

Power is extremely fundamental infrastructure on the whole extension of many nations in the world. The requirement for electrical energy is rising speedily in the world. It is being realized that renewable energy sources can supplement the available energy and provide a reasonable option in broad range of applications and plays a significant role in resolving the doppelganger problem of energy supply in the decentralized applications. Micro hydro power plant is considered to be the promising source surrounded by renewable energy. Renewable energy is a major constraint in the economic development of the rural areas which includes solar energy, biomass, wind, tidal, geothermal energy and flowing water stream and these sources are effortlessly accessible in remote areas which are island, ships, villages, military, hilly areas etc. Commercial sources that are produced from the exhaustion of fossil fuels like kerosene, diesel, petrol, coal and petroleum etc include their own disadvantages such as air pollution and global warming.Micro hydro is a type of hydroelectric power which produces up to100 kW of electricity using the natural flow of water. Prime mover of the hydraulic turbine rives the induction generator, and its reactive power consumption is rewarded by the capacitor banks and this whole system is known as self-excited induction generator (SEIG). Induction generators is used now a days because of advantages over synchronous generators i.e. brushless construction with squirrel cage rotor, rugged, low cost, less maintenance,operational simplicity, reduced size, no dc supply is needed ,against faults self-protection, good dynamic reaction, and capability to produce power at varying speed.Induction generator offers poor voltage regulation, frequency regulation under varying speedand its value depends on the prime mover speed, capacitor bank size.

Now a days wind as a significant proportion of non pollutant energy generation is widely used .If a large wind farm, which electrically is far away from its connection point to power system, is not fed by adequate reactive power, it present major instability problem. Various methods to analyze and improve wind farm stability have been performed. The stability of wind driven self excited induction generator SEIG s is analyzed. A breaking resistor to absorb active power during fault to enhance the system stability is developed . Flexible AC transmission system FACTS devices such as Static Synchronous Compensator STATCOM to improve the stability in wind farm is studied .

As a consequence, it will become necessary to require wind farms to maintain continuous operation during grid disturbances and thereby support the network voltage and frequency. In addition, in the area of a deregulated electricity industry, the policy of open access to transmission systems, which helped create competitive electricity markets, led to a huge increase in energy transactions over the grid and possible congestion in transmission systems. The expansion of power transfer capability of transmission systems has been a major problem over the past two decades. Under these conditions, the modern power system has had to confront some major operating problems, such as voltage regulation, power flow control, transient stability, and damping of power oscillations, etc. FACTS devices can be a solution to these problems . They are able to provide rapid active and reactive power compensations to power systems, and therefore can be used to provide voltage support and power flow control, increase transient stability and improve power oscillation damping. Suitably located FACTS devices allow more efficient utilization of existing transmission networks.

The STATCOM is used to provide rapid and fast control of voltage during during steady state and transient stability. This issue is even more critical in the case of microgirds, since certain FACTS controllers, particularly STATCOMs, are being considered as a possible solution for some of the voltage and angle stability problems inherent to these power grids. Consequently, typical STATCOM models are validated here using system identification techniques to extract the relevant electromechanical mode information from time-domain signals . System identification techniques are used to readily and directly compare fairly distinct STATCOM models, thus avoiding matrix based eigenvalue studies of complex system models and/or modeling approximations.

In this paper, a STATCOM is added to the power network to provide dynamic voltage control for the wind farm, dynamic power flow control for the transmission lines, relieve transmission congestion and improve power oscillation damping. Simulation results show that the STATCOM devices significantly improve the performance of the wind farm and the power network during transient disturbances.

II. Hydro Power Plant And Electric Generator Model

Hydropower represents 21% of the world power production. The development of hydroelectricity will be increased because of the interest in utilizing the renewable sources. basic principle of hydropower plant is to convert the hydraulic energy to mechanical energy which inturn is converted to electrical energy. Hydropower plants relay on dam which acts as a water reservoir. Gravity causes the water to fall through the penstock. At the end of penstock there is propeller ,which rotates by moving water .rotation in propeller will drive generator to produce the alternating current AC. transformers provided in switchyard of powerhouse converts it into higher voltage currents. Transmission lines are provided which carry the electricity from these transformers to the consumers. outflow carries used water through the pipe downstream which may be used for irrigation purpose.
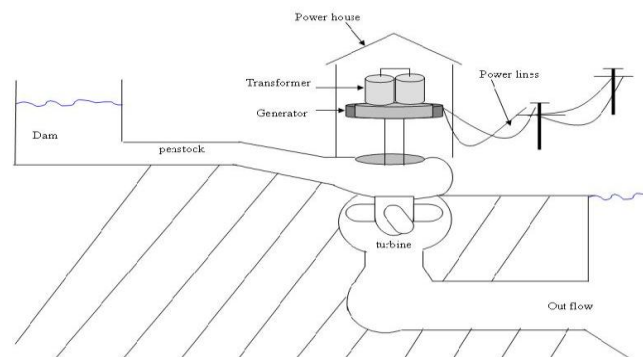
Statcom Model

Figure 1
shows the basic model of a STATCOM which is connected to the ac system bus through a coupling transformer. In a STATCOM, the maximum compensating current is independent of system voltage, so it operates at full capacity even at low voltages. A STATCOM's advantages include flexible voltage control for power quality improvement, fast response, and applicability for use with high fluctuating loads.
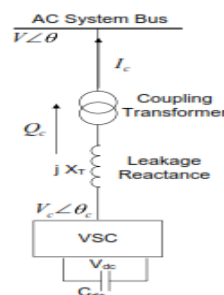
Figure 1. Basic model of a STATCOM

The output of the controller Qc is controllable which is proportional to the voltage magnitude difference (Vc −V) and is given by (1)

$$Q_c = V(V_c - V) / X \qquad\qquad (1)$$

The shunt inverter, transformer and connection filter are the major components of a STATCOM. The control system employed in this system maintains the magnitude of the bus voltage constant by controlling the magnitude and/or phase shift of the voltage reactive power exchange is achieved. By properly controlling i_q, reactive power exchange is achieved. The DC capacitor voltage is maintained at a constant value and this voltage error is used to determine the reference for the active power to be exchanged by the inverter. The STATCOM is a static var generator whose output can be varied so as to maintain or control certain specific parameters of the electric power system. The STATCOM is a power electronic component that can be applied to the dynamic control of the reactive power and the grid voltage. The reactive output power of the compensator is varied to control the voltage at given transmission network terminals, thus maintaining the desired power flows during possible system disturbances and contingencies. STATCOMs have the ability to address transient events at a faster rate and with better performance at lower voltages than a Static Voltage Compensator (SVC). The maximum compensation current in a STATCOM is independent of the system voltage. Overall, a STATCOM provides dynamic voltage control and power oscillation damping, and improves the system's transient stability. By controlling the phase angle, the flow of current between the converter and the ac system are controlled A STATCOM was chosen as a source for reactive power support because it has the ability to continuously vary its susceptance while reacting fast and providing voltage support at a local node. Figure 2 show the block diagram of the STATCOM controller. The values for all the variables in the figure are presented in the appendix
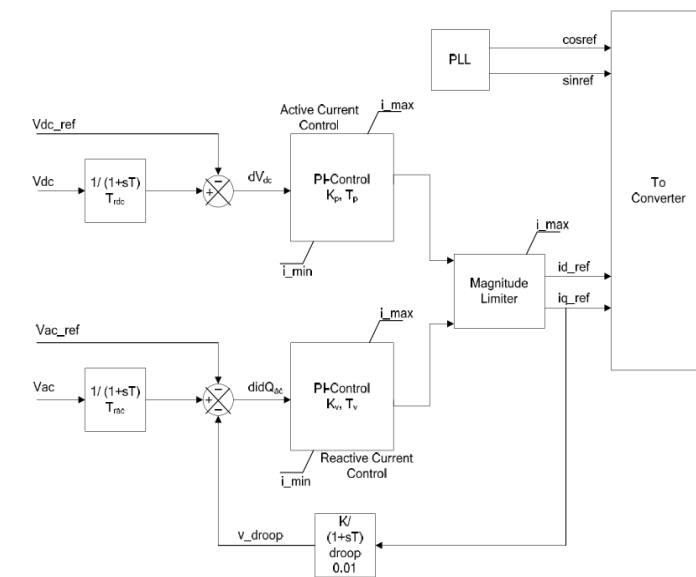
Figure 2 control scheme of the statcom

By controlling the phase and magnitude of the STATCOM output voltage, the power exchange between the ac system and the STATCOM can be controlled effectively. The outputs of the controller are i_d_ref and i_q_ref which are the reference currents in the dq coordinates which are needed to calculate the power injections by the STATCOM as in (2) and (3).

$$P_{inj} = Vi\ (\ i_d\cos\theta_i + i_q\sin\theta_i) = v_d\ i_d + v_q\ i_q \qquad (2) \qquad\qquad Q_{inj} = v_i\ (i_d\sin\theta_i - i_q\cos\theta_i) = -v_d i_q + v_q i_q \qquad (3)$$

Where i_d and i_q are the reference d and q axis currents of the ac system. The control variables are the current injected by the STATCOM and the reactive power injected into the system. The STATCOM ratings are based on many parameters which are mostly governed by the amount of reactive power the system needs to recover and ride through typical faults on the power system and to reduce the interaction of other system equipment that can become out of synchronism with the grid. Although the final rating of the STATCOM is determined based on system economics, the capacity chosen will be at least adequate for the system to stabilize after temporary system disturbances. The type of faults that the system is expected to recover from also determines the size of the STATCOM. For example, a three phase impedance fault of low impedance requires a very high rating STATCOM while a high impedance short circuit fault needs a lower rating device to support the system during the fault and help recover after the fault. The converter current ratings and the size of the capacitor also decide the capability of the STATCOM. The STATCOM can be connected to the system at

any voltage level by using a coupling transformer. The devices in a voltage source converter are clamped against over-voltages across the DC link capacitor bank to minimize losses and not have to withstand large spikes in reverse over-voltage.

III. Location Of Statcom

Simulation results show that STATCOM provides effective voltage support at the bus to which it is connected to. The STATCOM is placed as close as possible to the load bus for various reasons. The first reason is that the location of the reactive power support should be as close as possible to the point at which the support is needed. Secondly, in the studied test system the location of the STATCOM at the load bus is more appropriate because the effect of voltage change is the highest at this point. The location of the STATCOM is based on quantitative benefits evaluation. The main benefits of using a STATCOM in the system are reduced losses and increased maximum transfer capability. The location of STATCOM is generally chosen to be the location in the system which needs reactive power. To place a STATCOM at any load bus reduces the reactive power flow through the lines, thus, reducing line current and also the I^{2}R losses. Shipping of reactive power at low voltages in a system running close to its stability limit is not very efficient. Also, the total amount of reactive power transfer available will be influenced by the transmission line power factor limiting factors. Hence, sources and compensation devices are always kept as close as possible to the load as the ratio $\Delta V/V_{nom}$ will be higher for the load bus under fault conditions.

Newton-Raphson Approach

The Newton-Raphson (NR) method is a powerful method of solving non-linear algebraic equations. Because of its quadratic convergence, Newton's method is mathematically superior to the *Gauss*-Seidel method and is less prone to divergence with ill-conditioned problems. It works faster, and is sure to converge in most cases as compared to the Gauss-Siedel (GS) method. It is indeed the practical method of load flow solution of large power networks. Its only drawback is the large requirement of computer memory, which can be overcome through a compact storage scheme. One of the main strengths of the Newton-Raphson method is its reliability towards convergence. Contrary to non Newton-Raphson solutions, convergence is independent of the size of the network being solved and the number and kinds of control equipment present in the system. Hence in the proposed work Newton-Raphson method is preferred .

The Sample Five Bus Network
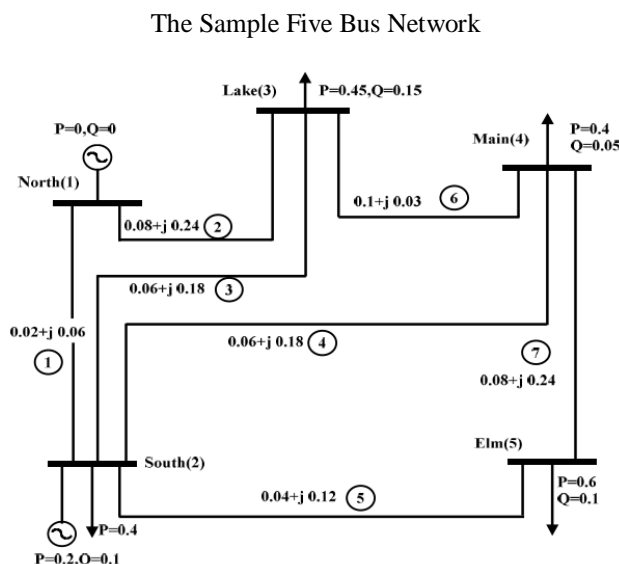
Fig 3 The 5 bus network

For study we have considered the five bus system as shown in Fig. 3, which is a seven line, two generator and three load bus. The input data for the considered system are given in Table 1 for the bus and Table 2 for transmission line . The transmission line impedances and line charging admittances are in per unit.

Table 1 Input bus data(p.u.)

Bus No.	type	Generation		Load		Voltage	
		P	Q	P	Q	|V|	θ
1	Slack	0	0	-	-	1.06	0
2	P-V	0.4	0	0.2	0.1	1	0
3	P-Q	-	-	0.45	0.15	1	0
4	P-Q	-	-	0.4	0.05	1	0
5	P-Q	-	-	0.6	0.1	1	0

Assuming Base Quantity of 100MVA and 100KV

Table 2 Input transmission line data (p.u)

Line no	Line Code	Impedance(R+jX)	Linecharging admittance
1	1-2	0.02+j0.06	0+j0.06
2	1-3	0.08+j0.24	0+j0.05
3	2-3	0.06+j0.18	0+j0.04
4	2-4	0.06+j0.18	0+j0.04
5	2-5	0.04+j0.12	0+j0.03
6	3-4	0.01+j0.03	0+j0.02
7	4-5	0.08+j0.24	0+j0.05

The load flow result and Power flow diagram for the 5-bus
system is shown in Table 3 and Fig 4 respectively.

Table 3 Power flow result without FACTS devices(p.u.)

Parameter	Bus 1	Bus 2	Bus 3	Bus 4	Bus 5
VM(p.u.)	1.06	1	0.985	0.986	0.9717
VA(deg)	0	-2.05	-4.62	-4.95	-5.78

It is observed from the above table that all the nodal voltages are within acceptable voltage magnitude limits. From the power flow diagram it is clear that the largest power flow takes place in the transmission line connecting the generator buses: 89.42 MW, and 73.93MVAR leave north and 86.63 MW and 72.73 MVAR arrive at South. This is also the transmission line that incurs higher active power loss (i.e. 2.79 MW). The operating conditions demand a large amount of reactive power generation by the generator connected at North (i.e.90.61 MVAR). This amount is well in excess of the reactive power drawn by the system loads (i.e. 40MVAR). The generator at South draws the excess of reactive power in the network (i.e.61.4 MVAR). This amount includes the net reactive power produced by several of the transmissionlines
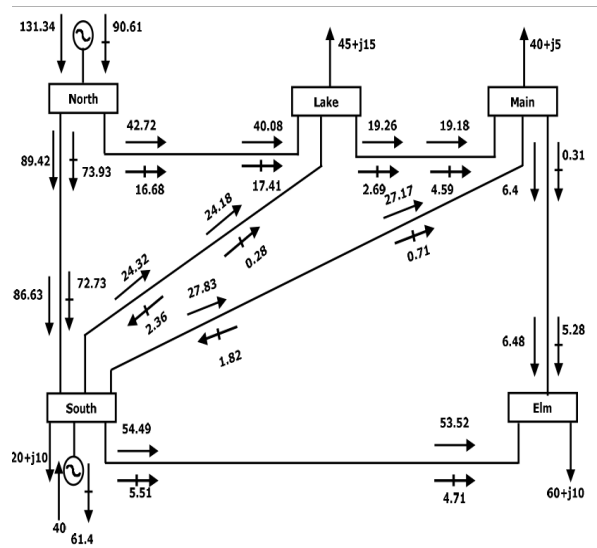
Fig 4 The five bus network and power flow result

Power Flow Model of STATCOM

The STATCOM is the static counterpart of the rotating synchronous condenser but it generates or absorbs reactive power at a faster rate because no moving parts are involved. It is even possible to increase the reactive current in a STATCOM under transient conditions if the devices are rated for the transient overload. The bus at which STATCOM is connected is represented as a PV bus, which may change to a PQ bus in the events of limits being violated. The power flow equations for the STATCOM are derived below from the first principles and assuming the following voltage source representation .
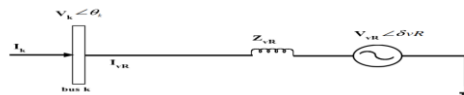
Fig 5 STATCOM-equivalent circuit

Based on the shunt connection shown in Fig 5, the following may be written as

$$E_{vR} = V_{vR}(\cos\delta_{vR} + j\sin\delta_{vR}) \qquad (4)$$

$$S_{vR} = V_{vR} I^*_{vR} = V_{vR} Y^*_{vR} (V^*_{vR} - V^*_k) \qquad (5)$$

Where V_{vR} and δ_{vR} are the controllable magnitude ($V_{vR}min \leq V_{vR} \leq V_{vR}max$) and phase angle ($0 \leq \delta_{vR} \leq 2\pi$) of the voltage source representing the shunt converter. The following are the active and reactive power equations for the converter at bus k,

$$P_{vR} = V^2_{vR}G_{VR} + V_{vR}V_k [G_{vR} Cos(\delta_{vR} - \theta_k) + B_{vR} Sin(\delta_{vR} - \theta_k)] \quad (2.3)$$

$$Q_{vR} = -V^2_{vR}B_{VR} + V_{vR}V_k[G_{vR}Sin(\delta_{vR} - \theta_k) - B_{vR}Cos(\delta_{vR} - \theta_k)] \quad (6)$$

$$P_k = V^2_kG_{vR} + V_kV_{kR} [G_{vR} Cos(\theta_{k-} \delta_{vR}) + B_{vR} Sin(\theta_{k-} \delta_{vR})] \qquad (7)$$

$$Q_k = -V^2_kB_{vR} + V_kV_{kR} [G_{vR} Sin(\theta_{k-} \delta_{vR}) - B_{vR} Cos(\theta_{k-} \delta_{vR})] \qquad (8)$$

Power Flow Stud with Statcom

The STATCOM is included in the bus 3 of the sample system to maintain the nodal voltage at 1 p.u.. Here the STATCOM data are: the initial source voltage magnitude is 1 p.u, Phase angle is 0 degrees   and the converter reactance is 10 p.u.
The load flow result and power flow diagram result for the 5-bus system with STATCOM at bus 3 is shown in Table 4 and Fig 6 respective.

Table 4 Result with STATCOM included at bus 3

Parameter	Bus 1	Bus 2	Bus 3	Bus 4	Bus 5
VM(p.u)	1.06	1	1	0.9953	0.9754
VA(deg)	0	-2.06	-4.752	-4.823	-5783
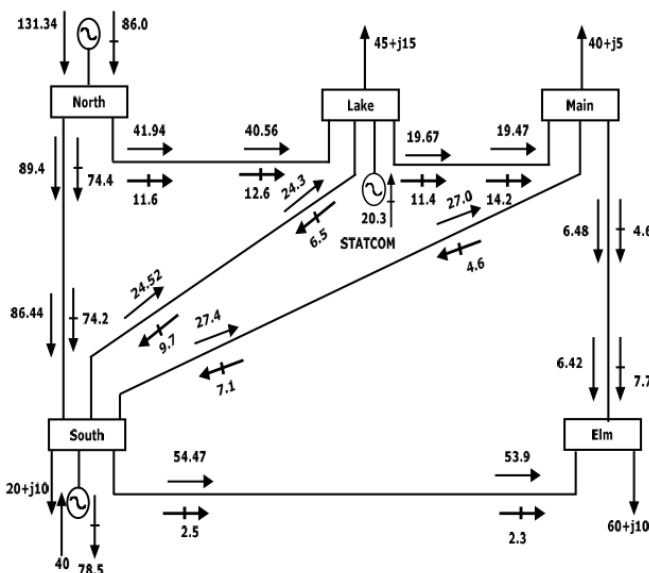
Fig.6 STATCOM-upgraded test network and power flow result

Here the power flow result indicates that the STATCOM generates 20.3 MVAR in order to keep the voltage magnitude at 1 p.u. at bus 3. The largest reactive power flow takes place in the transmission line connecting North and South, where 74.4 MVAR leaves North and 74.2 MVAR arrives at South. In general, more reactive power is available in the network than in the base case, and the generator connected at South increases its share of reactive power absorption compared with the base case. Active power flows are only marginally affected by the STATCOM installation the power flow of the five bus system has been studied without and with FACTS devices performing the Newton-Rapson method. Power flow without FACTS devices shows that the operating conditions demand a large amount of reactive power generation by the generator connected at bus 1 (i.e. 90.61 MVAR). This amount is well in excess of the reactive power drawn by the system loads (i.e. 40 MVAR). The generator at bus 2 draws the excess of reactive power in the network (i.e. 61.4 MVAR).

Use of STATCOM results in an improved network voltage profile, except at bus 5, which is too far away from bus 3 to benefit from the influence of STATCOM. The power flow result indicates that the STATCOM generates 20.3 MVAR in order to keep the voltage magnitude at 1 p.u at bus 3. The SVC injects 20.28 MVAR into bus 3 and keeps the nodal voltage magnitude at 1p.u. The action of the SVC results in an overall improved voltage profile. The STATCOM is superior to the SVC in providing voltage support under large system disturbances during which the voltage excursions would be well outside of the linear operating range of the compensator

The Sample Nine Bus System

For the proposed work we have considered the three- machine, nine- bus WSCC (Western System Coordinating Counsel) system as shown in Figure 7
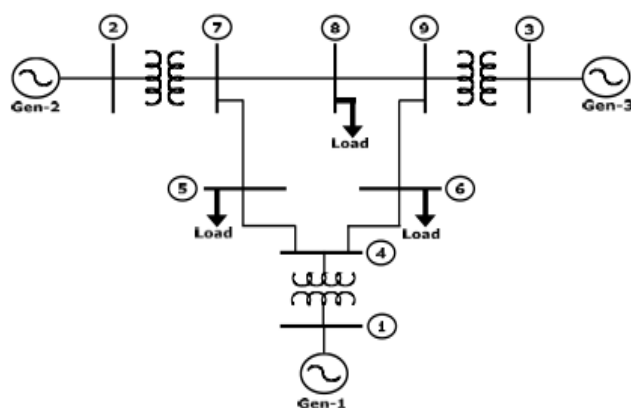
Figure 7

Thae input data for the considered system are given in table 5 for the bus and table 6 for the transmission line.the transmission line impedances and the line charging admittances are in per unit

Table input 5 Bus data (p.u)

Bus no	Type	Generation		Load		Voltage	
		P	Q	P	Q	|V|	θ
1	Slack	0	0	0	0	1,04	0
2	P-V	1.63	0	0	0	1.025	0
3	P-V	.85	0	0	0	1.025	0
4	P-Q	0	0	0	0	1	0
5	P-Q	0	0	1.25	.50	1	0
6	P-Q	0	0	.90	.30	1	0
7	P-Q	0	0	0	0	1	0
8	P-Q	0	0	1.0	.35	1	0
9	P-Q	0	0	0	0	1	0

Assuming base quantity of 100 MVA and 100 KV

Table 6 input transmissinion line data (p.u)

Bus No	Line Code	Impedance (R+jX)	Line Charging Admittance
1	1-4	0+j.0576	0+j0
2	2-7	0+j.0625	0+j0
3	3-9	0+j.0586	0+j0
4	4-5	0.01+j.0850	0+j.088
4	4-6	.017+j.0920	0+j.079
5	5-7	.0320+j.161	0+j.153
6	6-9	.0390+j.17	0+j.179
7	7-8	.0085+j.072	0+j.0745
8	8-9	.0119+j.1008	0+j.1045

The disturbances for the sample system are 3-phase faults at each end of each line (3-phase to earth), followed by clearing the fault via removing one of the lines connected to the faulted bus, followed by a successful three phase reclosure of the faulted line.

IV. Modelling

A three-phase fault is simulated in one of the lines of the nine-bus system i.e. three phase to earth fault. The simulation is done in three phases. To start with, the pre-fault system is run for a small time. Then a symmetrical fault is applied at one end of a line (Fig. 3.8). Simulation of the faulted condition continues until the line is disconnected from the buses at both of the ends of the faulted line after a fault clearing time tcl s. Then the post-fault system is simulated for a longer time (say,10 s) to observe the nature of the transients. We start with tcl = 0.1 s (which is six cycles for a 60-Hz system) and then tcl =.15s. Now the STATCOM is connected to the midpoint of one of the lines. To ensure the reactive power injection mode of operation, the magnitude of the voltage of the STATCOM is set at a value higher than the magnitudes of the pre-fault line midpoint voltage.

Plots of relative machine angles delta-(1-2) and (1-3) are shown in Fig. 7.1 and Fig. 7.2 with fault clearing time tcl = .1 (s) in line 5-7 respectively.

Fig. 7.1. Response of relative machine angles delta 1-2 for fault at bus 7, line removed at 5-7 without STATCOM and with STATCOM

Fig. 7.2. Response of relative machine angles delta 1-3 for fault at bus 7,line removed at 5-7 without STATCOM and with STATCOM

Plots of relative machine angles delta-(1-2) and (1-3) are shown in Fig. 7.3 and Fig. 7.4 with fault clearing time tcl = .15 (s) in line 5-7 respectively.

Fig. 7.3. Response of relative machine angles delta 1-2 for fault at bus 7, line removed at 5-7 without STATCOM and withSTATCOM

Fig. 7.4. Response of relative machine angles delta 1-3 for fault at bus 7, line removed at 5-7 without STATCOM and with STATCOM

Plots of relative machine angles delta-(1-2) and (1-3) are shown in Fig. 7.5 and Fig. 7.6 with fault clearing time tcl = .1 (s) in line 4-5 respectively.

Fig. 7.5. Response of relative machine angles delta 1-2 for fault at bus 5, line removed at 4-5 without STATCOM and with STATCOM

Fig. 7.6. Response of relative machine angles delta 1-3 for fault at bus 5, line removed at 4-5 without STATCOM and with STATCOM

Plots of relative machine angles delta-(1-2) and (1-3) are shown in Fig. 7.7 and Fig. 7.8 with fault clearing time tcl = .15 (s) in line 4-5 respectively.
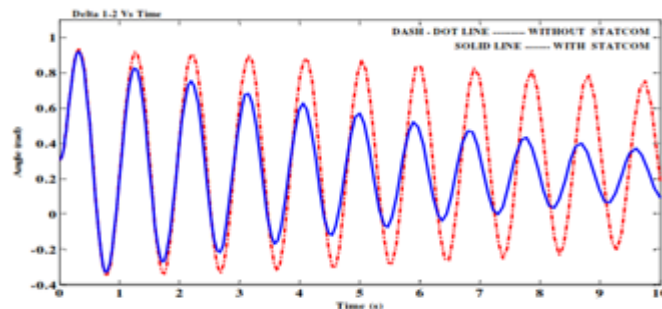
Fig.7.7. Response of lative machine angles delta 1-2 for fault at bus 5, line removed at 4-5 without TATCOM and with STATCOM.
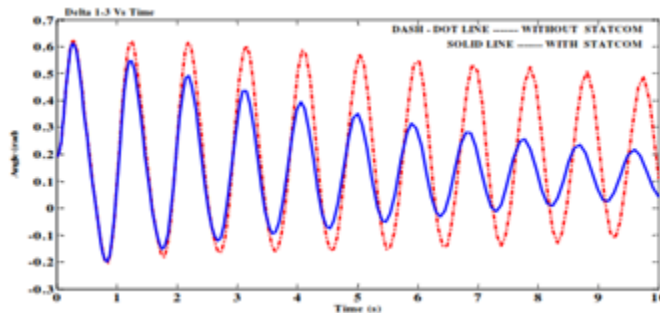
Fig. 7.8. Response of relative machine angles delta 1-3 for fault at bus 5,   line removed at 4-5 without STATCOM and with STATCOM.

Plots of relative machine angles delta-(1-2) and (1-3) are shown in Fig. 7.9 and Fig. 4.10 with fault clearing time tcl = .1(s) in line 6-9 respectively.
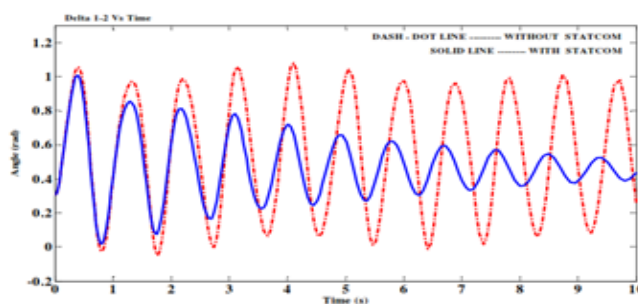
Fig. 7.9. Response of relative machine angles delta 1-2 for fault at bus 9, line removed at 6-9 without STATCOM and with STATCOM.
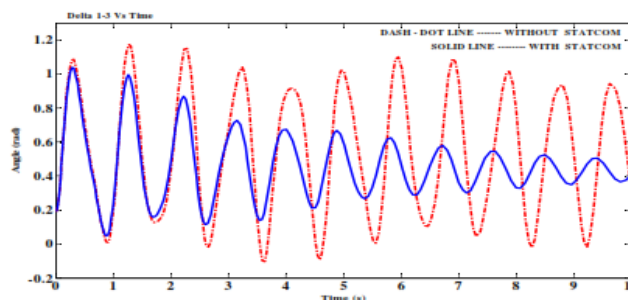
Fig. 7.10. Response of relative machine angles delta 1-3 for fault at bus 9, line removed at 6-9 without STATCOM and with STATCOM.

Plots of relative machine angles delta-(1-2) and (1-3) are shown in Fig. 7.11 and Fig. 7.12 with fault clearing time tcl = .15 (s) in line 6-9 respectively.
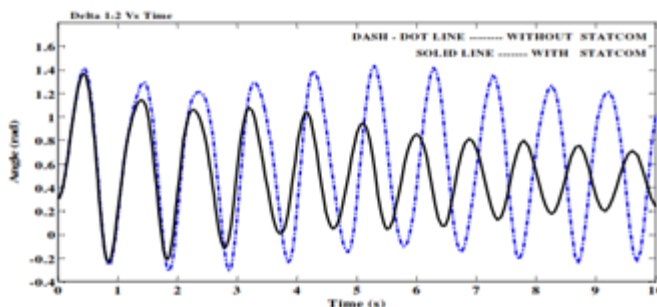
Fig. 7.11. Response of relative machine angles delta 1-2 for fault at bus 9, line removed at 6-9 without STATCOM and with STATCOM
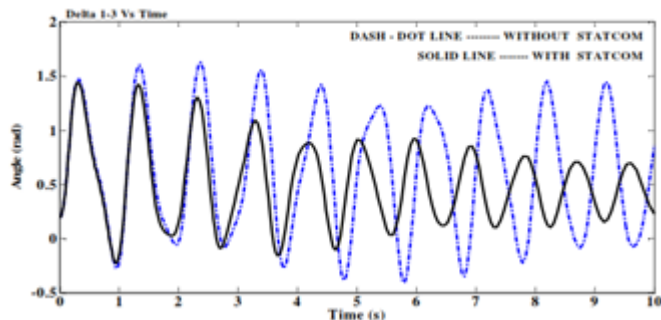
Fig. 7.12. Response of relative machine angles delta 1-3 for fault at bus 9, line removed at 6-9 without STATCOM and with STATCOM.

Plots of relative machine angles delta-(1-2) and (1-3) are shown in Fig. 7.13 and Fig. 7.14 with fault clearing time tcl = .1(s) in line 7-8respectively.
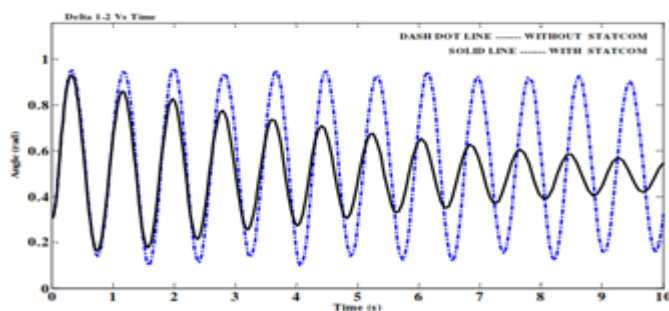
Fig. 7.13. Response of relative machine angles delta 1-2 for fault at bus 8, line removed at 7-8 without STATCOM and with STATCOM
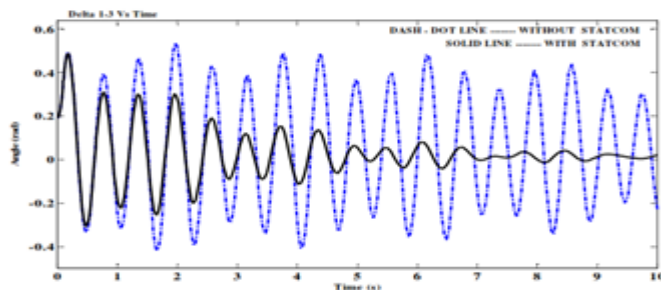
Fig. 7.14. Response of relative machine angles delta 1-3 for fault at bus 8, line removed at 7-8 without STATCOM and with STATCOM.

Plots of relative machine angles delta-(1-2) and (1-3) are shown in Fig. 7.15 and Fig. 7.16 with fault clearing time tcl = .15(s) in line 7-8 respectively.
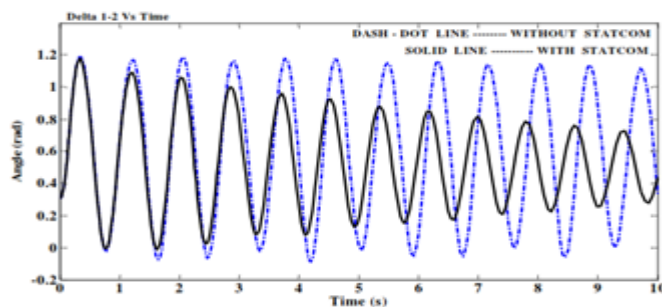
Fig. 7.15. Response of relative machine angles delta 1-2 for fault at bus 8, line removed at 7-8 without STATCOM and with STATCOM.

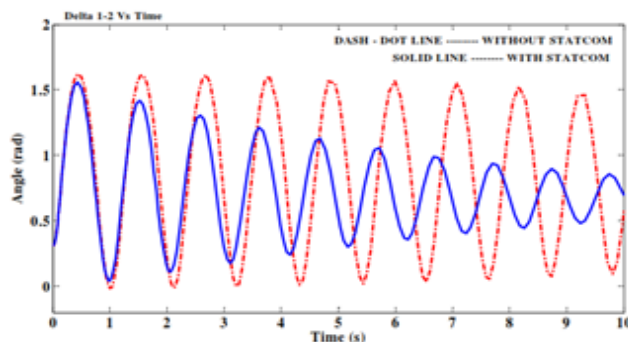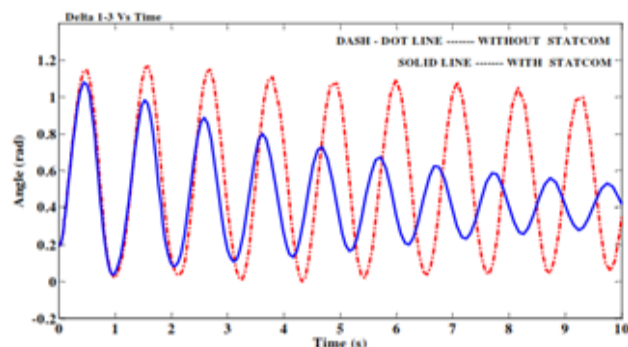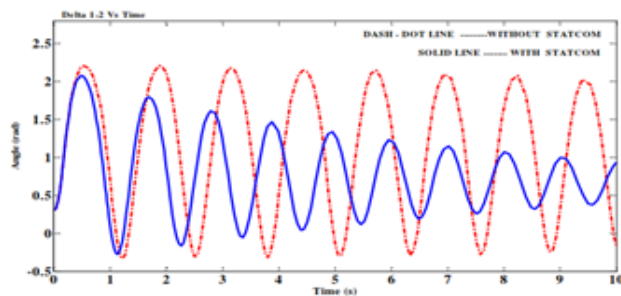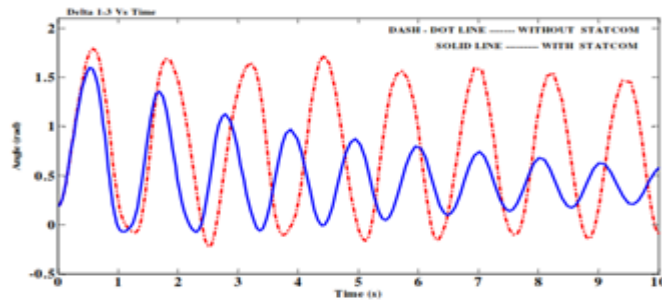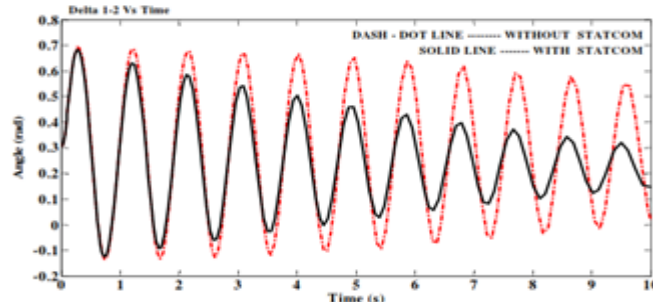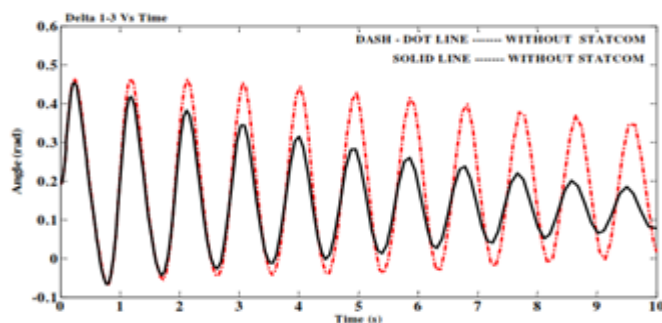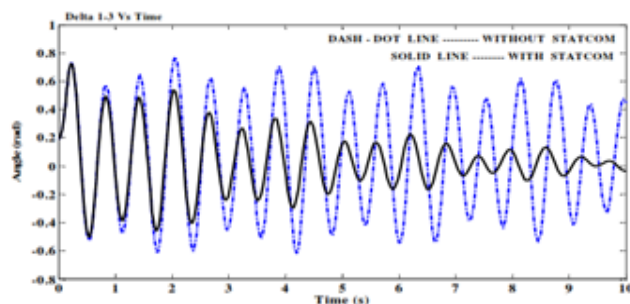Fig. 7.16. Response of relative machine angles delta 1-3 for fault at bus 8, line removed at 7-8 without STATCOM and with STATCOM.

From the above simulation results we conclude that STATCOM not only considerably improves transient stability but also compensates the reactive power in steady state. The STATCOM is used to control power flow of power system by injecting appropriate reactive power during dynamic state. The best possible location of the FACTS device (STATCOM) is found to vary with the location of the fault and the operating criteria of the device. We also conclude that if the fault clearing time is less, more stability improvement. On the other hand less transient stability improvement occurs if fault clearing time is more.

V. Conclusion

In this thesis, the effect of STATCOM for improving transient stability of the multi- machine power system is investigated in terms of the Fault Clearing Time. The STATCOM is used to control power flow of power system by injecting appropriate reactive power during dynamic state. Computer simulation results show that STATCOM not only considerably improves transient stability but also compensates the reactive power in steady state. Therefore STATCOM can increase reliability and capability of AC transmission system .It is also found that the best possible location of the STATCOM for transient stability improvement is not fixed for the nine-bus system; rather it varies depending on the fault location.

It is quite clear that before compensating a power system with FACTS device to improve transient stability, we need to assess the system stability conditions for different locations of the fault and the compensator and also with different amounts of compensation. The transient stability improvement of the multi-machine power system at different fault condition is investigated in this work. The proposed work is also analyzed for different fault clearing times.

REFERENCES

[1]   P. Kundur, "Power System Stability and Control", McGraw-Hill, 1994.
[2]   Y.H. Song and A.T. Johns, "Flexible ac transmission systems (FACTS)", The Institute ofElectrical Engineers, London, 1999.
[3]   N.G. Hingorani and L. Gyugyi, "Understanding FACTS: concepts and technology of flexible ac transmission systems", IEEE Press, NY, 1999. [4]   E. Muljadi, C.P. Butterfield, "Wind Farm Power System Model Development," World Renewable Energy Congress VIII, Colorado, Aug-Sept 2004
[5]   S.M. Muyeen, M.A. Mannan, M.H. Ali, R. Takahashi, T. Murata, J. Tamura, "Stabilization of Grid Connected Wind Generator by STATCOM," IEEE Power Electronics and Drives Systems, Vol. 2, 28-01 Nov. 2005
[6]   Z. Saad-Saoud, M.L. Lisboa, J.B. Ekanayake, N. Jenkins, G. Strbac, "Application of STATCOMs to wind farms," IEE Proceedings – Generation, Transmission, Distribution, vol. 145, pp.1584-89, Sept 1998
[7]   L. Chun, J. Qirong, X. Jianxin, "Investigation of Voltage Regulation Stability of Static Synchronous Compensator in Power System," IEEE Power Engineering Society Winter Meeting, vol. 4, 2642-47, 23-27 Jan. 2000
[8   E. Muljadi, C.P. Butterfield, A.Ellis, J.Mechenbier, J. Hochheimer, R. Young,N.Miller, R. Delmerico, R. Zavadil, J.C. Smith, "Equivalencing the Collector System of a Large Wind Power Plant," IEEE Power Engineering Society General Meeting, 18-22 June 2006
[9]   J.G. Slootweg, W.L. Kling, "Modeling of Large Wind Farms in Power System Simulations," IEEE Power Engineering Society Summer Meeting, vol. 1, 503-508, 2002
[10]   I. Etxeberria-Otadui, U. Viscarret, I. Zamakona, B. Redondo, J. Ibiricu,"Improved STATCOM operation under transient disturbances for wind power applications," 2007 European Conference on Power Electronics and Applications,2-5 Sept. 2007 [11] P.Kumkratug;, "The Effect of STATCOM on Inter-Area Power System Stability Improvement," Computer Modeling and Simulation, 2008. EMS '08. Second UKSIM European Symposium on , vol., no., pp.359-363, 8-10 Sept. 2008.
[12]   A. Ghosh, D.Chatterjee; , "Transient Stability Assessment of Power Systems Containing Series and Shunt Compensators," Power Systems, IEEE Transactions on , vol.22, no.3, pp.1210-1220, Aug. 2007.

[13]   T.Kondo, A.Yokoyama, M.Goto, H. Konishi, M. Sekoguchi, Lu. Qiang ; "Power system transient stability enhancement by STATCOM with nonlinear control system," Power System Technology, 2002. Proceedings. PowerCon 2002. International Conference on , vol.3, no., pp. 1908- 1912 vol.3, 2002.

[14]   V. Mahajan ; "Power System Stability Improvement with Flexible A.C. Transmission System   (FACTs) Controller," Power System Technology and IEEE Power India Conference, 2008. POWERCON 2008. Joint International Conference on , vol., no., pp.1-7, 12-15 Oct. 2008.

[15]   Brian Stott,"Review of Load-Flow Calculation Methods", Proceedings of the IEEE , Vol.62, No. 7, July 1974. pp 916-929. [16] S.W. Steven, "Wind parks as power plants," IEEE PES General Meeting, 2006 [17]   Heping Zou, Hui Sun, Jiyan Zou, "Fault Ride-through Performance of Wind Turbine with Doubly Fed Induction Generator," 2nd IEEE Conference on Industrial Electronics and Applications, pp. 1607-11, 23-25 May 2007

[18   M.L. Crow, "Power System Stability – Course material," Missouri University of Science and Technology, 2007

[19]   Wenjuan Zhang, "Optimal sizing and location of static and dynamic reactive power compensation," a dissertation submitted to the University of Tennessee, Knoxville, Dec. 2007

[20]   N.G. Hingorani, L. Gyugyi, Understanding FACTS: Concepts and Technology of Flexible AC Transmission Systems, New York, Wiley-IEEE Press, 1999

[21]   J.P. Aditya, A. Nikhil, B.H. Chowdhury, "Application of STATCOM for improved reliability of power grid containing a wind turbine," 2008 IEEE Power Engineering Society General Meeting, July 2008

[22]   P. Lehn, "Exact modeling of the voltage source converter," IEEE Trans. Power Delivery, vol. 17, pp. 217–222, Jan. 2002.

[23]   G.N.Stagg and A.H. El-Abiad "Computer Methods in Power System Analysis", McGrawn Hill International Publication, 1988.

[24]   P. M. Anderson and A. A. Fouad, "Power System Stability and Control". Ames, IA: Iowa State Univ. Press, 1977.

MOHD. ILYAS *was born on 2nd April 1976. He is an assistant professor in department of electrical & electronics with Al-Falah University Faridabad, Haryana. He received his B.Tech in electrical engineering & M.Tech in electrical power system & management from Jamia Millia Islamia, New Delhi. Now he is pursuing PhD. from MD University, Rohtak. He has more than 13 years experience in teaching. He taught various subjects such as Power Electronics, Electrical measurement & Measuring Instrument, Electric Power Generation etc. He attended many national and international Seminars and conferences. He has guided number of B.Tech and M.Tech projects in teaching.*

STATCOM for Improved Dynamic Performance of Wind Farms in Power Grid

Mohammad Ilyas[1], Mohammad Ubaid Soherwardi[2]

[1, 2](Department of Electrical and Electronics Engineering, Al-Falah School of Engineering and Technology, Faridabad (Haryana)

Abstract: *Application of FACTS controller called Static Synchronous Compensator STATCOM to improve the performance of power grid with Wind Farms is investigated .The essential feature of the STATCOM is that it has the ability to absorb or inject the reactive power with power grid. Therefore, the voltage regulation of the power grid with STATCOM FACTS device is achieved. Moreover restoring the stability of the power system having wind farm after occurring severe disturbance such as faults or wind farm mechanical power variation is obtained with STATCOM controller. The dynamic model of the power system having wind farm controlled by proposed STATCOM is developed. To validate the powerful of the STATCOM FACTS controller, the studied power system is simulated and subjected to different severe disturbances. The results prove the effectiveness of the proposed STATCOM controller in terms of fast damping the power system oscillations and restoring the power system stability.*
Keywords: *STATCOM, Wind Generation, Transient Stability.*

I. Introduction

Now a days wind as a significant proportion of non pollutant energy generation is widely used .If a large wind farm, which electrically is far away from its connection point to power system, is not fed by adequate reactive power, it present major instability problem. Various methods to analyze and improve wind farm stability have been performed. The stability of wind driven self excited induction generator SEIG s is analyzed. A breaking resistor to absorb active power during fault to enhance the system stability is developed . Flexible AC transmission system FACTS devices such as Static Synchronous Compensator STATCOM to improve the stability in wind farm is studied.

As a consequence, it will become necessary to require wind farms to maintain continuous operation during grid disturbances and thereby support the network voltage and frequency. In addition, in the area of a deregulated electricity industry, the policy of open access to transmission systems, which helped create competitive electricity markets, led to a huge increase in energy transactions over the grid and possible congestion in transmission systems[1]. The expansion of power transfer capability of transmission systems has been a major problem over the past two decades. Under these conditions, the modern power system has had to confront some major operating problems, such as voltage regulation, power flow control, transient stability, and damping of power oscillations, etc. FACTS devices can be a solution to these problems .

They are able to provide rapid active and reactive power compensations to power systems, and therefore can be used to provide voltage support and power flow control, increase transient stability and improve power oscillation damping. Suitably located FACTSdevices allow more efficient utilization of existing transmission networks.The STATCOM is used to provide rapid and fast control of voltage during during steady state and transient stability. This issue is even more critical in the case of microgirds, since certain FACTS controllers, particularly STATCOMs, are being considered as a possible solution for some of the voltage and angle stability problems inherent to these power grids. Consequently, typical STATCOM models are validated here using system identification techniques to extract the relevant electromechanical mode information from time-domain signals . System identification techniques are used to readily and directly compare fairly distinct STATCOM models, thus avoiding matrix based eigenvalue studies of complex system models and/or modeling approximations.

In this paper, a STATCOM is added to the power network to provide dynamic voltage control for the wind farm, dynamic power flow control for the transmission lines, relieve transmission congestion and improve power oscillation damping. Simulation results show that the STATCOM devices significantly improve the performance of the wind farm and the power network during transient disturbances.

II.   Wind Farm And Electric Generator Model

A wind turbine is a device that converts kinetic energy from the wind into electrical power. Wind turbine use squirrel cage induction generator output power to its nominal value for high wind speeds. In order to generate power the induction speed must be slightly above the synchronous speed but the speed variation istypicallysosmallthattheWTIGisconsideredtobeaffixed-speedwindgenerator.

A wind turbine used for charging batteries may be referred to as a wind charger[2].The result of over a millennium of windmill development and modern engineering, today's wind turbines are manufactured in a wide range of vertical and horizontal axis types. The smallest turbines are used for applications such as battery charging for auxiliary power for boats or caravans or to power traffic warning signs. Slightly larger turbines can be used for making small contributions to a domestic power supply whilst selling unused power back to the utility supplier via the electrical grid. Arrays of large turbines, known as wind farms, are becoming an increasingly important source of renewable energy and are used by many countries as part of a strategy to reduce their reliance on fossil fuels. Unlike the trend toward large-scale grid connected wind turbines seen in the West, the more immediate demand for rural energy supply in developing countries is for smaller machines in the 5 - 100 kW range[3]. These can be connected to small, localised micro-grid systems and used in conjunction with diesel generating sets and/or solar photovoltaic systems (see hybrid systems section later in this fact sheet). Currently, the use of wind power for electricity production in developing countries is limited, the main area of growth being for very small battery charging wind turbines (50 - 150 Watts). In Inner Mongolia there are over 30,000 such machines used by herders for providing power for lighting, televisions, radios, etc.
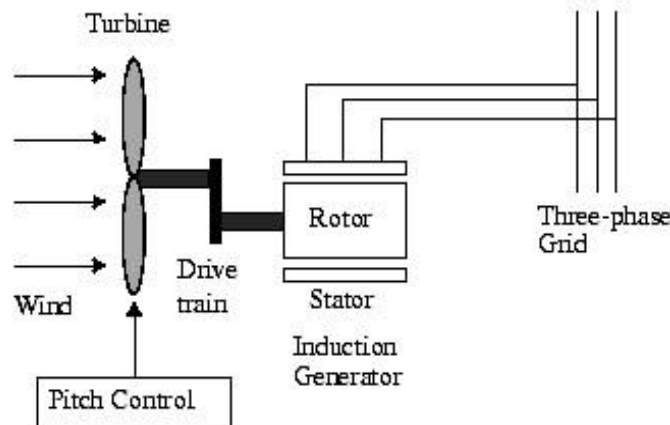
Figure 1: Wind turbineandinductiongenerator

Where you choose to build your wind turbine is important. Remember that if nearby houses, tree lines and silos obstruct the full force of the wind from your wind turbine, you will not be able to generate as much power.Wind speeds tend to be higher on the top of a ridge or hill, and for that reason it is a good idea to locate wind turbines at hilly locations[4]. Just remember to keep your turbine away from high turbulence. Neighbours must also be taken into consideration when picking a spot to build your turbine. The farther your wind turbine site is from neighbouring houses, the better.Do not expect your wind turbine to generate the same amount of power all the time. The wind speed at a single location may vary considerably, and this can have a significant impact on the power production from a wind turbine.Even if the wind speed varies by only 10%, the power production from a wind turbine can vary by up to 25%.
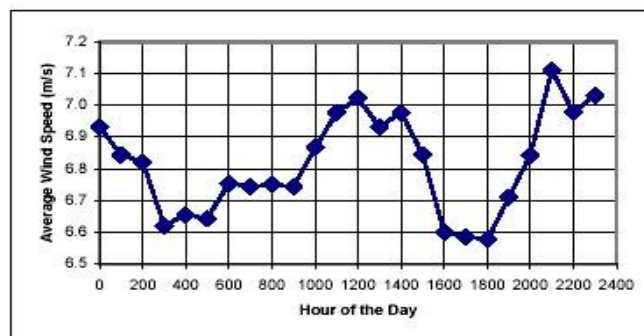
Figure 2: Example of wind speed distribution by hour of the day. Values shown are monthly averages of measurements made by anemometers. (Source: US Department of Energy).

The power available in the wind is proportional to the cube of its speed. This means that if wind speed doubles, the power available to the wind generator increases by a factor of 8 (2 x 2 x 2 = 8) [7].
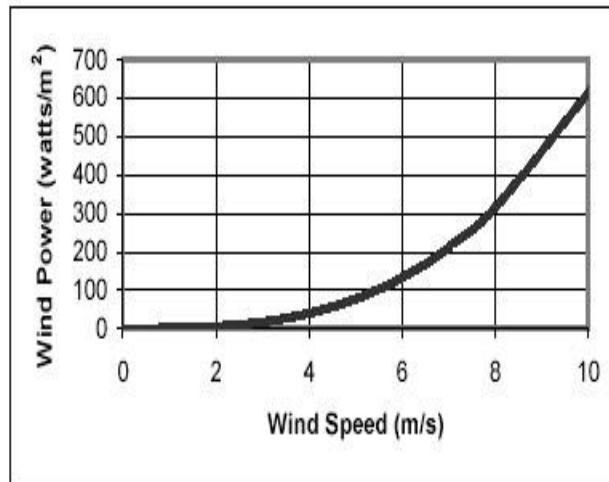
Figure 3: Relationship between wind speed and wind power.

III. Statcom Model

A static synchronous compensator (STATCOM), also known as a "static synchronous condenser" ("STATCON"), is a regulating device used on alternating current electricity transmission networks. It is based on a power electronics voltage-source converter and can act as either a source or sink of reactive AC power to an electricity network. If connected to a source of power it can also provide active AC power. It is a member of the FACTS family of devices

Usually a STATCOM is installed to support electricity networks that have a poor power factor and often poor voltage regulation. There are however, other uses, the most common use is for voltage stability. A STATCOM is a voltage source converter (VSC)-based device, with the voltage source behind a reactor. The voltage source is created from a DC capacitor and therefore a STATCOM has very little active power capability. However, its active power capability can be increased if a suitable energy storage device is connected across the DC capacitor. The reactive power at the terminals of the STATCOM depends on the amplitude of the voltage source. For example, if the terminal voltage of the VSC is higher than the AC voltage at the point of connection, the STATCOM generates reactive current; on the other hand, when the amplitude of the voltage source is lower than the AC voltage, it absorbs reactive power.
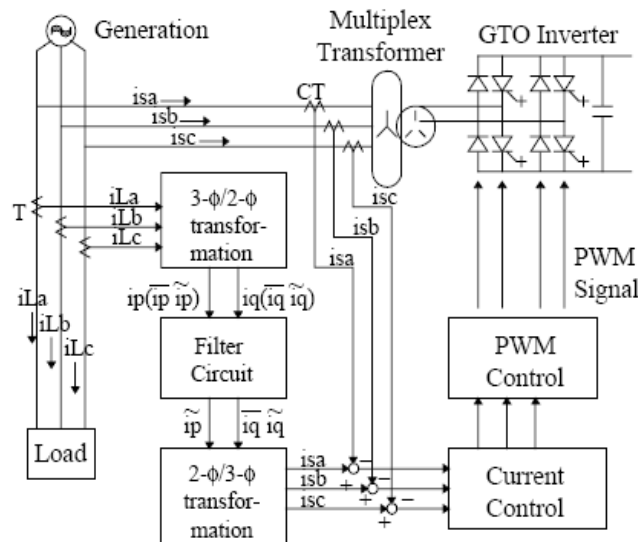
Figure 4: A typical control circuit of the STATCOM

The three-phase load currents to be compensated (iLa,iLb, and iLc shown in the last Figure) are measured from the system and transformed to two phase orthogonal components (ip and iq) on rotating coordinates synchronized with the line voltage. The outputs of the filter circuit are inversely transformed to

three-phase components (i_{sa}, i_{sb} and i_{sc} shown in Figure). The output current of the STATCOM is controlled by three-phase current feedback control using i_{sa}, i_{sb}, and i_{sc} as reference signals for each phase. The output signals of the current control added by a sensed system voltage signal becomes the voltage reference signal of the PWM control. The PWM control circuit generates the firing signal of the GTO by comparing triangular wave carrier signals to the voltage reference signal.

The response time of a STATCOM is shorter than that of an SVC, mainly due to the fast switching times provided by the IGBTs of the voltage source converter. The STATCOM also provides better reactive power support at low AC voltages than an SVC, since the reactive power from a STATCOM decreases linearly with the AC voltage (as the current can be maintained at the rated value even down to low AC voltage). A static VAR compensator (SVC) can also be used for voltage stability. However, a STATCOM has better characteristics than a SVC. When the system voltage drops sufficiently to force the STATCOM output current to its ceiling, its maximum reactive output current will not be affected by the voltage magnitude. Therefore, it exhibits constant current characteristics when the voltage is low under the limit. In contrast the SVC's reactive output is proportional to the square of the voltage magnitude. This makes the provided reactive power decrease rapidly when voltage decreases, thus reducing its stability. In addition, the speed of response of a STATCOM is faster than that of an SVC and the harmonic emission is lower. On the other hand STATCOMs typically exhibit higher losses and may be more expensive than SVCs, so the (older) SVC technology is still widespread.

IV. Modelling

A wind farm consisting of six 1.5-MW wind turbines is connected to a 25-kV distribution system exports power to a 120-kV grid through a 25-km 25-kV feeder. The 9-MW wind farm is simulated by three pairs of 1.5 MW wind-turbines. Wind turbines use squirrel-cage induction generators (IG). The stator winding is connected directly to the 60 Hz grid and the rotor is driven by a variable-pitch wind turbine. The pitch angle is controlled in order to limit the generator output power at its nominal value for winds exceeding the nominal speed (9 m/s).
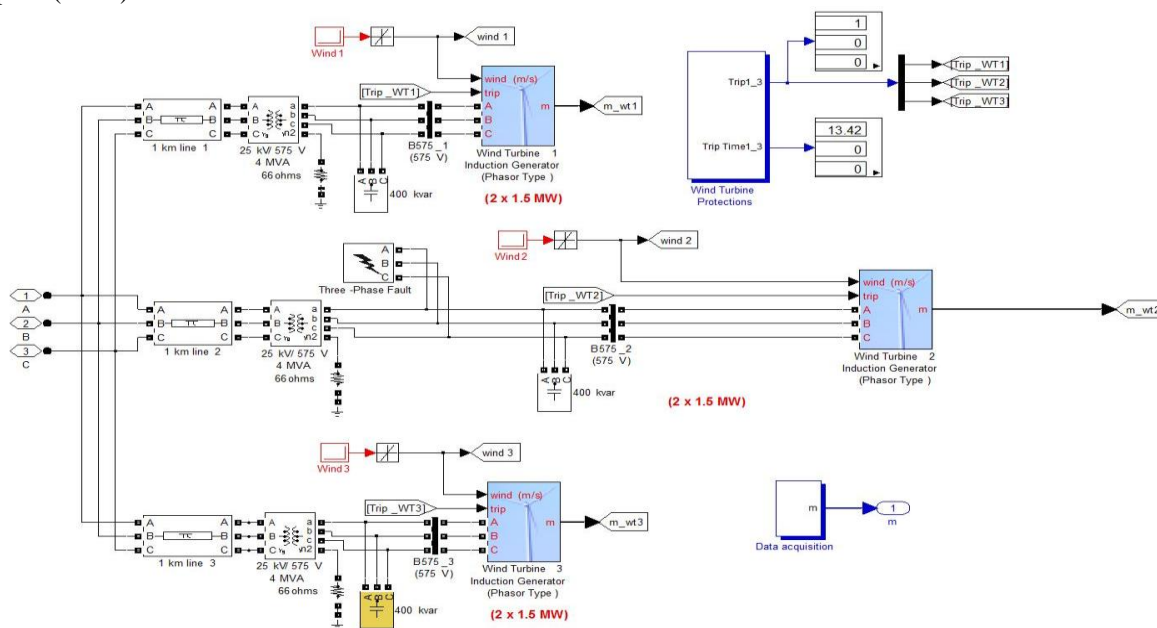
Fig 5.Wind farm consisting of 6 wind turbine induction generator

In order to generate power the IG speed must be slightly above the synchronous speed. Speed varies approximately between 1 Pu at no load and 1.005 Pu at full load. Each wind turbine has a protection system monitoring voltage, current and machine speed. Reactive power absorbed by the IGs is partly compensated by capacitor banks connected at each wind turbine low voltage bus (400 kvar for each pair of 1.5 MW turbine). The wind speed applied to each turbine is controlled by the "Wind 1" to "Wind 3" blocks. Initially, wind speed is set at 8 m/s, then starting at t=2s for "Wind turbine 1", wind speed is rammed to 11 m/s in 3 seconds. The same gust of wind is applied to Turbine 2 and Turbine 3, respectively with 2 seconds and 4 seconds delays. Then, at t=15 s a temporary fault is applied at the low voltage terminals (575 V) of "Wind Turbine 2".Start simulation and observe the signals on the "Wind Turbines" scope monitoring active and reactive power, generator speed, wind speed and pitch angle for each turbine.

From the Fig.6 it is clear that to keep the voltage close to 1 Pu, the STATCOM installed in the system provides 3 Mvar. So this amount of reactive power supplied by the STATCOM keeps the voltage constant irrespective of changes in the wind speed which otherwise is not possible if wind system is directly connected to the grid. So it is important to keep the voltage constant in the distribution system, hence voltage regulation is required in the distribution network. Voltage Source Converter (VSC) based STATCOM achieves voltage regulation in the connected bus by absorbing/supplying the required reactive power .For each pair of turbine the generated active power starts increasing smoothly (together with the wind speed) to reach its rated value of 3 MW in approximately 8s. Over that time frame the turbine speed will have increased from 1.0028 Pu to 1.0047 Pu. Initially, the pitch angle of the turbine blades is zero degree. When the output power exceed 3 MW, the pitch angle is increased from 0 deg to 8 deg in order to bring output power back to its nominal value. Observe that the absorbed reactive power increases as the generated active power increases.At nominal power, each pair of wind turbine absorbs 1.47 Mvar. For 11m/s wind speed, the total exported power measured at the B25 bus is 9 MW and the STATCOM maintains voltage at 0.984 Pu by generating 1.62 Mvar (see "B25 Bus" and "Statcom" scopes).
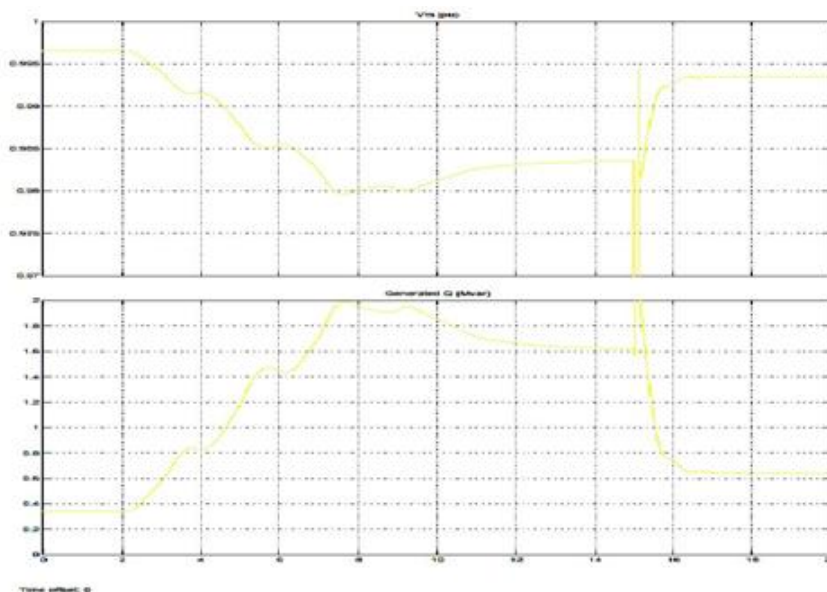
Figure 6: Reactive power and voltage at STATCOM terminals

At t=15 s, a phase to phase fault is applied at wind turbine 2 terminals, causing the turbine to trip at t=15.11 s. If you look inside the "Wind Turbine Protections" block you will see that the trip has been initiated by the AC Under-voltage protection. After turbine 2 has tripped, turbines 1 and 3 continue to generate 3 MW each.
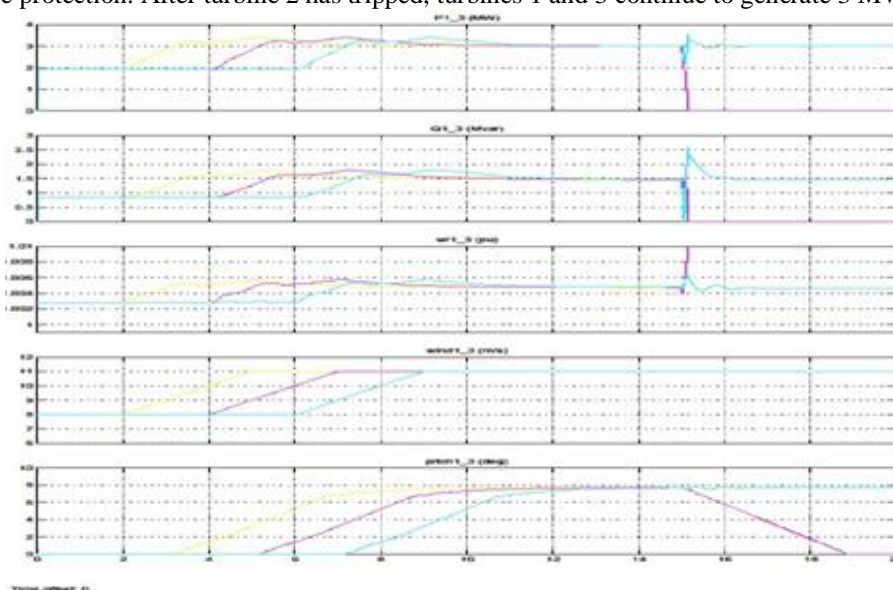
Figure7: Phase to phase fault

4.1 WITH STATCOM

The rest of reactive power required to maintain the 25-kV voltage at bus B25 close to 1 Pu is provided by a 3-Mvar STATCOM with a 3% droop setting. Open the "Wind Farm" block and look at "Wind Turbine 1". Open the turbine menu and look at the two sets of parameters specified for the turbine and the generator. Each wind turbine block represents two 1.5 MW turbines. Open the turbine menu, select "Turbine data" and check "Display wind-turbine power characteristics". The turbine mechanical power as function of turbine speed is displayed for wind speeds ranging from 4 m/s to 10 m/s. The nominal wind speed yielding the nominal mechanical power (1pu=3 MW) is 9 m/s. The wind turbine model (from the DR library) and the Statcom model (from the FACTS library) are phasor models that allow transient stability type studies with long simulation times. In this demo, the system is observed during 20 s.
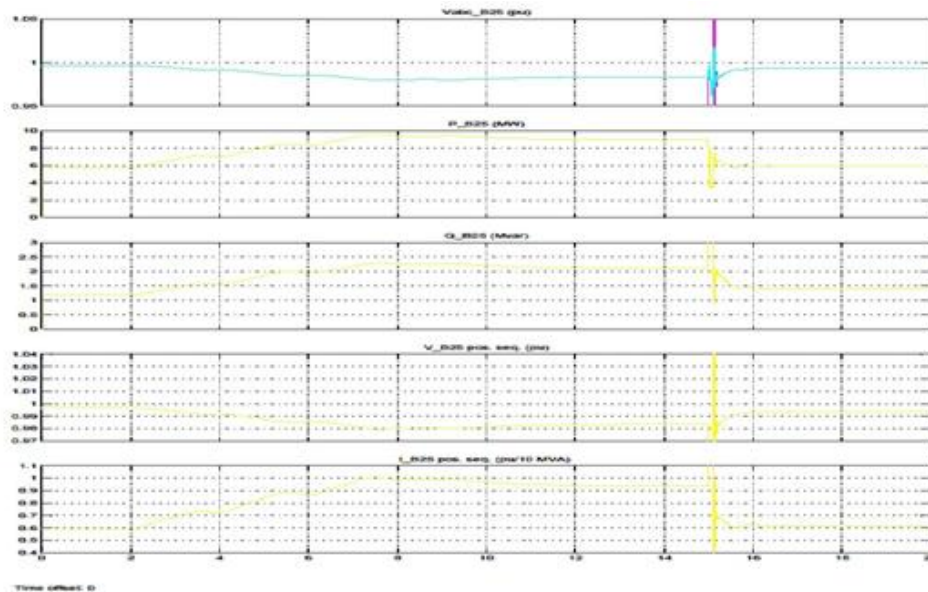
Figure**8:** Waveforms of different quantities with STATCOM

4.2 WITHOUT STATCOM

Observe on " B25 Bus" scope that because of the lack of reactive power support, the voltage at bus "B25" now drops to 0.91pu[Fig.10]. This low voltage condition results in an over load of the IG of "Wind Turbine 1". "Wind Turbine 1" is tripped at t=13.43 s. If you look inside the "Wind Turbine Protections" block you will see that the trip has been initiated by the AC Over current protection.
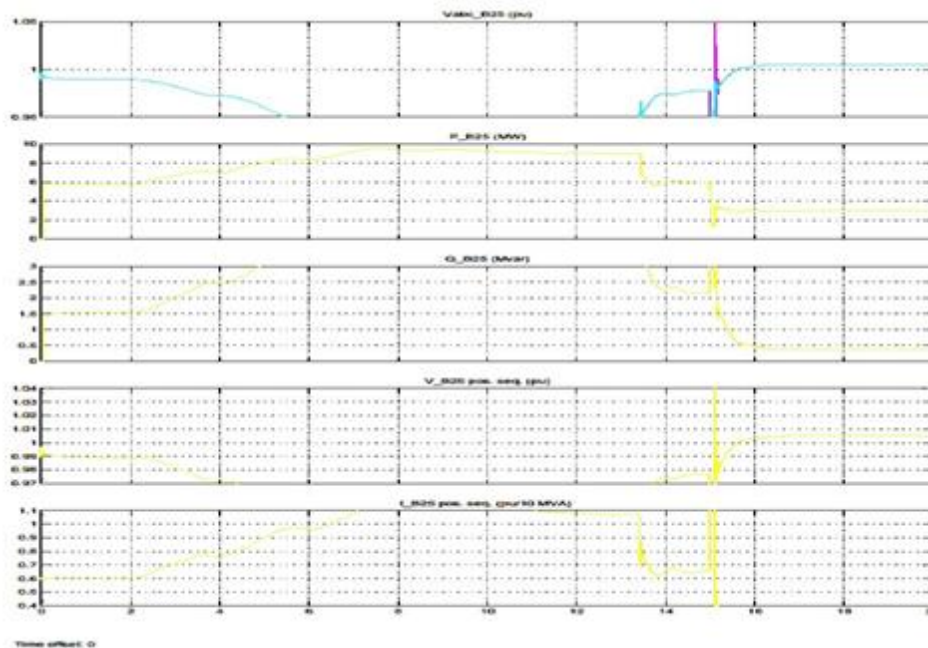
Figure9**:** Waveforms of different quantities without STATCOM

V. CONCLUSION

Power system with wind farms performance can be improved using FACTS devices such as STATCOM. The dynamic model of the studied power system is simulated using Simulink Matlab package software. To validate the effect of the STATCOM controller of power system operation, the system is subjected to different disturbances such as faults and power operating conditions. The digital results prove the powerful of the proposed STATCOM controller in terms of Stability improvement, power swings damping, voltage regulation, and increase of power transmission and chiefly as a supplier of controllable reactive power to accelerate voltage recovery after fault occurrence.

REFERENCES

[1]   V. Akhmatov, Knudsen, A.H. Nielsen, J.K.pedersen, and N.K. poulsen,"A dynamic stability limit of grid connected induction generators", Pro.International IASTED conference on power and energy systems,marbella, spain, 2000.

[2]   L. holdsworth, X.G. Wu, J.B. EKanayake, and N. Jenkins, "Comparison of fixed-speed and doubly-fed induction generator wind turbines during power system disturbances", IEEE proc. C-Gener. Transm. Distrib. , vol.150, no. 3, pp. 343-352, 2003.

[3]   S.M. Bolik, "Grid requirments challenges for wind turbines", Fourth International Workshop on large-scale Integration of Wind Power and transmission networks for Offshore Wind Farms, Oct .2003.

[4]   L. Holdsworth, N.Jenkins, and G. Strbac, "Electrical stability of large,offshore wind farms", IEEE seventh International Conference on AC-DC power Transmission, pp.156-161-2001.

[5]   Lie Xu Liangzhong Yao Sasse, C.," Comparison of using SVC andSTATCOM for wind farm integration", International Conference on
Power System Technology, pp. 1-7, Oct 2006.

[6]   N. G. Hingorani and L. Gyugyi, "Understanding FACTS: Concepts and Technology of Flexible AC Transmission Systems", IEEE, New York,2000, ISBN 0-7803, pp. 3455-3458, 2000.

[7]   EL-Moursi, M.S. and Sharaf,A.M, "Novel STATCOM controllers for voltage stablization of wind energy scheme", Int. J. Global Energy Issues,vol. 26, 2006.

[8]   F.G.R. de campos and A.A. Jr. penteado, "Wind Energy generation Simulation with asynchronous generator connected to ENERSUL distribution System", IEEE/PES Transmission and Distribution conference and Exposition, Latin America, pp. 149-154, 2004.

[9]   Siegfried Heier, "Grid integration of wind energy conversion systems", Jon Wiley & Sons Ltd, 1998.

[10]   E. Uzunovic, "Transient Stability and Power Flow Models of VSC FACTS controllers," Ph.D. dissertation, University of Waterloo,Waterloo, ON, Canada, 2001.

[11]   N. Mithulananthan, C. A. Canizares, J. Reeve, and G. J. Rogers,"Comparison of PSS, SVC and STATCOM controllers for dampingpower system oscillations", IEEE Trans. Power Systems, vol. 18, no. 2,pp. 786–792, May 2003.

Modeling Of Converter "Single Phase to Three Phase by Using Single Phase Supply"

Manikant Kumar[1], Er. Sudhanshu Tripathi[2]

[1] *(PG student, Electrical Department, SHIATS-DU, Allahabad-211007)*
[2] *(Faculty, Electrical Department, SHIATS-DU, Allahabad-211007)*

Abstract: *In Industrial application, two form of Electrical Energy is used. Direct current (DC) form and Alternative current (AC) form. In this paper single phase to three phase converter model is developed with the help of SIMULINK tool box of the MATLAB software. First of all single phase AC power is converted into DC power using diode rectifier bridge after this DC power is converted into three phase AC power with the help of three arms IGBT Inverter bridge. After the three phase conversion Three phase Induction Motor is run. They are ideal for future workshops, small industry, large building. Using the simulation result output of the model can be varied as per requirement of the applications.*
Keywords: *AC source, two arm universal bridge, Transformer, inverter, PWM generator*

I. INTRODUCTION

A wide variety of commercial and industrial electrical equipment requires three-phase power. Electric utilities do not install three-phase power as a matter of course because it costs significantly more than single-phase installation. As an alternative to utility installed three-phase, rotary phase converters, static phase converters and phase converting variable frequency drive have been used for decades to generate three –phase power from a single-phase source.

1. Single- phase –In electrical engineering, single-phase electric power refers to the distribution of alternating current electric power .unison system in which all the voltages of the supply vary in unison. Single-phase distribution is used when loads are mostly lighting and heating, with few large electric motors. A single-phase supply connected to an alternating current electric motor does not produce a revolving magnetic field. Single-phase motors need additional circuits for starting, and such motors are uncommon above 10 or 20 KW in rating.

2. Three-phase- In electrical engineering, three-phase electric power system have at least three conductors carrying alternating current voltages that are offset in time by one-third of the period. A three-phase system may be arranged in delta (Δ) or star (Y). A delta system arrangement only provides one voltage magnitude, however it has a greater redundancy as it may continue to operate normally with one of the three supply windings offline, albeit at 57.7% of total capacity. Harmonic currents in the neutral may become very large if non linear loads are connected. Power electronics is a very interesting technology to produce a circuit which is very small size. In olden days people were using a very complicated circuit, which was bulky, costly and low efficient. But power electronics has made it less weight, low cost and produce high efficiency .Embedded system is used along with power electronics to reduce the component size ,easy to handle but it require a high maintenance for the circuit.

Power electronic system is virtually in every electronics device. For example AC/DC converters (rectifiers) are used every time an electronic device is connected to television and computer. Inverter is broadly classified into two types namely voltage source inverter and current source inverter. Converting a single phase to three phase power supply uses semiconductor devices such as BJT (full form).

DC/AC converter are used primarily in UPS (full form) or emergency light .During blackout time the AC will be used to produce AC electricity at its output to power up the appliances

IGT (full form) is a current controlled device which operates only at low frequencies. The main disadvantages of using BJT is that high switching losses but lower conduction loss.

II. PROPOSED MODEL

"Single phase to three phase converter using BJT bridge" is our proposed model which uses an advanced technique such as converter to generate DC current .this paper represented single phase AC supply to converted three phase .

Converting a single phase to three phase power supply consists of two main circuits. These circuits are used to convert AC to DC supply and DC to AC supply for converting a single phase of low voltage to three phase of high voltage. They are

1. Power circuit

   Rectifier circuit

   Two arms universal bridge

   Liner Transformer

   3Φ Inverter circuit

2. Control circuit

   Power supply circuit

   PWM Generator

Control circuit is provided pulse three phase inverter. Power circuit is used to convert the single phase power supply to three phase power supply. It includes conversion of AC to DC supply using rectifier and DC to AC supply inverter.

III. BLOCK DIAGRAM

As we all know any invention of latest technology cannot be activated without the source of power. All the electronic or electrical components needs power supply of AC supply. So, we are converting power from single phase AC supply into three phase AC supply. Using these three phase power supply, we can drive any motor. Block diagram of converting single phase to three phase power supply units consists of.

Single phase AC supply

Liner transformer

Two arm universal bridge

Rectifier

3Φ inverter

3Φ transformer

Load
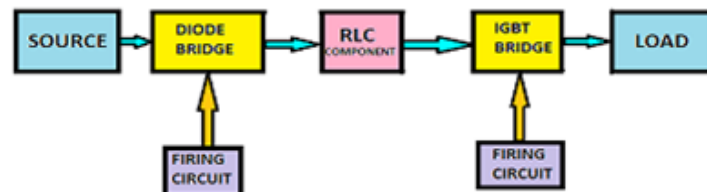
AC power supply of 380 volt is connected to liner transformer and liner transformer connected to two arms universal bridge converter, converter converted to DC 100 volt power supply to the rectifier .Rectifier rectifies the voltage and transferred to three arms IGBT .IGBT converts three phase power supply. It is mainly used in small industry, large building, workshop, etc.

The two arm universal bridge converter convert AC single phase power to DC power and rectifier, rectified DC power an inverter invert three phase power supply

IV. CIRCUIT EXPLANATION
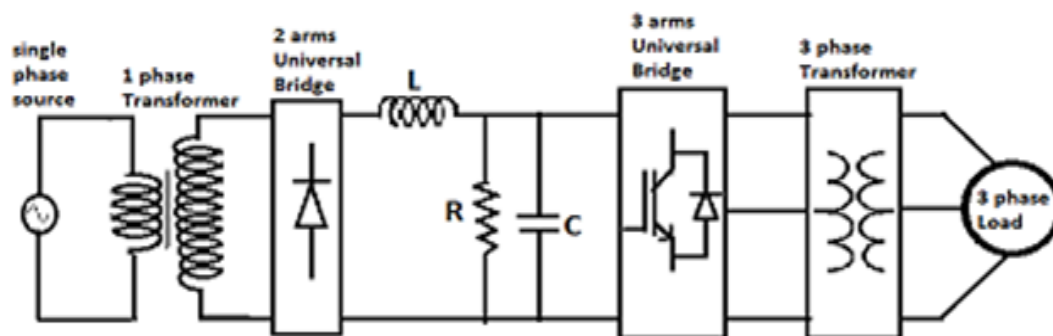
Power supply units consist of
1 Single phase supply
2 Liner transformers
3 Bridge circuit

When AC voltage is applied to the primary of the transformer, it can be stepped up depending upon the value of AC voltage needed. In our circuit the transformer of 380 volt and supply three phase power 180 volt. Changing transformer rating and three phase power also change. A commonly used circuit for supply AC source is bridge rectifier. A bridge rectifier of four diodes is used to achieve full wave rectification. Two diode will conduct during the positive half cycle and other two will conduct during negative half cycle. The AC voltage at the output terminals of bridge rectifier is less than 90% of RMS value.

The inverter converts DC supply to AC supply. Three winding transformer is connected with inverter to step up the voltage from the output and feed it to rectifier.

Three Phase Inverter
In three phase inverter there are three types they are

2 Level output
3 Level output
5 Level output

Matlab Simulink Tools
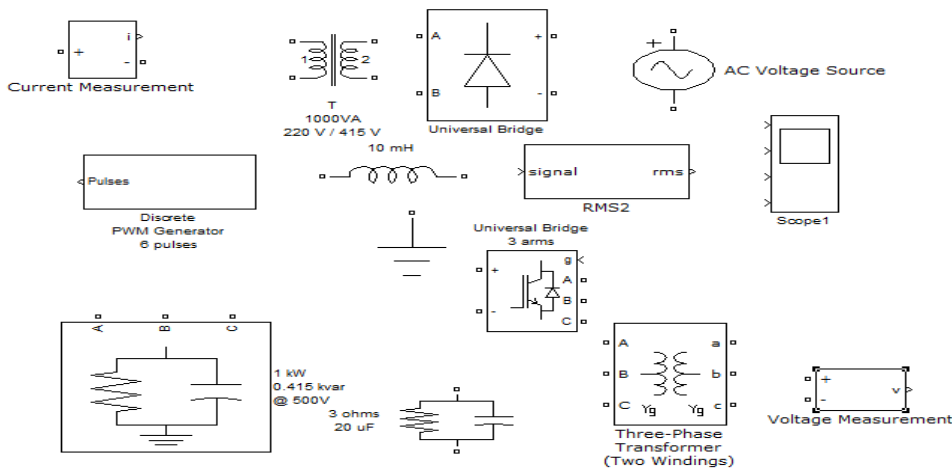
AC source	Peak amplitude(V) 325, frequency(HZ)50
Liner transformer	**Nominal Powe1000 VA ,frequency 50 HZ, primary winding voltage 220,resistance(pu)0.01,inductance(pu)0.002 ,secondary winding voltage 415,resistance o.01,inductance 0.02,magnetization resistance 25(pu) and reactance 25(pu0**
Two arm universal bridge	**Snubber resistance 25(ohms), snubber capacitance 0.1e-6(F), power electronics diode**
Three arms IGBT diode bridge	**Snubber resistance 100(ohms),forward voltage device I, forward voltage diode1**
Three phase transformer	**Nominal power 1000 VA, Power frequency 50 HZ, primary winding voltage220, resistance0.002, inductance 0.04, secondary winding voltage 770,resistance 0.002,and inductance 0.04**
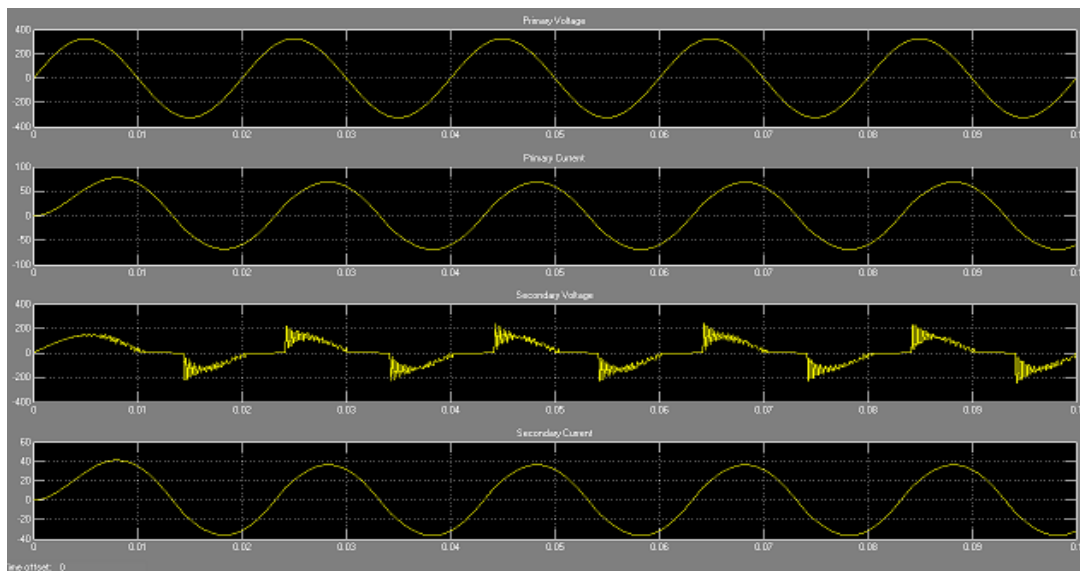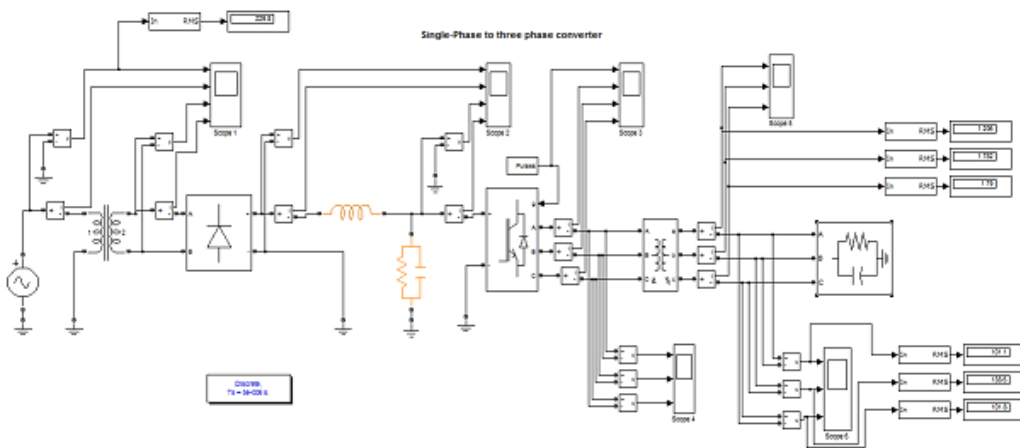
Transformer primary and secondary voltage and current
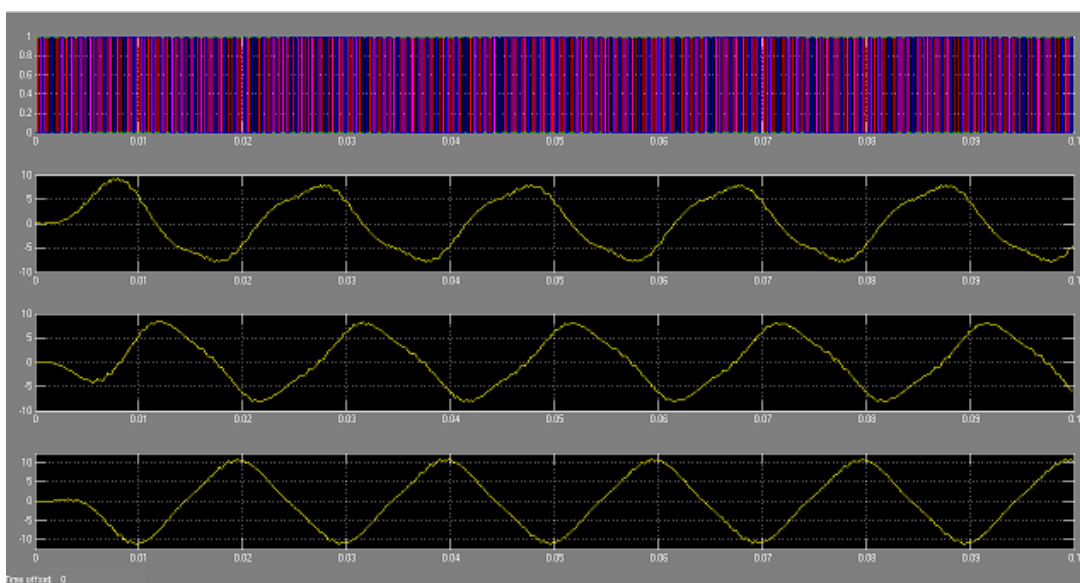
Pulses and inverter current
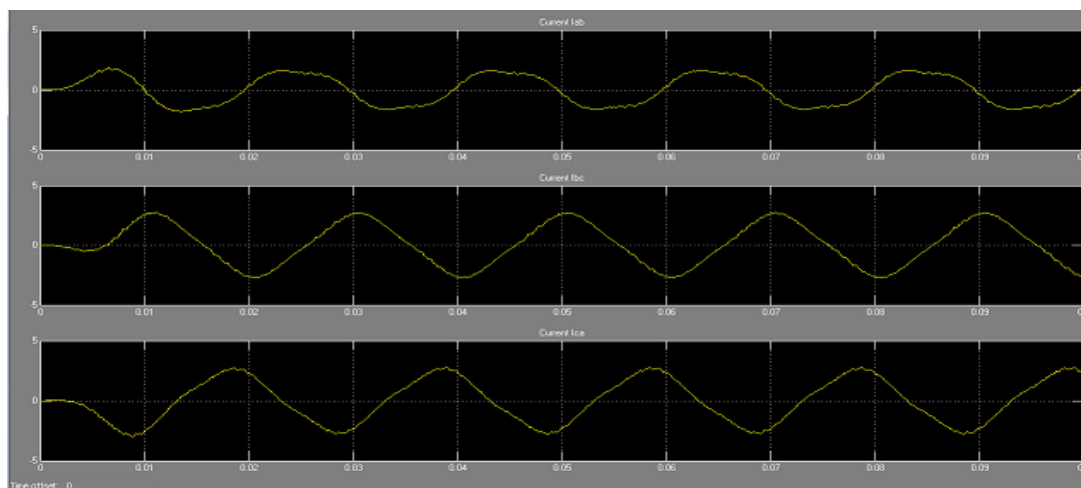
Phase currents Iab, Ibc, Ica
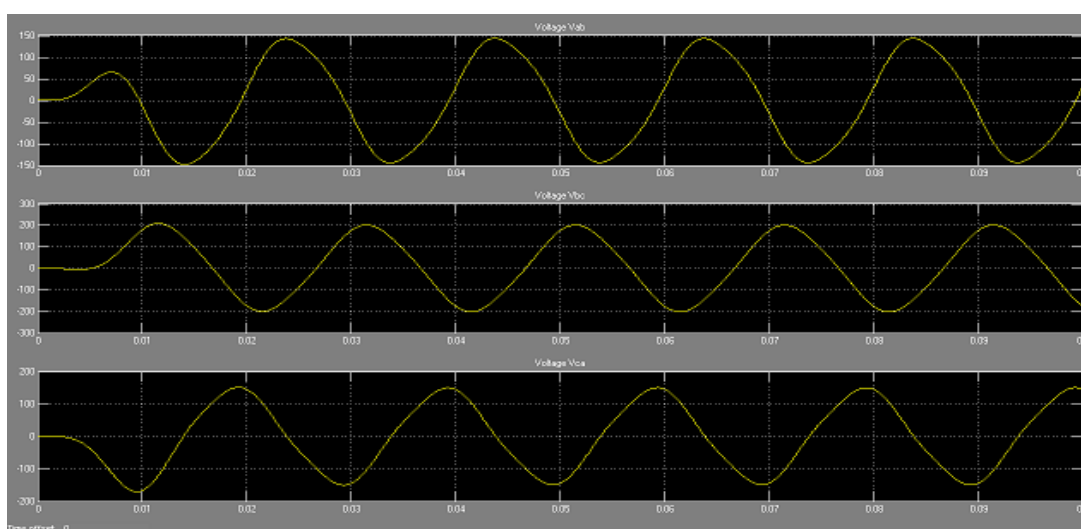
Phase voltage Vab , Vbc ,Vca

V. CONCLUSION

The propose model of single phase to three phase converter is mainly used in starting three phase induction motor, small industry, large building , workshop areas. The main advantage of our model is input AC single phase source but output is three phase supply. The output of the proposed model is increased by increasing the transformer rating and other components involved in converting single phase to three phase converter using inverting cost is also increased according to the required output. Simulation result is shown using MATLAB software is used to verify operation principle.

REFERENCES

[1]   H.S. Patel and R.G. Hoft, "Generalized techniques of harmonic elimination and voltage control in thyristor inverters: Part I- Harmonic elimination," IEEE Trans. Lod.Applicat,vol.IA-9,no.3,pp.310-317,May/June 1973

[2]   Z. Ye, D. Boroyevich, J.-Y. Choi, and F. C. Lee, ―Control of circulating current in two parallel three-phase boost   rectifiers,‖ IEEE Trans. PowerElectron., vol. 17, no. 5, pp. 609–615, Sep. 2002.

[3]   C. B. Jacobina, M. B. de R. Correa,A.M. N. Lima, and E. R. C. da Silva, ―AC motor drive systems with a reduced switch count converter,‖ IEEETrans. Ind. Appl., vol. 39, no. 5, pp. 1333–1342, Sep./Oct. 2003

[4]   Mazin, Hooman Erfanian; Gallant, Joey (August 14,2009, 2010) " A Probabilistic Analysis on the Harmonic Cancellation Characteristics of the Scott Transformer Electromagnetic Analysis & Applications 2: 18-24.Retrieved 20 December 2011

[5]   Sunil Kumar Mahapatro, "MPPT Based Solar PV System for 3 Phase Grid connected IGBT Inverter System using POWER-GUI Environment" International Journal of Engineering Research & Technology (IJERT) Vol. 2 Issue 4. April-   2013.

Books
[6]   Muhammad H. Rashid, "Power electronics: circuits, devices, and application "3rd ed .2004, Pearson /prentice Hall.
[7]   P.C. Sen, "Power Electronics", Tata Mcgraw-hill,
[8]   Dr. P. S.Bimbra (2011) "Power Electronics" in Fourth Edition

Manikant Kumar is a research scholar pursuing M.Tech in Power Electronics from Sam Higginbottom Institute of Agriculture Technology & Science Allahabad ,(U.P) India. He Secured Degree of B.Tech in Electrical Engineering from V.B.S.P.U Jaunpur (U.P) India 2012

Sudhanshu Tiwari presently working as Assistant Professor in Electrical & Electronics Engineering at Sam Higginbottom Institute of Agriculture Technology & Sciences, Allahabad, (U.P) India. The degree of B.Tech secured in Electrical & Electronics Engineering from U.P TECH University 2004 and M.Tech. in Digital Communication I from Moti Lal Nehru National Institute of Technology, Allahabad in 2007.

.

Matlab Simulation And Comparison Of Single Phase To Three Phase Converter Fed Induction Motor Drive Using One And Two Rectifier

Ashish Dongre[1], Sanjay Dhamse[2]

[1,2] *(Electrical Engineering Department, Government College of Engineering Aurangabad, India)*

Abstract: *This paper presents MATLAB simulation and comparison of three phase induction motor drive supplied from single phase supply with one rectifier and two rectifiers systems. To meet the new harmonic regulation produced by converters both system incorporates an active input current shaping feature that results in sinusoidal input current at close to unity power factor. Even with the increase in the number of switches, the total harmonic distortion in supply current of the parallel connected two rectifier system is lower than that of a conventional one. The model of the system is developed in MATLAB software. All simulation results and comparison are presented as well.*

Keywords: *AC to DC to AC converter, high power factor converters, parallel converter, Vector control.*

I. INTRODUCTION

In many villages only single phase supply is available. Farming, residential appliances require motors of different type for various operations such as pumping, grinding, material movement *etc*. Motors used in such operations may be rated in kilo watt power range and single phase motor is not suitable for such higher power ratings. Further three phase motors have many advantages over single phase motors in terms of machine efficiency, power factor, and torque ripples. The idea of operating a three phase motors from single phase supply is not new [1]-[3].

Conventionally a three phase induction motor drive consists of a front end full bridge controlled rectifier, dc link capacitor and an inverter as shown in figure 1. It consists of maximum ten switches. This type of configuration requires higher power rating switches in rectifier compared to inverter side [4]. Whereas a parallel connected system consists of a parallel connected full bridge front end controlled rectifier, dc link capacitor bank and a regular six-switch pulse width modulated (PWM) inverter to power a three-phase induction motor from a single-phase ac mains. The block diagram of parallel rectifier system is shown in figure 2. This parallel connected rectifier configuration in all consists of 14 switches. Due to parallel connection the power rating of the rectifier switches is reduced. There has been a considerable increase in the use of parallel converters to improve the power capability, reliability, efficiency, redundancy, and to decrease the cost.
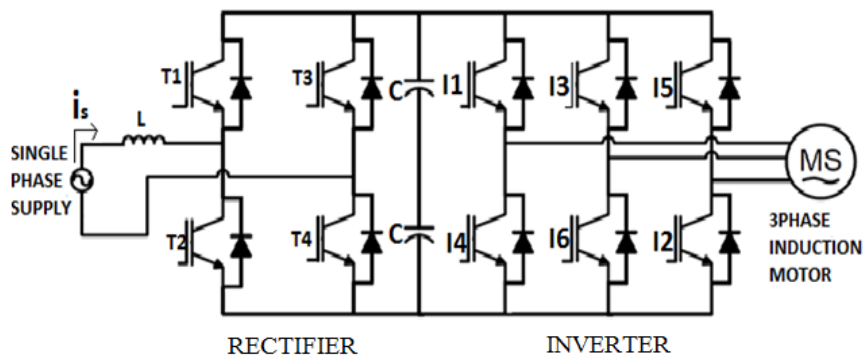
Figure 1: Conventional single phase to three phase induction motor drive

New regulations impose more strict limits on current harmonics injected by power converters [5]. These limits can be achieved with the help of pulse width-modulated rectifiers. These PWM converters, consists of power switches like insulated gate bipolar transistors (IGBTs), gate-turn-off thyristors (GTOs), or integrated gate

controlled thyristors (IGCTs) in the power circuit of the rectifier to change actively the waveform of the input current, reducing the distortion [6]-[7].
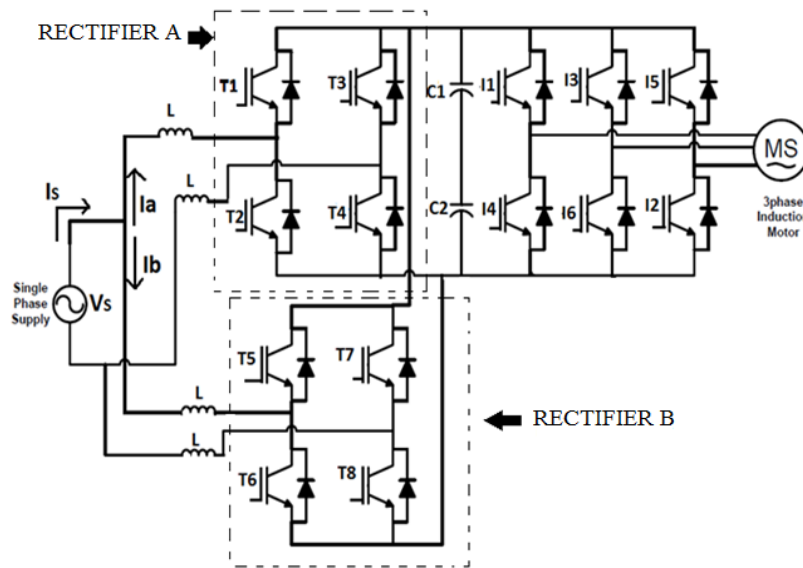
Figure 2: Parallel rectifier connected single phase to three phase induction motor drive

II.   Two Rectifier System

The two rectifier system as shown in figure 2 (control circuit for rectifier and inverter is not shown) consist of parallel connected front end rectifier supplied from single phase supply, input inductors, dc link capacitor bank and an inverter whose control signals are generated from vector control method which is discussed later in this paper. Upper rectifier is made up of switches T_1, T_2, T_3 and T_4 and lower rectifier is made up of switches T_5, T_6, T_7 and T_8. These two rectifiers are connected in parallel. The three phase inverter is composed of three legs having switches I_1, I_2, I_3, I_4, I_5, and I_6. The dc link capacitor banks which are connected between rectifiers and inverter helps in removing the ripple content of rectifier output. All switches are IGBT switches. Three phase induction motor is supplied from the three phase inverter output. Considering all the supply inductor equal the equations of the parallel connected configuration can be given as

Supply current	$i_s = i_a + i_b$	(2.1)
Output voltage	$V_o = V_a + V_b$	(2.2)
Rectifier A voltage	$V_a = V_s - 2(r + pl_a)i_a$	(2.3)
Rectifier B Voltage	$V_b = V_s - 2(r + pl_b)i_b$	(2.4)

Where $p = \dfrac{d}{dt}$ & r & l represents resistance and inductance of the inductor

III.   Rectifier Circuit Working Principle and MATLAB Implementation.

3.1. Working Principle of PWM rectifier

To understand the working, consider the conventional circuit of fully controlled single phase PWM rectifier as shown in figure 3 below. It consists of four controlled power switches with anti-parallel diode. For the proper working of this rectifier the output voltage V_o must be greater than input voltage V_s any time [7].This rectifier can work in two or three levels. The possible combination is as follows.

1.	$T_1 = T_4 =$ ON $T_2 = T_3 =$ OFF	$V_{PN} = V_o$	Fig3.2(a)
2.	$T_1 = T_4 =$ OFF $T_2 = T_3 =$ ON	$V_{PN} = -V_o$	Fig3.2(b)
3.	$T_1 = T_3 =$ ON $T_2 = T_4 =$ OFF	$V_{PN} = 0$	Fig 3.2(c)

And the voltage across inductor can be given as

$$V_l = L\frac{di_s}{dt} \qquad (3.1)$$

$$V_l = V_{s(t)} - KV_o \qquad (3.2)$$

Where K= 1, - 1 or 0.

If k=1 then the inductor voltage will be negative, so the input current will decrease its value.

If K=-1 then the inductor voltage will be positive, so the input current will increase its value.

If K=0 the input current increase or decrease its value depending on V_s. This allows for a complete control of the input current [7].
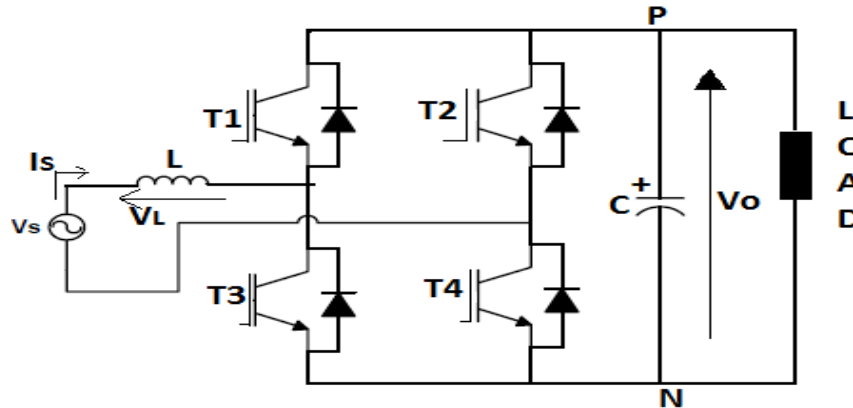
Figure 3.1: Single-phase PWM rectifier power circuit
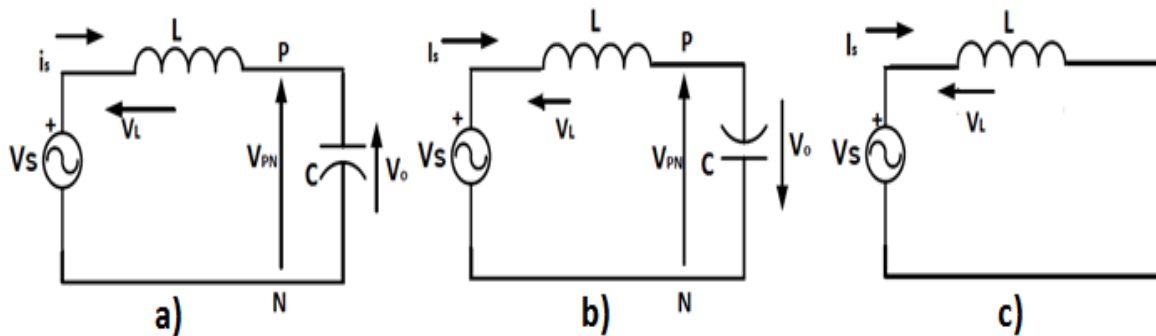
Figure 3.2: Single-phase PWM rectifier power circuit
a) $T_1=T_4$=ON   b) $T_1=T_4$=OFF c) $T_1=T_3$=ON

3.2. Control Scheme in MATLAB

The main objective of PWM rectifier is to maintain dc link voltage constant and to maintain input power factor close to unity. The dc-link voltage V_c is adjusted to its reference value V_c^* using the standard PI controller. This controller provides the amplitude of the reference supply current I_s^* as shown in figure 4.1. To control the power factor and harmonics in the supply side, the instantaneous reference current I_s^* is synchronized with voltage V_s, as given in the voltage-oriented control (VOC) for three-phase system [8]-[9].This synchronization is obtained by a phased locked loop (PLL) scheme in MATLAB. The reference currents I_a^* is again given to the controller which defines the input reference voltages V_a^* and then it is compared with the triangular wave to obtain the gating signals for rectifier as shown in figure 4.2. This scheme can be further extended to two rectifiers system. The only thing which needs to be done in two rectifier system is to divide grid current equally to obtain pulses for both the rectifiers.
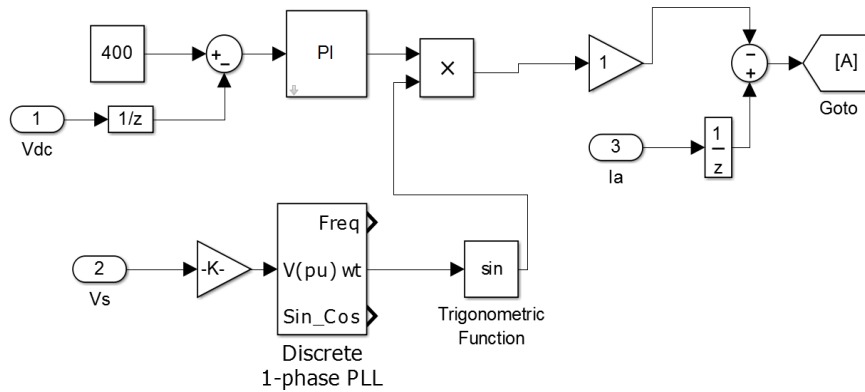
Figure 4.1: Control circuit of rectifier (part1)
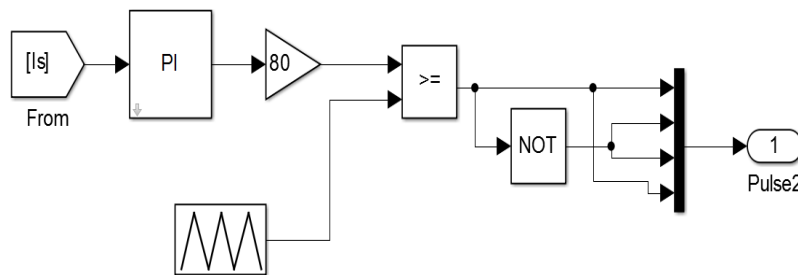
Figure 4.2: Control circuit of rectifier (part2)

IV. Vector Control Induction Motor

The three phase induction motor is fed by current controlled inverter. The control signals for inverter are derived from vector control method which helps in controlling the motor. Figure 7 shows the block diagram of vector controlled induction motor.
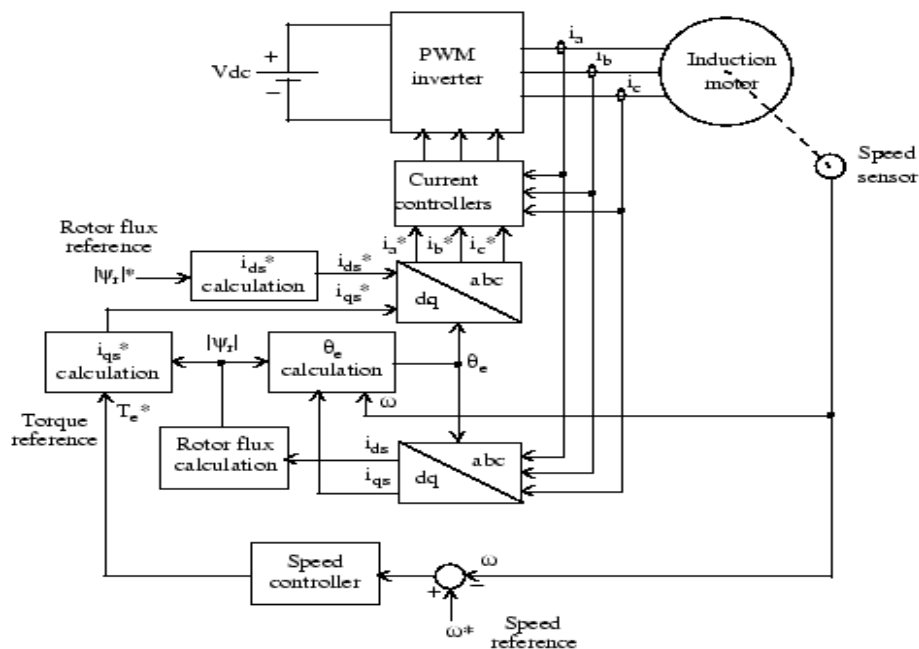
Figure 5: Block diagram of vector control induction motor

In vector control the motor speed ω is compared to the reference speed ω^* and the error is processed by the speed controller to produce a torque command T_e^*. The stator quadrature axis current reference i_{qs}^* is calculated from torque reference T_e^* using equation (4.1). The flux component of current i_{ds}^* for the desired

rotor flux is calculated from equation (4.4). The rotor flux position θ_e required for coordinates transformation is generated by integrating the rotor speed ω_m and slip frequency ω_{sl} given by equation (4.5). The reference quadrature axis i_{qs}^* and direct axis i_{ds}^* current are converted into three reference currents i_a^*, i_b^*, i_c^* for the current regulators by two phase to three phase transformation [10]. The regulators process the measured actual and reference currents to produce the inverter gating signals.

$$i_{qs}^* = \frac{2}{3} \cdot \frac{2}{p} \cdot \frac{L_r}{L_m} \frac{T_e^*}{\psi_r} \qquad (4.1)$$

Where

$$\psi_r = \frac{L_m \cdot i_{ds}}{1 + \tau_r \cdot s} \qquad (4.2)$$

And

Rotor time constant is given by

$$\tau_r = \frac{L_r}{R_r} \qquad (4.3)$$

$$i_{ds}^* = \frac{\psi_r^*}{L_m} \qquad (4.4)$$

$$\theta_e = \int (\omega_m + \omega_{sl})\, dt \qquad (4.5)$$

The slip frequency ω_{sl} can be calculated by

$$\omega_{sl} = \frac{L_m}{\psi_r} \frac{R_r}{L_r} i_{qs}^* \qquad (4.6)$$

Figure 6 shows the block diagram of vector control method implementation in MATLAB. Internal structure of each block of vector control is shown in figure 7.
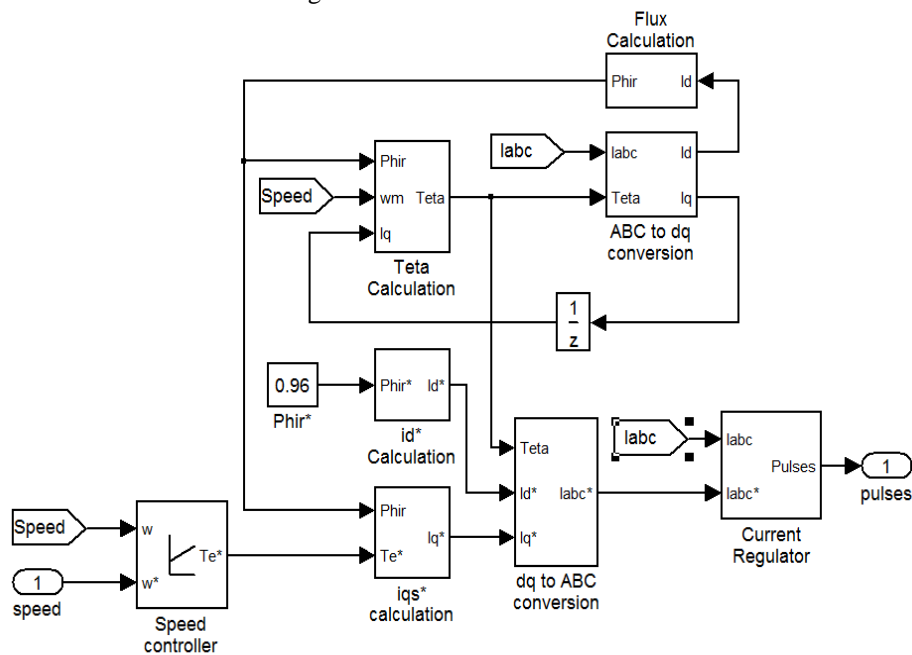
Figure 6: Block diagram of vector control in MATLAB
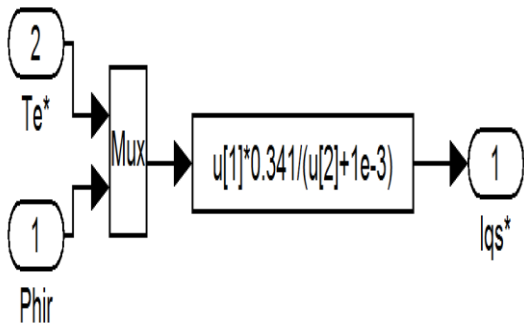
Figure 7.1: i_{qs}^* Calculation
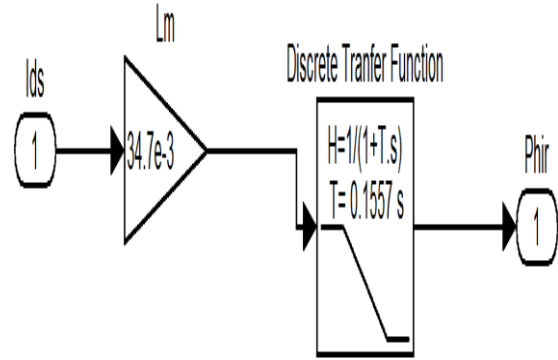
Figure 7.5: ψ_r or Phir Estimation
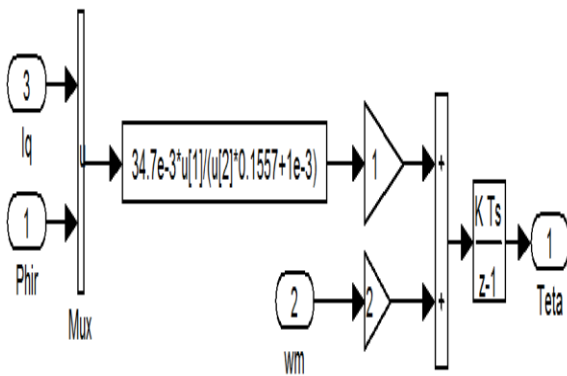
Figure 7.2: Theta or Θ_e Calculation
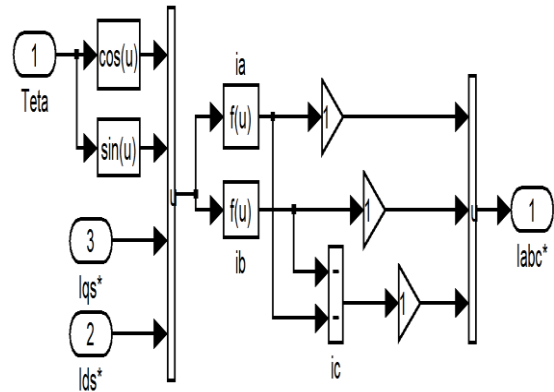
Figure 7.6: Two phase to three phase transformation
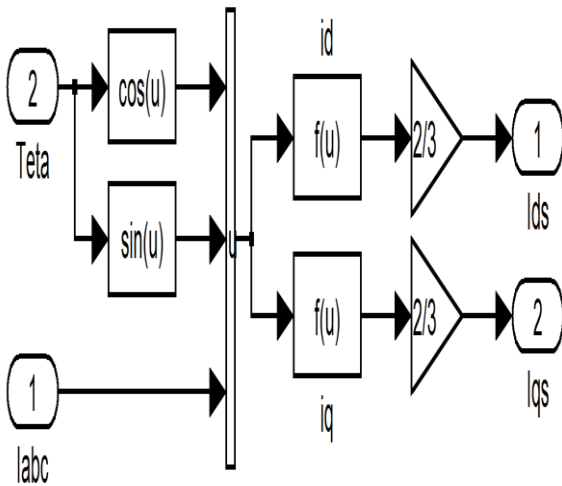
Figure 7.3: Three phase to two phase Transformation
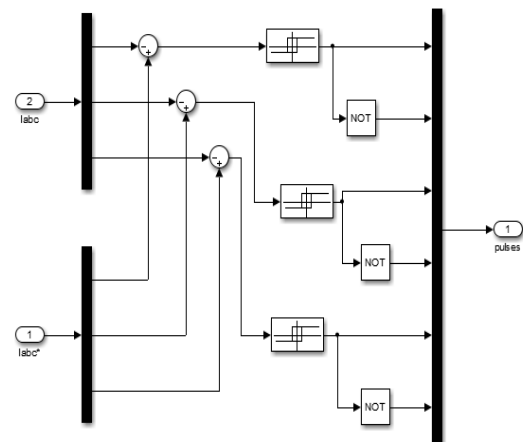
Figure 7.7: Hysteresis current controller
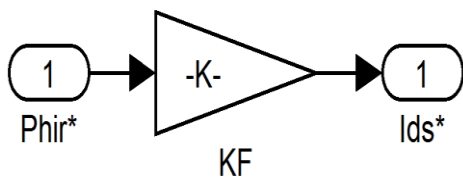
Figure 7.4: i_{ds}^* Calculation

Motor Used in Modeling

1 Hp, 3 phase squirrel cage induction motor		
Parameters		Value
R_s, L_{ls}	Stator resistance and leakage inductance	0.087 Ω, 0.8e-3H
L_m	Magnetizing inductance	34.7e-3H
p	Number of pole pairs	2
$R_r^{'}, L_{lr}^{'}$	Rotor resistance and leakage inductance	0.228Ω, 0.8e-3H
F	frequency	50 *Hz*
V_{L-L}	Line to line voltage	400v (Rms)

V. Complete System Model In MATLAB
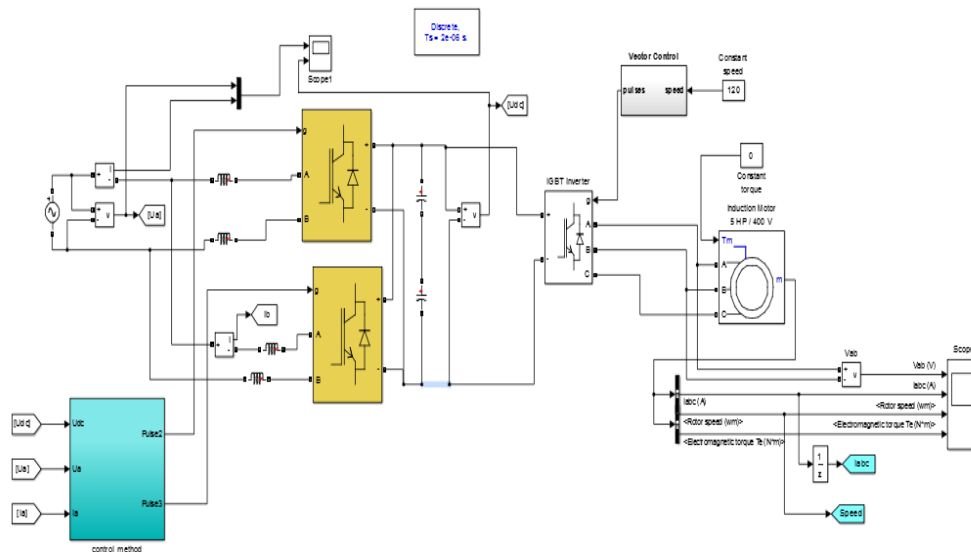
Figure 7: MATLAB model of two rectifier system
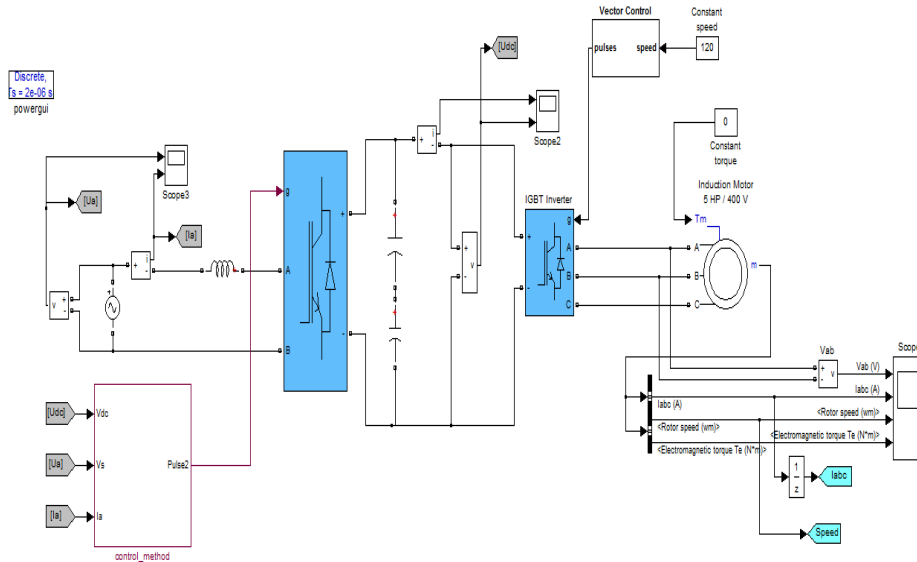
Figure 8: MATLAB model of one rectifier system (Conventional)

Both systems are developed in MATLAB software. The specification of the motor used in simulation is given in table 1. Figure 7 shows the complete developed model of two rectifier system and figure 8 shows the developed model of single rectifier system in MATLAB.

VI.   Simulation Results Of One Rectifier System (Conventional)
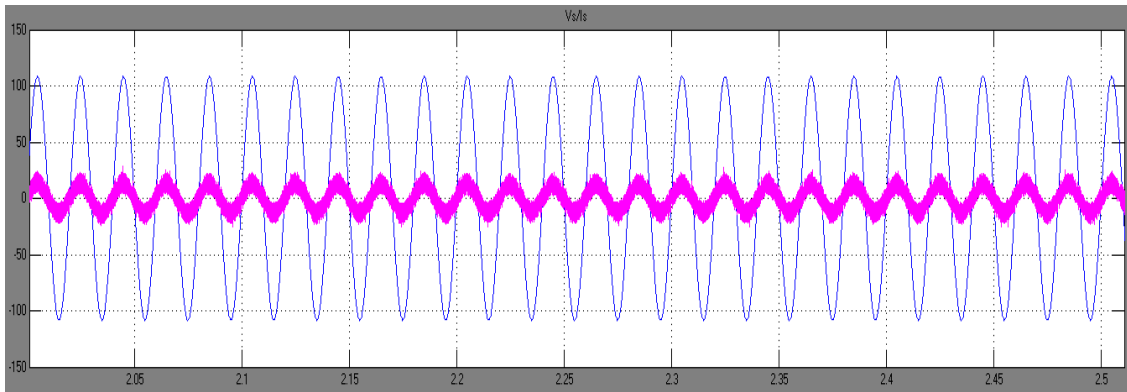
Figure 9.1: Input voltage and current
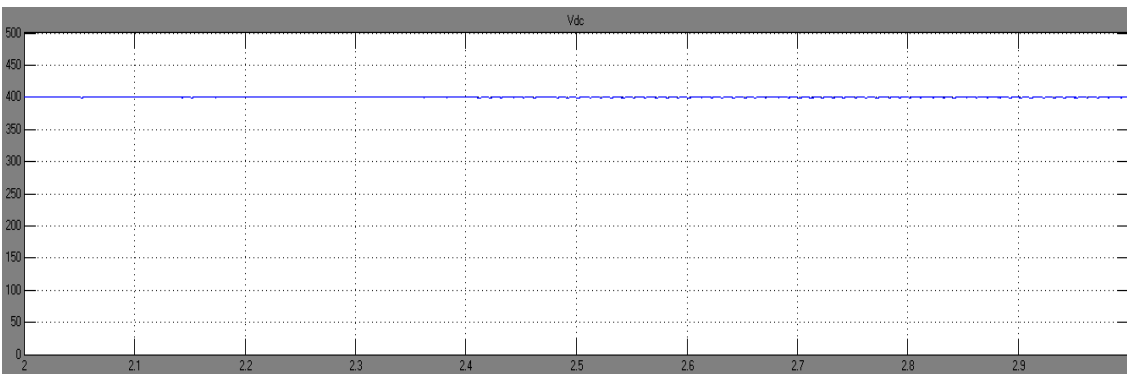
Figure 9.2: Dc link voltage
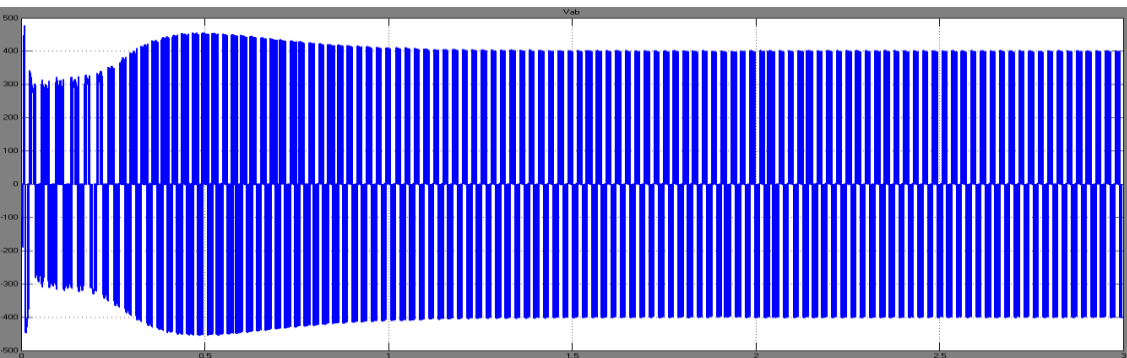
Figure 9.3: Phase voltage V_{a-b}
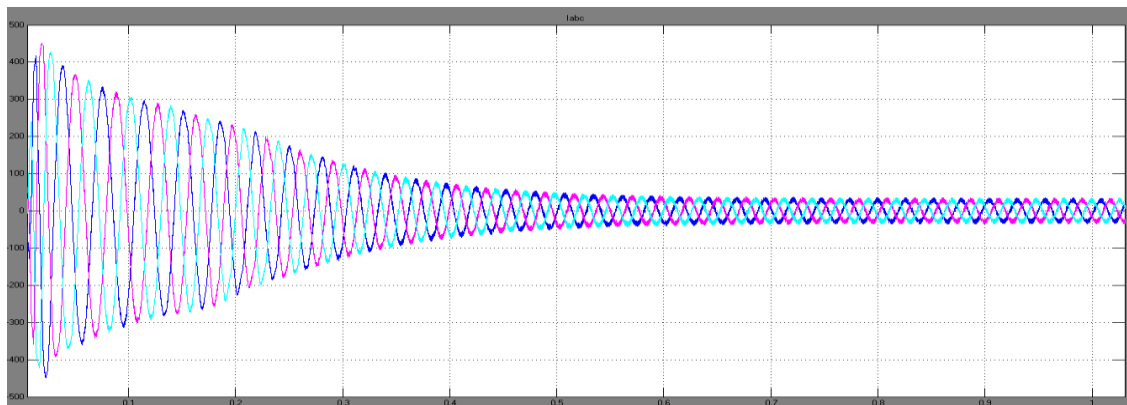
Figure 9.4: Three phase current
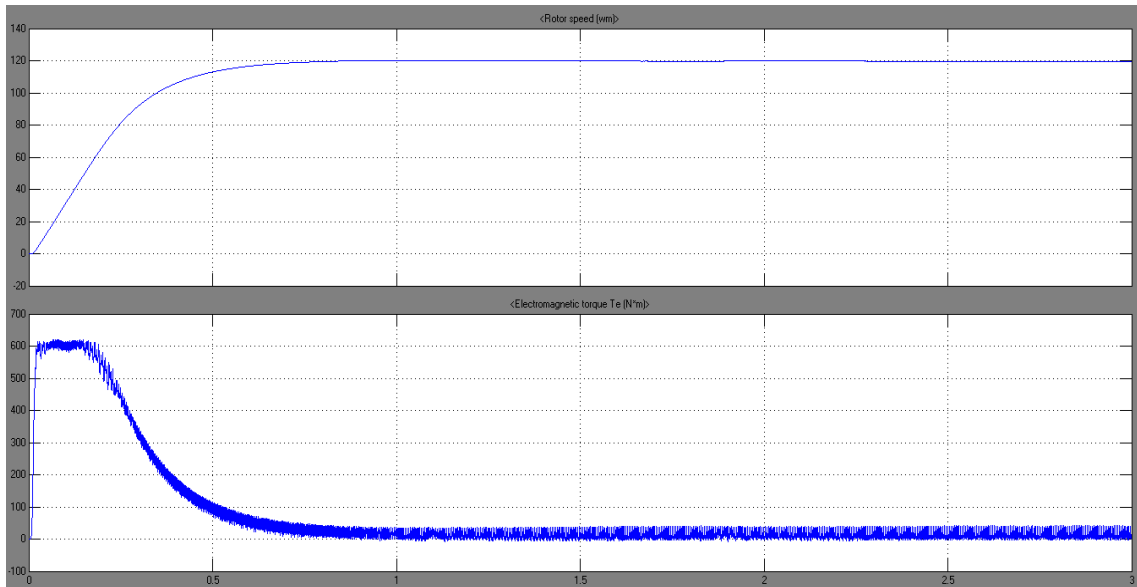
Figure 9.5: Speed and Electromagnetic torque T_e (Free acceleration $T_e = 0$)
Figure 9 Simulation result of one rectifier system

Figure 9 shows the simulation results of one rectifier system. Where figure 9.1 shows input voltage and current of supply. Figure 9.2 shows the dc link voltage whereas figure 9.3 phase voltage between phase a and b of the inverter output. The three phase current motor current is shown in figure 9.4. Speed and electromagnetic torque of motor for free acceleration is given in figure 9.5 similarly the simulation results of two rectifier system are given figure 10.

VII.   Simulation Results Of Two Rectifier System

Figure 10. Simulation result of two rectifier system
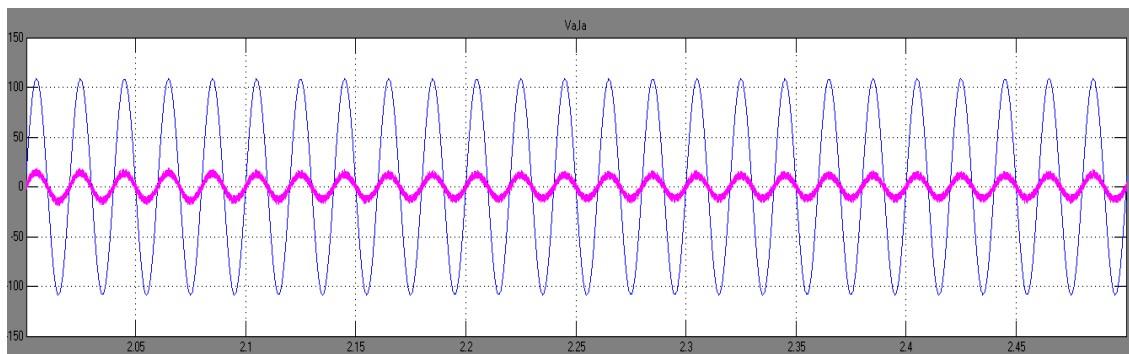
Figure 10.1: Input voltage and current
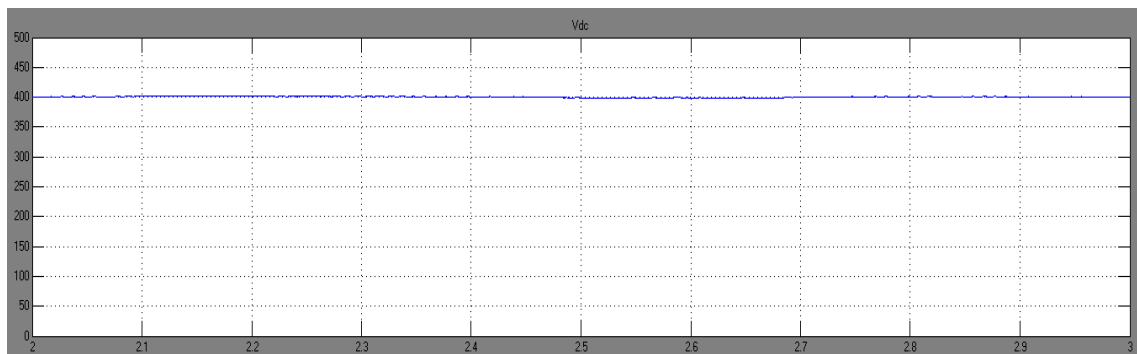
Figure 10.2: Dc link voltage
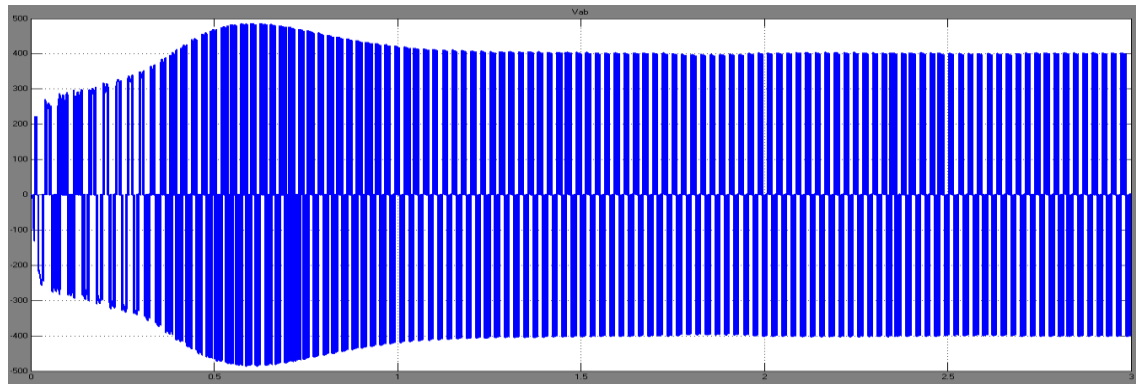
Figure 10.3: Phase voltage V_{a-b}
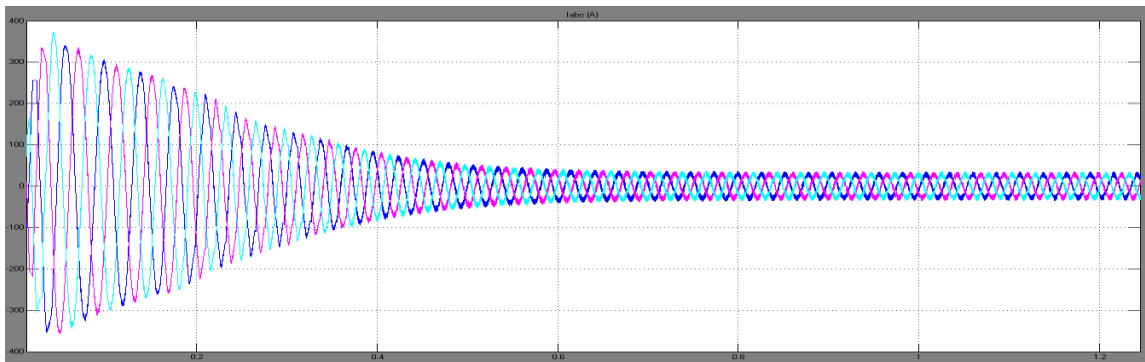
Figure 10.4: Three phase current
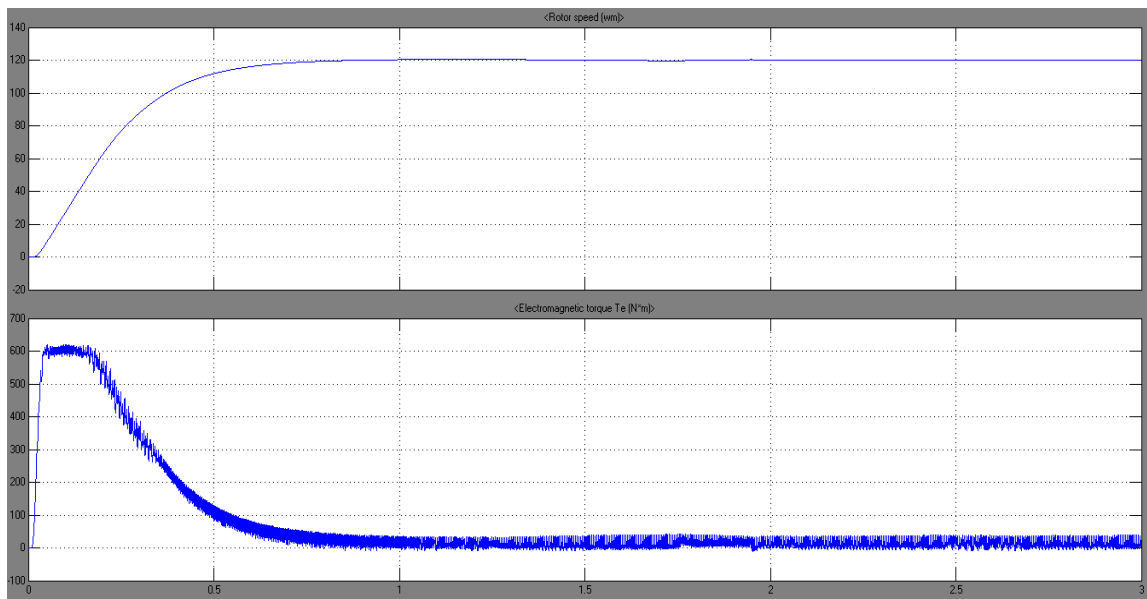
Figure 10.5: Speed and Electromagnetic torque T_e (Free acceleration $T_e = 0$)

Figure 10 shows the simulation results of two rectifier system. Where figure 10.1 shows input voltage and current of supply. Figure 10.2 shows the dc link voltage whereas figure 10.3 phase voltage between a-b phase of the inverter output. The three phase current motor current is shown in figure 10.4. Speed and electromagnetic torque of motor for free acceleration is given in figure 10.5

VIII.   Total Harmonic Distortion (THD) Analysis Of   Input Current

Simulation is run for 150 cycles and FFT analysis of input current is done. Following table shows the THD readings for different number of cycles. THD are measured from initial time i:e from zero

CONFIGURATION	PERCENTAGE THD IN INPUT SUPPLY CURRENT	NUMBER OF CYCLES	PERCENTAGE REDUCTION IN TWO RECTIFIER SYSTEM
One rectifier system	7.52	150	2.41
Two rectifier system	5.11		
One rectifier system	18.82	100	0.75
Two rectifier system	18.07		
One rectifier system	18.81	50	1.15
Two rectifier system	17.66		

Table 3 Comparison of two systems

Sr. No	Parameters	One rectifier (Conventional system)	Two rectifier (Parallel System)
1	THD	More	less
2	No of component	10	14
3	Cost	More	less
4	Input current shaping	Yes	Yes
5	Boost inductor	1	4

IX.   Conclusion

MATLAB simulation of three phase induction motor drive supplied from single phase supply with parallel connected rectifier and with one rectifier is developed in this paper. The parallel rectifier system helps to reduce the rectifier switch Currents, and the total harmonic distortion (*THD*) of the grid current with same switching frequency . In addition, the losses of the proposed system may be lower than that of the conventional counterpart. The system control strategy is fully developed and all the simulation results are presented. Because of the decrease in the rectifier switch current, the rating of switches decreases in rectifier circuit of proposed configuration which may helps in reducing cost of the system.

REFERENCES

[1]   P. Enjeti and A.Rahman, Jul./Aug. 1993. "A new single phase to three phase converter with active input current shaping for low cost AC motor drives," IEEE Trans. Ind. Appl., vol. 29, No.2, pp. 806–813.
[2]   Dong-Choon L and Young-Sin K, April 2007, "Control of Single-Phase-to-Three-Phase AC/DC/AC PWM Converters for Induction Motor Drives," IEEE Trans. On Ind. Electronics, vol. 54, No. 2 .
[3]   Euzeli C D S, Cursino B J, Edison R C d S, and Nady R, MAY 2012, "Single-Phase to Three-Phase Power Converters: State of the Art" IEEE Trans. On Power Electronics,VOL.27, NO. 5.
[4]   Euzeli Cipriano dos Santos, Cursino Brand˜ao Jacobina, MAY 2012, "Single-Phase to Three-Phase Power Converters: State of the Art" IEEE TRANSACTIONS ON POWER ELECTRONICS, VOL. 27, NO. 5.
[5]   Limits for Harmonic Current Emissions (Equipment Input Current up to and Including 16 A Per Phase), IEC 61000-3-2 International Standard, 2000.
[6]   B. Singh, B. N. Singh, A. Chandra, K. Al-Hadad, A. Pandey, and D. Kothari, "A review of single-phase improved power quality AC-DC converters, "IEEE Trans. Ind. Electron., vol. 50, no. 5, pp. 962–981, Oct. 2003
[7]   José R. R, Juan W. D, José R. E, Jorge P and Pablo L, Febrary 2005 ,"PWM Regenerative Rectifiers: State of the Art," IEEE Trans. On Ind. Electronics, vol. 52, no.1.
[8]   Cursino B J, Euzeli C d S, Nady R, and Edgard L L F, MAY 2010 ,"Single-Phase to Three-Phase Drive System Using Two Parallel Single-Phase Rectifiers" IEEESTrans. On Power Electronics, VOL. 25, NO. 5.
[9]   Mariusz M, Marian P. Kazmierkowski, and Andrzej M. T, November 2003 ,"A Comparative Study of Control Techniques for PWM Rectifiers in AC Adjustable Speed Drives," IEEE Trans. Power Electron., vol. 18, no.6.
[10]   Krause, P. C. Analysis of Electric Machinery. New York: McGraw-Hill, 1994.

Industrial Microcontroller Based Neural Network Controlled Autonomous Vehicle

D. Praveen Kumar[1], G. Sai Sudarsan[2], P. Dinesh[3], K Anil[4], Y. Govardhan[5]

[12345](*Department of Electronics and control Engineering, Sree Vidyanikethan Engineering College, India*)

Abstract: *This paper essentially deals with the design and implementation of a low cost autonomous vehicle which is controlled by neural network and is based on micro controller. The autonomous vehicle is equipped with a ultrasonic sensor for hurdle distance measurement, a GPS receiver for goal position information, a GSM modem for changing destination place on run time and a nonvolatile RAM for storing waypoint data; all these are interfaced to a Renesas RL78 microcontroller. This microcontroller processes the information acquired from the sensors and generates robot motion commands accordingly through neural network. The neural network which is running inside the microcontroller is a multilayer feed-forward network with back-propagation training algorithm which is trained offline with tangent-sigmoid as activation function for neurons and is implemented in real time with piecewise linear approximation of tangent-sigmoid function. This autonomous vehicle is tested to navigate inside college campus and has achieved better results.*

Keywords: *autonomous vehicle; ultrasonic sensors ;compass; GPS receiver ;GSM modem ;nonvolatile RAM ;tangent-sigmoid function approximation ;neural network ;microcontroller implementation.*

I. INTRODUCTION

Autonomous robots are robots that can perform desired tasks in unstructured environments without continuous human guidance. Many kinds of robots have some degree of autonomy. Different robots can be autonomous in different ways. A high degree of autonomy is particularly desirable in fields such as space exploration, cleaning floors, mowing lawns, and waste water treatment. Navigation is the ability of a mobile robot to reach the target safely without extended human assistance. So the main issues that are needed to be addressed in mobile robot navigation are obstacle avoidance and target acquisition.

Navigation comprises two tasks hurdle avoidance and goal reaching. Hurdle avoidance is achieved with the help of ultrasonic sensors and IR sensors. The data from these sensors is given to neural network running inside the primary microcontroller. To minimize the computational burden on the microcontroller, a neural network is implemented with piecewise linear approximation of tangent-sigmoid activation function for neurons. Goal reaching behavior involves the data from the ultrasonic sensors, IR sensors and GPS receiver which is processed by another microcontroller. The goal is a set of latitude and longitude location to which the robot need to navigate. The primary microcontroller fetches the desired data and generates motion commands for robot. A GSM modem which is interfaced to the main controller is used for selecting start and goal stations for robot inside the university campus.

II. PROTOTYPE

The prototype is implemented on a two wheeled mobile robot which is a made on chassis. The two microcontrollers, primary and secondary along with ultrasonic sensors, IR sensors, GPS sensor and GSM modem will be on the chassis while the chassis will be placed on the wheels that are driven by DC stepper motors along with a pivot wheel. The whole setup is driven by 18v DC power supply either from a battery or AC/DC adapter. The Quectel M10 GSM modem will be a used to communicate with the robot like sending the GPS coordinates or receiving the GPS coordinates of the robot. The GPS sensor which will work based on satellite navigation system will be continuously sensing the location which can be known through the commands. The Design of the prototype starts with mechanical design after which the circuit design is done. The mechanical design is done in such a way that all sensors are placed such that they cover the maximum area, which makes it easy to detect the sensors. All the other components are placed in appropriate places. Then circuit design was carried out in two phases, sensor part design and the control board design.
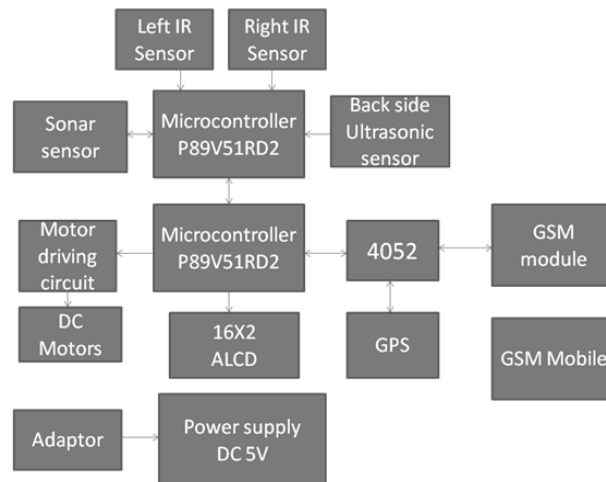
Figure 1.Block diagram

III. NAVIGATION SYSTEM

Navigation problem is decomposed into obstacle avoidance and goal reaching problems.
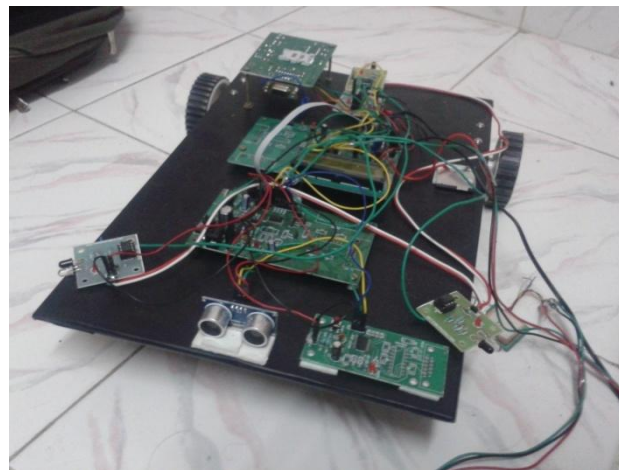
Figure 2. Experimental Prototype

A. Obstacle Avoidance

When a mobile robot is traveling towards its final target, it might face a variety of obstacles in its way. A neural network controller is designed to cope up with these situations.

***Neural network design*:** The neural network used is multi layer feed-forward network with back propagation learning algorithm and is designed using MATLAB® programming environment. The employed configuration contains 3 neurons in the input layer, 6 in the hidden layer and 4 in the output layer as shown in Fig. 4. The numbers of neurons in hidden layer are selected on trial and error basis. Three inputs to the neural network are distance information from 4 sensors. Centre and back sensors are combined to form one input while other two inputs are from left and right sensors. The outputs from the neural network are direct commands for motors. The activation function used for hidden layer is tangent-sigmoid function while pure linear function is employed in output layer.
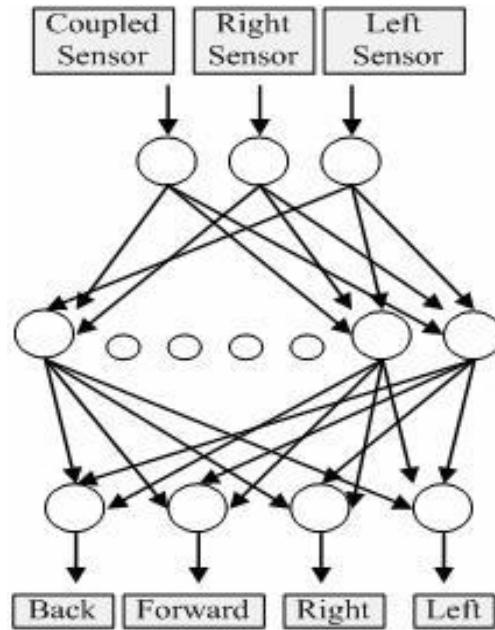
Figure 3. Neural Network Model

The output of a neuron can be expressed by the equation:
$$Yi = T (\Sigma j (Xj * Wij)) (1)$$
where T is the transfer function which is made user selectable, either sigmoid, threshold or custom made. This equation will be applied to calculate the output of hidden and output layer. For hidden layer, (1) will be
$$Hj = tansig (\Sigma j (Xj * Wij)), j = 1 \text{ to } 6, i = 1 \text{ to } 3 (2)$$
Similarly for output layer, (1) will be:
$$Oj = purline (\Sigma j (Xj * Wij)), j = 1 \text{ to } 4, i = 1 \text{ to } 6 (3)$$
Experimental data is divided into two sets: training data set and validation data set. During training, for each sample value, error is calculated between the desired output 'H' and network calculated output 'Y'. The following figure is the schematic of the neural network.

B. Goal Reaching:
$$E = H-Y (4)$$
The error is minimized by using backpropagation training algorithm. The algorithm minimizes the error by updating the weights and biases of the network. For a tangent-sigmoid function, new weights are calculated according to the relation:
$$Wnew = Wold + \eta (1 − \alpha) \Delta W + \alpha \Delta Wold (5)$$
where ΔW is the weight correction factor and α is the momentum factor used for convergence of network output to desired behavior by speeding up the iterative process. After performance goal is met in training phase, the network is tested with validation data set. This data set is used to avoid over-fitting the network to the training data. The training error graph showing the performance of network is shown in Fig. 5. 3) Neural network implementation: After Offline training in MATLAB®, the neural network is implemented using Renesas Microcontroller. Keeping in view the low memory and processing power of the microcontroller, tangent sigmoid function is converted in piecewise linear function for implementation in microcontroller and the converged weights are converted into integer form. The approximated function is described in the following equations.
The following equations are coded in the microcontroller.
$$f(x)=0.8x \text{ if } 0 \leq x <1 \; 0$$
$$f(x)=.2x + 0.6 \text{ if } 1 \leq x <1.8 (6)$$
$$f(x) = 0.05x + 0.87 \; 1.8 \leq x < 2.5 +1 \; x \geq 2.5$$

During navigation, if the obstacle avoidance system detects an obstacle, the control commands for avoiding the obstacle will override the normal commands provided by goal reaching system. In this case, vehicle will travel more distance than desired. The extra distance traveled by vehicle after avoiding the obstacle is recorded. Then knowing the current and destination (active waypoint) vehicle orientation, a new path is

generated along with new distance to be traveled to reach that waypoint. When the vehicle reaches within 5 meter of current waypoint, position value is read with the help of GPS receiver and new waypoint is loaded.

IV. RESULTS

Experiments performed with the prototype and the neural network simulations done on Matlab has proven better results for navigation in university campus the following are the results of the neural network toolbar are as follows.
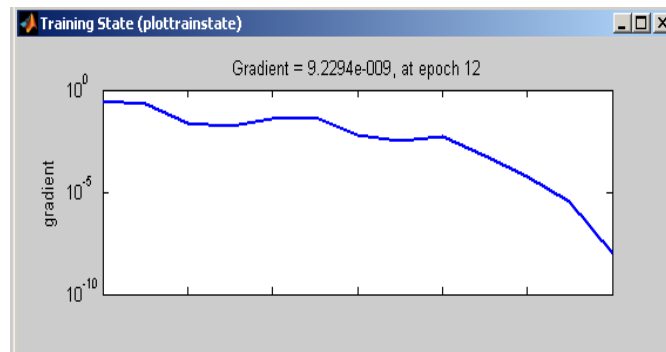
Figure 4. Training state

V. CONCLUSIONS

In this paper, design of a low cost autonomous vehicle based on neural network is presented for navigation inside the university campus. Equipped with various sensors, the vehicle has the capability of navigating in complex environments avoiding the obstacles in its way and reaching the target. The complexity of the system is reduced by making it modular i.e., more modules can easily be added to system by setting their priority level in the main controller.

REFERENCES

Journal Papers:
[1]   Nielsen L., "Automated Guidance of Vehicles using Vision and Projective Invariant Marking", Automatica 24:2, pp. 135-148, 1988.
[2]   Schraft R.D., "Mechatronics and Robotics for Service Applications", IEEE Robotics & Automation Magazine, pp. 31-37, December 1994.
[3]   Harris G., "Robotics Decontamination Keeps Operators Clear of Danger", Industrial Robot, 20:3, pp. 30-33, 1993.
[4]   Weisbin C.R., D.Lavery, " NASA Rover and Telerobotics Technology Program " , IEEE Robotic & Automation Magazine, pp. 14-20, December 1994.
[5]   Evans J., Krishnamurthy B., "Handling Real World Motion Planning A Hospital Transport Robot", IEEE Control Systems, pp.15-19, February 1992.
[6]   Orwig T, "Cybermotion's Roving Robots", Industrial Robot, 20:3, pp. 27-29, 1993.
[7]   Khaldoun K. Tahboub, Munaf S. N. Al-Din, "A Neuro-Fuzzy reasoning system for mobile robot navigation," Jordan Journal of Mechanical and Industrial Engineering, vol. 3 (1), pp. 77-88, March 2009.
[8]   Jonathan Milton Turner, obstacle avoidance and path traversal using interactive machine learning , M.S Thesis, Brigham Young University, August 2007.
[9]   Alexander Schepelmann, Henry H. Snow, Bradley E. Hughes, Frank L. Merat, Roger D. Quinn, "Vision-Based Obstacle Detection and Avoidance for the CWRU Cutter Autonomous Lawnmower"M Ozaki, Y. Adachi, Y. Iwahori, and N. Ishii, Application of fuzzy theory to writer recognition of Chinese characters, *International Journal of Modelling and Simulation, 18(2),* 1998, 112-116.

Control Chart Analysis of E_k/M/1 Queueing Model

T.Poongodi[1], Dr. (Mrs.) S. Muthulakshmi[2]

[1, 2] *(Assistant Professor, Faculty of Engineering, Professor, Faculty of Science, Avinashilingam Institute for Home Science and Higher Education for Women, Coimbatore, India)*

Abstract: *Queueing problems are most common features not only in our daily-life situations such as bank counters, post offices, ticket booking centres, public transportation systems, but also in more technical environments such as in manufacturing, computer networking and telecommunications. For any queueing system average queue length, average system length, average waiting time in the queue and average waiting time in the system are the main observable performance characteristics. Control chart is a graph used to study how a process changes over time and it is also used to control ongoing processes. In this paper control limits are established to study the behavior of E_k /M /1 queueing model using the performance characteristics. Numerical results are given to highlight its applications.*

Keywords: *queue length, waiting time, Erlang arrival, exponential service, control limits.*

I. INTRODUCTION

Queueing model with Erlang arrival has been discussed by Gross and Harris (1998) and several others. Control chart is a quality control technique evolved initially to monitor production processes. Montgomery (2005) proposed a number of applications of Shewhart control charts in assuring quality in manufacturing industries. Shore (2000) developed control chart for random queue length of M /M /s queueing model by considering the first three moments and also Shore (2006) developed Shewhart-like general control charts for G/G/S queueing system using skewness. Khaparde and Dhabe (2010) constructed the control chart for random queue length of M/M/1 queueing model using method of weighted variance. Poongodi and Muthulakshmi (2012) analyzed number of customers in system of M/E_k/1 queueing model using control chart technique. The Erlang arrival queueing system is applicable to many real-life situations:

(i) In military recruits a recruit first lines up to have blood test at one station, an eye examination at the next station, mental test by a psychiatrist at the third, and is examined by a doctor for medical problems at the fourth and so on. Recruit needs to pass all phases before entering for selection.

(ii) In a typical polling system, voters have to pass through many phases like showing identity cards, signing, getting ink mark etc., before voting.

(iii) In an airline counter, passengers are expected to check in which consists of many phases, before entering into the plane.
    and so on.

This motivated the author to study the construction of Shewhart control charts for number of customers in the queue, number of customers in the system, waiting time in the queue and waiting time in the system of E_k/M/1 queueing model.

II. E_k/ M/1 MODEL DESCRIPTION

Consider a queueing system in which the inter-arrival times follow k-Erlang distribution with mean $1/\lambda$ in which an arrival has to pass through k phases, each with a mean time $1/k\lambda$ prior to entering the service. Service times follow an exponential distribution with mean $1/\mu$.

Let p_n be the probability that there are n customers in E_k/M/1 queueing system. Then

$$p_n = \sum_{j=nk}^{nk+k-1} p_j^{(P)} \quad (1)$$

where $p_j^{(P)}$ is the probability of completion of j phases and is given by

$$p_j^{(P)} = \frac{k\lambda \, p_0^{(P)}}{\mu} r_0^{\,j-k} \qquad (j \geq k) \qquad (2)$$

where $r_0 \in (0,1)$ is the root of the characteristic equation

$$\mu \, z^{k+1} - (k\lambda+\mu) \, z + k\lambda = 0$$

since $p_0^{(P)} = \dfrac{1 - r_0}{k}$ taking $\rho = \lambda/\mu$, equation (2) becomes

$$p_j^{(P)} = \rho(1 - r_0)r_0^{\,j-k}$$

Therefore equation (1), reduces to

$$p_n = \rho\,(1 - r_0^{\,k})\,(r_0^{\,k})^{n-1}$$

which is a geometric distribution.

Control chart analysis of E_k/M/1 queueing model is carried out in the following sections.

III.   NUMBER OF CUSTOMERS IN THE QUEUE

Let L_q denote the number of customers in the queue.

The expected number of customers in the queue, $E(L_q)$ is given by

$$E(L_q) = \sum_{n=1}^{\infty} (n-1)\; p_n$$

$$= \frac{\rho\, r_0^{\,k}}{(1 - r_0^{\,k})} \quad (3)$$

and $$E(L_q^2) = \sum_{n=1}^{\infty} (n-1)^2 p_n$$

$$= \frac{\rho\, r_0^{\,k}(1 + r_0^{\,k})}{(1 - r_0^{\,k})^2}$$

Then variance of L_q is

$$\mathrm{Var}(L_q) = E(L_q^2) - (E(L_q))^2$$

$$= \frac{\rho\, r_0^{\,k}(1 + r_0^{\,k} - \rho\, r_0^{\,k})}{(1 - r_0^{\,k})^2} \quad (4)$$

Upper control limit (UCL), central line (CL) and lower control limit (LCL) of Shewhart control chart, under the assumption that the number of customers in the queue follows normal distribution, are given by

$$\left.\begin{array}{ll} \text{UCL} & = E(L_q) + 3\sqrt{\mathrm{Var}(L_q)} \\ \text{CL} & = E(L_q) \\ \text{LCL} & = E(L_q) - 3\sqrt{\mathrm{Var}(L_q)} \end{array}\right\} (5)$$

The parameters of the control chart are obtained by using (3) and (4) in (5) as

$$\text{UCL} = \frac{\rho\, r_0^{\,k} + 3\sqrt{\rho\, r_0^{\,k}(1 + r_0^{\,k} - \rho\, r_0^{\,k})}}{(1 - r_0^{\,k})}$$

$$\text{CL} = \frac{\rho\, r_0^{\,k}}{(1 - r_0^{\,k})}$$

$$\text{LCL} = \frac{\rho\, r_0^{\,k} - 3\sqrt{\rho\, r_0^{\,k}(1 + r_0^{\,k} - \rho\, r_0^{\,k})}}{(1 - r_0^{\,k})}$$

IV.   NUMBER OF CUSTOMERS IN THE SYSTEM

Let L_s denote the number of customers in the system (both in queue and in service).

The expected number of customers in the system is given by

$$E(L_s) = \sum_{n=1}^{\infty} n\,p_n$$

$$= \sum_{n=1}^{\infty} n\rho\,(1 - r_0^{\,k})\,(r_0^{\,k})^{n-1}$$

$$= \frac{\rho}{(1 - r_0{}^k)} \qquad (6)$$

and $\qquad E(L_s{}^2) = \sum_{n=1}^{\infty} n^2 p_n$

$$= \rho(1 - r_0{}^k) \sum_{n=1}^{\infty} n^2 (r_0{}^k)^{n-1}$$

$$= \frac{\rho(1 + r_0{}^k)}{(1 - r_0{}^k)^2}$$

Then variance of L_s is

$$Var(L_s) = E(L_s{}^2) - (E(L_s))^2$$

$$= \frac{\rho(1 + r_0{}^k - \rho)}{(1 - r_0{}^k)^2} \qquad (7)$$

The parameters of Shewhart control chart, under the assumption that the number of customers in the system follows normal distribution, are given by

$$\left. \begin{array}{ll} UCL & = E(L_s) + 3\sqrt{Var(L_s)} \\ CL & = E(L_s) \\ LCL & = E(L_s) - 3\sqrt{Var(L_s)} \end{array} \right\} \qquad (8)$$

Using (6) and (7) in (8), the parameters of the control chart are obtained as

$$UCL = \frac{\rho + 3\sqrt{\rho(1 + r_0{}^k - \rho)}}{(1 - r_0{}^k)}$$

$$CL = \frac{\rho}{(1 - r_0{}^k)}$$

$$LCL = \frac{\rho - 3\sqrt{\rho(1 + r_0{}^k - \rho)}}{(1 - r_0{}^k)}$$

V. WAITING TIME IN THE QUEUE

Distribution of waiting time of a customer in the queue for the model under study is given by

$$W_q(t) = 1 - r_0{}^k e^{-\mu(1 - r_0{}^k)t}, \qquad t \geq 0.$$

Then the pdf of waiting time is

$$w_q(t) = \mu r_0{}^k (1 - r_0{}^k) e^{-\mu(1 - r_0{}^k)t}$$

Let w_q denote the waiting time of customers in the queue.

The mean of w_q is

$$E(w_q) = \mu r_0{}^k (1 - r_0{}^k) \int_0^{\infty} t\, e^{-\mu(1 - r_0{}^k)t} dt$$

$$= \frac{r_0{}^k}{\mu(1 - r_0{}^k)} \qquad (9)$$

and $\qquad E(w_q{}^2) = \mu r_0{}^k (1 - r_0{}^k) \int_0^{\infty} t^2 e^{-\mu(1 - r_0{}^k)t} dt$

$$= \frac{2 \, r_0^{\ k}}{\mu^2 (1 - r_0^{\ k})^2}$$

Then variance of w_q is

$$\mathrm{Var}(w_q) = E(w_q^2) - (E(w_q))^2$$

$$= \frac{r_0^{\ k}(2 - r_0^{\ k})}{\mu^2 (1 - r_0^{\ k})^2} \tag{10}$$

The parameters of Shewhart control chart, under the assumption that the waiting time of customers in the queue follows normal distribution, are given by

$$\left.\begin{aligned}
\mathrm{UCL} &= E(w_q) + 3\sqrt{\mathrm{Var}(w_q)} \\
\mathrm{CL} &= E(w_q) \\
\mathrm{LCL} &= E(w_q) - 3\sqrt{\mathrm{Var}(w_q)}
\end{aligned}\right\} \tag{11}$$

The parameters of the control chart are obtained by using (9) and (10) in (11) as

$$\mathrm{UCL} = \frac{r_0^{\ k} + 3\sqrt{r_0^{\ k}(2 - r_0^{\ k})}}{\mu(1 - r_0^{\ k})}$$

$$\mathrm{CL} = \frac{r_0^{\ k}}{\mu(1 - r_0^{\ k})}$$

$$\mathrm{LCL} = \frac{r_0^{\ k} - 3\sqrt{r_0^{\ k}(2 - r_0^{\ k})}}{\mu(1 - r_0^{\ k})}$$

VI. WAITING TIME IN THE SYSTEM

Let w_s denote the waiting time of customers in the system.

The expected waiting time of customers in the system, $E(w_s)$ is given by

$$E(w_s) = E(L_s)/\lambda$$

$$= \frac{\rho}{\lambda(1 - r_0^{\ k})} \tag{12}$$

Also the variance of w_s is given by

$$\mathrm{Var}(w_s) = \mathrm{Var}(L_s)/\lambda^2$$

$$= \frac{\rho(1 + r_0^{\ k} - \rho)}{\lambda^2 (1 - r_0^{\ k})^2} \tag{13}$$

The parameters of Shewhart control chart, under the assumption that the waiting time of customers in the system follows normal distribution, are given by

$$\mathrm{UCL} = E(w_s) + 3\sqrt{\mathrm{Var}(w_s)} \tag{14}$$

$$\mathrm{CL} = E(w_s)$$

$$\mathrm{LCL} = E(w_s) - 3\sqrt{\mathrm{Var}(w_s)}$$

The control chart parameters are obtained by using (12) and (13) in (14) as

$$\mathrm{UCL} = \frac{\rho + 3\sqrt{\rho(1 + r_0^{\ k} - \rho)}}{\lambda(1 - r_0^{\ k})}$$

$$\mathrm{CL} = \frac{\rho}{\lambda(1 - r_0^{\ k})}$$

$$LCL = \frac{\rho - 3\sqrt{\rho(1 + r_0{}^k - \rho)}}{\lambda\,(1 - r_0{}^k)}$$

VII. NUMERICAL ANALYSIS

Numerical analysis is carried out to analyze the performance of queueing system with reference to the parameters λ, μ and k. As LCL values are negative for the selected values of the parameters, they are considered as zero and therefore not shown in the table as a separate column.

Table gives the control chart parameters for number of customers in the queue, number of customers in the system, waiting time of customers in the queue and waiting time of customers in the system for certain selected values of λ, μ and k.

TABLE - CONTROL CHART PARAMETERS FOR L_Q, L_S, W_Q AND W_S

λ	μ	k	ρ	r_0	L_q		L_s		w_q		w_s	
					CL	UCL	CL	UCL	CL	UCL	CL	UCL
4			0.40	0.7690	0.0756	1.0171	0.4756	2.4411	0.0189	0.2119	0.1189	0.6103
4.5			0.45	0.7991	0.1183	1.3421	0.5683	2.7810	0.0263	0.2576	0.1263	0.6180
5	10	7	0.50	0.8259	0.1776	1.7428	0.6776	3.1873	0.0355	0.3099	0.1355	0.6374
5.5			0.55	0.8500	0.2595	2.2430	0.8095	3.6842	0.0472	0.3712	0.1472	0.6699
6			0.60	0.8720	0.3731	2.8792	0.9731	4.3088	0.0622	0.4452	0.1622	0.7181
	15		0.67	0.8851	0.6174	4.1412	1.2904	5.5491	0.0617	0.3909	0.1290	0.5549
	20		0.50	0.8046	0.1862	1.8021	0.6862	3.2428	0.0186	0.1596	0.0686	0.3243
10	25	6	0.40	0.7425	0.0805	1.0595	0.4805	2.4775	0.0081	0.0880	0.0481	0.2478
	30		0.33	0.6920	0.0411	0.7090	0.3707	2.0803	0.0041	0.0553	0.0371	0.2081
	35		0.29	0.6496	0.0232	0.5109	0.3135	1.8612	0.0023	0.0375	0.0314	0.1862
		5	0.60	0.8343	0.4070	3.0796	1.0070	4.5047	0.1357	0.9445	0.3357	1.5016
		10	0.60	0.9045	0.3471	2.7250	0.9471	4.1586	0.1157	0.8485	0.3157	1.3862
3	5	15	0.60	0.9329	0.3271	2.6053	0.9271	4.0424	0.1090	0.8157	0.3090	1.3474
		20	0.60	0.9483	0.3173	2.5466	0.9173	3.9856	0.1058	0.7996	0.3058	1.3286
		25	0.60	0.9580	0.3120	2.5147	0.9120	3.9548	0.1040	0.7908	0.3040	1.3183

Numerical values in the table reveal the following features:
For all the performance measures of E_k/M/1 queueing system
  (i)   increase in the arrival rate λ, increases the parameters and UCL for fixed values of μ and k.
  (ii)   increase in the service rate μ, decreases the parameters CL and UCL for fixed values of λ and k.
  (iii)   increase in the number of phases k, decreases the parameters CL and UCL for fixed values of λ and μ.

VIII. CONCLUSION

In this paper control chart technique is applied to analyze the system characteristics of E_k/M/1 queueing system. These characteristics provide the arrivals to decide whether to join the system or not. In addition it gives the information on the waiting time.

REFERENCES
[1]   D. Gross and M. Harris, Fundamentals of queueing theory(5th edition, John Wiley & Sons, Inc.,1998).
[2]   D.C. Montgomery, Introduction to statistical quality control(5th edition, John Wiley & Sons, Inc.,2005).
[3]   H. Shore, General control charts for attributes, IIE transactions, 2000, 32, 1149-1160.
[4]   H. Shore, Control charts for the queue length in a G/G/S System, IIE Transactions, 2006, 38, 1117-1130.
[5]   M.V. Khaparde and S.D. Dhabe, Control chart for random queue length N for (M/M/1): (∞/FCFS) Queueing model, International Journal of Agricultural and Statistical sciences,2010, Vol.1,319-334.
[6]   T. Poongodi. and S. Muthulakshmi, Random queue length control chart for (M/E_k/1): (∞/FCFS) queueing model, International Journal of Mathematical Archive- 3(9),2012, 3340- 3344.

CFD Analysis and Fabrication of Aluminium Cenosphere Composites

Christy Oommen Jacob[1], S. Immanuel[2], A. Sabik Nainar[3], M. Gokulraj[4]

[1] *Graduate Scholar[1], Department of Aeronautical, Nehru Institute of Engg and Tech, Coimbatore*
[2] *Assistant Professor[2], Department of Mechanical Engineering, PSN Engineering College, Tirunelveli*
[3] *Assistant Professor[3], Excel Engineering College, Komarapalayam, Nammakkal*
[4] *Post Graduate Scholars, Department of Aeronautical Engineering, Nehru Institute of Engg and Tech, Coimbatore.*

Abstract: *Metal matrix composites are engineered materials with a combination of two or more dissimilar materials, to obtain enhanced properties. Aluminium alloys reinforced with ceramic particles exhibit superior mechanical properties when compared to unreinforced aluminium alloys and hence are candidate for engineering applications. In the present investigation aluminium alloy is used as the matrix and cenosphere as the reinforcing material. The hybrid metal matrix composite is produced using conventional foundry techniques by casting route. The cenosphere is to be added in 2%, 4% and 6% by volume and also with the influence of the particle size of cenosphere, to the molten metal with Magnesium, which is the main parameter for the wet ability of cenosphere and aluminium alloy. The hybrid composite is to be tested for hardness, density, mechanical properties and impact strength. The density decreases with increase in cenosphere content. The impact strength increases with increase in cenosphere content. The resistances to dry wear and slurry erosive wear increases with increase in cenosphere content and hence this material can be used as bearing material. This composite material being less dense than aluminium can therefore be used in place of conventional aluminium alloys in aircraft components*

Keywords: *Metal matrix composites, Aluminium alloy, Cenosphere.*

I. Introduction

Conventional monolithic materials have limitations with respect to achievable combinations of strength, stiffness and density. In order to overcome these shortcomings and to meet the ever increasing engineering demands of modern technology, metal matrix composite are gaining importance, In recent years discontinuously reinforced aluminium based metal matrix composites have attracted worldwide attention as a result of their potential to replace their monolithic counterparts primarily in aerospace, automobile and energy sector.The present investigation has been focused on utilization of waste fly ash particle in a useful manner by dispersing it in aluminium matrix to produce a composite. In the present work, fly ash particle which mainly consists of refractory oxides like silica, alumina and iron oxides will be used as the reinforcing phase and to increase the wettablity, magnesium or silicon were added. Further these composites will be characterized with help of optical microscopy. Fly ash particle used in current work is called as cenosphere or micro balloon. It is a hollow sphere made up of ceramic outer surface. cenospheres as a filler in Al casting reduces cost, decreases density and increases hardness, stiffness, wear and abrasion resistance. It also improves the maintability, damping capacity, coefficient of friction etc, which are needed in various industries like aerospace, automobile.etc

II. Parameter Selection

Only three specimens are casted and the experiments are conducted for these specimens alone. The particle size is taken constant because theoretically valid result will be encountered at this size interval only and it is expected that the tensile strength of the composite decreases with increase in the particle size. The Mg proportion is also taken constant at 2% by weight during experimentation.

The spcimen A is casted with cenosphere proportion% of 2% by volume aluminium, The specimen B is casted with cenosphere proportion% of 4% by volume aluminium and the Specimen C is casted with 6% by volume of aluminium and all the three specimen has and mg proportion of 2% by weight of aluminium and particles size of 0-200 µm.
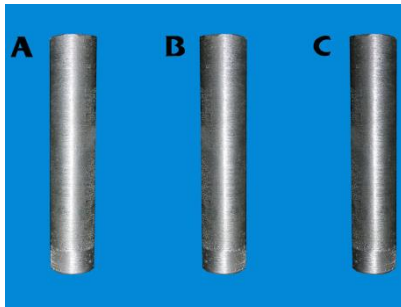
Figure 1. Specifications of various specimens
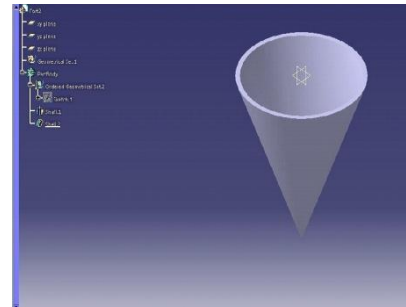
Figure 2. CATIA Cone Model

SPECIFICATION OF THE SPECIMENS

Table.1 Three specimens volume percentage, Mg proportion and particle size of the cenosphere.

Specimens	cenosphere proportion(%)by volume of aluminium	mg proportion(%)by weight of aluminium	cenosphere particle size in μm
Specimen A	2	2	0-200
Specimen B	4	2	0-200
Specimen C	6	2	0-200

TEST EXPERIMENTS

Following tests are carried out with the selected parameters

- SEM Analysis to check the dispersion of particles.
- Tensile Test in UTM Machine.
- Hardness test in Brinell & Vickers Hardness Machine.
- Impact test in Izod Machine.

Specimens are created based on ASTM standard and number of specimens was decided based on number of parameters and levels.

SEM ANALYSIS REPORT
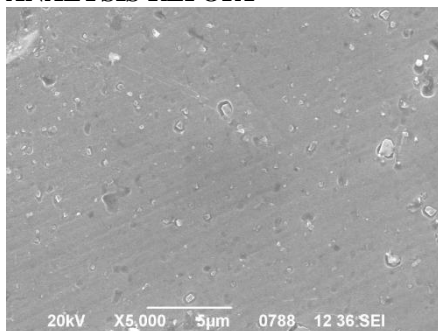
Figure 3. Image at a Magnification of 5000.
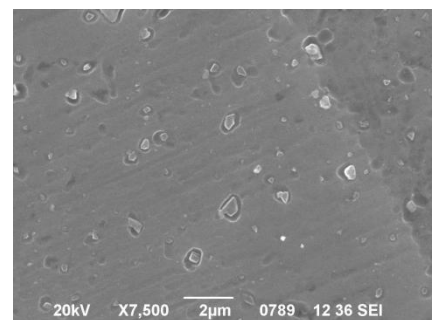
Figure 4. Image at a Magnification of 7500.
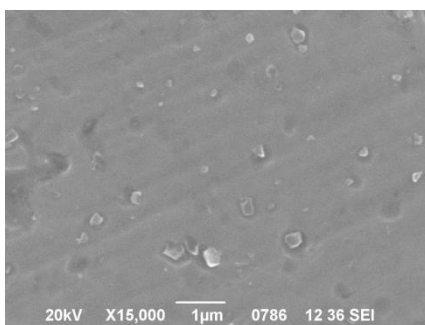
Figure 5. Image at a Magnification of 15000.
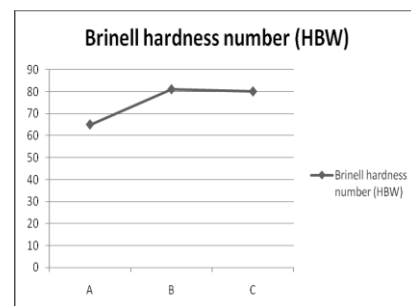
Figure 6. Comparison of Brinell hardness number of the specimens.
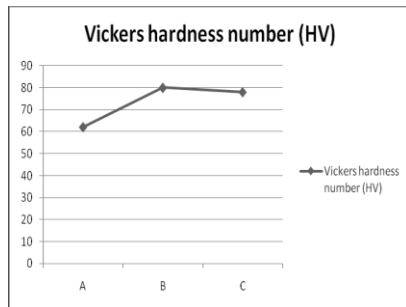
Figure 7. Comparison of Vicker hardness number of the specimens.
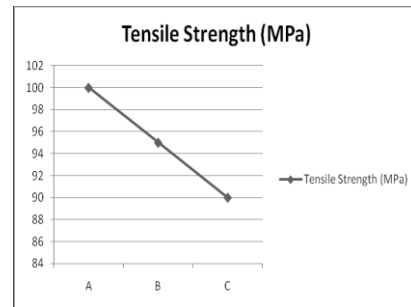
Figure 8. Comparison of Tensile Strength of the specimens.
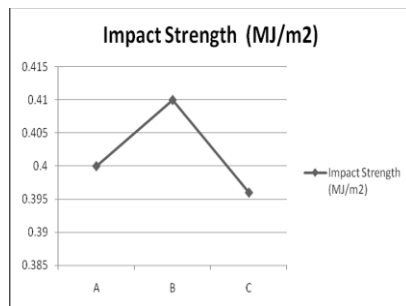
Figure 9. Comparison of Impact strength of the specimens.
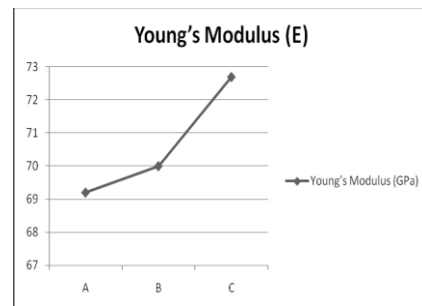
Figure 10. Comparison of Young's Modulus of the specimens.

SEM test was carried out under an accelerating voltage of 20kV Figure 3 gives the Image at a Magnification of 5000, Figure 4 gives Image at a Magnification of 7500 and Figure 5 gives Image at a Magnification of 15000. Figure 6 gives the image of graph of Comparison of Brinell hardness of specimens, The result gives that the Specimen A, B and C has the Brinell hardness number of 67, 82, and 81 respectively. Figure 7 gives the image of graph of comparison of Vickers hardness, The result gives that The Specimen A, B and C has the Vickers hardness number of 61, 81, and 79 respectively. Figure 8 gives the image of graph of comparison of Tensile strength number of the specimens, the result shows that the specimen A, B and C has the Tensile strength of 101Mpa, 96Mpa, and 89Mpa respectively. Figure 9gives the image of graph of comparison of impact strength of the specimens, the result shows that the specimen A, B, and C has the impact strength 0.401 MJ/m2, 0.411 MJ/m2, 0.397 MJ/m2 respectively. Figure 10gives the image of graph of Comparison of Young's Modulus of the specimens, the result shows that The Specimen A, B, and C has the Young's Modulus of 69.1Gpa, 70Gpa, 72.6Gpa respectively.

III.   Results of the Analyzed Inlet Cone

An inlet cone for the turbojet engine is made with material of the new specimen casted and it is analyzed in ANSYS for stress and strain analysis, and in FLUENT for its flow analysis, and the results are given below

Design of The Inlet Cone
The cone is designed using CATIA V5R17 software as shown in figure 2.
The specifications of the inlet cone are,
- Diameter, D = 160 mm,
- Length,   L = 250 mm,
- Thickness, t = 5 mm.

Inlet Cone with the Properties of Specimen A
When the load acting at the point P2 = 36 mm from the base of the cone.
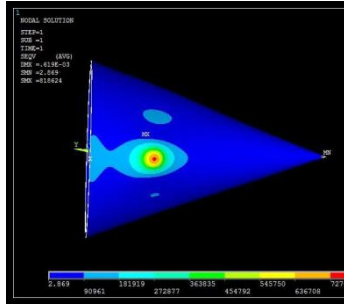
Figure 11.Von Mises Stress acting on the Cone
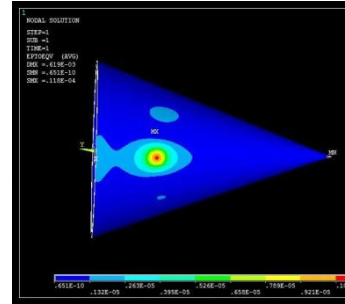
Figure 12. Von Mises Strain acting on the Cone

Inlet Cone with the Properties of Specimen B
When the load acting at the point P1 = 138.5mm from the base of the cone.
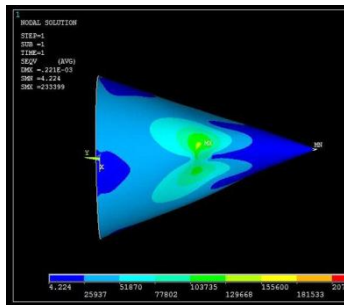
Figure 13.Von Mises Stress acting on the Cone
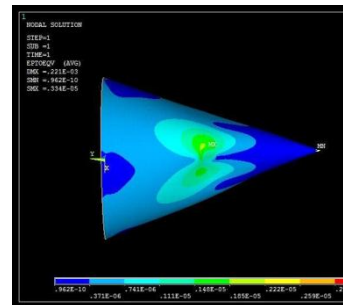
Figure 14.Von Mises Strain acting on the Cone

Inlet Cone with the Properties of Specimen C
When the load acting at the point P3 = 25 mm from the base of the cone.
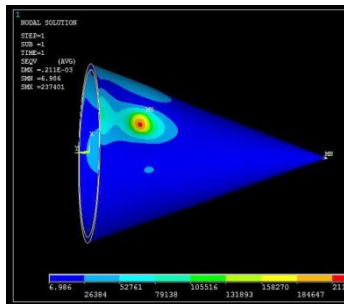
Figure 15. Von Mises Stress acting on the Cone
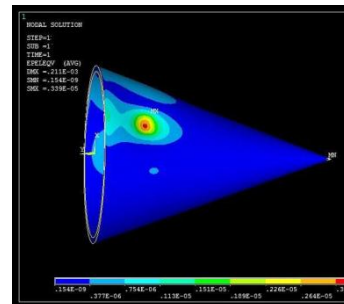
Figure 16.Von Mises Strain acting on the Cone

Flow Analysis
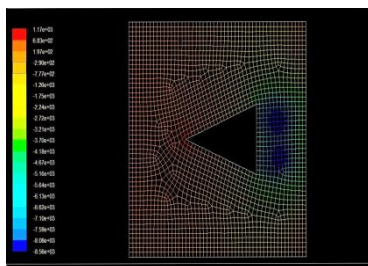
Figure 17.Pressure Distribution over the Cone
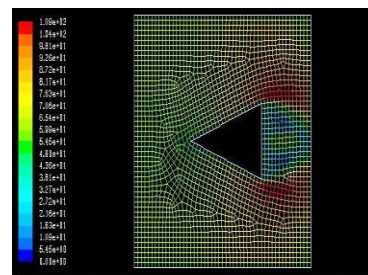
Figure 18. Velocity Distribution over the Cone

IV. Conclusion

Thus, the aluminium cenosphere composites were fabricated and tested for studying their mechanical properties. The tested results reveal that the Impact strength, Hardness and Young's modulus increases due to the presence of the cenosphere and the variation in these properties are shown. The density of the material decreases and it is less compared to the aluminium alloy which makes the composite lighter. The aluminium cenosphere composites show good mechanical properties when compared with its monolithic counterpart and are well suited for the aeronautical structural applications.

REFERENCES

[1.] Alok Satapathy, Suvendu Prasad Sahu and Debadutta Mishra , "Development of protective coatings using fly ash premixed with metal powder on aluminium substrates", Waste Management & Research,2009.
[2.] Sathyabalan, P, Selladurai, V and Sakthivel, V. P, "ANN Based Prediction of Effect of Reinforcements on Abrasive Wear Loss and Hardness in a Hybrid MMC", American Journal of Engineering and Applied Sciences, Vol.2, No. 1,pp. 50-53, 2009.
[3.] Williams Alozie Uju , "Synchrotron X-Ray Absorption Spectroscopy and Thermal Analysis Study Of Particle-Reinforced Aluminium Alloy Composites", Master of Science Thesis, University of Saskatchewan Saskatoon, Saskatchewan, Canada, 2009.

Monthly Monitoring Of Some Physico-Chemical Parameters in Domestic Wastewater Treatment Plant in Turkey: A Case Study On Selected Plant

Serpil SAVCI[1], Ayça DURAK[2]

[1, 2] *(Bozok University Arthitecture Faculty, 66100, Yozgat, Turkey)*

Abstract: *In this paper, monitoring of some parameters in wastewater from domestic wastewater treatment plant is evaluated. The wastewater from the selected plant is characterized by COD, BOD_5, pH, TSS. The wastewater samples were collected from the inlet and outlet to monthly from a wastewater treatment plant to the city of Yozgat in Turkey for eight months from May 2013 to December 2013. Results of a detailed survey on the performance of a selected plant was given both in terms of influent and effluent quality and in comparision with the current legislation on discharge limits to receiving waters. The results of effluent showed that the values of these parameters are ranged on average between 16,7 and 27,2 mg/L for biological oxygen demand (BOD_5), between 22,3 and 36,2 mg/L for chemical oxigen demand and between <10 and 21 total suspanded solid. All these values are beyond World Health Organization and Turkish Standards recommendations for wastewater discharge.*
Keywords: *sewage, monitoring,WHO, Turkey.*

I. Introduction

Over the last century, environmental problems related to human activities have increased as a consequence of population growth. Pollution of water resouces has become a major concern for environmental monitoring physical, chemical and bacteriological parameters associated to water quality. In this context, wastewater treatment plants play an important role as human activity closely associated with sustainable. Activated sludge treatment has been used worldwide in secondary treatment systems. The wastewater purification performance of activated sludge treatment depends heavily on the metabolism with bacteria playing a key role in the purification process.

Sewage water is a complex matrix. These include high concentration of BOD, COD, high dissolved solid. Traditionally, the quality of treated wastewater is defined by the measurement of parameters such as chemical oxigen demand (COD), biological oxigen demand (BOD), nitrate, sulphate, etc. These parameters provide crucial information on the quality of the influent, effluent wastewater and performance of treatment plants [1]. Previous studies, on domestic sewage treatment systems have mainly focused on removal of chemical oxygen demand, biochemical oxygen demand, total suspanded solid and nitrogen [2]. Information about the monitoring of these in domestic treatment systems is limited. Yozgat is a city in Turkey. The city is located at an elevation of 4380 ft (1,335 m), situated 170 km east of Ankara, near the head of a narrow valley through which the Ankara-Sivas road runs. According to 2009 census, population of the district is approximately 113,614 of which 73,835 live in the city of Yozgat. The main industries in Yozgat are textiles, food, cement, manufacturing and metallurgy [3-13].

According to national standards (Table 1), the receiving the water standards are based on organik load/ population equivalency [4]. The standards cover four main parameters without considering the bacteriological status.

Table 1.Discharge standards of domestic wastewater to receiving waters in Turkey [11].

Parameter	Composite sample (2h), Pop. 1000-10000	Composite sample (24h), Pop.1000-10000	Composite sample (2h), Pop>100000	Composite sample (24h), Pop. >100000
BOD_5 mg/L	50	45	40	35
COD mg/L	160	110	120	90
TSS mg/L	60	30	40	25
pH	6-9	6-9	6-9	6-9

In this study, wastewater samples (influent and effluent) were collected monthly from WWTP in Turkey for 8 months from May 2013 to December 2013. Typical pollution parameters measured in wastewater treatments plants such as chemical oxigen demand (COD), biological oxigen demand (BOD_5), pH and total suspanded solids.

II. Materials and methods

2.1. Waste water treatment plant operation
Wastewaters in WWTP are treated by mechanical-biological method by using active sludge. In order to maintain quality raw and treated wastewater, the quality of activated sludge and optimal operating conditions, and the operation of wastewater treatment plant are daily monitored. Measurements of different physical quantities such as temperature, flow, redox potential, pH of water and conductance are performed daily bu using standard laboratory equipment, instrument Sesinon (model 51935-00). Before and after treatment, the composition and quality of wastewater are determined daily by using standard analytical methods [5].

2.2. Water Samples
Water samples used in this study were collected from the effluents of secondary sedimantation in a WWTP. The WWTP has a treatment capacity of 26.000 m^3/d, serving a community in the middle of Turkey. The basic treatment process of the WWTP is primary sedimentation, followed by an anaerobic–anoxic–oxic process as its secondary treatment. Eight groups of samples were collected from May 2013 to December 2013. The water samples were transported to laboratory on ice, stored at 4 °C and analyzed on the day of collection.

2.2. Analysis of waste water
The study was conducted sewage treatment plant Yozgat in Turkey. Samples were collected from the influent and effluent waste water at biological wastewater treatment plant. Samples were collected in first week of every month during the year 2013 from May to December. Samples were collected in glass containers, pre-cleaned by washing with non-ionic detergents,
rinsed with tap water, 1:1 hydrochloric acid and finally with deionised water. Before sampling, the bottles were rinsed three times with sample water pH, temperature, BOD_5, COD and TSS were analyzed according to the methods prescribed by the APHA [5].

III.   Result and Discussion
The wastewater quality analysis of influent of sewage treatment plant has been carried out for physico-chemical parameters like, pH, COD, BOD_5 and TSS. The results are given in Table 2.

Table 2. Physicochemical parameters of influent of sewage treatment plant

Parameters/ Months	May	June	July	Au	Sep	Oc	Nov	Dec
pH	8.82	8.50	8.63	8.52	8.54	8.58	8.52	8.55
COD	810	680	630	777	806	791	820	840
BOD_5	607	510	472,5	583	604	593	615	630
TSS	198	212	161	205	228	178,5	185,5	192,2

The wastewater quality analysis of effluent of sewage treatment plant has been carried out for physico-chemical parameters like, pH, COD, BOD_5 and TSS. The results are given in Table 3.

Table 3. Physicochemical parameters of effluent of sewage treatment plant

Parameters/ Months	May	June	July	Au	Sep	Oc	Nov	Dec
pH	7,70	7,20	7,60	7,70	7,80	7,70	7,90	7,90
COD	33,2	28,6	35,4	26,7	22,3	27,1	33,4	36,2
BOD_5	25	22	26,5	20	16,7	20	25	27,2
TSS	11	<10	15	<10	<10	11	18	21

Temperature also measured in WWTP. It usually depends on the season, geographic location and sampling time. During the period of investigation temperature values in beetwen 13.5 to 20.6 ^{0}C. The minimum value was observed in month of December and the maximum value was observed in month of May. The variation in the water temperature may be due to different timings of collection and influence of season.

3.1 Chemical Oxigen Demand

The mean COD in the untreated wastewater was from 630 to 840 mg/L (Table 2). There was strong variation in COD concentrations over the sampling period. The minimum value was observed in the month of July while the maximum value was observed in the month of December in the influent of biological waste water plant in Yozgat in Turkey. The COD of the treatment wastewater is low in comparision to the range of COD values reported in the literature for domestic wastewater; including representative concentrations reported by Metcalf&Eddy Inc. (1991) of 250 mg/L, 430 mg/L and 800 mg/L for weak, medium and strong wastewater, respectively [6].
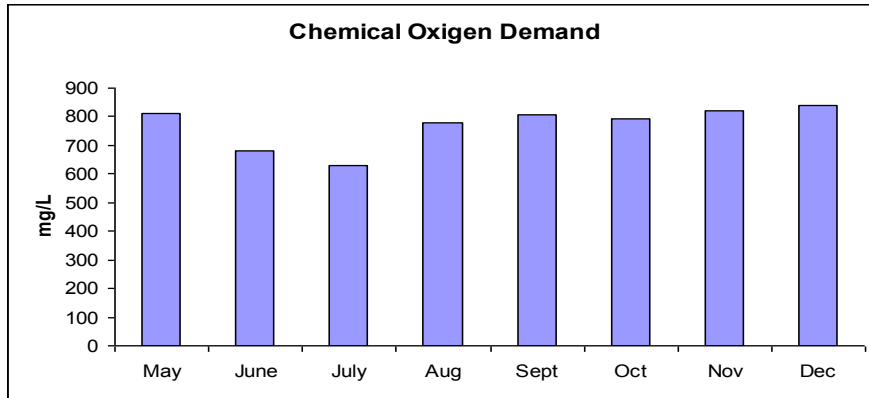
Figure 1. Variation of COD in Influent of WWTP
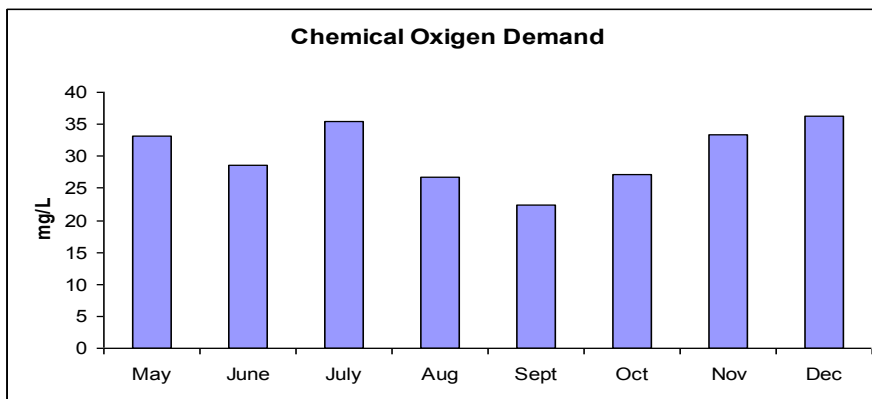
Figure 2. Variation of COD in Effluent of WWTP

3.2 Biological Oxigen Demand

In the present study, BOD_5 varied from 16,7 mg/L to 27,2 mg/L in the effluent of domestic waste water treatment plant. The minimum value was observed in the month of September while maximum value was observed in the month of December. BOD_5 indicates the present of microbial activities and dead organic matter. BOD_5 is directly linked with decomposition of dead organic matter present in the wastewater and hence the higher values of BOD_5 can be directly related with pollution status of the wastewater. The higher values of BOD_5 means present of more biodegradable organic matter [9-10].
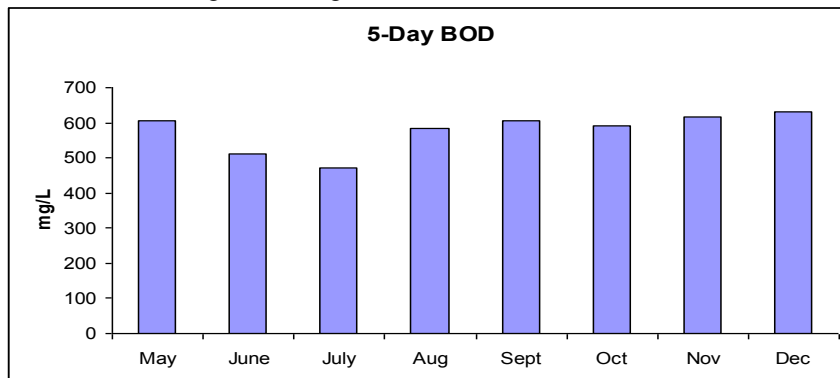
Figure 3. Variation of BOD_5 in Influent of WWTP

5-Day BOD
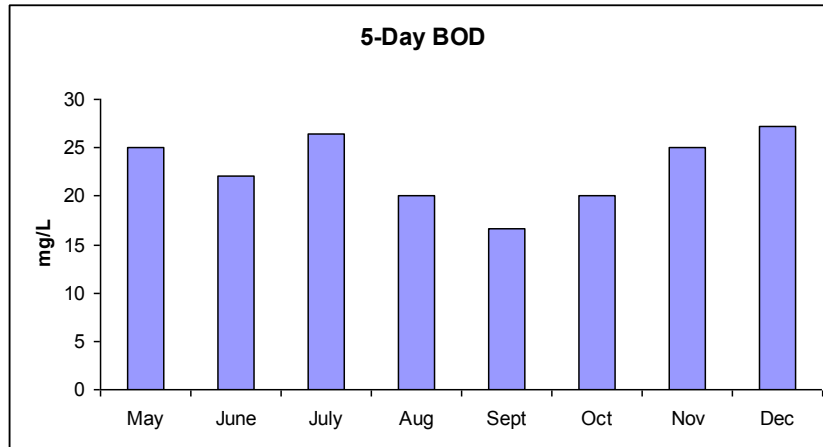
Figure 4. Variation of BOD_5 in Effluent of WWTP

Total Suspanded Solids

The concentration of suspanded solids (TSS) in the untreted sewage was 161 ± 212 mg/L, whereas from treated effluent varied from <10-21 mg/L respectively. Figure 5-6 shows the variation of suspanded solids from the inlet and outlet of wastewater treatment plant. The values shows suspanded solids are in permissible limit as compared with Turkish Standards [12].
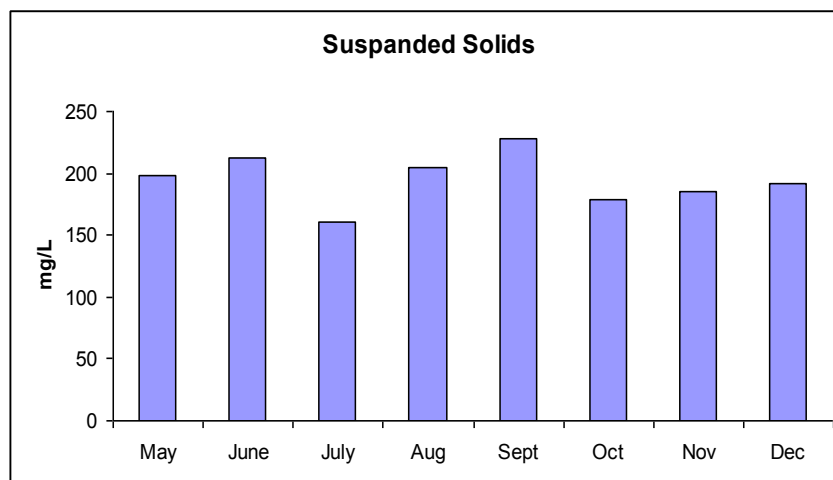
Suspanded Solids

Figure 5. Variation of Suspanded Solids in Influent of WWTP
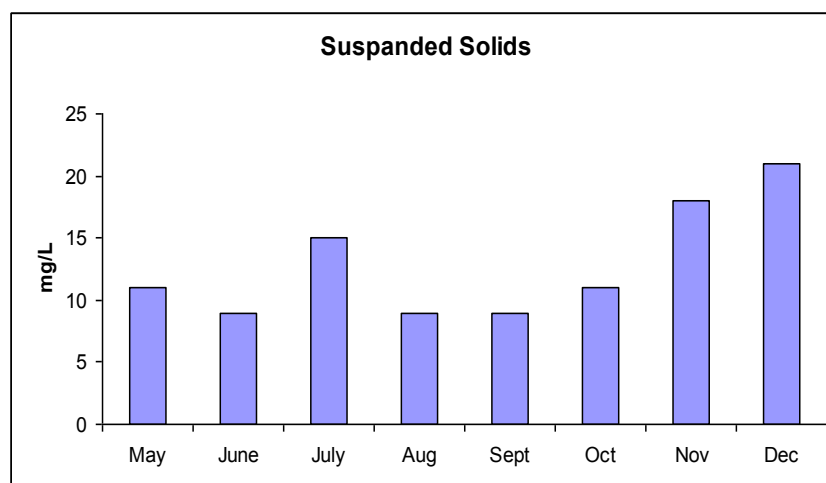
Suspanded Solids

Figure 6. Variation of Suspanded Solids in Effluent of WWTP

Water pH

pH measurements are common in wastewater treatment plant. The pH of the raw sewage was 8.52-8.82 and the system reduced the pH to values close to 7.20-7.90. These results are consistent with the behavior of pH in other treatment plants. There was no significant difference. WHO recommended maximum pemissible limit of pH from 6.5 to 9.2 [7-8]. pH value of different samples is within the desirable and suitable range. Figure 7-8 shows the variation of suspanded solids from the inlet and outlet of wastewater treatment plant
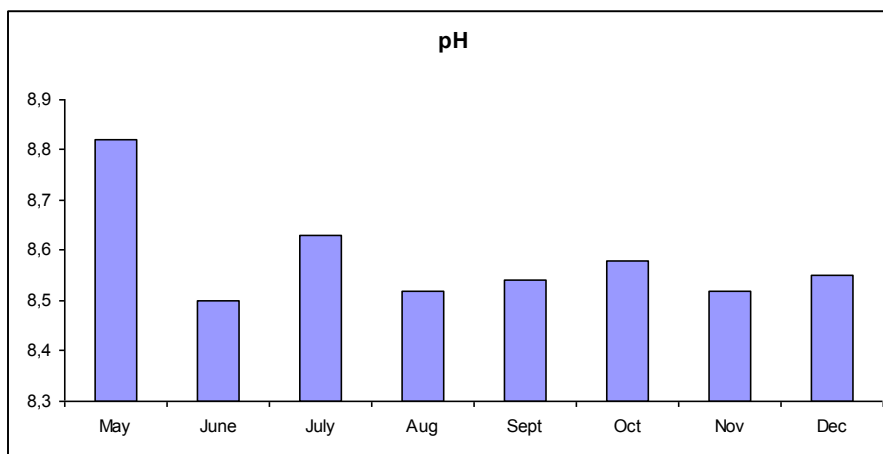
Figure 7. Variation of pH in Influent of WWTP
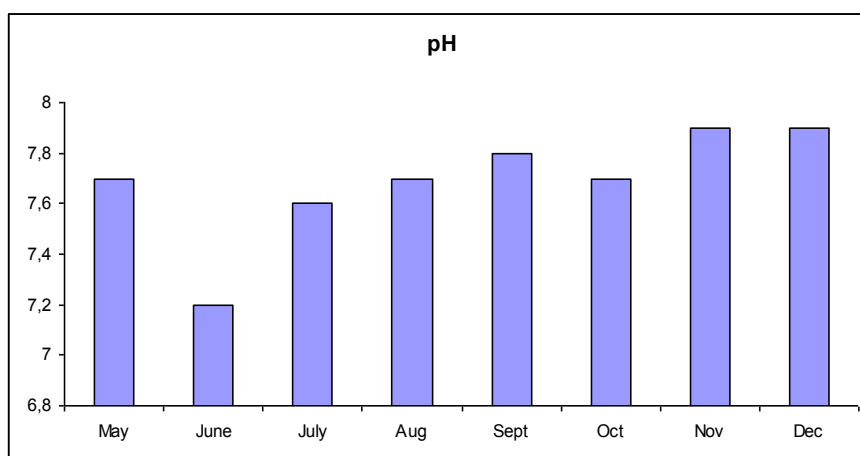
Figure 8. Variation of pH in Effluent of WWTP

IV. Conclusion

This study evaluated the physico-chemical properties rather than bacteriological parameters of a domestic wastewater treatment plant in Turkey. The physico-chemical characteristics of effluent is light brown in colour, pH shows alkaline nature of the effluent, TSS, BOD_5, COD are the parameters from the treated effluent is low in concentrations compared to Turkish standars. The concentration of the investigated in the water samples from Yozgat/Turkey were found below the guidelines for waste water given by WHO. The study showed a need for a continuous pollution monitory program.

REFERENCES

[1.]   LOOS, R., CARVALHO, R., ANTÓNIO, D. C., COMERO, S., LOCORO, G., TAVAZZI, S., PARACCHINI, B., GHIANI, M., LETTIERI, T., BLAHA, L., JAROSOVA, B., VOORSPOELS, S., SERVAES, K., HAGLUND, P., FICK, J., LINDBERG, R. H. EU-wide monitoring survey on emerging polar organic contaminants in wastewater treatment plant effluents. Water Research, 47:17:6475-6487, 2013.

[2.]   H. LIANG, M. GAO, J. LIU, Y. WEI, X. GUO. A novel integrated step-feed biofilm process for the treatment of decentralized domestic wastewater in rural areas of China. J Environ Sci, 22 (3) pp. 321–327, 2010.

[3.]   SAVCI, S., BELLITURK, K. Assesment of Irrigation Water Quality of Some Provinces of Turkey. International Journal of Modern Engineering Research, 3:1 pp:19-22, 2013.

[4.]   ALATON, I. A., TANIK, A., OVEZ, S., ISKENDER, G., GUREL, M., ORHON, D. Reuse potential of urban wastewater treatment plant effluents in Turkey: a case study on selected plants. Desalination. 215:159-165, 2007.

[5.]   Standard methods standard methods for the Examination of water and wastewater (20th Edition) APHA, American water works association (AWWA) and water Environment federations. Washington., 1325 pp., 1999.

[6.]   Metcalf&Eddy Inc. Wastewater Engineering,Treatment, Disposal, and Reuse, thirded. McGraw-Hill Inc., New York, p. 1333 (revised by Tchobanoglous, G. and Burton, F.L.) 1991.

[7.]   A.K DE. Environmental Chemistry 4th Edition, New Age International Publishers, New

[8.]   Delhi, 245-252, 2002.

[9.]   WHO, Rollingr evision of the WHO guidelines for drinking -water quality, Draft for review and comments. Nitrates and Nitrites in drinking -water, World Health Organization. (WHO/SDE/WSH/04.08/56), 2004.

[10.]   WQM Report., Annual report on water quality monitoring of upper and lower lakes Bhopal, Volumes I and II, 1999.

[11.]   10. KADLEC, R.H., KNİGHT, R.L., Treatment Wetlands. CRC Press, Lewis Publishers,   Boca Raton, FL, p. 893, 1996.

[12.]   11.WPCR, National Water Pollution Control Regulation (revised), Official Newspaper,   Reference no:25687, dated: 31 December 2004.

[13.]   12. Water Pollution Control Regulation of Turkish Authorities (WPCRTA) (Su Kirliligi Kontrol Yonetmeligi) No:19919,T.C. Resmi Gazete (4.9.1989).

[14.]   13. SOYLAK, M, ARMAĞAN AYDIN, f, SARACOGLU, S., ELCI, L., DOGAN, M., Chemical Analysis of Drinking Water Samples from Yozgat, Turkey. Polish Journal of Environmental Studies, 11,2, 151-156, 2001.

International Journal of Modern Engineering Research (IJMER)

Contents :

Modeling and Manufacturing of Powered vehicle for physically challenged people

G. Vijay Prakash[1], Dr. A. V. Ratna Prasad[2]

Reg.No:1050048. Ph.D (Mechanical Engineering), University College Of Engineering And Technology, Anu,
Nagarjuna Nagar-522510
M.TECH, Ph.D Prof. & HOD of Mechanical Dept, Department Of Mechanical Engineering, V. R. Siddardha
Engineering College, Kanuru, Vijayawada

Abstract: *This vehicle is suitable for physically challenged or disabled people. I proposed complete customized solutions for physically challenged drivers and patents also. This proposed vehicle successfully dealing with electric and Hybrid vehicle Conversions. In the market they are so many vehicles are designed for physically challenged peoples but my proposed system is a luxurious vehicle. Luxurious means vehicle which is automotive electrical vehicle and provide good hospitality to PCP's. Vehicle conversion products which enable the person to drive a vehicle with the help of his/her hands or using only one limb. With a disability, it can be very difficult to drive. Hand controls can make this much easier with more control and faster response times. Vehicle hand controls are suitable for almost any make and model car on the road today.*
Key words: *Motor electrical, Battery, Tubeless Tires, Controllers, velding, Operations.*

Different operating options available are:
- Hand Operated Brake.
- Hand Operated Accelerator.
- Automatic Clutch
- Fitting Universal Handel for any Point of Disabilities

The Hand Controls are customized & specially made for each user.

Various disability measures and their solutions:
- Persons with Right Limb Disability can use a Manual Transmission Vehicle fitted with a Hand Operated Brake & Accelerator

Persons with Both Limbs Disability can use an Automatic Transmission Vehicle fitted with a Hand operated Brake & Accelerator.

I. Introduction

Power wheelchair for use by people with various types and degrees of handicap. The intelligent wheelchair project intends to establish a methodology to design, implement, and test an effective add-on autonomy management system for use in conjunction with most common commercially available power wheelchairs.

Proposed vehicle is different than any other vehicle from the previous.

Some of the vehicles are look like my vehicle but that vehicles are did not provide much hospitality and facilitates. This vehicle truly designed based on my thoughts and urges of pcp's. and I had took some references regarding structure. And also proposed vehicle is electric(powered) vehicle.

This is a different structure and it gives a peaceful life to pcp's. in future it makes a rapid evaluation on pcp vehicles .

The proposed vehicle manufacturing cost is low compare to other powered vehicles . its available price is less than are equal to Rs.35000/. It gives a rich look,fashion and luxurious facilities.

And also it carries more than 150kg weight. And the main advantage of my proposed vehicle is easy to drive with single limb.

The luxurious facilities are provided in the vehicle is as follows:

Cooking
Drinking water
Sleeping

Laptop
Charging fan
Note: if people required any sensors and applications for their urges we provide much room for that.

The thought of design p.v for p.c.p's for a common man(pcp's) also live with a luxurious life with a minimal cost. It is designed based on Indian economical statics in physically challenged peoples(p.c.p's).
In market so many p.v are there but it cost is very high so a common man(pcp's) did not capture. that's why I designed this vehicle and it may be solve some of p.c peoples problems.

Literature survey on physically challenged vehicles:
The intelligent wheelchair project, now called the TAO Project, intends to establish a methodology to design, implement, and test an effective add-on autonomy management system for use in conjunction with most common commercially available power wheelchairs. In order to demonstrate the principle, the project will build, during its life, an autonomy management system for several well-established electric wheelchair models currently available on the market throughout North America and Japan.
In late 1995, a sister R&D company was established in Japan exclusively for the development of intelligent robotic technologies for the disabled and the aged. With the initiative of this new R&D group, the development of TAO-2 autonomous wheelchair using a commercially available Japanese wheelchair began in the spring of 1996.
Based on our experience, methods used and some issues related to the application of the behavior-based approach to realize an intelligent wheelchair and possibly other assistive technologies are discussed. A brief survey is also presented of other groups who are working in this area.

Brief survey of the field
Below is a description of research on intelligent wheelchairs that has been conducted and still ongoing at some institutions. The survey is not intended to be complete but to provide an idea of the different approaches used.

IBM T.J. Watson Research Center
Some of the earliest work in the development of intelligent wheelchairs was a system implemented by Connell and Viola, [Connell & Viola, 90] in which a chair is mounted on top of a robot to make it mobile. Mr. Ed, as the chair was called, could be controlled by the user using a joystick mounted on the arm of the chair and connected to the robot. The user could also delegate control to the system itself to perform certain functions such as avoid obstacles or follow other moving objects. In addition to the joystick, input to the robot comes from bumper switches at the front and rear of the robot, eight infrared proximity sensors for local navigation and two sonar sensors at the front of the robot for following objects. Control is passed from the user to the robot through a series of toggle switches.
A set of layered behaviors were used to control the chair's movement. These were broken into competencies with each small set of rules becoming a toolbox to achieve a particular goal. These groups could be enabled or disabled by means of switches controlled by the operator. It worked as a partnership in which the machine took care of the routine work and the user decided what needed to be done.

KISS Institute for Practical Robotics
The KISS Institute for Practical Robotics (KIPR), located in Virginia is a non-profit educational corporation performing R&D on the integration of robotics in assistive technology, space robotics and autonomous underwater vehicles as well as education in robotics and related fields.
David Miller and Marc Slack at KISS Institute have developed a supplementary wheelchair controller is installed between the joystick and the standard wheelchair motor controller. Along with sensors installed on the chair, the chair avoids obstacles and goes through openings with minimum input from the user. It has been tested with two power wheelchairs, Dynamics and Penny & Giles.

CALL Centre, University of Edinburgh
CALL Centre at the University of Edinburgh has developed the CALL Centre Smart Wheelchair. It was originally developed as a motivating educational and therapeutic resource for severely disabled children. The chairs were designed to assist in the assessment and development of physical, cognitive, social and communicative skills. Thirteen chairs have been built and evaluated in three local school, one in a residential hospital and three others in pre-vocational establishments.
The chairs are adapted, computer-controlled power wheelchairs which can be driven by a number of methods such as switches, joysticks, laptop computers, and voice-output. The mechanical, electronic and

software design are modular to simplify the addition of new functions, reduce the cost of individualized systems and create a modeless system. Since there are no modes and behaviors are combined transparent to the user, an explicit subsystem called the *Observer* was set up to report to the user what the system is doing. The *Observer* responds and reports its perceptions to the user via a speech synthesizer or input device.

The software runs on multiple 80C552 processors communicating via an I2C serial link monitoring the sensors and user commands. Objects or groups of objects form modules which encapsulate specific functional tasks. It is multitasking with each object defined as a separate task.

The architecture of behaviors each performing a specific functional task is similar to Brooks' Subsumption Architecture.

2.4 University of Michigan

Simon Levine, Director of Physical Rehabilitation at the University of Michigan Hospital began development of NavChair in 1991 with a grant for a three year project from the Veteran's Administration [Bell et al, 94]. The Vector Field Histogram (VFH) method was previously developed for avoiding obstacles in autonomous robots and was ported to the wheelchair. However, this method was designed for fully autonomous robots and it was soon determined that there were sufficient differences in the power base between robots and wheelchairs and in the requirements of human-machine systems that significant modifications were required. This resulted in a new method, called Minimum VFH (MVFH) which gives greater and more variable control to the user in manipulating the power wheelchair.

The Nav Chair has a control system designed to avoid obstacles, follow walls, and travel safely in cluttered environments. It is equipped with twelve ultrasonic sensors and an on-board computer. This team uses a shared-control system in which the user plans the route, does some navigation and indicates direction and speed of travel. The system does automatic wall following and overrides unsafe maneuvers with autonomous obstacle avoidance. Since it is desirable that the system change the user's commands as little as possible, the system and user must cooperat ively adapt to environmental or function conditions. A new method called "Stimulus Response Modelling" has been developed in which the system qualitatively monitors changes in the user's behavior and adapts in realtime. It is designed so that the adaptation is smooth and the change in modes intuitive to the user. By adjusting the degree of autonomy of obstacle avoidance the control modes of NavChair can be changed giving the user more or less control depending on the situation.

Nagasaki University and Ube Technical College Existing ceiling lights in an indoor environment are used as landmarks for self-localization of a motorized wheelchair by [Wang et al, 97]. The chair is therefore restricted to use within one the layout of which is known in advance. An azimuth sensor is used to give the angle between a fixed point and a particular object and a vision sensor detects the ceiling lights. The ceiling lights are used as the landmarks but if the lights are missed then the azimuth sensor and the rotating angle of both wheels provide the information necessary to continue the navigation.

A laser range finder is used to detect obstacles in the chair's path. Two CCD cameras are used, one is used to detect the ceiling light landmarks and the other is used in conjunction with the laser range finder to detect objects. A slit-ray is emitted from the laser emitter and this is detected by the CCD camera. The image signal is processed by a logic circuit constructed with an FPGA which informs the controller if passage is clear or where obstacles exist. In twenty test runs in a room with ten ceiling lights the maximum position error was 0.35 meters and the maximum orientation error was 17 degrees.

TIDE Programme

Technology initiative for disabled and elderly people (TIDE) programme of the European Union began in 1991 as a pilot action with 21 development projects and a budget of ECU18 million. The SENARIO project (SENsor Aided intelligent wheelchair navigatIOn), one of the initial projects within TIDE, includes 6 member companies from Greece, Germany, the UK, and France to introduce intelligence to the navigation system of powered wheelchairs. The system consists of five subsystems: risk avoidance, sensoring, positioning, control panel, and power control. The risk avoidance subsystem includes the central intelligence and inputs information from the sensoring and positioning subsystems. The sensoring subsystem includes ultrasonic, odometer, and inclinometer sensors. The positioning subsystem identifies the initial position of the chair by means of a laser range finder and allows the chair to be used in known environments. The control panel subsystem accepts user's instructions and the power control subsystem converts the system's instructions into vehicle movements.

The system has two modes of operation, the Teach mode and Run mode. In the Teach mode the user selects the desired paths from a topological diagram. In the Run mode (on a predefined path) the user selects a path and the system will follow it based on stored information obtained during the Teach mode. On a free route, the system takes instructions from the user and navigates semiautonomously while monitoring safety and taking action or warning the user of the level of risk.

Wellesley College, MIT

Wheeelesley is the name given to the chair used for experimental development by Holly Yanco, first at Wellesley College and now at MIT [Yanco et al, 95]. This chair has Subsumption Architecture-like layered approach to its performance. By means of a graphical interface the user of the chair points to the direction in which the chair should head. The chair then goes in that direction while performing other tasks such as obstacle avoidance. The interface also allows the user to tell the chair when specific tasks such as going up a ramp are required and to have a record of a particular environment and important features of that environment.

The chair is designed in such a way that it can turn in place. It has 12 proximity sensors, 6 ultrasonic range sensors, 2 shaft encoders and a front bumper with sensors. A 68332 computer is onboard and the interface runs on a Macintosh Powerbook. Work is underway to incorporate information from the angle of the eyes of the user to control the computer as a replacement for the mouse.

Northeastern University

The long-term goal of Crisman and Cleary [Crisman & Cleary,96] is to develop a robot which can go to a destination, retrieve an object and return it to the operator. A teleoperated and autonomous approach each has its strength and weaknesses. Therefore, a shared control approach is suggested to divide the task between the user and the robot, taking advantage of the strengths of each. The user performs high-level functions such as object recognition and route planning while the robot performs safety and motion controls. Since the user points the objects out explicitly in a video image, the robot has been named "Deictic". The robot, after receiving instructions how to move relative to the object, performs the local motion and waits for further instruction. This means there is continuous interaction between the user and the robot with the user giving instructions to the robot every minute or so. Commands are given to the robot by means of a button interface in which a verb description describes the desired motion of the robot and a noun describes the object relative to which the motion should be performed. The robot is able to navigate in almost any situation using its vision system to identify corners, edges, and polygonal patches. The initial work was done in simulation followed by an implementation on an Invacare Arrow wheelchair. Motion controller cards, optical encoders, and a vision system were added to the wheelchair New directional ultrasonic transducers were developed to detect obstacles at a wide angle in one direction and at a narrow angle in the opposite direction. This gave the robot the ability to detect objects not at standard height. A bumper with piezo-electric film embedded was installed to detect when the chair didbump an obstacle. A Puma 200 was used for the reaching experiments.

Powered vehicle Design Requirement:

I had studied so many litterateur survey regarding powered wheel chairs nothing will great on its working. its very expensive and operation and driving is critical compare to my proposed vehicle. its not a wheel chair it is a vehicle. My total vision is to help the PCPeoples, towards their required needs.

Required blocks to manufacture Proposed Vehicle:
1. Motor(Electro-Craft tape drive motor)
2. Controller
3. Batteries
4. Driven system
5. Tiers `
6. Dynamic braking
7. Bearings
8. Bolts and nuts
9. Belt
10. Body construction (Blue print)
11. Chassis formation

Above all are the requirements for the construction of powered vehicle for physically challenged peoples. And the following operations are performed to construct the vehicle

Design Operations:
➢ Marking operation
➢ Bending operation
➢ Drilling operation
➢ Threads cutting
➢ Step turning
➢ Groove cutting
➢ Cutting operation

- ➤ Welding operation
- ➤ Grinding operation

Motor:

      The motor is an electro craft tape drive motor from a reel to reel computer tape drive. The model number of motor was rubbed off. This motor firstly used to design cyclic motor vehicle. The specification of this motor is 5/8 inches diameter shaft and 14 gauge wire for power. Dimensions are 4 inches in diameter and 6.75 inches long. The motor has a fairly high winding resistance measured 0.5ohms which was one of the criteria that made me go with a 60 volt system.

Controller:

      The bike uses a 60 volt electrical system to take advantage of the characteristics of the motor and to lower battery losses due to high amperage . 60 volts is fairly nonstandard and there is a bite more difficulty finding compatible equipment than with the more typical 36v or 48v. luckily there are cheep scooter controllers and chargers available that work with 60v system. A key switch is used in-line with the throttle and accessory power circuit for security.

Fig.9: Block diagram of working of controller
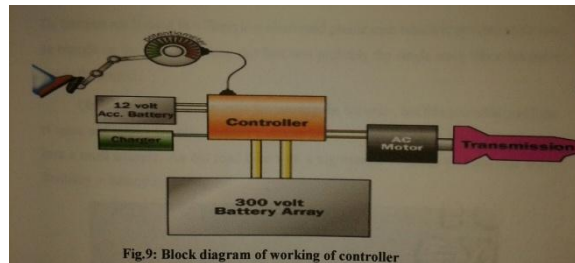
Batteries:

      Lead acid batteres were the default choice at least for the initial build/proof of concept. Five (5) 7 amp-hour, 12 volt "bricks" in a series string were used to get a nominal 60 volts. The battery pack weight is 13.6kg. The typical rules of lead acid and avoiding discharges of over 50% this battery pack has capacity of 210 watt hours:60v*7ah*0.5.

The batteries are house hold in a fiberglass reinforced plastic case which is molded to fit into the triangle on the frame making this box was probably the single most labor-intensive item in the project.

Drive system:

      The drive system of this powered vehicle is open belt drive. The open belt drive is used with shafts arranged parallel in the same direction. In this the driver pully pulls the belt from one side and delivers it to the other side. Thus the tension in the lower side belt will be more than that in the upper side belt. The lower side belt is known as tight side where as the upper side belt is known as slack side the open belt drive is as shown in the figure.

Tires:

      A venire stretcher pavement tires was installed. They were inexpensive and had good ratings

Dynamic breaking:

Given the heavy weight of the vehicle braking became more of a problem. The typical bicycle rim brakes worked but it was certain that wear of breaks pads and rims would be horribly quick if they were the only mode of braking.

Since the motor generates electricity when coasting down long steep hills for more power than the batteries could ever asorb inn regenerative braking a braking resistor was added. Its nothing more than a coil of stainless steel wire that gives a resistance of about 4ohms. Using the d_brake active a relay which switches the motor off of the controller and across this resistor.

Above all are the main requirements of my powered vehicle. And my pv structure is as following it will shown in engineering drawing . it is look like a auto structure because the handle of the auto controls all the momentum of vehicle so I also proposed auto structure and I placed an application i.e it will be drive suitable single limb peoples that's y I had selected this structure.

Above requirements are to design inner means the engine structure and the body.

Body Structure:

Body Frame represented in the form of Engineering drawing :

FIG. DIAGRAMATIC REPRESENTATION
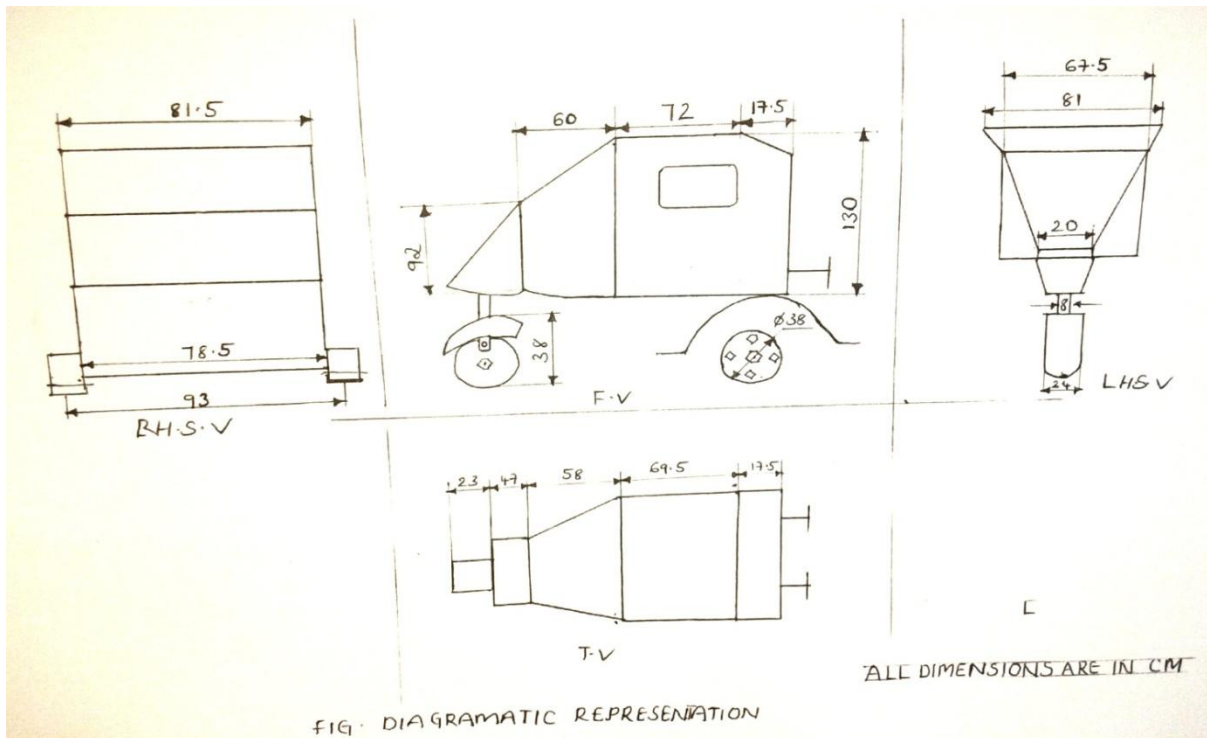
Facilities and Advantages:
➢ Cooking.
➢ Dust bin.
➢ Sleeping.
➢ Laptop.

ADVANTAGES:
1. More Facilities
2. Pollution Free
3. Noise free
4. Emergency Toilet
5. Less Cost
6. Less Vibrations
7. No fuel requirement
8. Easy maintenance

TECHNICAL DETAILS

6.1 TECHNICAL SPECIFICATIONS:

Vehicle type	: 3 Wheeler
Vehicle capacity	: Single person

Dimensions:

Powered vehicle length	: 218cm
Powered vehicle width	: 82cm
Powered vehicle height	: 152cm

Motor:

Motor weight	: 10kg
No of motors used	: 1
Motor type	: BLDC motor
Rated power	: 250W
Total vehicle weight	: 75kg

Battery:

Type	: Sealed lead acid
Voltage	: 48V
Capacity	: 12Ah
No of batteries used	: 4

Charger:

Rating	: 48V2A
Charging time	: 8-10 hrs
Range per charging	: 50 Kmpc
Power required	: 1 unit per full charging

No of controllers used : 1

Estimate speed : 25km per hour

No of wheels : 3

Wheel diameter : 38cm

No of bearings used : 2

No of shafts used : 1

Total shaft length : 100cm

No of pulleys used : 1

Pulley type : Flat

No of belts used : 1

Belt type : Flat

6.2 MATERIAL SPECIFICATIONS

Material type : MS Square pipes, circular pipe, flats and play wood

Square pipes thickness : 2.5mm

Circular pipes thickness : 3mm

Play wood thickness : 3mm

Belt material : Cotton

Pulley material : cast iron (built)

Shaft material : cast iron

II. Conclusion

This powered vehicle is not implemented .Our main criterian of this powered vehicle is economy of manufacturing.Despite of economy can any one can adopt automatic technologies for automatic opening and closing and openings of provided facilities so far cost factor we adopt simple technique in manufacturing of this multifaciltated vehicle.

The number of facilities provided in this power vehicle is helpful not only physically challenged people but also common .In personal intrest any one can adopt this vehicle.

These vehicles for challenged persons meet the expextations as the advanced technologies the person adopt this vehicle will satisfy more than expect. This vehicle provides almost all facilities without considerable moving of the person. Future Extension of my powered vehicle is automatic charging system by solar arrangement on the

top of the vehicle, automatic seasonal dome opening, and advanced suspension system for avoiding quick fatigue of driver.

The vehicle specifications at glance
Voltage: 48v
Millage: 50K.m per Charge
Load: 150 K.g
Weight: 75Kg

REFERENCES

[1]   "Production Technology" by R.K.JAIN KHANNA PUBLISHERS
[2]   "Machine Drawing" by K.L NARAYANA NEW AGE PUBLISHERS
[3]   "Machine Design" by R.S KHURMI , S.SHAND
[4]   "Automobile Engineering" by DR.KIRPAL SINGH,STANDARD PUBISHERS
[5]   "Theautomotive .chassis":Engineering principles" BY BUTTERWORTH-HEINEMANN
[6]   "D.C.Machines" by SESHAGIRI RAO,FALCON PUBLISHERS
[7]   "Machine Design" by THEREJA,S.CHAND PUBLICATIONS
[8]   "Electrical Technology" by THEREJA, S.CHAND PUBLICATIONS
[9]   "production Drawing" byK.L NARAYANA,NEW AGE PUBLISHERS
[10]   "Engineering Drawing" by N.D BHATT, CHARTOR PUBLISHERS
[11]   "Machine Design" by PANDEY AND SHAH, CHARTOR PUBLISHERS
[12]   "Automobile Engineering"by M.SREENIVASULU,FACCON PUBLISHERS
[13]   "Production Technology"by K.L KRISHNA REDDY, BS PUBLICATIONS
[14]   "Automobile Engineering" by RAMALINGAM scitech publications.

Finite Element Analysis of Anti-Roll Bar to Optimize the Stiffness of the Anti-Roll Bar and the Body Roll

Bankar Harshal[1], Kharade Rushikesh[2], P. Baskar[3]

[1,2](M.Tech Automotive Students VIT University, Vellore, Tamil Nadu)
[3] (Professor SMBS VIT University, Vellore, Tamil Nadu)

Abstract: *The objective of this paper is to analyze the main geometric parameters which affecting the stiffness of anti-roll bar. Further these parameters are also affecting the body roll angle. By the optimization of these geometric parameters we can able to increase the stiffness of bar and which will help to reduce the body roll angle. To calculate the stiffness of anti-roll bar Finite Element software ANSYS is used. The deflection for the change in internal angle, arm length, moment of inertia, distance between bushes found by static analysis. To calculate the body roll angle equation used from the literature survey, however they haven't taken all the suspension characteristics in the calculation of moment caused by the suspended and non-suspended masses. The equilibrium condition is considered between the moments of the force acting on the suspended and non-suspended masses and moments of reaction of the springs and anti-roll bar used in suspensions. The comparison of different anti-roll bar is based on the basis of stiffness per weight. The anti-roll bar which having more ratio of stiffness per weight can be used in the vehicle. As it will improve the stiffness of bar with small increase in weight, which will result in the improving roll stability of the vehicle.*

Keywords: *moments, non suspended, stability, stiffness, suspended*

I. INTRODUCTION

Automobile industry focus on producing element which give handling and performance of the vehicle better than today's vehicle but such element should not produce the extra cost and also it should be improve the comfort level of the vehicle that is to the passenger.

Anti roll bar is one of the inventions in the automobile industry which is also called as sway bar or stabilizer bar. Structure of such anti roll bar are U shaped bar which connect two wheel that is left and right wheel and bar is fixed to the chassis of the vehicle by bush.Anti roll bar may be solid or hollow tube. The main function of anti roll bar is reducing body roll motion when the vehicle is at the cornering condition. Body roll condion occurs due to the load transfer and changes takes place in the camber of vehicle which directly affect the steering behavior of the vehicle and vehicle loses its stability therefore to eliminate the roll effect in case of under steer and over steer anti roll bar is used. Anti roll bar give comfort in driving condion and safety in case of such roll situation.
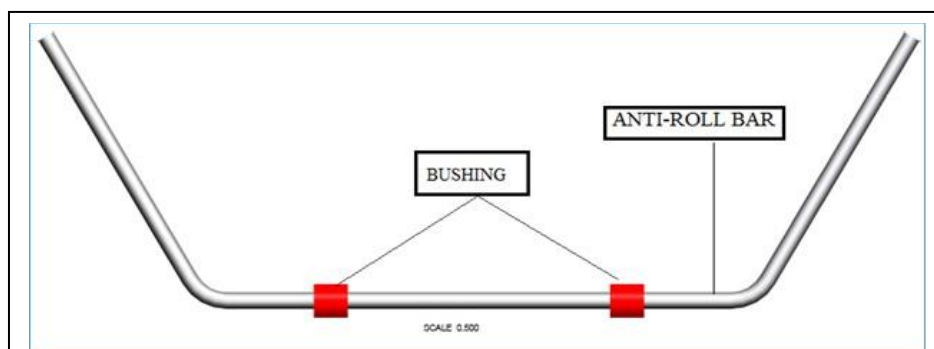
Figure-1 anti-roll bar with bus

When both the suspension affected simultaneously then the effect of the anti roll bar is eliminated. when one of the wheel moves opposite of the other then anti roll bar acts like the torsion spring and it will provide the torque such that it will oppose the motion of the vehicle so that tilting motion of the vehicle will

balanced that is neutralize the vehicle[1].Another important advantage of the anti roll bar is that it allow to use the less stiff spring therefore it can absorb the uneven road shocks which can give ultimately comfort to the passengers[2].In case of anti roll bar, SAE (society of automotive engineers) will provide the information of process of manufacturing of anti roll bar, equation to find out the stiffness of anti roll bar where load is applied at the end of the bar but only simple shapes of anti roll bar is used to apply these equation[3].To develop anti roll bar different design technique should be used

The effect of anti-roll bar when used at the front suspension is studied by[4].In this paper vehicle used for study is bus and considered effect without or with anti-roll bar and finally given equation which gives information of roll angle and rigidity of anti-roll bar.

The effect of different variable which affect the roll motion of the body and stiffness of anti-roll bar is important factor to study. When the anti-roll bar is used in the vehicle then   reduces the body roll by 48.4 % which gives stability to the vehicle [5].In this paper author also used finite element method to find the stiffness of the anti-roll bar and also show that lowest stiffness to the weight ratio is achieved by using the shortest length of side length of the bar.

The main objective of this paper is to analyze the anti-roll bar for stiffness and body roll of the vehicle by varying the various geometric condion of the anti-roll bar. In this paper we also find the variation which will give the lowest value of stiffness to the weight ratio.

II. METHODOLOGY

To achieve target of the paper we have done different geometrical variation in anti-roll bar that is we have variation in length of bar, variation in the distance of bush, variation in the angle between two arms of bar, varying the moments of inertia of the bar and by using the different cross section at the end of ant-roll bar. For analysis we have used simple geometry of anti-roll bar and to calculate the stiffness of the anti-roll bar we have used the finite element method that is by using software. In this paper we consider the use of anti-roll bar at the rear suspension of the vehicle.

1. Stiffness of Bar

Stiffness of the anti-roll is given by the equation,

$$k_e = F/\Delta x \qquad\qquad (1)$$

To calculate the roll stiffness divide the applied force by summation of absolute value of the deflection at the bar end which is find in the CAD software that is we have used the ansys workbench 14 for simulation and analysis of anti-roll bar. We have considered only static analysis means we have eliminated the effect of the dynamic condion. We have applied load at the end of ant-roll bar which is of 1KN which is of linear type and bush is fixed. In this paper material considered is steel for anti-roll bar. Properties of steel used are density, modulus of elasticity and Poisson's ratio. Load applied at one end is 1 KN in one direction but for other end we have applied the same load in opposite direction.
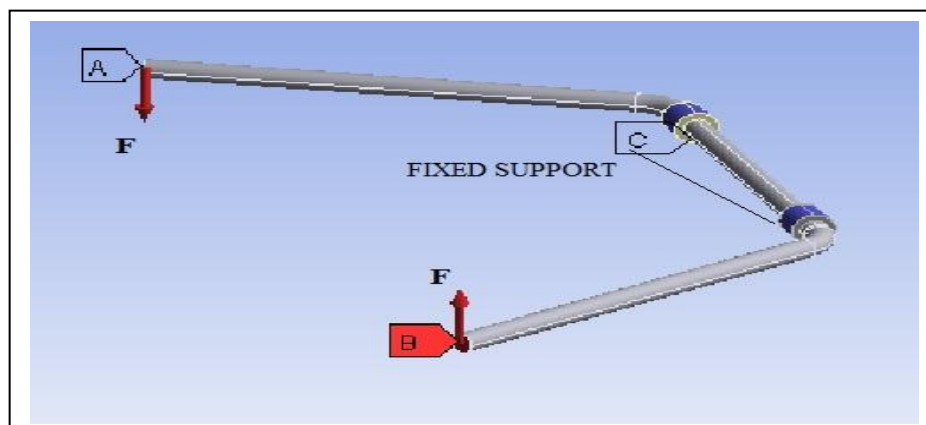
In this paper we have considered the geometrical variation of anti-roll bar and considered the response in terms of deformation by applying the load which having magnitude of 1KN after applying this load deflection is found in software. We have considered the absolute value of deflection only. The main purpose to find the deflection of the anti roll bar is found out the rigidity of the anti roll bar. In this analysis we have draw

---

simple model of anti-roll bar which mean that obtained result will not be result in the reality that is we can get the variation in the stiffness of bar and roll motion of the vehicle.
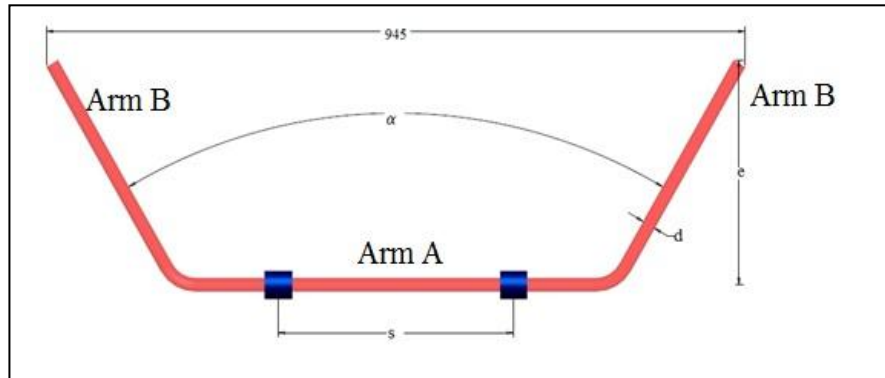
For analyze anti-roll bar we have the modification in the variation of 'e', variation between angle of two arms that is angle alpha, varying the moment of inertia of bar A and B by considering the different inner and outer diameter, varying the distance between arms that is 'S' and by considering the rectangular section at the one end of anti roll bar. In this work we have not changed the distance between the two arm ends.

1.1 Variation in the distance between horizontal arm and end of bar that is 'e' in the vertical direction.
In first part of the analysis we have changed the distance 'e' which is will show in the TABLE

Table-1

Anti-roll bar	1	2	3	4	5
e (mm)	220	270	320	370	420

In first case we have considered the following parameters
1. α (alpha) = 60^0.
2. S = 350 mm.
3. A and B: solid geometry having an outer diameter of 20 mm, A_o = 314.2 mm^2, I = 7854 mm^4 e, J =15708 mm^4.
4. Different weights of the anti-roll bar

Whereas I is moment of inertia, A_o is the outer diameter of the bar and J is the polar moment of inertia. The profile of the anti roll bar, moment of inertia, area of cross section is same in case of the analysis of first case. We can get the weight increase of the anti-roll bar which is due to the increase in the length of bar.
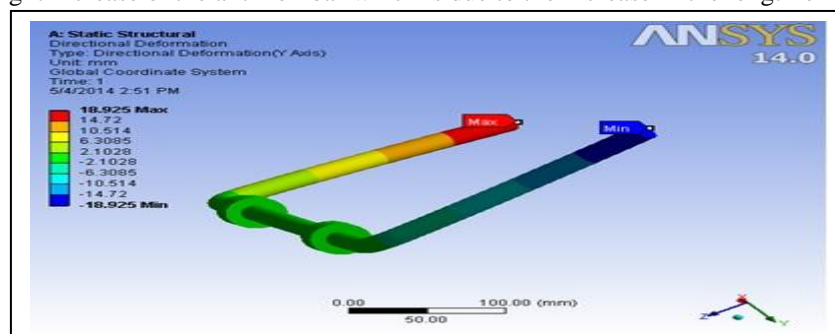
Above Fig shows that when first condion of the 'e' variation where we have applied 1 KN load and maximum deflection is noted. Maximum deflection observed is 18.925 mm on one side of bar. Total deflection will be summation of the both side deflection where absolute value should be taken.

1.2 Variation in the moments of inertia of A and B
Second analysis mainly to observe the change in the stiffness of bar but weight of anti-roll bar is not considered that we have not changed the cross section of the bar. Polar moment of inertia, moment of inertia of A and B changed.

Table-2

Anti-roll bar	6	7	8	9	10
$\emptyset_o$ (mm) of arm A & B	21	22	23	24	25
$\emptyset_i$ (mm) of arm A & B	6.4	9.2	11.4	13.3	15
I (mm^4) of arm A & B	9464	11147	12907	14750	16689
J (mm^4) of arm A & B	18928	22294	25815	29500	33379

In second case we have considered the following parameters
1 .e=420 mm
2. α =60^0
3. S=350 mm
4. A and B having area equal to 314.2 mm^2
5. Weight 40.14 N

1.3 Variation of the distance between the bush 'S'
In this section we have done variation in the distanced between the bush which is fixed to the chassis and give support to the anti-roll bar. The following TABLE gives information about this variation.

Table-3

Anti-roll bar	11	12	13	14	15
s (mm)	100	150	200	250	300

For third case we have considered the following parameter
1. e =420 mm
2. α =60^0
3. A and B section having outer diameter equal to 20 mm and area is 314.2 mm^{2}and moment of inertia I =7854 mm^4, polar moment of inertia equal to J=15708 mm^4.
5. Weight is equal to 40.14 N

1.4. Variation in angle between the two arms 'α'
In case of forth study we have done variation in angle between A and B.

Table-4

Anti-roll bar	16	17	18	19	20
α (^{0})	0	12	24	36	48

For forth we have considered the following parameter
1. e =420 mm
2. S =350 mm
3. A and B section having outer diameter equal to 20 mm and area is 314.2 mm^{2}and moment of inertia I =7854 mm^4, polar moment of inertia equal to J=15708 mm^4.
4. Different weights.

1.5. Variation in the profile of 'B' with changes in moment of inertia.
In this section we have changed the cross section of the B section from tubular section to the rectangular section this gives rigidity to the part.
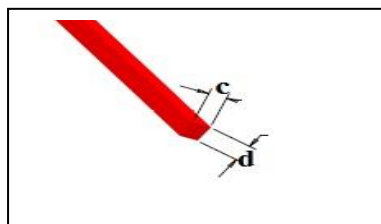
Figure-5 Changes made in profile B

Above Fig shows that rectangular cross section of profile B with variation made in the dimension of C and D but we have taken the same profile of A.

Following TABLE shows variation done on the cross section of profile B.

Table-5

Anti-roll bar	21	22	23	24	25
Height *c* (mm)	20	22.5	25	27.5	30
Width *d* (mm)	20	17.8	16	14.5	13.3
I (Stretch B) (mm4)	13333	16896	20833	25129	29925

For fifth study we have considered the following parameters
1. e =420 mm
2. α =60
3. S =350 mm
4. Profile B with area equal to 400 mm^2
5. Profile A having an outer diameter of 20 mm, Ao = 314.2 mm2, I = 7854 mm4 e, J =15708 mm4.
6. Weight 46.19 N

1.6 Variation in the profile of A without changes in the moment of inertia of section.
In this section we done variation in tubular section of the A but we have maintained the moment of inertia.
Following TABLE gives information about variation in the profile A.

Table-6

Anti-roll bar	26	27	28	29	30
Ø$_o$ (mm) of arm A	21	22	23	24	25
Ø$_i$ (mm) of arm A	13.6	16.5	18.6	20.4	21.9
A (mm^2) of arm A	285.6	363	427.8	489.6	547.5
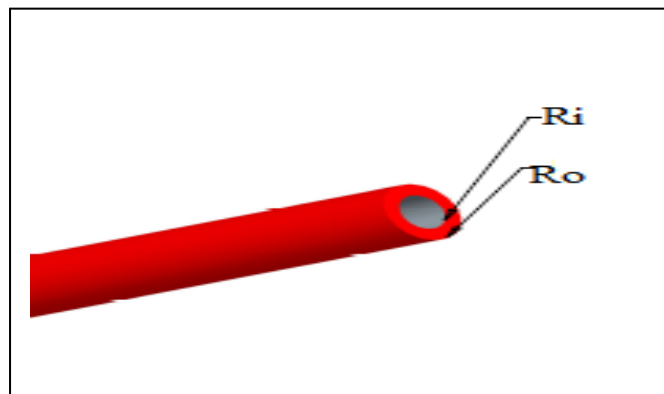
For sixth we have considered the following parameters where moment of inertia is maintained constant
1. e =420 mm
2. α =60^0
3. S=350 mm
4. Profile A having tubular section with the I= 7854 mm^4 and J=15708 mm^4
5. Profile B having outer diameter is equal 25 mm and 19174.8 mm^4
6. Different weight is considered

2. Roll Angle Calculation
In this section roll angle calculation is done based on method given by [6].In this method roll angle is actually tire grip coefficient between the wheel and road track. In this section we have taken μ$_s$ is equal to the 0.7.
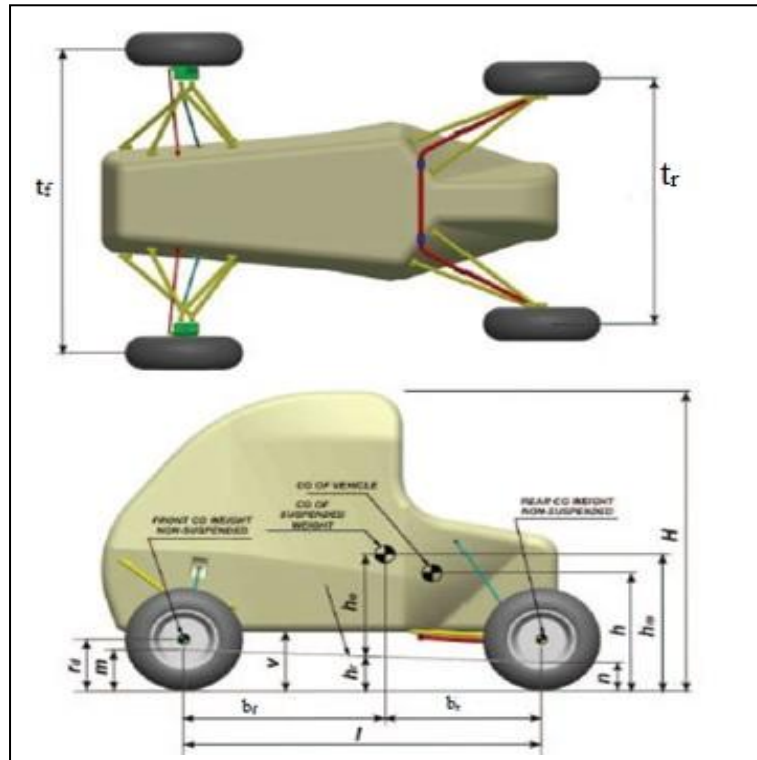
Figure-7 gives dimension of the vehicle which is to be considered in this paper [5].

Following TABLE gives information about dimension of the vehicle [5], Table-7 [5]

v	275 mm	Free vain
H	1400 mm	Total height
l	1450 mm	Distance between axles
h	550 mm	Height of center of gravity (CG)
r_d	240 mm	Dynamic radius of the tire
t_f	1420 mm	Front axle width
t_r	1150 mm	Rear axle width

In cornering situation the distribution of the weight is important. Following TABLE gives weight distribution Table-8 [5]

G	2452.5 N	Total vehicle weight with driver
		% Of the weight on the front axle
G_f	1103.625 N	Weight on front axle
Wn_f	274.68 N	Weight of the non-suspended masses on front axle
W_f	828.945 N	Weight of the suspended masses on the front axle
G_r	1348.875 N	Weight on the rear axle
Wn_r	274.68 N	Weight of the non-suspended masses on rear axle
W_r	1074.195 N	Weight of suspended masses on rear axle
W	1903.14 N	Weight of suspended masses
R_{0f}	1103.625 N	Reaction of the front wheels on the ground when the vehicle is stationary
R_{0r}	1348.875 N	Reaction of the rear wheels on the ground when the vehicle is stationary

Calculation of the b_f and b_r is done by following formulas,

$$b_f = \frac{R_{or} - W_{nr}}{W} l$$

(2)

$$b_r = \frac{R_{of} - W_{nf}}{W} l \tag{3}$$

Location of the center of gravity of the mass which is to be suspended mass gives the tilt of the vehicle which is due to moment produced at the axis of the vehicle. To calculate this it is considered that it will act the location of center of the wheel that is W_{nr} and W_{nf}.[6].Following formulas gives height of center of gravity of the suspended mass

$$h_m = \frac{\lfloor Gh - (W_{nf} + W_{nr})r_d \rfloor}{W} \tag{4}$$

Following TABLE gives information of center of gravity of the suspended mass based calculation done by using the equation (4).

Table-9 [5]

b_f	818.4 mm	distance of the CG of the suspended masses until the front axle
b_r	631.6 mm	distance of the CG of the suspended masses until the rear axle
h_m	639.5 mm	height of the CG of the suspended masses

Wheel will rotate at the instantaneous center of rotation which is known as reaction point and that of suspension system considered as roll center [6]. Value of that corresponding to front and rear we have taken from the paper [5].The Following TABLE gives information about front and rear point.

Table-10 [5]

m	192.1 mm	Height of the front roll center
P_f	-731.9 mm	Height of the front reaction point
n	133.7 mm	Height of the rear roll center
P_r	275.0 mm	Height of the rear reaction point

The distance between the c.g. of the suspended mass and roll axis of the vehicle is given by following equation (5) [6].

$$h_o = h_m - \frac{(nb_f + mb_r)}{l} \tag{5}$$

The calculation of the h_o is given in the following TABLE

Table-11[5]

h_o	480.3 mm	Distance of the center of gravity of the suspended mass to the roll axis
h_r	159.1 mm	Height of the roll axis to the ground

While taking the turn momentum is produced due to the centrifugal force of the suspended mass also load transfer takes place from inner wheel to the outer wheel which gives the inclination of the vehicle [6]. When extreme condion of the transverse arm is considered then spring constant is given by function of the stiffness of the spring and u position which is attached to the arm length of v. the following equation (6) gives relation between them[6]

$$K = k \left(\frac{u}{v}\right)^2 \tag{6}$$

The value of the stiffness at the front suspension is given by Following TABLE

Table-12 [5]

k_f	15 KN/m	Front spring stiffness
u_f	250 mm	Spring fixing position on the front arm
v_f	361 mm	Front arm length
K_f	7.2 KN/m	Spring constant in the extreme of the front arm

The value of the stiffness at the rear suspension is given by following TABLE.

Table-13 [5]

k_r	10 KN/m	rear spring stiffness
u_r	485 mm	Spring fixing position on the rear arm
v_r	596 mm	rear arm length
K_r	6.6 KN/m	Spring constant in the extreme of the rear arm

The spring constant effectively of the anti roll bar when the transverse arm is at the extreme condion is given by following equation [6]

$$K_E = k_e \left(\frac{u}{v}\right)^2$$

(7)

We have calculated only K_{EI} and K_{EII} because we have considered the anti-roll bar is only at the rear suspension. Value of the u and v gives the spring constant in the extreme condition of the rear arm.
To calculate the roll angle we have considered the moment between the moment of the stabilizer as well as moment of spring which is balanced by force of the suspended mass and unsuspended mass [6].
Momentum caused due to the suspended mass is given by following equation [6]

$$M_{RO} = \mu_s W h_O$$

(8)

Momentum caused due to the non suspended mass of the front axle is given by following equation [6]

$$M_{R1} = \mu_s W_{nf} r_d \left(1 - \frac{m}{P_f}\right)$$

(9)

Momentum caused due to the non suspended mass of the rear axle is given by following equation [6] ,

$$M_{R2} = \mu_s W_{nr} r_d \left(1 - \frac{m}{P_r}\right)$$

(10)

Roll angle of the vehicle body is given by following equation [6]

$$\varphi = \frac{M_{RO} + M_{R1} + M_{R2}}{\left(\frac{t_f^2}{2}\right) K_f + \left(\frac{t_r^2}{2}\right) K_r + \left(\frac{t_f^2}{2}\right) K_{Ef} + \left(\frac{t_r^2}{2}\right) K_{Er}}$$

(11)

'f' is the lateral displacement at the top most point of the vehicle when the vehicle occurs with the body roll.
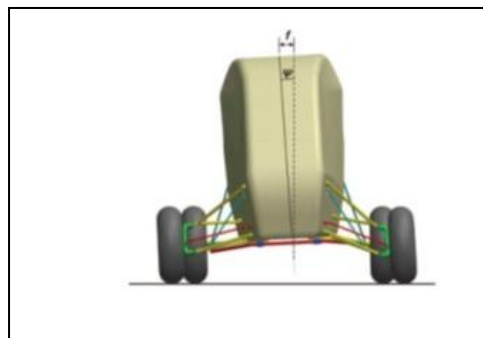
Figure-8 lateral displacement at top most point of the vehicle [5]

III. Result

Roll angle of the vehicle is calculated without considering the anti-roll bar. For calculation purpose we have used above procedure. Spring constant of the bar is zero in both the case that is in front and rear suspension. To find the roll momentum the weight of the bar is to be added to the weight of non suspended mass but this effect is very small to the roll of the vehicle.The main aim is to get the higher stiffness to the weight ratio to decrease the rolling effect of the body. Anti roll bar should be strong to the bending as well as twisting moment to reduce roll and it have less weight so that non suspended weight is less that why vehicle will follow the contour of the road due to its less inertia.
Following tables as well as graph shows result when the different geometrical variation done on the anti-roll bar, depending on that variation stiffness to the weight ratio is important to find the best suitable anti-roll bar.

3.1 Variation in the arm length 'e'
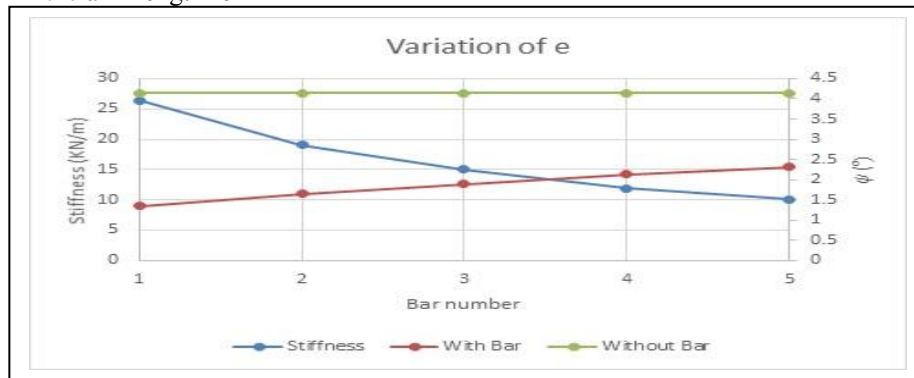
Figure-9 Effect of varying the length of arm 'e'

Following TABLE shows the effect of varying the arm length

Table-14

Anti-roll bar	1	2	3	4	5
e (mm)	220	270	320	370	420
Weight (N)	33.42	35.95	37.35	38.74	40.14
K_{er} (KN/m)	26.42	19.07	14.99	11.92	10.02
Stiffness/Weight (1/m)	0.79	0.53	0.40	0.31	0.25
Ψ (°)	1.34	1.65	1.89	2.13	2.31
f (mm)	28.98	35.70	40.97	46.12	49.97

Spring constant of the anti-roll bar decrease when the length of bar 'e' is increased. It is observed that when the factor of rigidly is declined then roll angle of the vehicle is increased. The Table-14 shows that stiffness to weight ratio is decreased so bar becomes flexible which will to reduce the effect of reducing roll of the body. Out of Five bars first anti-roll bar shows best result which shows the minimum roll angle.

The best performance on the stiffness/weight ratio for the five configurations analyzed was achieved by the first bar, which provided the greatest reduction of the roll angle and displacement of 67.68% when compared to the vehicle without the anti-roll bar

3.2 *Variation* in the moment of inertia of A and B
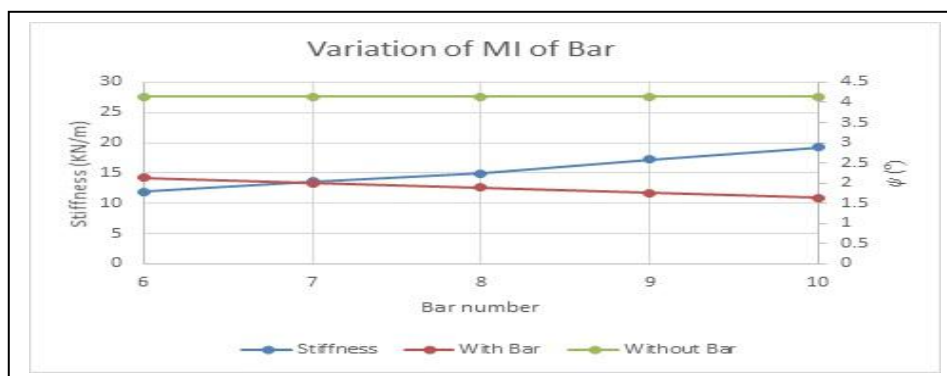
Following TABLE shows the Effect of varying the moment of inertia of A and B on the stiffness to the weight ratio.

Table-15

Anti-roll bar	6	7	8	9	10
$\emptyset_o$ (mm) of arm A & B	21	22	23	24	25
$\emptyset_i$ (mm) of arm A & B	6.4	9.2	11.4	13.3	15
I (mm^4) of arm A & B	9464	11147	12907	14750	16689
J (mm^4) of arm A & B	18928	22294	25815	25900	33379
Weight (N)	40.14	40.14	40.14	40.14	40.14
K_{er}(KN/m)	11.87	13.59	14.91	17.24	19.22
Stiffness/Weight (1/m)	0.30	0.34	0.37	0.43	0.48
Ψ (°)	2.13	1.99	1.90	1.75	1.64
f (mm)	46.20	43.17	41.10	37.90	35.54

Variation in the stiffness of the anti-roll bar takes place due to the changes takes place in the momentum of the inertia. Flexural strength resistance is more if the momentum of inertia the bar is more and bar will have maximum torsion resistance when polar moment of inertia have maximum value. If the momentum of inertia and polar moment of inertia is more the bar will be have more rigidity.

Stiffness to weight ratio will be more in last bar which is the best result among the five bar .Roll angle and upper travel will be reduced in this anti-roll bar when we compared with anti-roll bar. The roll angle and the upper travel for this case were reduced by 60.37%, compared with the values of the vehicle without the anti-roll bar.

3.3. Variation of the distance between the bush 'S'
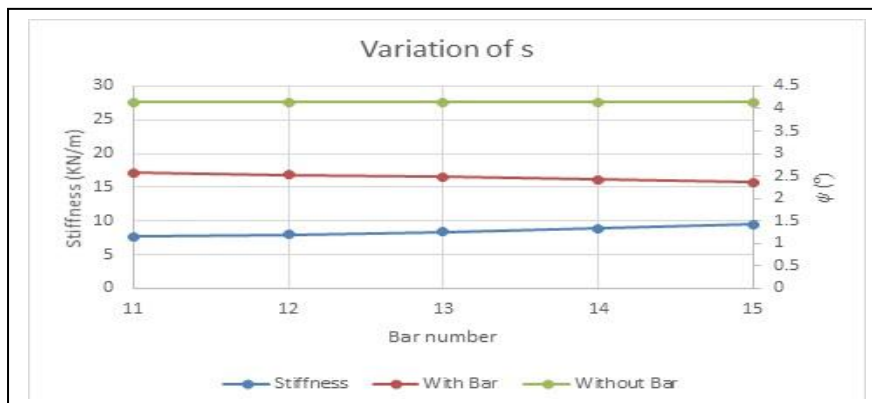
Figure-10 Effect of varying the distance between the bush

Following TABLE shows effect when distance between the bushes is changed.

Table-16

Anti-roll bar	11	12	13	14	15
s (mm)	100	150	200	250	300
Weight (N)	40.14	40.14	40.14	40.14	40.14
K_{eii}(KN/m)	7.64	8.00	8.42	8.92	9.51
Stiffness/Weight (1/m)	0.19	0.20	0.21	0.22	0.24
Ψ (°)	2.58	2.53	2.48	2.43	2.36
f (mm)	55.85	54.87	53.79	52.53	51.12

When bushing is far then the rigidity of the bar will increase as well as stiffness also increased .Rigidity to the assembly is given if bushing are away from each other but it will possible if extra support should not required for that arrangement and this will not add extra weight to the vehicle arrangement.

The best stiffness to weight ratio is given by last bar .Roll and 'f' that is upper travel is reduced by 43%, when compared with the values of the vehicle without the anti-roll bar.

3.4. Variation in angle between the two arms 'α'
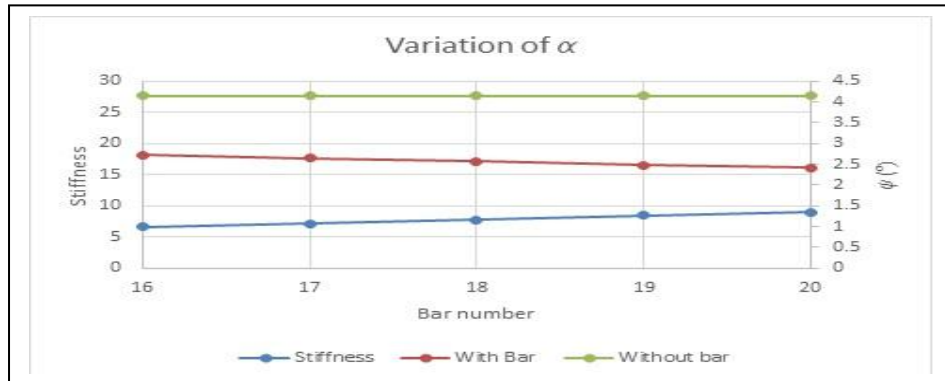
Figure-11 Effect of varying the angle between the arms

Following TABLE shows the effect of changing the angle between arms

Table-17

Anti-roll bar	16	17	18	19	20
α (⁰)	0	12	24	36	48
Weight (N)	47.95	46.16	44.50	42.96	41.51
K_{eII}(KN/m)	6.60	7.13	7.71	8.49	9.01
Stiffness/Weight (1/m)	0.14	0.15	0.17	0.20	0.22
Ψ (º)	2.72	2.65	2.57	2.47	2.41
f (mm)	58.88	57.31	55.65	53.60	52.31

From above figure it is observed that if angle between the arms is more the rigidity will be more. If angle small the length of the bar that subjected to the bending is greater than other bars, If the angle is increase then weight of the bar is reduced hence we got ratio of stiffness to the weight is increased and rigidity will improved Stiffness to the weight ratio is more in last result of bar 20. Roll angle and length of upper travel is reduced Over 41.67% when compared to the values of the vehicle without the anti-roll bar.

3.5. Changes in momentum of inertia of profile B of rectangular cross section.
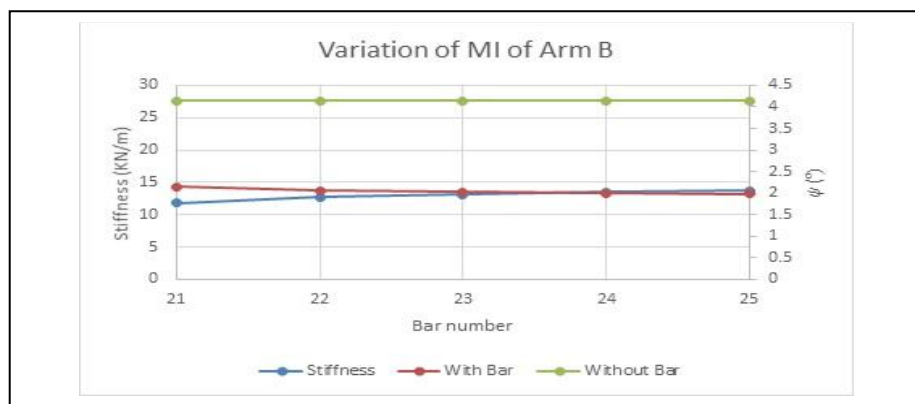
Figure-12 Shows the Effect of changing the momentum of inertia of profile B

Following TABLE shows changes in momentum of inertia of the cross section B.

Table-18

Anti-roll bar	21	22	23	24	25
Height c (mm)	20	22.5	25	27.5	30
Width d (mm)	20	17.8	16	14.5	13.3
I (Stretch B) (mm4)	13333.33	16896.09	20833.33	25129.56	29925
Weight (N)	46.22	46.26	46.22	46.13	46.15
K_{all}(KN/m)	11.78	12.69	13.06	13.50	13.74
Stiffness/Weight (1/m)	0.25	0.27	0.28	0.29	0.30
Ψ (°)	2.14	2.06	2.03	2.00	1.98
f (mm)	46.37	44.70	44.06	43.32	42.92

In this section another way to improve the stiffness is increasing momentum of inertia by varying the width and height of the profile B that is rectangular section. Weight is approximately constant in all bars and area also constant. Best result is for bar five in terms of stiffness to the weight ratio. The roll angle of body and 'f' that is upper travel is reduced by to 52.13% when compared with the values of the vehicle without the anti-roll bar.

3.6. Variation in the profile of A without changes in the momentum of inertia of section.
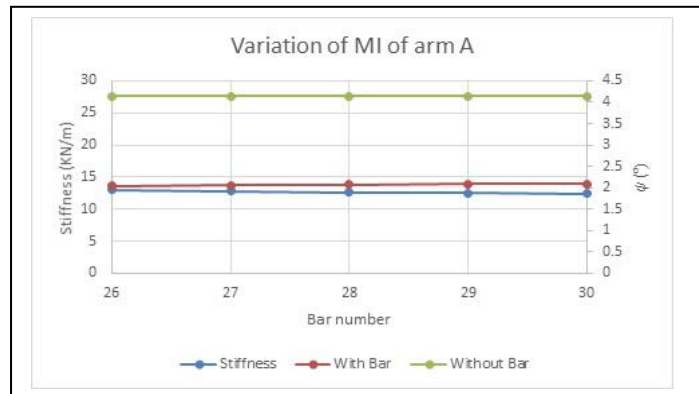
Figure-12 shows the effect of variation in profile A

Following TABLE shows changes in momentum of inertia of A profile.

Table-19

Anti-roll bar	26	27	28	29	30
$\emptyset_o$ (mm) of arm A	21	22	23	24	25
$\emptyset_i$ (mm) of arm A	13.6	16.5	18.6	20.4	21.9
A (mm²) of arm A	285.6	363	427.8	489.6	547.5
Weight (N)	48.89	48.59	47.68	46.89	45.72
K_{all}(KN/m)	12.96	12.77	12.61	12.46	12.38
Stiffness/Weight (1/m)	0.27	0.26	0.26	0.27	0.27
Ψ (°)	2.04	2.06	2.07	2.08	2.09
f (mm)	44.23	44.57	44.85	45.12	45.26

In sixth analysis we can get that if profile is changed and polar moment of inertia is constant then stiffness does not changes which shown by practically also. By variation in cross section and loss in weight we can get same rigidity. After analysis last bar give good result in terms of stiffness to the weight ratio. Roll angle and 'f' upper travel length reduced by more than 49.53%, when compared to the values of the vehicle without the anti-roll bar.

IV. Conclusion

We have got satisfactory result of anti-roll bar in terms of reducing the roll of the body that is roll angle of the vehicle by using the simple geometry of anti-roll bar. we can reduce body roll up to 67.68 % than vehicle without anti-roll bar so finally we can conclude that if implementation of the our modified bar is used then finally stability of the vehicle will improved.

Best stiffness to weight which is having the minimum length of the arm 'e'. Rigidity of the anti-roll is important criteria which is achieved if the less portion of bar is subjected to bending and in terms of flexibility of bar we can conclude that bush should be away from with one another.

We have changed profile of bar, momentum of inertia of bar increased then we got that stiffness of bar is improved but without increment in weight this conclusion give idea about we can achieve our target but with reduced cost of the vehicle. Stiffness to weight ratio give conclusion about the rigidity of the bar ,in this paper we have done modification in anti-roll bar to analyze performance in terms of this ratio

In this project we have found the stiffness of bar by using the software of finite element method and for roll angle calculation we have used equation proposed by literature review author. Future work of this project is that stress analysis of the anti-roll bar which will show which areas of bar subjected to more stress and depending on that use of anti-roll bar.

REFERENCES

[1]   Bernd Heibing, Metin Ersoy Chassis Handbook (Wiesbaden, Germany, 2011)
[2]   Thomas D. Gillespie Fundamentals of Vehicle Dynamics (Society of Automotive Engineers, Warrendale, USA, 1992)
[3]   SAE Spring Committee Spring Design Manual (Society of Automotive Engineers, 1996)
[4]   Uhlmann, C., Análise da influência da barra estabilizadora no ângulo de rolagem da suspensão dianteira de ônibus Universidade Federal do Rio Grande do Sul, Porto Alegre, Brazil, 2009.
[5]   Sérgio Yuri Ribeiro, Márcio Eduardo Silveira Application of Finite Element Method in the Study of Variables that Influence the Stiffness of the Anti-Roll Bar and the Body Roll Society of Automotive Engineers(SAE) journal 2013-36-0643
[6]   Leal, L., Rosa, E.,Nicolazzi, L.,Uma Introdução à Modelagem Quase-Estática de Veículos Automotores de Rodas Internal Publication, Universidade Federal de Santa Catarina, Florianópolis, Brazil, 2008.
[7]   Ian Czaja, Mohammad Hijawi , Automotive Stabilizer Bar System Design and Reliability Society of Automotive Engineers(SAE) journal 2004-01-1550
[8]   Çalişkan, K., Automated design analysis of anti-roll bars Ankara, Turkey, 2003.
[9]   Reimpell, J., and Stoll, H., The Automotive Chassis: Engineering Principles (Society of Automotive Engineers, Warrendale, USA, 1996.

Numerical Investigation of Multilayer Fractal FSS

R. H. C. Maniçoba[1], A. F. Santos[2], A. V. Lovato[3], N. M. Oliveira-Neto[4],
D. B. Brito[5], A. L. P. S. Campos[6], A. G. d'Assunção[7]

[1, 2, 3, 4] *(Collegiate of Information Systems Course, State University of Southwest Bahia – UESB, Jequié-BA, Brazil)*
[5]*(Institute of Computing, Federal University of Alagoas, Maceió-AL, Brazil)*
[6, 7]*(Communication Engineering Department, Federal University of Rio Grande do Norte, Natal-RN, Brazil)*

Abstract: *Numerical investigations are presented for a multilayer frequency selective surface with Koch fractal (levels 1 and 2) conducting patch elements. The structure investigated is obtained using two FSS screens separated by an air gap layer. For the proposed investigation were used three different values an air gap height. The results obtained using the numerical method were compared with other technique and using the commercial software Ansoft Designer[TM]. A good agreement was observed in terms of the bandwidth.*
Keywords: *FSS, Numerical Method, Multilayer Structure, Fractal, Wideband*

I. INTRODUCTION

A periodic surface can be defined basically as a set of identical elements arranged in two or three dimensions forming an infinite array. A periodic array formed by conductive patch elements or opening elements is known as Frequency Selective Surface (FSS). FSS are periodic structures that can provide frequency filtering to incoming electromagnetic waves, and their frequency response is entirely determined by the geometry of the structure in one period called a unit cell [1, 2].

Traditional FSS has a long history of development and have been investigated over the years for a variety applications, e.g., frequency filters or diplexers in high performance reflector antenna systems, advanced radome designs, and smart surfaces for stealth applications [3].

The question of operating bandwidth is one of important problems in FSS theory, in some applications a multiband frequency response is desired; however in other applications a wideband frequency response is more preferred. FSS structures have been successfully proven as a mean to increase the communication capabilities of satellite applications. In space mission (Voyager, Galileo and Cassini), for example, the use of dual antenna system with FSS reflectors has made it possible to share the main reflector among different frequency bands, therefore FSS with multiband responses have been studied by several researchers. But, in some applications, such as separating successive frequency bands, FSS are required to have a wide transmission or reflection bands and rapid rolloffs [4-10].

Experimental and numerical investigations on cascading or multilayer FSS have been done, using full and simple (approximate methods) [11-14]. This paper presents a numerical investigation of multilayer or cascaded FSS using a simple but efficient method used to predict the frequency response (transmission coefficient) for these structures. In this work was analyzed a multilayer FSS structure, using conducting Koch fractal elements. This structure was first proposed in [15] and consists of two FSS, called structure 1 and structure 2 mounted on a dielectric isotropic layer, separated by an air gap layer. The dielectric substrate used was the RT-Duroid 3010, with 1.27 mm of height and relative permittivity equal to 10.2 and unit cell periodicity ($T_x = T_y$) equal to 10 mm. We used the commercial software Ansoft Designer[TM] to obtain the individual scattering parameters of each one FSS structure. To validate the results a comparison with results from other numerical method is performed.

II. FSS THEORY

Through the use of the spectral domain approach to analyzing the response of an FSS, which is assumed to have infinitesimal thickness, one can determine the electromagnetic fields on a plane $z = z_n$, see Fig. 1 and Fig. 2, These electric fields are expressed in terms of a discrete spectrum of plane waves known as Floquet harmonics.
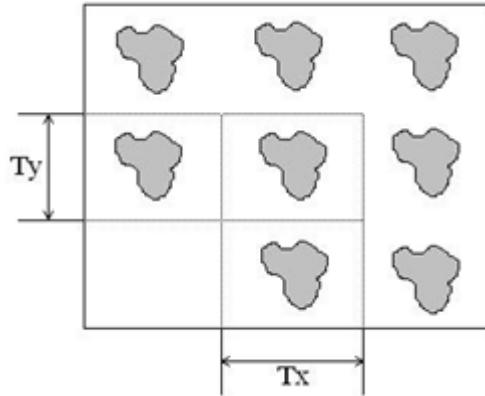
Fig. 1: Front (superior) view of a FSS.
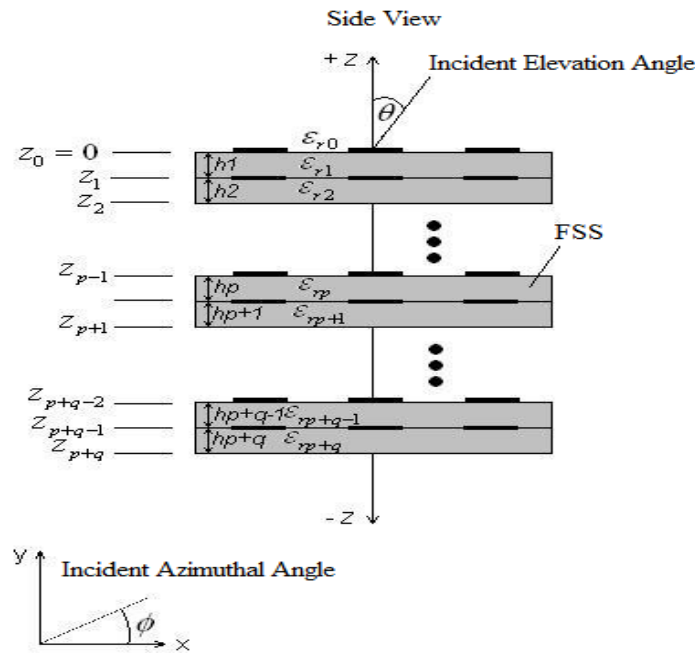
Fig. 2: FSS Cascading, side view.

Cwik in [16] has defined a set of scattering parameters that incorporates the vector nature of electromagnetic fields as follows [1]:

$$S_{11}(m,n,i,j) = \frac{V^{(+,-)}(k_{xm},k_{yn},k_{xi},k_{yj},z_L)}{\sqrt{P^{inc}(i,j)}}$$

$$S_{12}(m,n,i,j) = \frac{V^{(-,-)}(k_{xm},k_{yn},k_{xi},k_{yj},z_R)}{\sqrt{P^{inc}(i,j)}},$$

$$S_{21}(m,n,i,j) = \frac{V^{(+,+)}(k_{xm},k_{yn},k_{xi},k_{yj},z_L)}{\sqrt{P^{inc}(i,j)}},$$

$$S_{22}(m,n,i,j) = \frac{V^{(-,+)}(k_{xm},k_{yn},k_{xi},k_{yj},z_R)}{\sqrt{P^{inc}(i,j)}},$$

where z_R is the above interface and z_L is the below interface in Fig. 1, ie, $z_R = 0$ and $z_L = z_{p+q}$, $V^{(\pm,\pm)}$ are Floquet voltage waves given by [1]:

$$V^{(\pm,\pm)}(k_{xm},k_{yn},k_{xi},k_{yj},z_R) = \tilde{f}(m,n,i,j,z)^{(\pm,\pm)}\sqrt{P(m,n)},$$

With,

$$P(m,n) = (k_{xm}^2 + k_{yn}^2)Y_{mn},$$

Where:

$$Y_{mn} = \frac{\gamma_{mn}}{j\omega\mu},$$

The terms K_{xm} and K_{yn} (wave numbers of Floquet special harmonics) are defined as:

$$k_{xm} = \frac{2\pi}{T_x}m + k_x^{inc},$$

$$k_{yn} = \frac{2\pi}{T_y}n + k_y^{inc},$$

The incident harmonics are functions of elevation angle and the azimuthal angle, which are given as [1]:

$$k_x^{inc} = k_0 sen\theta_{inc}\cos\phi_{inc},$$

$$k_y^{inc} = k_0 sen\theta_{inc}sen\phi_{inc},$$

Referring to the coordinate system of Fig. 1, can be seen that the notation $(\pm, \pm)$ associated with the definition for the voltage waves indicates the direction, both +z or -z, of the incident and scattered energy in a FSS system. Regarding the scattering parameters, it is more convenient to express the potential vector, used in the definition of the Floquet voltage waves in terms of the electric fields transform.
The potential vector, expressed in terms of total electric fields, can be written as [1]:

$$\tilde{f}(m,n,i,j,z)^{(\pm,\pm)} = \frac{j(k_{yn}\tilde{E}_{x_{total}}^{\pm} - k_{xm}\tilde{E}_{y_{total}}^{\pm})}{k_{xm}^2 + k_{yn}^2},$$

The total electric field can be found as follows [1]:

$$\tilde{E}_{(x,y)_{total}}^{+}(k_{xm}, k_{yn}) = \tilde{E}_{(x,y)_S}^{+} + E_{(x,y)_{ref}}\delta(k_{xi} - k_{xm})\delta(k_{yj} - k_{yn}),$$

$$\tilde{E}_{(x,y)_{total}}^{-}(k_{xm}, k_{yn}) = \tilde{E}_{(x,y)_S}^{-} + E_{(x,y)_{trans}}\delta(k_{xi} - k_{xm})\delta(k_{yj} - k_{yn}),$$

Where $E_{(ref,\ trans)}$ are the reflected and transmitted electric fields, calculated in $z = 0$ and $z = z_{p+q}$. We can write the scattering parameters in terms of the electric field evaluated at the reference planes above (z_R) and below (z_L) of a FSS:

$$S_{11}(m,n,i,j) = \sqrt{\frac{Y_{mn}}{Y_{ij}}}\ \frac{j(k_{yn}\tilde{E}_{x_{total}}^{+} - k_{xm}\tilde{E}_{y_{total}}^{-})}{\sqrt{(k_{xm}^2 + k_{yn}^2)(k_{xi}^2 + k_{yj}^2)}}$$

$$S_{12}(m,n,i,j) = \sqrt{\frac{Y_{mn}}{Y_{ij}}}\ \frac{j(k_{yn}\tilde{E}_{x_{total}}^{-} - k_{xm}\tilde{E}_{y_{total}}^{-})}{\sqrt{(k_{xm}^2 + k_{yn}^2)(k_{xi}^2 + k_{yj}^2)}}$$

$$S_{21}(m,n,i,j) = \sqrt{\frac{Y_{mn}}{Y_{ij}}}\ \frac{j(k_{yn}\tilde{E}_{x_{total}}^{+} - k_{xm}\tilde{E}_{y_{total}}^{+})}{\sqrt{(k_{xm}^2 + k_{yn}^2)(k_{xi}^2 + k_{yj}^2)}}$$

$$S_{22}(m,n,i,j) = \sqrt{\frac{Y_{mn}}{Y_{ij}}}\ \frac{j(k_{yn}\tilde{E}_{x_{total}}^{-} - k_{xm}\tilde{E}_{y_{total}}^{+})}{\sqrt{(k_{xm}^2 + k_{yn}^2)(k_{xi}^2 + k_{yj}^2)}}$$

III. NUMERICAL METHOD

Since scattering parameters (scattering matrix) of finite dimension for a FSS are computed, many analytical procedures are available for obtaining multilayer composite representation. It is possible to make direct use of the scattering matrix along with the following equation to obtain the representation of a system with two FSS (multilayer or cascaded FSS), each FSS (individual structure) is viewed as a subsystem [1]. The scattering matrix for the multilayer FSS, using two FSS, is given by [17]:

$$S^C = \begin{bmatrix} S_{11}^{(1)} + S_{12}^{(1)} PTS_{11}^{(2)} PS_{21}^{(1)} & S_{12}^{(1)} PTS_{12}^{(2)} \\ S_{21}^{(2)} P(S_{21}^{(1)} + S_{22}^{(1)} PTS_{11}^{(2)} PS_{21}^{(1)}) & S_{21}^{(2)} PS_{22}^{(1)} PTS_{12}^{(2)} + S_{22}^{(2)} \end{bmatrix},$$

Where $S_{11}^{(1)}$, $S_{12}^{(1)}$, $S_{21}^{(1)}$ and $S_{22}^{(1)}$ are the scattering parameters which represent the first subsystem, namely, the first FSS, $S_{11}^{(2)}$, $S_{12}^{(2)}$, $S_{21}^{(2)}$ and $S_{22}^{(2)}$ are the scattering parameters associated with the second subsystem, and S^C is the scattering matrix for the system composed by two FSS (multilayer FSS).

And *T* is given by [17]:

$$T = (I - S_{11}^{(2)} PS_{22}^{(1)} P)^{-1},$$

P is a diagonal matrix that has $e^{(-j2kd)}$ as its elements, *k* is the wave number [45], in this work $k = k_0$ (because the multilayer FSS is formed by two single FSS separated by an air gap layer), and *I* is an identity matrix.

To validate the results, that will be presented, a comparison with results from other numerical method called "One Mode Interaction Technique" that can be seen in [17] and obtained by Method of Moments (MoM) using the commercial software Ansoft Designer™ is performed. The numerical results were computed using the commercial software MATLAB™ (MATrix LABoratory).

Using the One Mode Interaction (OMI) technique, the transmission (C_T) and reflection (C_R) coefficients for the multilayer FSS, in this case formed by two single FSS, are [18]:

$$C_T = \frac{T_1 T_2}{1 - R_1 R_2 e^{(-j2kd_1)}},$$

$$C_R = R_1 + \frac{T_1^2 R_2}{1 - R_1 R_2 e^{(-j2kd_1)}} e^{(-j2kd_1)},$$

Where d_1 is the spacing between the two structures. T_1, R_1 are the transmission and reflection coefficients for the first FSS, and T_2, R_2 are the transmission and reflection coefficients for the second FSS.

IV. MULTILAYER FSS STRUCTURE

The multilayer FSS used in this work consists of two FSS screens called structure 1 and structure 2, respectively, each one using Koch fractal patch elements printed on a dielectric substrate separated by an air gap layer. The first structure with Koch fractal level 1 is defined as structure 1 and the second FSS screen with Koch fractal level 2 is defined as structure 2, as can be seen in Table 1 with their respective resonant frequencies (*f*) and bandwidths (*BW*). The process to generate the Koch fractal elements used in this work can be seen in [14]. The element shapes and the multilayer structure considered in our investigation are shown in Fig. 3 and Fig. 4, respectively.

Table 1 – Identification of the elements

Structure	Element type	*f* (GHz)	*BW (GHz)*
1	Koch fractal level 1	9.115	1.951
2	Koch fractal level 2	8.333	1.618
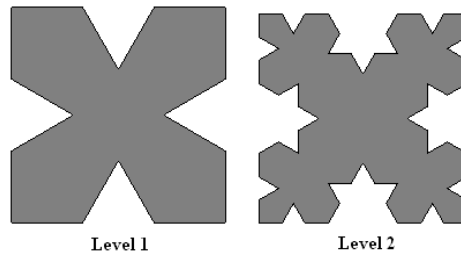
Fig. 3: Koch fractal shape elements.
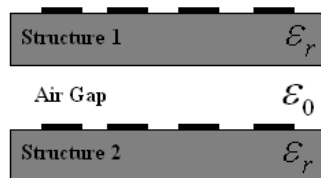
Fig. 4: Multilayer Structure.

V. RESULTS

In order to validate the results obtained with the numerical method presented before, they are compared with results obtained with the OMI technique and the results obtained using the commercial software Ansoft Designer^{TM}, the latter uses the full wave method, MoM, to compute its results.

Fig. 5 illustrates the results obtained with the numerical method for the case with an air gap height equal to 2.0 mm. For the multilayer FSS with an air gap height equal to 2.0 mm, the results obtained using the numerical method presents a bandwidth, for 20 dB insertion loss reference, equals to 3.420 GHz, a good agreement is observed between the results.

For the multilayer FSS with an air gap height equal to 4.0 mm, the results obtained using the numerical method presents a bandwidth, for 20 dB insertion loss reference, equal to 3.360 GHz, approximately. Fig 6. illustrates a comparison between the results.

Using an air gap height equal to 6.0mm, the numerical method presents a bandwidth, for the 20 dB insertion loss reference, equal to 3.290 GHz, approximately.
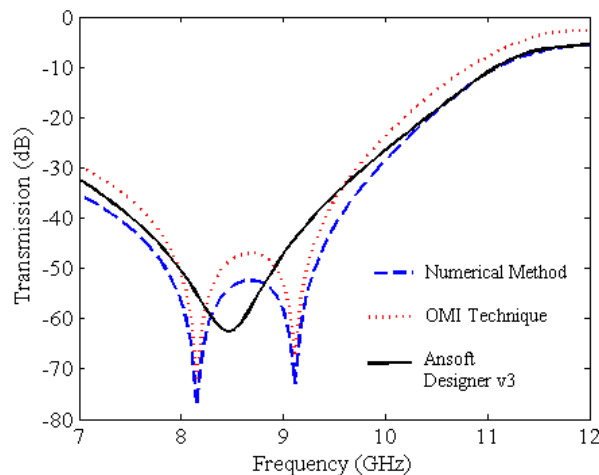
Fig. 5: Transmission coefficient for the multilayer FSS structure with an air gap height equal to 2.0 mm.
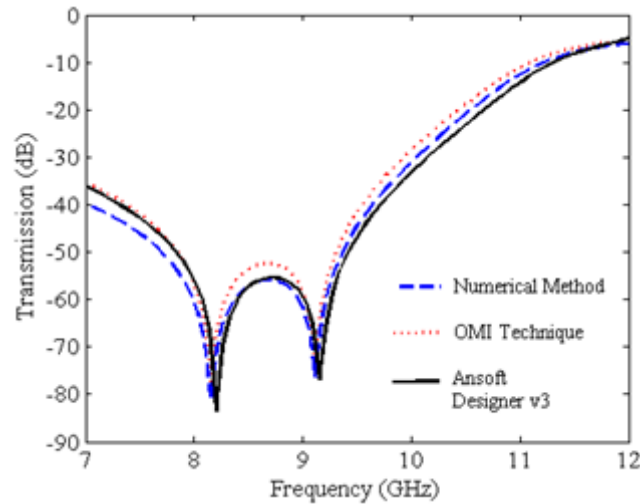
Fig. 6: Transmission coefficient for the multilayer FSS structure with an air gap height equal to 4.0 mm.
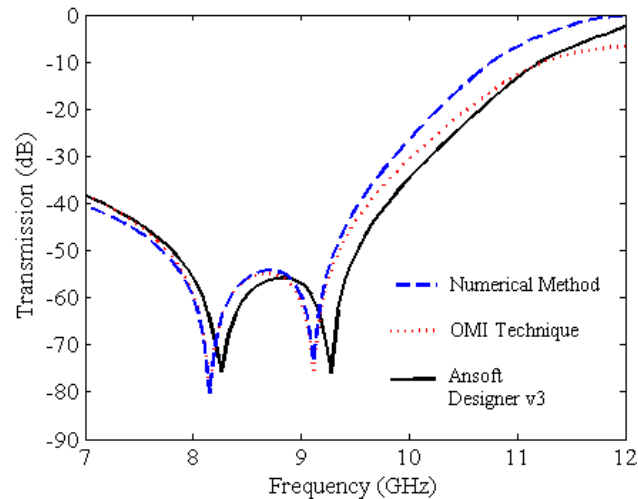
Fig. 7: Transmission coefficient for the multilayer FSS structure with an air gap height equal to 6.0 mm.

VI. CONCLUSION

In this paper, a multilayer FSS was investigated using a simple numerical method. This multilayer structure was formed by two FSS screens separated by an air gap layer, each one FSS screen using a conducting patch element with fractal geometry in the unit cell. The results were obtained for the numerical method and compared with other numerical technique called "One Mode Interaction". Moreover, both were compared with the results obtained using the commercial software Ansoft Designer™ for different values of spacing between the FSS screens. The numerical method is efficient and can be used in conjunction with other methods, like full wave methods such like: Finite Element Method, Wave Concept Iterative Procedure, and Equivalent Circuit Model, among others. For all the cases considered, the frequency responses have characteristics of a high-pass filter with a very large rejection band. A good agreement between the results was observed in terms of bandwidth.

REFERENCES

[1]   T. K. Wu, Frequency selective surface and grid array (Jonh Wiley & Sons, New York, E.U.A., 1995).
[2]   B. A. Munk, Frequency Selective Surfaces – Theory and Design (Jonh Wiley & Sons, New York, E.U.A., 2000).
[3]   F. Bayatpur and K. Sarabandi, Single-Layer High-Order Miniaturized-Element Frequency-Selective Surfaces, IEEE Transactions on Microwave Theory and Techniques, 56 (4), 2008, 774-781.
[4]   J. Romeu and Y. R. Samii, Fractal FSS: A novel dual-band Frequency selective surface, IEEE Transactions on Antennas and Propagation, 48 (7), 2000, 1097-1105.

[5]   J. P. Gianvittorio, Y. Rahmat-Samii and J. Romeu, "Fractal FSS: Various Self-Similar Geometries Used for Dual-Band and Dual-Polarized FSS", IEEE Antennas and Propagation International Symposium, Boston, MA, 2001, 640-643.

[6]   J. C. Zhang; Y. Z. Yin, and S. F. Zheng, Double Screen FSSs with Multi-Resonant Elements for Multiband, Broadband Applications, Journal of Electromagnetic Waves and Applications, 23 (16), 2009, 2209-2218.

[7]   A. L. P. S. Campos, T. L. Silva and A. G. Neto, Multiband Frequency Selective Surfaces with Simple Modification of a Rectangular Patch Element, Microwave and Optical Letters, 55 (12), 2013, 2206-2209.

[8]   F. C. G. S. Segundo, A. L. P. S. Campos and A. G. Neto, A Design Proposal for Ultrawide Band Frequency Selective Surface, Journal of Microwaves, Optoelectronics and Electromagnetics Applications, 12 (2), 2013, 2943-2946.

[9]   S. Baysakhia, R. Sivasamy, M. Kanagasabai and S. Periaswany, Novel Compact UWB Frequency Selective Surface for Angular and Polarization Independent Operation, Progress In Electromagnetics Research Letters, 40, 2013, 71-79.

[10]   M. V. Narayana, I. Govardhani, A. Vikranth, S. K. Nizamuddin, C. Venkatesh, V. V. V. S. Krishna and K. Rajkamal, Design of a Frequency selective surface with multiple four legged Slots, International Journal of Modern Engineering Research (IJMER), 2012, 2 (3), 807-810.

[11]   H. Oraizi and M. Afsahi, Analysis of Planar Dielectric Multilayers as FSS by Transmission Line Transfer Matrix Method (TLTMM), Progress in Electromagnetics Research, 74, 2007, 217-240.

[12]   T. L. Silva, A. L. P. S. Campos, A. G. d'Assunção and R. H. C. Maniçoba, A comparative Study Two Numerical Techniques to Analyze Double Screen Frequency Selective Surface, Microwave and Optical Technology Letters, 55 (9), 2013, 981-985.

[13]   A. L. P. S. Campos and T. L. Silva, Spectral domain analysis of double screen frequency selective surfaces, Journal of Microwaves, Optoelectronics and Electromagnetics Applications, 11(1), 2012, 81-92.

[14]   M. Titaouine, N. Raveu, A. G. Neto and H. Baudrand, Dual-band and Enhanced Band FSS Characterization Using WCIP Method, Microwave and Optical Technology Letters, 52 (4), 2010, 836-839.

[15]   R. H. C. Maniçoba, A. G. d'Assunção and A. L. P. S. Campos, Improving Stop-Band Properties of Frequency Selective Surface with Koch Fractal Elements, 2010 International Workshop on Antenna Technology (iWAT), Lisbon, 2010, 57-60.

[16]   T. Cwik and R. Mittra, The cascade connection of planar periodic surfaces and lossy dielectric layers to form an arbitrary periodic screen, IEEE Transactions on Antennas and Propagation, 35 (12), 1987, 1397 – 1405.

[17]   C. Wan and J. A. Encinar, Efficient computation of generalized scattering matrix for analyzing multilayered periodic structures, IEEE Transactions on Antennas and Propagation, 43 (11), 1995, 1233 – 1242.

[18]   S. W. Lee, G. Zarrillo and C. L. Law, Simple Formulas for Transmission Through Periodic Metal Grids or Plates, IEEE Transactions on Antennas and Propagation, 30 (5), 1982, 904 – 909.

Fabrication of Prototype Model of Infrared Sensor Based Regenerative Braking System Using Electromagnetic Clutch

Abhishek Gaikwad[1], Deepak Singh[2], Mohammad Adnaan Nizami[3], Siddhartha Tripathi[4], Zubair Abrar Khan[5]

[1](Assistant Professor, Dept. of Mechanical Engineering, SSET, SHIATS-Deemed University, Allahabad, India,
[2, 3, 4, 5](Scholars, B. Tech. Production & Industrial Engg, SHIATS-Allahabad, India)

Abstract: *The objective of this paper is to stored the kinetic energy dissipated in the brakes to accelerate the vehicle. This project is based on prototype model of Regenerative braking system using electromagnetic clutch. Regenerative braking results in an increase in energy output for a given energy input to a vehicle, the efficiency is improved. The amount of work done by the engine of the vehicle is reduced, in turn reducing the amount of prime energy required to propel the vehicle. In order for a regenerative braking system to be cost effective the prime energy saved over a specified lifetime must offset the initial cost, size and weight penalties of the system. The energy storage unit must be compact, durable and capable of handling high power levels efficiently. The energy can be directly provided to dynamo itself to generate current and will be displayed on the Ammeter installed in the set up. This set up also consists of an Infrared Sensor which helps to prevent the frequency of accidents increasing due to inefficient braking system and therefore can be considerably avoided using IR sensors. The vehicle instantly stops as any object appears in front of it where IR Sensors are installed.*

Keyword: *Dynamo, Efficiency, Electromagnetic Clutch, Infrared Sensor, Regenerative Braking.*

I. INTRODUCTION

Most commonly brakes use friction to convert kinetic energy into heat, though other methods of energy conversion may be employed. This work is based on regenerative braking which converts much of the energy to electrical energy, which may be stored for later use. Other methods convert kinetic energy into potential energy in such stored forms as pressurized air or pressurized oil. A regenerative brake is an energy recovery mechanism which slows a vehicle or object down by converting its kinetic energy into another form, which can be either used immediately or stored until needed. This contrasts with conventional braking systems, where the excess kinetic energy is converted to heat by friction in the brake linings and therefore wasted. The most common form of regenerative brake involves using an electric motor as an electric generator. In electric railways the generated electricity is fed back into the supply system, whereas in battery electric and hybrid electric vehicles, the energy is stored chemically in a battery, electrically in a bank of capacitors, or mechanically in a rotating flywheel. Hydraulic hybrid vehicles use hydraulic motors and store energy in form of compressed air.

Electromagnetic clutches operate electrically, but transmit torque mechanically. This is why they used to be referred to as electro-mechanical clutches. A sensor is a converter that measures a physical quantity and converts it into a signal which can be read by an observer or by an (today mostly electronic) instrument. An infrared sensor is an electronic instrument that is used to sense certain characteristics of its surroundings by either emitting and/or detecting infrared radiation. It is also capable of measuring heat of an object and detecting motion. Infrared waves are not visible to the human eye.

II. DESCRIPTION

Collision mitigation systems are forward-looking, radar-based systems comprised of collision warning and adaptive cruise control (ACC) with active braking. The collision warning component of collision mitigation systems provides audible and/or visual warnings of vehicles or objects that come within a predefined distance in the front of a vehicle with the system. A radar sensor mounted on the front bumper of the vehicle transmits and receives high frequency radio signals to determine the distance and speed of a target vehicle or object in front of it.

2.1 Techniques Involved

a) Anti-lock braking
b) Regenerative Braking System
c) Infrared sensor based auto braking

2.2 How anti-lock brakes work

Stopping a car in a hurry on a slippery road can be very challenging. Anti-lock braking systems (ABS) take a lot of the challenge out of this sometimes nerve-wracking event. In fact, on slippery surfaces, even professional drivers can't stop as quickly without ABS as an average driver can with ABS.
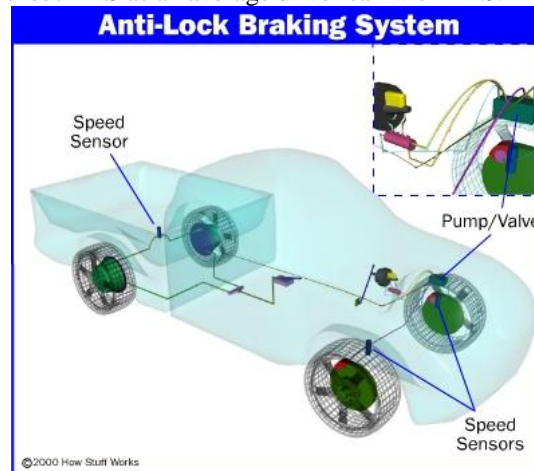
2.3 The ABS System

Anti-lock brake pump and valves

The theory behind anti-lock brakes is simple. A skidding wheel (where the tire contact patch is sliding relative to the road) has less traction than a non-skidding wheel. If you have been stuck on ice, you know that if your wheels are spinning you have no traction. This is because the contact patch is sliding relative to the ice by keeping the wheels from skidding while you slow down, anti-lock brakes benefit you in two ways: You'll stop faster, and you'll be able to steer while you stop.

There are four main components to an ABS system:

1. Speed Sensors: - The anti-lock braking system needs some way of knowing when a wheel is about to lock up. The speed sensors, which are located at each wheel, or in some cases in the differential, provide this information.
2. Pump: - Since the valve is able to release pressure from the brakes, there has to be some way to put that pressure back. That is what the pump does; when a valve reduces the pressure in a line, the pump is there to get the pressure back up.
3. Valves: - There is a valve in the brake line of each brake controlled by the ABS. On some systems, the valve has three positions:
3.1 In position one, the valve is open; pressure from the master cylinder is passed right through to the brake.
3.2 In position two, the valve blocks the line, isolating that brake from the master cylinder. This prevents the pressure from rising further should the driver push the brake pedal harder.
3.3 In position three, the valve releases some of the pressure from the brake.
4. Controller: - The controller is a computer in the car. It watches the speed sensors and controls the valves.

2.4 Anti-Lock Brake Diagram
Now let's put the parts together to see how anti-lock brakes work as a whole. This diagram provides both a close up view and an example of where the brakes are located in your vehicle.
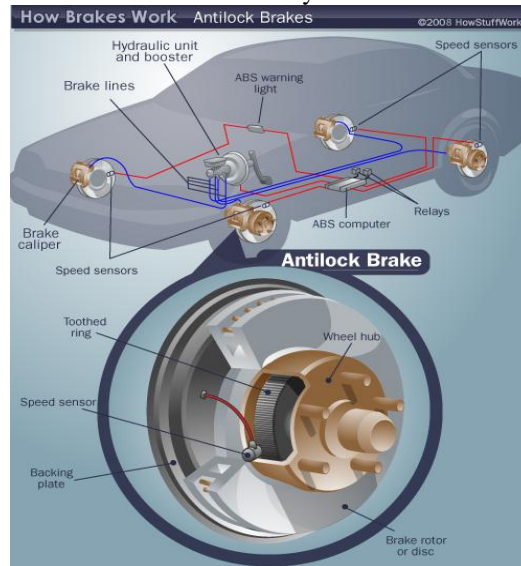
Anti-lock brake components

III. WHAT IS REGENERATIVE BRAKING?

Regenerative braking means reduce losses and regenerate power by using mechanical structure. Systems use friction to counteract the forward momentum of a moving car. As the brake pads rub against the wheels (or a disc connected to the axle), excessive heat energy is also created. This heat energy dissipates into the air, wasting up to 30% of the car's generated power. Over time, this cycle of friction and wasted heat energy reduces the car's fuel efficiency. More energy from the engine is required to replace the energy lost by braking.

Hybrid gas/electric automobiles now use a completely different method of braking at slower speeds. While hybrid cars still use conventional brake pads at highway speeds, electric motors help the car brake during stop-and-go driving. As the driver applies the brakes through a conventional pedal, the electric motors reverse direction. The torque created by this reversal counteracts the forward momentum and eventually stops the car.

But regenerative braking does more than simply stop the car. Electric motors and electric generators (such as a car's alternator) are essentially two sides of the same technology. Both use magnetic fields and coiled wires, but in different configurations. Regenerative braking systems take advantage of this duality. Whenever the electric motor of a hybrid car begins to reverse direction, it becomes an electric generator or dynamo. This generated electricity is fed into a chemical storage battery and used later to power the car at city speeds.

Regenerative braking takes energy normally wasted during braking and turns it into usable energy. It is not, however, a perpetual motion machine. Energy is still lost through friction with the road surface and other drains on the system. The energy collected during braking does not restore *all* the energy lost during driving. It does improve energy efficiency and assist the main alternator.

3.1 Regenerative Braking Diagram
This simple diagram shows how a regenerative braking system is able to recapture some of the vehicle's kinetic energy and convert it into electricity. This electricity is then used to recharge the vehicle's batteries.
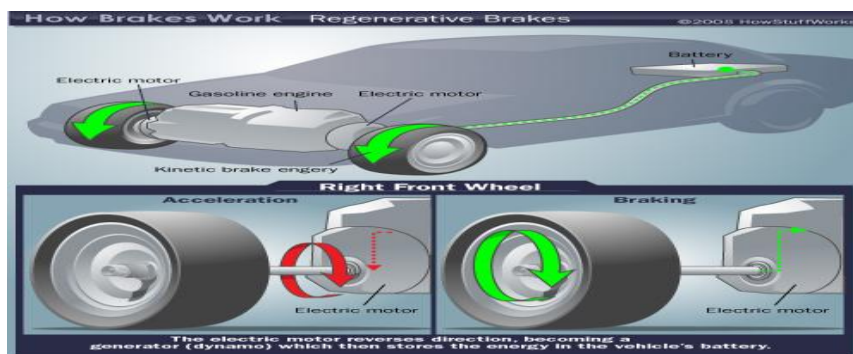
3.2 Construction & Working

We are using three different techniques in our project as mention above. We using electromagnetic clutch in our project as brake shoes and this electromagnetic brake shoe control by small ir based digital circuit. This ir sensor based electronic digital circuit work in auto braking mode at the minimum distance, if driver forget to press brake circuit applied brake in auto mode. Circuit transmit ir waves continuously if some obstruction comes circuit applied automatic braking and this automatic braking system transmit power to dynamo for current generation and braking.

3.2.1 Construction

SYSTEM IS WORKING
ir sensor transmitting waves

OBSTRUCTION

If IR SENSOR INTERRUPTER, ABS CIRCUIT CONTROL E.M. CLUTCH
FOR GRADUALLY BRAKING
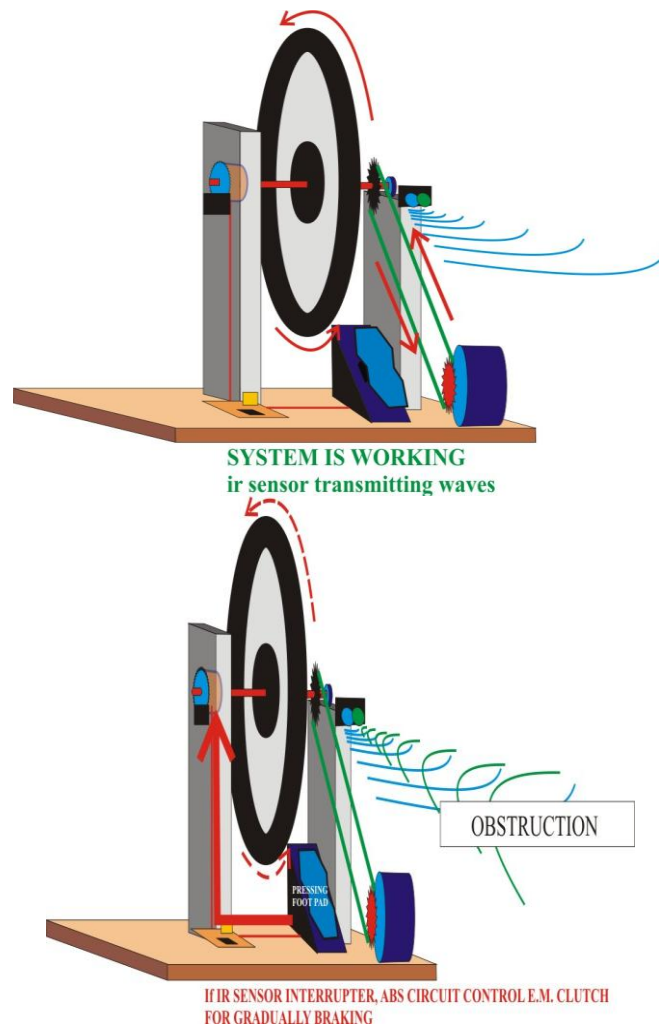
3.2.2 Working block diagram
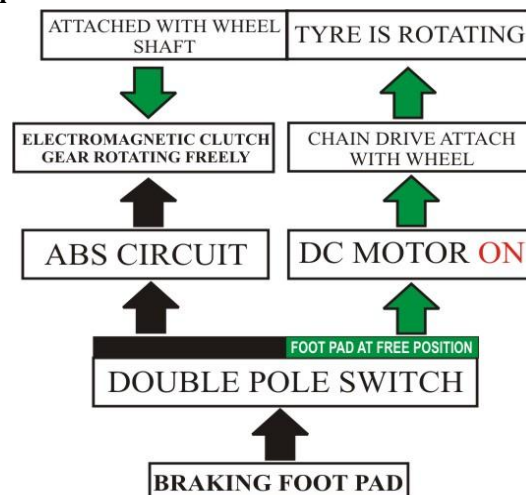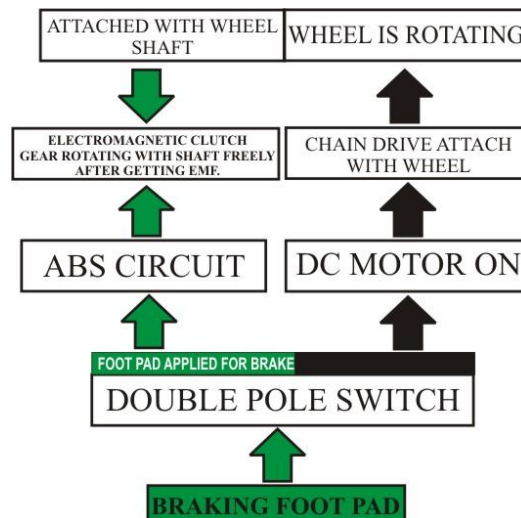
3.3 HARDWARE DESCRIPTION

3.3.1 MECHANICAL COMPOMENTS
1. Dynamo
2. Transformer
3. Electromagnetic clutch
4. Plastic wheel

3.3.2 Electronic Components
1. Relays
2. Transistor
3. Infrared sensor
4. Integrated circuit
5. Obstacles sensor unit
6. Tone Decoder

3.3 Electrical components
1. Power supply
2. Multimeter

IV. CONCLUSION

We using electromagnetic clutch in our project as brake shoes and this electromagnetic brake shoe control by small ir based digital circuit. This ir sensor based electronic digital circuit work in auto braking mode at the minimum distance, if driver forget to press brake circuit applied brake in auto mode.

Circuit transmit ir waves continuously if some obstruction comes circuit applied automatic braking and this automatic braking system transmit power to dynamo for current generation and braking.

A conclusion section must be included and should indicate clearly the advantages, limitations, and possible applications of the paper. Although a conclusion may review the main points of the paper, do not replicate the abstract as the conclusion. A conclusion might elaborate on the importance of the work or suggest applications and extensions.

Acknowledgements

I am deeply indebted to my parents, sisters, brother, friends and other family members for their constant Prayer support and inspirational encouragements and moral support which enabled me to pursue my studies. Thanking u all.

REFERENCES

[1.] Heaviside, O.W., Electromagnetic Theory, Vol I (London, 1893)

[2.] H.D. Wiederick, N. Gauthier, D.A. Campbell, & P. Rochan (1987), Magnetic braking: Simple theory and experiment, Journal of Physics, Vol 55 No.6, June 1987,500-502

[3.] Binggang Cao, Zhifeng Bai, Wei Zhang. Research on Control for Regenerative Braking of Electric Vehicle. 0-7803-9435-6, IEEE, 2005: 92-97. (Pubitemid 46049593)

[4.] Sasaki Y, Mtomo A, Kawahata F, et al. Toyota Braking System for Hybrid Vehicle with Regenerative System. Proceedings of the 14th International Electric Vehicle Symposium (EVS-14), Florida, 1997

[5.] Bradley Glenn, Gregory Washington, Giorgio Rizzoni. Operation and control strategies for hybrid electric automobiles. SAE2000-01-1537, 2000.

[6.] Eiji Nakamura, Masayuki Soga, Akira Sakai, AKihiro Otomo, Toshikazu Kobayashi. Development of Electronically Controlled Brake System for Hybrid Vehicle. SAE 2002-01-0300, 2002.

[7.] CHEN Qing-quan, SUN Feng-chun, ZHU Jia-guang. Modern Electric Vehicle Technology. Beijing Institute of Technology Press. 2002: 260-264.

[8.] HE Ren. Study on Methods of Regenerative Braking Energy of Automobile. Journal of Jiangsu University (Natural Science Edition), 2003, (6): 1-3.

[9.] Akshyakumar S.Puttewar Enhancement of Braking System in Automobile Using Electromagnetic Braking 2003

[10.] Sohel Anwar, An Anti-Lock Braking Control System for a Hybrid Electromagnetic/ Electrohydraulic Brake-By-Wire System, Proceeding of the 2004 American Control Conference Boston, Massachusetts June 30 - July 2, 2004

[11.] CHEN Quan-shi, QIU Bin, XIE Qi-cheng. Fuel cell Electric Vehicle. Tsinghua University Press. 2005

[12.] HE Ren, HU Qing-xun. Braking course of city bus with regenerative braking system. Journal of Jiangsu University (Natural Science Edition), 2005, (5): 391-392.

[13.] LUO Yu-gong, LI Peng, JIN Da-feng, etal. A Study on Regenerative Braking Strategy Based on Optimal Control Theory. Automotive Engineering. 2006, (4): 356-360.

[14.] LIANG Peng-fei, WANG Hai-gui, LING Hong. Research on Control Strategy of Regenerative Braking for HEV Diesel Engine, 2007, (3): 46-49.

[15.] Tatsuya Yamasaki, Masaaki Eguchi And Yusuke Makino, Development of an Electromechanical Brake, NTN Technical Review No.75（2007）

[16.] Kumar, K.P., Kadoli, R., Kumar, M.V.A., Mechanical and magnetic analysis of magnetostrictive disc brake system, Industrial and Information Systems (ICIIS), 2010 International Conference ,July 29 2010-Aug. 1 2010

[17.] Bharathram M , Kirubhahar Praveen P , Chandrakala D , Akshay Jalan , Gowtham Ram N, Brake Pad Actuation Using Electromagnetic Coils, Methods Enriching Power & Energy Developments (Meped'13)April 12 , 2013.

Performance analysis of Hybrid Transform, Hybrid Wavelet and Multi-Resolution Hybrid Wavelet for Image Data Compression

H. B. Kekre[1], Tanuja Sarode[2], Prachi Natu[3]

[1, 3](*Sr. Professor, Assistant Professor, Department of Computer Engineering, MPSTME/ NMIMS University, India*)
[2](*Associate Professor, Department of Computer Engineering, TSEC, Mumbai University, India*)

Abstract: Compression of digital images play vital role in transmission of multimedia data. This paper presents application of hybrid wavelet transform in image compression. Multi-resolution property of Wavelet transform helps to analyze the information contents of image effectively. This property has been used in image compression application. Hybrid wavelet transform is generated using two different component transforms. Various sizes of these component transforms can be used. In this hybrid wavelet, global and local properties of component transforms are incorporated and hence are called bi-resolution analysis. Different levels of resolutions can also be included in generated hybrid transform. Hence It is called multi-resolution analysis and is applied on images. At each level of resolution number of components can be changed. It provides great flexibility to generate hybrid transform matrix. Image is compressed using hybrid wavelet, hybrid wavelet with multi-resolution and hybrid transform. Their performance is compared and it has been observed that hybrid wavelet transform gives lower error values than multi-resolution analysis and hybrid transform. Along with Root mean Square Error (RMSE), Mean Absolute Error (MAE) and Average Fractional Change in Pixel Value (AFCPV) is used to measure error. AFCPV gives better perception to image quality as it is a fractional change in pixel values. Lower the value of AFCPV better is the image quality.
Keywords: AFCPV, Compression Ratio, Hybrid Transform, Hybrid Wavelet transform, Multi-Resolution Transform.

I. INTRODUCTION

In recent years, tremendous increase in internet usage has resulted in increased use of digital and multimedia data. Images are crucial part of this digital data as they represent the information effectively. Efficient storage manipulation and transmission of these digital images is equally important. Image compression serves this purpose. Aim of any compression technique is to eliminate redundant and irrelevant information while preserving the significant information [1]. This is possible as in case of images neighboring pixels are highly correlated and hence contain redundant information. Redundancy reduction removes the details in image which are not noticed by human visual system [2]. Data compression methods are usually classified into two categories: lossless compression and lossy compression. Image data compression is generally lossy compression. Lossy compression provides higher compression than lossless compression but decoded image approximately matches to original image [3]. Compression ratio is basic performance measurement criteria. It is defined as ratio of original data size and compressed data size. Higher compression ratio results in lower image quality and vice versa. Transform based coding is widely used for image compression in which image is transformed from spatial domain to frequency domain. Transforms have property to concentrate useful information into few low frequency coefficients. Initially Fourier transform was used for image compression. In Fourier transform local properties of signal are not detected easily. To overcome this drawback short time Fourier Transform (STFT) was introduced which is also called as window transform. It gives local properties at the cost of global properties [4]. The length of window limits the resolution in frequency. Discrete cosine Transform (DCT) [5] is popular transform used for image compression due to its good energy compaction property. Many compression systems use block based DCT where image is divided into blocks of uniform size and transform is applied on individual block. It does not take into account the discontinuities across the boundaries and results in degraded image. This is called as blocking effect [6]. Wavelets provide solution to these problems [7]. Wavelet transform gives time and frequency representation simultaneously [8]. Wavelet transform has higher energy compaction property. It is applied on entire image rather than on blocked image hence it eliminates blocking effect. Multi-resolution representation of an image is another most important characteristic of wavelet transform. Information contents of the image depend on the local variations of image intensity. Multi-resolution representation provides a hierarchical framework for interpreting the image

information. The wavelets can be scaled and shifted to analyze the spatial frequency contents of an image at different resolutions and positions. This paper focuses on use of multi-resolution property in image compression.

Remaining sections of this paper are organized as follows: section II contains review of literature, proposed method is presented in section III, results of experimental work are discussed in section IV and conclusion is outlined in section V.

II. REVIEW OF LITERATURE

So far wavelets of Haar transform have been studied because it is simple and fast. Modified fast Haar wavelet transform (MFHWT) has been discussed by Chang P. et al. [9]. It uses one dimensional approach and FHT is used to find N/2 detail coefficients at each level for a signal of length N. Extension of this work has been proposed by Anuj Bharadwaj and Rashid Ali [10]. It works for 2D images with the addition of considering the detail coefficients for N/2 elements at each level. Comparison of different wavelets in medical image compression is discussed in [**Error! Bookmark not defined.**]. It compares performance of Daubechies, Coeflits, Haar and biorthogonal transform. Image compression using Walsh transform has been studied in [11]. Image compression using approximate matching and run length coding is proposed in [12].

Compression using biorthogonal wavelet transform based on lifting scheme with SPIHT is proposed by Hong Liu et al. [13]. Wavelet based image compression using zero tree data structure is proposed by Tham Jo Yiew [14]. Wavelet transform decomposes the image hierarchically into oriented sub bands and then encodes the wavelet coefficients using zero tree data structure. Quad EZW method is further used to decompose higher frequency sub bands. Also blocks of wavelet coefficients are shifted with optimum translation factors prior to application of inverse wavelet transform to obtain better PSNR and reconstructed image quality. Column, row and full wavelet transform based image compression and comparison of their performances has been proposed by Kekre et al. [15]. In their paper simpler method of wavelet generation [16] has been used to generate the wavelet transform from orthogonal transform. Column wavelet transform can be used for compression to save computational overhead in full wavelet transform. Compressions using real Fourier transform and its wavelet transform has been presented in [17]. Wavelets of DCT, Discrete Sine Transform (DST), Hartley transform and Real-DFT have been used for image compression by Kekre et al. [18] by varying the sizes of their component orthogonal transforms. Different size combinations of component transforms give variation in error values. Proper component sizes can be selected to get acceptable image quality. Use of Kekre wavelet, Slant wavelet and Walsh wavelet is proposed in [19] by H.B. Kekre, Tanuja Sarode and Prachi Natu.

Use of hybrid techniques for image compression has also been done. Hybrid techniques combine two or more traditional approaches so that features of two individual techniques can be combined to get better performance. Transform coding combined with predictive coding was used by Clarke [20]. Recently hybrid DCT-VQ based approach for efficient compression of color images has been proposed by Arup Kumar Pal et al. [21]. Image compression based on DCT based compressive sensing and vector quantization is proposed by Dipti Bhatnagar and Sumeet Budhiraja [22]. It combines the advantages of compressive sensing and JPEG image compression standard. Compression based on discrete wavelet transform with arithmetic coding is proposed by Deepika Sunoriya et al. [23]. It applies Walsh Wavelet on blocks of image and then compression is achieved by arithmetic coding. Hybrid Wavelet transform using Kekre Transform [24] has been recently proposed [25] in which different orthogonal transforms can be combined with Kekre Transform to generate hybrid wavelet transform. Column hybrid wavelet transform can be used to save computations at small reduction in compression ratio.

III. PROPOSED TECHNIQUE

In this paper, Kekre transform (DKT) and Hartley transform is used to generate hybrid wavelet transform. By varying the global properties in hybrid wavelet transform hybrid transform is generated and used to compare its performance with hybrid wavelet. Also hybrid wavelet with multi-resolution is generated and its performance is compared with other two.

3.1 Hybrid Wavelet Transform

Hybrid wavelet transform matrix is generated using two different orthogonal component transform matrices. If A is a matrix of size pxp and B is matrix of size qxq then hybrid wavelet transform generated from A and B is of size nxn=pqxpq [**Error! Bookmark not defined.**]. In this paper Discrete Kekre transform (DKT) and Hartley transform (DHT) are used as component transforms to generate DKT-DHT hybrid wavelet transform.

3.2 Kekre Transform

Kekre Transform is an orthogonal transform in which all diagonal elements and the upper diagonal elements are one. Lower diagonal elements except the one exactly below the diagonal are zero. All other orthogonal transforms need to be in power of two. But this restriction is not there in Kekre transform.

3.3 Hartley Transform

Hartley transform is closely related to the Fourier transform. It was proposed as an alternative to the Fourier transform by R. V. L. Hartley in 1942, [**Error! Bookmark not defined.**] and is one of many known Fourier-related transforms. Compared to the Fourier transform, the Hartley transform has the advantages of transforming real functions to real functions (as opposed to requiring complex numbers) and of being its own inverse.

3.4 Generation of Hybrid Wavelet Transform

Hybrid wavelet is generated using Kronecker product as it reduces computations to great extent. Kronecker product is given as:

$$A \otimes B = a_{ij} [B] \tag{1}$$

Where a_{ij} is individual element in matrix A.

Generation of hybrid wavelet is given by following Kronecker product:

$$T_{AB} = \begin{bmatrix} A_p \otimes B_q (1) \\ I_p \otimes B_q (2) \\ I_p \otimes B_q (3) \\ . \\ . \\ . \\ . \\ I_p \otimes B_q (n) \end{bmatrix} \tag{2}$$

Here A and B are component matrices of size pxp and qxq respectively. B_q (1) indicates first row of matrix B, B_q (2) is second row of matrix B and so on. $A_p \otimes B_q$ (1) gives first p rows of pqxpq matrix which represents global properties of hybrid wavelet transform. Identity matrix I is used to translate the rows of matrix B. Thus matrix B contributes to local properties. In hybrid wavelet, properties of two different component transforms are combined which gives better results than the results obtained in single transform. Such hybrid wavelet transform gives bi-resolution because global and local properties are incorporated in transformation matrix T_{AB}. It means that it will analyze an image at global and local level of resolution. Generation of above hybrid wavelet matrix can be made more flexible to include analysis of image at various levels. Various levels of analysis can be introduced between global and local and hence called as semi global properties. It helps to analyze image at various resolutions. Hybrid wavelet transformation matrix which gives semi global properties is represented using Kronecker product in eq. (3) [**Error! Bookmark not defined.**]. In below matrix, Kronecker product in first row represents first p rows of hybrid wavelet. These rows represent global properties. Here r_0, $r_1, \ldots, r_{n-1}$ are divisors of p except 1 and p. Scaling operation is done using lower order matrices of A and shifting operation is done using Identity matrix 'I'. As size of matrix A decreases, size of 'I' increases by same scale. A and B are selected as two different matrices. Number of rows of matrix B selected for Kronecker product in each row can be varied by varying the values of $I_1, I_2, \ldots, I_n$ in each row of Kronecker product below such that size of T_{AB} remains pqxpq.

$$T_{AB} = \begin{bmatrix} A_p \otimes B_q (0:i_1) \\ I_{r0} \otimes (A_{p/r0} \otimes B_q (i_1+1:i_2)) \\ I_{r1} \otimes (A_{p/r1} \otimes B_q (i_2+1:i_3)) \\ . \\ . \\ . \\ . \\ I_{rn-1} \otimes (A_{p/rn-1} \otimes B_q (i_{n-2}+1:i_{n-1})) \\ I_p \otimes (B_q(i_n:q)) \end{bmatrix} \begin{matrix} \text{Global} \\ \text{Semiglobal 1} \\ \text{Semiglobal 2} \\ . \\ . \\ . \\ . \\ . \\ \text{Local} \end{matrix} \tag{3}$$

3.5 Performance Measurement Criteria
3.5.1 Root Mean Square Error (RMSE)

The Root Mean Square Error (RMSE) is a frequently used measure of the difference between values predicted by a model and the values actually observed. It is calculated as:

$$\text{RMSE} = \sqrt{\frac{\sum_{i=1}^{p}\sum_{j=1}^{q}(x_{ij}-y_{ij})^2}{p*q}} \tag{4}$$

Basically, the RMSD represents the sample standard deviation of the differences between predicted values and observed values. Here x_{ij} is reconstructed image, y_{ij} is original image and p is total number of rows and q is total number of columns in image.

3.5.2 Mean Absolute Error

It is a quantity used to measure how close the predicted values are to the actual outcomes. The mean absolute error is given by:

$$\text{MAE} = \frac{\sum_{i=1}^{p}\sum_{j=1}^{q}(|x_{ij}-y_{ij}|)}{p*q} \tag{5}$$

Where x_{ij}= original Image , y_{ij}=Reconstructed image, p= Number of rows and q=Number of columns.

3.5.3 Average Fractional Change in Pixel value (AFCPV)

This parameter is used to measure perceptibility of compressed image to human eye. Higher perceptibility is observed when AFCPV has lower value. It is calculated as:

$$\text{AFCPV} = \frac{\sum_{i=1}^{p}\sum_{j=1}^{q}(|x_{ij}-y_{ij}|)\Big/x_{ij}}{p*q} \tag{6}$$

where x_{ij}= original Image, y_{ij}=Reconstructed image, p= Number of rows and q=Number of columns.

3.6 General Steps applied for Image Compression

Using eq. (2) bi-resolution analysis of image is obtained using hybrid wavelet transform. To get multi-resolution analysis, hybrid wavelet transform is generated using eq. (3) and then following steps are repeated. Variation in results can also be observed by considering all global features of an image and no semi global and local properties. In that case hybrid wavelet matrix is generated using full Kronecker product of component transforms and is called as hybrid transform matrix.

Following are the general steps applied for image compression.

1. Generate hybrid wavelet transform of size equal to image size. Let the generated hybrid wavelet transform is T_{AB}.
2. Transform individual plane of an image.
3. Calculate energy of individual coefficient and Find highest energy coefficients in transformed image.
4. Retain high energy coefficients (low frequency coefficients) and discard those with low energy.
5. Reconstruct image using high energy coefficients obtained in above step.
6. Calculate Root Mean Square Error (RMSE), MAE and AFCPV between original image and reconstructed image for various compression ratios up to 32.
7. Repeat above steps using hybrid wavelet with multi-resolution analysis and also using Hybrid transform.

IV.   RESULTS AND DISCUSSIONS

Test set of images used for experimental purpose is shown in Fig. 1. Execution is performed on AMD dual core processor with 4 GB RAM using Matlab 7.0. Kekre Transform is selected as base transform and Hartley transform is used to contribute to local features. Hybrid wavelet (bi resolution analysis), hybrid wavelet with multi-resolution analysis and Hybrid transform is applied on images. Their performances are compared using three different parameters like: Root Mean Square Error (RMSE), Mean Absolute Error (MAE) and Average Fractional Change in Pixel value (AFCPV).

| Mandrill | Peppers | Grapes | Cartoon |

| Dolphin | Waterlili | Bud | Bear |

| Lena | Apple | Ball | Balloon |

| Bird | Colormap | Fruits | Hibiscus |

| Puppy | Rose | Tiger |
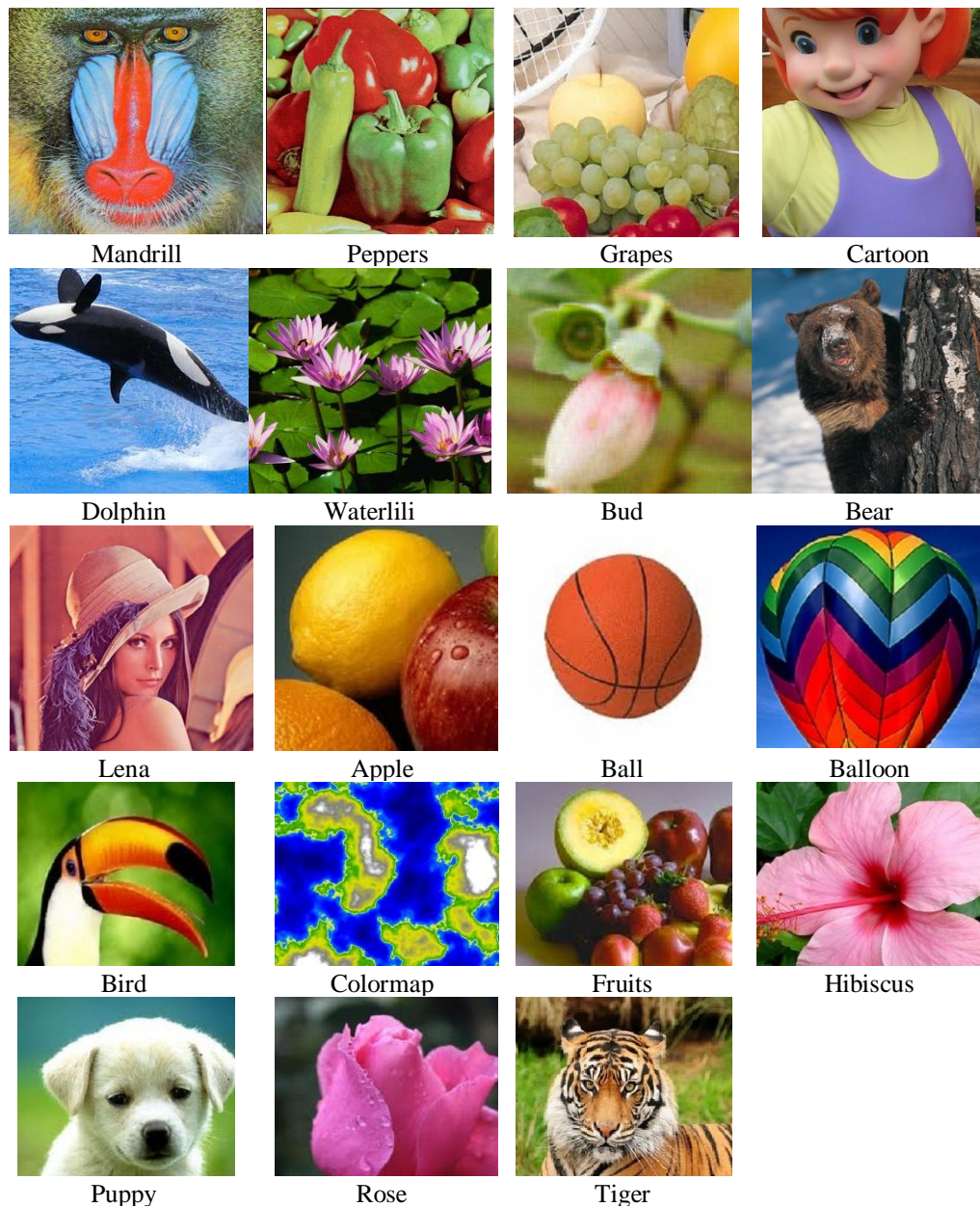
Fig. 1 Test set of Different Color images used for Experimental Purpose
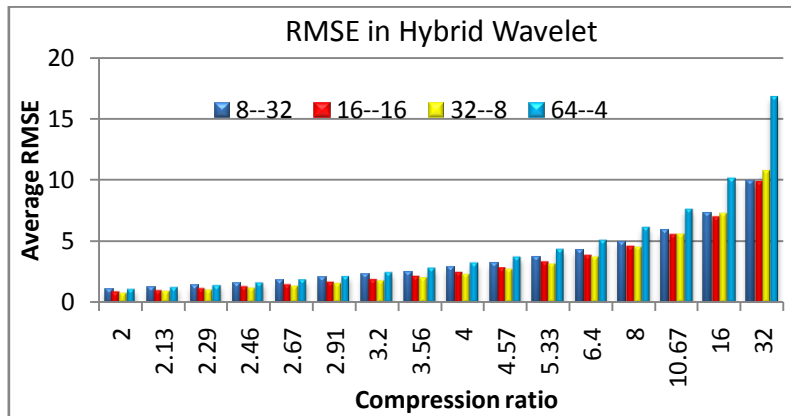
Fig. 2 Average RMSE against compression ratio using DKT-Hartley hybrid wavelet transform by varying the size of component transforms

Fig. 2 shows plot of RMSE vs. Compression ratio using DKT-Hartley hybrid wavelet transform. Here hybrid wavelet is generated using Kronecker product in eq. (1). Hence it gives bi-resolution analysis i.e. contain global and local properties. Size of component transforms is varied to get transform matrix of size 256x256. In above graph 8--32 indicate that first figure '8' is size of base transform i.e. Kekre transform and second figure '32' is size of Hartley transform. Similarly other size combinations like 16--16, 32--8 and 64--4 were tried. Up to compression ratio 16, size 16--16 and 32--8 give nearly equal values of RMSE but for higher compression ratio of 32, lesser error is given by 16--16 size DKT-Hartley hybrid wavelet.
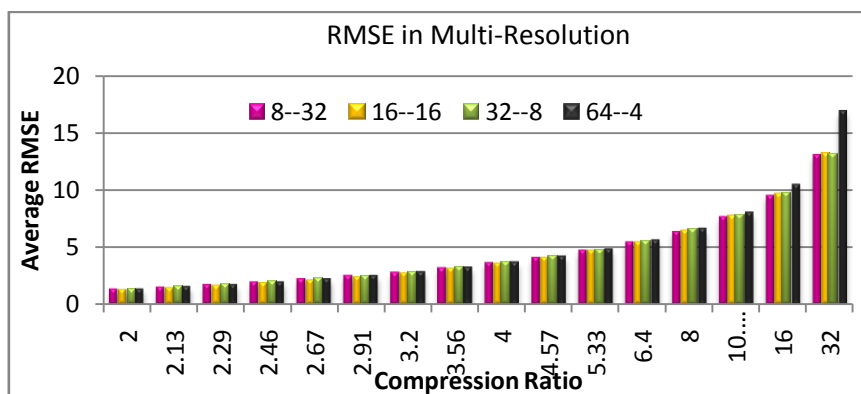
Fig. 3 Average RMSE against compression ratio using multi resolution analysis of DKT-Hartley hybrid wavelet transform by varying the size of component transforms

Fig. 3 shows graph of RMSE against Compression ratio using multi-resolution analysis of DKT-Hartley hybrid wavelet. Transform matrix is generated using eq. (2) to include semi global properties along with global and local properties. Size of component transforms is varied to select one which gives minimum RMSE. All size combinations except 64--4, give almost equal error.
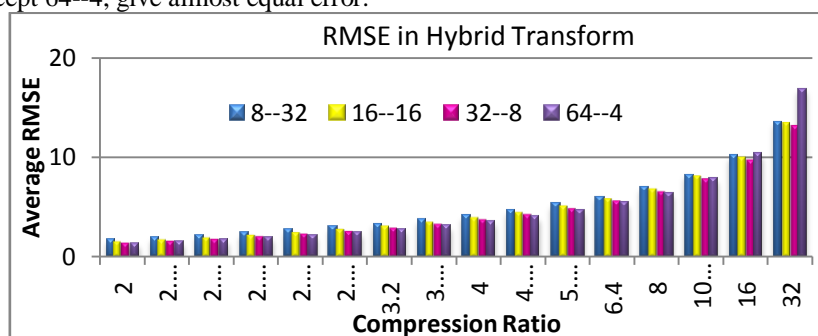
Fig. 4 Average RMSE against compression ratio using multi resolution analysis of DKT-Hartley hybrid transform by varying the size of component transforms

Fig. 4 shows RMSE vs. compression ratio using hybrid DKT-Hartley transform. Hybrid transform is Kronecker product of two component transforms. Hence it is the limiting case of hybrid wavelet where no local properties are included. DKT size 32x32 and Hartley size 8x8 gives lower RMSE at higher compression ratios like 16 and 32 than other combinations.

Fig. 5, 6 and 7 show plot of Mean Absolute Error (MAE) against compression ratio using hybrid wavelet, hybrid wavelet with multi-resolution analysis and hybrid transform respectively. In each of these cases, different size combinations of hybrid wavelet give better performance. In hybrid wavelet 8--32 sizes of components shows lowest MAE at compression ratio 32. In hybrid wavelet with multi-resolution analysis all combinations except 64-4 show nearly same performance whereas in hybrid transform, minimum MAE is obtained using DKT 32x32 and Hartley 8x8 size.
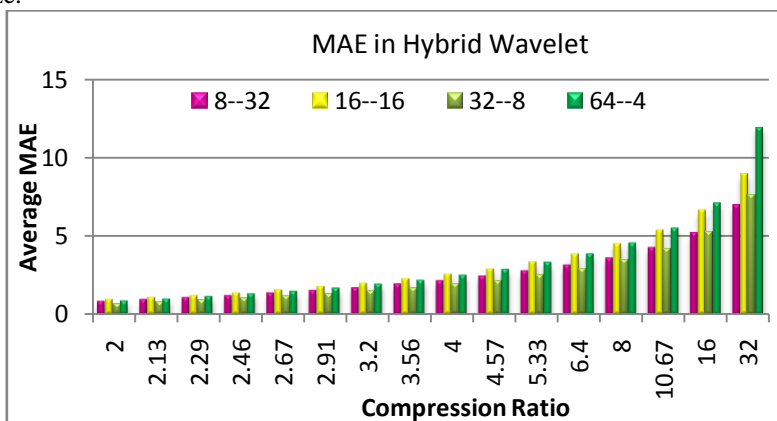
Fig. 5 Average MAE against compression ratio using DKT-Hartley hybrid wavelet transform by varying the size of component transforms
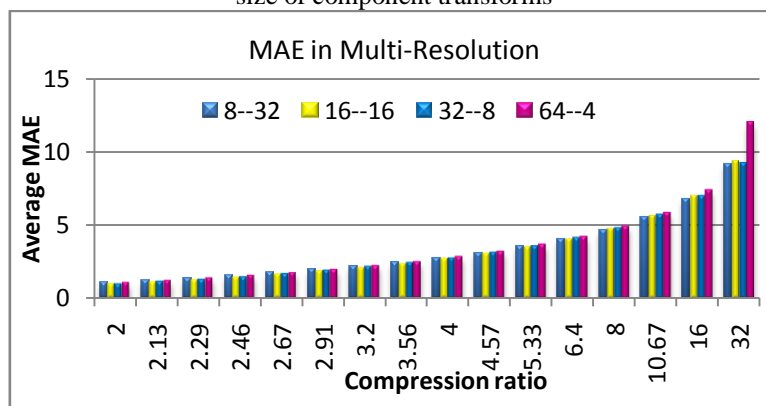
Fig. 6 Average MAE against compression ratio using multi resolution analysis of DKT-Hartley hybrid wavelet transform by varying the size of component transforms
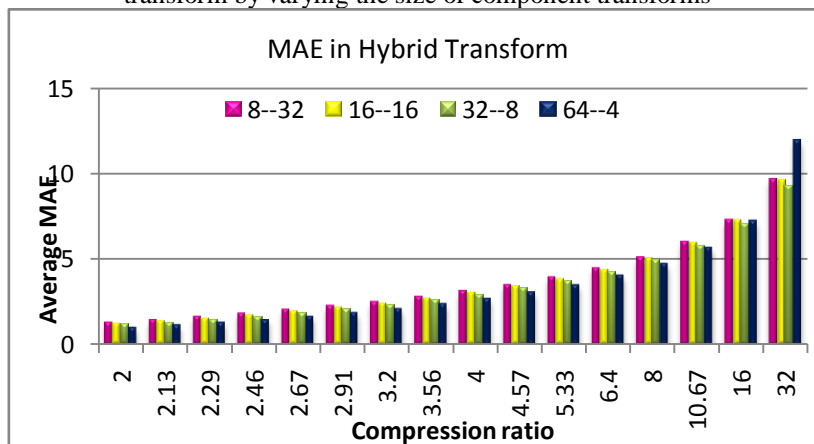
Fig. 7 Average MAE against compression ratio using multi resolution analysis of DKT-Hartley hybrid wavelet transform by varying the size of component transforms

Fig. 8, 9 and 10 show average fractional change in pixel value at various compression ratios. With increase in compression ratio, AFCPV increases. In each case it has been tried to select best suitable component size giving least value of AFCPV. As observed in fig. 8, hybrid wavelet 64-4 pair of DKT-Hartley gives lower AFCPV. But at higher compression ratio 32-8 size pair gives low AFCPV. For hybrid wavelet with multi-resolution analysis same observations are noted in Fig. 9 giving best size of component pair as DKT 32x32 and Hartley 8x8. Graph plotted for Hybrid transform in Fig. 10 also shows that DKT 32x32 and Hartley 8x8 is component size giving lowest value of AFCPV.
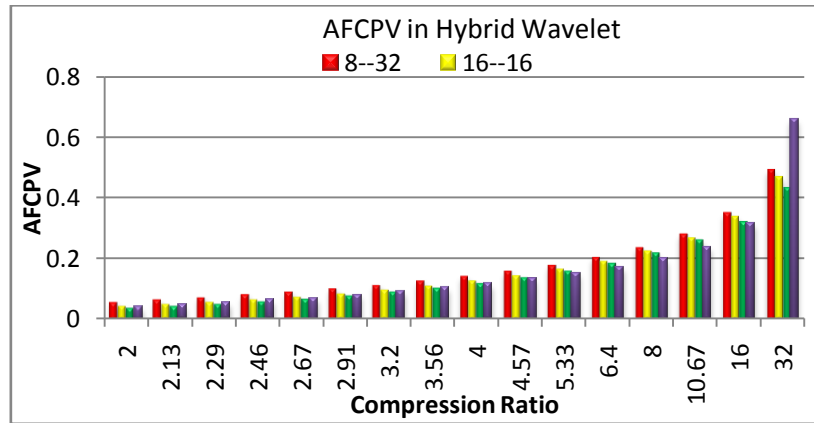
Fig. 8 AFCPV against compression ratio using DKT-Hartley hybrid wavelet transform by varying the size of component transforms

Fig. 9 AFCPV against compression ratio using multi resolution analysis of DKT-Hartley hybrid wavelet transform by varying the size of component transforms
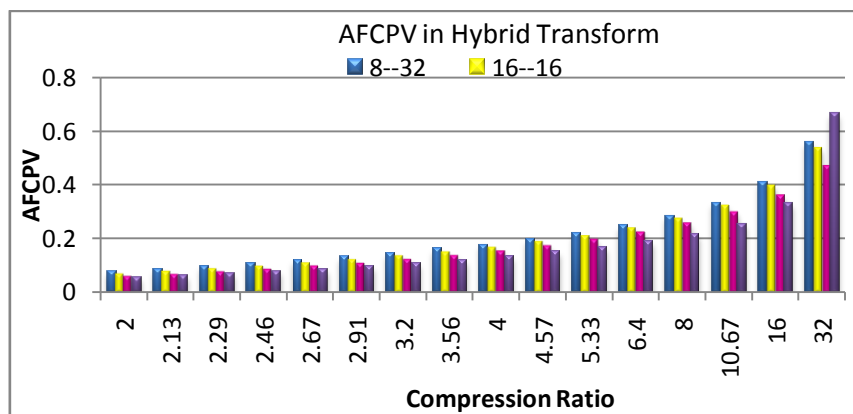
Fig. 10 AFCPV against compression ratio using DKT-Hartley hybrid transform by varying the size of component transforms
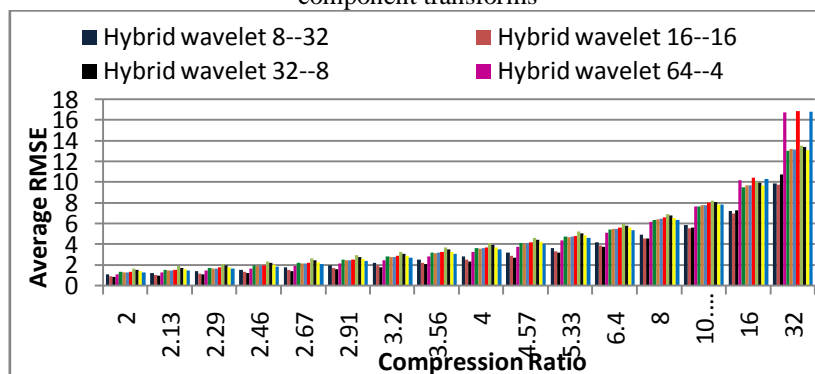
Fig. 11 Comparing RMSE of hybrid wavelet, multi resolution and hybrid transform using DKT-Hartley pair

Fig. 11 shows overall comparison of RMSE calculated in Hybrid wavelet transform, hybrid wavelet with multi-resolution analysis and hybrid transform with their possible sizes of component transforms. It has been observed that, values obtained in multi-resolution analysis are greater than those in hybrid wavelet transform. Further, values in hybrid transform are still greater than values in multi-resolution analysis for all sizes of component transforms except 64-4 pair. It indicates that, inclusion of semi global properties of image introduces more error in compressed image. Hybrid wavelet with DKT 16x16 and Hartley 16x16 gives lowest RMSE 9.79 among all. In multi-resolution analysis as size of base transform increases, error increases and reaches maximum value of 16.87.
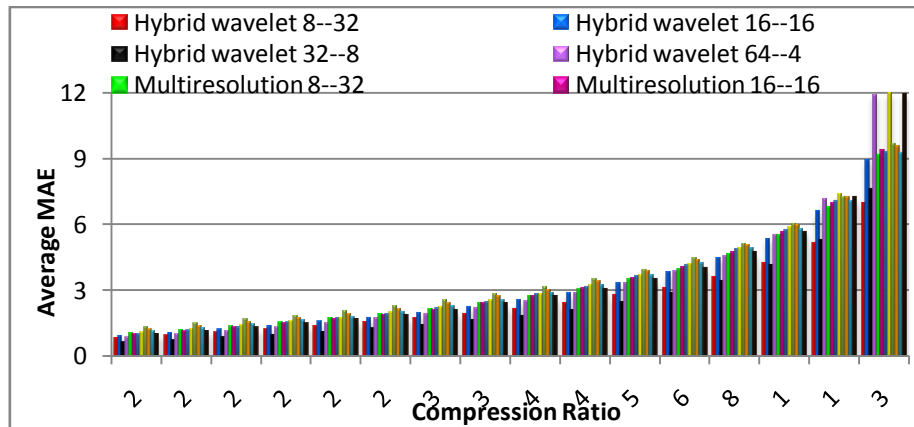
Fig. 12 Comparing MAE of hybrid wavelet, multi resolution and hybrid transform using DKT-Hartley pair

Fig. 12 shows overall comparison of MAE calculated in Hybrid wavelet transform, hybrid wavelet with Multi-resolution analysis and hybrid transform with their possible sizes of component transforms. Fig. 13 presents comparison of AFCPV in all possible cases of hybrid wavelet, its multi-resolution analysis and hybrid transform. Hybrid wavelet proves to be better than hybrid transform and multi-resolution analysis. 32x32 DKT and 8x8 Hartley gives lower value of AFCPV among all selected pairs.
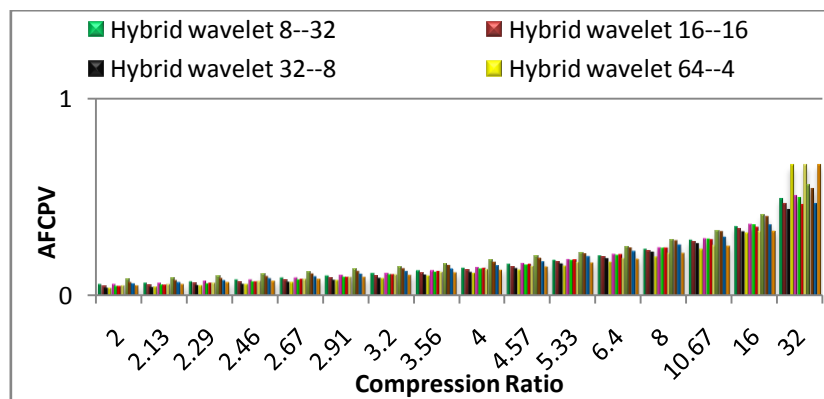
Fig. 13 Comparing AFCPV of hybrid wavelet, multi resolution and hybrid transform using DKT-Hartley pair.
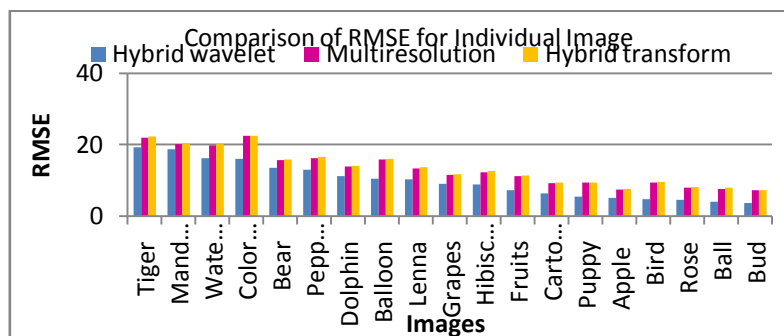
Fig. 14 RMSE of different images using three different techniques hybrid wavelet, multi resolution and hybrid transform

Fig. 14 shows RMSE values of individual image obtained by Hybrid wavelet, Multi-resolution analysis and hybrid transform respectively. For each image RMSE obtained using hybrid transform is greater than RMSE in Hybrid wavelet and multi-resolution technique. Same pattern is followed in MAE and AFCPV plot in Fig. 15 and Fig. 16. It has been observed that images containing more energy in high frequency components show higher error for same amount of data compression. Mandrill, Balloon, colormap, tiger show high error values.

Fig. 15 shows variation in MAE for three different techniques: Hybrid Wavelet, Multi-resolution analysis and hybrid transform. It has been observed that inclusion of semi global and global properties increases error for sharp image serroris more.
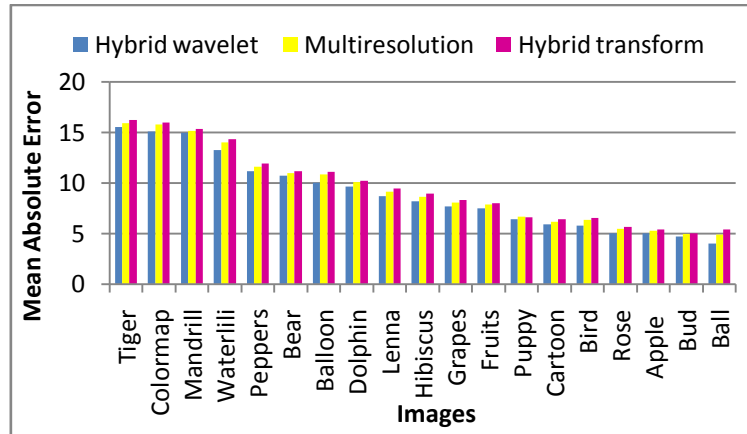
Fig. 15 MAE of different images using three different techniques hybrid wavelet, multi resolution and hybrid transform
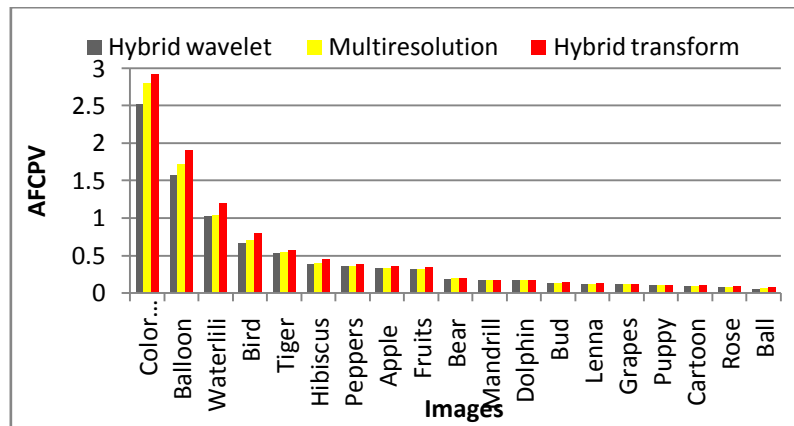
Fig. 16 AFCPV of different images using three different techniques hybrid wavelet, multi resolution and hybrid transform

Reconstructed 'Lena' image using component transform DKT 8x8, Hartley 32x32 at compression ratio 32		
Hybrid wavelet	Multi-Resolution	Hybrid Transform
RMSE= 10.56	RMSE= 13.08	RMSE= 13.67

Fig. 17 Reconstructed 'Lena' image using DKT-Hartley hybrid wavelet, multi resolution and hybrid transform with component sizes 8x8 and 32x32 i.e. (8-32), (16-16), (32-8) and (64-4) respectively

Fig. 17 shows reconstructed 'Lena' Image obtained at compression ratio 32 using three different techniques: hybrid wavelet, multi-resolution and hybrid transform. DKT-Hartley pair is used to generate hybrid wavelet transform. Component size is varied as 8-32, 16-16, 32-8 and 64-4. Blocking effect is observed in the reconstructed image but image quality is acceptable. For selected image 16-16 component size in hybrid wavelet gives lowest RMSE. Error is maximum in hybrid transform than all followed by multi-resolution analysis. Hence we can conclude that, inclusion of global and semi-global properties increases the error than hybrid wavelet with bi-resolution analysis.

V. CONCLUSION

This paper presents image compression technique based on hybrid wavelet transform with multi-resolution analysis. Kekre transform and Hartley transform are used to generate hybrid wavelet of size 256x256. Various combinations of these pairs (8-32, 16-16, 32-8 and 64-4 etc.) can be used to generate required size of transform matrix. In multi-resolution analysis semi global properties are introduced and their proportion in transformation matrix can be varied by changing the number of rows of second matrix. Since Kronecker product is used to generate the transformation matrix, this method is faster and simpler to implement. Inclusion of semi global properties increases error than usual bi resolution analysis. In hybrid transform where all global properties are present error is maximum. Along with RMSE, Mean Absolute Error (MAE) of these three

techniques is compared as it gives better perception of image quality than RMSE. Average Fractional Change in Pixel Value (AFCPV) gives still better perceptibility than MAE as it is a ratio of change in pixel values. At component size 16-16 lowest average RMSE 9.79 is obtained in hybrid Wavelet. MAE and AFCPV are 8.91 and 0.468 at this size.

REFERENCES

[1] Ataollah Ebrahim zadeh, Milad Azarbad, ECG Compression using Wavelet Transform and Three Level Quantization. IEEE Conference Procedeeings IDC. 2010, 250-254

[2] Vandendrope L, B. maison, F. Labeau, An Adaptive transform Approach for Image compression. IEEE Digital Signal Processing Workshop, 1997, 41-44

[3] Shawki A. Al Dubaee, Nesar Ahmad, Multilingual lossy Text Compression using Wavelet Transform. First IEEE International Conference on Integrated Intelligent Computing. 2010, 39-44.

[4] Strang G. Wavelet Transforms Versus Fourier Transforms. Bulletin of American Mathematical Society, (28), 1993, 288-305.

[5] N.Ahmed, T. Natarajan and K. R. Rao, Discrete Cosine Transform. IEEE Transaction Computers. (C-23), 1974, 90-93.

[6] S. Bauer, B. Zovko-Cihlar, and M. Grgic, The Influence of Impairments from Digital Compression of Video Signal on Perceived Picture Quality. 3rd International Workshop Image and Signal Processing, 1996, 245–248.

[7] S. Mallat, A Theory of Multiresolution Signal Decomposition: The Wavelet Representation. IEEE Trans. Pattern Analysis and Machine Intelligence, 1989, 674-693.

[8] Krishna Kumar, Basant Kumar & Rachna Shah, Analysis of Efficient Wavelet Based Volumetric Image Compression. International Journal of Image Processing. 6(2), 2012, 113-122

[9] Chang P, P. Piau, Modified fast and Exact Algorithm for Fast Haar Transform. In Proc. of World academy of Science, Engineering and Technology, 2007, 509-512

[10] Anuj Bharadwaj and Rashid Ali, Image compression using Modified Fast Haar Wavelet Transform. World Applied science Journal, 2009, 647-653.

[11] George Lazaridis, Maria Petrou, Image Compression By Means of Walsh Transform. IEEE Transaction on Image Processing. 15(8), 2006, 2343-2357

[12] Samir Kumar Bandyopadhyay, Tuhin Utsab Paul, Avishek Raychoudhury, Image Compression using Approximate Matching and Run Length. International Journal of Advanced Computer Science and Applications. 2(6), 2011, 117-121.

[13] Hong LIU, Lin-pei ZHAIV, Ying GAO , Wen-ming LI, Jiu-fei ZHOU, Image Compression Based on Biorthogonal Wavelet Transform. In proc. of IEEE conference on ISCIT, 2005, 578-581.

[14] Tham jo Yiew, Detail Preserving Image compression using Wavelet Transform. IEEE Region 10 student Paper Contest,1(9), 1995.

[15] H.B. Kekre, Tanuja Sarode, Prachi Natu, Image Compression Using Column, Row and Full Wavelet Transforms Of Walsh, Cosine, Haar, Kekre, Slant and Sine and Their Comparison with Corresponding Orthogonal Transforms. International Journal of Engineering Research and Development, 6(4), 2013, 102-113.

[16] H. B. Kekre, Tanuja Sarode, Sudeep Thepade, Sonal Shroff, Instigation of Orthogonal Wavelet Transforms using Walsh, Cosine, Hartley, Kekre Transforms and their use in Image Compression. International Journal of Computer Science and Information Security, 9(6), 2011, 125-133.

[17] H.B. Kekre, Tanuja Sarode, Prachi Natu, Image Compression using Real Fourier Transform, It's Wavelet Transform and Hybrid Wavelet with DCT. International Journal of Advanced Computer Science and Applications (IJACSA). 4(5), 2013, 41-47.

[18] H.B. Kekre, Tanuja Sarode, Prachi Natu, Image Compression using Wavelet Transforms of DCT, DST, Hartley and Real-DFT with Variation in Size of Component Transforms. International Journal of Scientific & Engineering Research, (IJSER), 4(10), 2013, 512-517.

[19] H.B. Kekre, Tanuja Sarode, Prachi Natu, Performance Comparison of Walsh Wavelet, Kekre Wavelet and Slant Wavelet Transform in Image Compression. International Journal of Advanced Research in Computer and Communication Engineering, 2(10), 2013, 3834-3840.

[20] Clarke, R.J. Hybrid intraframe transform coding of image data. IEEE Proceedings on Communications, Radar and Signal Processing,1984.

[21] Pal, A.K., Biswas G.P., Mukhopadhyay, S, (2010). A Hybrid DCT-VQ Based Approach for Efficient Compression of Color Images. Proc. International Conference on Computer and Communication Technology, Allahabad, 2010, 177-181.

[22] Dipti Bhatnagar, Sumeet Budhiraja, Image compression using DCT based Compressive Sensing and Vector Quantization. International Journal of Computer Applications, 50(20), 2012, 34-38

[23] Deepika Sunoriya, Uday Pratap Singh, Vineet Ricchariya, Comparison and Analysis of an efficient Image Compression Technique Based on Discrete 2-D wavelet transforms with Arithmetic Coding. International Journal of Advanced Computer Research, 2(3), 2012, 65-74.

[24] H.B. Kekre, Archana Athawale, Dipali Sadavarti, Algorithm to Generate Kekre's Wavelet Transform from Kekre's Transform. International Journal of Engineering Science and Technology (IJEST), 2(11), 2010, 756-767.

[25] H.B. Kekre, Tanuja Sarode, Prachi Natu, Performance Comparison of Column Hybrid Row Hybrid and full Hybrid Wavelet Transform on Image compression using Kekre Transform as Base Transform. International Journal of Computer Science and Information Security, (IJCSIS). 12(2), 2013, 5-17.

Network Performance Analysis of Dynamic Routing Protocols for Real Time Application

Saubhagya Das[1], Santosh Subedi[2] , N. Shekar V. Shet[3]
[1, 2, 3] *(Department of E&C, NITK, Surathkal, India)*

Abstract: *Routing protocol is taking a vital role in the modern internet era. A routing protocol determines how the routers communicate with each other to forward the packets by taking the optimal path to travel from a source node to a destination node in the network layer. Algorithms that are used for route selection and data structure are the main parts for the network layer. But in this paper we have explored four eminent dynamic routing protocols namely, Routing Information Protocol (RIP), Open Shortest Path First (OSPF) & Enhanced Interior Gateway Routing Protocol (EIGRP) and Interior Gateway Routing Protocol (IGRP) protocols. Evaluation of these routing protocols is performed based on the quantitative metrics such as Delay, FTP, E-mail, HTTP, VoIP and Video Conferencing through the simulated network models. The simulation results are analyzed, with a comparison between these protocols on the effectiveness and performance in network implemented. Results show that EIGRP will be best for delay, E-mail and FTP but for real time applications OSPF and RIP give better results.*
Keyword: *Network OPNET, Routing Protocols, FTP, HTTP, Video conference, Voice*

I. Introduction

Communication in the Internet has become a fundamental part of life. Transmission Control Protocol TCP / IP are the engine for Internet and interconnection networks worldwide. The main objective of the TCP / IP was to achieve interconnection, which led to the provision of universal communication through natural heterogeneous networks [2]. Routing links together small networks to form huge internetworks that span vast regions. This cumbersome task makes the network layer the most complex in the OSI reference model. The network layer provides the transfer of packets across the network. At the network layer, the Internet can be seen as a collection of sub networks or Autonomous Systems (AS-Autonomous Systems sites) that are connected together via the main backbone. The Internet connection is performed using IP protocol (Internet Protocol).

Routing protocols determine the mechanism by which routers obtain information on the state of the network topology respectively. Routing protocols are based on routing algorithms, which rely on various metrics to find the best path to transmit data across networks. Metrics include cost, bandwidth, packet delay, and hop count. Routing protocols utilize a routing table to store the results of these metrics. Based on whether the routing is within an Autonomous System (AS) or between ASs, there are two types of routing protocols: Interior Gateway Protocols (IGP) and Exterior Gateway Protocol (EGP). RIP, OSPF, EIGRP, IS-IS and IGRP are commonly used IGPs. A typical EGP is the Border Gateway Protocol (BGP).

II. DYNAMIC ROUTING PROTOCOL CONCEPT

Dynamic routing protocols play an important role in today's networks. They are used to facilitate the exchange of routing information between routers. They dynamically share information between routers, automatically update routing table when topology changes, and determine the best path to a destination. Compared to static routing, dynamic routing protocols have better scalability and adaptability and require less administrative overhead. Dynamic routing protocols allow routers to dynamically advertise and learn routes, determine available routes and identify the most efficient routes to a destination. Dynamic routing protocols have the capability to maintain the network operation in case of a failure or when network configuration or topology change [11].

Basically "Distance vector" and "link state" are used to describe routing protocols used by routers to forward packets. There are two groups of routing protocols, based on whether the routing protocol selects the best routing path based on a distance metric (the distance) and an interface (the vector) or selects the best routing path by calculating the state of each link in a path and finding the path with the lowest total metric to the destination. Distance vector protocols evaluate the best path based on distance, which can be measured in terms of hops or a combination of metrics calculated to represent a distance value. The IP Distance vector routing protocols in use today are RIP and IGRP. In link state routing, every node constructs a map of the connectivity to the network in the form of a graph showing connectivity of the nodes to each other. Each node then

independently calculates the next best logical path to every possible destination in the network [5]. The collection of best paths forms the node's routing table. Link state protocols have the routers announce their closest neighbors to every router in the network. Only a part of the table pertaining to its neighbors is distributed. EIGRP, OSPF, and Intermediate System-Intermediate System (IS-IS) are link state routing protocol.

2.1 Routing Information Protocol (RIP)

Distance vector routing algorithm assumes that each router maintains a table (e.g. a vector) that preserves the best known distance to each destination and the line to be followed to get there [3]. Distance vector routing algorithm is also known by other name such as distributed routing algorithm Bellman-Ford or Ford-Fulkerson algorithm; named researchers have proposed (Bellman, 1957 Ford and Fulkerson, 1962).
RIP is a distance vector dynamic routing protocol that employs the hop count as a routing metric. RIP is implemented on top of the User Datagram Protocol (UDP) as its transport protocol [11]. RIP prevents routing loops by implementing a limit on the number of hops allowed in a path from the source to a destination. The maximum number of permitted hops is 15. Hence a hop count of 16 is considered an infinite distance. RIP depends upon no of hop and selects paths that have the smallest hop counts. However, the path may be the slowest in the network. RIP is simple and efficient in small networks. However, it may be inefficient in larger networks. Every RIP router updates its own routing table by communicating with neighboring routers and transmits full updates in every 30 seconds [5]. RIP may take 30–60 seconds to converge based on the features of distance vector protocols. RIP has lower power consumption and memory than some other routing protocols.

2.2 Open Shortest Path First (OSPF)

OSPF uses a link state routing algorithm and it operates within a single AS. It exhibits faster routing compared to RIP. Each OSPF router stores the local network connection state with Link State Advertisement (LSA) and advertises to the entire AS. Each router receives the LSA generated by all routers within the AS. The LSA collection then forms Link State Database (LSDB). Each LSA is the description of the surrounding network topology of a router. Hence, the LSDB reflects the AS network topology [6]. When a new router is added to the network, it will broadcast hello messages to every neighbor and will receive the feedback hello messages from its neighbors. Eventually, routers establish connections with newly added router and synchronize their routing databases. Every router broadcasts link state update messages when network topology changes. Every router calculates the best paths to all destinations and indicates the closet router for each transmission. OSPF is the most widely used IGP in large enterprise networks.

2.3 Enhanced Interior Gateway Routing Protocol (EIGRP)

EIGRP is a Cisco proprietary routing protocol, which is an improved version of the interior gateway routing protocol (IGRP). EIGRP is being used as a more scalable protocol in both medium and large scale networks.
EIGRP is said to be an extensively used IGRP where route computation is done through Diffusion Update Algorithm (DUAL) [12]. EIGRP metrics are based on reliability, MTU, delay, load, and bandwidth. EIGRP collects data from three tables. The first is the neighbors' table, which stores data about neighboring routers that are directly accessible through interfaces that are connected. The second is the topology table, which contains the aggregation of the routing tables that are gathered from all neighbors that are directly connected. It contains a list of destination networks in the EIGRP routed network and their respective metrics. The third routing table stores the actual routes to all destinations. EIGRP does not rely on periodic updates to converge in the topology, instead building a table that will contain announcements on neighbours about changes in topology. The EIGRP router broadcasts to other neighbors if it cannot locate a router based on its routing database.

2.4 Interior Gateway Routing Protocol (IGRP)

IGRP is a Cisco-proprietary Distance-Vector protocol, designed to be more scalable than RIP. IGRP sends out the full routing table every periodic update every 90 seconds. IGRP metrics are based on bandwidth and delay. IGRP requires including an Autonomous System (AS) number in its configuration. Only routers in the same Autonomous system will send updates between each other. It support up to six parallel paths to the destination for load balancing. It provides loop free environment. It only support IP routing. By default it supports maximum 100 hops.

III. Simulation

In this paper, we used OPNET Simulator, a real time simulator specifically designed for network design and analysis, to compare these protocols, when considering a hypothetical network model. It enables simulation of heterogeneous networks by employing a various protocols [5]. The OPNET IT Guru provides a

GUI to create the virtual network conveniently. OPNET simulator is built on top of discrete event system (DES) and it simulates the system behavior by modeling each event in the system and processing it through user defined processes. It has several distinct methods of creating topologies. Modeler supports almost all network types and technologies [9].

3.1 Design and Analysis in OPNET

When implementing a real model of the system in the OPNET, some steps are to be followed to design on simulator. Figure 1 shows the workflow for OPNET.
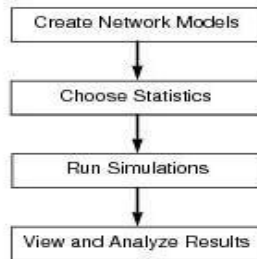
Fig.1: OPNET Analysis

3.2 Simulation Environment

The simulated network shown in Figure 2 consists of six subnets connected to each other with *Point to Point Protocol* (PPP) using Digital Signal 3 (DS3, 44.736 Mb/s). One subnet is acting as server at centre and remaining subnets are connected as shown in Fig 2. Each subnet consists of Ethernet4_slip8_gtwy routers, switches and 10BaseT LANs and nodes are connected with Ethernet 100BaseT cables as shown in Fig. 4. Server subnet is consists of three servers, two workstations and switches as shown in Fig 3. The network topology design in Fig. 1 is configured for RIP, OSPF, IGRP and EIGRP protocols with two scenarios such as Fail and No Fail. In order to analyze the network in terms of different parameters like upload and down load response time, packet end to end delay, throughput, etc., the global, node and link statistics are configured accordingly.
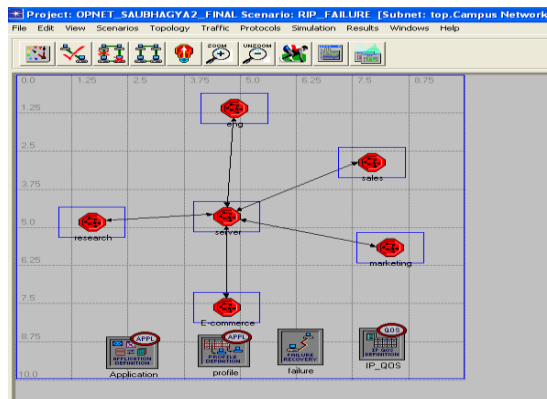
Fig.2: OPNET Simulated Network Topology
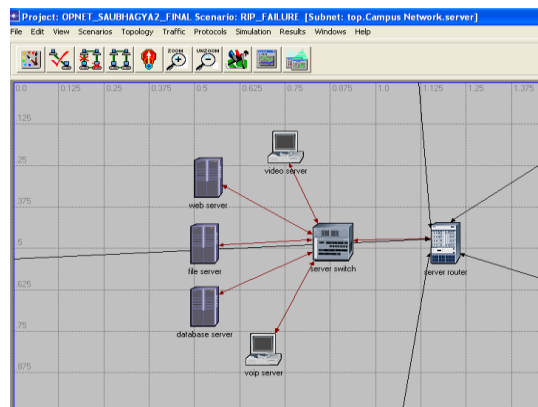
Fig.3: Design of server subnet
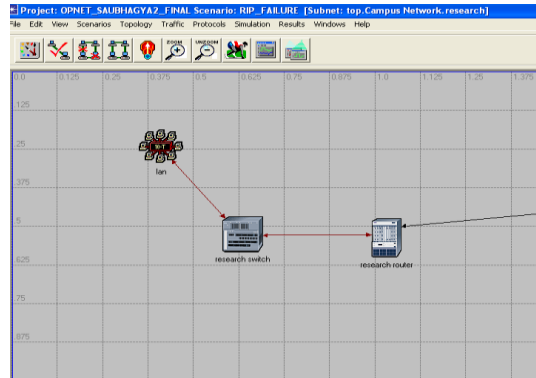
Fig.4: Design of client subnet

3.3 Design Parameters

(Ftp)Table		(Http)Table		(Video Conferencing)Table	
Attribute	Value	Attribute	Value	Attribute	Value
Command Mix(Get/Total)	50%	Http Specification	HTTP1.1	Frame interval time information	15 frames/sec
Inter-Request Time (seconds)	Constant(100)	Page Interval Time(sec)	Exponential (2000)	Frame size information	128×240 pixels
File Size(bytes)	Constant(100000)	Page Properties	(…)	Symbolic destination name	Video destination
Symbolic Server Name	FTP Server	Server Selection	(…)	Type of service	Streaming multimedia (4)
Type of Service	Best Effort(0)	Type of Service	Best Effort(0)	Traffic Mix	All discrete
(Database)Table		(Email)Table		(Voice)Table	
Transaction Mix(current/total)	100%	Send interval time	Exponential (3000)	Encoder scheme	G.711
Transaction interval Time	Constant(100)	Send group size	Constant(4)	Voice frames per packet	1
Transaction Size	Constant(512)	Receive interval time	Constant(10)	Type of Service	Interactive voice(6)
Symbolic Server Name	Database Server	Receive group size	Constant(4)	Symbolic destination	Voice destination
Type of Service	Best Effort(0)	Symbolic server name	Email server	RSVP Parameters	None

3.4 Simulation Results and Analysis

OPNET Modeller is used extensively to decide which protocols would be best suitable for applications. The metrics used for network performance are network convergence, queuing delay, throughput, QoS and CPU utilization. We consider a random network design so as to have a standard network with different profiles such as student, research, marketing, etc. each of which would require different applications, some of which would be real time while others non-real time. We start with the analysis of non-real time applications where on the topology shown in fig.2. It is necessary that we understand the effect of choice in routing protocols, the QoS that it offers, the effect of number of simultaneous users and applications which would add to the server load and hamper the QoS of real-time applications which work on a low latency QoS. The simulation time is set to fifteen minutes to all routing protocols.

Ethernet Delay: The Ethernet delay, representing the end to end delay of all packets received by all the stations in the network, is shown in Figure 5.
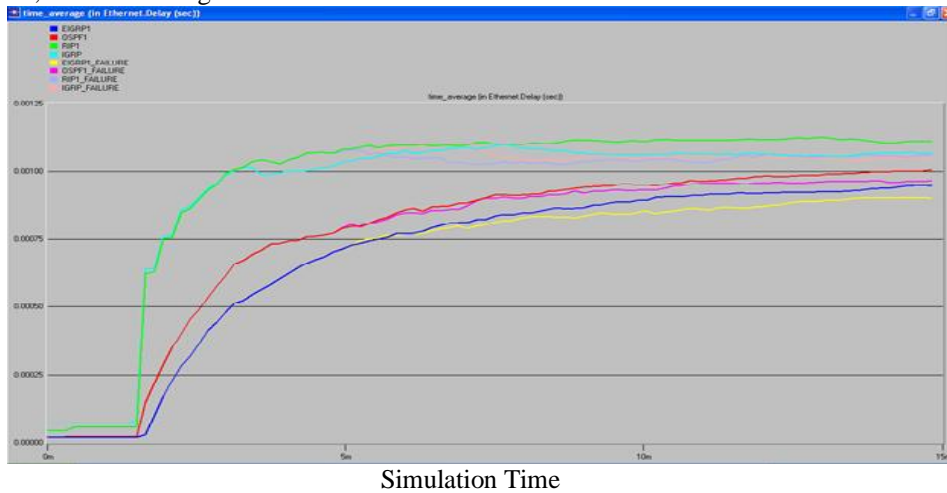
Simulation Time
Fig.5: Ethernet Delay

The lowest delay is experienced by EIGRP and the highest delay is experienced by RIP. EIGRP has very low usage of network resources during normal operation only *hello* packets are transmitted. When routing table changes, its convergence time is short and it reduces bandwidth utilization.

Email: The parameters which are considered for Email are Download response time and upload response time. The simulation is run for same time for all protocols.
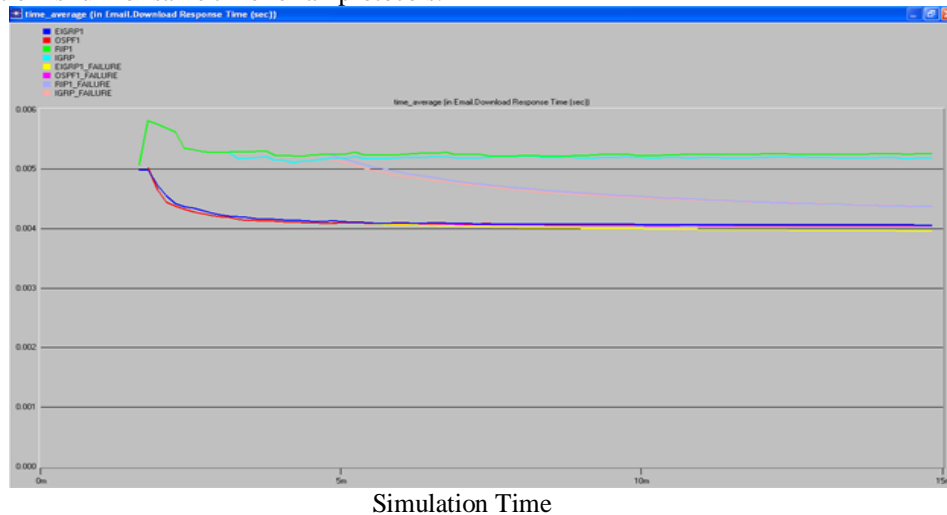
Simulation Time
Fig.6: Email down load Response time (sec)
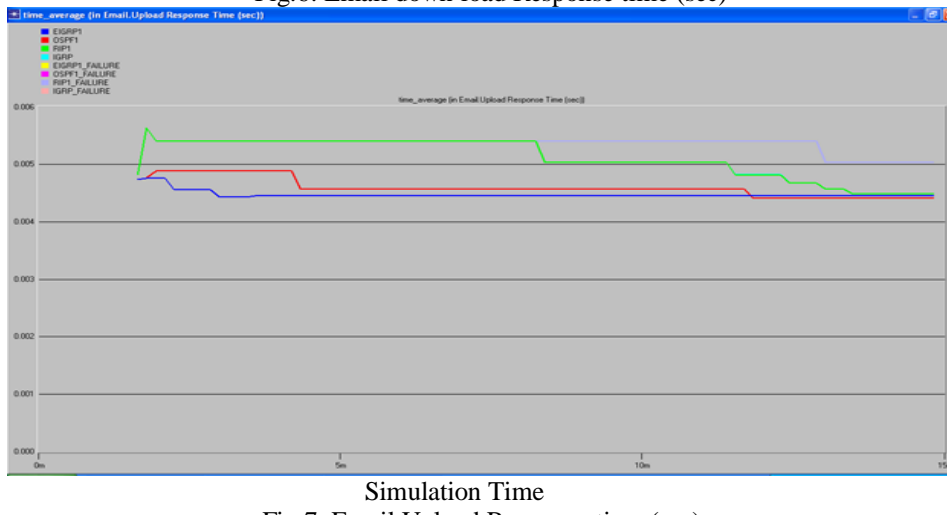
Simulation Time
Fig.7: Email Upload Response time (sec)

On the basis of simulation result, we observe that EIGRP protocol exhibits the shortest response time and RIP exhibits the highest response time for any simulation network in terms of convergence and latency for any standard simulated network. After failure also EIGRP exhibits shortest response time.

FTP: The parameters which are considered for ftp Download response time and upload response time. By default FTP application model transfers only one file at a time. FTP creates lots of packets which move through the network like a single packet. These packets tend to congest the flow through the network and affect the high priority traffic.
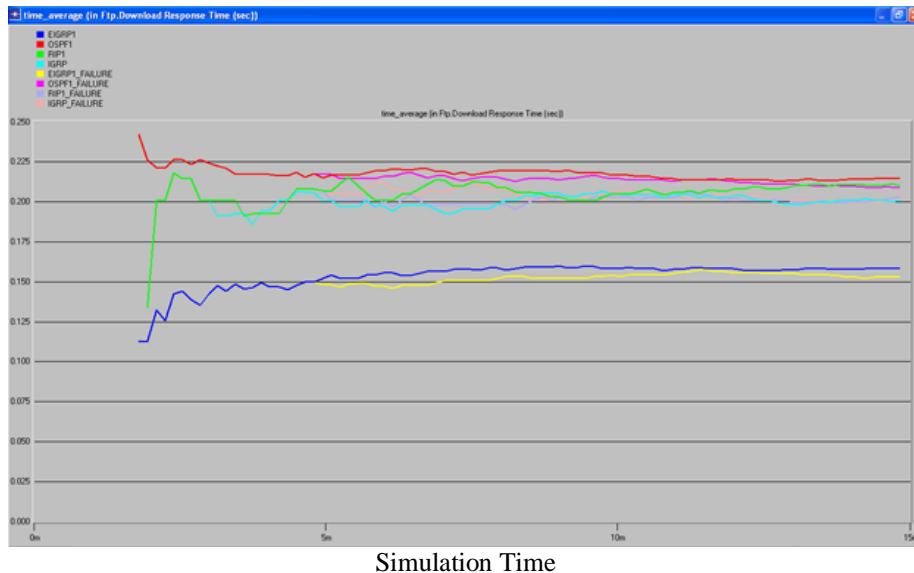
Simulation Time

Fig.8: Ftp down load Response time(sec)
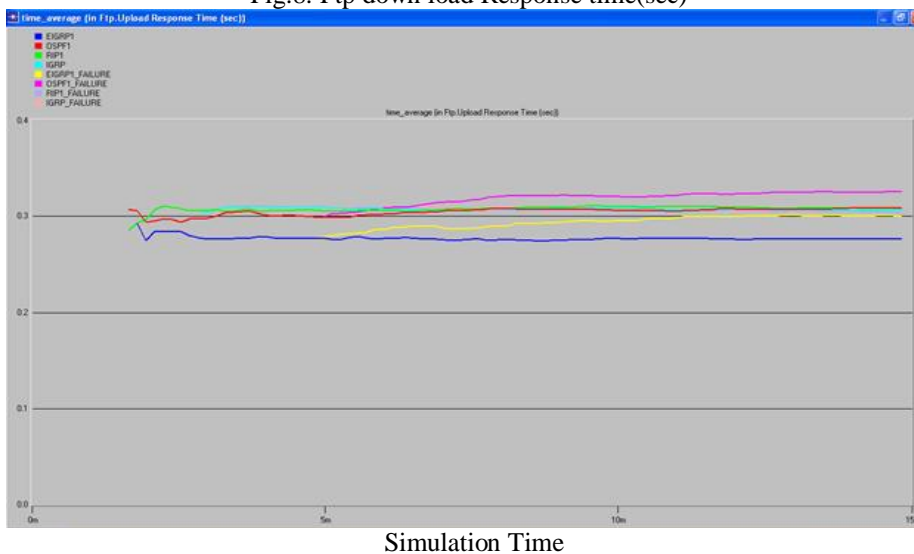
Simulation Time

Fig.9: Ftp down load Response time (sec)

We consider all routing protocols to determine which would provide most results for ftp. After simulation we conclude that EIGRP protocol would work best for ftp under standard network topology.

HTTP web browsing: The parameters which are considered for Http are page response time.
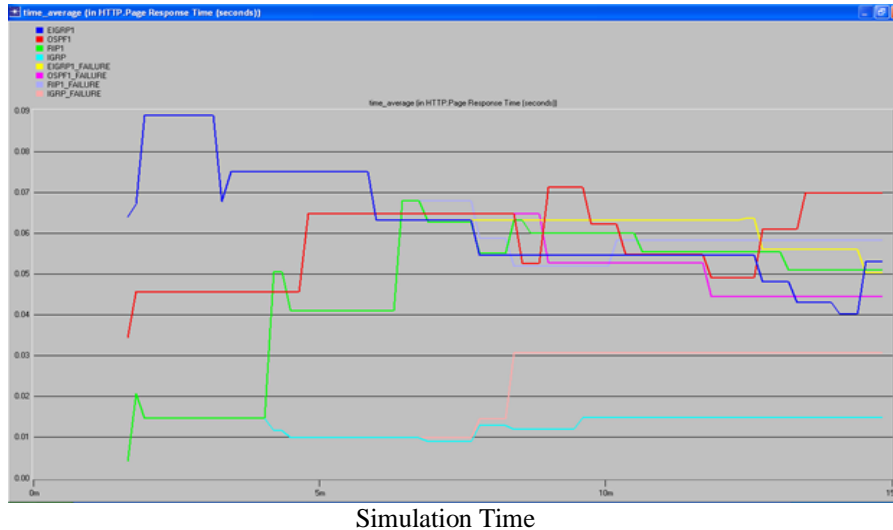
Simulation Time
Fig.10: Http page Response time (sec)

The HTTP web browsing takes both heavy as well as light traffic into account due to which scheduling of packets and congestion changes with time. Here the time average of page response time and object response time based on comparative results shown above we can say that IGRP is the best suited protocols for HTTP.

Real time applications

As seen in fig 3 the real time applications such as VoIP and video conferencing application are based on a peer to peer network and hence also can be termed as high bandwidth resource utiliser with improved QoS to meet demands of the user satisfaction. They are peer to peer applications and are more bandwidth dependant for better QoS.

Video Conferencing: The Video Conferencing application models transmission of video traffic between two nodes in the network. Video Conferencing application runs over the UDP transport protocol to avoid connection management and other delays associated with the TCP protocol. The selection of appropriate protocol for real time application is more important in terms of packet delay variation and End-to-End delay. The attribute for video conferencing is shown in design parameters.
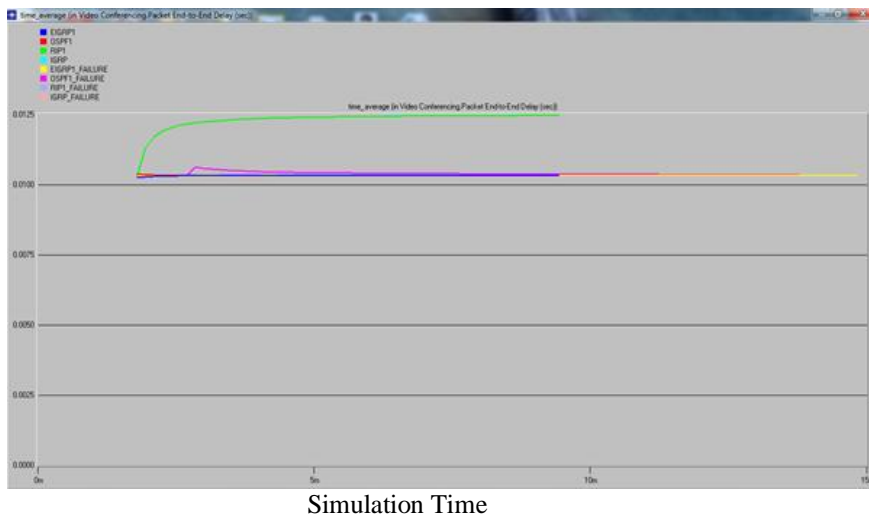
Simulation Time
Fig. 11: Video Conferencing packet End-to-End Delay (sec)

On the basis of simulation result we conclude that real time application for video conferencing and streaming packet End-to-End delay would work best with EIGRP routing protocol.

VoIP: Voice over IP technology integrates data and voice networks and offers flexibility by supplying device interoperability using standards-based protocols. Routing is an essential data networking function that provides an efficient real-time data delivery VoIP requires [10]. Best effort networks leverage IGP technologies to

determine path between hosts.The VoIP performance metrics include delay, jitter, and packet loss. The parameters which are considered for VoIP are voice packet delay and End-to-End Delay variation.
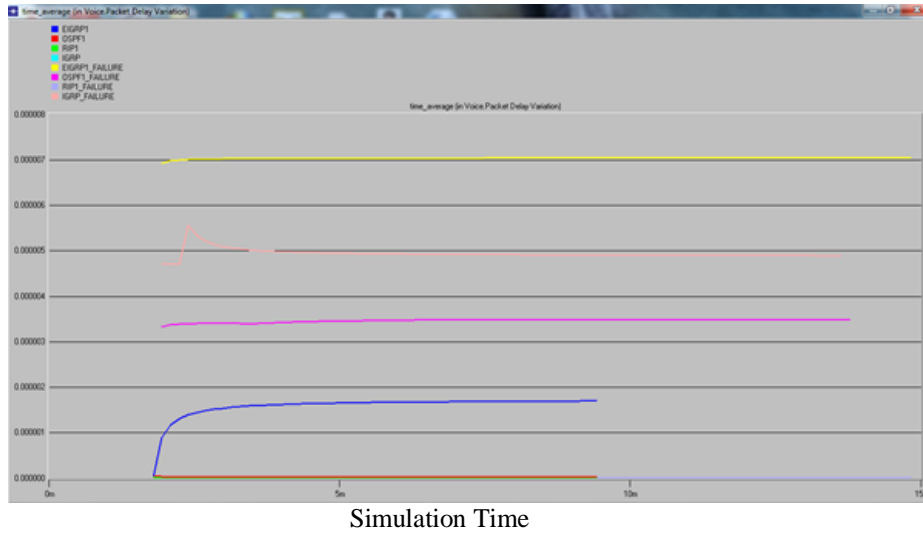
Simulation Time
Fig.12: Voice packet Delay variation (sec)
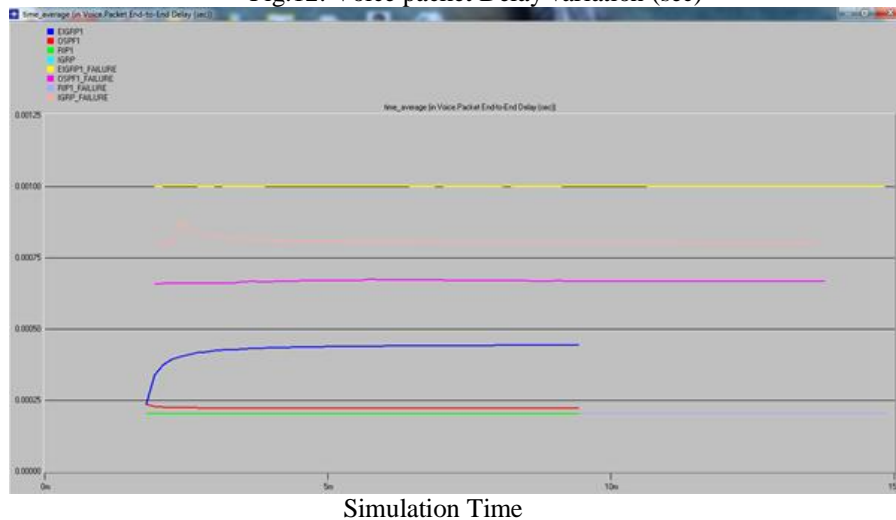
Simulation Time
Fig.13: Voice packet End-to-End Delay (sec)

As we expected, EIGRP carries out low-efficient routing in the network. RIP and OSPF perform with excellence because they computing the fastest possible route. On the basis of the above results we can conclude that based on the voice encoder schemes selected and the most optimal routing algorithm would be RIP and OSPF for real time VoIP application. RIP performs better in terms of voice packet delay because it is a simple routing protocol that relies on distance vector algorithms. OSPF has large protocol overhead when updating the routing table.

IV. Conclusions

In this paper we would like to find which routing protocol would serve best based on applications running in our network topology. Here we classified the application into real time and non-real time where RTP protocols are simulated over IGP protocols. EIGRP is a robust protocol, combines the attributes of distance-vector and link-state protocols attributes, resulting in a hybrid protocol that is easy to configure, efficient and also has a faster Convergence. We can conclude that EIGRP is the best choice for Delay, FTP and E-mail. We can use live requirement of video and voice applications to work with specific QoS to meet requirement of low latency and packet dropping. The best results for video and voice packet delay is OSPF and for video and voice end-to-end delay is EIGRP. As a future work we need to study the effect of newer applications on server load as well effect of nodes on QoS of applications. We can do new applications based on our current network topology using application and profile definition as a guideline.

REFERENCES

[1]   Andrew S. Tanenbaum, "Computer Networks 4Th Ed.", Prentice Hall, 2003.
[2]   Lydia Parziale, David T. Britt, Chuck Davis "TCP/IP Tutorial and Technical Overview" ibm. com/redbooks, December 2006.
[3]   Ioan Fiţigău, Gavril Toderean, "Network Performance Evaluation for RIP, OSPF and EIGRP Routing Protocols." Technical University of Cluj-Napoca, Str. George Baritiu, nr. 26-28, 978-1-4673-4937-6/13 ©2013 IEEE.
[4]   S. G. Thornier, "Communication service provider's choice between OSPF and IS-IS dynamic routing protocols and implementation criteria using OPNET simulator," in Proc. Second International Conference on Computer and Network Technology (ICCNT), Bangkok, Thailand, Apr. 2010, p. 38–4.
[5]   Don Xu and Ljiljana Trajković, "Performance Analysis of RIP, EIGRP, and OSPF using OPNET", Vancouver, Canada.
[6]   B. Fortz and M. Thorup, "Optimizing OSPF/IS–IS weights in a changing world," IEEE Journal on Selected Areas in Communications, vol. 20, no. 4, pp. 756–767, May 2002.
[7]   Wu, Bing, "Simulation Based Performance Analyses on RIP, EIGRP and OSPF Using OPNET".
[8]   Cisco,   Enhanced   Interior   Gateway   Routing   Protocol   [Online]. Available:http://docwiki.cisco.com/wiki/Enhanced_Interior_Gateway_Routing_Protocol.
[9]   Mohamad A. Yehia, Mohammed S. Aziz, Hussein A. Elsayed, "Analysis of IGP Routing Protocols for Real Time Applications: A Comparative Study", International Journal of Computer Applications, Volume 26-No3, July 2011.
[10]   Che, Xianhui, and Lee J. Cobley. "VoIP Performance over Different Interior Gateway Protocols." International Journal of Communication Networks and Information Security (IJCNIS) 1, no. 1 (2011).
[11]   http://www.cisco.com/en/US/docs/internetworking/
[12]   Mohammad Nazrul Islam, Md. Ahsan Ullah Ashiqu, "Simulation Based EIGRP over OSPF Performance Analysis", Master Thesis in Electrical Engineering Emphasis on Telecommunications Thesis no: 4983 May 14, 2010.
[13]   Bahl, Vasudha. "Performance Issues and Evaluation considerations of web traffic for RIP & OSPF Dynamic Routing Protocols for Hybrid Networks Using OPNET TM." International Journal 2, no. 9 (2012).
[14]   http://www.opnet.com [accessed in November, 2012]
[15]   B. Albrightson, J. J. G. L. Aceves, and J. Boyle. "EIGRP – a fast routing protocol based on distance vectors," in Proc. Of Networld/Interop, April 1994, pp.1-13.

A Novel Data mining Technique to Discover Patterns from Huge Text Corpus

Mohamed Younis Mohmed Alzarrous [1], Mr.Surya Prakash Mishra [2]

[1, 2] (*M.Sc, Asst. Prof, in Computer Science in Department of Computer Science and Information Technology in SHIATS, Allahabad, India)*

Abstract: *Data mining is the process of analyzing data from different perspectives and summarizing it into useful information - information that can be used to increase revenue, cuts costs, or both. Technically, data mining is the process of finding correlations or patterns among dozens of fields in large relational databases. Many techniques have been investigated on mining scenario from documents including the texts for required patterns respectively. There is a problem on dealing with this particular task for inventory patterns which are accurate. Research has done on this strategy; results have proven that this strategy is facing two problems, i.e., 1) synonymy and 2) polysemy (coexistence of many possible meanings for a word). So, in the text mining, we can use the techniques of pattern mining to find different text patterns, like co-occurring terms, frequent item-sets. Therefore now this present technique i.e., inventory pattern plays a crucial role in the investigation of the patterns. We first conduct a set of large-scale measurements with a collection of over different data sets into a database. We upload this database consisting of data sets for constructing the pattern taxonomy model, partial conflict tree and Chart. Based on the measurement results, we have proven that this technique works efficiently and effectively. It also provides good results for the implementation of task.*

Keywords: *Patterns, Associations, or Relationships, Sequence patterns, Classification of text.*

I. INTRODUCTION

Today, we have far more information than we can handle: from business transactions and scientific data, to satellite pictures, text reports and military intelligence. Information retrieval is simply not enough anymore for decision-making. Confronted with huge collections of data, we have now created new needs to help us make better managerial choices. These needs are automatic summarization of data, extraction of the "essence" of information stored, and the discovery of patterns in raw data. With this, Data mining with inventory pattern came into existence and got popularized. Data mining finds these patterns and relationships using data analysis tools and techniques to build models.

There are two main kinds of models in data mining. One is predictive models, which use data with known results to develop a model that can be used to explicitly predict values. Another is descriptive models, which describe patterns in existing data. All the models are abstract representations of reality, and can be guides to understanding business and suggest actions. These data provides many benefits and plays a vital role in the entire society in terms of managerial business and analyzing the market by the particular extraction respectively. Data mining is an important part of Knowledge discovery process that we can analyze an enormous set of data and get hidden and useful knowledge. Data mining is applied effectively not only in business environment but also in other fields such as weather forecast, medicine, transportation, healthcare, insurance, government…etc.

Figure 1.1: Data Mining is the core of Knowledge Discovery process
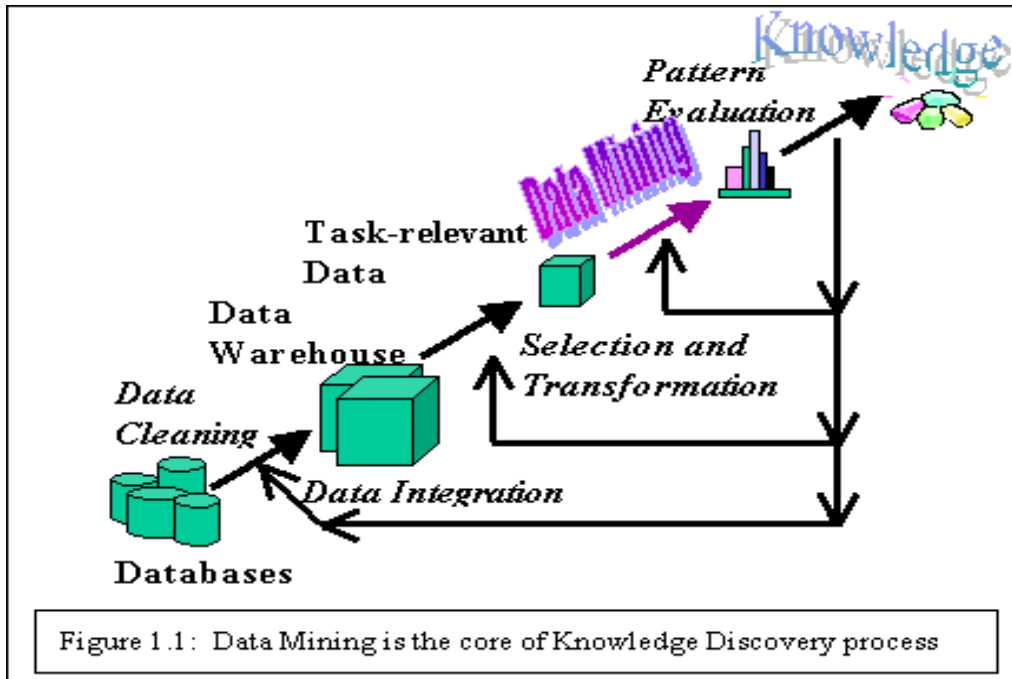
II. RELATED WORK

Necessity is the mother of invention. Since ancient times, our ancestors have been searching for useful information from data by hand. However, with the rapidly increasing volume of data in modern times, more automatic and effective mining approaches are required. Early methods such as Bayes' theorem in the 1700s and regression analysis in the 1800s were some of the first techniques used to identify patterns in data. After the 1900s, with the proliferation, ubiquity, and continuously developing power of computer technology, data collection and data storage were remarkably enlarged. As data sets have grown in size and complexity, direct hands-on data analysis has increasingly been augmented with indirect, automatic data processing. This has been aided by other discoveries in computer science, such as neural networks, clustering, genetic algorithms in the 1950s, Decision trees in the 1960s and support vector machines in the 1980s.

However, a well known one is a bag of words that uses keywords (terms) as elements in the vector of the feature space. Here the Rocchio system is used to improve performance. Also many other weighting schemes were given. The problem of the bag of words approach was how to select a limited number of features among an enormous set of words or terms in order to increase the system's efficiency.

Data mining techniques have been used for text analysis by extracting co-occurring terms as descriptive phrases from document collections. However, the effectiveness of the text mining systems using phrases as text representation showed no significant improvement. The likely reason was that a phrase-based method had lower consistency of assignment and lower document frequency for terms.

Pattern mining has been extensively studied in data mining communities for many years. A variety of algorithms such as Apriori-like algorithms, PrefixSpan, FP-tree, APADE, SLPMiner and GST have been proposed. These research works have mainly focused on developing efficient mining algorithms for discovering patterns from large data collection. However, searching for useful and interesting patterns and rules was still an open problem.

III. Proposed System

Even though after generating the patterns there is a problem in mining, they lend themselves discovering frequent item sets and the order they appear. So to overcome all these problems a particular method has been implemented which plays a key and crucial role in the field of mining of text in the form of extraction of the data accurately followed by a good updating process in the entire phenomena. Mining of text is the detection of knowledge based on the interest in the documents consisting of text respectively. Now there is a major challenging task involved in it where it must provide service for the user in the form of accurate extraction of the information in the mining of text in the form of generated patterns. There are large numbers of experimental analysis taken place in the collection of the data and also the retrieval of the text accurately

and precisely depending on the user's choice. Therefore our present methodology overcomes all the above problems accurately and carries the success.

IV. Problems in the Existing System

For the extraction of the information and knowledge, a large number of investigations had taken place in the mining of the data previously. There are some existing techniques that follow mining by the rule of association, Sequential patterns, mining by the help of item set phenomena, Mining by clustering, Mining by the classification, mining by the Prediction. There are some limitations to these presented techniques.

- They are implemented under one particular frame of time, i.e., under the restricted areas.
- Missing data; which poses a big hurdle in this current system
- The data is very large. So, it's not always very accurate
- Quality of the data is poor

V. Solutions to These Problems

To improve the performance in the mining of a text based aspects in the form of the patterns related to the closed strategy an extra information is used in the system for this purpose we are supposed to hold that particular phenomena by the name as D pattern respectively which is mainly used for the weight evaluation. Therefore these D patterns play a major role in the form of the technique by the name term in which there is no synonym for the greater value. Therefore this particular strategy is completely differed from the generalized scenario basis where it is completely inter dependent on the terms involved in the documentation in it. Further improving the performance of the system in the form of affectivity in the mining pattern of taxonomy where the differentiation of the algorithm takes place by the name of the mining based on SP method respectively in order to observe the relatively ordered patterns where the space of searching is got negotiated. Now moving towards the reciprocal documents that is the opposite of the normal scenario based documents where the reshuffling involves in it and also which provides support by the pattern D in the original form. In order to this a patterns generated by the noise gets nullified due to the less frequency oriented data and is termed as the evolution of the inner patterns. Here the consideration takes only with respect to the inner phenomena where as the outer phenomena got escaped from the system. Now here the major concern is similar and non similar data has to be differentiated therefore in order to separate between themselves, conditionality has to be set by the name of the threshold respectively. The defining of the threshold takes place by the help of the initialization of the setting D pattern. And therefore the threshold function is represented by the following equation

$$Threshold(D\ ') = \min_{p \in D} \left(\sum_{(t,w) \in \beta(p)} support(t) \right).$$

VI. Benefits

Using the D-pattern method, the text has the following benefits:-

- Improves the effectiveness by effectively
- Significantly improves the performance of information filtering
- Noise generated by the patterns are nullified due to less frequency data
- Provides accurate data
- Reduces the searching space

VII. Expected Result

In the present section by the evolution of patterns in the model of taxonomy, experimental results of PTM approach are presented and analyzed. The tabular column shows how frequently patterns occur in covering set and also displayed in the figure. As already mentioned earlier that mining of the data based on the item set where it is satisfied with rapid generation but it suffers from the implementation/ evaluation respectively. Here the comparison takes place by the experts and provides the data results accurately and in the much more efficient manner[3][4][6]. Our present method plays a crucial role on mining based on the terms and also on pattern dependent mining. and some of them includes support vector machine and the state of art.

Effective Inventory pattern
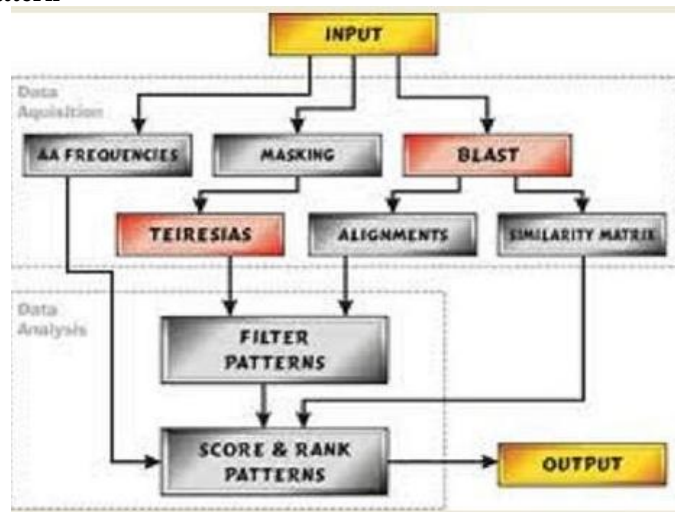
The above figure describes the step by step process of how the input has been converted to output i.e., inventory patterns.

Pattern Taxonomy model:

Upload DB File	Pattern Taxonomy	PTM IPE	
Frequent Pattern	Covering Set		Support
BOOKS,CD	P1,P5,P6		3.0
DVD,VIDEO	P2,P3,P4		3.0
BOOKS	P1,P5,P6		3.0
CD	P1,P5,P6		3.0
DVD	P2,P3,P4		3.0
VIDEO	P2,P3,P4		3.0

After uploading the database, we will get the above figure, which shows how frequent the patterns appear in covering set i.e., set of paragraphs and also shows the support value of each pattern.

Conflict tree:

Upload DB File   Pattern Taxonomy   PTM

ROOT
- {BOOKS,CD}[1,5,6]
- {DVD,VIDEO}[2,3,4]
- {KEYBOARD}[3,4,5,6]
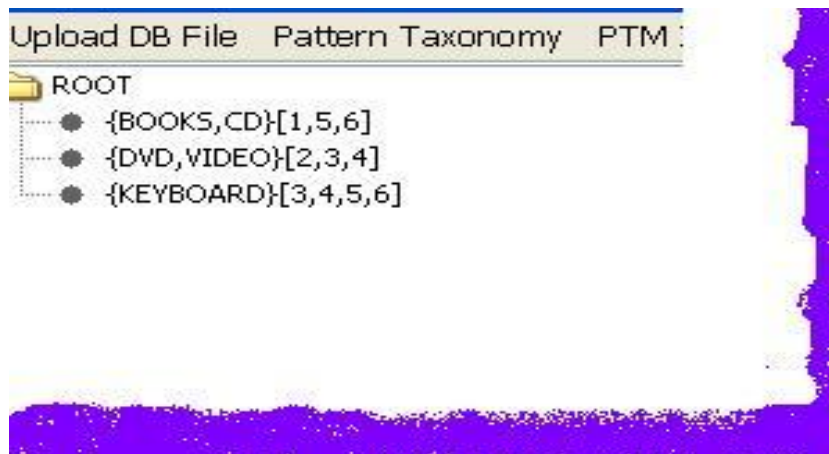
The above figure shows how set of different items appear in different paragraphs
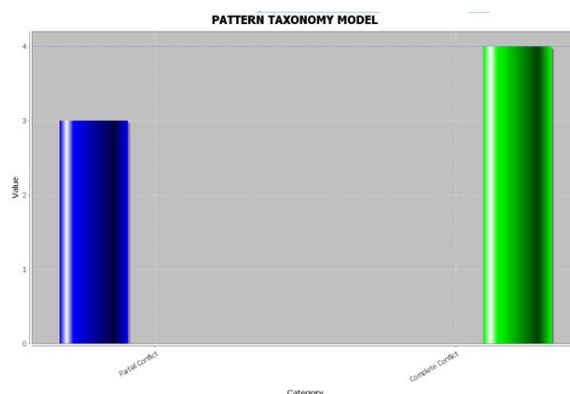
chart :
The above figure shows how the partial conflict differs from the complete conflict

VIII.   Conclusion

Research has been done on this particular problem. Many techniques have been involved before this methodology and some of them are mining by association, Sequential mining of the patterns, Pattern maximization, closeness of Pattern etc. The study of the above research oriented concepts involves lot of effort and is a huge tedious job in the stream of mining text and lacks efficiency and is less effective. In addition to the above problem it has the frequency issues. It has low frequency components. Low frequency means patterns generated with most of them are small and ineffective. In order to overcome these problems a new technique is implemented for studying low frequency data and also for studying mismatched problems respectively. The technique which is proposed in this paper deals with the evolution and deployment of the patterns in the mining of text. Practical approaches confirm that it not only used for the data text but also used for the state-of-art that is the support vector machine respectively.

REFERENCES

[1]   J. Han, J. Pei, and Y. Yin, "Mining Frequent Patterns without Candidate Generation," Proc. ACM SIGMOD Int'l Conf. Management of Data (SIGMOD '00), pp. 1-12, 2000.
[2]   W. Lam, M.E. Ruiz, and P. Srinivasan, "Automatic Text Categorization and Its Application to Text Retrieval," IEEE Trans. Knowledge and Data Eng., vol. 11, no. 6, pp. 865-879, Nov./Dec. 1999.
[3]   M.F. Caropreso, S. Matwin, and F. Sebastiani, "Statistical Phrases in Automated Text Categorization," Technical Report IEI-B4-07- 2000, Instituto di Elaborazione dell'Informazione, 2000.
[4]   R. Agrawal and R. Srikant, "Fast Algorithms for Mining Association Rules in Large Databases," Proc. 20th Int'l Conf. Very Large Data Bases (VLDB '94), pp. 478-499, 1994.
[5]   H. Ahonen, O. Heinonen, M. Klemettinen, and A.I. Verkamo, "Applying Data Mining Techniques for Descriptive Phrase Extraction in Digital Document Collections," Proc. IEEE Int'l Forum on Research and Technology Advances in Digital Libraries (ADL '98), pp. 2-11, 1998.
[6]   T. Joachims, "Transductive Inference for Text Classification Using Support Vector Machines," Proc. 16th Int'l Conf. Machine Learning (ICML '99), pp. 200-209, 1999.
[7]   T. Joachims, "A Probabilistic Analysis of the Rocchio Algorithm with tfidf for Text Categorization," Proc. 14th Int'l Conf. Machine Learning (ICML '97), pp. 143-151, 1997.
[8]   N. Cancedda, N. Cesa-Bianchi, A. Conconi, and C. Gentile,"Kernel Methods for Document Filtering," TREC, trec.nist.gov/pubs/trec11/papers/kermit.ps.gz, 2002.

Name:- Mohamed Younis Mohmed Alzarrous.
Gender :- male .
date of birth :- 01/12/1983
nationality of birth :- Libya .
present nationality :- Libya .
pervious certificate :- B.Sc in computer science - Libya - tragen .
current certificate :- M.Sc in computer science -India -Allahabad .
E-mail: moh_you83@yahoo.com

Name:-Mr. Surya Prakash Mishra .
gender :- male .
date of birth :- 05/07/1982
nationality of birth :- India .
present nationality :- India .
pervious certificate :- M.C.A in computer - UP. Tech University .
current certificate :- pursuing Ph.D
E-Mail :- surya.mishra@shiats.edu.in

Nonlinear Transformation Based Detection And Directional Mean Filter to Remove Random Valued Impulse Noise

Dr.Sivaagorasakthivelmurugan[1], P. Ravi Shankar[2]

[1, 2] (Associate Professor, Department of EEE, Department of EEE, Sree Sakthi Engineering College, Nehru Institute of Engineering and Technology, Coimbatore)

Abstract: *In this paper, a novel two stage algorithm for the removal of random valued impulse noise from the images is presented. In the first stage the noise pixels are detected by using an exponential nonlinear function. The transformation of the pixels increases the gap between noisy and noise free candidates which leads to an efficient detection. In the second stage, the directional differences between the pixels in the four main directions are calculated. The mean values of the pixels which lie in the direction of minimum difference are calculated and the noisy pixel values are replaced with the mean value of the pixels lying in the direction of minimum difference. Experimental results show that proposed method is superior to the conventional methods in peak signal to noise ratio.*

Index terms: *Impulse noise, mean, peak signal to noise ratio.*

I. Introduction

Noise Suppression from images is one of the most important concerns in digital image processing. The impulse noise is one kind of the most ubiquitous noise, which comes from transmission errors, malfunctioning pixel elements in the camera sensors, faulty memory locations, and timing errors in analog-to-digital conversion An important characteristic of this type of noise is that only part of the pixels are corrupted and the rest are noise-free. The amount of impulse noise is usually quantified by the percentage of pixels which are corrupted.Fixed valued impulse noise takes the values 0 and 255 where as the random valued impulse noise takes the values in the dynamic range of [0,255]. Various methods have been proposed in the literature for the removal of impulse noise.

One of the most popular methods is the median filter [2], which can suppress noise with high computational efficiency. However, since every pixel in the image is replaced by the median value in its neighborhood, the median filter often removes desirable details in the image and also blurs the image too. The weighted median filter and the center-weighted median filter [6] were proposed as remedy to improve the median filter by giving more weight to some selected pixels in the filtering window. Although these two filters can preserve more details than the median filter, they are still implemented uniformly across the image without considering whether the current pixel is noise-free or not. ROAD [5] mechanism provides a measure of how close a pixel value to its four most similar neighbors. But when the noise level is high it introduces blurring in the image.

Recently, directional weighted median filter [11] and has been reported in the literature to overcome the above draw backs and to improve the filtering performance in terms of noise removal and detail preservation. But the main drawback of these filters is that it uses large number of iterations for better noise removal and hence it takes large computation time.

PWMAD[6] is a robust estimator of variance, MAD (median of the absolute deviations from the median), is modified and used to efficiently separate noisy pixels from the image details. The median of the absolute deviations from the median-MAD is used to estimate the presence of image details, thus providing their efficient separation from noisy image pixels. An iterative pixel-wise modification of MAD (PWMAD) provides reliable removal of arbitrarily distributed impulse noise

The ACMF[8] devises a novel adaptive operator, which forms estimates based on the differences between the current pixel and the outputs of center-weighted median filters with varied center weights. It employs the switching scheme based on the impulse detection mechanisms. It utilizes the center-weighted median ilter that have varied center weights to define a more general operator, which realizes the impulse detection by using the differences defined between the outputs of CWM filters and the current pixel of concern. The ultimate output is switched between the median and the current pixel itself.

A new directional weighted median filter[2] for the removal of random-valued impulse noise algorithm uses a new impulse detector, which is based onthe differences between the current pixel and its neighbours aligned with fourmain directions. After impulse detection, it does not simply replace noisy pixels

identified by outputs of median filter but continue to use the information of the four directions to weight the pixels in the window in order to preserve the details as removing noise. It is an iterative method. This method repeats 8 to 10 times.

The methods which filters all the pixels irrespective of the corruption tends to blur the image, hence the techniques which follow the two stage process of detection of noise pixels and filtering of noise pixels are employed to achieve better performance in terms of peak signal to noise ratio.In order to overcome the difficulties in this paper, a two stage algorithm removal of impulse noise is proposed. The proposed method is simple and outperforms the existing methods in terms of the peak signal to noise ratio.

II. Principles Of Algorithm

The algorithm is a two stage algorithm. In the first stage the detection of noise pixels is done by widening the gap between the noise pixel and other pixels in the window. In the second stage detected pixels are subjected to the directional mean filtering process.

III. Two Stage Algorithm For Removal Of Impulse Noise.

Consider X to be a random valued noise corrupted image of size MxN and X(i,j) denote the grey level at the pixel location (i,j). The pixels in the detection window 'P' of size 3x3 is denoted as

$$P= [X_{i-1,j+1}, X_{i,j+1}, X_{i+1,j+1}, X_{i-1,j}$$
$$X_{i,j}, X_{i+1,j}, X_{i-1,j-1}, X_{i,j-1} X_{i+1,j-1}]$$

In the first stage the noise corrupted pixels are detected using the absolute deviation between the mean value and the centre pixel value and by comparing with threshold value. In the second stage, the detected noise pixels are replaced with the mean value of the pixels lying in the direction of the minimum difference.

A. Noise detection

Step 1:   A 3x3 sliding window (p) was chosen from the noise corrupted   image, and it runs from the top most left corner to the bottom most right corner, covering the entire size of the image. The centre pixel of the 3x3 window was treated as the test pixel.

Step 2: Usually the pixels located in the neighbourhood of a test pixel are correlated to each other and they process almost similar characteristics if the test pixel under consideration is noise free. The normalizedabsolute difference between the centre pixel value and its corresponding neighbours in the chosen 3X3 window is calculated.

$$ND = abs(p-p(i,j))/255$$

Step 3: The exponential nonlinear function is applied inorder to transform the pixel values within the filter window in a progressive manner. This operation widens the gap between noisy pixel and the other Pixels within the window.

$$NLF = exp(k*ND)-1$$

The values of k are varied in steps of 10 in each iteration. The
initial value of k is assigned to 10.

Step 4: The summatiom of least 'm' values from NLF are calculated .
$$Sum = \sum_{i=1}^{m} NLF(i)$$
Where m = 6 for the 3x3 window and 12 for 5x5 window under consideration.

Step 5: The threshold value 'T' is choosen adaptively for each window under consideration.
$$T = MAD(P);$$
Where MAD is the median of absolute deviation from the median of the window under consideration.

Step 6: The pixel under consideration is treated as noisy pixel if the absolute deviation is greater than the threshold value otherwise the   pixel is treated as noise free.

Step 7: Steps 3 to 6 are repeated until entire pixels in the noisy image 'X' are covered. The number of iterations varies from 2 to 6 depending on the noise density.

Step 8: Binary noise mask 'N' is created on the basis of step 6.
$$N(i,j) = \begin{cases} 1, & \text{if } d < T \\ 0, & \text{otherwise} \end{cases} \quad (5)$$

Step 9: Noise free pixels are sited directly to output image and Noisy pixels are subjected to filtering process.

B. Filtering stage:

In this stage the "noise pixels" marked with N(i,j) = 0 is replaced by an estimated correction term.

Step 1: Consider a 3x3 window, starting from the top-most left corner of the impulse noise corrupted image X.

Step 2: The absolute differences between the current pixel and its neighbors in the four main directions (i.e.) horizontal, vertical and direction along two diagonals are calculated.

$$Dk(i, j) = |X(i+u, j+v) − X(i−u, j−v)| \quad (6)$$

where, $(k, u, v) = \{(1, 1, 1), (2, 0, 1), (3,−1, 1), (4,−1, 0)\}$

Step 3: The direction along which the pixels giving the minimum difference value is calculated (i.e.) Min $\{ D_1, D_2, D_3, D_4 \}$.

Step 4: The median value of the pixels in the step 3 was calculated.

Step 5: Finally, the correction term to restore a detected "noise pixel" was obtained from the step 4 is replaced with the noise pixel value. The above steps 1 to 5 are repeated for all the pixels in the image.

IV. Illustration

To illustrate the proposed algorithm a 3x3 image segment from a lena image corrupted by 55% of random valued impulse noise is taken.

Original segment   Noisy segment

$$I = \begin{bmatrix} 151 & 156 & 157 \\ 156 & 156 & 157 \\ 151 & 156 & 157 \end{bmatrix} X = \begin{bmatrix} 82 & 156 & 186 \\ 156 & 218 & 157 \\ 31 & 58 & 157 \end{bmatrix}$$

A. Detection Stage

The normalized absolute difference between centre pixel value and its corresponding neighbours in X is given as:

$$ND = \begin{bmatrix} 0.533 & 0.243 & 0.1255 \\ 0.243 & 0 & 0.2392 \\ 0.7333 & 0.6275 & 0.2392 \end{bmatrix}$$

Calculation of the exponential nonlinear function is gives the values as

$$NLF = sort (Exp(10*ND)-1)$$

$$NLF = [0\ 2.5\ 9.9\ 9.9\ 10.4\ 10.4\ 206.1\ 206.1\ 528.9\ 529.5]$$

Summation of least six values of NLF are

Sum = 0+2.5+9.9+9.9+10.4+10.4 = 43.1

Calculation of Threshold value

Median(X) = 156.

Median (abs(X-Xmedian) = median(0 0 1 1 30 62 74 98 125)=30.

Since sum $> t$, the centre pixel in the noisy segment is treated as Noise candidate. Hence the corresponding element in the binary noise segment is N(i,j) = 0.

Binary Noise segment $N = \begin{bmatrix} 0 & 1 & 0 \\ 1 & 0 & 1 \\ 0 & 0 & 1 \end{bmatrix}$

B. Filtering Stage

By using the binary segment N , only the noise candidates are filtered.

calculation of mean of the pixels lying in the direction of minimum difference.

$$|82 − 157| = 75$$
$$|156 − 58| = 98$$
$$|186 − 31| = 155$$
$$|156 − 157| = 1 \ \rightarrow minimum$$

So mean of 156,157 is 156.5

The centre pixel in the noisy segment is replaced with the resultant value. The resultant segment is

$$R = \begin{bmatrix} 82 & 156 & 186 \\ 156 & 156.5 & 157 \\ 31 & 58 & 157 \end{bmatrix}$$

V. Results And Discussion

In this section, the feasibility of the proposed algorithm is compared to the other filters based on the quantitative measures. The PSNR (dB) evaluation scheme is used to access the strength of the filtered image, taken into consideration so as to measure the computational efficiency of the filter which was being implemented. In order to validate the proposed algorithm, Lena 512 ×512, Barbara 512x512, bridge 512x512 , 8- bit images are used in the analysis of the proposed algorithm.
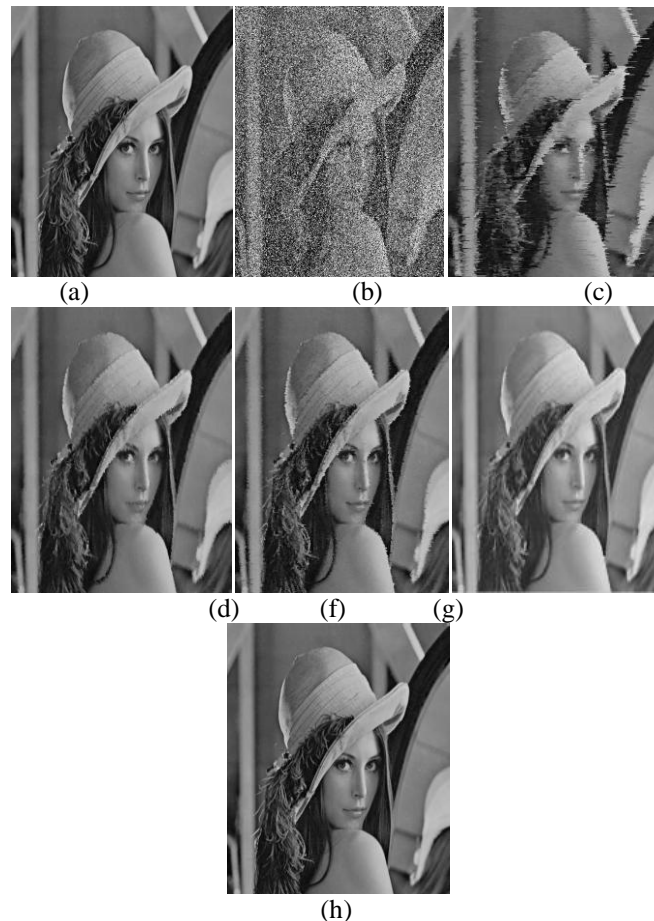
Figure 1: (a) original image (b) corrupted image (RVIN 50%) Restored image using (c) median filter (d) DWF (e) CWMF (f) CEF (g) proposed algorithm.
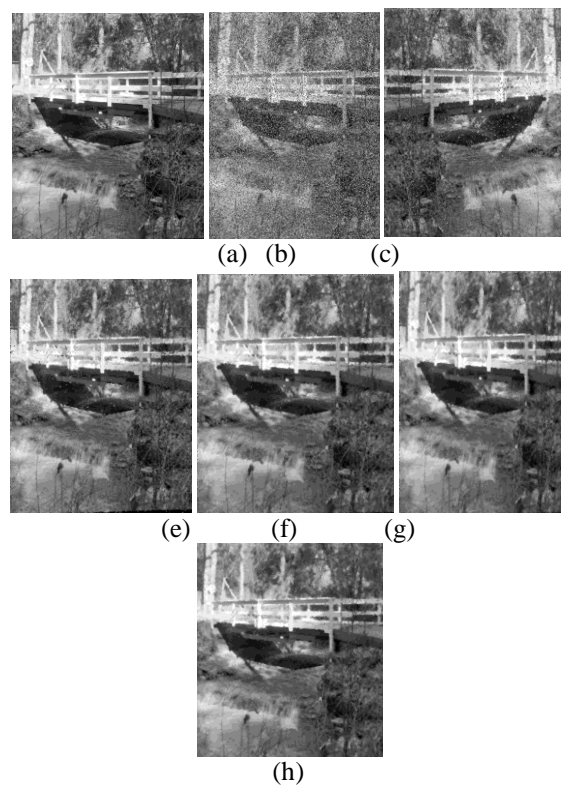
Figure 2: (a) original image (b) corrupted image (RVIN 40%) Restored image using (c) median filter (d) DWF(e) CWMF (f) CEF (g) proposed algorithm.

(a)   (b)   (c)   (d)

(e)   (f)   (g)

(h)
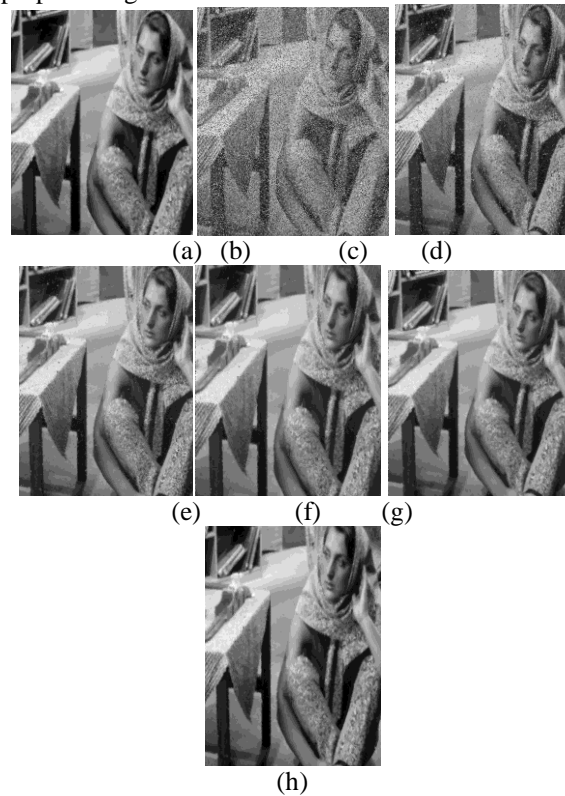
Figure 3: (a) original image (b) corrupted image (RVIN 40%) Restored image using (c) median filter (d) DWF (e) CWMF (f) CEF(g) proposed algorithm.

TABLE 1
COMPARATIVE PSNR VALUES OF VARIOUS NOISE FILTERS ON NOISY LENA IMAGE.

Noise density	Median	DWF	CWMF	CEF	PA
10	36.6	38.2	38.01	40.2	43.09
20	32.5	37.15	34.98	37.6	38.02
30	27.7	34.87	33.1	35.3	36.64
40	23.5	32.62	31.4	33.5	34.12
50	20	30.26	28.2	30.5	32.48
60	17.4	26.74	24.01	27.5	30.64

Restoration results are quantitatively measured by peak signal-to noise ratio (PSNR), Table 1 shows the comparison of PSNR values of proposed technique with existing techniques for 512x512 Lena image. It can be seen that our proposed filter provides the best results in PSNR. In particular, when the noise ratio is larger than 30%, the proposed algorithm produces PSNR values that are one decibel higher than the closest competing filters. By experimental results, the performance of the proposed algorithm is better than the competing filters in terms of the peak signal to noise ratio. It also removes most of the noise while preserving the edge details very well, and even thin lines.The algorithm has been implemented on the MATLAB platform, version 7.5 in core2duo processor with 2 GB RAM.

VI. Conclusion

The proposed algorithm deals with the removal of random valued impulsive Noise. Impulsive   noise being contaminated in some pixels based on probability densities. The detector utilises a threshold value to compare with a predefined parameter. Fixed threshold is not suitable and do not work well under different noise conditions as well as for different images. In this algorithm, adaptive threshold determination strategy based on given noisy image statistics was proposed. Various statistical parameters i.e. (μ, σ^2) are also used to predict the threshold value. The proposed filter is an impulsive noise removal scheme using the directional pixel wise difference method, replacing the corrupted pixel with the median value of pixels lying in the direction of minimum directional difference. The restored image, by this scheme exhibits the desirable properties of edge and detail preservation.

Extensive simulations and comparisons are done with competent schemes. It is observed, in general, that the proposed schemes are better in terms of peak signal to noise ratio suppressing impulsive noise at different noise densities than their counterparts.

REFERENCES

[1]   Umesh Ghanekar, Awadhesh Kumar Singh, and Rajoo Pandey" A Contrast Enhancement-Based Filter for Removal of Random Valued Impulse Noise"IEEE Signal Processing Lett, Vol. 17, No. 1,pp. 47 -51January 2010.
[2]   Y. Dong and S. Xu, "A new directional weighted median filter for removalof random-valued impulse noise," IEEE Signal Process. Lett.,   vol. 14, no. 3, pp. 193–196, Mar. 2007.
[3]   X. Zhang and Y. Xiong, "Impulse noise removal using directional difference based noise detector and adaptive weighted mean filter," IEEE Signal Process. Lett., Vol. 16, no. 4, pp. 295–298, Apr. 2009.
[4]   R C Gonzalez and R E Woods, Digital Image Processing. Prentice-Hall, India, second edition edition, 2007.
[5]   G. Pok, J. Liu, and A. S. Nair, "Selective removal of impulse noise based on homogeneity level information," IEEE Trans. Image Processing, Vol. 12, pp. 85 -92, Jan. 2003.
[6]   Crnojevi.C.V, Senk.V and Trpovski.Z "Advanced impulse detection based on pixel-wise MAD", IEEE Signal Processing Letters, Vol. 11,No. 6, pp. 589–592.Mar. 2004.
[7]   Chui.C, Garnett.R, Huegerich.T, and He.W."A universal noise removal algorithm with an impulse detector", IEEE Trans on Image Processing, Vol. 14,No. 5, pp. 1747–1754. June. 2005.
[8]   Ko .S.J. and Lee S.J., "Adaptive centre weighted median filters and   their applications to image enhancement", IEEE Transactions on Circuits and Systems, Vol. 15, No. 6, pp. 984–993. Nov. 1991.
[9]   Bovik A. C., Ed (2000), "Nonlinear filtering for image analysis and   enhancement", Handbook of Image & Video Processing. San Diego,CA: Academic, ch. 3.2 (G. R. Arce), pp. 95–95. Oct.2000.
[10]   M. K. Ng, R. H. Chan, and W.-C. Tang, A fast algorithm for deblurringmodelswith Neumann boundary conditions, SIAM J. Sci. Comput. 21 , 851–866 (1999).
[11]   Eduardo Abreu, Michael Lightstone, Sanjit K. Mitra, and Kaoru Arakawa, "A New Efficient Approach for Removal of Impulse Noise from Highly Corrupted Images", IEEE Transactions on image processing, vol. 5, no. 6, June 1996.
[12]   T. Chen, K.-K.Ma, and L.-H. Chen, "Tri-state median filter for image denoising," IEEE Trans. Image Process., vol. 8, no. 12, pp. 1834–1838, Dec. 1999.
[13]   A. S.Awad and H. Man, "High performance detection filter for impulse noise removal in images," Electron. Lett., vol. 44, no. 3, pp. 192–194, Jan. 2008.
[14]   W. Luo, "An efficient algorithm for the removal of impulse noise from corrupted images," Int. J. Electron. Commun.(AEU), vol. 61, no. 8, pp. 551–555, Sep. 2007.

A Novel Approach for User Search Results Using Feedback Sessions

Miss. T.Yogeshwari[1], Mr. S. Balamurugan[2]

[1, 2]*(PG Student, Assistant Professor, Sri Manakula Vinayagar Engineering College, Pondicherry-605106)*

Abstract: *In present scenario user search results using Fuzzy c-means algorithm focuses queries are submitted to search engines to represent the information needs of users. The proposed feedbacks sessions are clustered by data are bound to each cluster by means of a membership function. Feedback sessions are constructed from user click-through logs and can efficiently reflect the information needs of users. Pseudo-documents are generated to better understand the clustered feedbacks. Fuzzy C-means clustering algorithm is used to cluster the feedbacks. Clustering the feedbacks can effectively reflect the user needs. Fuzzy c-means algorithm uses the reciprocal of distances to decide the cluster centers. Ranking model is used to provide ranks to the URL based on the user search feedbacks. Evaluate the performance using "Classified Average Precision (CAP)" for user search results.*

Keywords: *Fuzzy c means algorithm, member function, feedback sessions, pseudo documents, classified average precision.*

I. Introduction

It is a novel approach for user search result with their feedback session. First, we have to cluster the feedback session by using Fuzzy c-means algorithm. Second, a novel optimization method to map feedback sessions to pseudo-documents which can efficiently reflect user information needs. Third, evaluate the CAP of restructured web search results.Generally, data mining (sometimes called data or knowledge discovery) is the process of analyzing data from different perspectives and summarizing it into useful information - information that can be used to increase revenue, cuts costs, or both. Data mining software is one of a number of analytical tools for analyzing data. It allows users to analyze data from many different dimensions or angles, categorize it, and summarize the relationships identified. Technically, data mining is the process of finding correlations or patterns among dozens of fields in large relational databases.

Data mining is the process of choosing, discovering, and exhibiting huge volumes of data to determine unknown patterns or associations useful to the data analyst. The objectives of data mining can be classified into two tasks: description and prediction. While the purpose of description is to mine understandable forms and relations from data, the goal of prediction is to forecast one or more variables of interest.

Clustering is the most important concept used here. Clustering analyzes data objects without consulting a known class label. The objects are grouped or clustered based on the principle of maximizing the intra class similarity and minimizing the inter class similarity. Apriori algorithm is a methodology of association rule of data mining, is used to findout the frequently used URL.

II. Feedback Session

The proposed feedback session consists of both clicked and unclicked URLs and ends with the last URL that was clicked in a single session. It is motivated that before the last click, all the URLs have been scanned and evaluated by users. The clicked URLs tell what users require and the unclicked URLs reflect what users do not care about. It is more efficient to analyze the feedback sessions than to analyze the search results or clicked URLs directly.

First, we are extracting the titles and snippets of the returned URLs appearing in the feedback session. Each URL in a feedback session is represented by a small text paragraph that consists of its title and snippet.Each URL's title and snippet are represented by a Term Frequency-Inverse Document Frequency (TF-IDF) vector, respectively, as in

$$T_{ui}=[t_{w1};t_{w2};...;t_{wn}]^{T};$$
$$S_{ui}=[s_{w1};s_{w2};...;s_{wn}]^{T};$$

whereT_{ui}andS_{ui} are the TF-IDF vectors of the URL's title and snippet, respectively. ui means the$i$th URL in the feedback session. And w_j(j=1;2;...;n) is the jth term appearing in the enriched URLs.t_{wj} and s_{wj} represent the TF-IDF value of the jth term in the URL's title and snippet, respectively.

The distributions of different user search goals can be obtained conveniently after feedback sessions are clustered. A novel optimization method isused to combine the enriched URLs in a feedback session to form a pseudo-document, which can effectively reflect the information need of a user. We infer the user goals by clustering, feedback sessions are proposed. Clustering the feedbacks can effectively reflect the user needs.

III. Forming Pseudo Document

We propose an optimization method to combineboth clicked and unclicked URLs in the feedback session. Let F_{fs} be the feature representation of a feedback session and f_{fs} (w) is the value for the term w. Let F_{ucm}(m=1;2,...;M) and F_{ucl}(l=1;2, ...;L) be the feature representations of the clicked and unclicked URLs in this feedbacksession, respectively. Let f_{ucm} (w) andf_{ucl}(w)be the values for the term win the vectors. We want to obtain such a F_{fs} that the sum of the distances between F_{fs} and each F_{ucm} is minimized and the sum of the distances betweenF_{fs} and each F_{ucl} is maximized.

$$F_{fs}= \left[f_{fs}(w1); f_{fs}(w2); ... f_{fs}(wn)^{T}; \right]$$

$$F_{fs}(w)=\arg\min{}_{ffs(w)} \sum \left[f_{fs}(w) - \left[f_{ucm}(w)\ ^{2} - \lambda^{2} \right] \right.$$

$$\sum f_{fs} \left[(w) - f_{ucl}(w)\ ^{2} \right] ; \left] f_{fs}(w) \in Ic \right.$$

Let I_c be the interval $\left[\mu\ f_{uc}(w) - \sigma\ f_{uc}(w),\ \mu\ f_{uc}(w) + \sigma\ f_{uc}(w) \right]$ and I_{ucl} be the interval $\left[\mu\ f_{ucl}(w) - \sigma\ f_{ucl}(w),\ \mu\ f_{ucl}(w) + \sigma\ f_{ucl}(w) \right]$,where $\mu\ f_{uc}(w)$ and $\sigma\ f_{uc}(w)$ represent the mean and mean square error of f_{uc} (w)respectively, and $\mu\ f_{ucl}(w)$and $\sigma\ f_{ucl}(w)$ represent the mean and mean square error of $f_{ucl}(w)$,respectively.Even if people skip some unclicked URLs because of duplication. Each dimension of F_{fs} indicates the importance of a term in this feedback session. F_{fs} is the pseudo-document that we want to introduce. It reflects what users desire and what they do not care about. It can be used to approximate the goal texts in user mind.
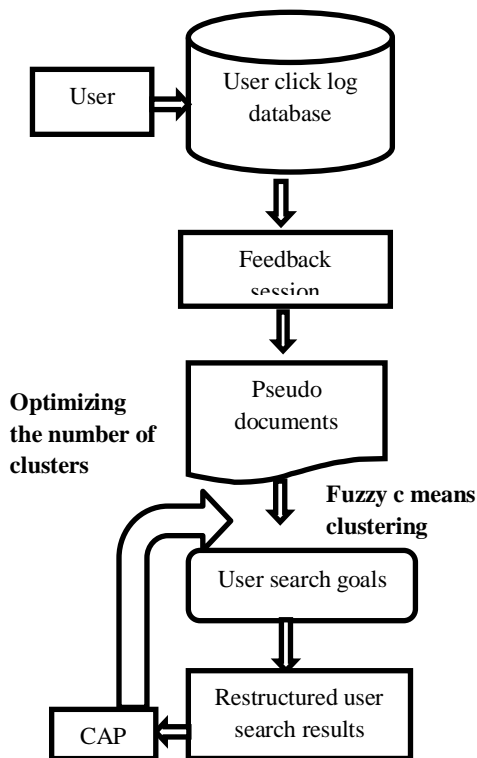
IV. Fuzzy C Means Algorithm

In Fuzzy clustering (also referred to as soft clustering), data elements can belong to more than one cluster, and associated with each element is a set of membership levels. These indicate the strength of the association between that data element and a particular cluster. Fuzzy clustering is a process of assigning these membership levels, and then using them to assign data elements to one or more clusters.In many situations, fuzzy clustering is more natural than hard clustering. Objects on the boundaries between several classes are not forced to fully belong to one of the classes, but rather are assigned membership degrees between 0 and 1 indicating their partial membership

The Fuzzy C-Means algorithm (FCM) is used in the areas like computational geometry, data compression and vector quantization, pattern recognition and pattern classification. Fuzzy C-Mean (FCM) is an unsupervised clustering algorithm that has been applied to wide range of problems involving feature analysis, clustering and classifier design.

The main features of that algorithm were the (i) use of a fuzzy local similarity measure, (ii) shielding of the algorithm from noise-related hypersensitivities.FCM clustering techniques are based on fuzzy behavior and they provide a technique which is natural for producing a clustering where membership weights have a natural interpretation but not probabilistic at all.In fuzzy clustering, every point has a degree of belonging to clusters, as in fuzzy logic, rather than belonging completely too just one cluster. Thus, points on the edge of a cluster may be in the cluster to a lesser degree than points in the center of cluster.

FCM clustering which constitute theoldest component of software computing, are really suitable for handling the issues related to understand ability of patterns, incomplete/noisy data, mixed media information, human interaction and it can provide approximate solutions faster.

FCM has a wide domain of applications such as agricultural engineering, astronomy, chemistry, geology, image analysis, medical diagnosis, shape analysis, andtarget recognition.More the data is near to the cluster center more is its membership towards the particular cluster center. The basic idea of fuzzy c-means is to find a fuzzy pseudo-partition to minimize the cost function.Fuzzy c-means has been a very important tool for image processing in clustering objects in an image. In the 70's, mathematicians introduced the spatial term into the FCM algorithm to improve the accuracy of clustering under noise.Fuzzy c-means algorithm uses the reciprocal of distances to decide the cluster centers.

This algorithm works by assigning membership to each data point corresponding to each cluster center on the basis of distance between the cluster center and the data point. More the data is near to the cluster center more is its membership towards the particular cluster center. Clearly, summation of membership of each data point should be equal to one. After each iteration membership and cluster centers are updated according to the formula. The FCM algorithm converges to a local minimum of the c-means functional. Hence, different initializations may lead to different results.The minimization of the c-means functional represents a nonlinear optimization problem that can be solved by using a variety of methods, including iterative minimization, simulated annealing or genetic algorithms.

The Algorithm Fuzzy C-Means (FCM) is a method of clustering which allows one piece of data to belong to two or more clusters. This method is frequently used in pattern recognition. It is based on minimization of the following objective function:

$$J_m = \sum_{i=1}^{N} \sum_{j=1}^{C} u_{ij}^m \left\| x_i - c_j \right\|^2 \quad , \quad 1 \leq m < \infty$$

where m is any real number greater than 1, u_{ij} is the degree of membership of x_i in the cluster j, x_i is the ith of d-dimensional measured data, c_j is the d-dimension center of the cluster, and $\|*\|$ is any norm expressing the similarity between any measured data and the center.

Time complexity of FCM is **O (ndc²i).**

V. Clustering Pseudo-Documents Using Fuzzy C Means Algorithm

Each feedback session is represented bypseudo-document and the feature representation of the pseudo-document is F_{fs}. We cluster pseudo-documents by Fuzzy c-means clustering which is simple and effective Fuzzy partitioning is carried out through an iterative optimization of the objective function shown above, with the update of membership u_{ij} and the cluster centers c_j by

$$u_{ij} = \frac{1}{\sum_{k=1}^{c} \left[\frac{d_{ij}}{d_{ik}} \right]^{\frac{2}{m-1}}}$$

$$v_j = \frac{\sum\limits_{i-1}^{N} u_{ij}{}^m \cdot x_i}{\sum\limits_{i-1}^{N} u_{ij}{}^m},$$

$\vee$j=1, 2 ….c. This iteration will stop when

$$\max_{ij}\left[\left|\left| u_{ij}{}^{(k+1)} - u_{ij}{}^{(k)} \right| < \varepsilon_\nu \right|\right]$$

whereis a termination criterion between 0 and 1, whereas *k* is the iteration steps. This procedure converges to a local minimum or a saddle point of J_m.

FCM clustering is an iterative process. The process stops when the maximum number of iterations is reached, or when

the objective function improvement between two consecutive iterations is less than the minimum amount of improvement specified.

5.1 STEPS

1) Randomly select *'c'* cluster centers.
2) calculate the fuzzy membership *'μ$_{ij}$'* using:

$$u_{ij} = \frac{1}{\sum\limits_{k-1}^{c}\left[\dfrac{d_{ij}}{d_{ik}}\right]^{\frac{2}{m-1}}}$$

3) compute the fuzzy centers *'v$_j$'* using:

$$v_j = \frac{\sum\limits_{i-1}^{N} u_{ij}{}^m \cdot x_i}{\sum\limits_{i-1}^{N} u_{ij}{}^m}$$

$\forall$j=1,2 ….c.

4) Repeat step 2) and 3) until the minimum 'J' value is achieved or *$||U^{(k+1)} - U^{(k)}|| < \beta$*.

Where,
  k' is the iteration step.
  β' is the termination criterion between [0, 1].
  'U = (μ$_{ij}$)$_{n*c}$' is the fuzzy membership matrix.
  'J' is the objective function.
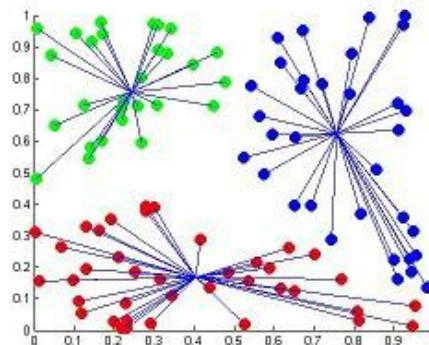
FCM is also called as Fuzzy ISODATA. FCM employs fuzzy partitioning such that a data point can belong to all groups which different membership grades between 0 and 1.

5.2 Parameters of the FCM algorithm
Before using the FCM algorithm, the following parameters must be specified:
- the number of clusters, *c*,
- the fuzziness exponent, *m*,
- The termination tolerance, *ε*.
- norm-inducing matrix, A

Norm inducing matrixes are 3 types. They are
- Euclidean norm
- diagonal norm
- Mahalanobis norm

After clustering all the pseudo-documents, each cluster can be considered as one user search goal.

VI. Evaluating Cap (Classified Average Precision)

CAP (classified Average Precision) is used toevaluate the performance of user search goal inference based on restructuring web search results. A possible evaluation criterion is the average precision (AP) which evaluates according to user implicit feedbacks. AP is the average of precisions computed at the point of each relevant document in the ranked sequence,

$$AP = 1 / N^+ \sum_{r=1}^{N} rel(r) R_r / r \ ,$$

Where N^+ is the number of relevant (or clicked) documents in the retrieved ones, r is the rank, N is the total number of retrieved documents, rel() is a binary function on the relevance of a given rank, and R_r is the number of relevant retrieved documents of rank r or less. "Voted AP (VAP)"
which is the AP of the class including more clicks namely votes. There should be a riskto avoid classifying search results into too many classes by error. We propose the risk as follows

$$Risk = \frac{\sum_{i,j=1(i<j)}^{m} d_{ij}}{C^2_m}$$

It calculates the normalized number of clicked URL pairs that are not in the same class, where m is the number of the clicked URLs. If the pair of the ith clicked URL and the jth clicked URL are not categorized into one class, d_{ij} will be 1; otherwise, it will be 0. $C^2_m = m(m-1) / 2$ is the total number of the clicked URL pairs.

We can further extend VAP by introducing the above Risk and propose a new criterion "Classified AP," as shown below

CAP = VAP × (1-Risk)$^\gamma$is used to adjust the influence of Risk on CAP, which can be learned from training data.

VII. Conclusion

In this paper, a novel approach has been proposed to user search results for a query by clustering its feedback sessions represented by pseudo-documents. Clustering feedback sessions are more efficient than clustering search results or clicked URL's directly. A new criterion called classified average Precision is used to evaluate the performance of restructured web search results. In this paper , we used Fuzzy c means clustering which constitute the oldest component of software computing, are really suitable for handling the issues related to understand ability of patterns, incomplete/noisy data, mixed media information, human interaction and it can provide approximate solutions faster. The execution time of FCM clustering algorithm for arbitrary data points depends only on the number of clusters and not on the data points. The distance between data points and some shape of the distribution, has the effect on the performance and behavior of the algorithm. Gives best result for overlapped data set and comparatively better then k-means algorithm.

REFRENCES

[1] Gayathri A, Nandhakumar C, Gokulavani M, Santhamani V," Inferring User Goals Using Customer Feedback and Analyzing Customer Behavior", International Journal of Computer Applications Technology and Research Volume 3– Issue 2, 125 - 129, 2014.
[2] T. Velmurugan, T.Santhanam," Implementation of Fuzzy C-Means Clustering Algorithm for Arbitrary Data Points", International Conference OnSystemics, Cybernetics And Informatics

[3]   ZhengLu,HongyuanZha, XiaokangYang,Weiyao Lin, and ZhaohuiZheng," A New Algorithm for Inferring User Search Goals with Feedback Sessions",IEEE TRANSACTIONS ON KNOWLEDGE AND DATA ENGINEERING, VOL. 25, NO. 3 MARCH 2013.

[4]   SoumiGhosh , Sanjay Kumar Dubey , "Comparative Analysis of K-Means and Fuzzy C Means Algorithms", ((IJACSA) International Journal of Advanced Computer Science and Applications, Vol. 4, No.4, 2013.

[5]   "A New Algorithm for Clustering Search Results" GIANSALVATOREMECCA, SALVATORERAUNICH, ALESSANDROP APPALARDO Dipartimento di Matematica e InformaticaUniversitàdella Basilicata Potenza – Italy.

[6]   T. Joachims, "Evaluating Retrieval Performance Using Clickthrough Data," Text Mining, J. Franke, G. Nakhaeizadeh, and I. Renz, eds., pp. 79-96, Physica/Springer Verlag, 2003..

[7]   J.-R Wen, J.-Y Nie, and H.-J Zhang, "Clustering User Queries of a Search Engine," Proc. Tenth Int'l Conf. World Wide Web (WWW '01), pp. 162-168, 2001.

[8]   D.Kavitha, K.M.Subramanian, Dr.K.Venkatachalam,"SURVEY ON INFERRING USER SEARCH GOAL USING FEEDBACK SESSION", International Journal of Advanced Research in Computer Engineering & Technology (IJARCET)Volume 2, Issue 12, December 2013.

[9]   D. Shen, J. Sun, Q. Yang, and Z. Chen, "Building bridges for web query classification," in Proceedings of the 29th annual international ACM SIGIR conference on Research and development in information retrieval. ACM, 2006, pp. 131–138.

[10]   Charudatt Mane, PallaviKulkarni," A Novel Approach to Discover User Search Goals Using Clickthrough Data", Charudatt Mane et al, / (IJCSIT) International Journal of Computer Science and Information Technologies, Vol. 5 (1) , 2014, 20-24.

[11]   X. Wang and C.-X Zhai, "Learn from Web Search Logs toOrganize Search Results," Proc. 30th Ann. Int'l ACM SIGIR Conf. Research and Development in Information Retrieval (SIGIR '07), pp. 87-94, 2007.

International Journal of Modern Engineering Research (IJMER)

Contents :

The Queue M/M/1 with Additional Servers for a Longer Queue

G. S. Mokaddis[1], S. A. Metwally[2], B. E. Farahat[3]

[1, 2, 3,] *(Ain Shams University, Department Of Mathematics, Faculty of Science, Cairo, Egypt)*

Abstract: *This paper deals with the queuing system M/M/1 with additional servers for a longer queue. Clearly the traffic intensity for this system will depend on the number of additional servers. The expected number of customers in the system, the probability of the additional of one server and the probability of the additional of two servers are obtained under the assumption that the number of additional servers depends on the number of customers in the system. The condition under which the M/M/1 queuing system with additional servers is profitable is discussed. A MATLAB program is used to illustrate this condition numerically. Finally, the maximum likelihood estimators of the parameters for this queuing system are obtained.*

Keywords: *Queuing system, traffic intensity, additional servers, customers, maximum likelihood estimate, queuing length.*

I.   Introduction

In many queuing situations, normally the number of servers is dependent on the queue length. For instance, in a bank more and more windows are opened for service when the queues in front of the already open windows get too long. This procedure is sometimes used even in the case of airlines, buses, etc. The basic advantage in such a system is the inherent flexibility of service. Here we shall consider a simplified system of this type.

Suppose we deal with a queuing system in which the arrivals are individually in a Poisson process with parameter λ, and service times of customers are negative exponential with mean μ^{-1}. The first customer to come is the first to be served. As long as there are enough customers for service. As long as the number of customers in the system is greater than or equal to zero and less than or equal to N, there is only one server in the system. As the number of customers in the system increases to more than N and is still less than or equal to 2N, an additional server is added. This additional server is removed when the number of customers in the system decreases to N or less. As soon as the number of customers in the system goes beyond 2N, the number of servers will be three. Similarly, the third server will be taken off when the number of customers falls to 2N or below. Let λ_n and μ_n be the arrival and service rates, respectively, when there are n customers in the system and so, for the described queuing model, we have

$$\lambda_n = \lambda \qquad \text{for every } n \geq 0 ,$$

$$\mu_n = \begin{cases} \mu ; & \text{if } 0 < n \leq N , \\ 2\mu; & \text{if } N < n \leq 2N, \\ 3\mu; & \text{if } 2N < n , \end{cases}$$

where, λ, μ and $\rho = \lambda/\mu$ be the arrival rate, service rate and traffic intensity respectively.

II.   System Equations

Assuming the limiting distribution of the number of customers in the system to be $\{P_n\}$. We obtain the following steady-state equations.

$$\lambda P_0 = \mu P_1 ,$$

$$(\lambda + \mu)P_n = \lambda P(n-1) + \mu P(n+1) , \qquad 1 \leq n < N ,$$

$$(\lambda + \mu)P_N = \lambda P(N-1) + 2\mu P(N+1) ,$$

$$(\lambda + 2\mu)P_n = \lambda P(n-1) + 2\mu P(n+1) , \qquad N < n < 2N ,$$

$$(\lambda + 2\mu)P_{2N} = \lambda P(2N-1) + 3\mu P(2N+1) ,$$

$$(\lambda + 3\mu)P_n = \lambda P(n-1) + 3\mu P(n+1) , \qquad n > 2N .$$

Solution of the System Equations

This system of equations can be solved recursively, or by using the general solution for single Markovian queuing models which is given as follows

For $0<n\leq N$;

$$P_n = \Pi_i(i=0)^{\dagger}(n-1) \; [((\lambda_i/\mu_i(i+1))P_i 0 \;]$$

$$= (\lambda/\mu)^n \, P_0 \qquad : \text{ (writing } \lambda/\mu = \rho \text{)}$$

$$= \rho^n P_0 \; . \tag{2.1}$$

For $N<n\leq 2N$;

$$P_n = \Pi_i(i=0)^{\dagger}(n-1) \; [((\lambda_i/\mu_i(i+1))P_i 0 \;]$$

$$= [\; \Pi_i(i=0)^{\dagger}(N-1) \; [((\lambda_i/\mu_i(i+1)) \;] \quad \Pi_i(i=N)^{\dagger}(n-1) \; [((\lambda_i/\mu_i(i+1)) \;] \quad]P_0$$

$$= (\lambda/\mu)^N . (\lambda/2\mu)^{n-N} \, P_0$$

$$= \frac{1}{2^{n-N}} \, \rho^n P_0 \; . \tag{2.2}$$

For $2N<n$;

$$P_n = \Pi_i(i=0)^{\dagger}(n-1) \; [((\lambda_i/\mu_i(i+1))P_i 0 \;]$$

$$=$$

$$[\Pi_i(i=0)^{\dagger}(N-1) \; [((\lambda_i/\mu_i(i+1)) \;] \quad \Pi_i(i=N)^{\dagger}(2N-1) \; [((\lambda_i/\mu_i(i+1)) \;] \quad \Pi_i(i=2N)^{\dagger}(n-1) \; [((\lambda_i/\mu_i(i+1)) \;] \;]P_0$$

$$= (\lambda/\mu)^N . (\lambda/2\mu)^N . (\lambda/3\mu)^{n-2N} \, P_0$$

$$= \frac{1}{2^N 3^{n-2N}} \, \rho^n P_0 \; . \tag{2.3}$$

Now, to determine P_0 we can use the normalizing condition $\sum_{n=0}^{\infty} P_n = 1$ and equations (2.1),(2.2) and (2.3) as follows

$$1 = \sum_{n=0}^{N} \rho^n P_0 \quad + \sum_{n=N+1}^{2N} \frac{1}{2^{n-N}} \rho^n P_0 \quad + \sum_{n=2N+1}^{\infty} \frac{1}{2^N 3^{n-2N}} \rho^n P_0 \qquad P_0^{-1} = \sum_{n=0}^{N} \rho^n \quad + \sum_{n=N+1}^{2N} \frac{1}{2^{n-N}} \rho^n \quad +$$

$$\sum_{n=2N+1}^{\infty} \frac{1}{2^N 3^{n-2N}} \rho^n$$

$$= \sum_{n=0}^{N} \rho^n \quad + \frac{\rho^{N+1}}{2} \sum_{n=0}^{N-1} \left(\frac{\rho}{2}\right)^n \quad + \frac{\rho^{2N+1}}{3(2^N)} \sum_{n=0}^{\infty} \left(\frac{\rho}{3}\right)^n$$

$$= \frac{1-\rho^{N+1}}{1-\rho} \; + \; \frac{\rho^{N+1}\left(1-\left(\frac{\rho}{2}\right)^N\right)}{2-\rho} \; + \frac{\rho^{2N+1}}{2^N(3-\rho)}$$

$$= \frac{1}{1-\rho} - \frac{\rho^{N+1}}{(1-\rho)(2-\rho)} - \frac{\rho^{2N+1}}{2^N(2-\rho)(3-\rho)} \quad ,$$

$$P_0^{-1} = \frac{2-\rho-\rho^{N+1}}{(1-\rho)(2-\rho)} - \frac{\rho^{2N+1}}{2^N(2-\rho)(3-\rho)} \; . \tag{2.4}$$

III. Profitable of using Additional Servers

Suppose the cost to the system due to the presence of a customer is \$$C_1$ and the cost of bringing in an additional server is \$$C_2$. It is profitable to use the additional server only if its cost is less than that due to the waiting customers see [4].

Let Q be the long-run queue length of the standard queue M/M/1 with the same parameters. It is evident that the M/M/1 queuing system with additional servers is recommended only if

$$C_1[E(Q)-E(Q_1)]>C_2[P_r(N<Q_1\leq 2N)+2P_r(2N<Q_1)], \tag{3.1}$$

where,

$E(Q)$=Expected number of customers in the system for the queuing model M/M/1 with no additional servers (standard).

$E(Q_1)$=Expected number of customers in the system for the queuing model M/M/1 with additional servers. We have

$$E(Q) = \frac{\sum\limits_{n=0}^{\infty} n p_n}{\sum\limits_{n=0}^{\infty} n \rho^n p_0}$$

$$= \frac{\rho}{1-\rho}.$$ (3.2)

Also,

$$E(Q_1) = \sum_{n=0}^{\infty} n p_n = \sum_{n=0}^{N} n \rho^n P_0 \sum_{n=N+1}^{2N} n \frac{1}{2^{n-N}} \rho^n P_0 \sum_{n=2N+1}^{\infty} n \frac{1}{2^N 3^{n-2N}} \rho^n P_0 .$$

(3.3)

Now we have to find

$$\sum_{n=0}^{N} n\rho^n P_0 = P_0 \rho \sum_{n=0}^{N} n \rho^{n-1}$$

$$= P_0 \rho \frac{d}{d\rho} \sum_{n=0}^{N} \rho^n$$

$$= \frac{P_0 \rho}{(1-\rho)^2} [1+N\rho^{N+1} -(N+1)\rho^N].$$

(3.4)

Similarly,

$$\sum_{n=N+1}^{2N} n \frac{1}{2^{n-N}} \rho^n P_0 = 2^N \rho P_0 \frac{d}{d\rho} [\left(\frac{\rho}{2}\right)^{N+1} \frac{1-\left(\frac{\rho}{2}\right)^N}{1-\frac{\rho}{2}}] =$$

$$\frac{\rho^{N+1}}{(2-\rho)^2} P_0 [2(N+1) - 2^{-N+1}(2N+1)\rho^N - N\rho + 2^{-N+1} N\rho^{N+1}].$$ (3.5)

And

$$\sum_{n=2N+1}^{\infty} n \frac{1}{2^N 3^{n-2N}} \rho^n P_0 = \frac{3^{2N+1}}{2^N} \rho P_0 \frac{d}{d\rho} [\left(\frac{\rho}{3}\right)^{2N+1} \frac{1}{3-\rho}] =$$

$$\frac{\rho^{2N+1}}{2^N (3-\rho)^2} P_0 [3(2N+1) - 2N\rho].$$

(3.6) Substituting by (3.4) , (3.5) and (3.6) into (3.3) it follows that

$$E(Q_1) = \rho P_0 \{ \frac{1}{(1-\rho)^2} [1+N\rho^{N+1} -(N+1)\rho^N]$$

$$+ \frac{\rho^N}{(2-\rho)^2} [2(N+1) - 2^{-N+1}(2N+1)\rho^N - N\rho + 2^{-N+1} N\rho^{N+1}]$$

$$+ \frac{\rho^{2N}}{2^N (3-\rho)^2} [3(2N+1) - 2N\rho] \}$$

$$= \rho P_0 [A/(2^N [(1-\rho)]^2 [(2-\rho)]^2 [(3-\rho)]^2)] ,$$

(3.7)
where

$$A = 2^N (2-\rho)^2 (3-\rho)^2 [1+N\rho^{N+1} -(N+1)\rho^N]$$
$$+ 2^N (1-\rho)^2 (3-\rho)^2 \rho^N [2(N+1) - 2^{-N+1}(2N+1)\rho^N - N\rho + 2^{-N+1} N\rho^{N+1}]$$
$$+ (1-\rho)^2 (2-\rho)^2 \rho^{2N} [3(2N+1) - 2N\rho] .$$

Also, we have to find the probability of the additional of one server,

$$P_r(N < Q_1 \leq 2N) = \sum_{n=N+1}^{2N} P_n = \sum_{n=N+1}^{2N} \frac{\rho^n}{2^{n-N}} P_0$$

$$= \frac{P_0\, 2^N \sum_{n=N+1}^{2N} \left(\frac{\rho}{2}\right)^n}{}$$

$$= \frac{P_0\, \rho^{N+1}\, \dfrac{1-\left(\frac{\rho}{2}\right)^N}{(2-\rho)}}{} \, . \tag{3.8}$$

And the probability of the additional of two servers ,

$$P_r(2N < Q_1) = \sum_{n=2N+1}^{\infty} P_n$$

$$= \sum_{n=2N+1}^{\infty} \frac{1}{2^N 3^{n-2N}} \rho^n P_0$$

$$= \frac{3^{2N}}{2^N} P_0 \left(\frac{\rho}{3}\right)^{2N+1} \sum_{n=0}^{\infty} \left(\frac{\rho}{3}\right)^n$$

$$= P_0 \frac{\rho^{2N+1}}{2^N(3-\rho)} \, . \tag{3.9}$$

Substituting by (3.2), (3.7), (3.8) and (3.9) into (3.1) it follows that the modified M/M/1 queuing system is recommended only when

$$\frac{C_2}{C_1} < \frac{E(Q) - E(Q_1)}{P_r(N < Q_1 \le 2N) + 2P_r(2N < Q_1)}$$

$$< \frac{\dfrac{\rho}{1-\rho} - \rho P_0 \left[\dfrac{A}{2^N(1-\rho)^2(2-\rho)^2(3-\rho)^2}\right]}{P_0\rho^{N+1}\dfrac{1-\left(\frac{\rho}{2}\right)^N}{(2-\rho)} + 2P_0\dfrac{\rho^{2N+1}}{2^N(3-\rho)}}$$

$$< \frac{\rho P_0 \left[\dfrac{P_0^{-1}}{1-\rho} - \dfrac{A}{2^N(1-\rho)^2(2-\rho)^2(3-\rho)^2}\right]}{\rho P_0 \left[\rho^N\dfrac{1-\left(\frac{\rho}{2}\right)^N}{(2-\rho)} + 2\dfrac{\rho^{2N}}{2^N(3-\rho)}\right]}$$

$$< \frac{\dfrac{P_0^{-1}}{1-\rho} - \dfrac{A}{2^N(1-\rho)^2(2-\rho)^2(3-\rho)^2}}{(3-\rho)\rho^N(2^N - \rho^N) + 2(2-\rho)\rho^{2N}} \Big/ 2^N(2-\rho)(3-\rho) \, .$$

Substituting by (2.4), we get

$$\frac{C_2}{C_1} < \frac{\left[\dfrac{2-\rho-\rho^{N+1}}{(1-\rho)^2(2-\rho)} - \dfrac{\rho^{2N+1}}{2^N(1-\rho)(2-\rho)(3-\rho)} - \dfrac{A}{2^N(1-\rho)^2(2-\rho)^2(3-\rho)^2}\right]}{2^N(2-\rho)(3-\rho)}$$

$$\overline{[(3-\rho)\rho^N(2^N - \rho^N) + 2(2-\rho)\rho^{2N}]}$$

$$< \frac{\left[\dfrac{2^N(3-\rho)(2-\rho-\rho^{N+1})}{(1-\rho)^2} - \dfrac{\rho^{2N+1}}{(1-\rho)} - \dfrac{A}{(1-\rho)^2(2-\rho)(3-\rho)}\right]}{1}$$

$$\overline{[(3-\rho)\rho^N(2^N - \rho^N) + 2(2-\rho)\rho^{2N}]}$$

$$< \frac{1}{1-\rho} \left[\frac{2^N(2-\rho)(3-\rho)^2(2-\rho-\rho^{N+1}) - (1-\rho)(2-\rho)(3-\rho)\rho^{2N+1} - A}{(1-\rho)(2-\rho)(3-\rho)[(3-\rho)\rho^N(2^N - \rho^N) + 2(2-\rho)\rho^{2N}]}\right].$$

Substituting by A from equation (3.7)

$$\frac{C_2}{C_1} < \frac{1}{1-\rho} \Bigg\{ 2^N(2-\rho)(3-\rho)^2 \left[\frac{(2-\rho-\rho^{N+1}) - (2-\rho)}{(1 + N\rho^{N+1} - (N+1)\rho^N)}\right]$$

$$- (1-\rho)(2-\rho)\, [(3-\rho)\,\rho^\uparrow(2N+1) + (1-\rho)(2-\rho)\rho^\uparrow 2N \quad (3(2N+1) - 2N \vdash \rho)]$$

$$- 2^N (1-\rho)^2(3-\rho)^2 \rho^N \, [2(N+1) - 2^{-N+1}(2N+1)\rho^N - N\rho + 2^{-N+1} N\rho^{N+1}] \Bigg\} \Big/$$

$$(1-\rho)(2-\rho)(3-\rho)[(3-\rho)\rho^N(2^N - \rho^N) + 2(2-\rho)\rho^{2N}] \, .$$

This can be simplified to

$$\frac{C_2}{C_1} < \frac{1}{\dfrac{(1-\rho)[(3-\rho)(2^N-\rho^N)+2(2-\rho)\rho^N]}{2^N(3-\rho)[2(N+1)-(3N+2)\rho+N\rho^2]}}$$

$$\left\{ \frac{}{(1-\rho)} \right.$$

$$- \frac{2^N(1-\rho)(3-\rho)[2(N+1)-2^{-N+1}(2N+1)\rho^N-N\rho+2^{-N+1}N\rho^{N+1}]}{(2-\rho)}$$

$$\left. - \frac{\rho^N[6(2N+1)-2(11N+3)\rho+(12N+5)\rho^2-2N\rho^3]}{(3-\rho)} \right\}. \tag{3.10}$$

From this inequality, depending on the decision variable, the largest value of C_2/C_1 can be determined when ρ and N are given. Table (1) has been obtained from the inequality (3.10) for the purpose of illustration. MATLAB program is used to perform these calculations.

Table (1)

$/N$ ρ	0.1	0.2	0.3	0.4	0.5
1	4.1765	4.6119	5.1762	5.9293	6.9778
2	6.5671	7.4620	8.5872	10.0580	12.0807
3	8.8032	10.0205	11.5852	13.6639	16.5562
4	11.0264	12.5286	14.4718	17.0736	20.7233
5	13.2486	15.0296	17.3346	20.4265	24.7769

From this table, we can conclude that for any given value of N, the largest value of c_2/c_1 decreases with decreasing values of ρ , that is with increasing values of service rates. The basic advantage in such a system is the inherent flexibility of service. Then there exists an optimal stationary policy (resulting in the least long-run expected cost) characterized by a single positive finite number N such that it is optimal to use the slow service rate μ when the number of customers in the system is less than or equal to N, faster service rate 2μ when the number in the system is greater than N or less than or equal to 2N and more fast service rate 3μ when the number in the system is greater than 2N.

III. Maximum Likelihood Estimators of The Parameters

To find the likelihood function it is necessary to find the three basic components see [5].

1. the stationary distribution of number of units in the system with contribution $\lim\limits_{t\to\infty} P_u(t) = P_u$,

2. the interarrival times of length t_i [each of which is exponential for n arrival units with contribution

$$\prod_{(i=1)}^{n} (e^{-(t_i})],$$

3. the service time of durations t_i for k units with contribution $\prod\limits_{(i=1)}^{k} \mu e^{-\mu t_i}$) .

Hence, the likelihood function may be written as.

$$L(\theta) = \prod_{i=1}^{n}(e^{-(t_i} \prod_{i=1}^{k} \mu e^{-\mu t_i} P_u(u) \quad ; \quad \theta = [(,\mu] \ ,$$

$$= \prod_{i=1}^{n}(e^{-(t_i} \prod_{i=1}^{k} \mu e^{-\mu t_i} \frac{1}{2^N 3^{u-2N}} \rho^u P_0 \quad ;$$

(use equation (2.3))

$$= P_{\downarrow}0 \ e^{\dagger}(-"(" \ T) \ e^{\dagger}(-\mu t) \ ({}^{\dagger}(n+u) \ \mu^{\dagger}(k-u) \ k_{\downarrow}1 \ ,$$

where ,

$$T = \sum_{i=1}^{n} t_i \ , \ t = \sum_{i=1}^{k} t_i \ \text{ and } k_1 \text{ is a constant .}$$

Thus

$$ln[L(\theta)] = lnP_{\downarrow}0 - (T - \mu t + (n+u)ln(+(k-u)ln\mu + lnk_{\downarrow}1.$$

By partial differentiation with respect to $($ and μ , respectively, and equating the results by zeros, one can obtain

$$-\left(\mathbb{K}\left[\partial lnL/\partial () \right]_\downarrow(\theta = \theta^\wedge) = {}^{-T+\frac{n+u}{(\hat{\Box})}} \right) = 0 \qquad (4.1)$$

and

$$\mu\left[\frac{\partial lnL}{\partial \mu} \right]_{\theta=\hat{\theta}} = \hat{\mu}\left[\frac{\partial lnP_0}{\partial \mu} - t + \frac{k-u}{\hat{\mu}} \right]_{=0}, \qquad (4.2)$$

where $\hat{\lambda}$ and QUOTE $\hat{\mu}\hat{\mu}$ are the maximum likelihood estimators for the parameters λ and μ, respectively.

To obtain $\hat{\lambda}$ and $\hat{\mu}$ we need to use the following important theorem
THEOREM (4.1),

For the birth-death process with rates, namely $0 \leq \lambda_n = \lambda g_\downarrow n$, $0 \leq \mu_n = \mu r_n$ for n positive integer and both g_n and r_n are bounded functions of n [1],
We have

$$E(n) = -\left((\partial lnP_\downarrow 0)/\partial (\right._{=}{}^{\mu\frac{\partial lnP_0}{\partial \mu}},$$

where P_0 = delay probability and
    E(n)= expected value of n .
Proof: It is clear that

$$P_n = P_\downarrow 0 \, \Pi_\downarrow(i = 0)^\intercal(n - 1)^{\underline{\underline{}}}(\lambda_i/\mu_\downarrow(i + 1) \qquad \forall n \geq 1$$

$$P_0 = \mathbb{K}[1 + \Sigma_\downarrow(n = 1)^\intercal\infty^{\underline{\underline{}}}\Pi_\downarrow(i = 0)^\intercal(n - 1)^{\underline{\underline{}}}(\lambda_i/\mu_\downarrow(i + 1)]\mathbb{X}^\intercal(-1)$$

Case (i): putting $\lambda_i = \lambda g_\downarrow i$, it follows that

$$P_0 = \mathbb{K}[1 + \Sigma_\downarrow(n = 1)^\intercal\infty^{\underline{\underline{}}}\mathbb{K}(\lambda^\intercal n \, \Pi_\downarrow(i = 0)^\intercal(n - 1)^{\underline{\underline{}}}g_\downarrow i/\mu_\downarrow(i + 1)\mathbb{X}]\mathbb{X}^\intercal(-1).$$

Taking the logarithm of both sides of this equation and differentiating the resulting equation partially with respect to λ $yield$

$$-(\partial lnP_\downarrow 0)/\partial (\right._{=} P_\downarrow 0 \, [\Sigma_\downarrow(n = 1)^\intercal\infty^{\underline{\underline{}}}\mathbb{K}n(\lambda^\intercal(n - 1) \, \Pi_\downarrow(i = 0)^\intercal(n - 1)^{\underline{\underline{}}}g_\downarrow i/\mu_\downarrow(i + 1)\mathbb{X}].$$

But,

$$E(n) = \Sigma_\downarrow(n = 1)^\intercal\infty^{\underline{\underline{}}}\mathbb{K}nP_\downarrow n = P_\downarrow 0 \, [\Sigma_\downarrow(n = 1)^\intercal\infty^{\underline{\underline{}}}\mathbb{K}n\Pi_\downarrow(i = 0)^\intercal(n - 1)^{\underline{\underline{}}}(\lambda_i/\mu_\downarrow(i + 1)\mathbb{X}]\mathbb{X}.$$

Therefore, it follows that

$$E(n) = -\left((\partial lnP_\downarrow 0)/\partial (\right..$$

Case (ii): putting $\mu_i = \mu r_i$, it follows that

$$P_0 = \mathbb{K}[1 + \Sigma_\downarrow(n = 1)^\intercal\infty^{\underline{\underline{}}}\mathbb{K}1/\mu^\intercal n \, \Pi_\downarrow(i = 0)^\intercal(n - 1)^{\underline{\underline{}}}(\lambda_i/r_\downarrow(i + 1)\mathbb{X}]\mathbb{X}^\intercal(-1).$$

Taking the logarithm of both sides of this equation, it follows that

$$lnP_0 = -ln[1 + \Sigma_\downarrow(n = 1)^\intercal\infty^{\underline{\underline{}}}\mathbb{K}1/\mu^\intercal n \, \Pi_\downarrow(i = 0)^\intercal(n - 1)^{\underline{\underline{}}}(\lambda_i/r_\downarrow(i + 1)\mathbb{X}].$$

Therefore,

$$\frac{\partial lnP_0}{\partial \mu} = P_\downarrow 0 \, [\Sigma_\downarrow(n = 1)^\intercal\infty^{\underline{\underline{}}}\mathbb{K}n/\mu^\intercal(n + 1) \, \Pi_\downarrow(i = 0)^\intercal(n - 1)^{\underline{\underline{}}}(\lambda_i/r_\downarrow(i + 1)\mathbb{X}].$$

Hence,

$$\mu\frac{\partial lnP_0}{\partial \mu} = P_\downarrow 0 \, [\Sigma_\downarrow(n = 1)^\intercal\infty^{\underline{\underline{}}}\mathbb{K}n/\mu^\intercal n \, \Pi_\downarrow(i = 0)^\intercal(n - 1)^{\underline{\underline{}}}(\lambda_i/r_\downarrow(i + 1)\mathbb{X}].$$

Thus, it is evident that

$$E(n) = {}^{\mu\frac{\partial lnP_0}{\partial \mu}},$$

Hence, the theorem is proved.
Using theorem (4.1), equation (4.1) can be written in the form

$$-\left(\hat{} (\partial lnP_\downarrow 0)/\partial (+(\hat{} T - (n + u) = 0,$$

$$E^\wedge(n) + \hat{} T - (n + u) = 0,$$

$$\hat{\Box} = \frac{1}{T[(n + u) - \hat{E}(n)]}. \qquad (4.3)$$

Also, by using theorem (4.1), equation (4.2) can be written in the form

$$\frac{\hat{\mu}(\partial lnP_0)}{\partial \mu} - \hat{\mu}t + (k - u) = 0,$$

$$\hat{E}(n) - \hat{\mu}t + (k - u) = 0,$$

$$\hat{\mu} = \frac{1}{t[(k-u)+\hat{E}(n)]}$$ (4.4)

Where $\hat{E}(n)$ is the maximum likelihood estimator of E(n) .

Obtaining the value of $\hat{E}(n)$ from each of the equations in (4.3), (4.4) and dividing the resulting values yields
From (4.3)

$$T\hat{C} = (n+u) - \hat{E}(n),$$
$$\hat{E}(n) = (n+u) - T\hat{C} .$$

From (4.4)

$$t\hat{\mu} = (k-u) + \hat{E}(n) ,$$
$$\hat{E}(n) = t\hat{\mu} - (k-u) ,$$
$$(t\hat{\mu} - (k-u))/(-T\hat{C} + (n+u)) = 1 .$$ (4.5)

Recalling that $\hat{\rho}$, the maximum likelihood estimator of the traffic intensity ρ , is given by $\hat{\rho} = \hat{C}/\hat{\mu}$ and using equations (4.3), (4.4)

$$\hat{\rho} = \hat{C}/\hat{\mu} = (t[(n+u) - \hat{E}(n)])/(T[(k-u) + \hat{E}(n)])$$ (4.6)

This equation can be written in the form

$$t[n+u - \hat{E}(n)] - \hat{\rho}T[k-u+\hat{E}(n)] = 0 .$$ (4.7)

Consider the special case M/M/1 on replacing $\hat{E}(n)$ by $\dfrac{\hat{\rho}}{1-\hat{\rho}}$ into equation (4.7)

$$t\left[n+u - \frac{\hat{\rho}}{1-\hat{\rho}}\right] - \hat{\rho}T\left[k-u+\frac{\hat{\rho}}{1-\hat{\rho}}\right] = 0 ,$$
$$t[(n+u)(1-\hat{\rho}) - \hat{\rho}] - \hat{\rho}T[(k-u)(1-\hat{\rho}) + \hat{\rho}] = 0 ,$$
$$T(k-u-1)\hat{\rho}^2 - [t(n+u+1) + T(k-u)]\hat{\rho} + t(n+u) = 0 .$$ (4.8)

Replacing (k-u-1) and (n+u+1) by (k-u) and (n+u), respectively, in (4.8) yields.

$$T(k-u)\hat{\rho}^2 - [t(n+u) + T(k-u)]\hat{\rho} + t(n+u) = 0 ,$$
$$T(k-u)\hat{\rho}(\hat{\rho}-1) - t(n+u)(\hat{\rho}-1) = 0 ,$$
$$(\hat{\rho}-1)[T(k-u)\hat{\rho} - t(n+u)] = 0 ,$$ (4.9)
$$T(k-u)\hat{\rho} - t(n+u) = 0 .$$

Then

$$\hat{\rho} = \frac{t(n+u)}{T(k-u)} ,$$ (4.10)

is a solution for the modified equation (4.9) of degree two in $\hat{\rho}$. Using (4.5) and (4.10) it follows that

$$\hat{\rho} = t(n+u)/T(k-u) * (t\hat{\mu} - (k-u))/(-T\hat{C} + (n+u)) ,$$
$$\hat{\rho} = (t^2\hat{\mu}(n+u) - t(k-u)(n+u))/(-T^2\hat{C}(k-u) + T(k-u)(n+u)) ,$$
$$-T^2\hat{\rho}\hat{C}(k-u) + T\hat{\rho}(k-u)(n+u) = t^2\hat{\mu}(n+u) - t(k-u)(n+u) ,$$
$$t^2\hat{\mu}(n+u) + T^2\hat{\rho}\hat{C}(k-u) = (n+u)(k-u)[T\hat{\rho} + t].$$ (4.11)

To find $\hat{\mu}$, put $\hat{C} = \hat{\rho}\hat{\mu}$ into equation (4.11)

$$t^2\hat{\mu}(n+u) + T^2\hat{\rho}^2\hat{\mu}(k-u) = (n+u)(k-u)[T\hat{\rho} + t],$$

$$\hat{\mu} = \frac{(n+u)(k-u)[T\hat{\rho}+t]}{t^2(n+u) + T^2\hat{\rho}^2(k-u)} \qquad \text{(use equation(4.10))}$$

$$= \frac{(n+u)(k-u)\left[T\dfrac{t(n+u)}{T(k-u)}+t\right]}{t^2(n+u) + T^2\dfrac{t^2(n+u)^2}{T^2(k-u)^2}(k-u)}$$

$$= \frac{t(n+u)[n+u+k-u]}{t(n+u)\left[t+\dfrac{t(n+u)}{k-u}\right]}$$

$$= \frac{n+k}{t+T\dfrac{t(n+u)}{T(k-u)}} \qquad \text{(from equation(4.10))}$$

Thus

$$\hat{\mu} = \frac{n+k}{t+T\hat{\rho}}$$

.

(4.12)

To find $\hat{l}$, put $\hat{\mu} = \hat{l}/\hat{\rho}$ into equation (4.12)

$$\hat{l}/\hat{\rho} = (n+k)/(T\hat{\rho} + t) \quad ,$$

$$\hat{l} = \frac{\hat{\rho}(n+k)}{T\hat{\rho} + t}$$

.

(4.13)

Then, by using (4.10) it follows that

$$\hat{\mu} = \frac{n+k}{T\hat{\rho} + t} = \frac{k-u}{t} \quad ,$$

(4.14)

$$\hat{l} = (\hat{\rho}(n+k))/(T\hat{\rho} + t) = (n+u)/T \quad .$$

REFERENCES

[1]. Feller W. An Introduction to Probability Theory and its Applications ,Vol. John Wiley, New Yourk,1972.
[2]. Gross, D., and Harris, C.M. Fundamentals Of Queuing Theory. John Wiley, New York, 1974.
[3]. Leonard, K. Queuing System, vol. I. John Wiley, New York , 1975 .
[4] Mokaddis , G. S and Zaki. S. S., The Problem Of The Queuing System M/M/1 With Additional Servers For A Longer Queue. Indian J . Pure Applied Math.1 Vol. 3, No. 3, PP.78-98, 2000.
[5]. Mokaddis, G.S. " The Statistical Point Estimation for Parameters of Some Queuing Systems" The Sixth International Congress for Statistical ,Computer Science ,Egypt,29 March-2 April pp.71-93,1981.
[6]. Narayan, U.B. An Introduction to Queuing Theory ,Boston Basel, Berlin 2008.

Design and Simulation of PV Based Two-Phase Interleaved Boost Converter

D.Umarani[1] and Dr.R.Seyezhai[2]

[1, 2] *(PG Scholar, Associate Professor, Department of EEE, SSN College of Engineering, Chennai, India)*

Abstract: *In this paper, simulation of PV based two phase interleaved boost converter has been discussed. Interleaved Boost Converter (IBC) serves several applications which require boost in output voltage such as fuel cells, photovoltaic cells and batteries etc., because it has several advantages over conventional DC-DC converters. The configuration of IBC comprises parallel combination of a number of boost converters with same phase shift and switching frequency. This paper deals with the design of two-phase IBC for a five level cascaded multilevel inverter (MLI). The source for each bridge of the MLI has been modelled as PV. The simulation has been carried out using MATLAB/SIMULINK.*

Keywords: *Multilevel Inverter, Interleaved boost converter, Boost converter & Photo-voltaic cells.*

I. INTRODUCTION

In recent days, Photovoltaic (PV) applications have become a great hit all over the world because of the abundant availability of the solar energy in almost all parts of the earth. Therefore there is a spurt in the area of photovoltaic research which in turn led to the development of suitability of converters to the photovoltaic systems. One such invention is the Interleaved Boost Converter (IBC) that has the boost and current sharing capability on high power application. It can be configured with many phases that allow the input current sharing and heat dissipation. Even though there are a number of DC boost converters that are available for the PV applications, they have objectionable level of ripples. In addition to the minimization of the ripples, it has higher modularity, reliability and power capability at the cost of additional inductors, diodes and switching devices. In this paper, the two phase IBC can be used with PV so as to get reduced current ripple that comes out of the PV cell. The boosted output voltage of the IBC is used as source of voltage for the five level cascaded (Multi level Inverter) MLI.

II. Two-Phase Interleaved Boost Converter

Application of interleaving technique is remarkable in the field power electronics. The voltage and current stress can go beyond the handling capability in high power applications. Therefore many power devices can be connected in parallel and/or in series. But voltage sharing and/or current sharing will always be a problem. Paralleling of power converters is an alternate solution instead of paralleling power devices which could be more beneficial. Figure 1 shows the two-phase interleaved boost converter topology[1]-[5].
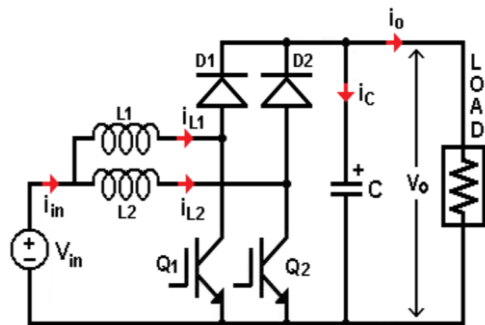
Figure 1.Two-Phase Interleaved Boost Converter   Figure 2. Timing signal of the two- phase IBC

The two-phase IBC consists of two parallel connected boost converter units. Each of the units in the IBC can be controlled by switching the devices with phase shift of $360^{o}/n$, where n is the number of parallel connected units. In this converter, there should be a phase shift implemented between the switching pulses of the both devices. A phase shift of 180° should be provided for each switch as there are two parallel units. The timing signal is shown in figure 2.

III. Operation Of The Two-Phase IBC

In general, the frequency and phase shift are same for each parallel connected unit in the IBC. Operation of two-phase IBC can be explained based on figure 1.The device Q1 is turned ON first. So, the current in the inductor i_{L1} increases linearly and at the same time energy is stored in inductor L1. When Q1 is turned OFF, diode D1 conducts and the stored energy in the inductor decreases with a slope of the difference in the input and output voltage. When the inductor discharges its energy, the transfer the current to the load takes place via the diode. Once half switching cycle of Q1 is completed, Q2 is also turned ON and completes same cycle of actions. The current ripple produced will be very small as there is a cancellation of ripples due to phase shift of 180° in the switching pulses[7]-[9].

IV. Design Equations Of Two-Phase IBC

The design of magnetic elements in the circuit plays an important role for storing energy and filtering. The two-phase IBC requires two identical inductors for achieving balanced current. The value of the inductor can be calculated as per the following equation.

$$L = \frac{V_{in} M}{f_s \Delta I_L} \qquad (1)$$

Where,
M - Modulation Index, V_{in} – Input Voltage, f_s-Switching frequency, ΔI_L - Inductor current ripple.
The value of the capacitor can be calculated by the following equation.

$$C = \frac{I_o M}{f_s \Delta V_C} \qquad (2)$$

Where,
M - Modulation Index, f_s-Switching frequency, ΔV_C – Change in output voltage, I_o –Output current.
The number of phases can be chosen based on the amount of ripple to be reduced. Increase in phase number will not result in much reduction in ripple. This poses a restriction to the increase in number of phases. The number of switches, inductors and diodes are equal in number with the phases.

V. PV Modeling

PV cell can be represented by the equivalent electrical circuit shown in figure 3.
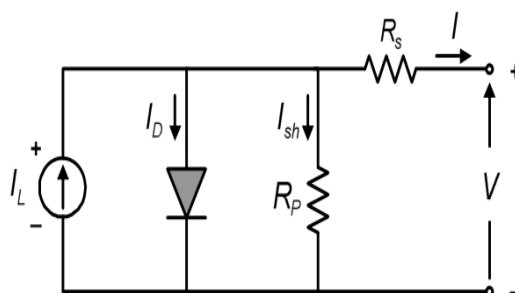
Figure 3. Equivalent circuit of a solar cell

The I-V and P-V characteristics of the solar cells are non linear in nature. The solar cell characteristics mainly depend on the existing atmospheric conditions such as temperature and irradiance. The P-V characteristics of solar cell are shown in figure 4.The I-V curve shown in figure 5 is for the PV module under sunlight and dark conditions.
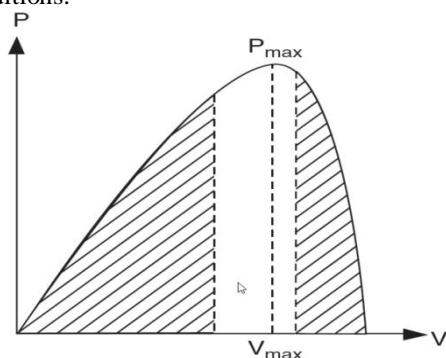
Figure 4. P-V characteristics of a PV cell
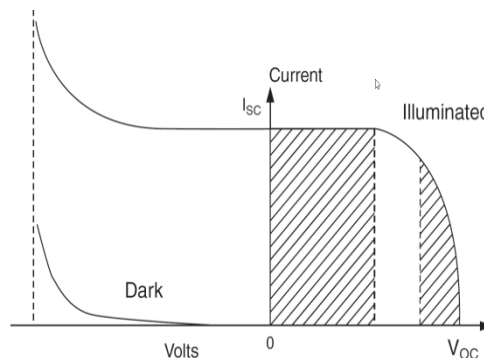
Figure 5. I-V characteristics of a PV cell

The PV cell can be mathematically modelled using the following equations.
The open circuit voltage given by V_{oc} is obtained when load current reaches zero.

$$V_{oc} = V + IR_{sh} \qquad (3)$$

The diode current expression is given by

$$I_d = I_D \left[e^{\frac{QV_{oc}}{AKT}} - 1 \right] \qquad (4)$$

The load current is given by the following equation

$$I = I_L - I_D \left[e^{\frac{QV_{oc}}{AkT}} - 1 \right] - \frac{V_{oc}}{R_{sh}} \qquad (5)$$

Where,
I_D – Diode saturation current
Q – Charge of an electron = 1.6×10^{-19} C
A - Curve fitting constant
k - Boltzmann constant = 1.38×10^{-23} J/K
T – Absolute Temperature in K

VI.   Maximum Power Point Tracking

Perturb and Observe algorithm has been implemented for tracking maximum power point in this paper. It is a very simple algorithm which requires the measurement of solar panel's output voltage and current. The perturbation at each step is used to find out the maximum power. The flow chart of the P & O algorithm is shown in figure 6.
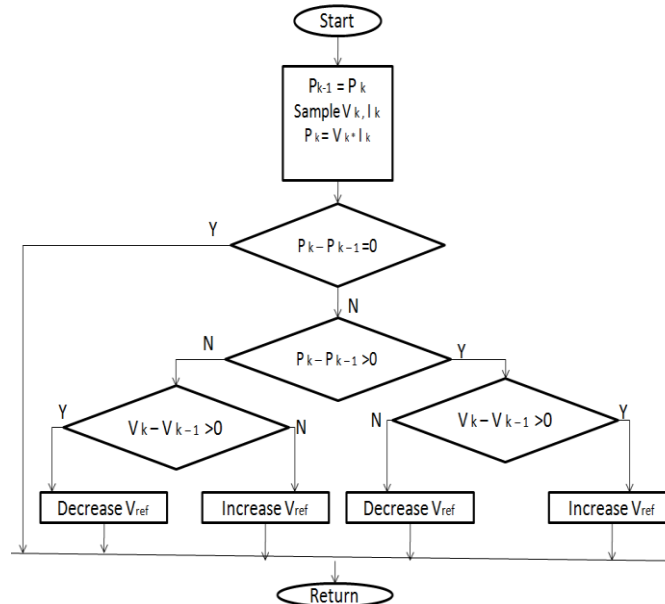
Figure 6. Flow chart of P & O MPPT algorithm

VII.   Simulation Results

7.1 Simulation Parameters

The simulation parameters for the PV panel and the IBC are listed in the table 1. The two-phase IBC simulation parameters are listed in the table 2.

Table 1. Simulation parameters of PV array

PV Parameters	Rating
Open circuit voltage V_{oc}	21.24 V
Short circuit current I_{sc}	2.55 A
No of cells Ns	36
Insolation G	1000 W/m^2
Ideality factor A	1.5
Operating temperature T	298 K

Table 2. Simulation parameters of Two-Phase IBC

Two-phase IBC Parameters	Rating
Input voltage	20 V
Inductor	0.015 mH
Capacitor	0.22 mF
Switching frequency	5 kHz

7.2 Mathematical model of PV array in MATLAB/Simulink along with P and O MPPT

The PV array has been modelled using the equations (3),(4) and (5). Single diode model of a solar cell is considered in this paper. Figure 7 shows the mathematical model of the PV array with perturb and observe maximum power point tracking technique (MPPT).For implementing MPPT, the current and the voltage of the PV panel has been taken and used as inputs for the P & O algorithm.
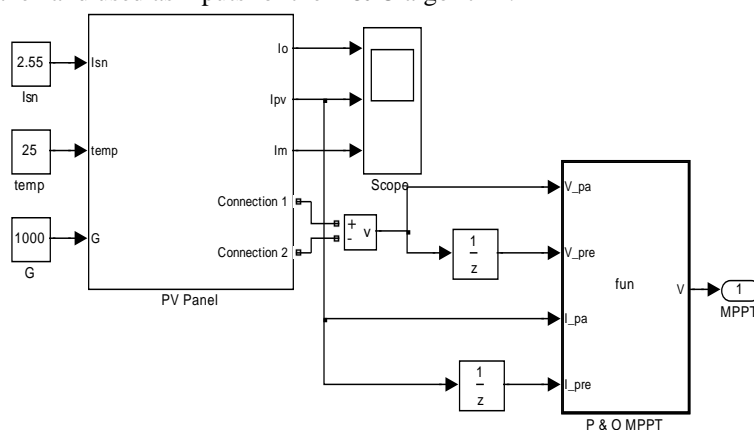
Figure 7. PV model with P & O MPPT

7.3 Simulink model of two-phase IBC

The two-phase IBC has been modelled with PV source implemented with MPPT in Matlab/Simulink. It is shown in the figure 8. The output voltage of the PV array is given to the two-phase IBC.
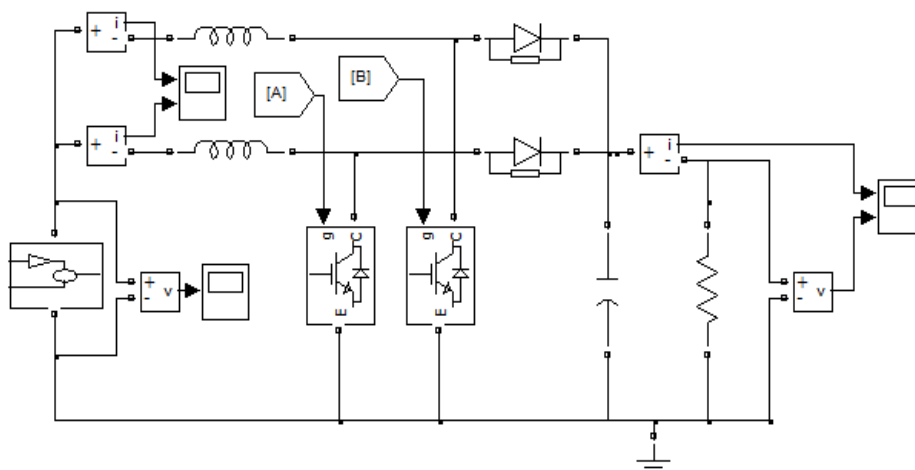
Figure 8. MATLAB/Simulink model of two-phase IBC with PV MPPT

7.4 Pulses for the switches of two-phase IBC

The switches of the two-phase IBC are required to be fired at 180° phase shift. Since there are two phases, the pulses are to be produced at the phase difference of $360^o/n$, where n=2.The pulse pattern for the two switches are shown in figure 9.
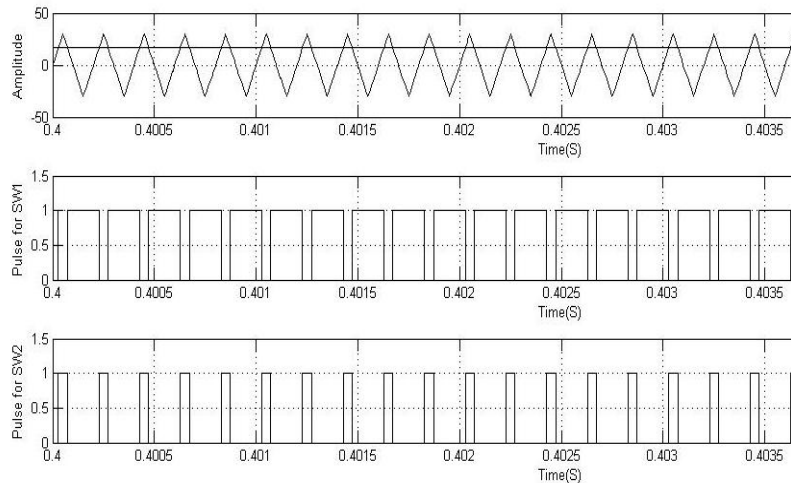
Figure 9. Pulses generated for switches of two-phase IBC

7.5 Inductor current ripple of two-phase IBC

The inductor current ripple of the two phase IBC is shown in figure 10 and it is found to be 6.89%.
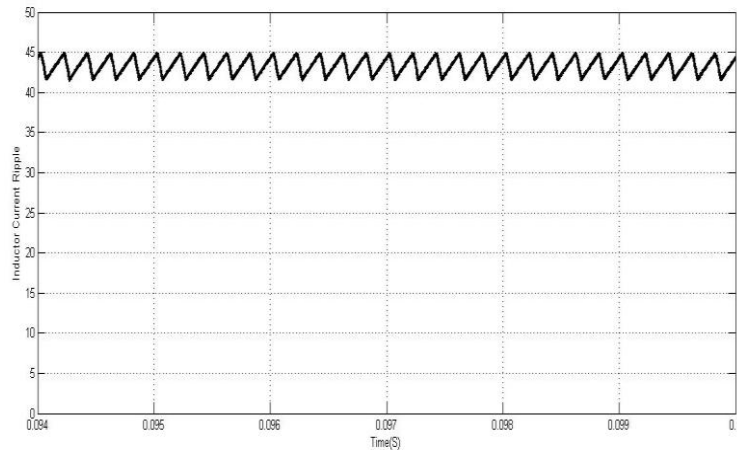
Figure10. Inductor current ripple of two-phase IBC

7.6 Output voltage waveform of two-phase IBC

The output voltage of the two-phase IBC is found to be 90 V for a resistive load of 10 Ω. The waveform is shown in figure 11.
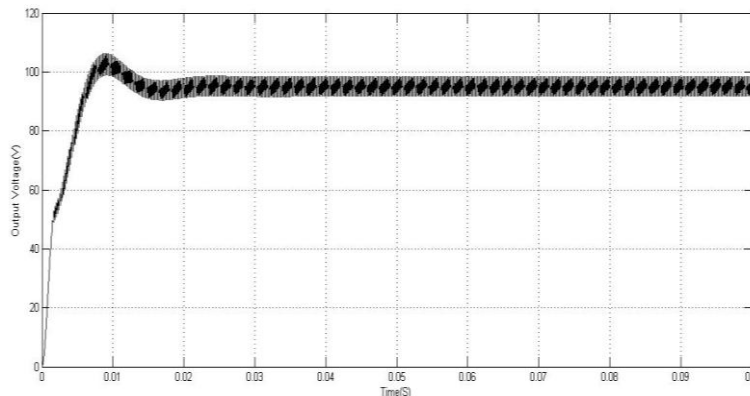
Figure 11. Inductor current ripple of two-phase IBC

7.7 Output voltage ripple of two phase IBC

Figure 12 shows the output voltage ripple of the two -phase IBC. It is found to be 6.31%
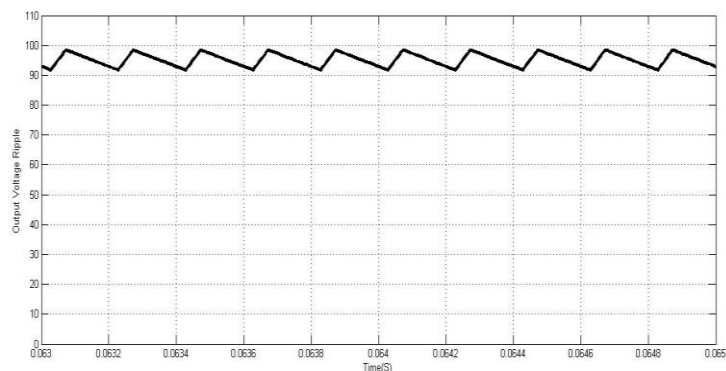
Figure 12.Output voltage ripple of two-phase IBC

7.8 Results of input inductor current ripple and output voltage ripple
Table 3. Calculated ripple values of Two- Phase IBC

Parameter	Ripple in %
Input inductor current	6.89
Output voltage	6.31

The values of input inductor current ripple and output voltage ripple has been calculated from the simulation results and tabulated in Table 3.

7.9 Application of two-phase IBC in a cascaded H-bridge five level inverter
The simulation model is shown in the figure 13.
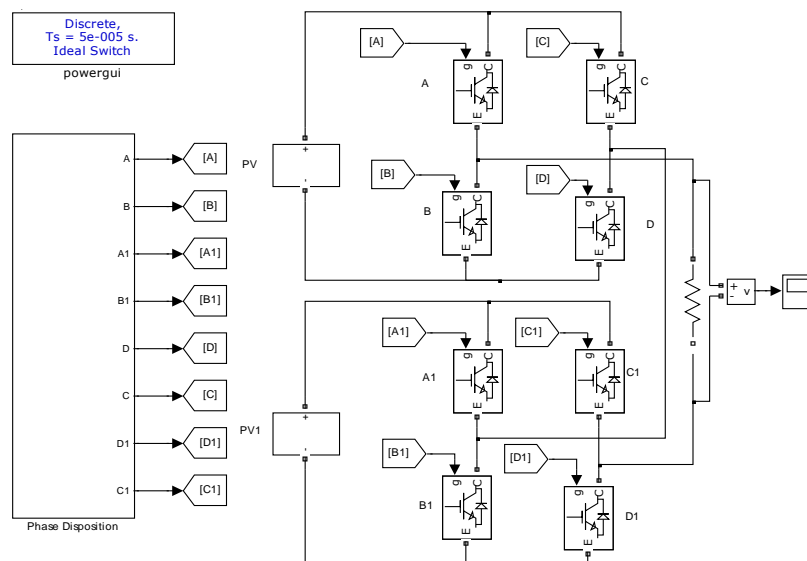
Figure 13. Five-level MLI interfaced to PV sourced two-phase IBC

The two-phase IBC can be used to boost the output voltage of the solar panel which can then be provided as input to the bridges of the multi level inverter. When compared to the conventional DC-DC boost converter, the two-phase IBC has reduced ripple content. It is more suitable for interfacing with the cascaded H-bridge MLI.

7.10Output voltage of MLI with two-phase IBC
The output voltage of the MLI connected to two-phase IBC is found to be 180 V. An input voltage of 90 V for each bridge is provided by two-phase IBC. The output voltage of five-level MLI with two-phase IBC is shown in figure 14.
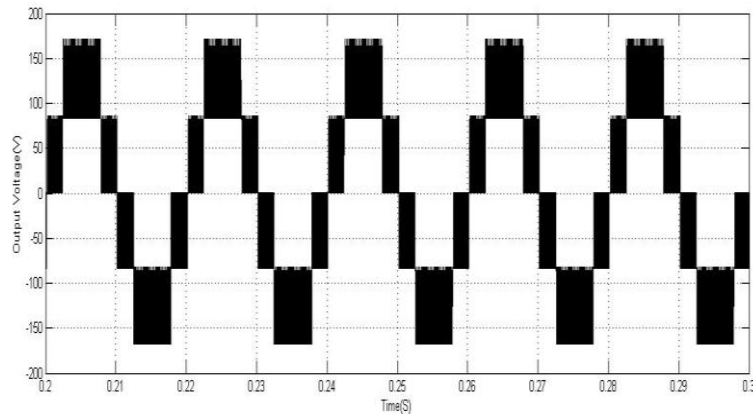
Figure 14. Output voltage of five-level MLI with two-phase IBC

7.11 THD of the output voltage of two-phase IBC

The THD of the output voltage of five-level MLI with two-phase IBC is found to be 22.61%.The frequency spectrum is shown in the figure 15.
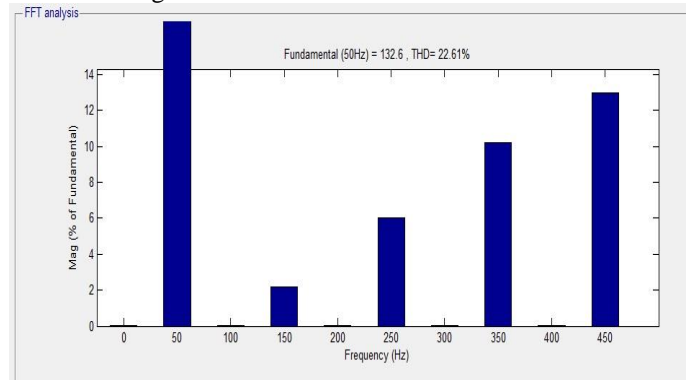
Figure 15. THD of output voltage of five-level MLI with two-phase IBC

VIII.   Conclusion

The PV array has been modelled using MATLAB/Simulink and then implemented with perturb and observe MPPT. The reference from the MPPT has been used to generate pulses for the two-phase IBC. The two-phase IBC has been modelled in MATLAB/Simulink and provided with PV source. The output voltage of PV panel is 20 V. It is boosted to 90 V by two-phase IBC. This 90 V is fed to each bridge of the five-level MLI. The output voltage is obtained as 180 V with a THD of 22.61%. The output voltage ripple is found to be 6.31% and the input inductor current ripple is found to be 6.89%. Thus, the two-phase IBC is suitable for interfacing with PV source and it can also act as boost converter for providing voltage for MLI.

REFERENCES

[1]   Geoffrey R. Walker, Paul C. Sernia,. "Cascaded DC-DC Converter Connection of Photovoltaic Modules". IEEE Transactions on power electronics,vol.19,no.4, 2004

[2]   Gyu-Yeong Choe, Hyun-Soo Kang, Byoung-Kuk Lee and Won-Yong Lee,. "Design Consideration of Interleaved Converters for Fuel Cell Applications", in Proceedings of International Conference on Electrical Machines and Systems ,Seoul, Korea, pp.238-243, 2007.

[3]   P.A.Dahono, S.Riyadi , A.Mudawari and Y.Haroen. "Output ripple analysis of multiphase DC–DC converter". IEEE International Conference on Power Electrical and Drive Systems, Hong Kong, pp. 626–631,1999.

[4]   L. Huber, B. T. Irving, M. M. Jovanovic, "Open-loop control methods for interleaved DCM/CCM boundary boost PFC converters", IEEE Transactions on Power Electronics., vol. 23, no. 4, pp.1649 – 1657,2008.

[5]   P.Thounthong, P.Sethakul, S.Rael and B.Davat ,"Design and implementation of 2- phase interleaved boost converter for fuel cell power source",' Int. Conf. Power Electronics, Machines, and Drives, PEMD 2008, pp. 91–95,2008.

[6]   P.Lee, Y.Lee, D.K.W. Cheng and X.Liu, "Steady-state analysis of an interleaved boost converter with coupled inductors", IEEE Transactions on Industrial Electronics, pp. 787–795,2000.

[7]   R. Seyezhai and B.L.Mathur, "Design and implementation of fuel cell based Interleaved Boost Converter', International Conference on Renewable Energy" , ICRE 2011 Jan 17-21, 2011, University of Rajasthan, Jaipur.

[8] H. B. Shin, J. G. Park, S. K. Chung, H. W. Lee and T. A. Lipo ,"Generalised steady-state analysis of multiphase interleaved boost converter with coupled inductors", IEE Electrical Power Applications, Vol.152, Issue.3, pp.584 – 594,2005

[9] R.Seyezhai and B.L.Mathur, "Analysis, design and experimentation of Interleaved Boost Converter for fuel cell power Source", IJRRIS Journal, Vol. 1, No: 2, June 2011.

Authors

D.Umarani received her B.E degree (Electrical and Electronics) in the year 2011 from Mepco Schlenk Engineering College, Sivakasi. Currently she is pursuing her Master of Engineering in Power Electronics and Drives from SSN College of Engineering, Chennai. Her areas of interest are Z-Source and Quasi Z-Source inverters, PV applications and AC Drives.

Dr.R.Seyezhai obtained her B.E. (Electronics & communication Engineering) from Noorul Islam College of Engineering, Nagercoil in 1996 and her M.E in Power Electronics & Drives from Shanmugha College of Engineering, Thanjavur in 1998 and Ph.D from Anna University, Chennai, in 2010 . She has been working in the teaching field for about 15 Years. She has published 120 papers in the area of Power Electronics & Drives. Her areas of interest include SiC Power Devices & Multilevel Inverters.

Distributed Utility-Based Energy Efficient Cooperative Medium Access Control in MANETS

Mr. M. Naresh[1], Mr. Gudditti.Viswanath[2], Mr. T. SunilKumarReddy[3]

[1]((M.Tech) Software Engineering, Sir Vishveshwaraiah Institute of Science&Tech., Madanapalle, Andhra Pradesh, India)

[2, 3](Asst.Professor, Dept of C.S.E, Sir Vishveshwaraiah Institute of Science & Tech. , Madanapalle, Andhra Pradesh, India)

Mail ids: *madakanaresh@gmail.com[1]*, *viswag111@gmail.com[2]*, *sunil_reddy1982@yahoo.co.in[3]*

Abstract: *Cooperative communication, that utilizes near terminals to relay the overhearing information to grasp the variability gains, choices a nice potential to strengthen the transmission potency in wireless networks. to the subsume the hard medium access interactions evoked by relaying and leverage the advantages of such cooperation, associate economical Cooperative Medium Access management (CMAC) protocol is required. throughout this paper, we've got an inclination to tend to propose a completely unique cross-layer Wide unfold Energy-adaptive Location-based CMAC protocol, notably WEAL-CMAC, for Mobile Ad-hoc Networks (MANETs). the design objective of WEAL-CMAC is to strengthen the performance of the MANETs in terms of network amount and energy potency. a wise energy consumption model is used throughout this paper, that takes the energy consumption on each transceiver instrumentation and transmit instrumentation into thought. A distributed utility-based best relay different strategy is incorporated, that selects the most effective relay supported location information and residual energy. moreover, with the aim of enhancing the spacial apply, associate innovative network allocation vector setting is provided to the subsume the variable transmission power of the beginning and relay terminals. we've got an inclination to tend to point that the planned WEAL-CMAC considerably prolongs the network amount below varied circumstances even for prime instrumentation energy consumption cases by comprehensive simulation study*

Keywords: *Network Lifetime, Cooperative Communication, Medium Access Control Protocol, Relay Selection.*

I. Introduction

The wireless network offers the advantages of present property and mobile access. However, with a lot of randomness and fewer stability, the wireless network still cannot succeed a similar dependableness and high rate as its wired counterpart, as a result of its distinctive options like attenuation, shadowing and path loss. to handle these issues, several techniques are planned, among that multiple-input and multiple-output (MIMO) [1,2] is one among the foremost promising solutions. sadly, it's not possible to equip palm-sized and powered mobile terminals with multiple receiving and transmission antennas [2]–[5], that limits the appliance of MIMO technique. Given the published nature of the wireless medium, information transmission from a begin terminal will be overheard by different terminals. As a result, it's doable for the beginning to work with these overhearing terminals (also called helpers) to create a virtual MIMO system. This user cooperation will offer several edges, together with system outturn improvement, interference mitigation and seamless service provision [6]. throughout the past decade, there area unit several studies on the cooperation at the physical layer [3,7]–[10]. several physical-layer cooperation protocols area unit planned, like amplify-and-forward (AF) [8], rewrite and-forward (DF) [8], compress-and-forward (CF) [9], and coded cooperation (CC) [10]. the look and analysis of those physical-layer relaying techniques area unit typically supported the subsequent assumptions:

_ A1: information is often transmitted during a cooperative manner.

_ A2: the beginning forever is aware of WHO the helpers area unit to work with.

_ A3: only 1 dedicated helper is usually concerned.

_ A4: Helpers area unit forever prepared and willing to assist.

Apparently, these assumptions might not be forever true in real network situations. concerning A1, if the relay channel is of caliber, cooperation might not be helpful or necessary. Moreover, the beginning might like to not transmit hand and glove as a result of energy or security issues. Indeed, from a physical-layer stance,

the beginning merely broadcasts its signal and doesn't ought to comprehend the helpers. However, from a higher-layer's purpose of read, a link between the beginning node and therefore the finish node ought to be established for non-broadcast services. the beginning should incorporate the address(es) of the chosen helper(s) because the finish of a frame in order that it'll not be born however forwarded by the helper(s). nevertheless, A2 may be invalid once helpers area unit moving. the beginning cannot have up-to-date information of the helpers to work with. moreover, A3 could be a robust assumption since it's difficult to pick a best helper among multiple candidates that catch the transmission from the beginning.

II. The Planned WEAL-CMAC Protocol

In this section, with the target of prolonging the network lifespan and increasing the energy potency, we tend to gift a unique CMAC protocol, particularly WEAL-CMAC, for multihop MANETs. once cooperative relaying is concerned, the channel reservation has to be extended in each house and time so as to coordinate transmissions at the relay. To touch upon the relaying and dynamic transmission power, besides the standard management frames RTS, CTS and ACK, extra management frames area unit needed. DELCMAC introduces 2 new management frames to facilitate the cooperation, i.e., Eager-To-Help (ETH) and Interference- Indicator (II). The ETH frame is employed for choosing the simplest relay during a distributed and light-weight manner, that is shipped by the winning relay to tell the beginning, finish and lost relays. during this paper, the simplest relay is outlined because the relay that has the utmost residual energy and needs the minimum transmission power among the capable relay candidates. The II frame is used to reassert the interference vary of allotted transmission power at the winning relay, so as to boost the spacial apply. Among all the frames, RTS, CTS, ETH and ACK area unit transmitted by mounted power. and therefore the transmission power for the II frame and information packet area unit dynamically allotted. we tend to denote the time durations for the transmission of RTS, CTS, ETH, ACK and II frames by TR_{RTS}, TR_{CTS}, TR_{ETH}, TR_{ACK} and TR_{II}, severally.

2.1 Protocol Description
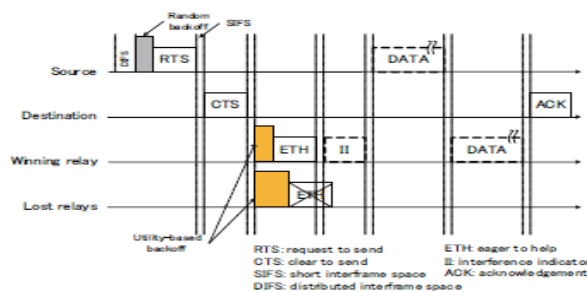
FIG1.TheFrameExchangingProcessOf WEAL-CMAC

Fig. 1. The frame exchanging method of WEAL-CMAC. The frame exchanging method of WEAL-CMAC is shown in Fig. 1. kind of like the IEEE 802.11 DCF protocol, the RTS/CTS shake is employed to order the channel initially. As we know, the cooperative transmission isn't necessary within the case that the sending power is little as a result of the extra overhead for coordinative the relaying overtakes the energy saving from diversity gain. Those inefficient cases square measure avoided by introducing a sending power threshold Λp. In WEAL-CMAC, upon receiving the RTS frame, the tip computes the desired sending power for the transmission mechanism PDs There square measure 2 cases looking on the calculated PDs

.• **Case (i):** PDs≤ Λp. the tip sends a CTS frame with FLAG_Field (FLAG-F) adequate to zero, which means that the transmission mechanism is adequate. Thus, once the sending power for the transmission mechanism is sufficiently low, WEAL-CMAC is reduced to the DCF protocol and therefore has backward compatibility with the gift 802.11 commonplace.

• **Case (ii):** PDs > Λp. FLAG-F within the CTS frame is about to one, that indicates that the cooperative relaying is desired. All the terminals having overheard RTS and CTS, and not interfere with alternative current transmissions square measure thought of because the relay candidates. when the relay candidates check if they're ready to cut back the energy consumption (given within the Eqn. (1)), the capable relay candidates contend for relaying by causation ETH when a utility-based go into reverse . Notice that there could exist the case that 2 relay candidates hidden with one another (outside the transmission range). However, they will still sense the message sent from one another (within the sensing vary that is about at one.9 times of the transmission point the machine by default). The case that multiple ETH frames collide thanks to hidden wouldn't exist. when SIFS (short entomb frame space), the winning relay broadcasts the II message to reassert the interference vary of the allotted sending power at relay, that is employed within the NAV setting when the on top of management frame exchanging, the beginning and relay hand in glove send an equivalent knowledge frames to the tip in 2

consecutive time intervals exploitation the allotted sending power Finally, the tip sends associate ACK back to the beginning if it decodes the message with success. The flow charts of the terminals square measure given within the Appendix B. The elaborated protocol operations square measure provided from the attitude of various terminals:

2.1.1 Operations at the Start

1. Once a begin desires to initiate the info transmission with payload LENGTH X bytes, it 1st senses the channel to ascertain if it's idle. If the channel is idle for DIFS, the beginning chooses a random backoff timer between zero and CW. once the backoff counter reaches zero, the beginning sends out a RTS to order the channel. Notice that completely different from DCF, the placement data of the beginning is carried within the RTS, that is employed within the best power allocation.

2. If the beginning doesn't receive a CTS at intervals $TR_{RTS}+TR_{CTS}+SIFS$, a retransmission method are performed. Otherwise, within the case that FLAG_F of CTS is zero, the WEAL-CMAC is reduced to DCF protocol, and that we omit its operations within the following. within the case that FLAG_F is one, the beginning waits for an additional $TR^{scoop}_{BackOff} +TR_{ETH}+SIFS$, wherever $TR^{max}_{Back Of f}$ is that the most backoff time for the relay . If ETH isn't received, which implies that no capable relay exist, the beginning sends the info by transmission mechanism with rate M.

3. If each CTS and ETH square measure received, when expecting TRII+SIFS, the beginning initiates a cooperative transmission with rate 2M exploitation the best sending power PCs that is piggybacked within the ETH. Notice that so as to keep up the end-to-end outturn, doubled rate is used within the cooperative transmission mode. we tend to assume that the terminal will support 2 transmission rates by completely different cryptography and modulation schemes.

4. If associate ACK isn't received when $16(X+XH)/2M+TR_{ACK}+2S$ IFS, wherever Xh is that the header length (in bytes), the beginning would perform a random backoff same as DCF. Otherwise, the transmission method succeeds and therefore the begin handles consecutive packet within the buffer if any. Notice that the unit for L and gonadotropic hormone is computer memory unit, and therefore the unit for rate is bits per second, therefore the UTC for one knowledge frame is 8(L + Lh)/2M.

2.1.2 Operations at the End:

1. Upon receiving the RTS, the top sends a CTS back when SIFS. The CTS contains the situation data of the top, the FLAG_F, and therefore the sending power for the transmission mechanism PDs (in the shape of dBm, occupying four bytes), that is employed for the doable relay competition.

2. within the case that FLAG_F is one, if the top has not detected any ETH inside TRmaxBack o f f +TRCTS +TRETH+SIFS, it assumes that the transmission mechanism are going to be performed and waits for the information packet from the beginning.

3. Otherwise, the top waits for the information packets from the beginning and winning relay. If the top will rewrite the combined signals properly, it sends back associate ACK. Otherwise, it simply lets the beginning timeout and convey.

2.1.3. Operations at the Relay

1. Any terminal that receives each RTS and CTS (with FLAG_F equals 1) and doesn't interfere with different transmissions in its neck of the woods may be thought to be a relay candidate. Upon receiving the CTS, every relay candidate checks whether or not it's able to scale back the whole energy consumption by

$(2PDs-PCs-PCr-2P')\times(X+Xh)/2M-$

$(PCrP')\times TRII-(P+3P)\times TR_{ETH}>0$ (1)

 PCs and PCr sit down with the sending power within the cooperative transmission mode for begin and relay PDs and P sit down with the sending power within the transmission mechanism mode for begin and therefore the mounted sending power severally.Term(2PDs-PCs-PCr- 2P')×(X+Xh)/2M denotes the saved energy consumption in sending the information by CC, term(PCr+P')×TR$_{II}$and(P+3P')×TR$_{ETH}$ denotes the extra energy consumption on management overhead. By Eqn. (1), the relay checks whether or not CC will scale back the whole energy consumption each on sending and receiving, compared to transmission mechanism. each capable relay candidate (satisfies Eqn. (1)), starts a backoff timer when SIFS interval.

2. Intuitively, the backoff at an improved relay expires earlier, thus the simplest relay can channel associate ETH initial. The lost relays quit competition once sensing the ETH. The ETH contains the best sending power PCs for the beginning (in the shape of dBm, occupying four bytes).

3. when SIFS, the winning relay broadcasts the II message mistreatment power PCr . II message is employed to confirm the interference vary of the relay with the target to reinforce the spacial recycle.

III. Performance Evaluation

In this section, we tend to assess WEAL-CMAC via in depth simulations examination with IEEE 802.11 DCF and Coop- macintosh [11]. Since the aim of our theme is to prolong the network period of time and increasing the energy potency, the analysis metrics during this paper square measure the sending power, total energy consumption, network period of time, aggregate

RTS	120bits	Noise power	-80 dbm
CTS	124bits	Fixedtransmit power	30 dbm
ACK	192bits	Data rate	3mbps
ETH	172bits	Pathloss exponent	5
II	60 bits	Initial energy E	3 j
PHYheader	162bits	Energy Threshold	30
MACheader	162bits	Powerthreshold ^p	2 dbm
Unit time T	0.1ms	Circuitry power	9,12,15db m

Table I.

The sending power denotes the facility consumed at transmit electronic equipment (without the facility consumed at transmit circuitry). the whole energy consumption is that the summation of the sending (including each transmit electronic equipment and circuitry) and receiving energy value at the beginning, finish and relay. The period of time is outlined because the length from the network low-level formatting to the time that the primary terminal runs out of power. To validate the performance enhancements in WEAL-CMAC, we tend to utilize each the single-hop situation and therefore the multi-hop multi-connection situation. The simulation is disbursed in QualNet network machine [13]. The initial energy of all the terminals square measure set to one J. The propagation channel of 2 ray path loss model is adopted. Constant rate with one Mbps is employed in WEAL-CMAC and DCF, whereas custom-made knowledge rates with one, 2, 5.5 Mbps square measure utilized in CoopMAC. The mounted sending power used for management frames is ready to twelve dBm and, the mounted sending power used for knowledge border CoopMAC is ready to seventeen dBm as a result of the high rate (the sending power for the information frames in WEAL-CMAC and DCF is dynamically allocated). The simulation settings and parameters are listed in Table I.

3.1. Single hop scenario
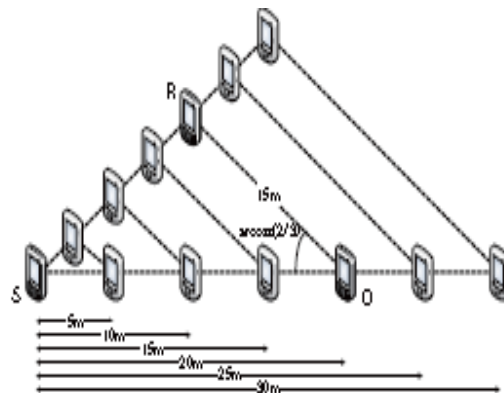
Fig.2 An Illustration Of The Single-Hop Scenario

We 1st compare our WEAL-CMAC with the IEEE 802.11 DCF during a single-hop state of affairs that solely consists of 3 terminals (one begin, one finish and one relay), to indicate the variations between cooperative and non-cooperative communication on energy consumption. As shown in Fig two, the space between begin and finish changes from five m to thirty m, and angles ∠SER and ∠ESR keep at arccos(2/3). Fig. 3shows the variance of the transmission power to satisfy totally different outage likelihood necessities, once the

space between begin and finish is twenty m. it's simple that prime outage likelihood demand results in high price in terms of transmission power. we have a tendency to observe that for the specified rate and outage likelihood, the transmission power for cooperative transmission is way but the one for transmission mechanism. Since the likelihood of success ninety nine.9% is suitable for many of the wireless network applications, the simulation study within the remainder of this paper square measure all supported the outage likelihood zero.1%.
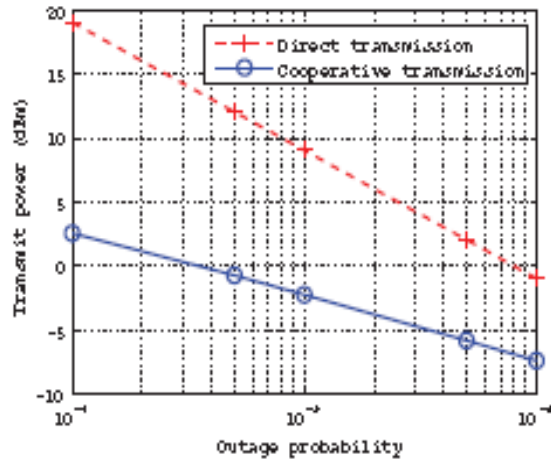
FIG3. Transmitting Power Versus Outage Probability
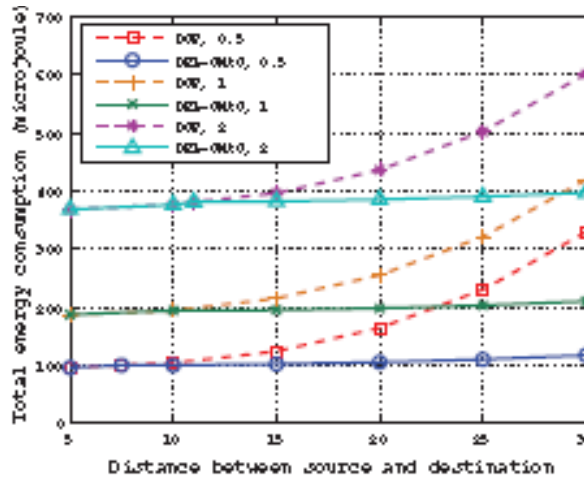
FIG4. Energy Consumption Versus S-D Distance

3.2 Multi-hopMulti-connection Scenarios

Next, we have a tendency to illustrate the performance of WEAL-CMAC in a very realistic multi-hop multi-connection state of affairs along side IEEE 802.11 DCF and CoopMAC. This complicated state of affairs takes the interference and collision caused by totally different connections under consideration. As shown in Fig. 5,
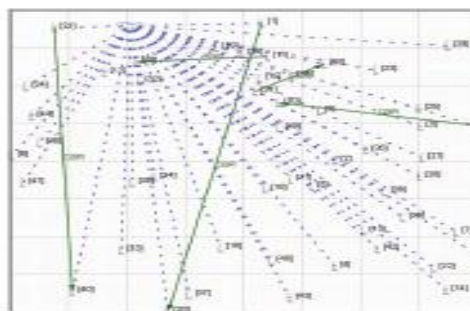
FIG5. A Snapshot Of The Multi-Hop Network

Square measure at random placed in a very sq. space of 250 × 250m2. The dotted lines indicate that every one the terminals belong to constant subnet. The five solid lines indicate that five Constant Bit Rate (CBR) connections, within which starts (nodes one, 11, 21, 31, 41) transmit UDP-based traffic at one packet per one hundred milliseconds to the ends (nodes thirty, 40, 50, 60, 20) through multi-hop. the info payload length is about to 1024 bytes (unless declared otherwise). AODV [14] routing protocol is employed to determine the routing methods, that is wide utilized in MANETs. different routing protocols as DSR or energy aware routing protocol may be used, the performance of the projected macintosh layer theme is freelance of network layer schemes.

IV. Conclusion

In this paper, we've got projected a completely unique distributed energy adaptational location-based cooperative macintosh protocol for MANETs. By introducing WEAL-CMAC, each energy advantage and placement advantage may be exploited so the network period is extended considerably. we've got additionally projected an efficient relay choice strategy to settle on the most effective relay terminal and a cross-layer best power allocation theme to line the sending power. Moreover, we've got increased the abstraction employ to attenuate the interference among totally different connections by exploitation novel NAV settings. we've got incontestable that WEAL-CMAC will considerably prolong the network period comparison with the IEEE 802.11 DCF and CoopMAC, at comparatively low outturn and delay degradation price. As a future work, we'll investigate our WEAL-CMAC for larger scale network size and with high quality. we'll additionally bear in mind to develop an efficient cross-layer cooperative diversity-aware routing formula along side our DELCMAC to conserve energy whereas minimizing the outturn and delay degradation.

REFERENCES

[1] K. J. R. Liu, A. K. Sadek, W. Su, and A. Kwasinski, Cooperative Communications and Networking. Cambridge, 2008.
[2] Y. W. P. Hong, W. Huang, and C. C. J. Kuo, Cooperation Communications and Networking: Technology and System Design. Springer,2010.
[3] A. Sendonaris, E. Erkip, and B. Aazhang, "User cooperation diversity - Part I: System description," IEEE Trans. Commun., vol. 51,no. 11, pp. 1927–1938, 2003.
[4] P. Liu, Z. Tao, S. Narayanan, T. Korakis, and S. S. Panwar, "CoopMAC: A cooperative MAC for wireless LANs," IEEE J. Select. Areas Commun., vol. 25, no. 2, pp. 340–354, 2007.
[5] R. Ahmad, "Performance analysis of relay based cooperative MAC protocols," Ph.D. dissertation, Victoria University, 2010.
[6] W. Zhuang and M. Ismail, "Cooperation in wireless communication networks," IEEE Wireless Commun. Mag., vol. 19, no. 2, pp.10–20, 2012.
[7] A. Sendonaris, E. Erkip, and B. Aazhang, "User cooperation diversity - Part II: Implementation aspects and performance analysis," IEEE Trans. Commun., vol. 51, no. 11, pp. 1939–1948, 2003.
[8] J. N. Laneman, D. N. C. Tse, and G. W. Wornell, "Cooperative diversity in wireless networks: Efficient protocols and outage behavior," IEEE Trans. Inform. Theory, vol. 50, no. 12, pp. 3062–3080, 2004.
[9] G. Kramer, M. Gastpar, and P. Gupta, "Cooperative strategies and capacity theorems for relay networks," IEEE Trans. Inform. Theory, vol. 51, no. 9, pp. 3037–3063, 2005.
[10] T. E. Hunter and A. Nosratinia, "Diversity through coded cooperation," IEEE Trans. Wireless Commun., vol. 5, no. 2, pp. 283–289, 2006.
[11] S. Cui, A. J. Goldsmith, and A. Bahai, "Energy-efficiency of MIMO and cooperative MIMO in sensor networks," IEEE Journal on Selected Areas in Communications, vol. 22, no. 6, pp. 1089.1098, Aug. 2004.
[12] P. Liu, Z. Tao, S. Narayanan, T. Korakis, and S. S. Panwar, "Coop- MAC: a cooperative MAC for wireless LANs," IEEE J. Selected Areas in Commun., vol. 25, pp. 340-354, Feb. 2007.
[13] http://www.scalable   networks.com/products/qualnet/
[14] C. E. Perkins, and E. Royer, "Ad-hoc On-demand Distance Vector Routing," IEEE Workshop on Mobile Computing Systems and Applications, 1999.

BIOGRAPHIES

M.Naresh is an PG Scholor in the Department of Computer science & engineering, Sir Vishveshwariah Institute of Science and Technology, Madanapalli. He received the B.Tech degree in information technology from JNTU University in 2012.His research include mobile computing, wireless networks.

Gudditti.Viswanath is born in 1982 in India. He is graduated in **B.C.A** from Osmania University, Hyderabad, post graduated in **M.C.A** from S.K. University and second post graduated in **M.Tech** from JNTU Anantapur. He is currently working as a Assistant professor in the department of Computer science and engineering at Sir Vishveshwariah Institute of Science and Technology, Madanapalli. , Chittoor.

T. Sunil Kumar Reddy is an associate professor in the Department of Computer science & engineering at Sir Vishveshwariah Institute of Science and Technology, Madanapalli. He received the B.Tech degree in Information Technology from Satyabhama University in 2005, the M.Tech degree in Information Technology from V.I.T University in 2007and he is pursuing PhD degree in computer science & engineering from JNTUA University, Anantapur. His research interests include Cloud Computing, High performance computers, Wireless Networks.

A Threshold Fuzzy Entropy Based Feature Selection: Comparative Study

Miss. K.Barani[1], Mr. R.Ramakrishnan[2]

[1, 2](PG Student, Associate Professor, Sri Manakula Vinayagar Engineering College, Pondicherry-605106)

Abstract: *Feature selection is one of the most common and critical tasks in database classification. It reduces the computational cost by removing insignificant and unwanted features. Consequently, this makes the diagnosis process accurate and comprehensible. This paper presents the measurement of feature relevance based on fuzzy entropy, tested with Radial Basis Classifier (RBF) network, Bagging(Bootstrap Aggregating), Boosting and stacking for various fields of datasets. Twenty benchmarked datasets which are available in UCI Machine Learning Repository and KDD have been used for this work. The accuracy obtained from these classification process shows that the proposed method is capable of producing good and accurate results with fewer features than the original datasets.*

Keywords: *Fuzzy entropy, Feature selection, RBF network, Bagging, Boosting, Stacking, Fuzzy C-means clustering algorithm.*

I. Introduction

Data mining is the process of efficient discovery of non-obvious valuable patterns from a large collection of data. It has been discussed widely and applied successfully in the field of medical research, scientific analysis and business applications. Feature selection has many advantages such as shortening the number of measurements, reducing the execution time and improving transparency and compactness of the suggested diagnosis.

Feature selection is the process of selecting a subset of'd' features of the set D, such that d ≤ D. the primary purpose of the feature selection is to reduce the computational cost and improve the performance of the learning algorithm. Feature selection deals with different evaluation criteria and generally, are classified into filter and Wrapper models. The filter model evaluates the general characteristics of the training data to select the feature subset without relation to any other learning algorithms, thus, it is computationally economical. Nevertheless, it carries the risk of selecting subset of features that may not be relevant. The wrapper models which requires a pre-determined induction algorithm, which assesses the performance of the features that are chosen. The selected features are related significantly to the choice of the classifier and do not generalize to other classifiers. However, this tends to be computationally expensive. Therefore, the filter and wrapper model would complement each other; wrapper models provide better accuracy, whereas filter models search the feature space efficiently.

This paper proposes a filter-based feature subset selection based on fuzzy entropy measures and presents the different selection strategies for handling the datasets. The proposed method is evaluated using RBF network, Bagging, Boosting and stacking for the given benchmarked datasets.

II. Literature Review

Recently, a number of researchers have focused on several feature selection methods and most of them have reported their good performance in database classification. Battiti [7] proposes a method called Mutual-Information-based Feature Selection (MIFS), in which the selection criterion is based on maximizing the mutual information between candidate features and the class variables, and minimizing the redundancy between candidate features and the selected features. Hanchuan et al. [8] follow a similar technique to MIFS, which has been called the minimal-redundancy-maximal-relevance (mRMR) criterion. It eliminates the manually tuned parameter with cardinality of the features already selected. Pablo et al. [9] present a Normalized Mutual Information Feature Selection algorithm. The mutual information among features should be divided by the minimum value of their entropies in order to produce a normalized value, which is to be measured by the redundant term. Yu and Liu [10] developed a correction-based method for relevance and redundancy analysis and then removed redundant features using the Markov Blanket method.

In addition, feature selection methods are analyzed by a number of techniques. Abdel-Aal [1] developed a novel technique for feature ranking and selection with the group method of data handling. Feature reduction of more than 50% could be achieved and improved in the classification performance. Sahanetal [11] built a new hybrid machine learning method for a fuzzy-artificial immune system with a k-nearest neighbour algorithm to solve medical diagnosis problems, which demonstrated good results. Jaganathan etal. [12] Applied a new improved quick reduct algorithm, which is a variant of quick reduct for feature selection and tested it on a classification algorithm called AntMiner. Sivagami Nathan et al. [13] proposed a hybrid method combining Ant Colony Optimization and Artificial Neural Networks (ANNs) to deal with feature selection, which produced promising results. Lin et al. [14] proposed a Simulated Annealing approach for parameter setting in Support Vector Machines, which is compared with a grid search parameter setting and was found to produce higher classification accuracy.

Lin et al. [15] applied a Particle-Swarm-Optimization-based approach to search for appropriate parameter values for a back-propagation network to select the most valuable subset of features to improve classification accuracy. Unler et al [16] developed a modified discrete particle swarm optimization algorithm for the feature selection problem and compared it with tabu and scatter search algorithms to demonstrate its effectiveness. Chang et al [17] introduced a hybrid model for integrating a case-based reasoning approach with a particle swarm optimization model for feature subset selection in medical database classification. Salamo et al [18] evaluated a number of measures for estimating feature relevance based on rough set theory and also proposed three strategies for feature selection in a Case Based Reasoning classifier. Qasem et al [19] applied a time variant multi-objective particle swarm optimization to an RBF Network for diagnosing medical diseases.

This paper describes in detail how to combine the relevance measures and feature subset selection strategies.

III. Fuzzy Entropy-Based Relevance Measure

In information theory, the Shannon entropy measure is generally used to characterize the impurity of a collection of samples. Assuming X as a discrete random variable with a finite set of n elements, where X={x1, x2, x3,…,xn}, then if an element x_i occurs with probability $p(x_i)$, the entropy H(X) of X is defined as follows:

$$H(X) = -\sum_{i=1}^{n} p(x_i) \log_2 p(x_i) \qquad (1)$$

Where n denotes the number of elements.

An extension of Shannon entropy with fuzzy sets, which is used to support the evaluation of entropies, is called fuzzy entropy. It was introduced in 1972, after which a number of modifications were introduced to the original fuzzy entropy method.

The proposed fuzzy entropy method is based on the utilization of the Fuzzy C-Means Clustering algorithm (FCM), which is used to construct the membership function of all features. The data may belong to two or more clusters simultaneously and the belonging of a data point to the clusters is governed by the membership values. Similar data points are placed in the same cluster and dissimilar data points normally belong to different clusters. The membership values of the data points are reorganized iteratively to reduce the dissimilarity. The Euclidean distance is used to measure the dissimilarity of two data points.

The FCM algorithm is explained as follows.

Step1: assume the number of clusters(C), where $2 \leq C \leq N$, C – number of clusters and N – number of data points.

Step2: calculate the jth cluster center C_j using the following expression

$$C_J = (\sum_{i=1}^{N} \mu_{ij}^{g} x_{ij}) / (\sum_{i=1}^{N} \mu_{ij}^{g}) \qquad (2)$$

where $g \geq 1$ is the fuzziness coefficient and μ_{ij} is the degree of membership for the ith data point x_i in cluster j.

Step3: calculate the Euclidean distance between the ith data point and the jth cluster center as follows:

$$d_{ij} = |C_{ij} - x_i| \qquad (3)$$

Step4: update the fuzzy membership values according to d_{ij}. If $d_{ij} \geq 0$, then

$$\mu = 1/(\sum_{m=1}^{C} (d_{ij}/d_{im})^{2/(g-1)}) \qquad (4)$$

If d=0, then the data point coincides with the jth cluster center (C) and it will have the full membership value, i.e., $\mu_{ij} = 1.0$

Step5: repeat Steps 2–4 until the changes in $[\mu]$ are less than some pre-specified values.

The FCM algorithm computes the membership of each sample in all clusters and then normalizes it. This procedure is applied for each feature. The summation of membership of feature 'x' in class 'c', divided by the membership of feature 'x' in all 'C' classes, is termed the class degree CDc($\check{A}$), which is given as:

$$CD_c(\check{A}) = \sum_{x \in c} \mu_{\check{A}}(x) / \sum_{x \in C} \mu_{\check{A}}(x) \qquad (5)$$

Where $\mu_{\check{A}}$ denotes the membership function of the fuzzy set and $\mu_{\check{A}}(x_i)$ denotes the membership grade of x belonging to the fuzzy set $\check{A}$.

The fuzzy entropy FEc ($\check{A}$) ofclass 'c' is defined as

$FE_c(\breve{A})=-CD_c(\breve{A})\log_2 CD_c(\breve{A})$ (6)

The fuzzy entropy $FE(\breve{A})$ of a fuzzy set X is defined as follows:

$FE(\breve{A})=\sum_{c\epsilon C} FE_c(\breve{A})$ (7)

The probability $p(x_i)$ of Shannon's entropy is measured by the number of occurring elements. In contrast, the class degree $CDc(\breve{A})$ in fuzzy entropy is measured by the membership values of the occurring elements and the highest fuzzy entropy value of the feature is regarded as the most informative one.

IV. Feature Selection Strategies

This section explains three different criteria for the feature selection process. The features are regulated with respect to decreasing values of the fuzzy entropy. A feature in the first position is the most relevant and the one in the last position is the least relevant in the resulting rank vector. The framework of feature selection is depicted in Fig. 1.
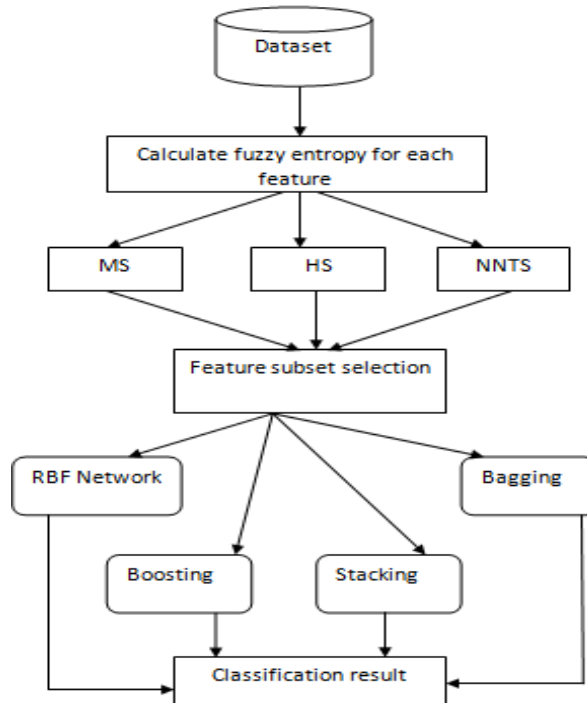
Fig 1

Mean Selection (MS) Strategy: A feature f ϵ F is selected if it satisfies the following condition:

$$\sigma(f) \geq \sum_{f \epsilon F} \sigma(f)/|F|$$

where $\sigma(f)$ is the relevance value of the features, which is selected if it is greater than or equivalent to the mean of the relevant values. This strategy will be useful in examining the suitability of the fuzzy entropy relevance measure.

Half Selection (HS) Strategy: The half selection strategy aims to reduce feature dimensionality to select approximately 50% of the features in the domain. The feature f ϵ F is selected if it satisfies the following condition:

$P_a \geq |F|/2$

Where Pa is the position of the feature in the rank vector. It represents the selected features having a relevance value higher than a given threshold, which is calculated as $|F|/2$. This strategy does produce great reductions, close to 50%. At the same time, some of the selected features are irrelevant despite them passing the threshold. Similarly, some of the omitted features may also be relevant despite them not being selected. This suggests that a new feature selection strategy must be based on the relevance value of each feature instead of a predefined number of features that are to be reduced. The last feature selection strategy described below has a relatively smaller number of features but at the same time, it retains the most relevant.

Neural Network for Threshold Selection (NNTS): An ANN is one of the well-known machine learning techniques and it can be used in a variety of applications in data mining. The ANN provides a variety of feed forward networks that are generally called back propagation networks. It possesses a number of inter- connected

layers that consist of an input layer, a hidden layer and an output layer. The fuzzy entropy value of each feature is an initial value for each node in the input layer. The value from the input layer to the output layer is achieved by hidden layers using weights and activation functions. A sigmoid function is used as an activation function and a learning rate coefficient determines the size of weight adjustments made at the each iteration. An output layer is used to represent an output value. The output value can be considered as a threshold value of the given fuzzy entropy.

V. Methodology Description

There are four methodologies used for calculating an accuracy after the features are selected using the above three strategies.

RBF Network:

An RBF network is a type of ANN, which is simpler network structure with better approximation capabilities. It is an artificial neural network that uses the radial basis function as the artificial network. Radial basis function is the real-valued function whose values depends on distance from origin or any other point called as C.RBF can be used as kernel in support vector classification.RBF network trains the hidden layer in unsupervised manner.

Bagging:

Bagging (Bootstrap Aggregating) is a machine learning ensemble meta algorithm that is used to find the stability and accuracy of the training data. This method creates separate samples of the training dataset and classifier for each sample. The result of multiple classifiers is combined to find accuracy.

Bagging leads to improvements in unstable procedures. It helps to reduce variance avoids over fitting. This is the special case of model averaging approach.

Boosting:

Boosting is an ensemble method that starts out with a base classifier that is prepared on the training data. A second classifier is then created behind it to focus on the instances in the training data that the first classifier goes wrong. The process continues to add classifiers until a limit is reached in the number of models or accuracy. It helps to remove noisy data and removes outliers.

Stacking:

Stacking also called Blending or Stacked generalization. It is an ensemble method where multiple different algorithms are prepared on the training data and a Meta classifier is prepared that learns how to take the predictions of each classifier and make accurate predictions on unseen data.

It involves training learning algorithms to combine predictions of several other learning algorithms. First, all of the other algorithms are trained using the available data, then a combiner algorithm is trained to make a final prediction using all the predictions of the other algorithms as additional inputs. It combines algorithms like ID3 and J48.

ID3: Generates decision tree from the dataset and is used in machine learning and natural language processing domains. It begins with original set S at the root node and iterates through unused attribute of the set. It is calculated using Entropy and information gain value.

J48: It is the extension of ID3 algorithm. It is used to generate decision tree that can be used for classification and so it is called as statistical classifier.

VI. Dataset Description

The performance of the proposed method is evaluated using several benchmarked datasets.

DATASET	NO OF FEATURES	NO OF INSTANCES
Diabetes	768	8
Hepatitis	155	19
Heart-Statlog	270	13
Wisconsin breast cancer	699	9
Grub damage	155	8
White clover	63	31
Squash unstored	52	23
Squash stored	50	23
Tic-tac-toe	51	9
Chess	42	6

Dermatology	105	34
Car	1117	6
Liver disorder	187	6
Hypothyroid	312	29
Pasture	36	22
Eggs	48	3
Fiber	48	4
Ionosphere	351	34
Balance	17	3
Cleveland heart disease	302	13

1. Wisconsin breast cancer:
The dataset was collected by Dr.William H.Wolberg (1989– 1991) at the University of Wisconsin– Madison Hospitals. It contains 699 instances characterized by nine features: (1) Clump Thickness, (2) Uniformity of Cell Size, (3) Uniformity of Cell Shape, (4) Marginal Adhesion, (5) Single Epithelial Cell Size, (6) Bare Nuclei, (7) Bland Chromatin, (8)Normal Nucleoli and (9)Mitoses, which are used to predict benign or malignant growths. In this dataset, 241(34.5%) instances are malignant and 458(65.5%) instances are benign.

2. Pima Indians diabetes:
The dataset is available at the National Institute of Diabetes and Digestive and Kidney Diseases. It contains 768 instances described by eight features used to predict the presence or absence of diabetes. The features are as follows: (1) number of pregnancies, (2) plasma glucose concentration, (3) diastolic blood pressure, (4) triceps skin fold thickness,(5) serum insulin, (6)body mass index, (7)diabetes pedigree function and (8)age in years.

3. Heart-Statlog:
The dataset is based on data from the Cleveland Clinic Foundation and it contains 270 instances belonging to two classes: the presence or absence of heart disease. It is described by13 features (age, sex, chest, resting blood pressure, serum cholesterol, fasting blood sugar, resting electro cardiographic, maximum heart rate, exercise induced angina, old peak, slope, number of major vessels and thal).

4. Hepatitis:
The dataset is obtained from the Carnegie–Mellon University and it contains 155 instances belonging to two classes: live or die. There are 19 features (age, sex, steroid, antivirals, fatigue, malaise, anorexia, liver big, liver film, spleen palpable, spiders, ascites, varices, bilirubin, alk phosphate, SGOT, albumin, protime and histology).

5. Cleveland heart disease:
The dataset was collected from the Cleveland Clinic Foundation and contains about 296 instances, each having 13 features, which are used to infer the presence or absence of heart disease. The features are (1) age, (2)sex, (3)chest pain type, (4)resting blood pressure, (5) cholesterol, (6)fasting blood sugar, (7)resting electro cardio- graphic results, (8)maximum heart rate, (9)exercise induced angina, (10)depression induced by exercise relative to segment, (11)slope of peak exercise, (12) number of major vessels and (13)thal.

6. Chess:
The dataset consist of 6 attributes namely:(1)White_king_file,(2) White_king_rank (3)White_rook_file, (4)White_rook_rank, (5) Black_king_file ,(6)Black_king_rank and two classes like win or lose for 42 instances.

7. Grub_damage:
The dataset consists of 158 instances consisting of attributes like year-zone, year, strip, pdk, damage- rankRJT, damage-rankALL, dry_or_irr and zone with two classes: low or high.

8. Pasture:
This dataset contains two classes like low or high with 22 attributes like fertilizer, slope, aspect_dev_NW, OLsenP, MinN, TS, Ca-Mg, LOM, NFIX, Eworms-main-3, Eworms-No-Species, KUnset, OM,Air-Perm, Porosity, HFRG-pct-mean, jan-mar-mean-TDR, Annual-mean-Runoff, root-surface-area and Leaf-p.

9. Squash-stored:
The dataset containing two class and 50 instances with 24 attributes like site, daf, fruit, weight, storewt, lene, solids, brix, a*, egdd, fgdd, ground slot a*, glucose, fructose, sucrose, total, glucose+fructose, starch, sweetness, flavor, dry/moist, fiber, heat inlut emerg and heat inlut flower.

10. Squash-Unstored:

The dataset containing two class and 52 instances with 23 attributes like site, daf, fruit, weight, lene, solids, brix, a*, egdd, fgdd, groundslot_a*, glucose, fructose, sucrose, total, glucose+fructose, starch, sweetness, flavor, dry/moist, fiber, heat_inlut emerg and heat inlut flower.

11. Tic-tac-toe:

This dataset contains 51 instances with 9 attributes like top-left-square, top-middle-square, middle-left-square, middle-middle-square, middle-right-square, bottom-left-square, bottom-middle-square and bottom-right-square with two classes.

12. White-clover:

The dataset contains 63 instances with two classes and with 31 attributes like strata, plot, paddock, whiteclover-91, bareground-91, cocksfoot-91, othergrasses-91, otherlegumes-91, RyeGrass-91, Weeds-91, whiteclover-92, bareground-92, cocksfoot-92, othergrasses-92, otherlegumes-92, RyeGrass-92, weeds-92, whiteclover-93, bareground-93, cocksfoot-93, othergrasses-93, otherlegumes-93, RyeGrass-93, weeds-93, whiteclover-94, bareground-94, cocksfoot-94, othergrasses-94, otherlegumes-94, RyeGrass-94, weeds-94 and strata combined. The classes may be either yes or no.

13. Balance:

The dataset contains two classes with 17 instances and 3 attributes like Subject no, forward-backward and side-side.

14. Car:

This contains 1117 instances with 6 attributes like buying, maint, doors, persons, lug boot and safety with two classes.

15. Dermatology:

This dataset contains 105 instances with 34 attributes and two classes. The attributes are like erythema, scaling, definite borders, itching, koebner phenomenon, polygonal papulus, follicular papulus, oral mucosal involvement, knee and elbow involvement, Scalp involvement, family history, melanin incontinence, eosinophils in the infiltrate, PNL infiltrate, fibrosis of the papillary dermis, exocytosis, acanthosis, hyperkeratosis, parakeratosis, clubbing of the rete ridges, thinning of the suprapapillary epidermis, spongiform pastule, munro microabcess, focal hypergranulosis, disappearance of the granular layer, vacuolisatio and damage of basal layer, spongiosis, saw-tooth appearance of the retes, follicular horn plug, perifollicular parakeratosis, inflammatory monoluclear inflitrate, band-like infiltrate and age. The class defines either present or absent.

16. Hypothyroid:

The dataset contains 29 attributes for 312 instances. The attributes are as: age, sex, on thyroxine, query on thyroxine, on antithyroid medication, sick, pregnant, thyroid surgery,I131 treatment, query hypothyroid, query hyperthyroid, lithium, goiter, tumor, hypopituitary, psych, TSH measured, TSH, T3 measured, T3, TT4 measured, TT4,,T4U measured, T4U,FTI measured, FTI, TBG measured, TBG, referral source with class negative or positive.

17. Eggs:

The dataset contains 3 attributes like Gat_content, Lab, and Technician with two classes G and H for 48 instances.

18. Fiber:

This dataset contains two classes yes or no with 4 attributes. The attributes considered are cracker, diet, and subject and digested.

19. Ionosphere:

This dataset contains 34 attributes from a01to a34 for 351 instances and consists of two classes 1 or 2.

20. Liver-disorder:

The dataset contains mcz, alkphos, sgpt, sgot, gammagt, drinks as attributes for 187 instances with two classes 1 or 2.

VII. Result

The selected features from the three strategies are tested with RBF network, Bagging, Boosting and stacking to calculate the accuracy.

7.1 Wisconsin Breast Cancer:

In fig 2, the report is clearly depicted and is found that Bagging and Boosting yields the highest accuracy of 99.57 in mean selection strategy.
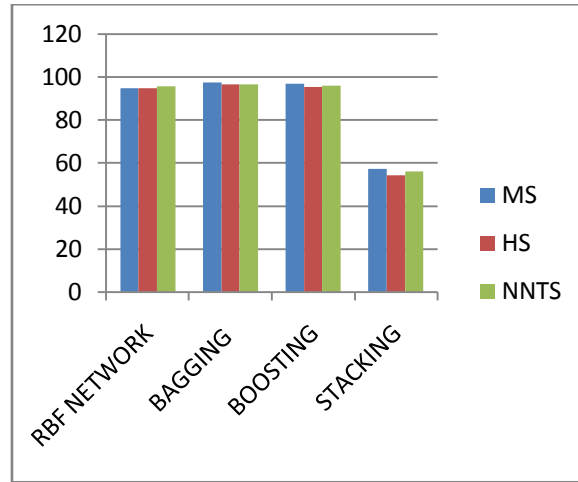
Fig 2

7.2 Pima Indian Diabetes:

In fig 3, the report is clearly depicted and is found that Bagging yields the highest accuracy of 100.0 in mean selection strategy.
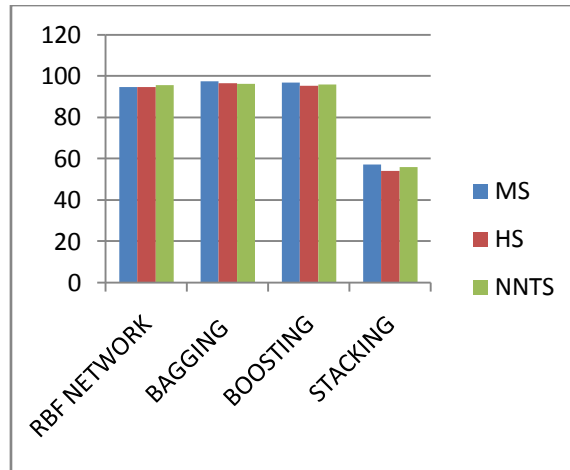
Fig 3

7.3 Heart- Statlog:

In fig 4, the report is clearly depicted and is found that Bagging and Boosting yields the highest accuracy of 99.62 in mean selection strategy.
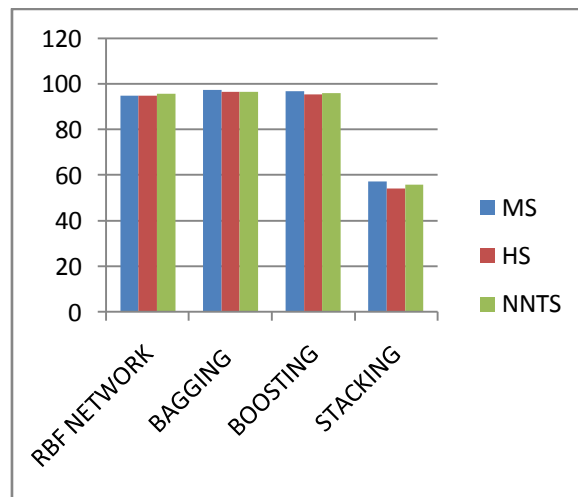
Fig 4

7.4 Hepatitis:

In fig 5, the report is clearly depicted and is found that RBF network yields the highest accuracy of 90.32 in half selection strategy.
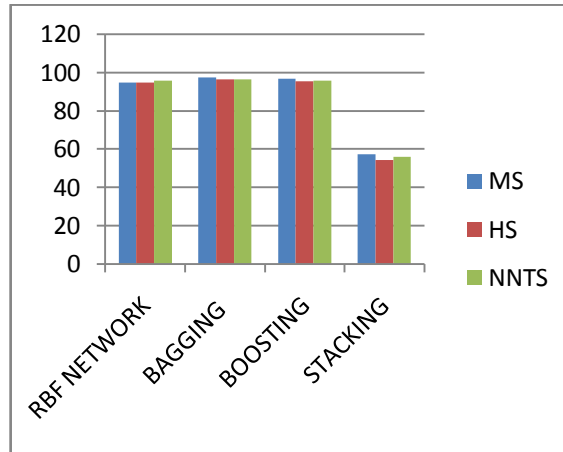
Fig 5

7.5 Cleveland heart Disease:

In fig 6, the report is clearly depicted and is found that RBF network yields the highest accuracy of 99.00 in neural network for threshold selection strategy.
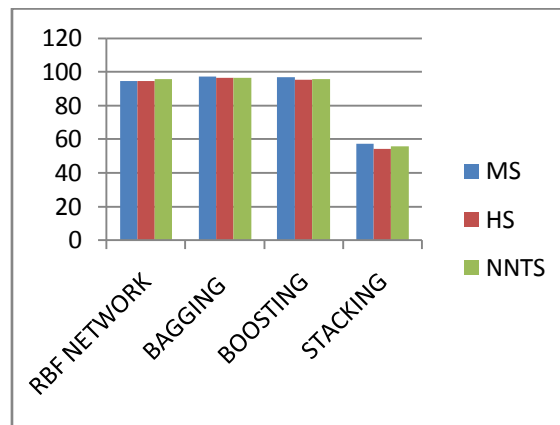
Fig 6

7.6 Chess:

In fig 7, the report is clearly depicted and is found that Bagging and Boosting yields the highest accuracy of 100 in mean selection strategy.
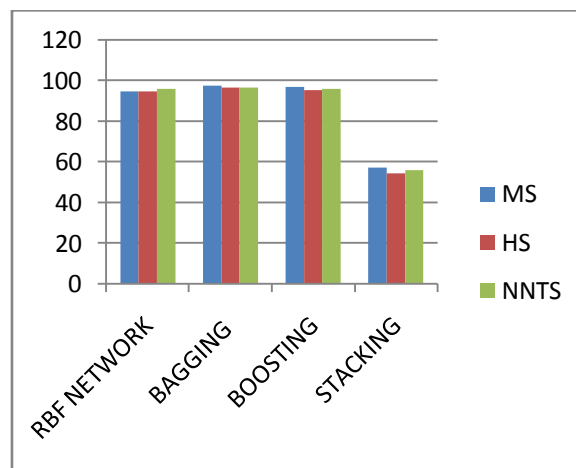
Fig 7

7.7 Grub Damage:
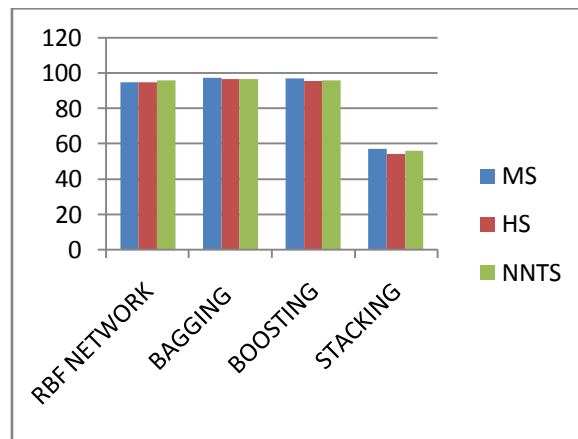
Fig 8

In fig 8, the report is clearly depicted and is found that Bagging and Boosting yields the highest accuracy of 98.06 in mean selection strategy.

7.8 Pasture:

In fig 9, the report is clearly depicted and is found that RBF network yields the highest accuracy of 100.0 in mean selection strategy.
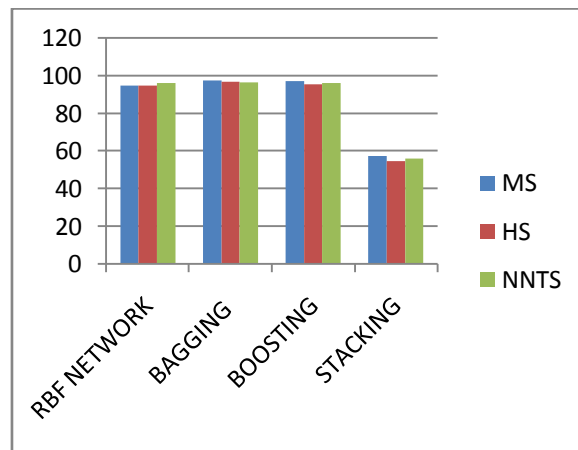
Fig 9

7.9 Squash-Stored:

In fig 10, the report is clearly depicted and is found that Boosting yields the highest accuracy of 98.0 in mean selection strategy.
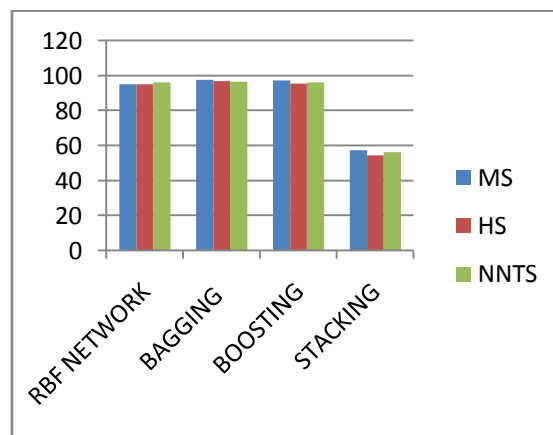
Fig 10

7.10 Squash-Unstored:

In fig 11, the report is clearly depicted and is found that Bagging yields the highest accuracy of 100.0 in mean selection strategy.
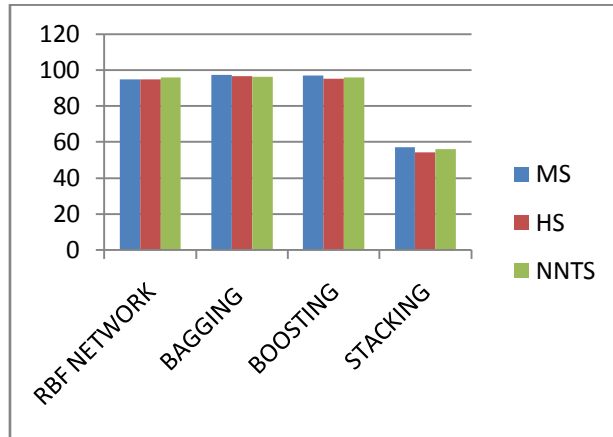
Fig 11

7.11 Tic-tac-toe:

In fig 12, the report is clearly depicted and is found that Bagging and Boosting yields the highest accuracy of 100.0 in mean selection strategy.
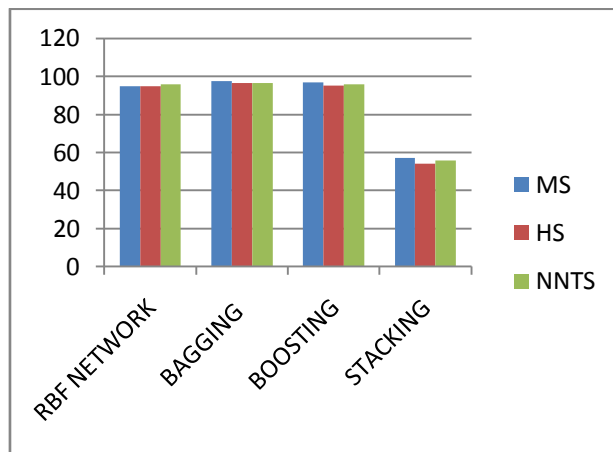
Fig 12

7.12 White- Clover:

In fig 13, the report is clearly depicted and is found that Bagging and Boosting yields the highest accuracy of 96.82 in mean selection strategy.
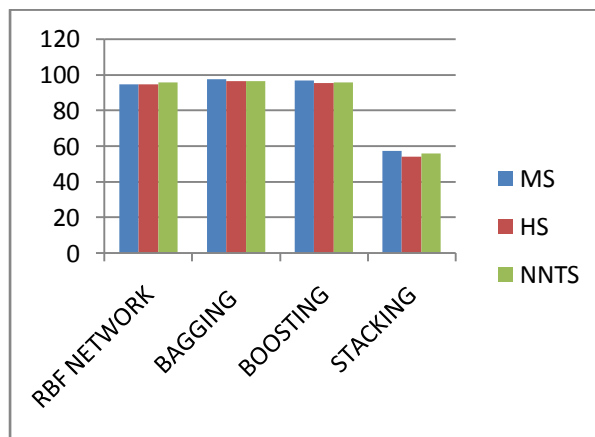
Fig 13

7.13 Balance:
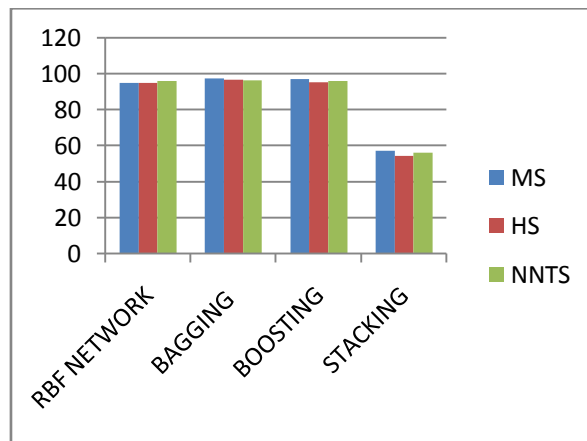
Fig 14

In fig 14, the report is clearly depicted and is found that Bagging and Boosting yields the highest accuracy of 100.0 in mean selection strategy and the same accuracy in RBF network using half selection.

7.14 Car:

In fig 15, the report is clearly depicted and is found that Bagging yields the highest accuracy of 98.06 in neural network for threshold selection strategy.
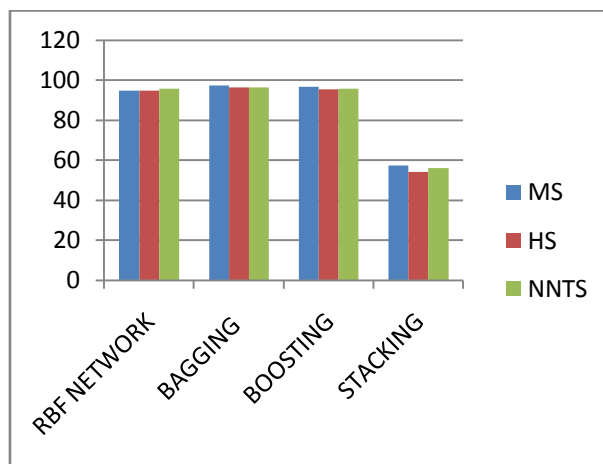
Fig 15

7.15 Dermatology:

In fig 16, the report is clearly depicted and is found that Bagging and Boosting yields the highest accuracy of 99.04 in mean selection strategy.
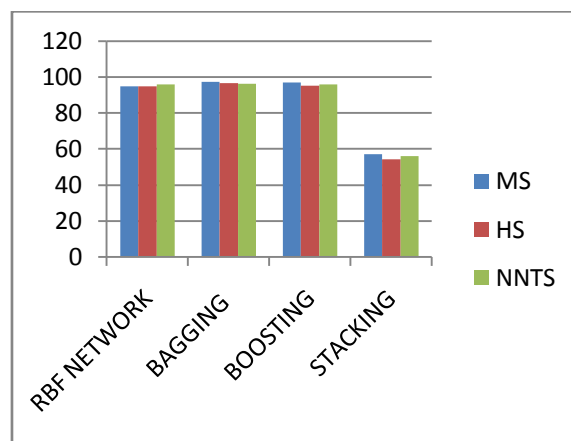
Fig 16

7.16 Hypothyroid:

In fig 17, the report is clearly depicted and is found that all the four methodologies yields the highest accuracy of 94.23 in mean selection strategy.
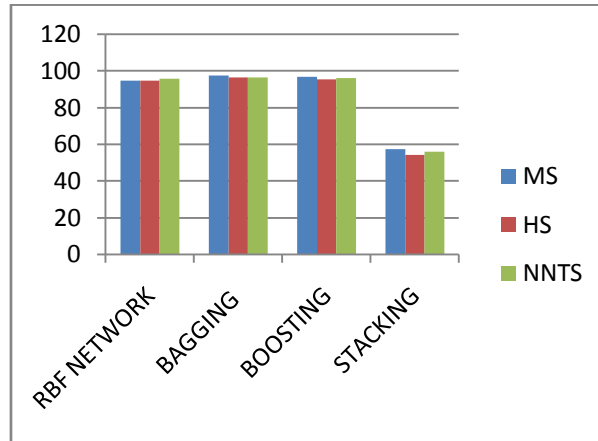
Fig 17

7.17 Eggs:

In fig 18, the report is clearly depicted and is found that RBF network yields the highest accuracy of 100.0 in mean selection strategy.
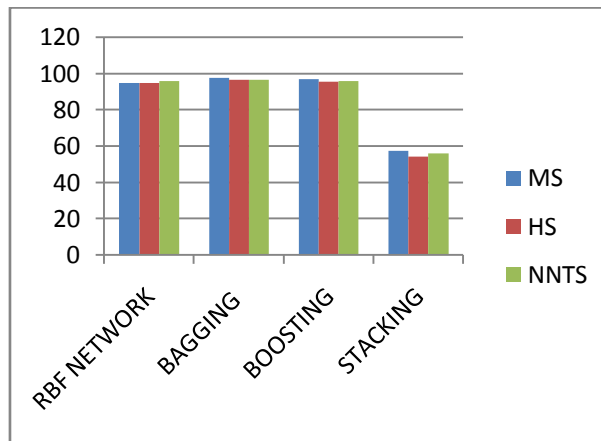
Fig 18

7.18 Fiber:

In fig 19, the report is clearly depicted and is found that Bagging and Boosting yields the highest accuracy of 97.91 in mean selection strategy.
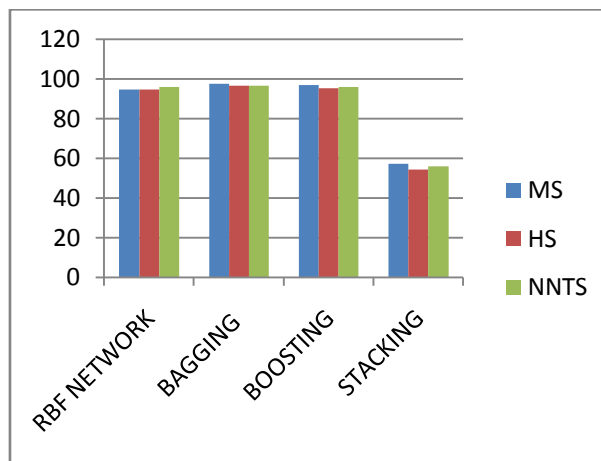
Fig 19

7.19 Ionosphere:

In fig 20, the report is clearly depicted and is found that Boosting yields the highest accuracy of 99.43 in mean selection strategy.
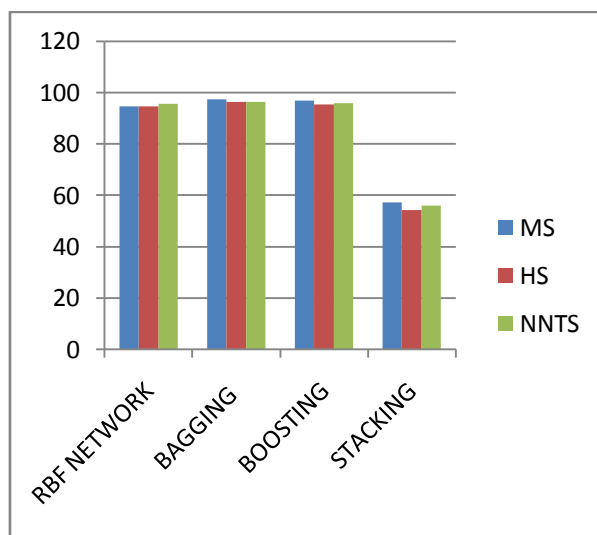
Fig 20

7.20 Liver Disorder:

In fig 21, the report is clearly depicted and is found that Bagging yields the highest accuracy of 97.32 in mean selection strategy.
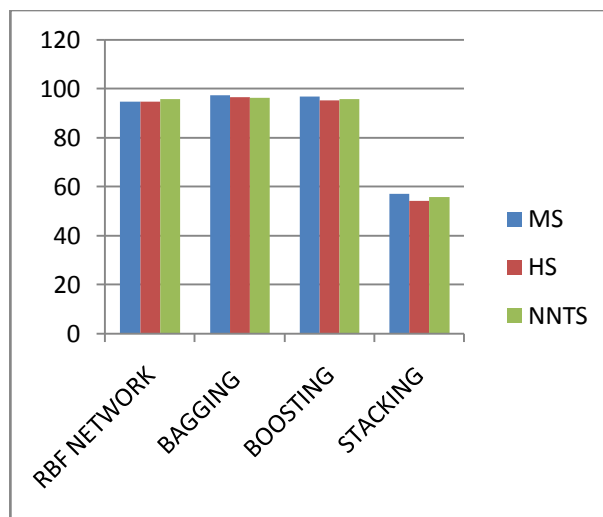
Fig 21

The overall result of the dataset being used is depicted in table 1 and table 2.

Table 1

S.NO	DATASET & ATTRIBUTES	STRATEGY	SELECTED FEATURES	RBF NETWORK	BAGGING	BOOSTING	STACKING
1	Wisconsin Breast Cancer(9)	MS	1,5	99.42	**99.57**	**99.57**	65.52
		HS	2,3,4,6,7,8,9	98.99	98.67	98.07	62.53
		NNTS	All	93.33	98.06	98.04	75.84
2	Pima Indian Diabetes (8)	MS	2,3	98.30	**100**	99.86	65.10
		HS	1,4,5,6,7,8	96.09	99.10	98.36	62.11
		NNTS	2,3	98.30	99.02	98.86	63.80
3	Heart Statlog (13)	MS	1,4,5,8	98.51	**99.62**	**99.62**	55.55
		HS	2,3,6,7,9,10,11,12,13	95.55	98.73	98.12	52.56
		NNTS	1,4,5,8	98.51	98.64	98.62	54.25
4	Hepatitis(19)	MS	1,15,16,18	84.51	89.67	89.67	79.35
		HS	2,3,5,6,7,8,9,10,11,12, 13,14,17,19,4	**90.32**	88.78	88.17	76.36
		NNTS	1,15,16,18	84.51	88.69	88.67	78.05
5	Cleveland Heart Disease(13	MS	4,5,8	98.34	98.67	98.67	3.63
		HS	1,2,3,7,9,10,11,12,13, 6	94.71	97.78	97.17	0.64
		NNTS	1,4,5,8	**99.00**	97.69	97.67	2.33
6	Chess(6)	MS	1,4,6	88.09	**100**	**100**	71.42
		HS	2,3,5	88.09	99.10	98.5	68.44
		NNTS	4,6	88.09	99.02	99.00	70.13
7	Grub Damage(8)	MS	2	96.77	**98.06**	**98.06**	68.38
		HS	1,3,4,5,6,7,8	83.87	97.16	96.56	65.40
		NNTS	2	96.77	97.08	97.06	67.08
8	Pasture(22)	MS	5,6,17,20,22	**100**	88.88	88.88	66.66
		HS	1,2,3,4,7,8,9,10,11,12, 13,14,15,16,18,19,21	80.55	87.99	87.38	63.68
		NNTS	2,3,4,5,6,10,13,16,17, 19,20,21,22	80.55	87.90	87.88	65.36
9	Squash stored(24)	MS	4,5,10,11,19,20,23,24	84.0	90.0	**98.0**	86.0
		HS	1,2,3,6,7,8,9,12,13,14, 15,16,17,18,21,22	86.0	89.10	96.5	83.01
		NNTS	All	86.0	89.02	97.0	84.70
10	Squash Unstored(23)	MS	4,9,10,18,19,22,23	82.69	**100**	98.07	5.76
		HS	1,3,5,6,7,11,12,13,14, 15,16,17,20,21,2	86.53	99.10	96.57	2.78
		NNTS	2,4,5,6,7,8,9,10,11,14, 15,16,17,18,19,20,21, 22,23,	78.84	99.02	97.07	4.47

Table 2

S. NO	DATASET & ATTRIBUTES	STRATEGY	SELECTED FEATURES	RBF NETWORK	BAGGING	BOOSTING	STACKING
11	Tic-tac-toe (9)	MS	2,4,5,7	96.07	**100**	**100**	56.86
		HS	1,3,6,8,9	88.23	99.103	98.5	53.87
		NNTS	All	87.30	95.84	95.82	59.01
12	White Clover(31)	MS	3,4,7,9,13,16,18,20,23,26,27,29	87.30	**96.82**	**96.82**	60.31
		HS	1,2,5,6,8,10,11,12,14,15,17,19,21,22,24,25,28,30,31	82.53	95.92	95.32	57.33
		NNTS	3,4,7,9,13,14,16,18,20,23,26,27,29	87.30	95.84	95.82	59.01
13	Balance(3)	MS	2,3	94.11	**100**	**100**	5.88
		HS	1	**100**	99.10	98.5	2.89
		NNTS	All	94.11	99.02	99.0	4.58
14	Car(6)	MS	3,4	97.31	96.50	96.50	68.66
		HS	1,2,5,6	94.89	95.61	95.0	65.68
		NNTS	All	93.33	**98.06**	98.04	75.84
15	Dermatology (34)	MS	34	93.33	**99.04**	**99.04**	77.14
		HS	34	95.23	98.15	97.54	74.15
		NNTS	34	93.33	98.06	98.04	75.84
16	Hypothyroid (29)	MS	1,22,26	**94.23**	**94.23**	**94.23**	**94.23**
		HS	All except 1	89.10	93.33	92.73	91.24
		NNTS	22,26	**94.23**	93.25	93.23	92.93
17	Eggs(3)	MS	2	**100**	93.75	95.83	2.08
		HS	1,3	87.5	92.85	94.33	0.92
		NNTS	All	91.66	96.93	96.91	63.28
18	Fiber(4)	MS	4	91.66	**97.91**	**97.91**	64.58
		HS	1,2,3	91.66	97.01	96.41	61.59
		NNTS	3,4	91.66	96.93	96.91	63.28
19	Ionosphere (34)	MS	All except 14	94.01	99.14	**99.43**	64.10
		HS	14,28	97.43	98.24	97.93	61.11
		NNTS	All	91.66	96.93	96.91	63.28
20	Liver Disorder(6)	MS	1,2	94.65	**97.32**	96.79	57.21
		HS	3,4,5,6	94.65	96.42	95.29	54.23
		NNTS	1,2,3,4	95.72	96.34	95.79	55.92

VIII. Conclusion

Feature selection aims to reduce the amount of unnecessary, irrelevant and redundant features. It helps retrieve the most relevant features in datasets and improves the classification accuracy with less computational effort. If the features are not chosen well, even the best classifier performs poorly. In this paper, we describe feature relevance measures based on fuzzy entropy values and devise three feature selection strategies: Mean

Selection, Half Selection and Neural Network Threshold Selection with an RBF Network classifier. The features selected using the above strategies is passed over RBF network, Bagging, Boosting and stacking to predict their accuracy. The intention is to select the correct set of features for classification when datasets contain noisy, redundant and vague information.

Twenty benchmark datasets from the UCI Machine Learning Repository from various fields like medicine, agriculture, sports and others are used for evaluation. The proposed feature selection strategies have produced accuracies that are acceptable or better when compared with the accuracy obtained for the entire feature set without any feature selection. Of all the proponents, the one that maximizes the accuracy is the fuzzy entropy with Mean Selection. It is also found that among the four methodologies used, Bagging yields highest accuracy in most of the cases. Thus, Bagging can be taken a Best case, Boosting and RBF network as Average case and Stacking as Worst case. In future, this can be applied to a wide range of problem domains with hybridization of different feature selection techniques to improve the performance of both the feature selection and the classification.

REFERENCE

[1]   R.E. Abdel-Aal, GMDH based feature ranking and selection for improved classification of medical data, J.Biomed.Inform.38 (6)(2005)456–468.
[2]   M.F.Akay, Support vector machines combined with feature selection for breast cancer diagnosis, Int.J.Expert Syst.Appl.36 (2)(2009)3240–3247.
[3]   Chin-Yuan Fan,Pei-Chann Chang, Jyun-Jie Lin,J.C.Hsieh, A hybrid model combining case-based reasoning and fuzzy decision tree for medical data classification, Int.J.Appl.Soft Comput.11(1)(2011)632–644.
[4]   Huan Liu, LeiYu, Toward integrating feature selection algorithms for classification and clustering, IEEE Trans.Knowl.Data Eng.17 (4)(2005)491–502.
[5]   R. Kohavi, George H.John, Wrappers for feature selection subset selection, Artif. Intell.97 (1–2) (1997)273–324.
[6]   II-Seok Oh, Jin-Seon Lee, Byung-RoMoon, Hybrid genetic algorithm for feature selection, IEEE Trans.Pattern Anal.Mach.Intell.26 (11)(2004)1424–1437.
[7]   R. Battiti, Using mutual information for selecting features in supervised neural net learning, IEEE Trans.Neural Netw.5(4)(1994)537–550.
[8]   Hanchuan Peng, Fuhui Long, Chris Ding, Feature selection based on mutual information: criterion of max-dependency, max-relevance and min- redundancy, IEEE Trans.Pattern Anal.Mach.Intell.27 (8) (2005)1226–1238.
[9]   Pablo A.Extevez, Michel Tesmer,Claudio A.Perez, JacekM.Zurada, Normalized mutual information feature selection, IEEE Trans. Neural Netw.20 (2) (2009)189–201. [10] Lei Yu, Huan Liu, Efficient feature selection via analysis of relevance and redundancy, J.Mach.Learn.Res.5 (2004)1205–1224.
[11]   Seral Sahan, Kemal Polat, Halife Kodaz, Salih Gunes, A new hybrid method based on fuzzy-artificial immune system and k-nn algorithm for breast cancer diagnosis, Int.J.Comput.Biol.Med.37(3)(2007)415–423.
[12]   P.Jaganathan,K.Thangavel, A.Pethalakshmi, M.Karnan, Classification rule discovery with ant colony optimization and improved quick reduct algorithm,IAENGInt.J.Comput.Sci.33(1)(2007)50–55.
[13]   Rahul Karthik Sivagaminathan, Sreeram Rama krishnan, A hybrid approach for feature subset selection using neural networks and ant colony optimization, Int. J.Expert Syst.Appl.33(1)(2007)49–60.
[14]   Shih-Wei Lin, Zne-Jung Lee,Shih-Chieh Chen, Tsung-YuanTseng, Parameter determination of support vector machine and feature selection using simulated annealing approach,Int.J.Appl.Soft Comput.8(4)(2008)1505–1512.
[15]   Shih-WeiLin, Shih-Chieh Chen, Wen-Jie Wu, Chih-Hsien Chen, Parameter determination and feature selection for back-propagation network by particle swarm optimization, Int.J.Knowl.Inf.Syst.21(2)(2009)249–266.
[16]   Alper Unler, Alper Murat, A discrete particle swarm optimization method for feature selection in binary classification problems, Eur.J.Oper.Res.206(3) (2010)528–539.
[17]   Pei-Chann Chang, Jyun-JieLin, Chen-Hao Liu, An attribute weight assignment and particle swarm optimization algorithm for medical database classification, Int. J.Comput.Methods Progr.Biomed.107(3)(2012)382–392.
[18]   Maria Salamo, MaiteLopez-Sanchez,   Rough set based approaches to feature selection for case-based reasoning classifiers, Int.J.Pattern Recognit.Lett.32 (2) (2011)280–292. [19] Sultan Noman Qasem, Siti Mariyam Shamsuddin, Radial basis function network based on time variant multi-objective particle swarm optimization for medical diseases diagnosis, Int.J.Appl. Soft Comput.11(1) (2011)) 1427–1438.

Development of a Suitable Load Balancing Strategy In Case Of a Cloud Computing Architecture

Dayananda RB[1], Prof. Dr. G. Manoj Someswar[2]

[1](Associate Professor, Department of CSE, RRIT, Bangalore – 90, Karnataka, India)
[2](Professor & HOD, Department of CSE & IT, Nawab Shah Alam Khan College of Engineering & Technology, Affiliated to JNTU, Hyderabad, Malkpet, Hyderabad – 500024, India)

Abstract: *Cloud computing is an attracting technology in the field of computer science. In Gartner's report, it says that the cloud will bring changes to the IT industry. The cloud is changing our life by providing users with new types of services. Users get service from a cloud without paying attention to the details. NIST gave a definition of cloud computing as a model for enabling ubiquitous, convenient, on-demand network access to a shared pool of configurable computing resources (e.g., networks, servers, storage, applications, and services) that can be rapidly provisioned and released with minimal management effort or service provider interaction. More and more people pay attention to cloud computing. Cloud computing is efficient and scalable but maintaining the stability of processing so many jobs in the cloud computing environment is a very complex problem with load balancing receiving much attention for researchers. Since the job arrival pattern is not predictable and the capacities of each node in the cloud differ, for load balancing problem, workload control is crucial to improve system performance and maintain stability. Load balancing schemes depending on whether the system dynamics are important can be either static or dynamic. Static schemes do not use the system information and are less complex while dynamic schemes will bring additional costs for the system but can change as the system status changes. A dynamic scheme is used here for its flexibility. The model has a main controller and balancers to gather and analyze the information. Thus, the dynamic control has little influence on the other working nodes. The system status then provides a basis for choosing the right load balancing strategy. The load balancing model given in this research article is aimed at the public cloud which has numerous nodes with distributed computing resources in many different geographic locations. Thus, this model divides the public cloud into several cloud partitions. When the environment is very large and complex, these divisions simplify the load balancing. The cloud has a main controller that chooses the suitable partitions for arriving jobs while the balancer for each cloud partition chooses the best load balancing strategy.*

Keywords: *Load Balancing Strategy, User Interface Design, Requirements Traceability Matrix, Application Execution, Database Staging, Effective Network Performance*

I.   Introduction

The mysticism of cloud computing has worn off, leaving those required to implement cloud computing directives with that valley-of-despair feeling. When the hype is skimmed from cloud computing—private, public, or hybrid—what is left is a large, virtualized data center with IT control ranging from limited to non-existent. In private cloud deployments, IT maintains a modicum of control, but as with all architectural choices, that control is limited by the systems that comprise the cloud.

In a public cloud, not one stitch of cloud infrastructure is within the bounds of organizational control. Hybrid implementations, of course, suffer both of these limitations in different ways. But what cloud computing represents—the ability to shift loads rapidly across the Internet—is something large multi-national and even large intra-national organizations mastered long before the term "cloud" came along. While pundits like to refer to cloud computing as revolutionary, from the technologists' perspective, it is purely evolutionary. Cloud resources and cloud balancing extend the benefits of global application delivery to the smallest of organizations. In its most basic form, cloud balancing provides an organization with the ability to distribute application requests across any number of application deployments located in data centers and through cloud-computing providers.

Cloud balancing takes a broader view of application delivery and applies specified thresholds and service level agreements (SLAs) to every request. The use of cloud balancing can result in the majority of users being served by application deployments in the cloud providers' environments, even though the local application deployment or internal, private cloud might have more than enough capacity to serve that user. A variant of cloud balancing called cloud bursting, which sends excess traffic to cloud implementations, is also being implemented across the globe today. Cloud bursting delivers the benefits of cloud providers when usage is high, without the expense when organizational data centers—including internal cloud deployments—can handle the workload. In one vision of the future, the shifting of load is automated to enable organizations to configure clouds and cloud balancing and then turn their attention to other issues, trusting that the infrastructure will perform as designed.

II. Existing System

Cloud computing is efficient and scalable but maintaining the stability of processing so many jobs in the cloud computing environment is a very complex problem with load balancing receiving much attention for researchers. Since the job arrival pattern is not predictable and the capacities of each node in the cloud differ, for load balancing problem, workload control is. crucial to improve system performance and maintain stability. Load balancing schemes depending on whether the system dynamics are important can be either static and dynamic. Static schemes do not use the system information and are less complex while dynamic schemes will bring additional costs for the system but can change as the system status changes. A dynamic scheme is used here for its flexibility.

Disadvantages of Existing System

Load balancing schemes depending on whether the system dynamics are important can be either static and dynamic. Static schemes do not use the system information and are less complex.

III. Proposed System

Load balancing schemes depending on whether the system dynamics are important can be either static and dynamic. Static schemes do not use the system information and are less complex while dynamic schemes will bring additional costs for the system but can change as the system status changes. A dynamic scheme is used here for its flexibility. The model has a main controller and balancers to gather and analyze the information. Thus, the dynamic control has little influence on the other working nodes. The system status then provides a basis for choosing the right load balancing strategy.

The load balancing model given in this research article is aimed at the public cloud which has numerous nodes with distributed computing resources in many different geographic locations. Thus, this model divides the public cloud into several cloud partitions. When the environment is very large and complex, these divisions simplify the load balancing. The cloud has a main controller that chooses the suitable partitions for arriving jobs while the balancer for each cloud partition chooses the best load balancing strategy.

Advantages of Proposed System

Load balancing schemes depending on whether the system dynamics are important can be either static and dynamic . Static scheme does use the system information and are less complex.

IV. The Study Of The System

To conduct studies and analyses of an operational and technological nature, and to promote the exchange and development of methods and tools for operational analysis as applied to defense problems.

Logical design

The logical design of a system pertains to an abstract representation of the data flows, inputs and outputs of the system. This is often conducted via modeling, using an over-abstract (and sometimes graphical) model of the actual system.

Physical design

The physical design relates to the actual input and output processes of the system. This is laid down in terms of how data is input into a system, how it is verified / authenticated, how it is processed, and how it is displayed as output. In Physical design, following requirements about the system are decided.
1. Input requirement,
2. Output requirements,
3. Storage requirements,
4. Processing Requirements,

5. System control and backup or recovery.

Put another way, the physical portion of systems design can generally be broken down into three sub-tasks:
1. User Interface Design
2. Data Design
3. Process Design

   User Interface Design is concerned with how users add information to the system and with how the system presents information back to them. Data Design is concerned with how the data is represented and stored within the system. Finally, Process Design is concerned with how data moves through the system, and with how and where it is validated, secured and/or transformed as it flows into, through and out of the system. At the end of the systems design phase, documentation describing the three sub-tasks is produced and made available for use in the next phase. Physical design, in this context, does not refer to the tangible physical design of an information system. To use an analogy, a personal computer's physical design involves input via a keyboard, processing within the CPU, and output via a monitor, printer, etc. It would not concern the actual layout of the tangible hardware, which for a PC would be a monitor, CPU, motherboard, hard drive, modems, video/graphics cards, USB slots, etc. It involves a detailed design of a user and a product database structure processor and a control processor. The H/S personal specification is developed for the proposed system.

V. Input & Output Representation

Input Design

   The input design is the link between the information system and the user. It comprises the developing specification and procedures for data preparation and those steps are necessary to put transaction data in to a usable form for processing can be achieved by inspecting the computer to read data from a written or printed document or it can occur by having people keying the data directly into the system. The design of input focuses on controlling the amount of input required, controlling the errors, avoiding delay, avoiding extra steps and keeping the process simple. The input is designed in such a way so that it provides security and ease of use with retaining the privacy. Input Design considered the following things:

- What data should be given as input?
- How the data should be arranged or coded?
- The dialog to guide the operating personnel in providing input.
- Methods for preparing input validations and steps to follow when error occur.

Objectives

   Input Design is the process of converting a user-oriented description of the input into a computer-based system. This design is important to avoid errors in the data input process and show the correct direction to the management for getting correct information from the computerized system. It is achieved by creating user-friendly screens for the data entry to handle large volume of data. The goal of designing input is to make data entry easier and to be free from errors. The data entry screen is designed in such a way that all the data manipulates can be performed. It also provides record viewing facilities.

   When the data is entered it will check for its validity. Data can be entered with the help of screens. Appropriate messages are provided as when needed so that the user will not be in maize of instant. Thus the objective of input design is to create an input layout that is easy to follow.

Output Design

   A quality output is one, which meets the requirements of the end user and presents the information clearly. In any system results of processing are communicated to the users and to other system through outputs. In output design it is determined how the information is to be displaced for immediate need and also the hard copy output. It is the most important and direct source information to the user. Efficient and intelligent output design improves the system's relationship to help user decision-making.
   a. Designing computer output should proceed in an organized, well thought out manner; the right output must be developed while ensuring that each output element is designed so that people will find the system can use easily and effectively. When analysis design computer output, they should Identify the specific output that is needed to meet the requirements.
   b. Select methods for presenting information.
   c. Create document, report, or other formats that contain information produced by the system.
The output form of an information system should accomplish one or more of the following objectives.
- Convey information about past activities, current status or projections of the future.

- Signal important events, opportunities, problems, or warnings.
- Trigger an action.
- Confirm an action.

VI. Process Model Used With Justification

SDLC is nothing but Software Development Life Cycle. It is a standard which is used by software industry to develop good software.

SDLC (Umbrella Model):
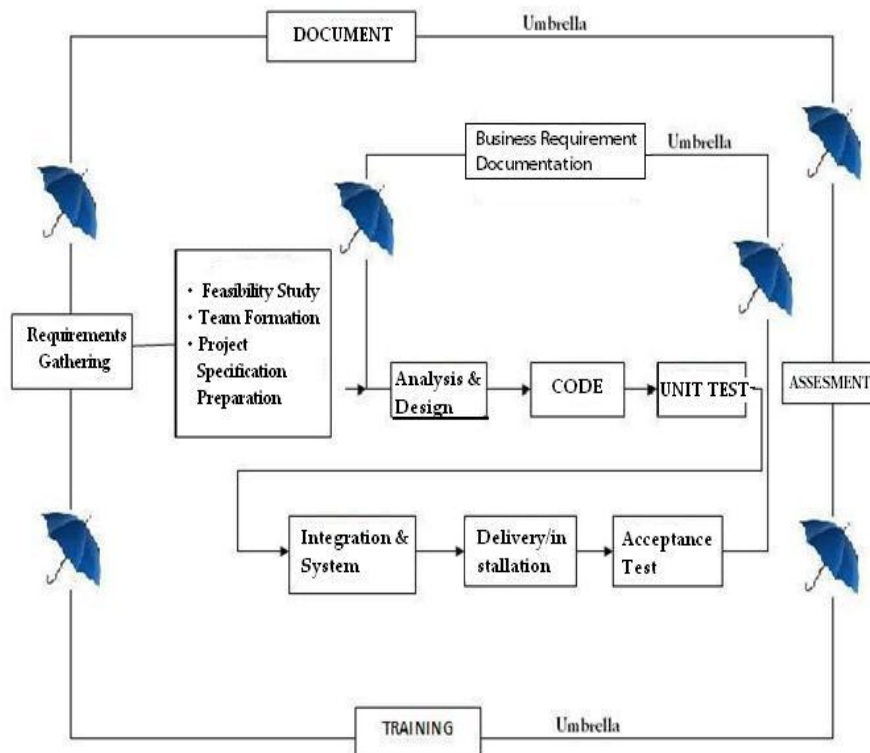
Stages of SDLC:
- Requirement Gathering and Analysis
- Designing
- Coding
- Testing
- Deployment

Requirements Definition Stage and Analysis

The requirements gathering process takes as its input the goals identified in the high-level requirements section of the project plan. Each goal will be refined into a set of one or more requirements. These requirements define the major functions of the intended application, define operational data areas and reference data areas, and define the initial data entities. Major functions include critical processes to be managed, as well as mission critical inputs, outputs and reports. A user class hierarchy is developed and associated with these major functions, data areas, and data entities. Each of these definitions is termed a Requirement. Requirements are identified by unique requirement identifiers and, at minimum, contain a requirement title and textual description.
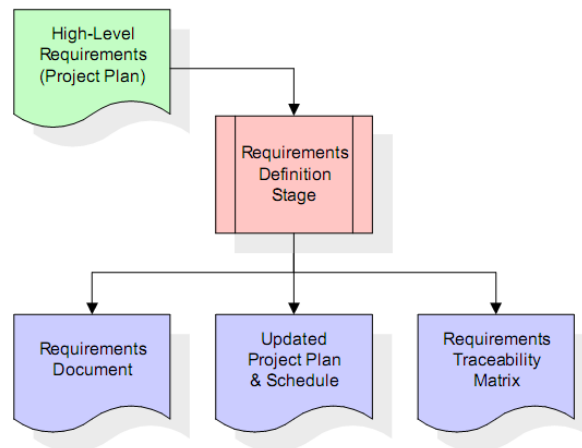
These requirements are fully described in the primary deliverables for this stage: the Requirements Document and the Requirements Traceability Matrix (RTM). the requirements document contains complete descriptions of each requirement, including diagrams and references to external documents as necessary. Note that detailed listings of database tables and fields are *not* included in the requirements document. The title of each requirement is also placed into the first version of the RTM, along with the title of each goal from the project plan. The purpose of the RTM is to show that the product components developed during each stage of the software development lifecycle are formally connected to the components developed in prior stages.

In the requirements stage, the RTM consists of a list of high-level requirements, or goals, by title, with a listing of associated requirements for each goal, listed by requirement title. In this hierarchical listing, the RTM shows that each requirement developed during this stage is formally linked to a specific product goal. In this format, each requirement can be traced to a specific product goal, hence the term *requirements traceability*. The outputs of the requirements definition stage include the requirements document, the RTM, and an updated project plan.

Design Stage

The design stage takes as its initial input the requirements identified in the approved requirements document. For each requirement, a set of one or more design elements will be produced as a result of interviews, workshops, and/or prototype efforts. Design elements describe the desired software features in detail, and generally include functional hierarchy diagrams, screen layout diagrams, tables of business rules, business process diagrams, pseudo code, and a complete entity-relationship diagram with a full data dictionary. These design elements are intended to describe the software in sufficient detail that skilled programmers may develop the software with minimal additional input.
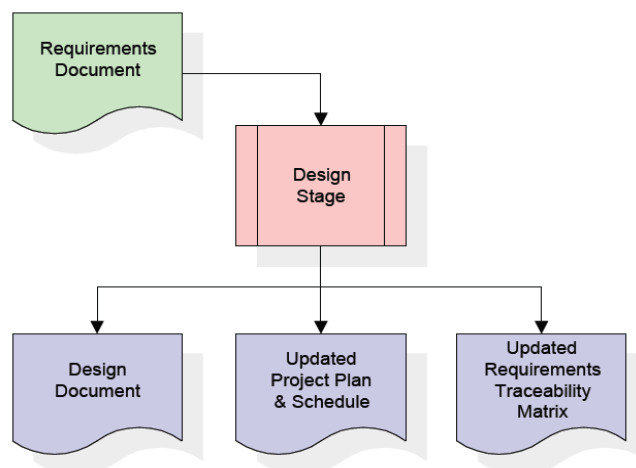
When the design document is finalized and accepted, the RTM is updated to show that each design element is formally associated with a specific requirement. The outputs of the design stage are the design document, an updated RTM, and an updated project plan.

Development Stage

The development stage takes as its primary input the design elements described in the approved design document. For each design element, a set of one or more software artifacts will be produced. Software artifacts include but are not limited to menus, dialogs, data management forms, data reporting formats, and specialized procedures and functions. Appropriate test cases will be developed for each set of functionally related software artifacts, and an online help system will be developed to guide users in their interactions with the software.
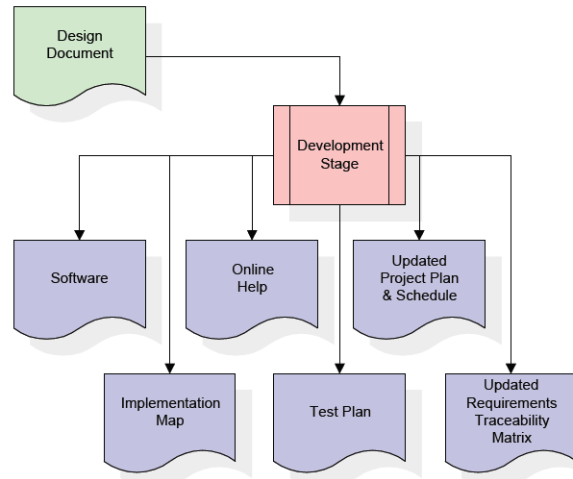
The RTM will be updated to show that each developed artifact is linked to a specific design element, and that each developed artifact has one or more corresponding test case items. At this point, the RTM is in its final configuration. The outputs of the development stage include a fully functional set of software that satisfies the requirements and design elements previously documented, an online help system that describes the operation of the software, an implementation map that identifies the primary code entry points for all major system functions, a test plan that describes the test cases to be used to validate the correctness and completeness of the software, an updated RTM, and an updated project plan.

Integration & Test Stage

During the integration and test stage, the software artifacts, online help, and test data are migrated from the development environment to a separate test environment. At this point, all test cases are run to verify the correctness and completeness of the software. Successful execution of the test suite confirms a robust and complete migration capability. During this stage, reference data is finalized for production use and production users are identified and linked to their appropriate roles. The final reference data (or links to reference data source files) and production user list are compiled intothe Production Initiation Plan.
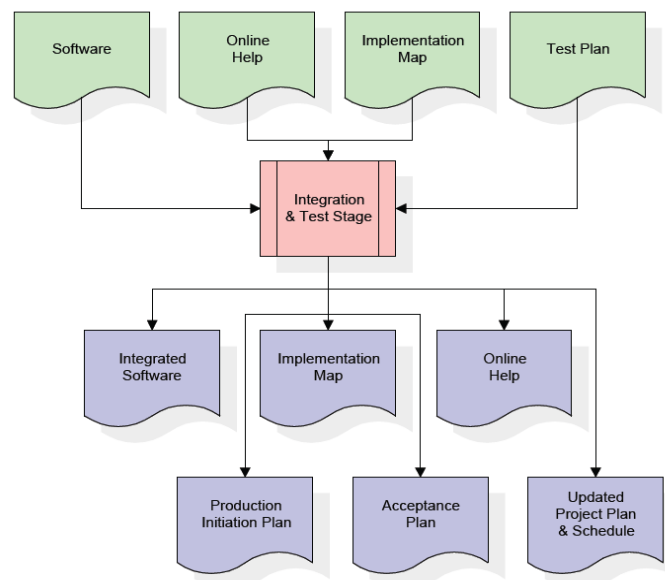
The outputs of the integration and test stage include an integrated set of software, an online help system, an implementation map, a production initiation plan that describes reference data and production users, an acceptance plan which contains the final suite of test cases, and an updated project plan.

Installation & Acceptance Stage

During the installation and acceptance stage, the software artifacts, online help, and initial production data are loaded onto the production server. At this point, all test cases are run to verify the correctness and completeness of the software. Successful execution of the test suite is a prerequisite to acceptance of the software by the customer. After customer personnel have verified that the initial production data load is correct and the test suite has been executed with satisfactory results, the customer formally accepts the delivery of the software.
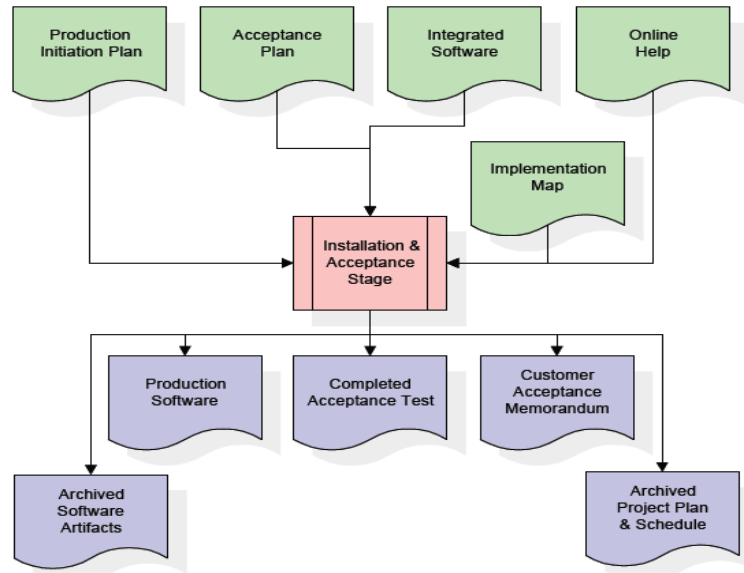
The primary outputs of the installation and acceptance stage include a production application, a completed acceptance test suite, and a memorandum of customer acceptance of the software. Finally, the PDR enters the last of the actual labor data into the project schedule and locks the project as a permanent project record. At this point the PDR "locks" the project by archiving all software items, the implementation map, the source code, and the documentation for future reference.

VII.   System Architecture

Architecture Flow

Below architecture diagram represents mainly flow of request from the users to database through servers. In this scenario overall system is designed in three tiers separately using three layers called presentation layer, business layer, data link layer. This project was developed using 3-tier architecture.
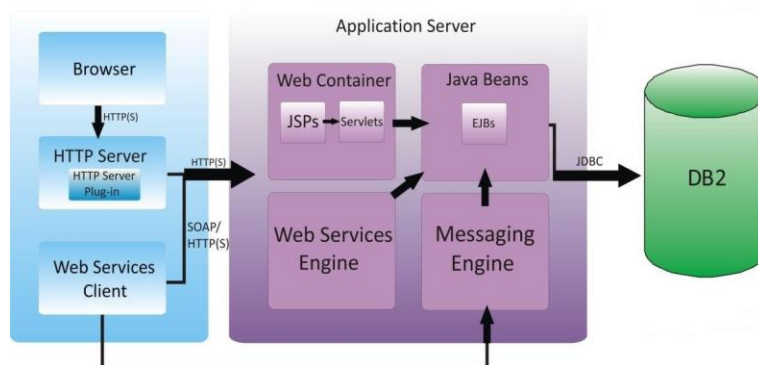
3-Tier Architecture

The three-tier software architecture (a three layer architecture) emerged in the 1990s to overcome the limitations of the two-tier architecture. The third tier (middle tier server) is between the user interface (client) and the data management (server) components. This middle tier provides process management where business logic and rules are executed and can accommodate hundreds of users (as compared to only 100 users with the two tier architecture) by providing functions such as queuing, application execution, and database staging.

The three tier architecture is used when an effective distributed client/server design is needed that provides (when compared to the two tier) increased performance, flexibility, maintainability, reusability, and scalability, while hiding the complexity of distributed processing from the user. These characteristics have made three layer architectures a popular choice for Internet applications and net-centric information systems

Advantages of Three-Tier
- Separates functionality from presentation.
- Clear separation - better understanding.
- Changes limited to well define components.
- Can be running on WWW.
- Effective network performance**.**

System Design Introduction:

The System Design Document describes the system requirements, operating environment, system and subsystem architecture, files and database design, input formats, output layouts, human-machine interfaces, detailed design, processing logic, and external interfaces.

VIII.   UML Diagrams

1. Global Use Case Diagrams:

Identification of actors:

Actor: Actor represents the role a user plays with respect to the system. An actor interacts with, but has no control over the use cases.

Graphical representation:
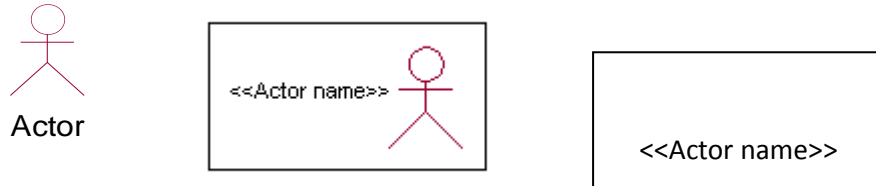
An actor is someone or something that:

Interacts with or uses the system.
- Provides input to and receives information from the system.
- Is external to the system and has no control over the use cases.

Actors are discovered by examining:
- Who directly uses the system?
- Who is responsible for maintaining the system?
- External hardware used by the system.
- Other systems that need to interact with the system.

Questions to identify actors:
- Who is using the system? Or, who is affected by the system? Or, which groups need help from the system to perform a task?
- Who affects the system? Or, which user groups are needed by the system to perform its functions? These functions can be both main functions and secondary functions such as administration.
- Which external hardware or systems (if any) use the system to perform tasks?
- What problems does this application solve (that is, for whom)?
- And, finally, how do users use the system (use case)? What are they doing with the system?

The actors identified in this system are:
  a. **System Administrator**
  b. **Customer**
  c. **Customer Care**

Identification of use cases:
Usecase: A use case can be described as a specific way of using the system from a user's (actor's) perspective.

IX. Graphical Representation
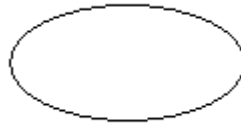
A more detailed description might characterize a use case as:
- Pattern of behavior the system exhibits
- A sequence of related transactions performed by an actor and the system
- Delivering something of value to the actor

Use cases provide a means to:
- capture system requirements
- communicate with the end users and domain experts
- test the system

Use cases are best discovered by examining the actors and defining what the actor will be able to do with the system.

Guide lines for identifying use cases:
- For each actor, find the tasks and functions that the actor should be able to perform or that the system needs the actor to perform. The use case should represent a course of events that leads to clear goal
- Name the use cases.
- Describe the use cases briefly by applying terms with which the user is familiar.

This makes the description less ambiguous
Questions to identify use cases:
- What are the tasks of each actor?
- Will any actor create, store, change, remove or read information in the system?
- What use case will store, change, remove or read this information?
- Will any actor need to inform the system about sudden external changes?
- Does any actor need to inform about certain occurrences in the system?
- What use cases will support and maintains the system?

Flow of Events

A flow of events is a sequence of transactions (or events) performed by the system. They typically contain very detailed information, written in terms of what the system should do, not how the system accomplishes the task. Flow of events are created as separate files or documents in your favorite text editor and then attached or linked to a use case using the Files tab of a model element.

A flow of events should include:
- When and how the use case starts and ends
- Use case/actor interactions
- Data needed by the use case
- Normal sequence of events for the use case
- Alternate or exceptional flows

Construction of Use case diagrams:

Use-case diagrams graphically depict system behavior (use cases). These diagrams present a high level view of how the system is used as viewed from an outsider's (actor's) perspective. A use-case diagram may depict all or some of the use cases of a system.

A use-case diagram can contain:
- actors ("things" outside the system)
- use cases (system boundaries identifying what the system should do)
- Interactions or relationships between actors and use cases in the system including the associations, dependencies, and generalizations.

Relationships in use cases:
1. Communication:
  The communication relationship of an actor in a use case is shown by connecting the actor symbol to the use case symbol with a solid path. The actor is said to communicate with the use case.
2. Uses:
  A Uses relationship between the use cases is shown by generalization arrow from the use case.
3. Extends:
  The extend relationship is used when we have one use case that is similar to another use case but does a bit more. In essence it is like subclass.

Main Use Case Diagram in our system:
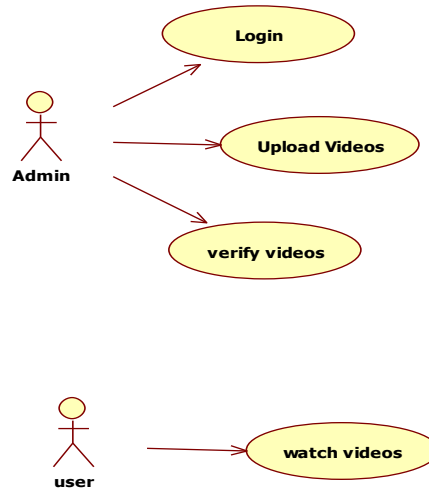
X. Activity Diagram

  Activity diagrams provide a way to model the workflow of a business process, code-specific information such as a class operation. The transitions are implicitly triggered by completion of the actions in the source activities. The main difference between activity diagrams and state charts is activity diagrams are activity centric, while state charts are state centric. An activity diagram is typically used for modeling the sequence of activities in a process, whereas a state chart is better suited to model the discrete stages of an object's lifetime. An activity represents the performance of task or duty in a workflow. It may also represent the execution of a statement in a procedure. You can share activities between state machines. However, transitions cannot be shared. An action is described as a "task" that takes place while inside a state or activity. Actions on activities can occur at one of four times:

- **on entry** ---- The "task" must be performed when the object enters the state or activity.
- **on exit** ---- The "task" must be performed when the object exits the state or activity.
- **do** ---- The "task" must be performed while in the state or activity and must continue until exiting the state.
- **on event** ---- The "task" triggers an action only if a specific event is received.
- An **end state** represents a final or terminal state on an activity diagram or state chart diagram.
- A **start state** (also called an "initial state") explicitly shows the beginning of a workflow on an activity diagram.
- **Swim lanes** can represent organizational units or roles within a business model. They are very similar to an object. They are used to determine which unit is responsible for carrying out the specific activity. They show ownership or responsibility. Transitions cross swim lanes
- **Synchronizations** enable you to see a simultaneous workflow in an activity diagram Synchronizations visually define forks and joins representing parallel workflow.
- A **fork** construct is used to model a single flow of control that divides into two or more separate, but simultaneous flows. A corresponding join should ideally accompany every fork that appears on an activity diagram. A **join** consists of two of more flows of control that unite into a single flow of control.

All model elements (such as activities and states) that appear between a fork and join must complete before the flow of controls can unite into one.

- An **object flow** on an activity diagram represents the relationship between an activity and the object that creates it (as an output) or uses it (as an input).
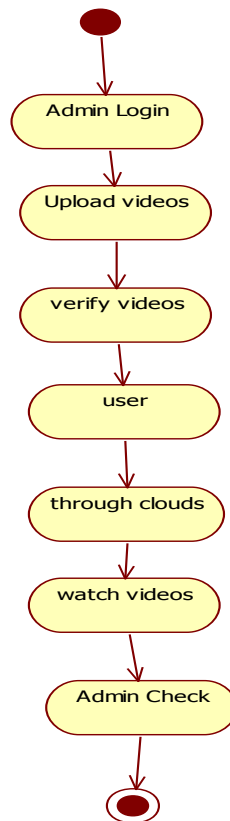
XI. Sequence Diagrams

A sequence diagram is a graphical view of a scenario that shows object interaction in a time-based sequence what happens first, what happens next. Sequence diagrams establish the roles of objects and help provide essential information to determine class responsibilities and interfaces. There are two main differences between sequence and collaboration diagrams: sequence diagrams show time-based object interaction while collaboration diagrams show how objects associate with each other. A sequence diagram has two dimensions: typically, vertical placement represents time and horizontal placement represents different objects.

Object:

An object has state, behavior, and identity. The structure and behavior of similar objects are defined in their common class. Each object in a diagram indicates some instance of a class. An object that is not named is referred to as a class instance. The object icon is similar to a class icon except that the name is underlined:An object's concurrency is defined by the concurrency of its class.

Message:

A message is the communication carried between two objects that trigger an event. A message carries information from the source focus of control to the destination focus of control. The synchronization of a message can be modified through the message specification. Synchronization means a message where the sending object pauses to wait for results.

Link:

A link should exist between two objects, including class utilities, only if there is a relationship between their corresponding classes. The existence of a relationship between two classes symbolizes a path of communication between instances of the classes: one object may send messages to another. The link is depicted

as a straight line between objects or objects and class instances in a collaboration diagram. If an object links to itself, use the loop version of the icon.

Admin Sequence:
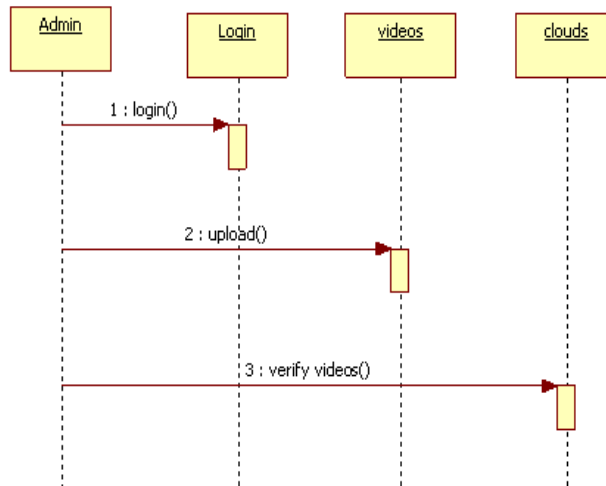
Admin Collaboration:
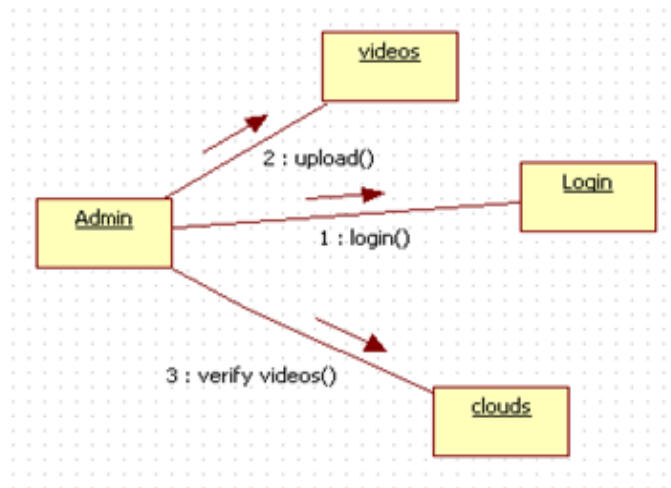
User Sequence:
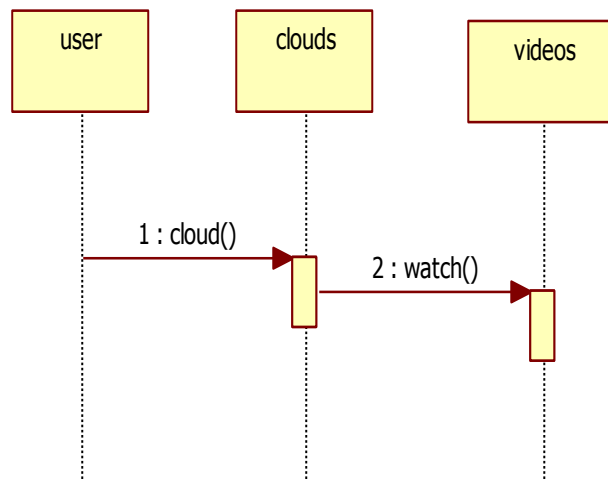
User Collaboration:
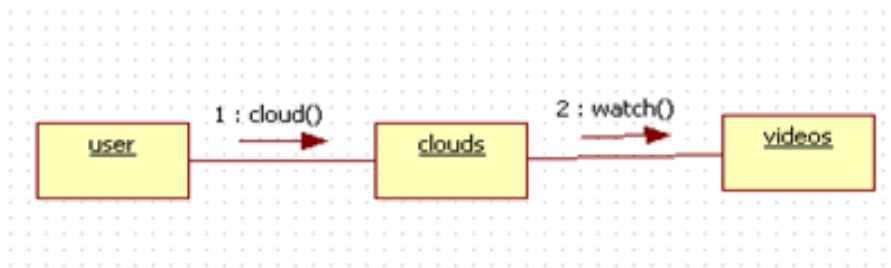
XII. Class Diagram

Identification of analysis classes:

A class is a set of objects that share a common structure and common behavior (the same attributes, operations, relationships and semantics). A class is an abstraction of real-world items.

There are 4 approaches for identifying classes:
a. Noun phrase approach:
b. Common class pattern approach.
c. Use case Driven Sequence or Collaboration approach.
d. Classes , Responsibilities and collaborators Approach

1. Noun Phrase Approach:

The guidelines for identifying the classes:
- Look for nouns and noun phrases in the use cases.
- Some classes are implicit or taken from general knowledge.
- All classes must make sense in the application domain; Avoid computer
- Implementation classes – defer them to the design stage.
- Carefully choose and define the class names After identifying the classes we have to eliminate the following types of classes:
- Adjective classes.

2. Common class pattern approach:

The following are the patterns for finding the candidate classes:
- Concept class.
- Events class.
- Organization class
- Peoples class
- Places class
- Tangible things and devices class.

3. Use case driven approach:

We have to draw the sequence diagram or collaboration diagram. If there is need for some classes to represent some functionality then add new classes which perform those functionalities.

XIII. CRC Approach

The process consists of the following steps:
- Identify classes' responsibilities (and identify the classes)
- Assign the responsibilities
- Identify the collaborators.

Identification of responsibilities of each class:

The questions that should be answered to identify the attributes and methods of a class respectively are:
a. What information about an object should we keep track of?
b. What services must a class provide?

Identification of relationships among the classes:
Three types of relationships among the objects are:
Association: How objects are associated?
Super-sub structure: How are objects organized into super classes and sub classes?
Aggregation: What is the composition of the complex classes?
Association:
The **questions** that will help us to identify the associations are:
a. Is the class capable of fulfilling the required task by itself?
b. If not, what does it need?
c. From what other classes can it acquire what it needs?

Guidelines for identifying the tentative associations:
- A dependency between two or more classes may be an association. Association often corresponds to a verb or prepositional phrase.
- A reference from one class to another is an association. Some associations are implicit or taken from general knowledge.

Some common association patterns are:
Location association like part of, next to, contained in…..
Communication association like talk to, order to ……
We have to eliminate the unnecessary association like implementation associations, ternary or n-ary associations and derived associations.
Super-sub class relationships:
Super-sub class hierarchy is a relationship between classes where one class is the parent class of another class (derived class).This is based on inheritance.
Guidelines for identifying the super-sub relationship, a generalization are:
1**. Top-down***:*
Look for noun phrases composed of various adjectives in a class name. Avoid excessive refinement. Specialize only when the sub classes have significant behavior.
2. **Bottom-up***:*
Look for classes with similar attributes or methods. Group them by moving the common attributes and methods to an abstract class. You may have to alter the definitions a bit.
3. **Reusability***:*
Move the attributes and methods as high as possible in the hierarchy.
4. **Multiple inheritances***:*
Avoid excessive use of multiple inheritances. One way of getting benefits of multiple inheritances is to inherit from the most appropriate class and add an object of another class as an attribute.
Aggregation or a-part-of relationship:
It represents the situation where a class consists of several component classes. A class that is composed of other classes doesn't behave like its parts. It behaves very difficultly. The major properties of this relationship are transitivity and anti symmetry.
The **questions** whose answers will determine the distinction between the part and whole relationships are:
- Does the part class belong to the problem domain?
- Is the part class within the system's responsibilities?
- Does the part class capture more than a single value?(If not then simply include it as an attribute of the whole class)
- Does it provide a useful abstraction in dealing with the problem domain?

There are three types of aggregation relationships. They are:
Assembly:
It is constructed from its parts and an assembly-part situation physically exists.
Container:
A physical whole encompasses but is not constructed from physical parts.
Collection member:
A conceptual whole encompasses parts that may be physical or conceptual. The container and collection are represented by hollow diamonds but composition is represented by solid diamond.
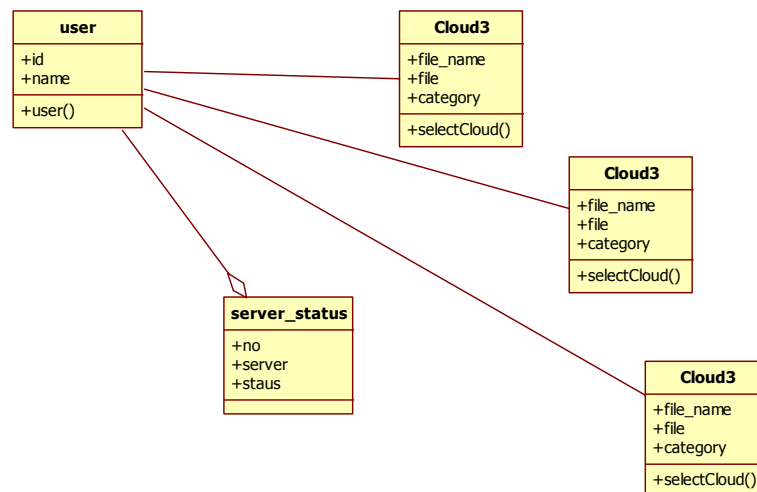
XIV. Conclusion

Till now we have discussed on basic concepts of Cloud Computing and Load balancing. In addition to that, the load balancing technique that is based on Swarm intelligence has been discussed. We have discussed how the mobile agents can balance the load of a cloud using the concept of Ant colony Optimization. The limitation of this technique is that it will be more efficient if we form cluster in our cloud. So, the research work can be proceeded to implement the total solution of load balancing in a complete cloud environment. Our objective for this paper is to develop an effective load balancing algorithm using Ant colony optimization technique to maximize or minimize different performance parameters like CPU load, Memory capacity, Delay or network load for the clouds of different sizes.

REFERENCES

[1]   R. Hunter, The why of cloud, http://www.gartner.com/ DisplayDocument?doc cd=226469&ref= g noreg, 2012.
[2]   M. D. Dikaiakos, D. Katsaros, P. Mehra, G. Pallis, and A. Vakali, Cloud computing: Distributed internet computing for IT and scientific research, Internet Computing, vol.13, no.5, pp.10-13, Sept.-Oct. 2009.
[3]   P. Mell and T. Grance, The NIST definition of cloud computing, http://csrc.nist.gov/ publications/nistpubs/800-145/SP800-145.pdf, 2012.
[4]   Microsoft Academic Research, Cloud computing, http:// libra.msra.cn/Keyword/6051/cloud-computing?query= cloud%20computing, 2012.
[5]   Google Trends, Cloud computing, http://www.google. com/trends/explore#q=cloud%20computing, 2012.
[6]   N. G. Shivaratri, P. Krueger, and M. Singhal, Load distributing for locally distributed systems, Computer, vol. 25, no. 12, pp. 33-44, Dec. 1992.
[7]   B. Adler, Load balancing in the cloud: Tools, tips and techniques, http://www.rightscale. com/info center/white-papers/Load-Balancing-in-the-Cloud.pdf, 2012.

Harmonic Analysis of VFD's

Poonam Kaur[1], Ritula Thakur[2]
[1, 2] *(ME student, Asstt. Prof. , Deptt. Of Electrical Engg. NITTTR Chandigarh)*

Abstract: *VFD's are the power electronic control devices that provide unique and beneficial opportunities for AC induction motors control. VFD's offer process control through speed variation and starting control for motors. VFD's convert/rectify voltage from a constant frequency alternating current (AC) power system to create a direct current (DC) voltage link, and then electronically invert the DC voltage link to create a variable voltage variable frequency output. While doing this conversion the supply is rectified and inverted using power semiconductor devices. This conversion process generates harmonics in the line current waveform and power gets polluted.*
Keywords: *Variable frequency drives, Total harmonic distortion, Power harmonic analyzer.*

I. Introduction

The harmonic distortion depends on the network impedance, the technology used in the VFD incoming rectifier and the impedance values of the components used in the VFD power circuit. The most commonly used frequency converter is of a type called pulse width modulation (PWM). This uses a 6-pulse diode rectifier. Many manufacturers are using inductances to reduce the harmonic distortion level. With the inductances, the typical THD (total harmonic distortion in current) value is around 30%. Without the inductance, it can be 70% to 120%. Industries with heavy motor load and VFDs generate harmonics and thus pollute the power. It also affects other consumers also. Therefore consumers are required to evaluate the impact of their plants on the power system. For this reason, it is necessary to measure harmonics at the Point of Common Coupling (PCC).
Three phase ac power supply is rectified into dc voltage by the rectifier unit and smoothed by a bank of smoothing capacitors. These smoothing capacitors act as a constant voltage source for the inverter stage of the VFD. Hence the name voltage source inverter type of VFD. The dc bus voltage is inverted using pulse-width modulation strategies and fed into the induction motor. The output frequency of the inverter is controlled by a control circuit to meet different load conditions. Theses VFD's area major source of the harmonics in the power system and thereby pollute power. VFD's control speed of the motor over the entire load range. Therefore for harmonic mitigation VFD's must be analyzed taking into account load variation.

II. Harmonic analysis of VFD

Variable Frequency Drives (VFD's) have grown rapidly in their usage in recent years because of many advantages. An unfortunate side effect of their usage however, is the introduction of harmonic distortion in the power system. As a non-linear load, a VFD draws current in a non-sinusoidal manner, rich in harmonic components. These harmonics flow through the power system where they can distort the supply voltage, overload electrical distribution equipment (such as transformers) and resonate with power factor correction capacitors among other issues.
In Harmonic Spectrum of VFD:

- Lower harmonic orders have the higher magnitudes
- Magnitudes should decline as the harmonic order increases

If the harmonic spectrum exhibits abnormal magnitudes, it is a good sign of harmonic resonance typically caused by interaction with Power Factor Correction Capacitors. The following VFDs were analyzed and 5th harmonic component was recorded at various frequencies. Harmonic signatures of the VFD were taken at different frequencies. Equipment taken under consideration is a Cooling Tower Fan motor, Make- Marathon, V= 415 V, F = 50 Hz, kW =18.5,HP =25, RPM =1460, % Eff =90.5, P.F =0.85 Amp =33.5
VFD details: Model Power Flex 700, Make Allen Bradley, Normal duty Power= 30 Kw 40 HP, Heavy duty Power = 22 kW 30 HP, Input 3 Ph. - 47- 63 Hz, AC voltage Range =342 - 440 V, Amp = 53, Output 3 Ph. 0- 400 Hz, AC voltage Range 0- 400, Base Hz = 50, Continuous Amp =56, 1 Min over Load Amp =64, 3 sec Overload Amp =86
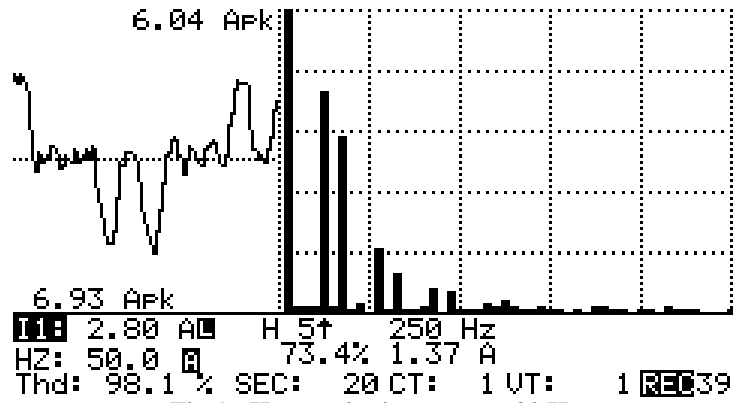
Fig 1 : Harmonic signature at 20 Hz
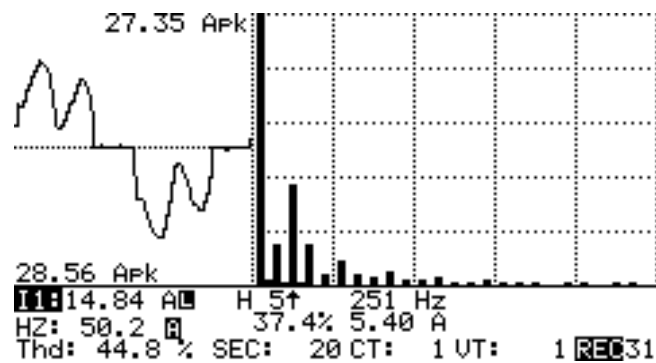
Fig 2: Harmonic signature at 40 Hz
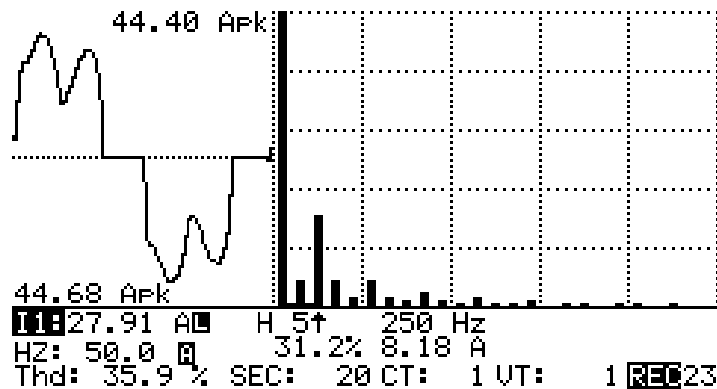
Fig 3: Harmonic signature at 50 Hz
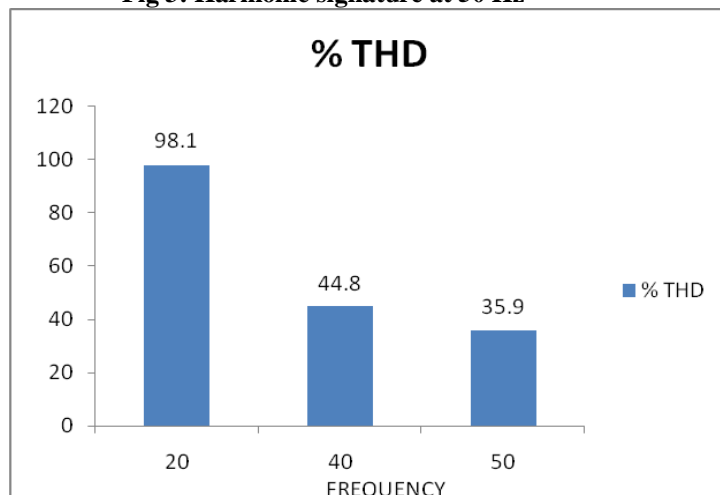
Fig 4: %THD Vs Frequency in Hz

Fig. 5 Photograph of actual experimental set up

III. Conclusion

- In all the VFDs, %THD falls with the increase in frequency.
- In all the cases, 5th harmonic component was the highest one.
- As the harmonic order increases its value decreases i.e. 7th , 11th and so on all the components are smaller than 5th harmonic component. Thus there is no harmonic resonance

IV. Future Scope

Based on the work done filter can be designed to mitigate harmonics generated by the variable frequency drives considering the variations introduced in the THD % age because of variation in thefrequency of the drive.

REFERENCES

[1] Barreiro J, Hernandez M, Ramos G, " Systematic Evaluation for harmonic distortion limits from IEEE 519", IEEE, 2013.
[2] Verma Vishal, Singh Bhim, Chandra Ambrish, Haddad Al Kamal , "Power Conditioner for Variable-Frequency Drives in Offshore Oil Fields", IEEE transactions on industry applications, Vol. 46, No. 2, pp 731-739, April 2010
[3] Issouribehere P. E, Barbera G. A, Issouribehere F., Mayer H. G., "Power Quality Measurements and Mitigation of Disturbances Due To PWM AC Drives", IEEE, pp 1-8, 2008
[4] Singh Bhim, Gairola Sanjay, " A Novel Harmonic Mitigation Converter for Variable Frequency Drives", IEEE, 2006
[5] Swamy Mahesh, Rossiter Steve, "Typical problems encountered with Variable frequency drives in the industry", IEEE, pp 503-510, 1993.
[6] KhanShoaib, Eldehaibi Nazem, "System and equipment problems associated with Variable frequency drives in the pulp and paper industry", IEEE, pp 131-136, 1995
[7] Chan W.L., Suen S.M., So A.T.P., "A Study on Electrical Performance of Modern VVVF Drivesfor HVAC Applications", Proceedings of the 4th International Conference on Advances in Power System Control, Operation and Management, pp 825-830, 1997.
[8] Larsen and Tourbo, Eco care, complete solutions for energy efficiency and harmonic Mitigation, www.larsentoubro.com
[9] Barton J Sauer, Patrick A Brady, "Application of AC Induction motors with variable frequency Drives", IEEE, 2009.

Energy Audit of a Food Industry

Poonam Kaur[1] Ritula Thakur[2]

[1,2]*(ME student, Asstt. Prof., Deptt. Of Electrical Engg. NITTTR Chandigarh)*

Abstract: The Energy Audit would give a positive orientation for implementing the energy cost reduction, preventive maintenance and quality control programmes which are vital for production and utility activities. Energy Audit is the translation of conservation ideas into realities, by lending technically feasible solutions with economic and other organizational considerations within a specified time frame. This thesis deals with the identification of nature of losses in industry that manufacturers food products. The energy accounting with the use of measuring instruments like lux-meter, power and harmonic analyzer etc. helps to record and analyze data of energy usage. With the help of this data, energy wastage and losses are calculated and recommendations are given to reduce these losses and improve savings. Lastly, to deal with the issues of power quality, power quality assessment is done at PCC.

Keywords: Energy audit, Point of common coupling, Power harmonic analyzer, ILER.

I. Introduction

Energy audit process is a planned and organized approach to identify energy wastage in a facility, finding how this wastage can be removed at a reasonable cost within a suitable time limit. Energy audit is widely used in all the areas like industries small scale or large scale, commercial buildings, institutes etc. Energy auditing of a premises can vary from a short walkthrough of the area to a detailed analysis. Energy audit not only serves to identify energy use among the various services and to identify opportunities for energy conservation but it is also first step in establishing an energy management program. The audit will produce the data on which such a program is based. Such kind of study must reveal to the owner or management team the options available for reducing energy waste, the costs involved, and the benefits achievable from implementing those energy-conserving opportunities (ECOs). A "Detailed Energy Audit" is a type of audit which is most comprehensive type of energy audit. This includes the use of instruments to measure the energy use of whole building and energy systems within the building. An audit aims at analyzing and identifying possible energy saving measures, which can be implemented in a factory. This will help the factory to reduce their monthly electrical energy consumption thus reducing the cost of production

In the energy audit the first is the Lighting audit, which is performed during the premises assessment process which includes a visit to the premises in order to identify areas for the Energy Conservation process. The second one is the harmonics analysis. Harmonics reflect the distortion of the wave form and pollute the quality of the power which leads to increased transformer heating and transmission losses. Harmonics can be defined as periodic, steady-state distortion of voltage or may be current waveform in a power system. These distortions are injected by devices which have non-linear relationship between current and voltage. Poor power quality due to harmonic distortion has come up as a serious issue. The effects of harmonics can often be serious, computer systems may fail to operate properly, capacitor banks, such as those used for power factor correction, can become overload and fail, and the interference may occur on communication lines.

II. Lighting Based Audit

The first and important part of lighting based energy audit is the input data collection. Although industry contains bulk load like motors, compressors, etc. 10% of the total load is of lighting and out of this 2-4% of the energy consumption can be reduced by installing efficient fixtures. Secondly, proper illumination at the working place is much important for the safety of the employees working in the plant, keeping all these points the lighting based energy audit has been conducted in production office and engineering workshop. Before conducting lighting based energy audit some terminologies and definitions should be known and there must be a process flowchart through which it becomes easier to understand the steps to be performed during energy audit. Two areas have been considered as case A(Process Hall) and B(workshop). Cases are further divided into three categories as:

1. With only day light is on
2. With day light as well as Luminaries on

3. With Luminaries only at night time.

For all the three cases mentioned above ILER is calculated.
Installed Load Efficacy Ratio = Lux per watt square meter / Target Lux

Table 1: ILER calculated for three categories of both cases

Case A	Installed Load Efficacy Ratio	Case B	Installed Load Efficacy Ratio
A1	0.3	B1	.48
A2	0.78	B2	1.2
A3	0.71	B3	.78

Table 2: ILER as recommended by BEE

ILER	Assessment
0.75 or above	Satisfactory to good
0.51 to 0.74	Review suggested
0.5 or less	Urgent action required

Table 3: Results for both cases

Cases	Suggestion	Cases	Suggestion
A1	Poor illuminance level	B1	Poor illuminance level
A2	Good lighting condition	B2	Good lighting condition
A3	Action required for better lluminance	B3	Good lighting condition

Case A: Though ILER for this case is satisfactory, it was found that mounting height was approximate 8 meters of the fixture therefore illuminance can be increased or improved further by reducing the mounting height. Also MV lamps can be replaced by more efficient fixtures such as Metal Halide or LED panels.

Case B: In workshop, the mounting height was also nearly 4.5 meters, the illuminance level measured was not found good in case B1. Main reason behind poor illuminance level was the mounting height and no proper utilization of day light, fixtures are not clean. This requires additional installation of the lamps therefore the cost as well as wastage of energy increased. For improvement in illuminance level & increasing the savings, avoid such problem by decreasing the mounting height and keep the fixtures clean, therefore get better illuminance level.

III. Harmonic Analysis

Harmonic analysis at point of common coupling (PCC) is very important as harmonic currents produced by non-linear loads are injected back into power distribution systems through the point of common coupling (PCC). With the help of Power and Harmonic Analyzer, total harmonic distortions (THD) are recorded at Point of Common Coupling (PCC).The industrial consumer falls in the category in which maximum allowed THD is 4%.

Table 4: Thd V and I measured at PCC

		Voltage- Thd V	Current – Thd I
33kv side	R	1.9	3.017
	Y	2.1	4.6
	B	2.1	4.7

Table 5: Current Distortion Limit of IEEE-519-1992 Standard

Isc/IL	<11	$11 \leq h<17$	$17 \leq h<23$	$23 \leq h<35$	$35 \geq h$	TDD
<20	4.0	2.0	1.5	0.6	0.3	5.0
20-50	7.0	3.5	2.5	1.0	0.5	8.0
50-100	10.0	4.5	4.0	1.5	0.7	12.0
100-1000	12.0	5.5	5.0	2.0	1.0	15.0
>1000	15.0	7.0	6.0	2.5	1.4	20.0

IV. Conclusion

From the survey it was found that, illuminance level is poor, in few areas. This dissertation implemented the concept of energy audit for the calculation of lighting parameters manually. This dissertation implemented the concept of lighting methodology that calculated the lighting parameters like ILER, energy wastage, etc manually. Power Quality Assessment was done at Point of common Coupling (PCC) of the industry. The harmonic components at Point of common Coupling (PCC) were measured, recorded and analyzed with the help of harmonic analyzer. With the help of measured data, total harmonic distortion (THD%) and total harmonic distortion (TDD%) were calculated. From the calculated THD% and TDD%, it was found to be within permissible limit.

V. Future Scope

The energy audit conducted at food industry was done. The tedious manual calculations can be done simply with the help of development of software programme.

REFERENCES

[1] Sunil M. Jaralikar and Mangalpady Aruna, "Energy Audit of a 400/220 kV Substation", IEEE, pp 1-8, 2012.
[2] Young Li, Jian Jun Wang, Tie Liu Jiang, Bing Wen Zhang, " Energy Audit and its application in coal fired power plant", IEEE, 2009.
[3] Danielle M Lorimer, Patrick Murray, "Industrial strategies to help reduce energy consumption: A holistic approach for cement producers", IEEE , 2010.
[4] Barreiro J, Hernandez M, Ramos G, " Systematic Evaluation for harmonic distortion limits from IEEE 519", IEEE, 2013.
[5] F.M. Sánchez, A. Filgueira, M.A. Seijo , M.E. Muñoz , E. Muñoz, "Energy Audit Model for a Waste Water Treatment Plant", IEEE, pp 550-554, 2009.
[6] Putri Zalila Yaacoh and Dr.Abdullah Asuhainu Mohd. Zin, "Electrical Energy management in Small and medium size industries ", IEEE, pp 379-382, 1993
[7] Wuwei. Cao, Xin.Wang and Chen Huang, "Energy Audit of Building: A Case Study of a Commercial Building in Shanghai".
[8] Guide Books for the National Certificate Examination for Energy Managers and Energy Auditors, Book I General Aspect of Energy Management and Energy Auditing Book, Book II Energy Efficiency in Electrical Utilities, http://www.energymanagertraining.com.
[9] Official website of the Bureau of Energy Efficiency, Govt. of India, http://www.beeindia.nic.in.
[10] Energy Efficiency Guide for Industry in Asia, www.energyefficiencyasia.org.

Study of Roller Conveyor Chain Strip under Tensile Loading

Jagtap M. D. [1], Gaikwad B. D.[2], Pawar P. M. [3]

1(PG Student ME Mechanical (CAD/CAM), SVERI's C.O.Engg, Pandharpur, Solapur University, India)
2, 3 (Associate Professor, Department of Mechanical Engineering, C.O.Engg, Pandharpur, Solapur University, India)

Abstract: *Conveyor chain drives are one of the primary systems used in industry to transmit power and convey products. Conveyor chain that suffers from premature elongation due to wear and needs to be replaced on a frequent basis will negatively impact productivity and increase the cost of the operation. Roller conveyor chains are the critical component in sugar mills, paper mill, food processing, fertilizer industry, pharmaceutical industry, cement industry, foundry industry, heat treatment units, coal mines etc. The scope of this paper is to study the behavior of chain strip under tensile loading. In turn it will help in reducing down time and maintenance cost related chain assembly in various above said industries. Today, few literatures on the wear of conveyor chain are available. In this paper we study the analytical, experimental and numerical behavior of strip under tensile loading.*
Keywords: Chain strip, Link plate, Roller conveyor chain, Tensile loading.

I. INTRODUCTION

From a theoretical viewpoint chain is a continuous flexible rack engaging the teeth on a pair of gears. Cetrainly a sprocket being a toothed wheel whose teeth are shaped to mesh with a chain, is a form of gear. Based on its history and development, chian is a mechanical belt running over sprockets that can be used to transmit power or convey materials. Chain strips are machine elements that are subjected to extreme service conditions, such as high tensile loads, friction, and sometimes aggressive operating environment (e.g. presence of humidity, seawater, chemicals). Apart from tensile overload fracture, double shear is also an important failure mechanism which occurs under lower applied loads. Chain is the most important element of the industrial processes required for transmitting power and conveying of materials. As these chains operate under various forces, failure of chain assembly is the major problem. Causes of these failures are improper material selection, uncertainties in manufacturing, faulty manufacturing processes. It is important to study the influence of these parameters on the strength of the chain which governs the failure modes of the chain. The faulty manufacturing processes are another source of failure initiation.

Ledvina and Hummel [1] have developed a randomized sprocket for roller chain. A roller Chain and sprocket drive with a randomized sprocket which modulates the roller position on the sprocket by varying the radial seating position of the roller while maintaining a constant chordal dimension between the Seated rollers. Payet [2] has developed a process and conveyor device for feeding sugar cane in a Mill Train. Various known processes were used in sugar refineries for feeding sugar cane to mills or for conveying the bagasse from one mill to the next. The purpose of this invention was to produce a device enabling very high conveying speeds to be obtained and a regular feed to the three-roller crushing mills. White and Fraboni [3] have demonstrated roller chain sprockets oriented to minimize strand length variation. Numerous methods have been developed to reduce the radiated noise levels generated by the engagement of roller chains with sprockets.

A roller chain strip plate profile was developed by Moster et al., [4]. Material is added to the profile of the strip plates at the location on the strip plate where fatigue failure originates. The added material decreases the maximum stress levels effectively making the strip plate stronger, which provides for a stronger chain. A static stress analysis of strip plate of roller chain using finite element method and some design proposals for weight saving investigated by Noguchi et al., [5]. Roller chains have a long history as mechanical elements for transmission. Although they had clear advantages over belts in terms of performance and efficiency, but their larger weight has always been a disadvantage. Failure of engineering components due to presence of defects in the material was common issue. Sujata et al., [6] discovered a failure analysis of conveyor chain strips. These defects were either present in the material from the casting stage or get developed during subsequent hot working and thermal treatment operations.

Bhoite et al., [7] studied FEA based effect of radial variation of outer strip in a typical roller chain strip assembly. They summarized various design variables, such as wall thickness of strip, breaking area of strip and shape of the strip to formulate an idea of the system. Sapate and Didolkar [8] discovered metallurgical investigation of failure of coal mill drag chain pin. They done metallurgical investigation of fractured connecting pins of drag chain conveyors used for coal conveying from raw coal hopper to grave gate in coal mill of a cement plant.

II. Basic structure of roller conveyor chain.

Chains are used in a variety of applications in engineering practice. In general, there are three basic types of system; hoisting and securing chains, conveying and elevating chains and power transmission chains. Conveyors chains are used when material are to be moved frequently between specific points. Depending on the materials to be handled and the move to be performed, a variety of conveyors can be used. All roller chains are constructed so that the rollers are evenly spaced throughout the chain. Several types of roller chains are used in conveyors, many of single-pitch or double-pitch conveyors chain but here below Fig.1 shows the basic structure of roller conveyor chain.
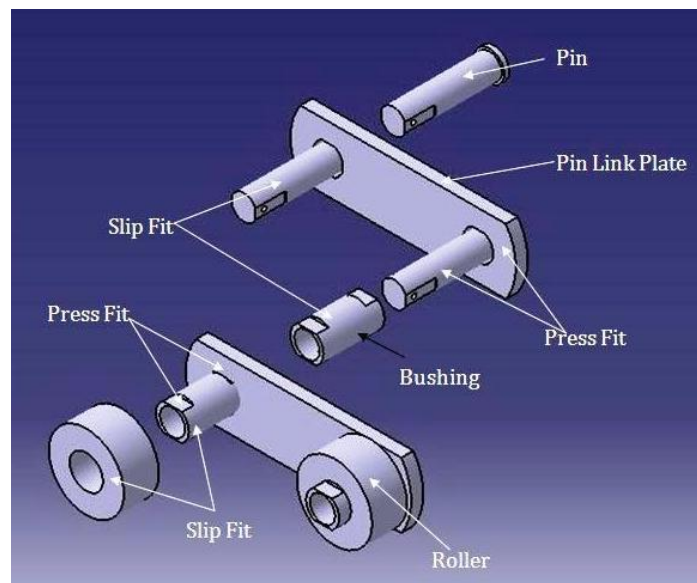
Fig.1 Basic structure of roller conveyor chain

Above Fig.1 shows the basic structure and components of roller conveyor chain and the different types of fits assembled under working conditions. Main components of roller conveyor chain are pin, link plate (strip), bushing and roller. The pin link plate i.e. strip is the assemblies of two pins that are press fitted into the holes of two pin link plates. The press fit between pin and the pin link plate prevents the pin from rotating. Usually there is a repeated loading, sometimes accompanied by shock. The pin is subject to shearing and bending forces transmitted by the plate. There is slip fit between bushing and pin.

The bushing is subject to shearing and bending stresses transmitted by the plate and roller, and also gets shock loads when the chain engages the sprocket. In addition, when the chain articulates, the inner surface forms a load-bearing part together with the pin. The outer surface also forms a load-bearing part with the roller's inner surface when the roller rotates on the rail or engages the sprocket. There is slip fit between the bushing and the roller. The roller is subject to impact load as it strikes the sprocket teeth during the chain engagement with the sprocket. After engagement, the roller changes its point of contact and balance. It is held between the sprocket teeth and bushing, and moves on the tooth face while receiving a compression load. A major advantages of roller chian is that the rollers rotate when contacting the teeth of the sprocket.

III. Analytical Study of Chain Strip

Roller conveyor chain or bush roller conveyor chain is the type of chain drive most commonly used for transmission of mechanical power on many kinds of domestic, industrial and agricultural machinery, including conveyors, wire and tube drawing machines, printing presses, cars, motorcycles, and bicycles. It consists of a series of short cylindrical rollers held together by side strips i.e. link plates as we had seen the basic structure

in Fig.1. It is driven by a toothed wheel called a sprocket. It is a simple, reliable, and efficient means of power transmission.
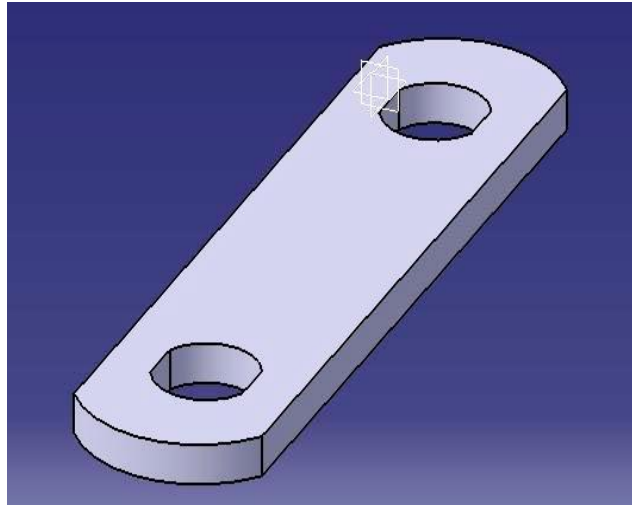
Fig.2 Strip dimensions (55mm x 150mm (Pitch) x 10mm)

Fig.2 shows the Strip of dimensions 55mm x 150mm (Pitch) x 10mm. Now by using the analytical formulae we find out the value of maximum stress i.e. ultimate tensile strength for

Values from design data book
Tensile strength = 67-71kgf = 630 N/mm^2 to 710 N/mm^2
Modulus of elasticity = 2.05*10^5 N/mm^2
Poisson's ratio = 0.3

$$Working\ stress = \frac{Maximum stress}{Factor of safety}$$

$$Working\ stress = \frac{710}{1.5}$$

$$Working\ stress = 473.33 N/mm^2$$

So as per the above analytical calculations we got working stress of 473.33 N/mm^2, now by using that working stress value we calculate the working load the strip can carry by using the following formulae.

$$Working\ stress = \frac{Working Load}{\operatorname{Re} sisting Area}$$

$$473.33 = \frac{Working Load}{27 \times 10}$$

$$Working\ Load = 473.33 \times 270$$

$$Working\ Load = 1,27,799 N$$

So as per the above analytical calculations we got working load of 1, 27,799 N. Now we can check these values with experimental and numerical results.

IV. Experimental Study of Chain Strip

For Experimental testing of chain strip of dimensions 55mm x 150mm x 10mm of EN353 material were taken to study the working stress of the strip. For this testing we are using a Universal Testing Machine of 40tonne capacity. The Experimental test setup for this experiment is shown in Figure 2.

Fig.3 Testing of Chain strip

As shown in above Fig.3 the strip of dimensions 55mm x 150mm x 10mm was clamped on the Universal Testing Machine with the help of two fixtures. The load was given by the application of the hydraulic pressure.
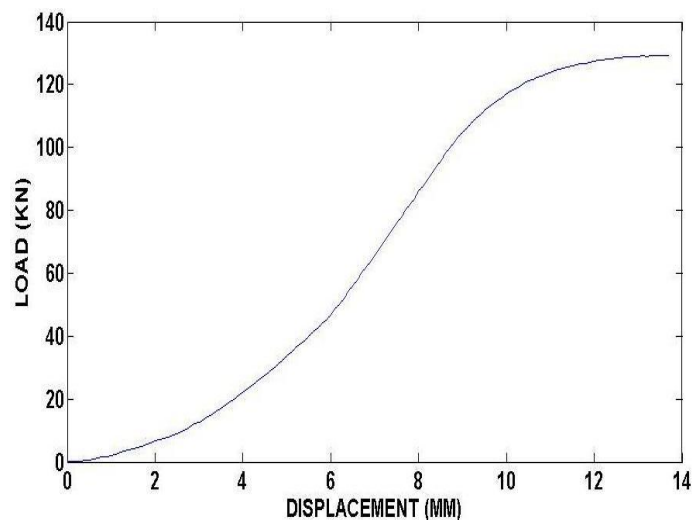
Fig.4 Graph of Load v/s Displacement

As shown in the above Fig.4 displacement in MM is shown on x-axis and load in KN is shown on Y-axis. The max load of 129.2KN is taken by the strip and then it fails elliptical hole. The maximum tensile strength of 490 N/mm^2 was gained by the strip.

Tensile strength = 490 N/mm^2
Maximum load = 129.2KN

V. Numerical Results of Chain Strip

In the assembly of roller conveyor chain on the outer sidebars i.e. on strips tensile forces are applied by pins that are assembled through holes in the sidebars. The holes in the sidebars are significant stress risers. The outer sidebars are primarily tension members, and they also are subjected to substantial bending and stress concentrations around the holes. The outer sidebars must have enough strength to withstand the tensile forces without deforming or breaking, and they must have enough ductility to withstand substantial bending and to resist fatigue.

Table.1 Input parameters for the simulation.

INPUT PARAMETERS	
Young's Modulus	2.05e+005 N/mm^2
Poisson's Ratio	0.3
Define By	Components
Coordinate System	Global Coordinate System
X Component	0. N
Y Component	0. N
Z Component	128000N

The strip is first modeled in CATIA V-5 and then exported to ANSYS where it is further meshed, constrained and loaded and simulated further. As far as loading and geometry of strip is concerned, it is necessary to carry out three dimensional analysis .Therefore; Strip is fine meshed. Material properties of EN353 are entered as an input. The above Table.1 shows the input parameters required for the simulation.
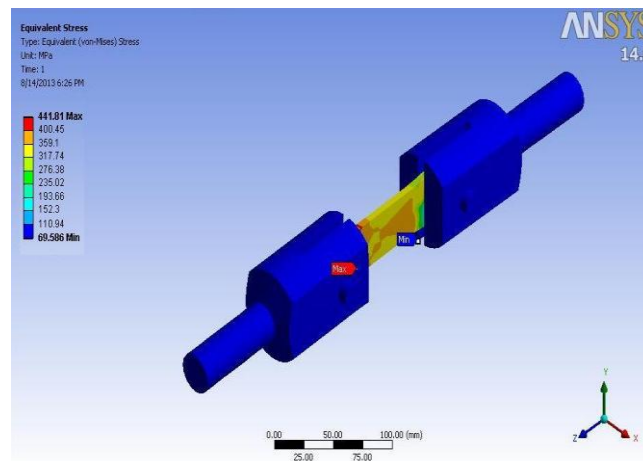
Fig.5 FEA set up with fixture

Finite element analysis (FEA) of strip has been carried out as shown in above Fig.5. As far as boundary conditions are concerned, total 128000N static load is applied in positive Z at one end of strip i.e.at fixture. Red colored arrows show reaction of applied forces. Maximum stress developed in strip has been found out. Also, region of failure for strip was observed after simulation.
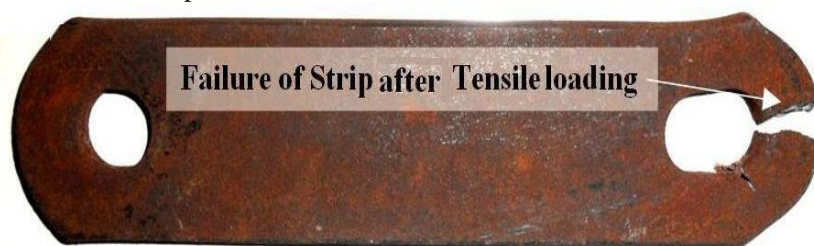
Fig.6 Failure of Strip

The above Fig.6 shows the actual failure of strip under tensile loading. It is observed that the round hole of strip becomes elliptical under tensile loading. Further while gradually increasing of load it fails near to elliptical hole.
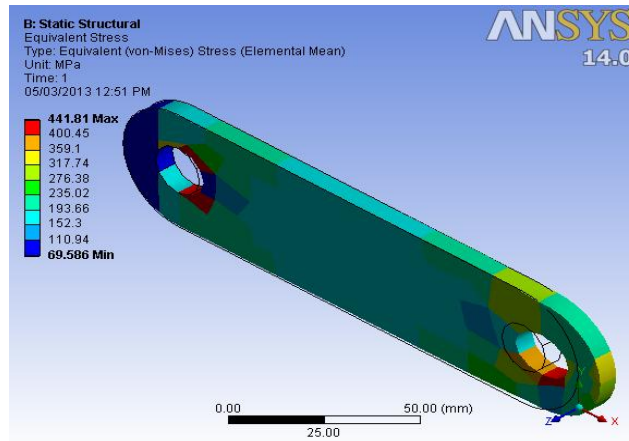
Fig.7 Finite element model of strip

From above Fig.7 it is observed that there is stress concentration near to elliptical hole in the strip, so the strip will fail in that region. It can sustain maximum stress of 441.81 N/mm^2. If stress value at any point in strip crosses 441.81 N/mm^2 strip starts yielding and it will fail.

VI. Conclusion

We studied the analytical, experimental and numerical behavior of strip under tensile loading. The fatigue initially nucleated at the external cracks of the link, and later propagated to the inside of the links until sudden fracture occurred. Below table shows the comparison results.

Table.2 Comparison of results

Tests	Analytical result	Experimental result	Numerical result
Tensile Stress(N/mm^2)	473.33	490	441.81

As above table shows all the results are within +/- 10% of the calculated working stress, so the strip is safe under the maximum working load of 1,28,000 N. A roller chain drives may be subjected to all of the tensile loads, thus the roller chain must have several tensile strength properties to withstand the wide range of tensile loads that may be imposed on it.

REFERENCES

[1]   Ledvina T. J. and Hummel J. A. (2002) Randomized Sprocket for Roller Chain, European Patent # EP0907041
[2]   Payet P. R. (1964) Process and Conveyor Device for Feeding Sugar Cane in a Mill Train, U. S. Patent # 3,120,173.
[3]   White D. C. and Fraboni H. J. (2001) Roller Chain Sprockets Oriented to Minimize Strand Length Variation, United States Patent # 6213905.
[4]   Moster A. and Ledvina T. J. (2003) Roller Chain Link Plate Profile, European Patent # EP0833078
[5]   Noguchi S, Nagasaki K., Nakayama S., Kanada T., Nishino T., Ohtani T., "Static Stress Analysis of Link Plate of Roller Chain Using Finite Element Method and Some Design Proposals for Weight Saving", Journal of Advanced Mechanical Design, Systems, and Manufacturing, (2009), Vol. 3, No. 2.
[6]   Sujata M., Venkataswamy M., Parameswara M., Bhaumik S., "Failure Analysis of Conveyor Chain Links", Engineering Failure Analysis, (2006), 13(6), 914-924.
[7]   Bhoite T., Pawar P., Gaikwad B., "FEA Based Study of Effect of Radial Variation of Outer Link in A Typical Roller Chain Link Assembly", International Journal of Mechanical and Industrial Engineering (IJMIE), (2012), ISSN No. 2231 –6477, Vol-1, Issue-4.
[8]   Sapate S., Didolkar V., "Metallurgical Investigation of Failure of Coal Mill Drag Chain Pin", Materials and Design, (2009), 30(7) 2623-2629.

Design &Analysis of Waste Heat Recovery System for Domestic Refrigerator

S. B. Lokhande[1], Dr. S. B. Barve[2]

[1] *(Mechanical Engineering Department, MIT College of Engineering, Pune, University of Pune, India)*
[2] *(Professor, Mechanical Engineering Department, MIT College of Engineering, Pune, University of Pune, India)*
sbl2070@gmail.com, sbbarve@rediffmail.com / sbbarve@gmail.com

Abstract: *Heat is energy, so energy saving is one of the key matters from view point of fuel consumption and for the protection of global environment. So it is necessary that a significant and concrete effort should be made for conserving energy through waste heat recovery too. The main objective of this paper is to study "Waste Heat recovery system for domestic refrigerator". An attempt has been made to utilize waste heat from condenser of refrigerator. This heat can be used for number of domestic and industrial purposes. In minimum constructional, maintenance and running cost, this system is much useful for domestic purpose. It is valuable alternative approach to improve overall efficiency and reuse the waste heat. The study has shown that such a system is technically feasible and economically viable.*
Keywords: *Waste heat recovery, 165 liter Domestic refrigerator, COP of refrigerator, Refrigerating effect.*

I. INTRODUCTION

Waste heat is generally the energy associated with the waste streams of air, gases and liquids that leaves the boundary of the system and enter into environment. Waste heat which is rejected from a process at a temperature enough high above the ambient temperature permits the recovery of energy for some useful purposes in an economic manner. The essential quality of heat is not the amount but its value. Waste heat recovery and utilization is the process of capturing and reusing waste heat for useful purposes. Not all waste heat is practically recoverable. The strategy of how to recover this heat depends on the temperature of the waste heat sources and on the economics involves behind the technology incorporated.

Cooling generates considerable quantities of heat. If not utilized, this energy simply becomes waste heat. The cooling may be for the process cooling, air conditioning or other use. Thus all the heat removed from the process, plus most of the energy added by the compressor and ancillary pumps, is rejected to the local environment. This rejected heat can often be economically recovered and be used instead of heat generated from fossil fuels. While there is a cost in running the refrigeration plant, this heat is effectively close to 'free'.

Stinson et al. [1] conducted research in dairy refrigeration by recovering the heat from condenser. They found out that by using the water cooled condenser COP of the system is enhanced by 10% to 18%. They also found that increase in condenser pressure reduces COP, and inclusion of heat recovery heat exchanger reduces head loss. Rane et al. [2] developed sensible heat recovery unit and carried out experiments. Waste heat recovered is utilized for water heating. Their findings are: (i) chiller cooling capacity enhanced by 30% and COP by 20%. Kulkarni,Barve [3] *discussed in studies on* to heat water by recovering the heat released on the level of the condenser of the cooling systems such as refrigerator, air-conditioner, cold room etc.They have also shown that such a system is economically viable. Energy consumption by the system and environmental pollution can still further be reduced by designing and employing energy saving equipments. F.N.Yu, K.T.Chan [4] discussed the improved condenser design for air cooled chillers.

II. System Description and Design

The present work was with the aim to recover and utilize waste heat from the domestic refrigerator which as such is let off to the surrounding through its surface condenser. To assess the viability of this concept a very common house hold appliance known as hot case was selected and its energisation is replaced from high quality electrical power to low grade waste heat of hot refrigerant vapors keeping in view the likelihood of more effective cooling of high pressure hot refrigerant vapors from the compressor.For that purpose some calculations are made regarding size and length of condenser and then WHRS is designed. But after different discussions and calculations for heat transfer rates we approached to the final design of insulated cabin with compact construction and with reasonable cost. So as to extract more and more heat, we have mounted a hot case on top,

left and right side of refrigerator. The main advantage of this design is that we can get maximum heat with minimum losses.

2.1 Fabrication and assembly work:-

2.1.1 Major equipments and parts:-

Since the concept gives brief idea about utilizing waste heat at domestic level, hence we have decided to use a "GODREDE" second hand working domestic refrigerator of capacity 165 liters. Parts of domestic refrigerator are as follows. Compressor, Modified Air cooled Condenser, Capillary Tube, Plate type Evaporator & Insulated Cabin. The insulated cabin is a peripheral component which is used for utilizing the waste heat from refrigerator. This insulated cabin is fabricated by using galvanized iron sheets.

Table 2.1: Equipments with Specifications

SR.NO	Equipment	Type/ Material	Specification/ Capacity	Manufacturer
1	Refrigerator a. Compressor b. Condenser c. Evaporator	Domestic Type 2 Hermetically sealed Water cooled Plate type	165 Liters 1/8th HP No. of Tubes – 18	Godrej Kirloskar Kirloskar \ Roll bond
2	Refrigerant	CCl_2F_2	110 gms	Innotech technology
3	Insulated Cabin 1.on both side of refrigerator 2.on top of the refrigerator 3 Insulation	Galvanized Iron Galvanized Iron Thermocole	(70cmX35cmX2cm)X 2 = 9.8 liters =1.2 liters Thickness:- 3.50cm	-----------------
4	Energy Meter	DJ01 A.C.1 Phase 2 wire static kwh meter	Rating:5-30 Amp 240 V. 50Hz	U.G. Jaipur Industries (India)
5	Temperature Indicator	Multipoint Temp. detector	Power: 230 VAC .50 Hz Input:RTD-PT100 x4 NO Range:-25 to 100 ^{0}c	Kristech solution ltd ,pune

1.1.2..Experimental Setup:

Figure shows the assembly and the connection of the hot case, energy meter, temperature detector with the refrigerator.

III. EXPERIMENTAL RESULT AND ANALYSIS

3.1.1Actual COP of System Based On Theoretical Data

For Refrigerator of 165 liters capacity, given data from Kirloskar Ltd manual follows-
Refrigerator cooling capacity:(PROVIDED BY GODREJ)

=76 kcal/hr

$= 76 \times 4.187 \times 1000/3600 = 88.392$ W

Power required running the compressor

= 1/8 HP

$= 1/8 \times 746 = 93.25$ W

The coefficient of performance (COP) :

$$= \frac{\text{Refrigeration effect}}{\text{Work supplied}}$$

$$= \frac{88.392}{93.25}$$

$$= 0.958$$

3.1.2 Practical Cop of System

Pot filled with known quantity of water is put inside evaporator and main cabin and outide compartment and temperatures are noted after specific interval of time. By following above procedure, observations are noted and time V_s temperature and COP graphs are plotted.

3.1.2.1. Refrigerator with Hot Case

Sr. No	Time	Energy Meter reading K.W.Hr.	Power watts	Temp. of water in evapora-tor °C	Temp. of water in main cabin °C	Temp of water in outside cabin °c	Refrigerating effect in evaporator (watt)	Refrigerating effect in main cabin watts	Total refrigeration effect watts	C.O.P
1	11:00	12.50	-------	34	34	34	-----------	-----------	-----------	-------
2	11:30	12.61	220	20	28	36	97.53	309	306.53	1.410
3	12:00	12.70	200	05	24	39	104.5	139.33	243.63	1.299
4	12:30	12.78	160	00	20	40.9	36.83	139.33	176.16	1.106
5	01:00	12.85	140	-5.3	16.7	45.7	36.92	114.05	150.97	1.083
6	01:30	12.91	120	-8.3	13.6	48.6	22.99	107.3	130.2	1.082
7	02:00	12.96	100	-11.0	11.2	50.6	18.81	90.086	108.89	1.081

3.1.2.2. Refrigerator without Hot Case

Sr. No	Time	Energy Meter reading K.W.Hr.	Power watts	Temp. of water in evapora-tor °C	Temp. of water in main cabin °C	Temp of water in outside cabin °c	Refrigerating effect in evaporator (watt)	Refrigerating effect in main cabin watts	Total refrigeration effect watts	C.O.P
1	11:00	17.14	-------	34	34	-----------	-------------	-----------	-----------	-------
2	11:30	17.26	220	19	28.5	-----------	104.12	209.4	313.16	1.363
3	12:00	17.37	200	09	23.1	-----------	69.66	188.1	257.76	1.229
4	12:30	17.46	160	0	17.3	-----------	34.83	160.23	195.06	1.146
5	01:00	17.53	140	-4	13.6	-----------	28.86	128.88	157.74	1.123
6	01:30	17.59	120	-8.3	10.9	-----------	28.56	96.04	124.60	1.101

TIME VS POWER

TIME VS COP

TIME VS TEMPRATURE OF WATER IN OUTSIDE COMPARTMENT
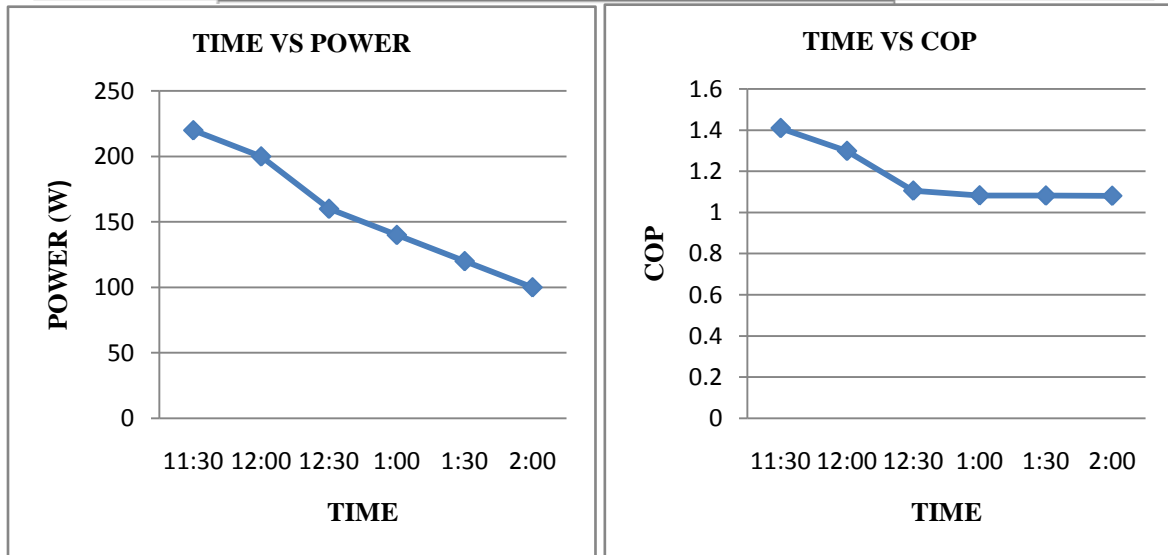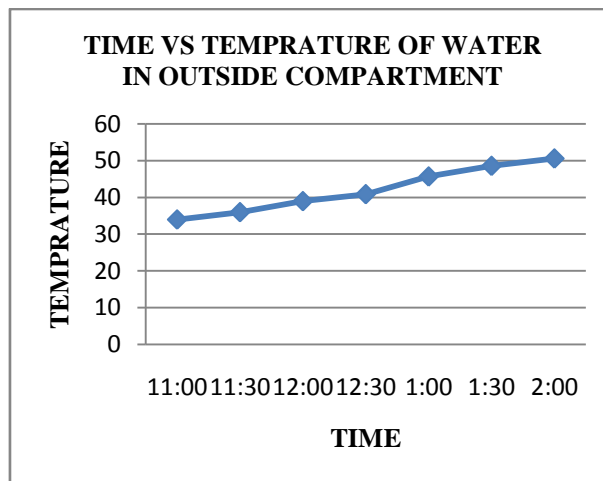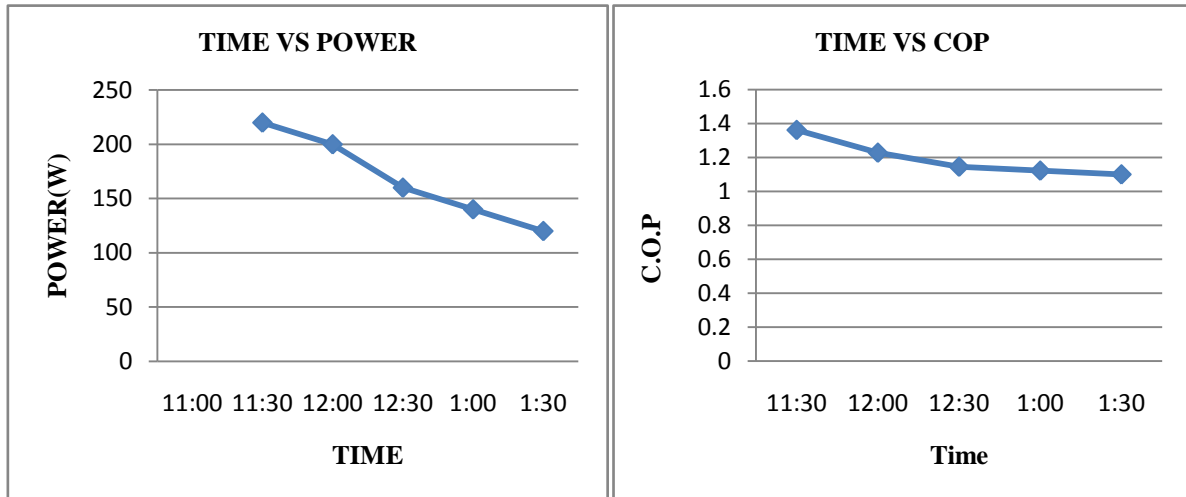
IV. CONCLUSION

From the results tabulated it can be concluded that with time the energy consumption of the refrigerator decreases for certain time and then it remain constant.The refrigerating effect keeps decreasing as the temperature difference between the refrigerant and article placed Is decreased.The C.O.P. remains almost constant though it decreases a little bit.

With hot case, as if we add up heating effect in desired effect, then the c.o.p. is increased also otherwise it is almost little bit more than the unit with the hot case.

Thus the hot case has not bad effect on the refrigerator. Here with use of hot case, we can keep some food stuff, is hot condition, also temperature of food/milk, etc can be increased without change in taste, so amount of electrical energy used for hot case, as in case of conventional system, can be saved.

REFERENCES

[1]   G. E. Stinson, C. J. Stuman, D. J. Warburton, " A dairyrefrigeration heat recovery unit and its effects on refrigeration operation" , J. agric. Engng Res. (1987) 36, 275-285.
[2]   Milind V. Rane, Madhukar S. Tandale, "Benefits of superheat recovery on chillers case study for a hotelinstallation", International Congress of Refrigeration 2003, Washington, D.C.
[3]   S. C. Walawade,B.R Barve, P. R. Kulkarni,"Design and Development of Waste Heat Recovery System for Domestic Refrigerator", IOSR Journal of Mechanical and Civil Engineering, ISSN: 2278-1684, PP: 28-32

[4]   F.N.Yu, K.T.Chan, "Improved condenser design and condenser-fan operation for air-cooled chillers", Applied Energy, Vol.83 (2006) 628-648..

[5]   Alexander Cohr PachaiJohnson Controls Building Efficiency "Energy consumption and heat recovery of refrigeration systemin modern Arena".

Enhance Example-Based Super Resolution to Achieve Fine Magnification of Low Resolution Images Using Neighbour Embedding Method

Nisarg Patel [1] Rahul Joshi [2]

[1,2] *(Master in Computer Engineering, Department of Information technology, Parul Institute of Engineering & Technology, Vadodara, Gujarat, India)*

Abstract: *Images with high resolution (HR) often required in most electronic imaging applications. There are two types of resolution first is high resolution and other one is low resolution. Now high resolution means pixel density with in an image is high and low resolution means pixel density with in an image is low. Therefore high resolution image can offer more detail compare to low resolution image that may be critical in many application. Super resolution is the process to obtain high resolution image from one or more low resolution images. Here in paper explain such robust methods of image super resolution. This paper describes the learning-based SR technique that utilizes an example-based algorithm. This technique divides a large volume of training images into small rectangular pieces called patches and patch pairs of low-resolution and high-resolution images are stored in dictionary. After that there are low resolution patch is extracted from the input images. The most alike patch pair is searched in the dictionary to synthesize high resolution image using the searched high resolution patch in the pair.*

Index Terms: *Super resolution (SR), training, example based, patch, image restoration.*

I. Introduction

Image super resolution plays important role in multimedia application. Super resolution is a technique to achieve a clear high resolution image from a low resolution image. This technique is widely adopted to improve a quality of images shots by a digital camera. When image captured by low resolution camera three main artefacts occur, namely aliasing, blurring and additive noise. An aliasing occurs due to the low sampling rate. This causes the loss of high frequency contents from the image. High frequency having information about edges and textures, so there are ultimate artefacts occurs at the edges in the image. A blurring occurs due to the relative motion between image and camera. An atmospheric noises like rainy atmosphere and dusty atmosphere cause additive noise in image. So, one can say that the super resolution is the process of recovering the missing high frequency details and removing the degradation that arise during the image acquisition process. Super-resolution techniques can be applied in various domains. Image processing applications are like remote sensing, enlarging consumer photographs, medical imaging, and online image exchange, image viewing and converting NTSC video content to HDTV demands high resolution image.

Super-resolution techniques can be applied in various domains. Image processing applications are like remote sensing, enlarging consumer photographs, medical imaging, and online image exchange, image viewing and converting NTSC video content to HDTV demands high resolution image. The high resolution image not only gives the viewer pleasing appearance but also gives additional information that important for the analysis in many applications like medical imaging. There are many practical applications of SR reconstruction.

Satellite imagery is one obvious application. If the slight offsets between images taken from separate orbits are of sub-pixel accuracy, SR image reconstruction is viable. Land-cover-mapping is an area where SR techniques are necessary for resolving landscape features, especially rural hedges and other thin formations. Also, at some position image captured by satellite is LR image then it has to wait until it complete one revolution to recapture the same scene. In such case SR technique helpful to obtain HR image.

Super-resolution methods can also be used to create high resolution still pictures or video from video sequences. The sub-pixel motion requirement necessary for SR image reconstruction does not have to come from movement of the imaging system. In the case of a video sequence, global motion of objects in the scene may be adequate in the temporarily shifted frames, even if the camera remains static. For static scenes, SR image reconstruction is viable so long as long as sub-pixel accuracy can be attained due to vibrations in the camera. The same techniques can also be applied to improve the resolution of existing (low resolution) video content for use in high definition television sets.

The enhancement of smaller, ROI objects within a field of view (FOV) is very important in imaging, especially surveillance. An example of this is digital zoom, where a ROI is up-sampled ("blown up") to the dimensions of the original FOV. Super resolution reconstruction is also used to obtain HR image by some form of using single LR image. Surveillance system like License Plate Recognition (LPR) system needs to identify the vehicle license plate images taken from the camera. Most LPR systems are designed for toll gates and parking place or any other places for security purpose. In order to full fill this need we can use technique to reconstruct HR image from low resolution images or single LR image. In medical imaging, SR image reconstruction is useful in resolution-limited imaging systems such as computed tomography (CT) and magnetic resonance imaging (MRI) which can easily acquires multiple images of the same scene. Apart from these, there are number of application of super resolution reconstruction used to obtain the HR image from multiple LR images or single LR image.

II.   Super Resolution Image Reconstruction

The generation of the low resolution image can be modeled as a combination of smoothing and down-sampling operation of natural scenes by low quality sensors. Super resolution is the inverse problem of this generation process. One criteria of solving this inverse problem is minimizing the reconstruction error. Various methods are proposed in literature to deal with the inverse problem. In following section I categorize the different SR methods available in existing literature.

In this method [9] super-resolution problems can use flexible method that in principle with arbitrary magnification factors up to some fundamental limits. Propose a new, using the training examples in more general way so that simultaneously the generation of each image patch can be used multiple training examples in the high-resolution image. This formula is very important when generalization over the training examples is possible and hence there are required limited numbers of training examples.

In this Method [2] a robust first-order regression model for image super-resolution based on justified in-place self-similarity. Model leverages the two most successful super-resolution methodologies of learning from an external training database and learning from self-examples. Taking advantage of the in-place examples, learn a fast and robust regression function for the otherwise ill-posed inverse mapping from low- to high-resolution patches. On the other hand, by learning from an external training database, the regression model can overcome the problem of insufficient number of self-examples for matching. Compared with previous example-based approaches, new approach is more accurate and can produce natural looking results with sharp details. In many practical applications where images are contaminated by noise or compression artefacts, our robust formulation is of particular importance.

In this Method [4] learning patch pairs of low- and high-resolution images use to synthesizes a high-resolution image. However, since a low-resolution patch is usually mapped to multiple high-resolution patches, unwanted artefacts or blurring can appear in super-resolved images. Here propose a novel approach to generate a high quality, high-resolution image without introducing noticeable artefacts. Introducing robust statistics to a learning-based super-resolution, we efficiently reject outliers which cause artefacts. Global and local constraints are also applied to produce a more reliable high-resolution image. Learning-based super-resolution algorithms are generally known to provide HR images of high quality. However, their practical problem is the one-to-multiple mapping of an LR patch to HR patches, which results in image quality degradation.

This algorithm [5] uses learning method to construct super resolution image. The main contributions of these algorithms are: (1) a class-specific predictor is designed for each class in our example-based super-resolution algorithm – this can improve the performance in terms of visual quality and computational cost; and (2) different types of training set are investigated so that a more effective training set can be obtained. The classification is performed based on vector quantization (VQ), and then a simple and accurate predictor for each category, i.e. a class-specific predictor, can be trained easily using the example patch-pairs of that particular category. These class-specific predictors are used to estimate, and then to reconstruct, the high-frequency components of a HR image. Hence, having classified a LR patch into one of the categories, the high-frequency content can be predicted without searching a large set of LR-HR patch-pairs.

In this Algorithm [3] a learning-based super resolution technique using an example-based approach that enables restoration of finely-magnified, high-resolution images by specifying target objects. The proposed method features the unique properties of minutely varied, training images as well as applying weighted searching/synthesizing. Therefore, it can achieve finely-magnified, high-precision super resolution of images efficiently, including those of texts and human faces. Results of text images, car license plate images and human face images demonstrate the great effectiveness of this method. This method consists of two phases, 1) A dictionary construction phase that performs extraction of patch pairs from both HR and LR images, and then stores them as training data in the dictionary, and 2) An super resolution phase that performs synthesizing of HR images by searching patches stored in the dictionary that are best matched to the input images.

Table 1: comparison between super-resolution techniques

	Methods	Advantages	Disadvantages
1	Nearest Neighbor Interpolation	Preserves the sharpness and does not produce the blurring effect	Produce aliasing.
2	Bi-linear Interpolation	Does not create an aliasing effect.	Produce some artefact
3	Bi-cubic Interpolation	Gives smooth image	Produce some artefact
4	An Efficient Example-Based Approach for Image Super-Resolution	Excellent performance in terms of both quality and computational complexity.	
5	Robust Learning-Based Super-Resolution	Provide high quality image	The one-to-multiple mapping of an LR patch to HR patches, which results in image quality degradation.
6	Fast Image Super-resolution Based on In-place Example Regression	Better at handling real applications	Does not handle noisy input images
7	Super-Resolution Through Neighbor Embedding	Smoothes the texture on the face, better effect on some edges.	Produce some artefact
8	Iterative back projection algorithm	Less complexity and low-less number of iteration is required	Edges are not improve compare to other methods

III. Proposed Method

In my proposed work it will use enhance example learning based super resolution method for avoiding artefact and improve image quality. My proposed method is dividing into two phase. First phase is dictionary construction phase. There is different types of low resolution images classified by minute variations are generated out of a large volume high resolution training images. Patches are extracted from high resolution and low resolution image and patch pair of high resolution and low resolution images are stored in the dictionary. Second phase is Super resolution phase. There are low resolution patch is extracted from the input images. The most alike patch pair is searched in the dictionary to synthesize high resolution image using the searched high resolution patch in the pair.

There are k-mean tree used in dictionary construction phase for arrange the patch pair of low resolution and high resolution patch pair. Now in super resolution phase neighbor embedding method is used for searching the well match patch pair from dictionary and synthesize the high resolution.There are reconstructed high resolution image has some blur so for removing that blur used non-local mean algorithm, by using this algorithm we avoid the blur and improve the image quality.Here algorithm of proposed method,

3.1 Dictionary Construction Phase

There are three steps for develop this phase such as:

Step 1: Input different types of low resolution (LR) images classified by minute variation are generated out of a large volume of high resolution (HR) training images.
Step 2: Patches are extracted from HR and LR images using example based super resolution.
Step 3: Patch pair of HR and LR are stored in dictionary.

3.2 Super resolution Phase
There are four steps such as:

Step 1: LR patch is extracted from the input image.
Step 2: The most alike patch pair is search in dictionary using Neighbour Embedding algorithm
Step 3: Synthesize an HR image using the search HR patch in the pair.
Step 4: Reconstruction based enhancement.

IV. Experimental Results

In order to show the effectiveness of our proposed method, we introduce the results when our proposed method was applied to a low-resolution text image shot by a digital camera. Here in result input low resolution image and get $3 \times$ magnified output high resolution image.

| (a) | (b) | (c) | (d) | (e) |
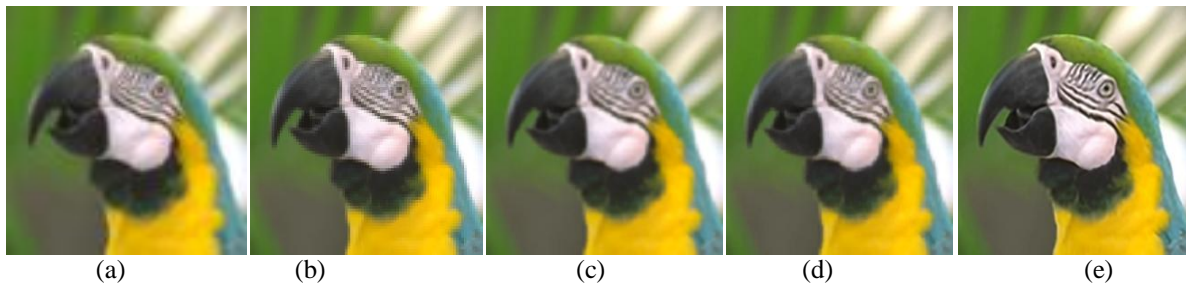
Figure 1: (a) Input Image (b) Nearest neighbor (b) Bi-cubic interpolation(PSNR= 26.02 dB) (d) SR image using Euclidean distance(PSNR = 26.15 dB) (e) SR image using Neighbor Embedding Method (PSNR = 30.10 dB).

| (a) | (b) | (c) | (d) | (e) |
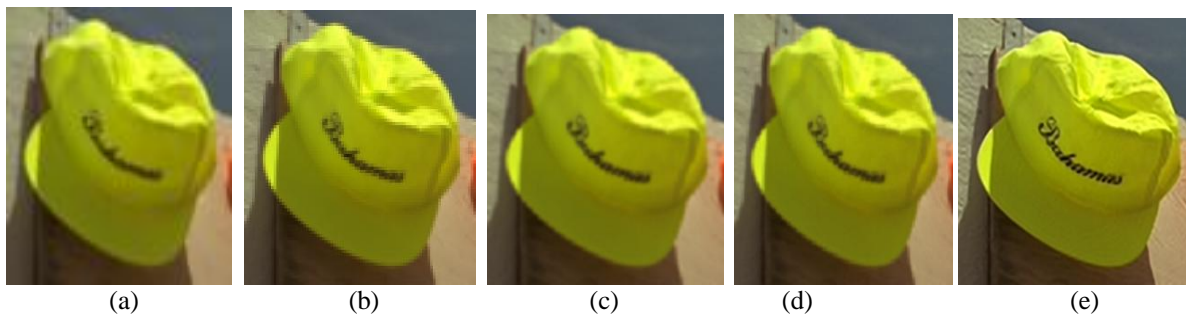
Figure 1 : (a) Input Image (b) Nearest neighbor (b) Bi-cubic interpolation(PSNR= 27.56 dB) (d) SR image using Euclidean distance(PSNR = 27.67 dB) (e) SR image using Neighbor Embedding Method (PSNR = 31.01 dB).

V. Conclusion

There are several methods used to improve the quality of low resolution image but some methods can produce blur in the image. Some may avoid blur but occur aliasing in the high resolution image. So, reconstructed image is reducing efficiency and performance due this artefact. So, here   developed a new approach of enhance example based super –resolution for magnified low resolution images using neighbour embedding method that reduce blur and artefact from image and improve the efficiency and quality of image . In future, improve quality of image using more number of training images.

Acknowledgements

REFERENCES

[1]   Dr. S. D. Ruikar and Mr. T.D. Wadhavane "A Single Image Super Resolution Using Advanced Neighbour Embedding" International Journal of Computer Science & Engineering Technology (IJCSET), Vol. 4 No. 04 April 2013.
[2]   Jianchao Yang, Zhe Lin, Scott Cohen, "Fast Image Super-resolution Based on In-place Example Regression" computer vision foundation, CVPR2013.

[3]   SENDA Shuji, SHIBATA Takashi, IKETANI Akihiko" Example-based Super Resolution to Achieve Fine Magnification of Low-Resolution Images" NEC TECHNICAL JOURNAL, Vol.7 No.2/2012.

[4]   Changhyun Kim and Kyuha Choi "Robust learning-based super-resolution", Proceedings of IEEE 17th International Conference on Image Processing, 2010, pp 2017 – 2020

[5]   Xiaoguang Li and Kin Man Lam "An efficient example-based approach for image super- resolution"   IEEE   Int. Conference Neural Networks & Signal Processing Zhenjiang, China,   June 2008, pp 575 – 580

[6]   M.V.Joshi and S.Chaudhuri " A learning based method for image super-resolution from zoomed observations " Proc. of 5th Int. Conf. on Advances in Pattern Recognition (ICAPR'03) pp.179-182, Calcutta, India, Dec.2003.

[7]   S. Dai, M. Han, Y. Wu, and Y. Gong, "Bilateral Back-Projection for Single Image Super Resolution," IEEE Conference on Multimedia and Expo (ICME), 2007, pp. 1039-1042.

[8]   W.T. Freeman, T.R. Jones, and E.C. Pasztor "Example-Based Super- Resolution," IEEE   Computer Graphics and Applications, vol. 22, no. 2, 2002, pp. 56-65.

[9]   Hong Chang, Dit-Yan Yeung, Yimin Xiong" Super-Resolution Through Neighbor Embedding"

[10]   R. Gonzalez and R. Woods, "Digital Image Processing", 3rd Edition, Pearson Eduction, Inc, Publishing as Prentice Hall, pp. 714-715.

[11]   W.T. Freeman, T.R. Jones, and E.C. Pasztor, "Example- Based Super- Resolution," IEEE Computer Graphics and Applications, vol. 22, no. 2, 2002, pp. 56-65.

[12]   M.V.Joshi and S.Chaudhuri," A learning based method for image super-resolution from zoomed observations," Proc. of 5th Int. Conf. On Advances in Pattern Recognition (ICAPR'03) pp.179-182, Calcutta, India, Dec.2003.

[13]   Nunez J, Otazu X, Fors O, Prades A, Pala V, Arbiol R. "Multiresolution-based image fusion with additive wavelet decomposition". IEEE Transactions on Geoscience and Remote Sensing, vol 37, no 3, 1999, pp 1204−1211

[14]   J.Ma, J. C.-W. Chan, and F. Canters, "Fully automatic sub-pixel image registration of multi-angle CHRIS/Proba data," IEEE Trans. Geosci. Remote Sens., vol. 48, no. 7, pp. 2829–2839, July 2010.

[15]   G. Yang, C. V. Stewart, M. Sofka, and C.-L. Tsai, "Registration of challenging image pairs: Initialization, estimation, and decision," IEEE Trans. Pattern Anal.Mach. Intell., vol. 29, no. 11, pp. 1973– 1989,Nov.2007.

[16]   Chen- Chiung Hsieh and Yo-Ping Huang "Video Super-Resolution by Motion Compensated Iterative Back-Projection Approach" journal of information science and engineering, vol 27, no 3, 2011, pp 1107-1122

[17]   H. Trussel and B. Hunt, "Sectioned methods for image restoration," IEEE Trans. Acoust., Speech Signal Process., vol. ASSP-26, no. 2, pp. 157–164, 1978.

International Journal of Modern Engineering Research (IJMER)

Contents :

CFD Analysis of Heat Transfer and Flow Characteristics in A 3D Cubic Enclosure

Mohd. Abdul Samad[1], Dr. Syed Nawazish Mehdi[2], Md. Abdul Raheem Junaidi[3],
Dr. M. Manzoor Hussain[4]

[1, 2, 3] (Sr. Assistant Professor, Professor, Assistant Professor Mechanical Engineering Department ,Osmania University, India)
[4] (Principal, JNTUH College of Engineering Sulthanpur, India)

Abstract: *Flow arising "naturally" from the effect of density difference, resulting from temperature or concentration difference in a body force field such as gravity, the process is termed as natural convection. There has been growing interest in buoyancy-induced flows and the associated heat and mass transfer over the past three decades, because of the importance of these flows in many different areas such as cooling of electronic equipment, pollution, materials processing, energy systems and safety in thermal processes. Steady state laminar natural convection in a cubic enclosure with a cold vertical wall and two square heaters with constant temperature on the opposite wall is studied numerically. The enclosure is fitted with various liquids. Three-dimensional Navier Stokes equations are solved by employing SIMPLE algorithm. Computations are performed for a range of Rayleigh number from 10^4 to 10^7 while enclosure aspect ratio varies from 0.1 to 1.25. The effects of Rayleigh number, enclosure aspect ratio, and Prandtl number on heat transfer characteristics are studied in detail. The results show that the flow field is very complex and heat transfer from the two heaters is not the same. The effect of Prandtl number is negligible in the range 5 to 100 with other parameters kept constant. This allows the use of liquids such as water for studying other dielectric liquids, provided the flow geometry and other non-dimensional parameters are similar. The overall Nusselt number increased markedly with Rayleigh Number. It is also affected by enclosure aspect ratio.*

Keywords: *Temperature, Aspect ratio, Computation, Three Dimensional, Rayleigh number.*

I. INTRODUCTION

Steady-state laminar natural convection in a cubic enclosure with a cold vertical wall and two hot squares heaters with constant temperature on opposite wall was studied numerically by Y.L.He, W.W.Yang and W.Q.Tao [1]. The enclosure is filled with liquid various liquids and three dimensional numerical analysis was carried and computations were performed for a range of Rayleigh numbers with various aspect ratios. The effect of Rayleigh number, enclosure aspect ratio and Prandtl number on heat transfer characteristics were studied in detail. The results show that the flow field is very complex and heat transfer from the two heaters is not the same. The effects of Prandtl number are negligible with other parameters kept constant. This allows the use of liquids such as water for studying other dielectric liquids, provided the flow geometry and other non dimensional parameters are similar. The overall Nusselt number increases markedly with Rayleigh number and was also affected by enclosure aspect ratio.

Natural convection in a cubical enclosure with an internal isolated heated vertically plate was investigated both experimentally and numerically by W. Yang and W.Q.Tao [2]. The internal plate was suspended under lower surface of the enclosure top wall and electrically heated. The six enclosure walls were at a lower constant temperature. The plate average Nusselt number and the air temperature in the enclosure symmetry plane were experimentally determined in the range of $8x10^4$ to $5x10^5$. Numerical simulations of laminar natural convection in the same configuration were performed. The agreement between the test data and the numerically predicted values is reasonably good, with a maximum deviation in plate Nusselt number of 12.3% and that in air temperature of 9.4%. Detailed temperature and velocity distribution in four cross sections were presented for the case of Ra=$6.57x10^5$. In the low Rayleigh number region, the plate average Nusselt number is quite close to that of the vertical plate situated in infinite space. The difference between the average Nusselt numbers of a vertical plate in a confined space and infinite space gradually becomes large with increasing Rayleigh number. It is revealed that the three dimensional effect i.e. the flow in the Z direction is

quite significant in the region around the end vertical plate, while for the plane normal to the plate and near the symmetry plane, the flow pattern is quite similar to that of the two dimensional results.

II. PROBLEM STATEMENT

The Steady state 3D numerical simulation was carried out inside a cavity by varying the aspect ratio, Rayleigh Number and the Prandtl number. The flow and heat transfer characteristics are functions of geometry and fluid properties. Varying the aspect ratio varied the geometry. The various aspects ratios considered for the analysis are 0.1, 0.25, 0.5, 1, and 1.25. In the analysis the fluid properties are varied in such a way the Prandtl number takes values of 5, 50 and 100. The body forces are increased or the viscous forces are reduced to attain a Rayleigh number of 10^4, 10^5, 10^6 and 10^7. The effect of the same on the flow analysis was determined numerically by using a commercial CFD code "FLUENT".
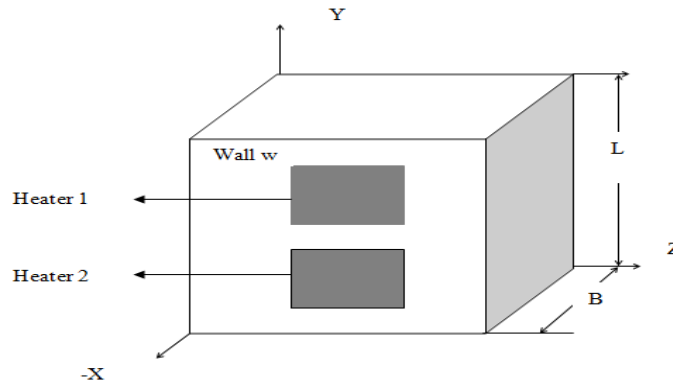
Fig.1: **Boundary Condition for the problem.**

Two heaters are maintained at a higher temperature on one side of the wall of the enclosure. The rest of the wall w on which heaters are installed is completely insulated. The opposite wall to the heaters is maintained at a low temperature i.e. cold wall. The rest of the four walls are completely insulated. No slip boundary condition is considered.

1.   At X=0: θ=1, for the isothermal region on the wall containing heaters.

2.   At X=0; $\dfrac{\partial \theta}{\partial X} = 0$ for the rest of the region on the wall containing heaters.

3.   At X=1: θ=0, for the wall opposite to the wall containing heaters.

4.   At Y=0 and Y=1 $\dfrac{\partial \theta}{\partial Y} = 0$.

5.   At Z=0 and Z=1 $\dfrac{\partial \theta}{\partial Z} = 0$.

III. GRID GENERATION

Before proceeding further, it is necessary to ascertain the reliability and accuracy of the present numerical model. A grid independence test was carried out, and the results were compared. Three sets of grid, 42×42×42, 50×50×50 and 62×62×62 were employed; the case with 50×50×50 grids was used for taking both the accuracy and convergence rate into account. Also quantitative comparisons were made with the results of various grid setting and it was observed that there were quite negligible variations in the results obtained after increasing the grid size beyond 50×50×50 hence it was treated as an optimum range for obtaining reliable results. Fig.2 shows detailed view of Grid for aspect ratio of 1.25.
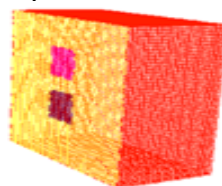
Fig.2

IV. RESULTS & DISCUSSION

A. RESULTS FOR ASPECT RATIO=0.1 AND PRANDTL NUMBER=5.

Ra=10^4

Ra=10^5

Ra=10^6

Ra=10^7
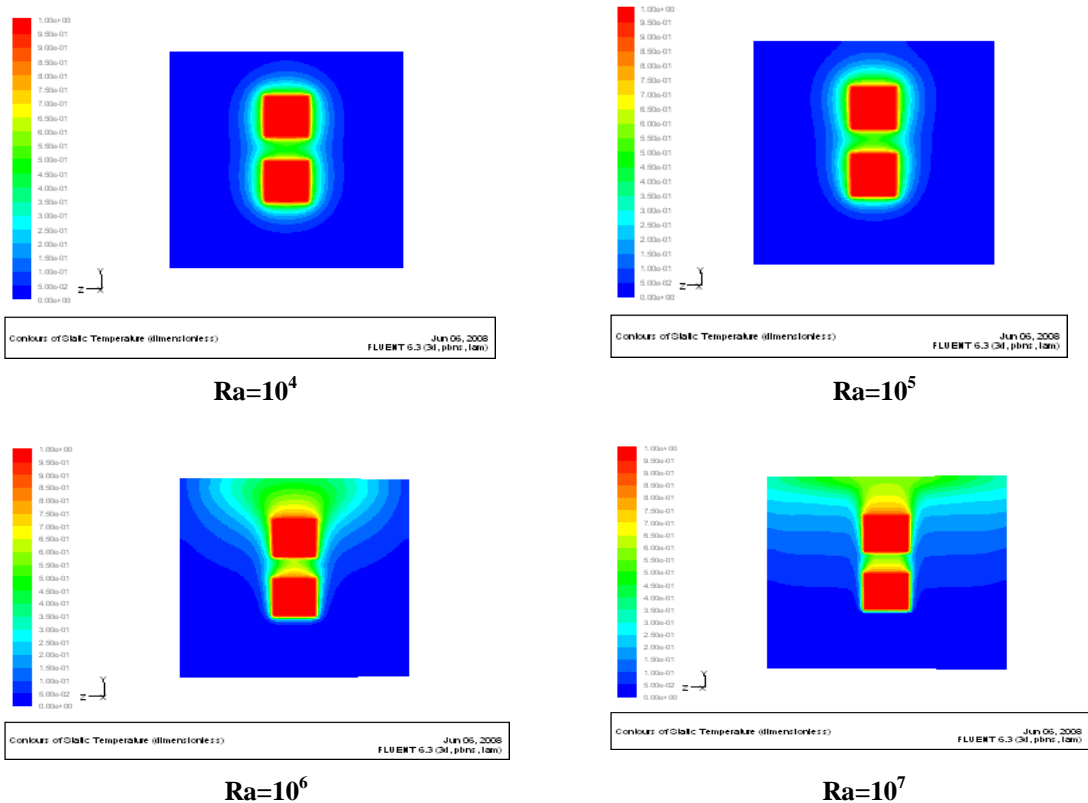
Fig. 3:-Temperature distributions on the plate of the enclosure containing the heaters at various Rayleigh numbers of 10^4, 10^5, 10^6 and 10^7 and **aspect ratio of 0.1**

Ra=10^4

Ra=10^5

Ra=10^6

Ra=10^7
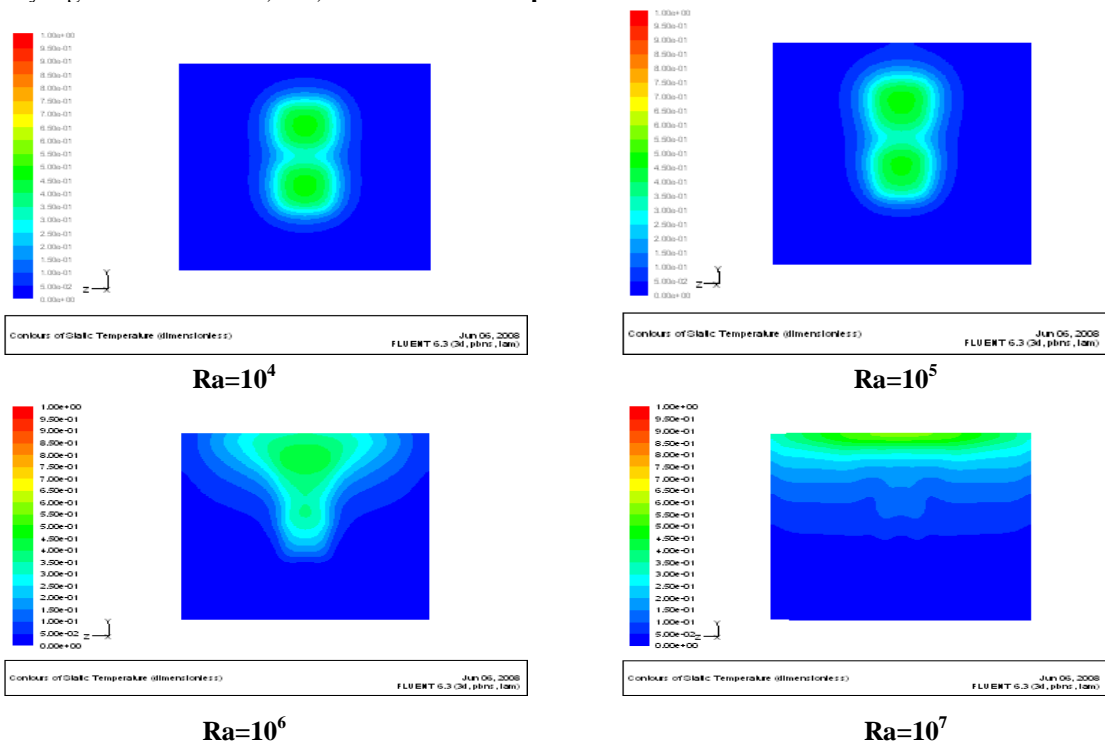
Fig. 4:-Temperature distributions at X=0.05 from the surface of enclosure containing the heaters for various Rayleigh numbers of 10^4, 10^5, 10^6 and 10^7 and **aspect ratio of 0.1.**

Rayleigh number =10^5
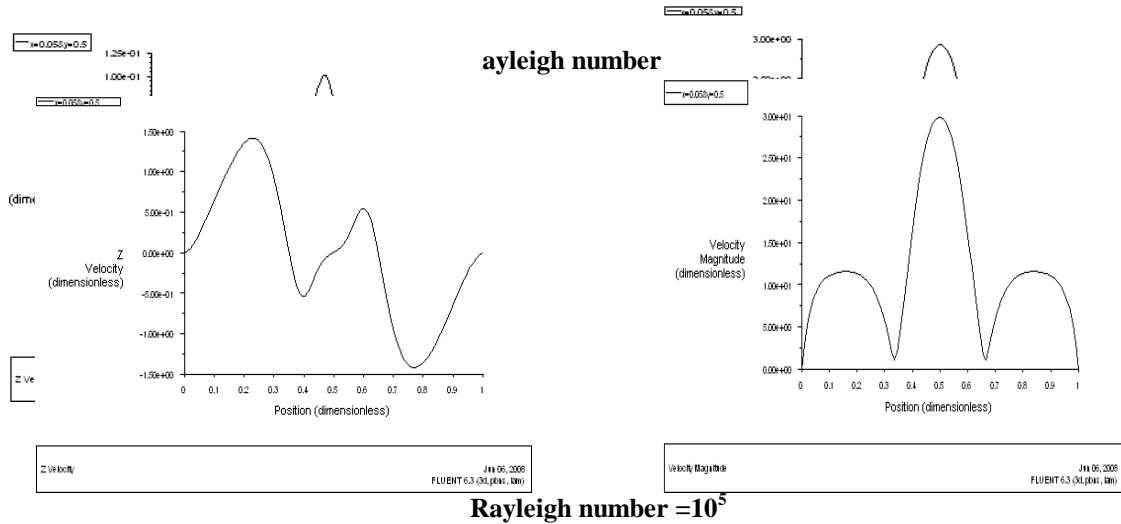
Fig.5:-Velocity distribution at X=0.05 from the surface of enclosure containing the heaters for Ra=10^4 and Ra=10^5 for **aspect ratio of 0.1** and Pr=5.

Rayleigh number =10^6

Rayleigh number =10^7

.
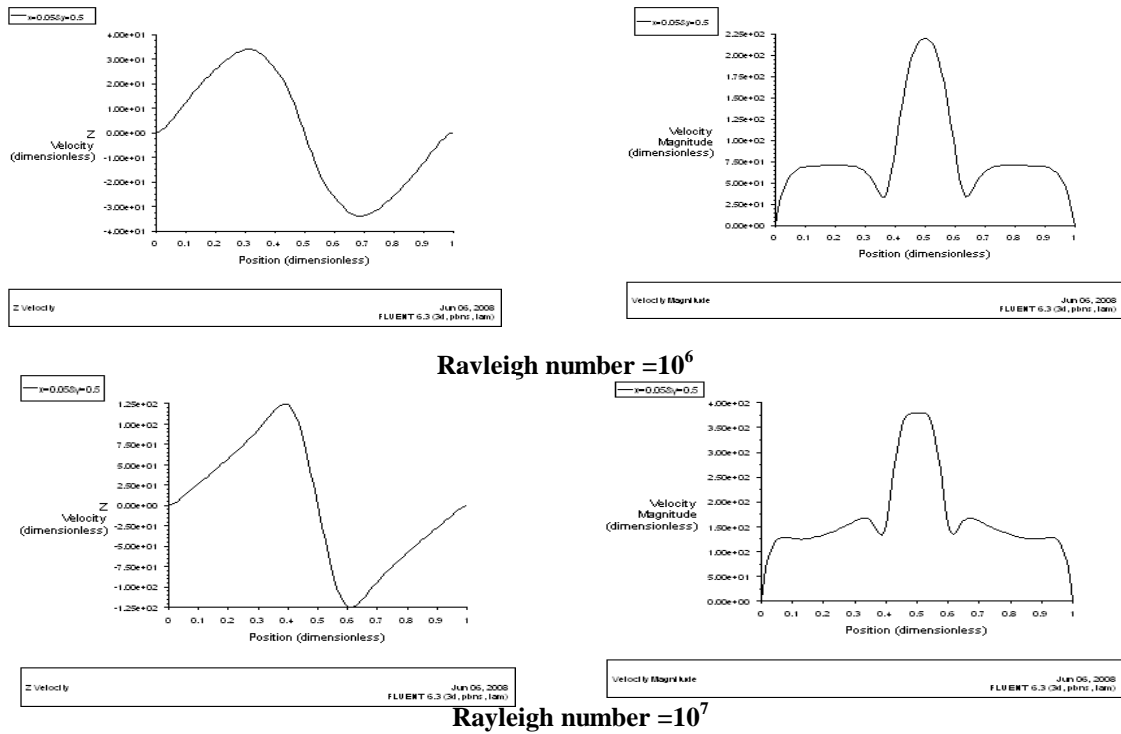
Fig.6: - Velocity distribution at X=0.05 from the surface of enclosure containing the heaters at Rayleigh numbers of 10^6 and10^7 for **aspect ratio 0.1** and Pr=5.

At postion X=0.01   At position X=0.02   At position X=0.03

At position X=0.04   At positoin X=0.05   At position X=0.06

At position X=0.07   At position X=0.09   At positon X=0.1
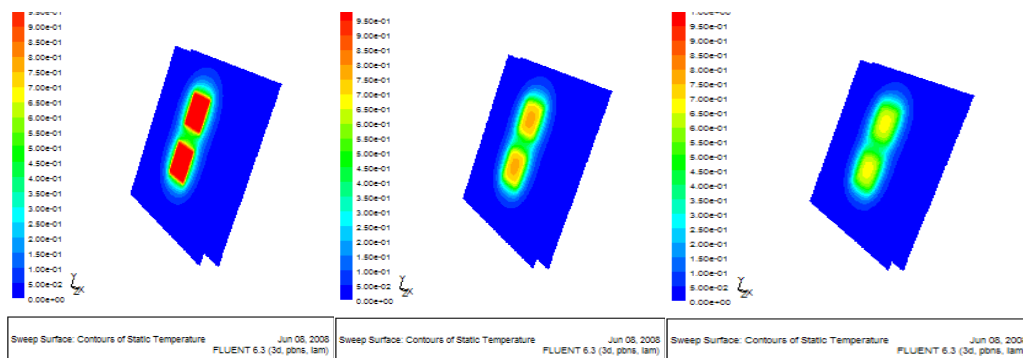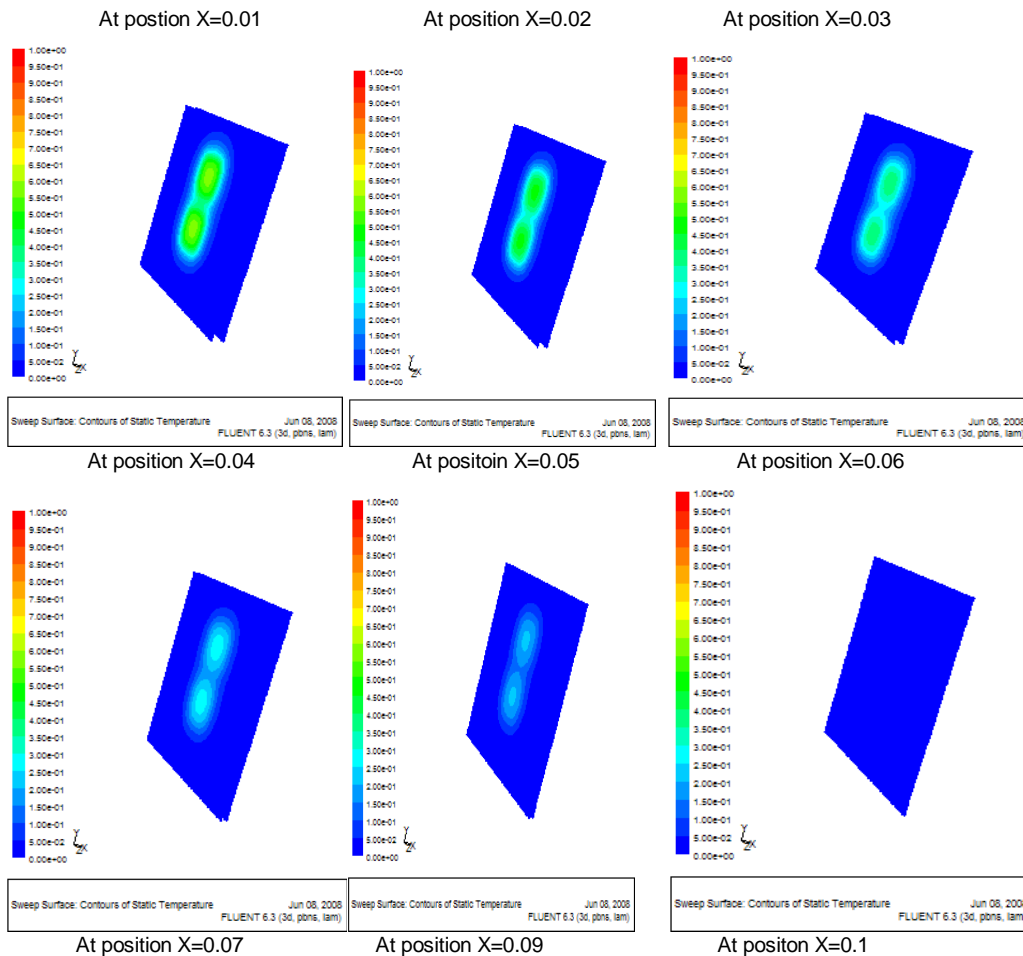
Fig.7:-The above fig shows the animated views of the flow of heat along the x- direction for an enclosure with **aspect ratio of 0.1**.

When the aspect ratio is 0.1, the temperature gradients on the plate containing the heaters are less (Fig. 3). This shows the effect of flow fields on the temperature variations is negligible. When the flow area is restricted as in the case of aspect ratio 0.1, the velocity fields are very small and less convection mode of heat transfer occurs inside the cavity. But as the Rayleigh number is increased the flow picks up and the temperature gradients near the heater picks up. As we move away from the plate containing the heaters, the temperature gradients decreases (Fig. 4 & Fig. 7) and most of the fluid inside the cavity is at rest as there is no density gradient. We can observe slight increase in the temperature gradients with increase in Rayleigh Number. From the temperature variation contour plots it is clear that the temperature gradients are more on heater 2 than Heater 1. Relatively the Nusselt number is greater on Heater 2.

Table 1:-Variation of Nusselt number with Rayleigh number for Aspect Ratio 0.1 for Heater 1 & Heater 2.

Aspect Ratio(0.1)	Nusselt number on Heater 1	Nusselt number on Heater 2
$Ra=10^4$	25.12	25.31
$Ra=10^5$	24.7	26.75
$Ra=10^6$	30.08	42.88
$Ra=10^7$	54.94	76.84

The Z component of velocities (Fig. 5) is very small as the temperature gradients are very small. This is the direction along which we have the density gradients. The magnitude of the velocities are also very small, viewed at X=0.05 and Y=0.5 line. The maximum velocity attained is 4 dimensionless units for a Rayleigh Number of 10^6(Fig. 6). 1 units of dimensionless velocity corresponds to approximately 10^{-6}m/sec, which is very small. Similarly, For aspect ratio of 0.25, the variation in the temperature distribution is more or less the same.

For low Rayleigh numbers the gradients are very small across the heaters and increases as the Rayleigh number is increased. Temperature variations at X=0.05 shows that the gradients are more confined to the upper part of the cavity and the lower part of the cavity have zero temperature gradients. This means the velocities are very low below the cavity. The variation of Nusselt number for different Rayleigh number is given below.

TABLE 2:-Variation of Nusselt number with Rayleigh number for Aspect Ratio 0.25 for Heater 1 & Heater 2.

Aspect Ratio(0.25)	Nusselt Number on Heater 1	Nusselt Number on Heater 2
Ra=10^4	3.91	4.42
Ra=10^5	4.55	6.32
Ra=10^6	7.89	10.98
Ra=10^7	14.14	19.78

Though the Nusselt number is increasing as Rayleigh number is increased, when compared to the aspect ratio of 0.1, the heat transfer rates are very small.

Also, for aspect ratio of 0.5, except for Rayleigh number of 10^7, the temperature gradients are less around the heater, so we cannot find much variation in the Nusselt number as compared with aspect ratio of 0.25. There is a slight decrease in the Nusselt number when compared with aspect ratio of 0.25.

TABLE 3:-Variation of Nusselt number with Rayleigh number for Aspect Ratio of 0.5 for Heater 1 & Heater 2.

Aspect Ratio(0.5)	Nusselt number on Heater 1	Nusselt number on Heater 2
Ra=10^4	3.03	4.08
Ra=10^5	4.57	6.39
Ra=10^6	7.80	10.82
Ra=10^7	14.01	19.5

Further, for aspect ratio of 1.0, drops in the heat transfer rates were observed. The temperature variations are more or less similar with the gradients getting increased with increase in Rayleigh number.

TABLE 4:-Variation of Nusselt number with Rayleigh number for Aspect Ratio 1 for Heater 1 & Heater 2.

Aspect Ratio(1.0)	Nusselt number on Heater 1	Nusselt number on Heater 2
Ra=10^4	2.69	3.83
Ra=10^5	4.38	6.11
Ra=10^6	7.62	10.57
Ra=10^7	13.79	19.25

Nusselt Number variation for aspect ratio of 1.25.

TABLE 5:-Variation of Nusselt number with Rayleigh number for Aspect Ratio 1.25 for Heater 1 & Heater 2.

Aspect Ratio(1.25)	Nusselt number on Heater 1	Nusselt number on Heater 2
Ra=10^4	2.56	3.65
Ra=10^5	4.30	6.00
Ra=10^6	7.54	10.45
Ra=10^7	13.45	18.77
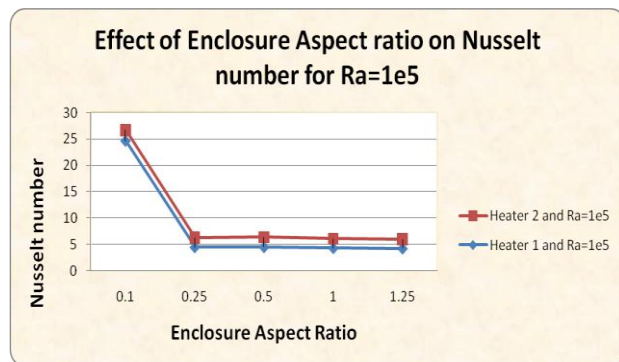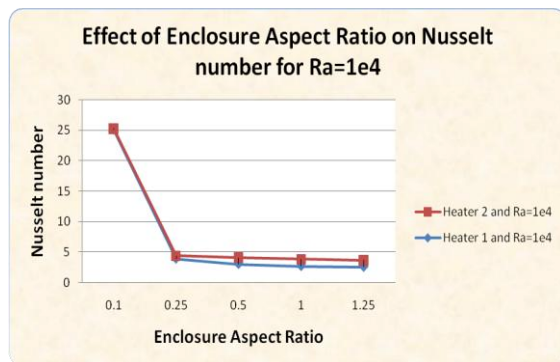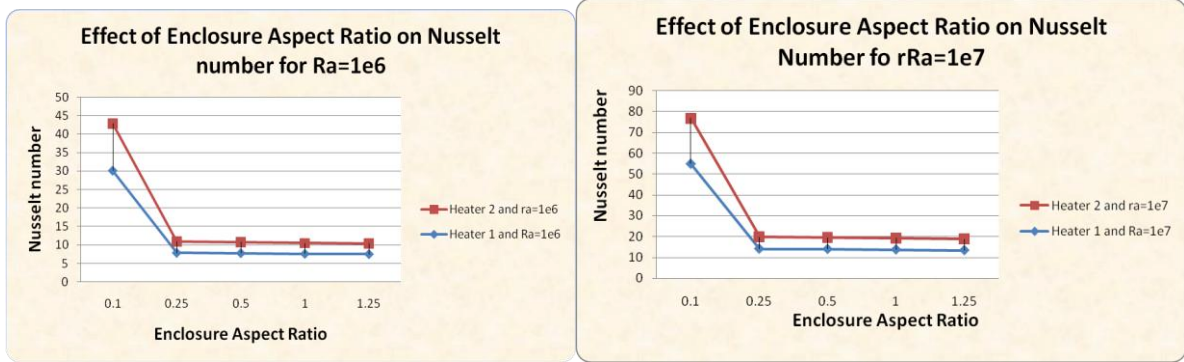
Fig 8:-The effect of enclosure aspect ratio on Nusselt number for heater 1 and heater 2 at Ra=10^4, 10^5, 10^6 and 10^7.
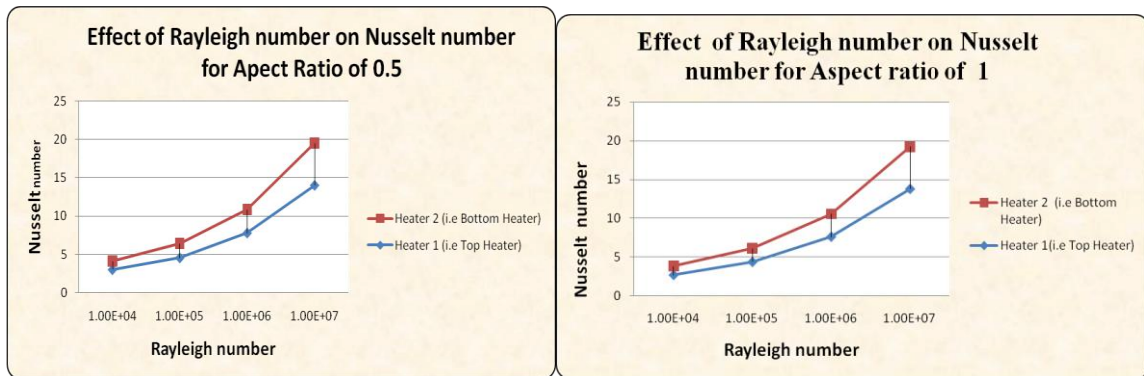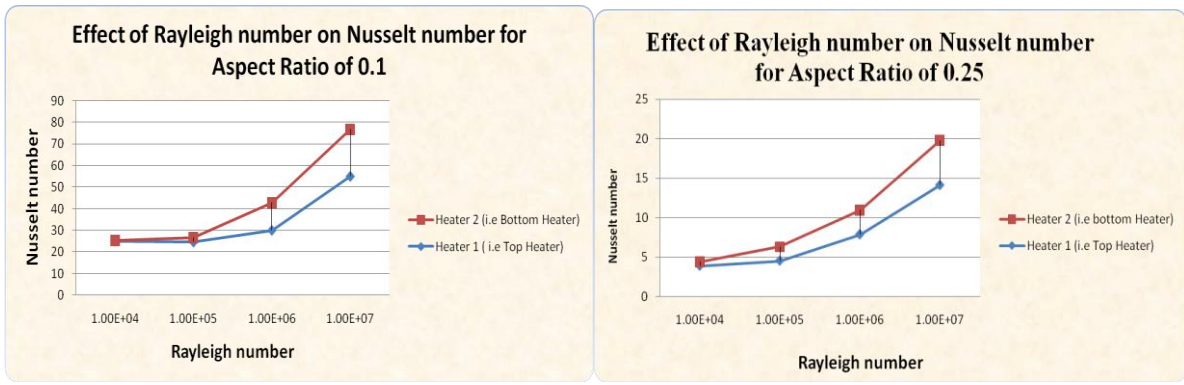
Fig 9:-Effect of Rayleigh number on Nusselt number for Heater1 and Heater 2 for Aspect Ratio of 0.25,0.5, 1 and 1.25.
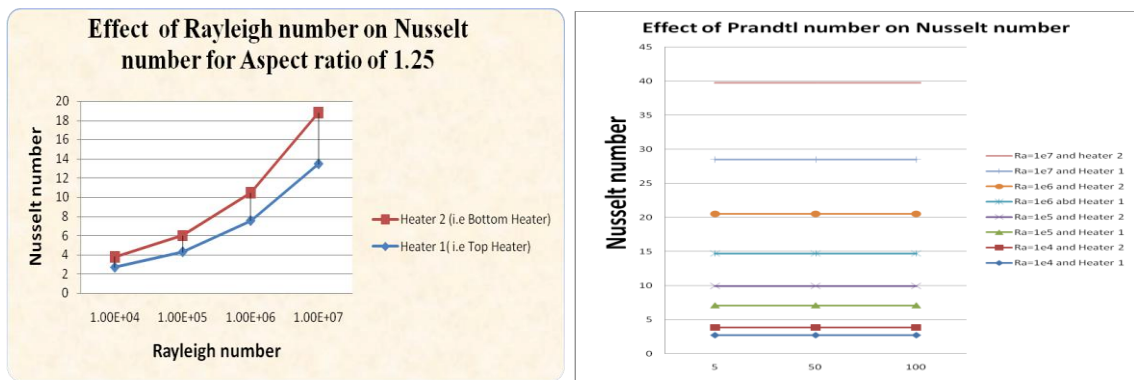
Fig 10:-Effect of Prandtl number on Nusselt number for Heater1&Heater 2.

V. CONCLUSION

The following are the conclusions derived from the numerical investigation carried out inside the cubical enclosure using FLUENT solver.

1. For all the aspect ratios considered for analysis, there was a gradual increase in the heat transfer rates, i.e. Nusselt number, with increase in Rayleigh number (Fig 9).

2. With increase in the aspect ratio from 0.25 to 1.25 there is a gradual reduction of heat transfer rates. Heat transfer rates reduced by 8-22% with increase in the aspect ratio. But there is a drastic reduction in heat transfer rates when the aspect ratio was varied from 0.1 to 0.25. Heat transfer rates reduced by 84%. (Fig 8).

3. From the velocity counters it is very clear that the location of the maximum z component of velocity varied unevenly which shows complex flow phenomena inside the enclosure.

4. With variation of Prandtl number from 1 to 100, the effect on flow and heat transfer characteristics is negligible (Fig. 8).

5. Nusselt number on heater 1 is less than that of heater 2 irrespective of aspect ratio, Prandtl and Rayleigh number (Fig 8) & (Fig 9).

Future Work

This analysis can be carried by including fins inside the cavity, which control the flow phenomena thereby effects the heat transfer rates. Aspect ratio of the heaters can be varied and analysis can be carried to find the optimum location at which the maximum heat transfer rates exists.

REFERENCES

[1] Y.L.He, W. W. Yang and W.Q. Tao, "Three-Dimensional Numerical Study of Natural Convective Heat Transfer of Liquids in a Cubic Enclosure", Numerical Heat Transfer, Part A, 47: pp. 917-934, 2005.

[2] M.Yang and W.Q.Tao, "Three Dimensional Natural Convection in an Enclosure with An internal Isolated Vertical Plate", Journal of Heat Transfer, Vol. 117, pp. 619-625.

[3] A.F. Emery and J. W. Lee, "The Effects of Property Variations on natural Convection in a Square Enclosure", Journal of Heat Transfer, Vol. 121, pp. 57-62.

[4] R.Selver, Y. Kamotani and S. Ostrach,"Natural Convection of a Liquid Metal in Vertical Circular Cylinders Heated Locally from the Side", Journal of Heat transfer, Vol. 120, pp. 108-114.

[5] Peter M. Teertstra, M. Michael Yovanovich & J. Richard Culham"Modelling of Natural Convection in Electronic Enclosures, Journal of Heat transfer, Vol. 128, pp.157-165.

[6] Vipin yadav & keshav Kan, "Convective Cooling of PCB like Surface with Mixed Heating Conditions in a Vertical Channel", Journal of Heat Transfer, Vol. 129, pp.129-143

[7] Y.L.He, W.W.Yang and W.Q.Tao, Numerical Heat Transfer, "Three dimensional numerical study of natural convection heat transfer of liquid in a cubical enclosure", Part A, 47: pp917-934.

[8] "Introduction to Finite Volume Methods", Malashekara and Versteeg, Cambridge Publications,

[9] J.P.Holman, "Heat Transfer", McGraw Hill Publications. [10] Ferziger and Peric "Computational Methods for Fluid Dynamics", Spinger Publications.

[11] S.V. Patankar, "Numerical Heat Transfer and Fluid Flow" Cambridge Publications.

[12] Frank and White, "Viscous Fluid Flow", McGraw Hill Publications 1999.

[13] T.Chung, "Computational Fluid Dynamics", Cambridge Publications 2000.

[14] Adrian Bejan and Allan Kraus, "Heat Transfer Handbook", John Wiley and Sons Publication.

Implementation of Wide Band Frequency Synthesizer Base on DFS (Digital Frequency Synthesizer) Controller Using VHDL

Md. Aamir Rauf Khan[1], Archana Yadav[2]

[1, 2]*(Department of ECE, Integral University, India)*

Abstract: *A frequency synthesizer is an electronic system for generating any of a range of frequencies from a single fixed time base or oscillator. They are found in many modern devices, including radio receivers, mobile telephones, radiotelephones, walkie-talkies, CB radios, satellite receivers, GPS systems, etc. Direct Digital Synthesis (DDS) is a kind of frequency synthesizer that use electronic methods for digitally creating arbitrary waveforms and frequencies from a single, fixed source frequency. Direct Digital Frequency Synthesis (DDFS) is a mixed signal part i.e. it has both digital and analog parts. DDFS's digital part is also known as Numerically Controlled Oscillator (NCO), which consists of a Phase Register, a Phase Accumulator (PA) and a ROM. The analog part has Digital-to-Analog Converter and a filter. NCO is a digital computing block which renders digital word sequences in time at a given reference clock frequency, which thereafter are converted into analog signals to serve as a synthesizer. The phase accumulator (PA) clocked with, generates the phase value sequence. Application of the DDFS ranges from instrumentation to modern communication systems, which employs spread-spectrum and phase shift-keying modulation techniques.*
The focus of this paper is on design, analysis and simulation of DDFS, using tools like Xilinx and Cadence. Traditional designs of high bandwidth frequency synthesizers employ the use of a phase locked- loop (PLL). DDFS provides many significant advantages over the PLL approaches, such as fast settling time, sub-Hertz frequency resolution, continuous-phase switching response and low phase noise.
Keywords: *DFS, Modelsim 10.2a, VHDL, Wide Band Frequency Synthesizer, Xilinx ISE 14.2.*

I. INTRODUCTION

Wide Band Frequency Synthesizer has become essential components in wireless communication systems. They are used as frequency synthesizers with precise and convenient digital control in both traditional electronics, such as televisions and AM/FM radios, and modern consumer products among which cellular mobile phone is a striking example.

IC fabrication technology advances have made monolithic integration possible. More and more electronic devices can be put on the same chip to reduce the number of external components and then the costs. Therefore, on a single chip we can accomplish many functions for which we might need to make several chips work together a few years ago. A monolithic wide-band PLL is of great interests to wireless communication applications due to both its low cost and convenience to switch between different communication standards. The focus of this work is to implement a wide-band Frequency Synthesizer using as few as possible building blocks and also as simple as possible structure.

Many of the concepts of DDS are illustrated by the way in which a sine wave is generated. The figure below shows a block diagram of a simple DDS function generator. The sine function is stored in a RAM table. The RAM's digital sine output is converted to an analog sine wave by a DAC. The steps seen at the DAC output are filtered by a low pass filter to provide a clean sine wave output.

The frequency of the sine wave depends on the rate at which addresses to the RAM table are changed. Addresses are generated by adding a constant, stored in the phase increment register (PIR), to the phase accumulator. Usually, the rate of additions is constant, and the frequency is changed by changing the number in the PIR.

Our intuition might suggest that a large number of samples are required for each cycle of the sine wave to achieve good spectral purity of the output. A sketch of a sine which is approximated by a small number of samples per cycle hardly looks like a sine wave. Remarkably, only about three samples are required during each cycle. In fact, if we could make an arbitrarily sharp, low-pass filter, we would need only two samples per cycle

II. RELATED WORK

The Fast frequency switching is crucially important in modern wireless communication systems such as TDMA/CDMA digital cellular systems and spectrum-spread wireless LANs. For example, the TDMA system may require that the carrier frequency have to be switched during a signal slot, that is, the change must be accomplished within 100us. Linear phase shifting is also crucial in any system that uses phase shift keying modulation techniques. Such system includes IS-95, IS-94, GSM, DCS-1800, CDPD and several others. Direct Digital Frequency Synthesizer (DDFS) can achieve fast frequency switching in small frequency steps, over a wide band. Also it provides linear phase and frequency shifting with good spectral purity. So, DDFS is best suited to use in the above communication systems. A further requirement for DDFS is low power consumption budget, especially for portable wireless terminals.

Woogeun Rhee et al (2013), worked on overview of fractional- N phase-locked loops (PLLs) with practical design perspectives focusing on a 0Σ modulation technique and a finite-impulse response (FIR) filtering method. Spur generation and nonlinearity issues in the 0Σ fractional-N PLLs are discussed with simulation and hardware results. High-order 0Σ modulation with FIR-embedded filtering is considered for low noise frequency generation. Also, various architectures of finite-modulo fractional-N PLLs are reviewed for alternative low cost design, and the FIR filtering technique is shown to be useful for spur reduction in the finite-modulo fractional-N PLL design [2].

Govind S. Patel et al (2013), worked on an optimized Direct Digital Frequency Synthesizer (DDFS) utilizing Piecewise Linear Approximation is introduced. The proposed technique allows successive read access to memory cells per one clock cycle using time sharing. The output values will be temporarily stored and read at a later time. The output of this system is a reconstructed signal that is a good approximation of the desired waveform. As a result, the DDFS only needs to store fewer coefficients and the hardware complexity is significantly reduced. The proposed DDFS has been analyzed using MATLAB. The SFDR of synthesized achieved is 84.2 dBc. To prove the better performance of proposed DDS architecture it is compared favorably with several existing DDS architectures. In future it can also be used to improve the performance of Hybrid DDS-PLL Synthesizers [3].

M. NourEldin M. et al (2013), proposed a algorithm for a low-power high-resolution ROM-less Direct Digital frequency synthesizer architecture based on FPGA Design is proposed. This work is equipped to generate a sinusoidal waveform with a new simple design method, which is endowed with high speed, low power and high spurious free dynamic range (SFDR) features. The proposed low power methodology is achieved by two methods: first, in a phase accumulator design by selecting a pipelined phase accumulator with 8-bit components that has lowest number of four input LUTs and number of occupied Slices. Second, in the circuit of TSC by proposing the circuit without an external power source. The output frequency of proposed design is 195.35 kHz using built in clock frequency of 50MHz. However, the maximum operating frequency is 190.93MHz. In addition, the design has frequency resolution of 0.012Hz, which is promising to get very high tuning frequency with SFDR of 42 dBc or 70 dBFS [4].

Eli Bloch wt al, (2013), worked on an integrated circuit (IC) for heterodyne optical phase locking in a 1–20-GHz offset range is hereby reported. The IC, implemented in a 500-nm InP HBT process, contains an emitter coupled logic digital single-sideband mixer to provide phase locking at a 20-GHz offset frequency, and a wideband phase-frequency detector designed to provide loop acquisition up to 40-GHz initial frequency offset. The all-digital IC design has phase-frequency detection gain independent of IC process parameters or optical signal levels, and provides a wide offset locking range. A 100-ps delay decreases the overall loop delay, making wideband loop filter design possible. In addition, a medium-scale high-frequency logic design methodology is presented and fully discussed [5].

Jochen Rust et al, (2012) said that nowadays Direct Digital Frequency Synthesizers (DDFS) are used in a vast area of applications, the demand for simple and efficient hardware design and implementation methods is a highly important aspect. In this work a new approach is introduced considering Automatic Nonuniform Piecewise linear function Approximation (ANPA). Automatic function generation is performed that enables quick HDL design by parameter specification in advance. For evaluation, several different configurations are simulated regarding approximation accuracy and complexity. In addition, logical and physical IC synthesis is performed for selected designs and their results are compared with actual references with respect to the common hardware constraints power, area and time [6].

III. METHODOLOGY

The concept of this technique is the same with that used in above quadrant compression technique [3]. Figure 1 shows the block diagram of the proposed DDFS architecture. The MSB2 is used to select the quadrants of the sine wave, while the MSB1 is used to control the format converter. The remaining W-2 bits are fed into Complement or whose output is split into two parts, the MSB part, with A bits long, represents the S segments and the LSB part with B bits long, represents an angle x in the interval $[0, \pi/(2S)]$. A multiplexer and its coefficients are the equivalent of a ROM which provide the segment initial amplitudes Q_i, represented with D bits. The proposed architecture also incorporates pulse forming circuit which controls the fetching and loading process of successive Q_i coefficients. This circuit along with the three storage registers and one Subtract or is essential to perform the task of the slope derivation during the segment interval. Besides the sine symmetry property, the linear approximation method has been used to approximate the first quadrant of sine function by S straight lines; each line is defined by two coefficients, P_i and Q_i. The coefficient M_i, which represents the slope of ith element. The first quadrant of sine function approximation segment can be calculated from the sine function as follows.

$$P_i = \{\sin[i\Delta x] - \sin[(i-1)\Delta x]\}/\Delta x \quad 1 \le i \le S \qquad (1)$$

where, Δx = the length of segment. Above Eq. (1) can be realized easily by subtracting the Sin [i.Δx] at successive phase angles and then dividing the result by Δx.

As Δx unsigned constant coefficient, the division can simply be realized by binary operation. The coefficients Q_i, is equal to [sin (i-1) Δx] points, As examples for segment number1, (Q_1= 0), yields K_1 = P_1x and for segment number 2, (Q_2 = sin Δx), in general, Q_i = sin [(i-1) Δx] for the ith segment and it can be realized by delaying the pervious sin (iΔx) by one clock period, hence the realization of the whole K_i (x) function is accomplished. It is clear that it must get two consecutive sine points at the same time to conduct the process of subtraction and extraction of the slope later.

These two sine points can be got only when the corresponding phase angles point simultaneously to their addresses in the sine LUT and that is an inconsequent assumption. As mentioned earlier, the accessing of the memory is valid only once at a specific clock cycle. In this study, we introduce architecture of pulse forming circuit which is performing the task of time sharing and propose the procedure enumerated below to get around this problem. The value of phase register at any clock period represents the phase of the sine function. As not all of the samples of the sinusoid are stored, only the first A bits of the W-2 phase accumulator output are used to select segment initial amplitudes Q_i. , i.e., it represents the MUX address inputs. The remaining B LSB's bits (B = W-2-A) represent an angle x in the interval Δx and are used to calculate the value of the interpolated sine point. It has three simple blocks: digital comparator, pulse narrowing circuit and tapped delay.

- At each clock cycle, the digital comparator examines the MUX Address inputs for detecting the changes in data select inputs i.e., transitions between the segments
- The detected signal will be applied to the Pulse Narrowing Circuit to produce a Δt pulse width signal i.e., trigger1 (tg1), which is usually a fraction of 1/fclk
- This signal, tg1 gives an order to advance the Data Select Inputs of MUX by 1, hence the output of the MUX during this time slot is Sin [(i+2)Δx]
- At the same time, the tg1 is used to load this value in register1 (R1)
- After Δt, the data select inputs get back to the previous address value, so the output of MUX will be Sin [(i+1)Δx]
- Trigger2 (tg2) enables register 2 (R2) to load this value
- The content of R2 will be subtracted from the content of R1 and the result will be loaded in register3 (R3), after a specific time which is precisely sufficient to give a chance for signals to be propagated through all gates and settle. Hence, the slope is simply derived and kept unchanged during the segment interval.
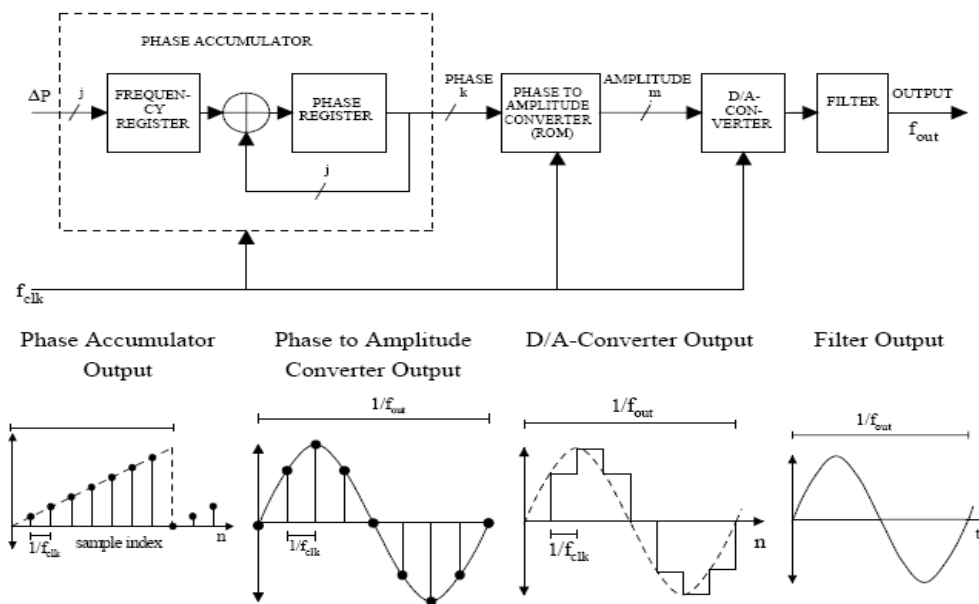
Fig 1: Block diagram of a direct digital frequency synthesizer

As shown in Figure 1, the main components of a DDFS are a phase accumulator, phase-to-amplitude converter (a sine look-up table), a Digital-to-Analog Converter and filter. A DDFS produces a sine wave at a given frequency. The frequency depends on three variables; the reference-clock frequency and the binary number programmed into the phase register (frequency control word,clkfM), length of n-bit accumulator. The binary number in the phase register provides the main input to the phase accumulator.

If a sine look-up table is used, the phase accumulator computes a phase (angle) address for the look-up table, which outputs the digital value of amplitude—corresponding to the sine of that phase angle—to the DAC. The DAC, in turn, converts that number to a corresponding value of analog voltage or current. To generate a fixed-frequency sine wave, a constant value (the phase increment—that is determined by the binary numberM) is added to the phase accumulator with each clock cycle. If the phase increment is large, the phase accumulator will step quickly through the sine look-up table and thus generate a high frequency sine wave. If the phase increment is small, the phase accumulator will take many more steps, accordingly generating a slower waveform.

Building Blocks of DDFS:
A DDFS is a mixed signal device i.e. it has both analog and digital blocks. These blocks are the Phase Register, Phase Accumulator, Phase-to-Amplitude Converter (ROM/LUT), Digital-to-Analog Converter, and Reconstruction Filter. The functionality of each of these blocks is discussed in the following section.

Phase Accumulator:
Continuous-time sinusoidal signals have a repetitive angular phase range of 0 to 360 degrees. The digital implementation is no different. The counter's carry function allows the phase accumulator to act as a phase wheel in the DDFS implementation.

Phase-to-Amplitude Converter (ROM/ LUT):
The DDFS's ROM is a sine Look up Table; it converts digital phase input from the accumulator to output amplitude. The accumulator output represents the phase of the wave as well as an address to a word, which is the corresponding amplitude of the phase in the LUT. This phase amplitude from the ROM LUT drives the DAC to provide an analog output. It is also called a digital Phase-to-Amplitude Converter (PAC)

Digital-to-Analog Converter and Filter:
The phase accumulator computes a phase (angle) address for the look-up table, which outputs the digital value of amplitude—corresponding to the sine of that phase angle—to the DAC. The DAC, in turn, converts that number to a corresponding value of analog voltage or current.

IV. SIMULATION RESULTS

We are generating the sine wave of 1 Hz frequency with different phases in below results. We are taking frequency 1 Hz converting it into decimal 2147483 then we converting this into hexadecimal we are getting 0020c49B. In the same way we are converting phase into angle to radian and then converting it into decimal and hexadecimal as well. In this case we are generating the sine wave of above said frequency with 0° phase (simple sine wave) shown in fig 2. In this case we are working on positive edge of clock and reset will be '0'.
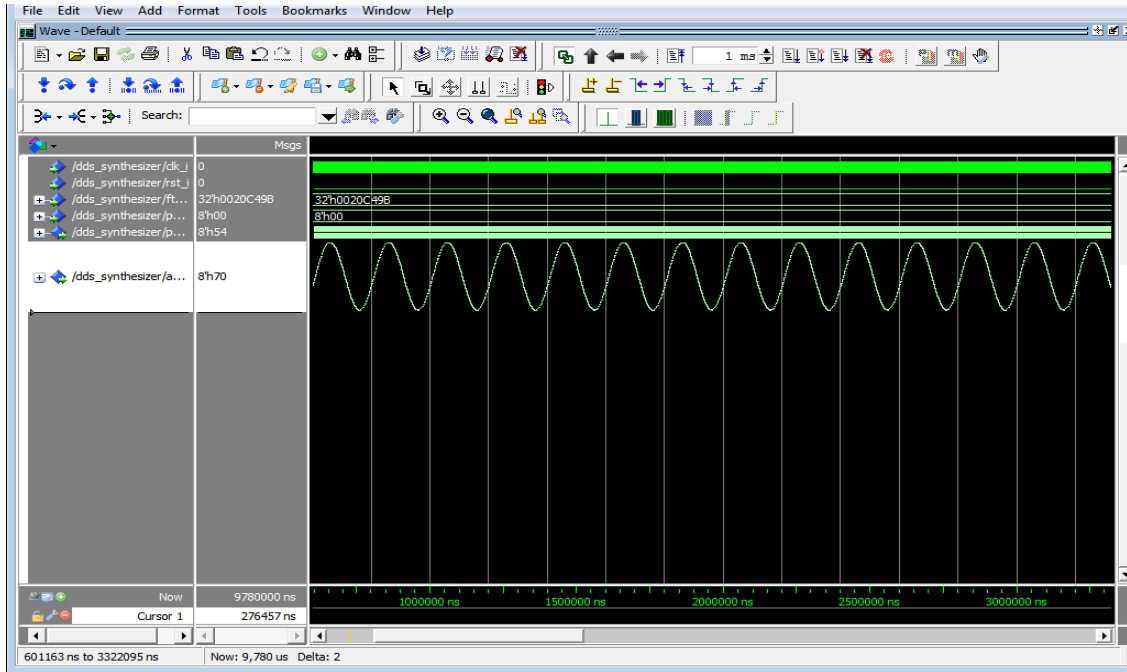
Fig 2: Simulation Results for 0° Phase.

In this case we are generating the sine wave of above said frequency with 90° phase shown in fig 3. In this case we are working on positive edge of clock and reset will be '0'.
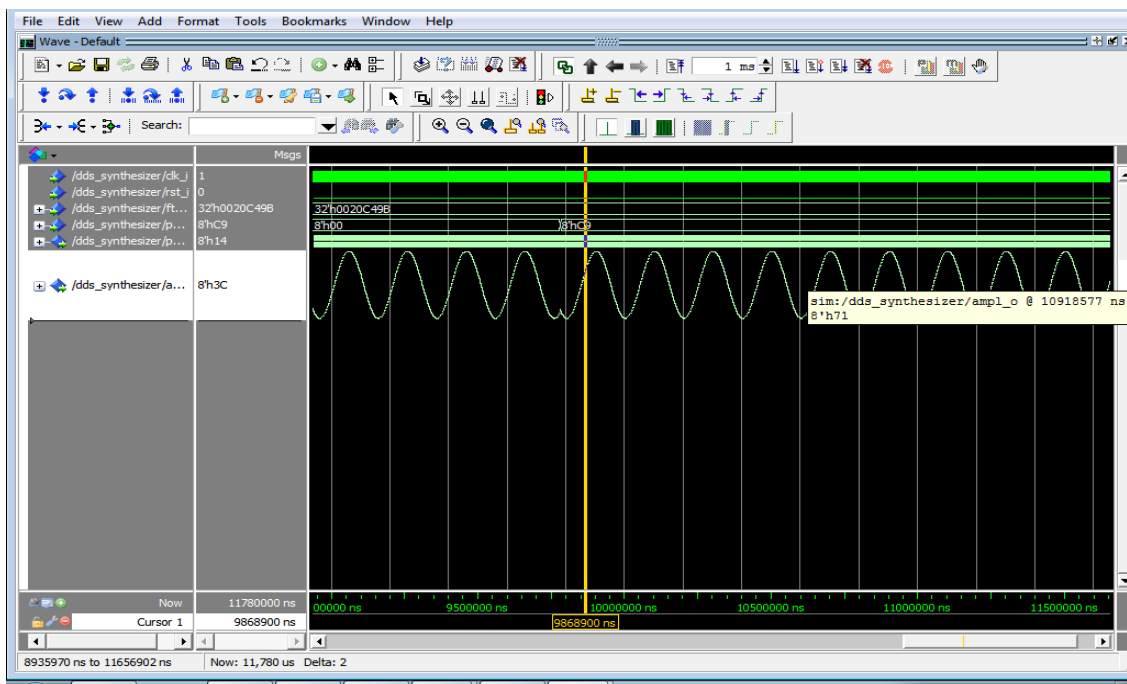
Fig 3: Simulation Results for 90° Phase Shift.

In this case we are generating the sine wave of above said frequency with 45° phase shift. In this case we are working on positive edge of clock and reset will be '0' shown in fig 4.
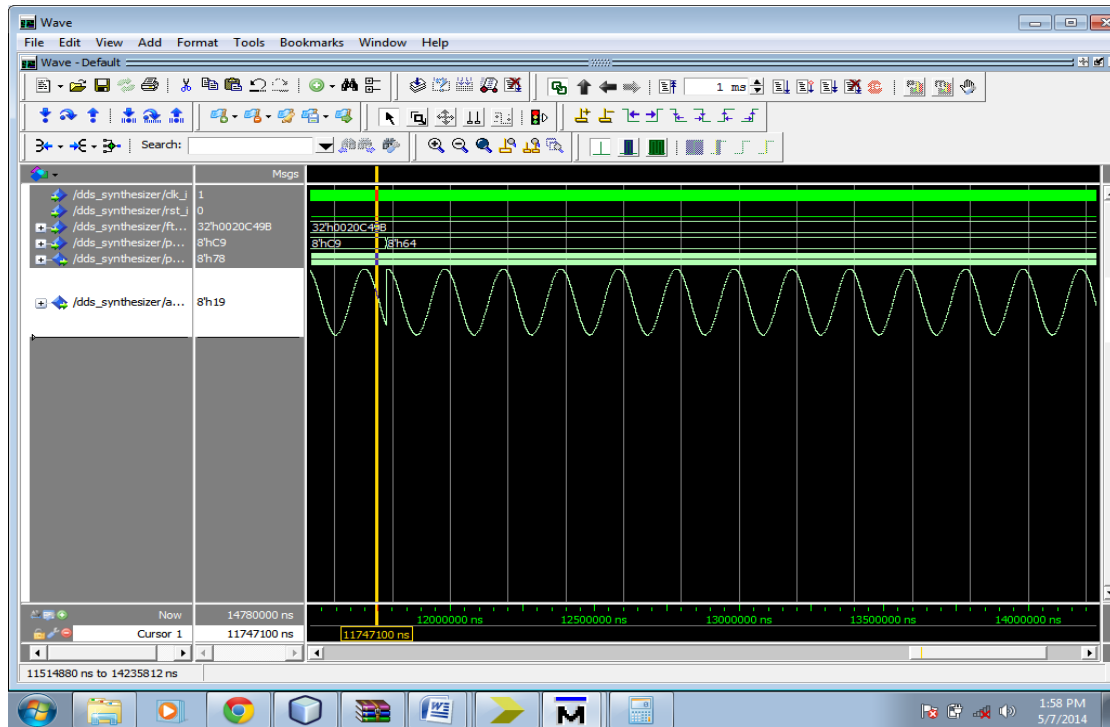
Fig 4: Simulation Results for 45° Phase Shift.

In this case we are generating the sine wave of above said frequency with -12° phase shift. In this case we are working on positive edge of clock and reset will be '0' shown in fig 5.
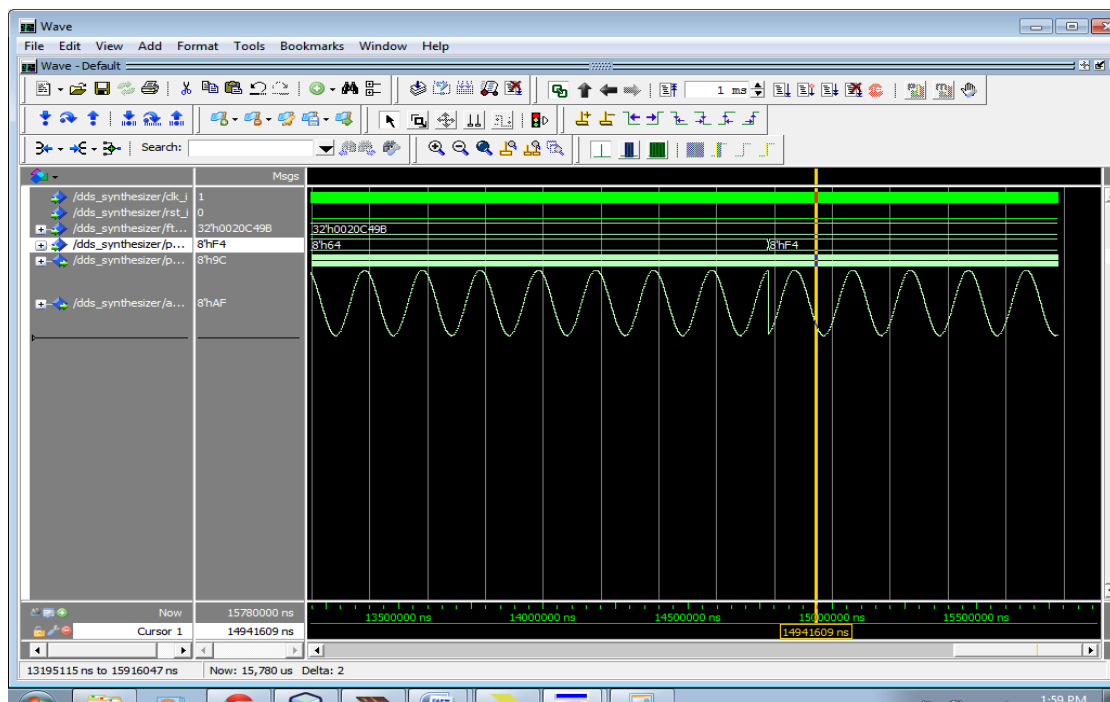
Fig 5: Simulation Results for -12° Phase Shift.

V. CONCLUSION

The DDS IP core (dds_synthesizer) is a implementation of a direct digital frequency synthesizer (DDS) (also called number controlled oscillator, NCO) which produces a sine wave at the output with a specified frequency and phase (adjustable at runtime). The resolution of the frequency tuning word (FTW), the phase and the amplitude are defined seperately. While the FTW resolution can be set by the generic ftw_width, phase and amplitude resolution are defined as constants phase_width and ampl_width in the seperate package sine_lut_pkg. We have Simulated the Direct Frequency Synthesizer for Sine wave generation from 1Hz to 100 MHz with Amplitude -1V to 1V. The output frequency range / Amplitude range can be change by manipulating the Bit width of Ampl_o or FTW.

We can further enhance our design to generate Triangular/ Square by using the presented design with some more logical gate inserting into it. For implementing on hardware side we must include a DAC.DAC is required to generate the analog pulses as most of the devices supports only analog input.

REFERENCES

[1]   C.S. Vaucher, Architectures for RF Frequency Synthesizers. Boston: Kluwer Academic Publishers, 2002.
[2]   Woogeun Rhee et al, "Fractional-N Frequency Synthesis: Overview and Practical Aspects with FIR-Embedded Design" Journal Of Semiconductor Technology And Science, Vol.13, No.2, April, 2013.
[3]   Govind S. Patel et al , " The Optimization of Direct Digital Frequency Synthesizer Performance by New Approximation Technique" Research Journal of Applied Sciences, Engineering and Technology 5(11): 3134-3139, 2013.
[4]   M. NourEldin M. et al, "A Novel Low-Power High-Resolution ROM-less DDFS Architecture" International Journal of Advanced Research in Electronics and Communication Engineering (IJARECE) Volume 2, Issue 12, December-2013.
[5]   Eli Bloch wt al, "A 1–20-GHz All-Digital InP HBT Optical Wavelength Synthesis IC" IEEE transactions on microwave theory and techniques, vol. 61, no. 1, january 2013.
[6]   Jochen Rust et al, "A Direct Digital Frequency Synthesizer Based On Automatic Nonuniform Piecewise Function Generation" 20th European Signal Processing Conference (EUSIPCO 2012) Bucharest, Romania, August 27 - 31, 2012.

Granger Causality Test: A Useful Descriptive Tool for Time Series Data

OGUNTADE, E. S[1]; OLANREWAJU, S. O[2]., OJENIYI, J.A.[3]

[1,2] *(Department of Statistics, University of Abuja, P.M.B.117, Abuja. Nigeria)*
[3] *(Department of Cyber-Security Science, Federal University of Technology, Minna)*

Abstract: *Interdependency of one or more variables on the other has been in the existence over long time when it was discovered that one variable has to move or regress toward another following the work done by Galton (1886); Pearson & Lee (1903); Kendall & Stuart, (1961); Johnston and DiNardo, (1997); Gujarati, (2004) etc. It was in the light of this dependency over time the researcher uses Granger Causality as an effective tool in time series Predictive causality using Nigeria GDP and Money Supply to know the type of causality in existence in the two time series variables under consideration and which one can statistically predicts the other.*

The research work aimed at testing for nature of causality between GDP and money supply for Federal Republic of Nigeria for the period of thirty years using the data sourced from Central Bank of Nigeria Statistical Bulletin. After observing the various conditions of Granger causality test such as ensuring stationarity in the variables under consideration; adding enough number of lags in the prescribed model before estimation as Granger causality test is sensitive to the number of lags introduced in the model; and as well as assuming the disturbance terms in the various models are uncorrelated, the result of the analysis indicates a bilateral relationship between Nigeria GDP and Money Supply. It implies Nigeria GDP Granger causes money Supply and vice versa. Based on the result of this study, both Nigeria GDP and money Supply can be successfully model using Vector Autoregressive Model since changes in one variable has a significant effect on the other variable.

Keywords: *Bilateral Causality, Time Series, VARMA Model, Stationarity, Wold representation GDP, Money Supply,*

I. Introduction

Two or more variables can be interdependence on one another if the occurrence of one causes the other to take place or vice versa, then one can talk of unidirectional causality and feedback causality. Changes in the first variable precede changes in the other. That is one Granger causes another knowing fully that the present with its lagged values can only predict the future but the future cannot predict the past.

A statistical relationship in itself cannot logically imply causation, to ascribe causality; one must appeal to a priori or theoretical considerations (Gujarati, 2004 pp23). A statistical relationship, however strong and however suggestive, can never establish causal connection: our ideas of causation must not from mere statistics but ultimately from some theory or other (Kendall & Stuart, 1961).

II. Model Description and Notations

2.1 Overview of ARMA Models

A set of repeated observations of the same variable such as Stock Returns, GDP, Money Supply, Interest Rates etc each one being recorded at a specific time are termed Time Series. These set of variables in their stationarity form can be modelled using ARMA model espoused in Box Jenkins &Reinsel, (1994).ARMA model of order (p,q) can be viewed as linear filter from of digital signal processing perspective,(Fangge and Peixian,(2011).

Consider the linear combination of the lagged variables in the equation (1) given below

$$\sum_{j=0}^{p} \alpha_j y_{t-j} = \sum_{j=0}^{q} \theta_j \mu_{t-j}, \ \phi_0 = \theta_0 = 1 \tag{1}$$

where

$$E(\mu_t) = 0 \, ; E\{\mu_s \mu_t\} = \sigma_{st}^2, \, \sigma > 0$$

μ_t are shocks or innovation series
and that

$$E(y_t) = E(y_s) \text{ for all } t \text{ and } s$$

$$E(y_t y_{t-j}) = E(y_s y_{s-j}) \text{ for all } t \text{ and } s$$

The letter **E** is use to denote the expectation operator.

The ARMA (p,q) in equation (1) is a combination of the autoregressive structure of the residues (moving average MA) and a linear relationship between the value predicted by the model at time t and the past values of the time series(autoregressive AR).

Construction of ARMA model requires four iterative steps which are made explicit in Box, Jenkins, & Reinsel ,(1994); Hamilton,(1994); Salau, (2003); Oguntade,(2010); Oguntade and Ogunfiditimi (2013) etc.

2.2 Runs Test for Stationarity

ARMA models can be used directly if the time series is wide sense stationary, (Fangge & Peixian, 2011).The stationary assumption of any given time series need be checked for proper identification and estimation of the model. This is achieved by Runs Test for randomness. The stationarity assumption is rejected if Asymp. Sig $\prec$ 0.05.Otherwise time series should be differenced or transformed using various time series transformation techniques until stationarity is achieved.

2.3 Granger Causality Test

If variable Y contains useful information for predicting variable X , then Y causes X .That is Y is Granger / Predictive causality of X .Then Y causes X is denoted as $(Y \rightarrow X)$ and X causes Y is denoted as $(X \rightarrow Y)$ where the arrow points to the direction of Causality. The Granger Causality Test assumes that the information relevant to the prediction of variables Y and X is contained in the time series data on these variables.

The bilateral causality are related by the following regression models

$$X_t = \sum_{i=1}^{n} \alpha_i X_{t-i} + \sum_{j=1}^{n} \beta_j Y_{i-j} + \ell_{t1} \tag{1}$$

$$Y_t = \sum_{i=1}^{n} \phi_i X_{t-i} + \sum_{j=1}^{n} \varphi_j Y_{i-j} + \ell_{t2} \tag{2}$$

Where ℓ_{t1} and ℓ_{t2} are orthogonal disturbances

From the regression equations, we test the hypothesis H^1_0 that lagged Y terms do not belong in the regression ($\sum_{j=1}^{n} \beta_j = 0$). That is Y do not cause X using F statistic given below with m and $(n-k)$ degrees of freedom

$$F = \frac{(RSS_R - RSS_{UR})/m}{RSS_{UR}/(n-k)} \tag{3}$$

Also, $H^2_0 : \sum_{i=1}^{n} \phi_i = 0$ versus $H^2_1 : \sum_{i=1}^{n} \phi_i \neq 0$ is also tested for the model above

Note: rejection of H_0 at certain critical value of F implies one variable Granger causes another
See Gujarati (2004) and Cochrane (2005)

2.4 VAR as a time series Econometric Model

Multivariate causality among dependent or response variables is made possible through Vector Autoregressive technique .Causality, Cointegration and VAR as time Series Econometrics terms are powerful tools in estimation and prediction of Vector Autoregressive Moving Average Models which takes its root from the popular Box Jenkins methodology. See for example Brockwell and Davis, (1990); Gujarati, (2004); Cochrane, (2005)

Consider the VAR given in (1) Y_t Granger causes X_t if Y_t helps to forecast X_t, given past X_t. But, Y_t does not Granger causes X_t if $\beta_j = 0$

That is if VAR in (1) is equivalent to

$$X_t = \sum_{i=1}^{n} \alpha_i X_{t-i} + 0 \sum_{j=1}^{n} Y_{i-j} + \ell_{t1} \tag{3}$$

$$Y_t = \sum_{i=1}^{n} \phi_i X_{t-i} + \sum_{j=1}^{n} \varphi_j Y_{i-j} + \ell_{t2}$$

Equation (1) in matrix notations becomes

$$\begin{bmatrix} X_t \\ Y_t \end{bmatrix} = \begin{bmatrix} a & b \\ c & d \end{bmatrix} \begin{bmatrix} X_{t-i} \\ Y_{t-j} \end{bmatrix} + \begin{bmatrix} \ell_{t1} \\ \ell_{t2} \end{bmatrix}$$

$$\begin{bmatrix} I - La & -Lb \\ -Lc & -Ld \end{bmatrix} \begin{bmatrix} X_t \\ Y_t \end{bmatrix} = \begin{bmatrix} \ell_{t1} \\ \ell_{t2} \end{bmatrix}$$

$$\begin{bmatrix} a^*(L) & b^*(L) \\ c^*(L) & d^*(L) \end{bmatrix} \begin{bmatrix} X_t \\ Y_t \end{bmatrix} = \begin{bmatrix} \ell_{t1} \\ \ell_{t2} \end{bmatrix} \tag{4}$$

Inverting the autoregressive representation, we have (5)

$$\begin{bmatrix} X_t \\ Y_t \end{bmatrix} = \frac{1}{a^*(L)d^*(L) - b^*(L)c^*(L)} \begin{bmatrix} d^*(L) & -b^*(L) \\ -c^*(L) & a^*(L) \end{bmatrix} \begin{bmatrix} \ell_{t1} \\ \ell_{t2} \end{bmatrix} \tag{5}$$

Equation (5) is moving average representation called Bivariate Wold representation.

From (5) Y does not Granger cause X Iff $b^*(L) = 0$, or if the autoregressive matrix lag polynomial is lower triangle.

Thus, Y does not Granger cause X if and only if the Wold moving average matrix lag polynomial is lower triangular. That is Y does not Granger cause X if and only if X "s bivariate Wold representation is the same as its univariate Wold representation. The projection of X on past X and Y is the same as projection of X on the past X, and that X is a function of its shocks only and does not respond to Y shocks while Y is a function of both X shocks and Y shocks. Details of these and others are available in Cochran, (2005).

III. Numerical Example

3.1 Data Description

The data for this research paper were extracted from the bulletin published by the Central Bank of Nigeria (CBN) (as shown in figure 1). The data on GDP and Money supply were used in the predicting multivariate model. The preliminary transformations were not left out as trends were discovered in the Figure 1
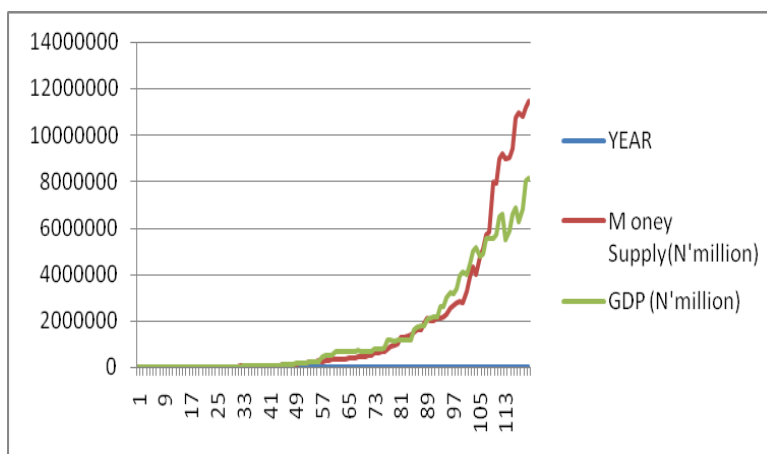
Fig1:Time Plot of Nigeria GDP and Money Supply

3.2 Empirical Results
Table 3.1 Null Unit Root Test for GDP
Hypothesis: D(GDP,2) has a unit root
Exogenous: Constant
Lag Length: 7 (Automatic - based on SIC, maxlag=12)

		t-Statistic	Prob.*
Augmented Dickey-Fuller test statistic		-8.234916	0.0000
Test critical values:	1% level	-3.490772	
	5% level	-2.887909	
	10% level	-2.580908	

*MacKinnon (1996) one-sided p-values.

Table 3.2 Null Unit Root Test for MS
Null Hypothesis: D(money supply,2) has a unit root
Exogenous: Constant
Lag Length: 12 (Automatic - based on SIC, maxlag=12)

		t-Statistic	Prob.*
Augmented Dickey-Fuller test statistic		-4.736734	0.0002
Test critical values:	1% level	-3.493747	
	5% level	-2.889200	
	10% level	-2.581596	

*MacKinnon (1996) one-sided p-values.

Table 3.3 Granger Causality Tests
Pairwise Granger Causality Tests
Date: 10/17/13   Time: 05:40
Sample: 1981Q1 2010Q4
Lags: 2

Null Hypothesis:	Obs	F-Statistic	Prob.
GDP does not Granger Cause Money supply	116	48.0658	9.E-16
money supply does not Granger Cause GDP		47.6875	1.E-15

Table 3.4:   Outcome of Unit Root Tests

ADF TEST	F	P-VALUE	DECISION
GDP	8.234916	0.0000	SIGNIFICANT AT 5% α
MS	4.736736	0.0002	SIGNIFICANT AT 5% α

3.2.1: Result of Stationarity Test
        Both GDP and money supply are not stationary in their level form but the desired level of stationarity was achieved after second difference with significant ADF values of 8.234916 and 4.736736 in absolute value respectively. We reject the Null hypothesis of presence of unit roots in both cases at **5% α** as the P –values in table 3.1 above are significant.

Table 3.5: Results of Causality Test

DIRECTION OF CAUSALITY	F	DECISION
MS $\rightarrow$ GDP	48.0658	REJECT
GDP $\rightarrow$ MS	47.6875	REJECT

3.2.2: Discussion of Results

The result suggests that the direction of causality is bi-direction in nature, since the estimated f values are significant at 5% level of significant; the critical F values are 48.0658 and 47.6875 respectively as elicited in Table 3.2

The granger causality test under the null hypotheses (H_o) GDP does not granger cause money supply and vice-versa are statistically significant, which implies that there is bilateral/feedback causality between GDP and money supply. The significant value of the test in the table above Implies the set of coefficients of GDP and Money Supply are statistically and significantly different from zero in both regressions.

Changes in either GDP or money supply causes changes in the other variable and hence changes in the economic growth and development of Nigeria. Investing more money into the economy leads to increase GDP.

REFERENCES

[1.] Box, G.E.P., Jenkins, G .N. and Reinsel G.C. (1994): Time Series Analysis: Forecasting and Control, 3th Edition, Prentice-Hall,New Jersey.
[2.] Brockwell, P and Davis R.A. (1990); Time Series: Theory and Methods. New York: Springer-Verlag.
[3.] Cochrane, J .H. (2005) Time series for Macroeconomics and Finance
[4.] Chicago: Spring pub.
[5.] Fangge, L. &Peixian, L. (2011)'AR MA Model for Predicting the Number of Outbreaks of Newcastle diseases During the Month' in IEEE. 660-663.
[6.] Galton F. (1886) 'Family Likeness in Stature' in Proceedings of Royal Society, London.Vol40:42-72
[7.] Gujarati, D.N. (2004): Basic Econometrics, 4th Ed. New York: Tata Graw – Hill Publishing Co. Ltd.
[8.] Kendall, M.G and Stuart, A. (1961): The Advanced Theory of Statistics. New York: Charles Griffin Publishers.
[9.] Hamilton, J.D. (1994): Time Series Analysis. Princeton: Princeton University Press.
[10.] Oguntade, E.S. (2010) 'Time Series Modelling of Malaria Pandemic in Nigeria' in Global Journal of Mathematics and Statistics. Vol.2 (1):61-68.
[11.] Oguntade, E.S. and Ogunfiditimi, F O (2013): 'On Recursive and Numerical Forecasts: An Interesting Characterization of the Behaviour of Time Series' in International Journal of Numerical Mathematics. Vol.7 (2):204-217.
[12.] Pearson K and Lee A. (1903) 'On the Laws of Inheritance 'in Biometrika.Vol2:357-462.

Development of a Integrated Air Cushioned Vehicle (Hovercraft)

S.V. Uma Maheswara Rao[1], V.S. Surya Prakash[2]

[1, 2] (Professor, M.E Student, Department of Marine Engineering, AUCE (A), Visakhapatnam-5300003)

Abstract: *The design and development of a hovercraft prototype with full hovercraft basic functions is reported by taking into consideration, size, material and component availability and intermediate fabrication skill. In-depth research was carried out to determine the components of a hovercraft system and their basic functions and in particular its principle of operation. Detailed research in design was done to determine the size of component parts, quite in accordance with relevant standard requirements as applicable in the air cushioned vehicles (ACV). The fabrication of the designed hovercraft by using materials that are readily available by taking into consideration the economic constraints and time constraints. It also includes the testing process which includes the tweaking of various parameters that govern lift and thrust of the hovercraft. Further research is recommended to improve on the efficiency of the craft.*
Keywords: *Hover craft, air cushioned vehicle, hybrid vessel, hull, skirt, air box.*

I. Introduction

A hovercraft is a vehicle that hovers just above the ground, or over snow or water, by a cushion of air trapped under the body creating lift. Air propellers, water propellers, or water jets usually provide propulsion. This type of vehicle is known as air cushion vehicle(ACV).it is a craft capable of travelling over land, water or ice and other surfaces both at moderate speeds, and even it could hover at stationary condition. It operates by creating a cushion of high pressure air between the hull of the vessel and the surface below. Fig1 illustrates the operational principles and basic components of a typical hovercraft. Specifically for our hovercraft, has three main design groups: the lift, thrust, and steering systems. The arrangement of the hovercraft is similar to that shown in Fig 1
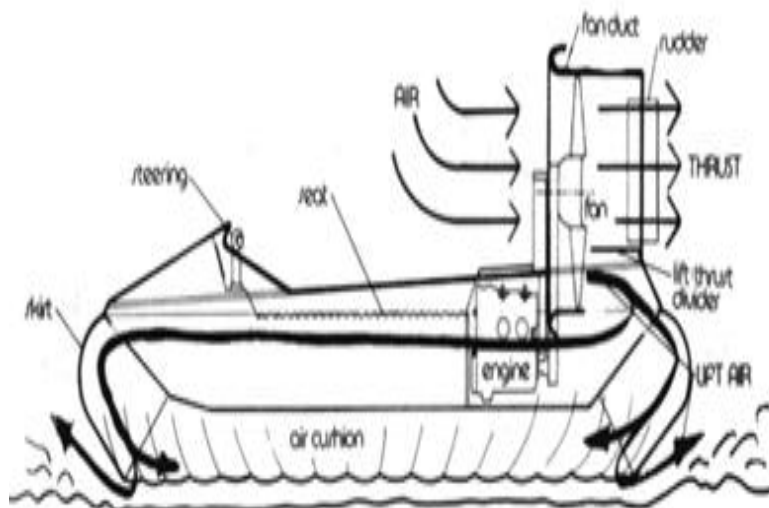
Fig 1: Air Cushioned Vehicle (Hover craft)

The propeller shown must be designed for a vehicle as typically a fan for creating vortices to mix the air, reducing the ejected air's translational kinetic energy to provide the necessary lift and thrust. Typically the cushioning effect is contained between a flexible skirt. Hovercrafts are hybrid vessels they typically hover at heights between 200mm and 600mm above any surface and can operate at speeds above 37km per hour. They can clean gradient up to 20 degree. Locations which are not easily accessible by landed vehicles due to

natural phenomena are best suited for hovercrafts. Today they are commonly used as specialized transport in disaster relief, coast ground military and survey applications as well as for sports and passenger services. Very large versions have been used to transport tanks, soldiers and large equipment in hostile environment and terrain. In riverine areas, there is great need for a transport system that would be fast, efficient, safe and low in cost. Time is spent in transferring load from landed vehicle to a boat. With hovercraft there is no need for transfer of goods since it operates both on land and water. It is said to be faster than a boat of same specifications which makes it deliver service on time.

II. Principle Of Operation

The hovercraft floats above the ground surface on a cushion of air supplied by the lift fan. The air cushion makes the hovercraft essentially frictionless. The hovercraft relies on a stable cushion of air to maintain sufficient lift. The air ejected from the propeller is separated by a horizontal divider into pressurized air utilized for the air cushion and momentum used for thrust. The weight distribution on top of the deck is arranged so that the air is distributed the air from the rear of the deck throughout the cushion volume in an approximately even fashion to provide the necessary support. The skirt extending below the deck provides containment, improves balance, and allows the craft to traverse more varied terrain. We maintain the rigidity of the skirt by filling the air-tight skirt with the same pressurized air diverted towards lift. The skirt inflates and the increasing air pressure acts on the base of the hull thereby pushing up (lifting) the unit. Small air gaps are left underneath the skirt prevent it from bursting and provide the cushion of air needed. A little effort on the hovercraft propels it in the direction of the push [7]. Steering effect is achieved by mounting rudders in the airflow from the blower or propeller. A change in direction of the rudders changes the direction of air flow thereby resulting in a change in direction of the vehicle. This is achieved by connecting wire cables and pulleys to a handle. When the handle is pushed it changes the direction of the rudders.

III. Conceptual Design

Integrated lift and thrust hovercraft
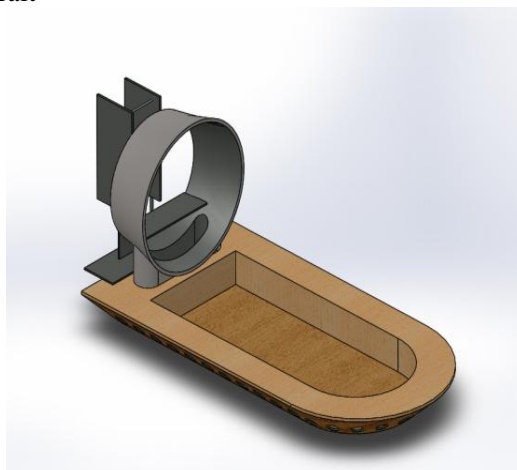
Fig2: Integrated Hover Craft

This design proposes an integrated system i.e. a single propeller is used for both the lift and thrust requirements. Here in this design the air from the shroud is split to cater to two requirements i.e. for the lift and thrust. 40% of the air is split and directed towards the base which will fulfil the lift requirements and the rest of the air is used to propel the hovercraft thereby fulfilling the thrust requirements. The salient feature of this design is that it requires only one source of power as shown in Fig 2 i.e. only one engine for thrust and lift [4] and therefore this design becomes an economically better option. However there are issues in this design such as air distribution that require further attention.

IV. Design Of Major Components

4.1 The hull, skirt calculations:

Our intention is to design a hovercraft for demonstration purpose. so a total weight of 200 kg is considered of this, 100 kg has been taken as passenger weight, and the remaining 100 kg as the hovercraft weight, which includes the weight of the base, the weight of the engine, impeller, shroud, the air box, steering mechanism, rudder system, the engine frame, the weight of the skirt, petrol tank etc.[3].
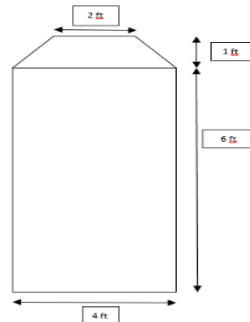
Fig3: Hull Dimensions

Total Weight = 200 kg
Length = 7 feet
Breadth = 4 feet
Area of Base, A = 28 sq.ft = 2.5 m^2
Cushion Pressure,

$$P_c = \frac{Weight}{Area of base} = \frac{200}{2.5} = 80 \text{ kg/m}^2$$
$$P_c = 80 \times 9.81 = 784.8 \text{ N/m}^2 \text{ (Pa)}$$

Escape Velocity,

$$V_e = \sqrt{\frac{2 \times P_c}{\rho}} = \sqrt{\frac{2 \times 80}{1.16}} = 11.75 \text{ m/s}$$

Perimeter of Skirt
5.25 + 5.25 + 2.5 + 2.5 = 15.5 ft = 4.72 m
Hover Gap
50 cm = 0.05 m

4.2 Lift and thrust calculations
Escape Velocity,

$$V_e = \sqrt{\frac{2 \times P_c}{\rho}} = \sqrt{\frac{2 \times 80}{1.16}} = 11.75 \text{ m/s}$$

Perimeter of Skirt = 5.25 + 5.25 + 2.5 + 2.5   = 15.5 ft = 4.72 m
Hover Gap = 50 cm = 0.05 m
Escape Area, A_e = 4.72 x 0.05 m = 0.236 m^2
Volume of Air Lost = V_e x A_e = 11.75 x 0.236   = 2.773 m^3/s
This much volume of air is required to lift the hovercraft of the total airflow generated by the impeller, 33% is used to lift the hovercraft. This 33% corresponds to 2.773 m^3/s. So the total volume of air that must be generated is three times this quantity
Therefore,
    Total Volume of Airflow required
    3.33 x 2.773 = 9.23 m^3/s
Hence, we need to select an impeller that can provide us with pressure of 785 Pa and airflow of 9.23 m^3/s.

4.3 Splitter Area and Thrust Area
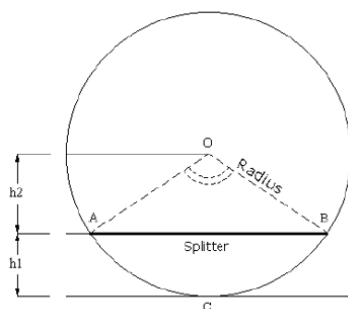
Fig 4: Splitter Area of Propeller

Area of the duct, $a_d = \frac{\pi}{4} (.9^2 - .2^2)$
$\qquad\qquad\qquad = 0.6048 \text{ m}^2$
For Splitter Height = 0.30 m
Splitter Area,

$$a_{sp} = \frac{1}{2} (\theta - \sin\theta)r^2, \qquad \theta = 140^0$$
$$a_{sp} = \frac{1}{2} \{((140 \times \frac{\pi}{180}) - \sin 140) \times 0.45^2\}$$

$\qquad = 0.2419 \text{ m}^2$

Thrust Area, $a_{th} = a_d - a_{sp}$
$\qquad\qquad\qquad = 0.3629 \text{ m}^2$
Thrust Ratio $= \frac{a_{th}}{a_d} = \frac{0.3629}{0.6048} = 60.0 \%$
Lift Ratio $= \frac{a_{sp}}{a_d} = \frac{0.2419}{0.6048} = 39.99\%$

4.4. Fan Selection
 The selection of a suitable impeller is a relatively tough task. In an integrated hovercraft, the impeller is used to provide both, the lift as well as the thrust. Usually, industrial fans are used for this purpose. Some of the most important factors that need to be considered while selecting an impeller are the size of the impeller, the number of blades, the pitch angle of the blade, and the power required. The power source (in our case – engine) should be able to provide enough power to run the impeller at the required working conditions [6].
Formulae:
For a change in speed:
The Rotational Frequency Ratio

$$(k) = \frac{N_2 \quad (NewSpeed)}{N_1 \quad (OldSpeed)}$$

To change the parameters for the fan at the new speed we can apply the following laws,
Airflow (q), $q_2 = q_1 \text{ x } k$
Pressure (p), $p_2 = p_1 \text{ x } k^2$
Power (P), $P_2 = P_1 \text{ x } k^3$
In our case, we required a pressure of 785 Pa and airflow of 10m^3/s. For selecting the fan we used sizing software called Multi-Wing Optimizer 7.0.1.144, provide by Multi-Wing India Pvt Ltd.
The specification of the impeller selected for our hovercraft is
$\qquad\qquad\qquad$ 900/3-6/31.5/PAG/5ZL
Breaking Down the Part Number Code:
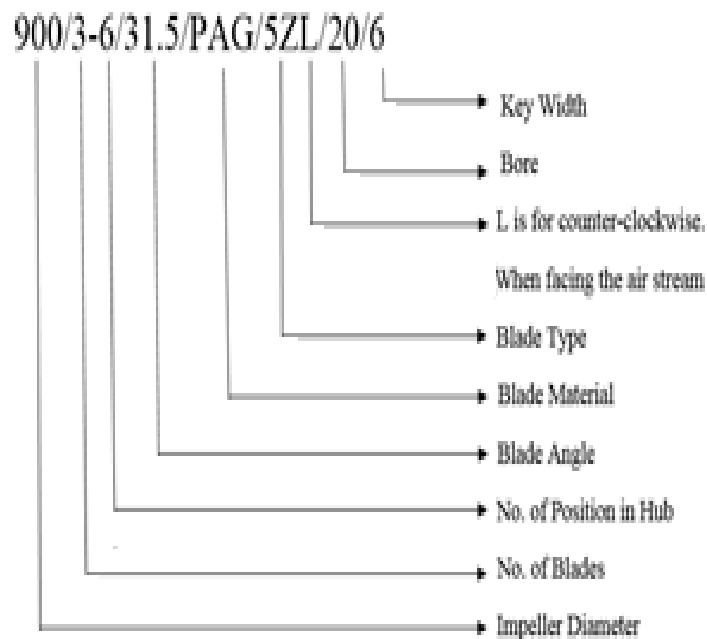
Fig 5: Breaking down the code

In the sizing software we input conditions such as Pressure required and airflow.

Fig 6: Sizing Software

Based on the data obtained from the calculation's the hovercraft has been modelled in the catia for understanding the 3-dimensonal design of how the hover craft looks like. The parts are modelled in individual workbenches and later on assembled.

Now the fabrication of the hovercraft (acv) is initiated. The materials availability according to the design is a big task.

V. Fabrication Of The Hover Craft

5.1 Hull:

Hull is made by sandwiching polystyrene sheets between plywood sheets; Industrial grade glue is used for this purpose. First plywood is cut according to the specifications given in Fig 7 glue is applied to a plywood sheet and 4 polystyrene sheets, and they are stuck together. Polystyrene sheets are kept horizontal to the plywood. Then another layer of polystyrene is adhered to the existing one to get required thickness, this time sheet are arranged vertical to plywood. Then another plywood sheet is adhered at the top. Prepared hull is kept under pressure overnight.

Fig 7: Hull

5.2 Air box:

We constructed two air boxes. One was of a height to divert 33% of the air driven by the propeller into the duct, and another one to divert 60% of the air. In the Fig 8 .First one was constructed by plywood of thickness 10mm and air tightened by applying fevicol glue at the edges. Second air box was constructed wooden pieces of 10mm thickness. Curved shape is cut in the wood, PVC sheet is fixed along the edges of the two curves with nails. Supports are provided at the base this makes the second air box. Both air boxes are used in the testing phase and appropriate one is selected.

Fig 8: Air Box

5.3. Skirt:

Skirt is kept along the craft and extra material is cut off. Both ends of useful part of skirt material is stitched so that it forms a loop. First, hole of 5mm are drilled along the hull, each 10 cm apart. Same is done on the aluminium sheets that are to be placed above the skirt so that it sticks to the hull completely. Skirt is held on the hull and holes are drilled at the same distance as before to match holes on the skirt, hull and aluminium sheets as shown in Fig 9. All three are fixed with the help of nuts and bolts. At the other end of the skirt is stitched so that a passage forms along the skirt, in which a rope is passed. Two ends of rope are tightened.

Fig 9: Skirt

5.4. Engine:

Engine mount is acquired from the scrap yard, we found that it does not support whole engine, but provides support to the base. Extra material of the mount is cut off to save the weight and to provide space for the new frame. New frame is constructed so as to support the upper part of the engine and hold two bearings that are kept parallel and aligned. Bearings house the shaft of diameter 25mm.diameter at one end of the shaft is reduced to 20 mm so as to fit into the fan hub. Manufacturer provided a 20 mm hole in the fan hub for the shaft to fit in, with a key of 6 mm. Shaft is also provided with the same dimension of key grove. Transmission consists of sprocket and chain arrangement. Sprocket is fixed on the shaft with Allen screws. Chain is fitted on the sprocket teeth and teeth on direct output of the engine. Bearing and frames so constructed that shaft is at the height of 475mm from the hull, or the centre of the duct. Washers are fitted so as not to leave the chain slack. Engine, engine mount, transmission assembly parts are fitted together to form power house assembly. This power house assembly is fixed on the hull 4 M10 bolts. To absorb the vibrations of the engine 4 rubber pads, 2 pads for each leg of the mount, of 8mm thickness are provided between engine mount base and hull.

Fig10: Engine Assembly

Fig 11: Final Assembly of the Hovercraft

VI. Result

The hovercraft was lifted and was propelled by the thrust system. It was able to carry one person of weight 75 kg and hovered with an air cushion of 70 mm .Manoeuvrability was achieved with the steering system.it covered a distance of 100 m in 20 sec which results in a speed just less than 20 km/hr.

VII. Conclusion

The concept of a hovercraft is very simple, but the actual construction of it is a tough task. The calculations involved are complex and they should be extremely accurate. The weight should be evenly distributed and the centre of gravity should be properly identified. The experience gained by doing this project taught us a lot about many things. It helped us understand a lot of concepts and saw those concepts put to use. After the hovercraft was built, a lot of testing and tweaking was required to make it work. All the testing and tweaking actually tested our patience and dedication towards the project. After days of up's and down's, the hovercraft finally hovered and was working fine.

VIII. Future Scope

The intension is to understand the basic principle of a hovercraft and to fabricate the same keeping the constraints such as monetary constraints, time constraints etc., in mind. The hovercraft attempted was a primitive one and as many aspect that needs to be optimized in the future such as

- Vibration and noise reduction
- Minimization of fuel consumption, etc.

REFERENCES

[1]   Development of a Hovercraft Prototype, Okafor, B.E.Department of Mechanical Engineering, Fed. University of Technology., Owerri-Nigeria.International Journal of Engineering and Technology Volume 3 No. 3, March, 2013, ISSN 2049-3444

[2]   A.K.Amiruddin, S.M.Sapuan, and A.A.Jaafar, Development of a hovercraft prototype with an aluminium hull base. International Journal of the Physical Sciences Vol. 6(17), pp. 4185-4194, 2 September, 2011.ISSN 1992 -1950

[3]   P.FitzPatrick – Hovercraft Club of Great Britain (S.E. Branch), Calculation of thrust in a ducted fan assembly for hovercraft.

[4]   RevD, A method for estimating the thrust and lift performance of an integrated hovercraft.

[5]   Kofi Anguah and Nick Szapiro, Design and Construction of a passenger hovercraft.

[6]   P.FitzPatrick – Hovercraft Club of Great Britain (S.E. Branch), Understanding and Selecting lift fans.

[7]   P.FitzPatrick – Hovercraft Club of Great Britain (S.E. Branch), the principles of hovercraft design.

[8]   Rose-Hulman Institute of Technology, Design and Fabrication of a model hovercraft.

[9]   LakhbirChauhan P.E, Pump Consulting Services, Inc, Propeller Design Considerations.

[10]   Perozzo, James. HovercraftingAs a Hobby. Maverick Publications, Bend, OR, p.27, 1995.

[11]   Okiishi, Munson and Young, Fundamentals of Fluid Mechanics, 5th Edition. Equation 3.20, pg122, Wiley Publishing, 2005.

[12]   Melissa Ernst, University of North Carolina, Hovercraft, NSF GK-12

[13]   Amyot J. R. (1989). Hovercraft Technology, Economics and Applications. Elsevier Science Publishing Co., New York.

Pathogenic Bacteria in Corals from Veracruz Reef System National Park

García-Fuentes J.L[1], Galaviz-Villa I[2], Lango-Reynoso F[3],
Castañeda-Chávez M. del R[4].

[1](Masters Student/ Instituto Tecnológico de Boca del Río, México)
[2, 3, 4] (Division of Graduate Studies and Research, Instituto Tecnológico de Boca del Río, México)

Abstract: *The Veracruz Reef System National Park (PNSAV) is situated in front of Veracruz-Boca del Río and Antón Lizardo conurbation with approximately 65,516 hectares. In 1992 this reef system was declared a Natural Protected Area and in 2006 it became Biosphere reserve. Despite this recognition, the PNSAV is exposed to anthropogenic effects such as river discharge, port traffic, tourism, and waste discharges; all this causes sediment and bacteria, which affect corals. Studies conducted by PNSAV show the presence of diseases and syndromes in scleractinian corals but do not denote the causal agent of the disease. For this reason, the present study aimed to make the diagnosis of bacteria causing damages to the scleractinian coral and its relation to discharges from areas of influence of PNSAV. 12 fixed 80 meter transects were established and coral samples were collected from the genera: Colpophyllia, Montastraea, Porites and Siderastrea. The lesions identified as criteria for the collection were bands, marks and spots on the body of the coral. The sample was run in duplicate, both the affected and the visually healthy. A microbiological analysis of wastewater from point sources of pollution was performed. The coral and water samples were analyzed by simple PCR in laboratory of the Instituto Tecnológico de Boca del Río in Veracruz (ITBOCA). Primers of pathogenic bacteria include species of the genera Oscillatoria, Vibrio, Serratia y Aurantimonas. There was a positive presence of Vibrio bacteria with an 87% in the water samples and a 27.1% in coral tissue. The bacteria Serratia marcescens was only present in water samples and the Aurantimona coralicida in diseased coral tissue. It was also noted that there is a relationship in bacteria in the positive presence of 3-point sources of pollution and coral tissue.*
Keywords: *Pathogenic bacteria, Corals, PCR.*

I. Introduction

In recent years it has been considered that coral reefs worldwide are threatened with extinction, this as a result of climate change and anthropogenic pollution, which generates a large-scale mortality and a difficult long-time regeneration [1] [2] [3]. The rapid growth of human population on coastal margins of the surrounding reefs has caused physical, chemical and biological changes in these systems [4]. Point sources of pollution are generally discharges through pipes and channels, which are taken to riverbeds, coastal waters and other water bodies. All these sources provide bacteria causing adverse effects difficult to control [5] [6].

Bacterial communities are known to be extremely important in many ecosystems. In coral reef systems, the bacteria are sensitive to environmental or anthropogenic changes and even after these changes occur they continue to cause effects over long periods of time [7].

This pathogenic bacteria causes degradation of coral tissue and during that process it quickly colonizes the coral structure altering significantly the microbial community (Holobiontes), and its interaction with the host [8]. The injuries caused by bacterial infection in the coral are identified as bands, irregular spots and dots.

The National Park Veracruz Reef System (PNSAV) is exposed to local effects such as discharges from the Jamapa River with a discharge volume of 670 million m3 per year, it also has the influence of the Papaloapan River with a discharge volume of 20,000 million m3 a year [9], and to the north is the influence of La Antigua River. The PNSAV is influenced by the port traffic, which admitted between 1505 and 1809 ships a year [10]. Added to this, there are multiple impact factors such as the flow of municipal, industrial and agricultural discharges, tourism including scuba diving, boat trips and visits to some of the beaches and shallow areas of the park, involving among other vessels anchoring, groundings, and oil spills [11].

The river discharges are rich in nutrients and sediment. These characteristics cause adverse affectations for coral reefs since these systems prefer oligotrophic conditions and clear water [12].

There is little information concerning the identification of pathogenic bacteria that cause damage to the health of corals in the Gulf of México. Understanding the need of information, this study generates the first diagnosis of pathogenic bacteria in corals of PNSAV.

II. Materials and Method

2.1 *Study area*

This study was conducted at the Veracruz Reef System National Park (PNSAV), it is located between the coordinates 19º00'00'' – 19º16'00'' N and 95º45'00'' – 96º12'00'' W, in the central portion of the state of Veracruz. The PNSAV extension is 65,516 hectares (Fig. 1).
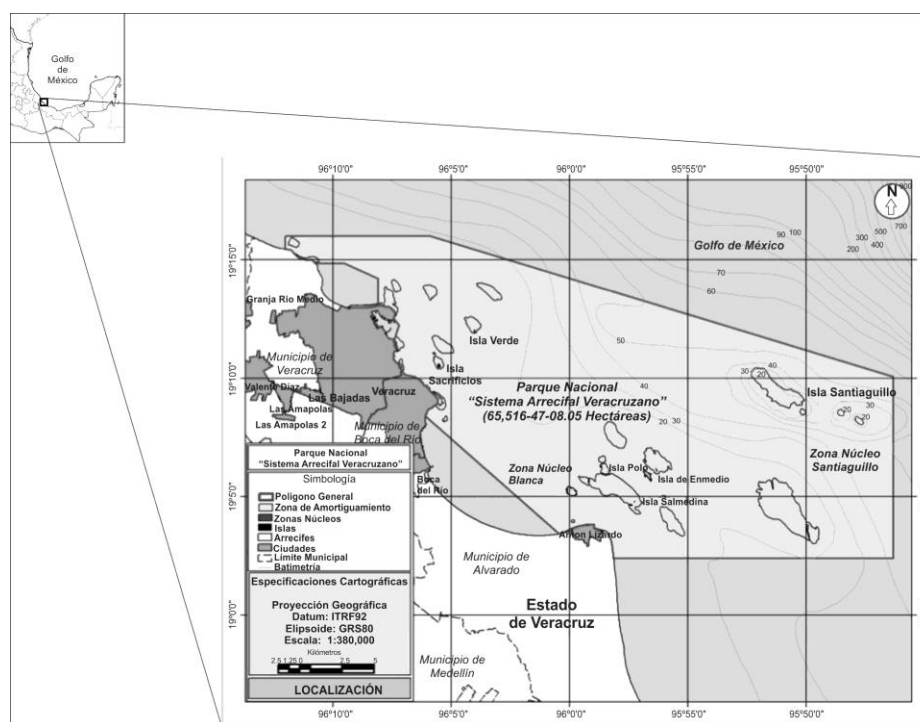
Figure 1.Schematic location of PNSAV.

2.2 Sample collection and process
2.2.1 Point sources of pollution (PSP)

Ten point sources of pollution were identified and selected; they are located throughout the metropolitan area of Veracruz-Boca del Río, Alvarado and Antón Lizardo. The sites selected were: Papaloapan River, Giote Stream, Jamapa River, Villa Rica Sump, América's Calzada, Simón Bolívar Collector, Yacht Club, Port Area, Shipyards and an open sky channel The Cable. There were obtained 10 samples with replicates at each sampling site. The water samples were placed in sterile polyethylene bags and transported in coolers at an approximate temperature of 4ºC for preservation until analysis in a maximum of 5 hours in the Research Laboratory and Aquatic Resources of the Instituto Tecnológico de Boca del Río (ITBOCA).

2.2.2 Corals

The coral tissue sampling was performed by setting 12 fixed 80 x 1m transects with a parallel pattern to the coast (northeast-southwest). A discriminatory table was performed as proposed criteria for the selection of coral species based on greater distribution and occurrence of diseases that resulted in the following species: *Colpophyllia natans, Montastraea cavernosa, Montastraea faveolata, Porites astreoides* and *Siderastrea siderea*.

The sampling consisted on removing an approximately 2cm³ piece of coral tissue; a chisel and a hammer were used as support tools for the extraction of the tissue sample. The tissue sample was extracted in

duplicate, both visually impaired and healthy part. These were collected separately in sterile bags and stored at an approximate temperature of 4ºC for storage until analysis in a maximum period of 5 hours at the laboratory of ITBOCA.

Water samples and corals were processed for DNA extraction using PROMEGA Corp. The molecular biology test that was performed was simple PCR and the primers used were pathogenic bacteria, as shown in the following table (Table 1).

2.2.3 Statistical analysis

The test of Cochran, a non-parametric statistical method was used by means of a randomized complete block design. The data generated were analyzed by the Statistica software V.10.

Bacteria	Primer	Sequence	Base pairs	References
Género Oscillatoria	Antx-f	CGCAAATCGATGCTCACTTA	650	[13]
	Antx-r	CCACTGGCTCCATCTTGATT		
Aurantimonas coralicida.	Ac-995F	TCG ACG GTA TCC GGA GAC GGA T	500	[14]
	UB-1492R	TAC GGY TAC CTT GTT ACG ACT T		
Vibrio complex	HA-F	CATGAGGTCAGCCACGGTTTTACTGAGCAG	225	[15]
	HA-R	CGCGCGGTTAAACACGCCACTCGAATGGTGAAC		
Serratia marcescens	Sm-456F	GGT GAG CTT AAT ACG TTC ATC A	1040	[14]
	UB-1492R	TAC GGY TAC CTT GTT ACG ACT T		
Vibrio coralliilyticus	Vc-76F	GTT RTC TGA ACC TTC GGG GAA CG	940	[14]
	Vc-1019R	CTG TCT CCA GTC TCT TCT GAG G		
Vibrio shilonii	Vs-457F	GGT ACG TTA ATA GCG TGC TCG	570	[14]
	Vs-1023R	ACC TGC GTC TCC GCT GGC		

Table 1. Pathogenic bacteria and primers reported by different authors for corals.

III. Results

3.1 Pathogenic bacteria on PSP

Pathogenic bacteria on PSP (n=10) shows the presence of 85% of Vibrio complex (Fig. 2), 45% of *Vibrio coraliilyticus*, 45% of *Vibrio shilonii*, 60% of *Serratia marcescens* and absence of *Aurantimonas coralicida* and Oscillatoria genus.
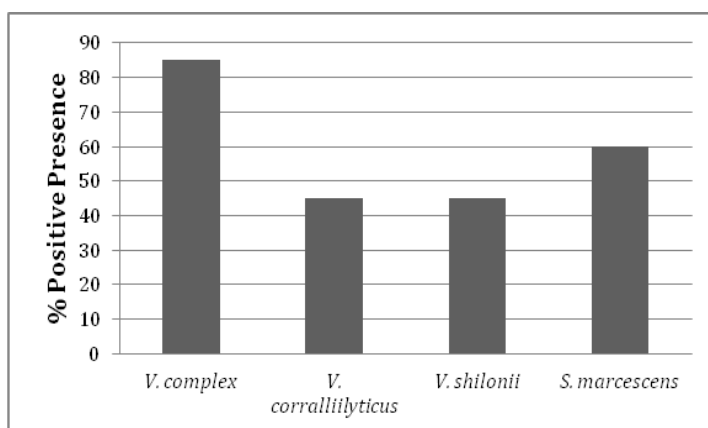
Figure 2. Positive presence of pathogenic bacteria in the point sources of pollution (PSP) of PNSAV.

Presence of pathogenic bacteria in the PSP of PNSAV showed to *V. complex* present in each sample point. *Aurantimonas coralicida* and the Oscillatoria genus were absent (Table 2).

Table 2. Presence of pathogenic bacteria in the PSP of PNSAV. (Vcom) *Vibrio complex*, (Vc)*Vibrio coralliilyticus,* (Vs)*Vibrio shilonii,* (Sm)*Serrata marcescens,* (Ac)*Aurantimonas coralicida,* (Os)*Oscillatoria*; (+) positive, (-) negative.

Point sources of pollution	V. com	Vc	Vs	Sm	Ac	Os
River Papaloapan	+	+	+	+	-	-
Stream Giote	+	+	+	+	-	-
River Jamapa	+	+	+	+	-	-
Lift station Villa Rica	+	+	-	+	-	-
Calzada de las Américas	+	-	-	-	-	-
Collector Simón Bolívar	+	-	-	-	-	-
Yacht club, Veracruz	+	+	+	+	-	-
Port area, Veracruz	+	+	+	+	-	-
Shipyard, Veracruz	+	-	-	-	-	-
Waterway El Cable	+	+	-	+	-	-

3.2 *Corals*

The pathogenic bacteria present in coral tissue (n=92) showed 42.3% for *Vibrio complex*, 27.1% for *Vibrio coraliilyticus*, 11% for *Vibrio shilonii*, 11% for *Aurantimonas coralicida* and absence of *Serratia marcescens* and *Oscillatoria* genus (Fig. 3).
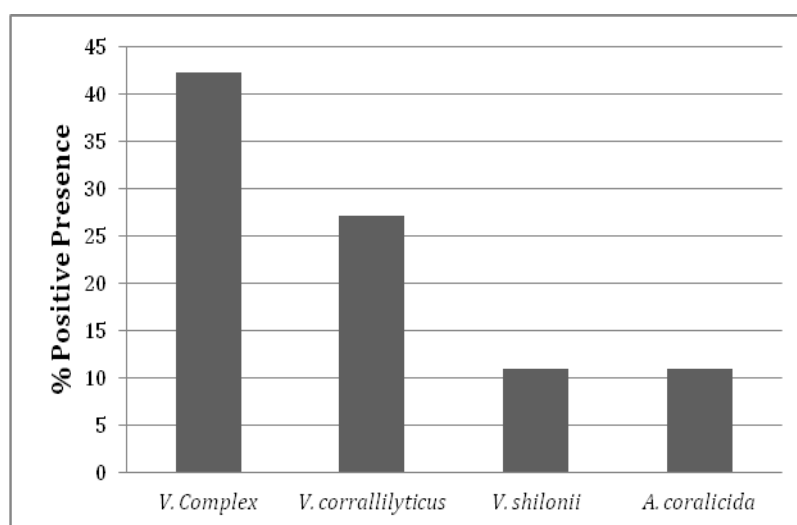
Figure 3. Positive presence of pathogenic bacteria *C. natans, M. Cavernosa, M. Faveloata, P. Astreoides, S. Siderea* identified in coral tissue in the PNSAV.

3.3 Relationship of pathogenic bacteria found in the PSP and the PNSAV.

The relationship between the two can be seen in the following comparison table, which was made with the results of the identification of pathogenic bacteria in the PSP and coral tissue (Table 4).

Table 4. Pathogenic bacteria such as (Vcom) *Vibrio complex,* (Vc) *Vibrio Coralliilyticus,* (Vs) *Vibrio Shilonii,* (Sm) *Serratia marcescens,* (Ac) *Aurantimonas coralicida,* (Os) *Oscillatoria* present in the PCP and coral tissue (*C. natans, M. Cavernosa, M. Faveolata, P. Astreoides, S. Siderea*). Superscripts [1][2][3][4] refer to the coral species present in each of the reefs of the corresponding row.

Point sources of pollution	Detected bacteria	Near reef	Coral species	Etiological characteristics	Detected bacteria	Bacteria in common
Papaloapan River	Vcom, Vc, Vs, Sm	Cabezo norte[1] Cabezo sur[2] Santiaguillo[3]	*Siderastrea siderea*[1,2]	Gray spots	Vcom, Vc	Vcom, Vc
			Siderastrea siderea[2]	Yellow spots	Vcom, Vc, Vs	
			Colpophyllia natans[1,2]	Bleaching	Vcom, Vc, Ac	
			Porites astreoides[3]	Yellow spots	Vcom, Vc, Vs	
Giote Stream	Vcom, Vc, Vs, Sm	Blanca[1] Giote[2] Sargazo[3] La palma[4]	*Siderastrea siderea*[1]	White band	Vcom, Vs	Vcom, Vc, Vs
			Siderastrea siderea[2]	White spots	Vcom, Ac	
			Siderastrea siderea[3]	Gray spots	Vcom, Vs	
			Siderastrea siderea[4]	Black band	Vcom, Vc	
			Colpophyllia natans[3]	Bleaching	Ac	
			Colpophyllia natans[4]	White band	Vcom, Vc	
			Montastraea faveolata[2]	Yellow spots	Vcom, Vc	
			Montastraea cavernosa[1]	White band	Vcom, Vc, Ac	
Jamapa River	Vcom, Vc, Vs, Sm	Verde[1] Bajo mersey[2] Blanca[3] Giote[4]	*Siderastrea siderea*[1]	Dark band	Vcom, Vc, Vs	Vcom, Vc, Vs
			Siderastrea siderea[3]	White band	Vcom, Vs	
			Siderastrea siderea[4]	White spots	Vcom, Ac	
			Porites astreoides[2]	Yellow spots	Vcom, Vs	
			Colpophyllia natans[1]	Bleaching	Ac	
			Montastraea cavernosa[2]	Dark band	Vcom	
			Montastraea cavernosa[3]	White band	Vcom, Vc, Ac	
			Montastraea faveolata[4]	Yellow spots	Vcom, Vc	
Villa Rica Sump	Vcom, Vc, Sm	Verde[1] Bajo mersey[2]	*Siderastrea siderea*[1]	Dark band	Vcom, Vc, Vs	Vcom, Vc
			Porites astreoides[2]	Yellow spots	Vcom, Vs	
			Colpophyllia natans[1]	Bleaching	Ac	
			Montastraea cavernosa[2]	Dark band	Vc	
América's Calzada	Vcom	Verde[1] Bajo mersey[2]	*Siderastrea siderea*[1]	Dark band	Vcom, Vc, Vs	Vcom
			Porites astreoides[2]	Yellow spots	Vcom, Vs	
			Colpophyllia natans[1]	Bleaching	Ac	
			Montastraea cavernosa[2]	Dark band	Vc	
Simón Bolívar Collector	Vcom	Bajo mersey[1]	*Porites astreoides*[1]	Yellow spots	Vcom, Vs	Vcom
			Montastraea cavernosa[1]	Dark band	Vcom	
Yacht Club, Veracruz	Vcom, Vc, Vs, Sm	Blanquilla[1] Verde[2] Bajo mersey[3]	*Siderastrea siderea*[2]	Dark band	Vcom, Vc, Vs	Vcom, Vc, Vs
			Porites astreoides[1,3]	Yellow spots	Vcom, Vs	
			Montastraea cavernosa[3]	Dark band	Vcom	
			Colpophyllia natans[2]	Bleaching	Ac	
Port Area, Veracruz	Vcom, Vc, Vs, Sm	Blanquilla[1] Verde[2] Bajo mersey[3]	*Siderastrea siderea*[2]	Dark band	Vcom, Vc, Vs	Vcom, Vc, Vs
			Porites astreoides[1,3]	Yellow spots	Vcom, Vs	
			Montastraea cavernosa[3]	Dark band	Vcom	
			Colpophyllia natans[2]	Bleaching	Ac	
Shipyards, Veracruz	Vcom	Gallega[1] Galleguilla[2] Blanquilla[3]	*Siderastrea siderea*[2]	Gray spots	-	Vcom
			Porites astreoides[1,3]	Yellow spots	Vcom, Vc	
Open Sky Channel El Cable	Vcom, Vc, Sm	Gallega[1] Galleguilla[2]	*Siderastrea siderea*[2]	Gray spots	-	Vcom
			Porites astreoides[1]	Yellow spots	Vcom, Vc	

IV. Discussion

Pathogenic bacteria of the genus Vibrio, which were positive, occurred in 85% of PSP of analyzed samples, unlike coral samples where the percentage of bacteria decreased by 42.3%. According to the primer used HA-F/HA-R (*Vibrio complex*), this amplifies the gene encoding the zinc-metalloprotease, which is characteristic of pathogenic bacteria of the genus Vibrio, such as *V. cholera*, *V. vulnificus*, *V. harveyi, V. anguillarum*, *V. parahaemolyticus*, including the species of *V. coralliilyticus* and *V. shilonii* [16]. *Vibrio complex* in coral tissue suggests that some of the species mentioned above could be present. Therefore, it is possible that there is a risk of causing alterations to coral with diseases like White syndrome, Syndrome of Dark Spots, Black Band disease and Yellow Band disease [17][18][19][20].

Serratia marcescens bacteria had positive presence in six out of ten PSP sampling points. Its appearance in the marine environment may be due to the contribution coming from the PSP since this bacteria is common in the intestinal tract of humans and animals [21]. This same bacterium was not present in the tissue of the coral species *Colpophyllia natans*, *Montastraea cavernosa*, *Montrastaea faveolata*, *Porites astreoides* and *Siderastrea siderea*. In studies, this bacterium is reported and known as pathogen of the coral genus Acropora and causes White Pox disease [22][23]. However, their

presence is not ruled out in other species, as the etiological characteristics of the disease in the coral Acropora are similar to other coral species.

The *Aurantimonas coralicida* bacteria only occurred in 11% of coral tissue *Colpophyllia natans*, *Siderastrea sidera* and *Montastraea cavernosa*, this bacterium is associated with a disease called White Plague; a sign of this disease is exposure of the limestone structure, showing no tissue in its periphery [24][25][26]. It was also found the presence of *A. Coralicida* and *Vibrio complex*, bacteria associated with the etiologic features of the aforementioned disease. So it is likely that this disease is caused by a bacterial complex and not just by the bacteria *Aurantimonas coralicida* in the previously mentioned coral species [27][28]. The genus Oscillatoria showed only in 4% of the tissue samples of analyzed coral, there were no etiologic lesions. Although there have been studies showing that it is a causative agent of the Black Band disease (BBD), which has affected more than 45 coral species.

The presence of pathogenic bacteria in different species of coral in the PNSAV, correspond to those identified in the PSP. By the distance of the reef with the PSP and according to the results obtained in this study, it reflects a potential risk for the contribution of pathogenic bacteria to the environment, which directly affect coral species. In 2005, it found a similar behavior due to the presence of diseases in corals that are located near to discharge zones [29]. Such is the case of the Veracruz Reef System National Park where these coral reefs found near urban coastal areas are exposed to excessive discharges of nutrients, sediment and pathogens that alter the survival of coral [30][31]. However, one of the affectations of greatest impact is the presence of pathogenic bacteria that cause diseases and threaten the ecological balance of the coral ecosystem [32].

V. Conclusion

The contribution of pathogenic bacteria from point sources of pollution is causing pathological affectations in corals, which are characteristic of the disease: White Band, Black Band, Yellow Band, White Plague and Bacterial Bleaching. This represents short-term negative impacts such as loss in coral cover, and long-term changes in the PNSAV faunal composition. However, the prevalence of pathogenic bacteria in corals could be related to the coral adaptation to these vulnerability conditions, this conclusion is reached since pathogenic bacteria were found in coral tissue without signs of injury or illness.

This problem represents potential risks to species of commercial interest that inhabit the reef, the above is a result of environmental impacts, loss of habitat for the species that live or depend on PNSAV, thus also reduction or migration of species, some modifications in life stage of the ecological niche and opportunities for invasive and opportunistic species. Socioeconomic impacts would be reflected in the decrease of the capture of species of commercial interest and an increment in prices as a result of fishing effort.

This study generated the first report of the presence of pathogenic bacteria from point sources of pollution and its direct effect on PNSAV coral reefs.

Acknowledgments

REFERENCES

[1] J.M West, & Slam, V.R. Resistance and resilience to coral bleaching: implications for coral reef conservation and management. Conservation Biology, 17(4), 2003, 956-967. http://dx.doi.org/ 10.1046/j.1523-1739.2003.02055.x

[2] J. E. N. Veron, Devantier, L. M., Turak, E., Green, A. L., Kininmonth, S., Stafford-Smith, M., & Peterson, N. Delineating the coral triangle. Galaxea, Journal of Coral Reef Studies, 11(2), 2009, 91-100. Retrieved from http://outremer.mnhn.fr/sites/outremer.mnhn.fr/files/coral_triangle.pdf

[3] M. Pandolfi, Connolly, S., Marshall, D., & Cohen, A. Projecting coral reef futures under global warming and ocean acidification. Science, 333(6041), 2011, 418-422. http://dx.doi.org/10.1126/science.1204794

[4] A. Dikou. Ecological Processes and Contemporary Coral Reef Management. Diversity, 2, 2010, 717-737. http://dx.doi.org/10.3390/d2050717

[5]   N. Rajendran, Suwa, Y., & Urushigawa, Y. Distribution of phospholipid ester-linked fatty acid biomarkers for bacteria in the sediment of Ise Bay, Japan. Marine Chemistry, 42(1), 1993, 39-56. http://dx.doi.org/10.1016/0304-4203(93)90248-M

[6]   W.D. Grant, Kamekura, M., McGenity, T.J., & Ventosa, A. Class III. Halobacteria class. nov. In D.R. Boone & R.W. Castenholz (Eds.), Vol. 1: The Archaea and the Deeply Branching and Phototrophic Bacteria. In G.M. Garrity (Ed.), Bergey's Manual of Systematic Bacteriology, 2nd ed., Springer-Verlag, New York. 294-334, 2001.

[7]   P. Schimel, Balser, T., & Wallenstein, M. Microbial stress-response physiology and its implications for ecosystem function. Ecology, 88, 2007, 1386–1394. http://dx.doi.org/10.1890/06-0219

[8]   T. Ainsworth, Kramasky-Invierno, E., Loya, H.O., & Fine M. Coral Disease Diagnostics: What's between a Plague and a Band. Applied and Environmental Microbiology, 73(3), 2007, 981–992. http://dx.doi.org/10.1128/AEM.02172-06

[9]   PEMEX. Evaluación de los corales escleractinios del sistema arrecifal del Puerto de Veracruz. PEMEX y SEMAR, México. GPTA-E-01/87, 1987.

[10]   APIVER. Resumen de movimientos de buques y carga. Administración Portuaria Integral de Veracruz, 2005. Retrieved from http://148.223.221.118/apiwww/op-movimiento2.htm

[11]   C.V. Gutiérrez-Ruiz, Román-Vives, M., Vergara, C.H., & Badano, E.I. Impact of anthropogenic disturbances on the diversity of shallow stony corals in the Veracruz Reef System National Park. Revista Mexicana de Biodiversidad, 82, 2011, 249-260. Retrieved from http://www.scielo.org.mx/pdf/rmbiodiv/v82n1/v82n1a22.pdf

[12]   J.E.N. Veron. Corals of the world. Vol 1-3. M. Stafford-Smith (Ed.) Australian Institute of Marine Science, Townsville, Australia, 2000. 1382 p.

[13]   S. Cadel-Six, C. Peyraud-Thomas., L. Brient., Tandeau de Marsac., R. Rippka., & A. Me'Jean. Different genotypes of anatoxin-producing cyanobacteria coexist in the Tarn River, France. Applied and Environmental Microbiology, 73, 2007, 7605–7614. Retrieved from http://aem.asm.org/content/73/23/7605.short

[14]   W.L. Polson, L. Higgins, & Woodley, M. PCR-based Assay for Detection of Four Coral Pathogens. 11th International Coral Reef Symposium. Lauderdale, Florida. Sesión 8, 2008, 247-251. Retrieved from http://www.nova.edu/ncri/11icrs/proceedings/files/m08-02.pdf

[15]   W. Sussman, Bette L., Steven, V., & Bourne, D. Coral pathogens identified for white syndrome (WS) epizootics in the Indo-Pacific. Public Library of Science ONE. 3(6), 2008, 1-14. http://dx.doi.org/10.1371/journal.pone.0002393

[16]   L. Gil-Agudelo & Garzon-Ferreira, J. Spatial and seasonal variation of dark spots disease in coral communities of the Santa Marta area (Colombian Caribbean). Bulletin of Marine Science, 69 (2), 2001, 619–629. Retrieved from http://www.ingentaconnect.com/content/umrsmas/bullmar/2001/00000069/00000002/art00033?crawler=true

[17]   M. Sweet & Bythell, J. Ciliate and bacterial communities associated with white syndrome and brown band disease in reef-building corals. Environmental Microbiology, 14, 2012, 2184–2199. http://dx.doi.org/ 10.1111/j.1462-2920.2012.02746.x

[18]   C. Sheridan, Kramarsky-Winter, E., Sweet, M., Kushmaro, A. & Costa, M. Diseases in coral aquaculture: causes, implicationsandpreventions,Review,Aquaculture,396-399,2013,124-135.http://dx.doi.org/10.1016/ j.aquaculture.2013.02.037.

[19]   A. Cróquer, C. Bastidas., A. Elliott., & M. Sweet. Bacterial assemblages shifts from healthy to yellow band disease states in the dominant reef coral Montastraea faveolata. Environmental Microbiology Reports 5, 2013, 90–96. http://dx.doi.org/10.1111/j.1758-2229.2012.00397

[20]   P. Sutherland, & K. Ritchie. White pox disease of the Caribbean elkhorn coral Acropora palmate. 289-300. En: Rosenberg, E. y Y. Loya. (Eds.). Coral health and disease. Springer-Verlag, Berlín. 2004, 488 pp. http://dx.doi.org/10.1007/978-3-662-06414-6_16

[21]   P. Sutherland, Shaban, S., Joyner, J., Porter, J. & Lipp E. Human pathogen shown to cause disease in the threatened eklhorn coral Acropora palmata. Public Library of Science ONE, 6(8), 2011. http://dx.doi.org/ 10.1371/journal.pone.0023468

[22]   B. Ritchie. Regulation of microbial populations by coral surface mucus and mucus-associated bacteria. Marine Ecology Progress Series, 322, 2006,1-14. http://dx.doi.org/ 10.3354/meps322001

[23]   P. Dustan. Vitality of reef coral population off Key Largo, Florida: recruitment and mortality. Environmental Geology, 2, 1977, 51-58. http://dx.doi.org/10.1007/BF02430665

[24]   L. Richardson. Coral diseases: what is really known? TREE, 13(11), 1998, 438-443. Retrieved fromhttp://www.denix.osd.mil/nr/crid/Coral_Reef_Iniative_Database/Coral_Reef_Information_files/Richardson,%201998.pdf

[25]   E. DenneR, G. Smith., J. Busse., P. Schumann., T. Narzt., & S. Polson. Aurantimonas coralicida gen. nov., sp nov., the causative agent of white plague type II on Caribbean scleractinian corals. International Journal of Systematic

and Evolutionary Microbiology, 53, 2003, 1115–1122. Retrieved from http://www.ncbi.nlm.nih.gov/pubmed/12892136.

[26]   E. Weil, Smith, G., & Gil-Agudelo, D. L. Status and progress in coral reef disease research. Diseases of Aquatic Organisms, 69(1), 2006, 1-7. http://dx.doi.org/ 10.3354/dao069001

[27]   S. Sunagawa, DeSantis, T.Z., Piceno M.Y., Brodie, E. L, DeSalvo, M.K., Voolstra, C.R, Weil, E., Andersen, G.L., & Medina M. Bacterial diversity and white plague disease-associated community changes in the caribbean coral Montastrea faveolata. The ISME Journal, 3(5), 2009, 512-521. http://dx.doi.org/ 10.1038/ismej.2008.131

[28]   L. Kaczmarsky, Draud, M., & Williams, E. Is there a relationship between proximity to sewage effluent and the prevalence of coral disease? Caribbean Journal of Science, 41(1), 2005, 37-124. Retrieved from http://www.denix.osd.mil/nr/crid/Coral_Reef_Iniative_Database/Conservation_files/Kaczmarsky%20etal%202005.pdf

[29]   M.D. Spalding, & Grenfell, A.M. New estimates of global and regional coral reef areas. Coral Reefs, 16(4), 1997, 225–230. http:// dx.doi.org/10.1007/s003380050078

[30]   K. Fabricius. Effects of terrestrial runoff on the ecology of corals and coral reefs: review and synthesis. Marine Pollution Bulletin, 50, 2005, 125-146. http://dx.doi.org/10.1016/j.marpolbul.2004.11.028

[31]   T.P. Hughes, Baird, A. H., Bellwood, D. R., Card, M., Connolly, S. R., Folke, C., Grosberg, R., Hoegh-Guldberg, O., Jackson, J. B., Kleypas, J., Lough, J. M., Marshall, P., Nystrom, M., Palumbi, S. R., Pandolfi, J. M., Rosen, B., & Roughgarden, J. Climate change, human impacts, and the resilience of coral reefs. Science, 301(5635), 2003, 929–933. http://dx.doi.org/ 10.1126/science.1085046

[32]   N. Knowlton. The future of coral reefs. Proceedings of the National Academy of Sciences, 98(10), 2001, 5419-5425. http://dx.doi.org/ 10.1073/pnas.091092998

Design and Development of Arm Manikin for Blood Pressure and Pulse Simulation

Mr. Mahavir K. Beldar[1], Mr. Prasanna Balan[2], Dr. B. B. Ahuja[3]

[1, 2, 3] *(Mechatronics Engineering, Deputy Director, Production Engineering, Government College of Engineering Pune, India)*

Abstract: *The purpose of this study is to develop an arm manikin for oscillometric methods of blood pressure measurement over full clinical range of blood pressure, heart rate. Blood pressure simulator helps to resolve the uncertainties common in teaching students to take blood pressure. Simulator allows the pre-setting of values for both systolic and diastolic pressures and provides an excellent means to practice listening and distinguishing blood pressure sounds prior to actual clinical experience. With this realistic unit, the student can find the preset results and the instructor can unfailingly know if the student has performed the procedure accurately. The arm manikin is a mould made up of rexine material which is coated with ethaflex as a skin material. A small rubber tube is used as blood vessel and a small micro-speaker for heart beat listening. An external electronic box is used to make students do the whole practice of blood pressure and pulse measurement. The compressed air with 2x2 NC solenoid valve and other pneumatic accessories are used to create the artificial pulses. A small micro-speaker with pre-recorded sound is used to generate heart beating sound in the antecubital area. A blood pressure sensor MPX5050GP is used to sense the sphygmomanometer dial pressure. PCB designed using a 16-bit micro-controller with on-chip ADC and DAC. It has five keys and graphical 16x2 LCD for setting the simulation parameters including the heart rate, systolic pressure, diastolic pressure.*

Keywords: *Mechatronics System Design, Components Selection-Pressure Sensor, Solenoid Valve, μC, PCB Design.*

I. Introduction

1.1 Introduction

Using patient simulators in medical, nursing, and pharmacy education has increased. Simulators can be used as an effective teaching strategy to facilitate learning and improve knowledge, provide controlled and safe practice opportunities, and aid in the development of strong clinical skills. Patient simulators can range from using technology and volunteers portraying patients to high-fidelity full-body human patient simulators. Blood pressure simulator arm is among one simulator. Using the simulator arm is an acceptable method for teaching blood pressure measurement skills to students. The simulator arm allows a student to practice the same skills and techniques in measuring a blood pressure as executed on a human subject. Systolic and diastolic pressure, heart rate settings are adjusted using an external control panel allowing for variability, as seen in clinical practice. The simulator arm closely resembles a human subject's arm anatomically, therefore the proper application of the blood pressure cuff and stethoscope is necessary to measure successfully the blood pressure.

1.2 Need of Blood Pressure Measurement Simulator Arm

This blood pressure simulator helps resolve the uncertainties common in teaching students to take blood pressure. This simulator allows the presetting of values for both systolic and diastolic pressures, provides an excellent means to practice listening to and distinguishing blood pressure sounds prior to actual clinical experience. Many times when working with a live subject, pressures are difficult to auscultate , making accurate evaluation of student proficiency almost impossible, and undermining the student's self-confidence. With this realistic unit, the student can find the preset results and the instructor can unfailingly know if the student has performed the procedure accurately. Teacher can easily calibrate the unit for use with any sphygmomanometer. Advantages of Blood pressure simulator arm are as follows

1) Helps to resolve the uncertainties common in teaching students to take Blood Pressure.
2) Avoid the Fatigue coming on the patient due to frequently checking of Blood Pressure.
3) Avoids the bursting of Artery due to Excessive blood Pressure.

1.3 Blood pressure measurement Method selected for making simulator

The auscultator method (from the Latin word for "listening") uses a stethoscope and a sphygmomanometer. Fig.1.1 shows the auscultatory method of blood pressure measurement. This comprises an inflatable cuff placed around the upper arm at roughly the same vertical height as the heart, attached to a mercury or aneroid manometer. The mercury manometer, considered the gold standard, measures the height of a column of mercury, giving an absolute result without need for calibration and, consequently, not subject to the errors and drift of calibration which affect other methods. The use of mercury manometers is often required in clinical trials and for the clinical measurement of hypertension in high-risk patients, such as pregnant women. A cuff of appropriate size is fitted smoothly and snugly, and then inflated manually by repeatedly squeezing a rubber bulb until the artery is completely occluded. Listening with the stethoscope to the brachial artery at the elbow, the examiner slowly releases the pressure in the cuff. When blood just starts to flow in the artery, the turbulent flow creates a "whooshing" or pounding (first Korotkoff sound). The pressure at which this sound is first heard is the systolic blood pressure. The cuff pressure is further released until no sound can be heard (fifth Korotkoff sound), at the diastolic arterial pressure. The auscultatory method is the predominant method of clinical measurement.

Fig.1.1 Auscultatory method aneroid sphygmomanometer with stethoscope

1.4 Medical Terms used in blood pressure measurement

Blood pressure-Blood pressure is the amount of force (pressure) that blood exerts on the walls of the blood vessels as it passes through them.

1.4.1) Systolic pressure

Systolic blood pressure is a measure of blood pressure while the heart is beating. Systolic pressure is peak pressure in the arteries, which occurs near the end of the cardiac cycle when the ventricles are contracting.

1.4.2) Diastolic pressure

Diastolic pressure is a measure of blood pressure while the heart is relaxed. Diastolic pressure is the minimum pressure in the arteries, which occurs near the beginning of the cardiac cycle when the ventricles are filled with blood.

1.4.3) Pulse pressure

The up and down fluctuation of the arterial pressure results from the pulsatile nature of the cardiac output, i.e. the heartbeat. The pulse pressure is determined by the interaction of the stroke volume of the heart, compliance (ability to expand) of the aorta, and the resistance to flow in the arterial tree. By expanding under pressure, the aorta absorbs some of the force of the blood surge from the heart during a heartbeat. In this way, the pulse pressure is reduced from what it would be if the aorta wasn't compliant. The loss of arterial compliance that occurs with aging explains the elevated pulse pressures found in elderly patients. The pulse pressure can be simply calculated from the difference of the measured systolic and diastolic pressures. According to American Heart Association the pulse pressure is given by,

$$P_{pulse} = P_{sys} - P_{dias}.$$

1.5) Actual Procedure for Measuring Blood Pressure

Blood pressure is the amount of force (pressure) that blood exerts on the walls of the blood vessels as it passes through them. Two pressures are required to be measure for a blood pressure reading:

1.5.1) Systolic blood pressure is a measure of blood pressure while the heart is beating

1.5.2) Diastolic pressure is a measure of blood pressure while the heart is relaxed, between heartbeats.

Blood pressure (BP), sometimes referred to as arterial blood pressure, is the pressure exerted by circulating blood upon the walls of blood vessels. During each heartbeat, blood pressure varies between a maximum

(systolic) and a minimum (diastolic) pressure. The blood pressure in the circulation is principally due to the pumping action of the heart. Differences in mean blood pressure are responsible for blood flow from one location to another in the circulation. A person's blood pressure is usually expressed in terms of the systolic pressure over diastolic pressure and is measured in millimeter of mercury (mmHg).

Example - 120/80 mmHg

        Systolic pressure -120mmHg

        Diastolic Pressure-80mmHg
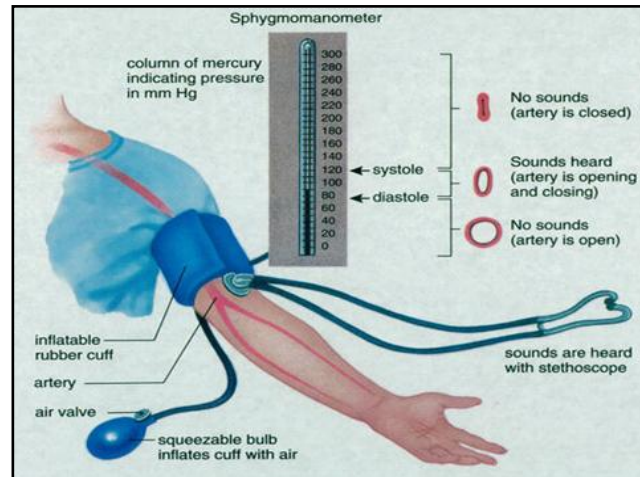
Fig. 1.3 Actual blood pressure measurement procedures

II. Design Procedure of Blood Pressure Simulator Arm

2.1) Block diagram of pulse generation and blood pressure measurement
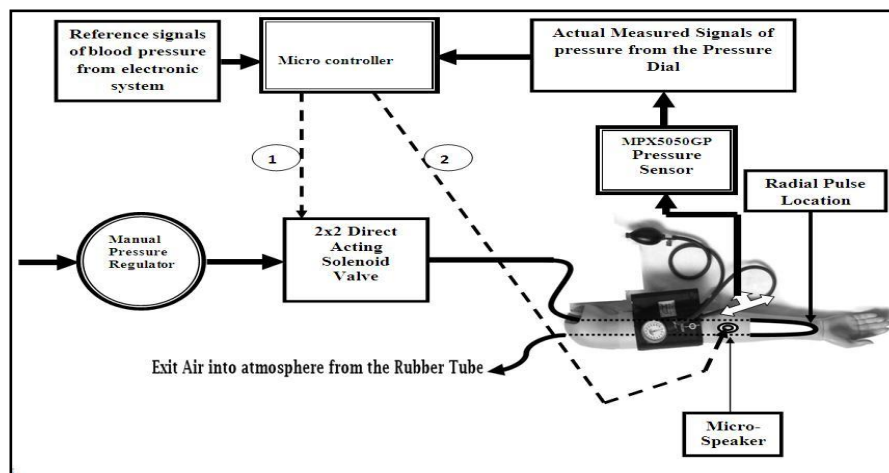
Fig. 1.4 Schematic of artificial blood pressure generation

2.2) Conditions for pressure readings and pulse rate in blood pressure simulators.

2.2.1) Systolic pressure range

In the actual blood pressure measurement the assumed minimum systolic pressure value is 50mmHg and maximum systolic pressure value is 300mmHg. So that, this requirements are considered in the blood pressure simulator arm.

2.2.2) Diastolic pressure range

In the actual blood pressure measurement the assumed minimum diastolic pressure value is 30mmHg and maximum diastolic pressure value is 250mmHg.

2.2.3) Maximum and minimum difference between the systolic and diastolic pressure

The minimum difference between two pressure is 20mmHg i.e.100/80 mmHg and the maximum difference between two pressure-50 i.e. 150/100mmHg

2.2.4) Pulse Rate
The minimum pulse rate value is 30 BPM (Beats per minute) and maximum pulse rate value is 150 beats per minute.

2.3) Connection between Pressure Sensor & Sphygmomanometer pressure line tube
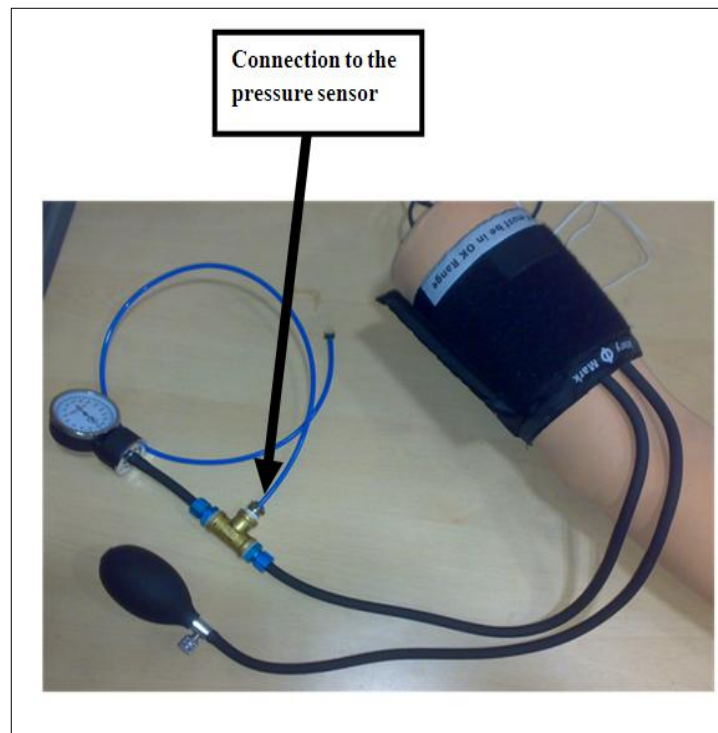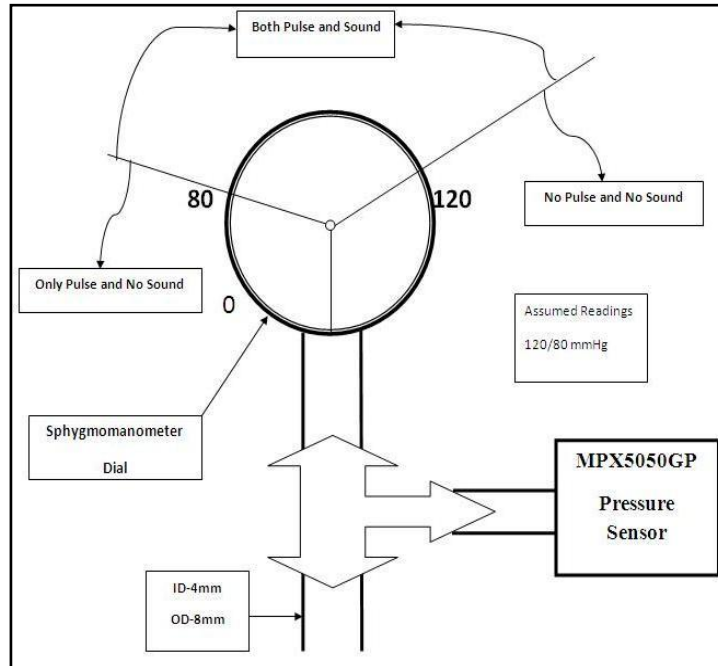
Fig.1.5 Block Diagram & picture of Connection between Pressure sensor & Sphygmomanometer tube

2.4) Reason for cutting of sphygmomanometer tube at some distance from pressure dial
2.4.1) Getting the pressure reading from the pressure dial of the sphygmomanometer is the major task.
2.4.2) For this purpose at some distance from the pressure dial the tube is cut and taken the T-fitting and insert it between the two ends of tubing that were previously cut.

2.4.3) Now the remaining open port of the T-fitting is connected to pressure sensor by using the connecting tube.

2.4.4) Now pressure sensor will show the similar pressure readings that the sphygmomanometer gauge will show. Fig.1.5 above shows the arrangement of pressure sensor and dial tube connection.

III. Working Procedure

3.1) Flow chart of working of blood pressure simulator system

3.2) Step by Step working of blood pressure simulator

[Assuming the set readings in the electronic display are 120/80 mmHg & Pulse rate-72BPM]

1. According to actual blood pressure measuring procedure the sphygmomanometer cuff is fitted on the upper side of the artificial arm where the brachial artery is present. This is shown in fig.1.3

2. Now inflate the cuff by the pressure valve provided with the cuff

3. Pressure in the cuff starts increasing and the pressure reading will appear on the gauge provided with sphygmomanometer

4. Actually we have cut the pressure line tube of sphygmomanometer at some distance from the pressure indicating gauge and that cut part of the tube is connected by the T-section and one end of the T-section will be open and to that end one pressure sensor is connected.

6. Now pressure sensor will show the similar pressure readings that of the sphygmomanometer gauge will show with the required calibration.

7. Now start the blood pressure measuring procedure by inflating the cuff

<div style="text-align:center">

Set readings on Electronic Display are   Systolic pressure -120mmHg

Diastolic Pressure - 80mmHg

Heart Rate   -72BPM

</div>

One micro-speaker is attached at the position where brachial artery is present and near the arm elbow where doctors used to check the pulses.

8. Inflate the cuff above 120mmHg so that when readings on the dial exceeds 120mmHg the pressure sensor will also sense same reading and sends signal to the electronic system when this actual reading is compared with reference reading, one electrical signal is generated to OFF the solenoid valve and micro-speaker

9. By using stethoscope no pulses will sense on the arm and no beating sound when reading is above 120mmHg

10. Deflate the cuff by releasing the air valve below 120mmHg so that when pressure sensor detect reading below 120mmHg i.e. 119mmHg it will send the same for comparison with reference reading and one signal is generated to ON the solenoid valve and micro-speaker. By using stethoscope beating sound will hear and pulses

sensation. Now the pressure reading at the time when first heart beating sound hears is called as systolic pressure.

12. Again deflate the cuff below 80mmHg i.e.79mmHg when sensor detect the same pressure reading and send it for comparison with reference reading and again system will generate one electrical signal to OFF the beating sound(micro-speaker) and remains ON the solenoid valve. By using the stethoscope no beating sound will detect and only pulse sensation takes place. Now the pressure reading at the time when last heat beating sound hears is called as diastolic pressure. Above procedure will repeat for different set of pressure readings. Assuming the set readings in the electronic display are 120/80 mmHg & Heart Rate-72BPM

3.3) Analogy of pulse and heart beating sound (Assuming the set readings in the electronic display are 120/80 mmHg & Pulse rate-72BPM)

Table 1.1 Analogy between pulse and heart beating

Pressure Readings	Actual Blood Pressure Measurement		Blood Pressure measurement using Simulator Arm	
	Pulses	Sound (Artery opening & closing)	Solenoid Valve	Micro-Speaker
Above 120mmHg	OFF	OFF	OFF	OFF
Between 120 & 80mmHg	ON	ON	ON	ON
Below 80mmHg	ON	OFF	ON	OFF

IV. Component's Selection

4.1) Selection of pressure sensor
4.1.1) Pressure sensor selection parameters
1) Range
The region between the limits within which an instrument is designed to operate for measuring, indicating or recording a physical quantity is called the range of the instrument. So that required lower range of the sensor is 0mmHg and upper range is 300mmHg.Which is shown in fig.1.6

Fig.1.6 sphygmomanometer Dial

2) Resolution
 The smallest amount of input signal change that the instrument can detect reliably. In the world of electronic equipment, the term "resolution" refers to the measurement of the finest detail that can be resolved by the sensors on a device. So that from the above picture of sphygmomanometer dial the sensor should be able to measure minimum 2mmHg pressure.

3) Accuracy
The accuracy is a measure of the degree of closeness of a measured or calculated value to its actual value. Accuracy required for the pressure sensor is ±1mmHg or less than ±0.33%FSS (full scale span) (Required full scalespanis300mmHg)

4) Precision
It prescribes the ability of the instrument to reproduce its readings over and over again for a constant input signal. For the pressure sensor it must be as high as possible.

5) Sensitivity

Sensitivity of an instrument or an instrumentation system is the ratio of the magnitude of the response (output signal) to the magnitude of the quantity being measured (input signal) i.e.

Change of output signal

Sensitivity= ----------------------------

Change of input signal

The sensitivity for the sensor should be linear or almost constant over wide range of readings.

6) Mounting type

The sensor should be panel mountable or preferably on the printed circuit boards (PCB) mountable.

7) Electrical Specifications

7.1) Supply Voltage

As circuit design for blood pressure simulator arm is operating at 5Vdc .So that supply voltage required for the sensor preferably 5Vdc supply.

7.2) Output Voltage

The micro-controller (µC) used in the circuit design is operating in the voltage range of 0 to 5Vdc so that the output of the sensor required for our application preferably in the volts (Vdc) instead of mill volts (mVdc).

4.1.2) Selected Pressure Sensor

The freescale semiconductors, Inc provides the MPX2050GP series device and it is a silicon piezoresistive pressure sensor providing a highly accurate and linear voltage output directly proportional to the applied pressure. The sensor is a single, monolithic silicon diaphragm with the strain gauge and a thin–film resistor network integrated on–chip. The chip is laser trimmed for precise span and offset calibration and temperature compensation.

Table 1.2. Operating Characteristic of pressure sensor [Model no.MPX2050GP]

Characteristics	Minimum	Typical	Maximum	Unit
Range	0	-	375	mmHg
Supply Voltage	4.75	5.0	5.25	Vdc
Supply Current	-	7.0	10	mAdc
Output Voltage	0.2	-	4.7	Vdc
Full Scale Span@ Vs=5.0Volts	-	4.5	-	Vdc
Accuracy	-2.5	-	+2.5	%V$_{FSS}$
Sensitivity	-	90	-	mV/kPa
Proof Pressure	-	-	200	kPa
Operating Temperature	-40		125	°C
Response Time	-	1.0	-	ms
Mounting of the sensor- PC Board Mountable				

.1.3) Works out calculations while selecting the pressure sensor are as follows

Minimum pressure measurement by the sensor should be 2mmHg. Let us calculate the resolution or the least count as follows.

MPX5050GP pressure sensor is connected to port, which is an input to the on-chip 10-bit analog-to-digital (A/D) converter. The pressure sensor provides a signal output to the microcontroller of approximately 0.2 Vdc at 0 mm Hg to 4.7 Vdc at 375 mm Hg of applied pressure. In this example, the input range of the A/D converter is set at approximately 0 Vdc to 5Vdc. This compresses the range of the A/D converter around 0 mm Hg to 300 mm Hg to maximize the resolution; 0 to 1023 counts is the range of the A/D converter. VRH and

VRL are the reference voltage inputs to the A/D converter. V_{ensor} is output of the sensor. The resolution is defined by the following:

$$\text{Count} = [(V_{sensor} - VRL) / (VRH - VRL)] \times 1023$$
$$\text{The count at 0 mmHg} = [(0.2 - 0)/ (5.0 - 0)] \times 1023 = 40.92 \approx 41$$
$$\text{The count at 300 mmHg} = [(5.0 - 0)/ (5.0 - 0)] \times 1023 \approx 1023$$
$$\text{Therefore the resolution} = 1023 - 41 = 982 \text{ counts}.$$

This translates to a system that will resolve to [300/982] 0.3054 mmHg. That is the sensor is used to measure 0.3054 mmHg minimum pressure so this MPX5050GP sensor is selected. The output of the pressure sensor is ratio metric to the voltage applied to it. Resolution= 0.3054 mmHg So that, the resolution of the selected sensor is 0.3054 mmHg which will be rounded to 1mmHg in the electronic system

5.3) Selection of other pneumatic Accessories
5.3.1) Requirement of the solenoid valve in the blood pressure simulator arm
      Reason for the use of the solenoid valve in the blood pressure simulator arm is to generate the artificial pulse with the use of electronic delay signals & which will be felt at the wrist location of the hand. Assuming the maximum and minimum heart beats of the human in the range of 40 to 140 beats per minute (BPM) so that accordingly solenoid valve is selected and having response time in the range of 0.42(for 140 beats) to 1.5(for 40 beats) second. After studying the specifications of different types of solenoid valves, the patcon pneumatics solenoid valve model number is PC22CD selected.

5.3.2) Details of the solenoid valve model PC22CD
      Patcon Pneumatics offers Direct Acting 2/2 Way NC Solenoid Valve. Patcon Pneumatics supplies pneumatic systems and equipments in wide ranges. Direct Acting 2/2 Way NC Solenoid Valve is applied in various sectors like- water treatment plants, nuclear power plants, domestic water purifiers, thermal power plants, welding industry and packaging industry etc. Direct Acting 2/2 Way NC Solenoid Valve is suited with 0-40 Bar pressure. Direct Acting 2/2 Way NC Solenoid Valve requires 1/8 inch to 1/2 inch BSP/NPT connections.

5.3.2a) Specifications of the solenoid valve
1) Operating pressure range- 0 to 10Bar
2) Coil Voltage- 24Vdc
3) Coil rating- Continuous duty rated
4) Fluids- Air, Inert gas.

5.3.2b) Technical Specifications of Direct Acting 2/2 Way NC Solenoid Valve

Table No. 1.3 Technical Specification of solenoid valve

Model Number	PC22CD	
Supply Voltage	24Vdc	
Coil Type	SI	
Port Size	1/8 inch to ½ inch BSP/NPT [G1/4X8 mm]	
Response Time (millisecond)	AC	15 ms
	DC	20 ms
Orifice (NW)	3.0 mm	
Maximum working pressure (Bar)	10 Bar	
Watts	AC	6 W
	DC	8 W

5.4) Selection of the connectors and Tubes

In order to connect the pneumatic nylon tubes with pressure regulator, solenoid valve and finally to the rubber tube which is artificial artery we require some pneumatic connectors and which are listed below. For our application we have selected and used nylon tubes having sizes are 8x6 mm and 4x2 mm.

Table No.1.4 Selected connectors and tubes

Connectors	Size	Quantity
Male Connector	G1/4 x 4mm	2
Male Connector	G1/4 x 8mm	3
Straight Union	Dia.4mm	1
Straight Union	Dia.8mm	1
T-Connector	G1/4 x 8mm	1
Socket	G1/4 x 8mm	1
Blue Nylon Tube	OD-8mm & ID-6mm	5 Meter
Blue Nylon Tube	OD-4mm & ID-2.5mm	5 Meter

5.5) Electronic components selection
5.5.1) Transformer
The Transformer used here is a 18-0-18 centre tap transformer which gives a final output of 36 V AC output. As we know that

$$VRMS = V_{Peak} /\sqrt{2}$$

The value here comes here to be 25.455 V sufficient inputs for a 24 V output of LM317.

5.5.2) Rectifier circuit
The rectifier circuit used here is commonly used when its output is to be fed to a linear regulator. The circuit here uses a centre tap transformer with two diodes to give a pulsating DC signal. This then is fed into a series of caps into a linear regulator. This technique is very simple and easy to build.

Fig.1.7 Rectifier circuit

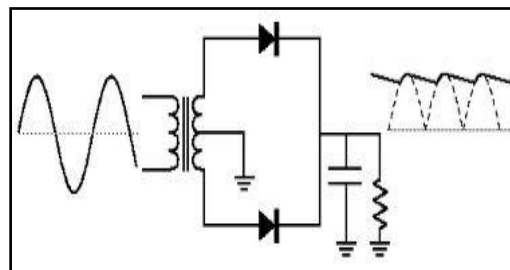**5.5.3) linear regulators**
 Linear regulator ICs are used primarily for regulating DC voltages. These are primarily used for getting a fixed/variable voltage when power losses are not much of a concern. Various power regulator ICs are available depending on power losses and voltage levels. The generic diagram of a power regulator is as below:
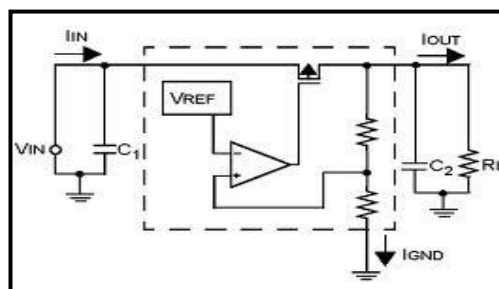

Fig.1.8 Basic operation of linear power regulator

As you can see, Vin is the input voltage and V_{out} or voltage across RL is the output voltage. The op-amp sees to it that voltage on both its inputs remains the same. This causes output to be equal to VREF. In fixed voltage regulators like the 78xx series, the reference voltage is fixed whereas in ICs like LM317 and so on, reference voltage is also variable and is set using a pair of resistances.
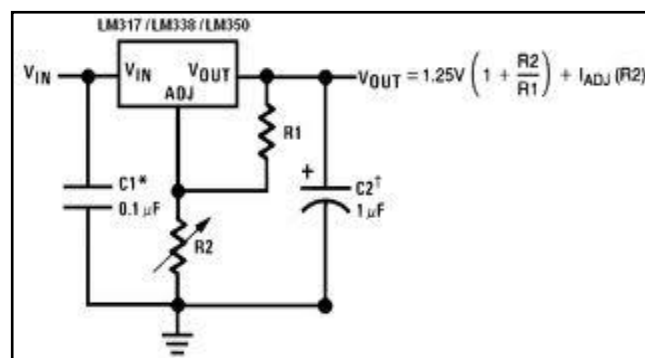

Fig.1.9 LM317 IC

Varying values of R2 gives different values at output. Changing the output value only means changing 1 (at most 2) resistances.

5.3.4) Micro-controller
The micro-controller is the heart of the circuit. It is technically a mini-computer which can be programmed and used in such smaller circuits. It has an internal RAM, ROM, ALU and peripherals that are used in getting the work done. There are many different companies manufacturing different types of micros. Popular amongst them are Microchip, Atmel, Parallax, Motorola etc. The micro-controller that we are using here is Atmega 16.
It's specifications are:
1. 8 bit CPU. This also means 8 bit ALU
2. 16 KB Internal Flash
3. 512 Bytes EEPROM
4. 1KB Internal SRAM
5. In System Programming Feature
6. Two 8 bit Timer/Counter and 1 16 Bit Timer/Counter with PWM
7. 8 channel 10 bit ADC
8. External and Internal Interrupt sources
9. 9. 32 programmable I/O lines
10. Support for USART and slave/master SPI

5.3.5) L293D IC
It is the most commonly used motor control driver IC. It is very highly used for controlling 2 DC motors or a single stepper motor. It is a very versatile tool and can be used wherever current limit is about 1.2 A. The main reason why such motor drivers are needed is because motors need a lot of current. The average current consumption of a micro is less than 100mA. That's not enough for a motor to rotate. Motor driver ICs have 2 sets of input voltages, supply voltage and logic supply voltage.
For L293D it is as below:
Max Supply Voltage: 36V
Max Logic Supply Voltage: anything from about 1.5V to supply voltage
Max Enable Voltage: 7V
Based on the logic voltage input and enable pin, supply voltage is given to the motors. Logic voltage can be taken from the micro-controller. In this way, motors can be controlled by a micro. It is this feature that makes these devices useful.

5.3.6) 16x2 LCD display
This display is used here to set the input and output and also as a tool for debugging in case some things go wrong. It has 2 lines of display, 16 characters per line. Hence, the name is 16x2. There are a lot of varieties of this display available. All of them use the IC HD44780 from Hitachi.

Fig 2.0 16X2 LCD Display

This display has:
1. 8 bit data bus. It can be used in 8 bit or 4 bit mode.
2. 3 control pins
    1. Enable pin to enable/disable the display
    2. R/S pin to set whether command or data
    3. RW pin to set whether to read or write to the LCD
3. 2 back light pins
4. 1 contrast pin to set contrast of output displayed
5. VCC and GND power inputs

5.4) Micro-controller ADC considerations and Works out calculations

There is one component of any system that is very important and must be studied in detail when using any such sensor that outputs analog data, ADC. Every processor or computer based circuit needs to have an ADC because computers/micros work in the digital world whereas sensors still work in the analog world. Atmega 16 has a 10 bit ADC. This basically means that the whole range is divided into 0 to $2^{10}-1$ (i.e.) 1023 levels. In the case of this project, overall voltage level is 0-5V.

Thus, 1 level= 5V/1023 = 4.88 mV .Thus, the least count of ADC should be more than 4.88 mV otherwise the ADC cannot show correct readings. Our least count of pressure is 2mm Hg as the dial cannot show 1 mm Hg.

Hence, least count of the sensor must be 4.88mV/2mmHg (i.e.) 2.44mV/mm Hg or less.

Also, care should be taken that multiple values don't round up to the same actual value. This care is taken here in the code.

5.5) Code for micro-controller

Code is compiled using avr-gcc and burnt using avrdude.

V. PCB Design And Complete Circuit Board

The diagram and the schematic have been made using eagle software. The board uses Eagle's maximum size of 10 cm by 8 cm. This is a single layer board full of through hole components.
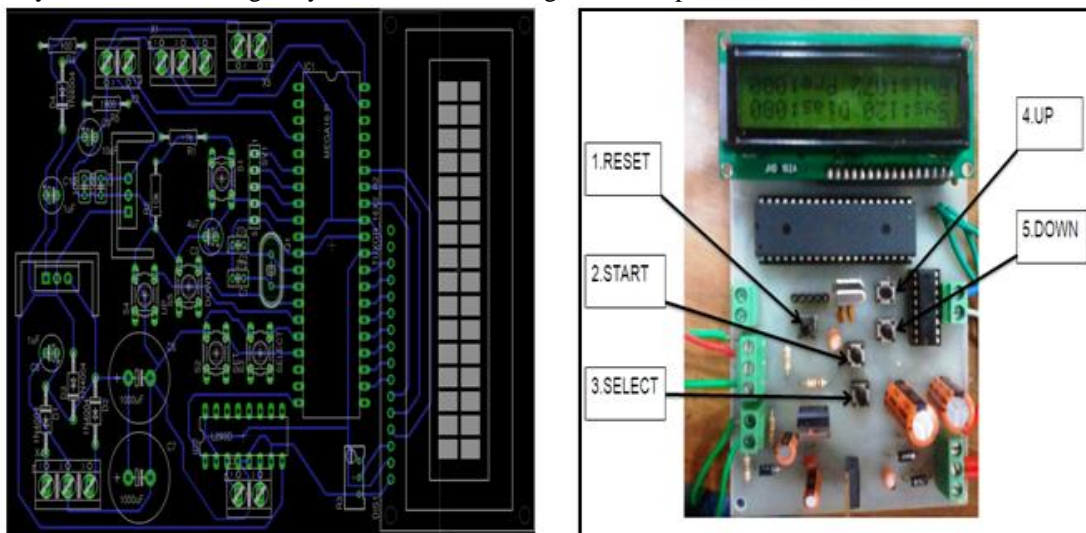
Fig2.1 PCB Design and Complete circuit
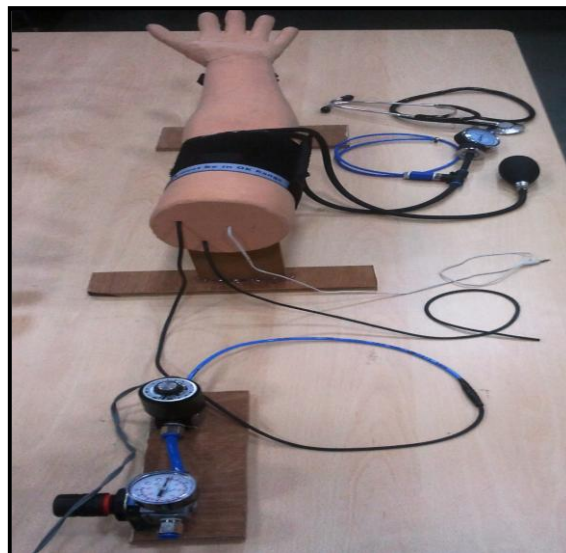
Fig.2.2 Complete arm manikin setup

VI.   Sensor Testing and Results

Calculations and graph plotting of sensor output voltage Vs Input pressure applied- Checking of the sensor output voltage with input pressure applied is very necessary. Transfer function for the output voltage provided by the freescale semiconductor Inc; is given by,

$$Vout = Vs (P \times 0.018 + 0.04)$$

Whereas, Vout- Output voltage of the sensor in Volts

Vs- Supply voltage to the sensor in Volts

P- Input pressure to the sensor in kPa

From the transfer function, Values of the actual output voltage of the sensor and measured output voltage of the sensor with input pressure are calculated as below.

Table1.4 Reading and Graph of Sensor output voltage (V) Vs Input pressure (kPa)

Input Pressure		True output voltage (Volts) (Vt)	Measured output voltage (Volts) (Vm)	Error E=Vm-Vt
mmHg	kPa			
0	0	0.2	0.19	-0.01
37.5	5	0.65	0.70	0.05
75	10	1.1	1.17	0.07
112.5	15	1.55	1.58	0.03
150	20	2.0	2.02	0.02
187.5	25	2.45	2.48	0.03
225	30	2.9	2.94	0.04
262.5	35	3.35	3.4	0.05
300	40	3.8	3.85	0.05
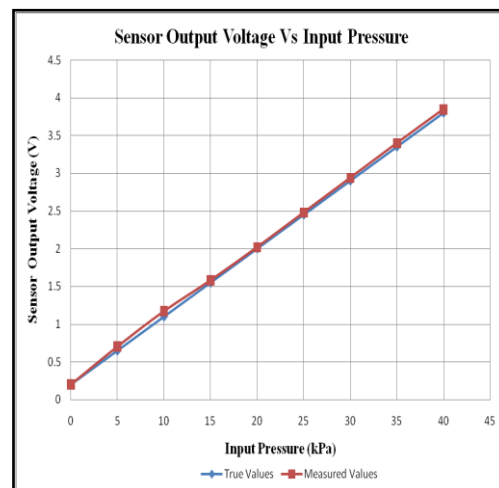
Repeatability of the blood pressure readings are explained below-

Above graph clearly shows that the true values and measured values of sensor output voltage coincides except some deviation. Above graph is plotted for 0 to 300mmHg pressure range   (i.e.0 to 40kPa) on X-axis and Sensor output voltage range 0.2 to 3.8V on Y-axis. The deviation in the output voltage occurs or rather graph is non-linear at the pressure points 5kPa (37.5mmHg), 10kPa (75mmHg), 35kPa (262.5mmHg).As this is the direct output measured from the pressure sensor with digital-multimeter (DMM). When pressure sensor output signal is interfaced with the micro-controller (µc) with proper analog to digital conversion (ADC) the results obtained

are much better that means whatever the readings on the pressure dial that same are shown by the pressure sensor with ±1mmHg accuracy.

Major functions offered by the new developed blood pressure simulator are as follows

1) Pulse rate generation using the pneumatic system

The pulse generation is achieved in this simulator by using rubber tube as a artificial artery and solenoid valve with compressed air. So that the main thing is to feel the pulse checking as natural as in the human pulse checking. Due to rubber tube inserted inside the arm manikin it feels like a natural artery and due to compressed air palpation is easily detected. While in the available simulators it is achieved by using programmable palpable radial pulse, so the feel of pulse is not similar to the developed blood pressure simulator.

2) Higher accuracy compared to available blood pressure simulators

Accuracy of the new developed simulator is ±2 mmHg so that it can measure any blood pressure readings from range 0 to 300mmHg. While the accuracy offered by the available simulator is ±3mmHg, So that this will not be able to measure all blood pressure readings ranging from 0 to 300mmHg.

VII. Conclusion and Future Work Of Project

7.1) Effective use of electronic and mechanical system to build a whole mechatronics system.

7.2) Made a manikin of arm with the help of KIMS, Karad which aesthetically looks better.

7.3) developed an electronics system that could change all three values (Systolic pressure, Diastolic pressure and Pulse rate) on runtime. Limitation of this blood pressure simulator arm is that, while using it as a trainer for medical students they are forced to use the sphygmomanometer cuff provided with the whole setup. This means that students cannot use different type of sphygmomanometer cuff.

7.4) Future work on blood pressure simulator arm manikin

At present, getting dial pressure is achieved by using MPX5050GP pressure sensor attached at certain position from the dial. Thus no other cuff can be used. To overcome this limitation, a force sensor which is capable of measuring pressure range from 0 to 300mmHg is needed.

The problem with the above arrangement is that the output will vary based on how tightly the cuff is placed over the force sensor. Thus each new cuff has to be calibrated.

REFERENCES

[1] Caro, Colin G. (1978). The Mechanics of the Circulation. Oxford [Oxford shire]: Oxford University Press. ISBN 0-19-263323-6.

[2] Kaunda, Richard (2005). Cardiovascular Physiology Concepts. Lippincott Williams & Wilkins. pp. 93–4. ISBN 978-0-7817-5030-1.

[3] "Understanding blood pressure readings" American Heart Association. 11 January 2011. Retrieved 30 March 2011.

[4] Dug dale, David. "Blood Pressure" Retrieved 1 April 2011.

[5] Kaunda, Richard. "Arterial Blood Pressure" Retrieved 31 March 2011. Available from: http://www.nhs.uk/chq/pages/what-is-blood pressure.aspx?categoryid=201&subcategoryid=201

[6] National Center for Health Statistics. Health, United States, 2009: With special feature on medical technology. Hyattsville, MD. 2010. Available from: http://www.cdc.gov/ nchs/hus.html and http://homepage.smc.edu/wissmann_paul/anatomy1/1bloodpressure.html

[7] Life/form® Blood Pressure Simulator (Item: W44085 [1005621]) and Blood Pressure Simulator Arm with PDA (Item: W44675 [1005775]). Available from: www.3bscientific.com

[8] Simulaids Blood pressure simulator with PDA Technology. Available from: www.simulaids.com

[9] S311.414 Blood Pressure Arm and S222.414 Blood Pressure Arm. Available from: www.gaumard.com

[10] BC Biomedical Group International, Inc. USA & Laerdal Medical India Pvt. Ltd

[11] NASCO Life/form® Blood Pressure Simulator. Available from: www.eNasco.com

[12] Unisense Technology co., Ltd. 9F NO.1, Jinshan7thst.Hsinchu 50080, Taiwan

[13] Bradley P. The history of simulation in medical education and possible future directions. Med Educ. 2006; 40(3):254–262. [PubMed]

[14] http://www.nlm.nih.gov/medlineplus/ency/article/002345.htm/Dacron graft

[15] www.festo.com and www.janatics.com

[16] Motorola Semiconductors (Freescale Semiconductor, Inc) H.K. Ltd Available from: www.freescale.com

[17] http://www.patconpneumatics.com/Standard%20Range%20of%20Solenoid%20Valves.htm Available from www.patconpneumatics.com

Exact Solutions of Convection Diffusion Equation by Modified F-Expansion Method

Priyanka M. Patel[1], Vikas H. Pradhan[2]

[1, 2] *(S.V. National Institute of Technology, Surat-395007, India)*

Abstract: *In this paper, the modified F-expansion method is proposed for constructing more than one exact solutions of nonlinear convection diffusion equation with the aid of symbolic computation Mathematica. By using this method, some new exact travelling wave solutions of the convection diffusion equation are successfully obtained. These exact solutions include the soliton-like solutions, trigonometric function solutions and rational solutions. Also, it is shown that the proposed method is efficient for solving nonlinear partial differential equations arising in mathematical physics.*

Keywords: *convection diffusion equation, modified F-expansion method, travelling wave solutions*

I. Introduction

It is well known that nonlinear partial differential equations (NLPDEs) play a major role in describing many phenomena arising in many fields of sciences and engineering. The investigation of exact solutions of NLPDEs plays an important role in the study of nonlinear physical phenomena. In recent years, direct search for exact solutions to NLPDE has become more and more attractive partly due to availability of computer symbolic system like Mathematica or Maple which allows us to perform some complicated and tedious algebraic calculation on computer. Different methods have been invented to obtain exact solutions of NLPDEs, such as homotopy perturbation method [3], homotopy analysis method [9,14], variational iteration method [11], tanh method [17] and so on. In the recent past F- expansion method [19,21] was proposed to construct exact solutions of NLPDEs. This method was later further extended in different manners, like the generalized F-expansion method [20], modified F-expansion method [6,7,8], improve F-expansion method [18], etc. in this study, the modified F-expansion method is used.

The objective of this paper is to apply modified F-expansion method to construct the exact travelling wave solutions of the following nonlinear convection-diffusion equation [10,12,15] for two cases.

$$u_t = \left(u^m\right)_{xx} + \left(u^n\right)_x \qquad (1)$$

This equation arises in many physical phenomena for different values of m and n. For example, $(m,n) = (1,2)$ eq.(1) converted into classic Burgers' equation [1,13,14,16] which has many application in gas dynamics, traffic flow, shock wave phenomena etc. Eq.(1) also arises in theory of infiltration of water under gravity through a homogeneous and isotropic porous medium for $n \geq m > 1$ [4]. In the case of $(m,n) = (4,3)$, eq.(1) models the flow of a thin viscous sheet on an inclined bed [5]. Act as a foam drainage equation for $(m,n) = (3/2,2)$ [8].

II. Outline Of The Modified F-Expansion Method

In this section, the description of the method is given.
Consider a given nonlinear partial differential equation with independent variables x, t and dependent variable u,

$$P\left(u, u_t, u_{xx}, u_{xt}, u_{tt}, \ldots.\right) = 0 \qquad (2)$$

Generally speaking, the left-hand side of eq.(2) is a polynomial in u and its various partial derivatives. The main points of the modified F-expansion method for solving eq.(2) are as follows:
[1]. Seek travelling wave solutions to eq.(2) by taking

$$u(x,t) = u(\xi) \text{ where } \xi = h(x + v t) \qquad (3)$$

where $h \neq 0$ and v are constants to be determined, inserting eq.(3) into eq.(2) yields an ordinary differential equation (ODE) for $u(\xi)$

$$P\left(u, u^{'}, u^{''}, \ldots\right) = 0 \tag{4}$$

where prime denotes the derivative with respect to ξ.

[2]. Suppose that $u(\xi)$ can be expressed as

$$u(\xi) = \sum_{i=-N}^{N} a_i F^i(\xi) \text{ where } a_N \neq 0 \tag{5}$$

where $a_i \left(i = -N, \ldots, -1, 0, 1, \ldots, N\right)$ are all constants to be determined and $F(\xi)$ satisfies following Riccati equation

$$F^{'}(\xi) = A + BF(\xi) + CF^2(\xi) \tag{6}$$

where A, B, C are constants and N is a integer which can be determined by considering the homogeneous balance between the governing nonlinear term(s) and highest order derivative of $u(\xi)$ in eq.(4) and

(i) when $N = \left(\dfrac{p}{q}\right)$ is fraction, let $u(\xi) = w^{p/q}(\xi)$

(ii) when N is negative integer, let $u(\xi) = w^N(\xi)$

By using (i) and (ii), we change eq.(4) into another ODE for $w(\xi)$ whose balancing number will be a positive integer.

[3]. Substitute eq.(5) into eq.(4) and using eq.(6) then left-hand side of eq.(4) can be converted into a finite series in $F^p(\xi)$, $\left(p = -N, \ldots, -1, 0, 1, \ldots, N\right)$. Equating each coefficient of $F^p(\xi)$ to zero yields a system of algebraic equations.

[4]. Solve the system of algebraic equations probably with the aid of Mathematica, a_i, h, v can be expressed by A, B, C. Substituting these results into eq.(5), we can obtain the general form of travelling wave solutions to eq.(4).

[5]. From the general form of travelling wave solutions listed in appendix, we can give a series of soliton-like solutions, trigonometric function solutions and rational solutions of eq.(2).

III. Implementation Of The Method

To solve eq.(1), following two cases are considered:

Case [I]: $n = m > 1$

Case [III]: $n = 2m - 1, \ m > 1$

Case [I]: $n = m > 1$

Considering $n = m$ in eq.(1), we get

$$u_t = \left(u^m\right)_{xx} + \left(u^m\right)_x \tag{7}$$

Let us start our analysis by using the transformation,

$$u(x, t) = u(\xi) \text{ where } \xi = h(x + vt) \tag{8}$$

where $h \neq 0$ and v are constants to be determined later. Substituting eq.(8) into eq.(7), we get ODE

$$hvu^{'} - h^2 m(m-1)u^{m-2}\left(u^{'}\right)^2 - h^2 m u^{m-1} u^{''} - hm u^{m-1} u^{'} = 0 \tag{9}$$

where prime denotes differentiation with respect to ξ. Balancing the orders of $u^{'}$ and $u^{m-1}u^{''}$ in eq.(9), we have $N = -\dfrac{1}{m-1}$. Now, we use $u(\xi) = w^{-1/m-1}(\xi)$ in eq.(9), we get ODE in the following form,

$$vww' + \frac{m(2m-1)}{m-1}hw^{-1}(w')^2 - mhw'' - mw' = 0 \tag{10}$$

Balancing the orders of ww' and w'' in eq.(10), we get $N=1$. So we can write solution of eq.(7) in the form,

$$u(x,t) = w^{-1/m-1}(\xi) \text{ where } w(\xi) = a_0 + a_{-1}F^{-1}(\xi) + a_1F(\xi) \tag{11}$$

Substituting eq.(11) into eq.(10) and using eq.(6), the left-hand side of eq.(10) can be converted into a finite series in $F^p(\xi)$, $(p = -4, -3, -2, -1, 0, 1, 2, 3, 4)$. Equating each coefficient of $F^p(\xi)$ to zero, we obtained the following set of algebraic equations with the aid of Mathematica:

$$F^{-4}(\xi): -2A^2hma_{-1}^2 - \frac{A^2hma_{-1}^2}{m-1} + \frac{2A^2hm^2a_{-1}^2}{m-1} - Aa_{-1}^3v = 0$$

$$F^{-3}(\xi): -2A^2hma_0a_{-1} + Ama_{-1}^2 - 3ABhma_{-1}^2 - \frac{2ABhma_{-1}^2}{m-1} + \frac{4ABhm^2a_{-1}^2}{m-1}$$
$$- 2Aa_0a_{-1}^2v - Ba_{-1}^3v = 0$$

$$F^{-2}(\xi): Ama_0a_{-1} - 3ABhma_0a_{-1} + Bma_{-1}^2 - B^2hma_{-1}^2 - 2AChma_{-1}^2 - \frac{B^2hma_{-1}^2}{m-1}$$
$$- \frac{2AChma_{-1}^2}{m-1} + \frac{2B^2hm^2a_{-1}^2}{m-1} + \frac{4AChm^2a_{-1}^2}{m-1} - 2A^2hma_{-1}a_1 + \frac{2A^2hma_{-1}a_1}{m-1}$$
$$- \frac{4A^2hm^2a_{-1}a_1}{m-1} - Aa_0^2a_{-1}v - 2Ba_0a_{-1}^2v - Ca_{-1}^3v - Aa_{-1}^2a_1v = 0$$

$$F^{-1}(\xi): Bma_0a_{-1} - B^2hma_0a_{-1} - 2AChma_0a_{-1} + Cma_{-1}^2 - BChma_{-1}^2 - \frac{2BChma_{-1}^2}{m-1}$$
$$+ \frac{4BChm^2a_{-1}^2}{m-1} - 4ABhma_{-1}a_1 + \frac{4ABhma_{-1}a_1}{m-1} - \frac{8ABhm^2a_{-1}a_1}{m-1} - Ba_0^2a_{-1}v$$
$$- 2Ca_0a_{-1}^2v - Ba_{-1}^2a_1v = 0$$

$$F^0(\xi): Cma_0a_{-1} - BChma_0a_{-1} - \frac{C^2hma_{-1}^2}{m-1} + \frac{2C^2hm^2a_{-1}^2}{m-1} - Am\ a_0a_1 - ABhma_0a_1$$
$$- 2B^2hma_{-1}a_1 - 4AChma_{-1}a_1 + \frac{2B^2hma_{-1}a_1}{m-1} + \frac{4AChma_{-1}a_1}{m-1} - \frac{4B^2hm^2a_{-1}a_1}{m-1}$$
$$- \frac{8AChm^2a_{-1}a_1}{m-1} - \frac{A^2hma_1^2}{m-1} + \frac{2A^2hm^2a_1^2}{m-1} - Ca_0^2a_{-1}v + Aa_0^2a_1v - Ca_{-1}^2a_1v$$
$$+ Aa_{-1}a_1^2v = 0$$

$$F^1(\xi): -Bma_0a_1 - B^2hma_0a_1 - 2AChma_0a_1 - 4BChma_{-1}a_1 + \frac{4BChma_{-1}a_1}{m-1}$$
$$- \frac{8BChm^2a_{-1}a_1}{m-1} - Ama_1^2 - ABhma_1^2 - \frac{2ABhma_1^2}{m-1} + \frac{4ABhm^2a_1^2}{m-1} + Ba_0^2a_1v$$
$$+ 2Aa_0a_1^2v + Ba_{-1}a_1^2v = 0$$

$$F^2(\xi): -Cma_0a_1 - 3BChma_0a_1 - 2C^2hma_{-1}a_1 + \frac{2C^2hma_{-1}a_1}{m-1} - \frac{4C^2hm^2a_{-1}a_1}{m-1}$$
$$- Bma_1^2 - B^2hma_1^2 - 2AChma_1^2 - \frac{B^2hma_1^2}{m-1} - \frac{2AChma_1^2}{m-1} + \frac{2B^2hm^2a_1^2}{m-1}$$
$$+ \frac{4AChm^2a_1^2}{m-1} + Ca_0^2a_1v + 2Ba_0a_1^2v + Ca_{-1}a_1^2v + Aa_1^3v = 0$$

$$F^3(\xi): -2C^2hma_0a_1 - Cma_1^2 - 3BChma_1^2 - \frac{2BChma_1^2}{m-1} + \frac{4BChm^2a_1^2}{m-1}$$
$$+ 2Ca_0a_1^2v + Ba_1^3v = 0$$

$$F^4(\xi): -2C^2hma_1^2 - \frac{C^2hma_1^2}{m-1} + \frac{2C^2hm^2a_1^2}{m-1} + Ca_1^3v = 0$$

(12)

Solving the above algebraic equations by Mathematica, we considered different cases as follows:
Case 1: $A = 0$, we have

$$a_0 = 0, a_{-1} = 0, a_1 = a_1, v = -\frac{Chm}{a_1(m-1)} \tag{13}$$

Case 2: $B = 0$, we have

$$a_0 = a_0, a_{-1} = 0, a_1 = a_1, v = \frac{2Chma_0 + ma_1}{2a_0 a_1} \tag{14}$$

Using cases 1,2 and appendix, we obtained the following exact generalized solutions of eq.(7)
<u>Soliton-like solutions:</u>
(1) $A = 0, B = 1, C = -1$

Assuming, $h = \frac{m-1}{m}$ in eq.(13), we get

$$a_0 = 0, a_{-1} = 0, a_1 = a_1, v = \frac{1}{a_1} \tag{15}$$

From appendix and eq.(15), we have

$$u_1(x,t) = \left\{ a_1 \left(\frac{1}{2} + \frac{1}{2} \tanh \left[\frac{m-1}{2m} \left(x + \frac{1}{a_1} t \right) \right] \right) \right\}^{-1/m-1} \tag{16}$$

(2) $A = 0, B = -1, C = 1$

Assuming, $h = -\frac{m-1}{m}$ in eq.(13), we get

$$a_0 = 0, a_{-1} = 0, a_1 = a_1, v = \frac{1}{a_1} \tag{17}$$

From appendix and eq.(17), we have

$$u_2(x,t) = \left\{ a_1 \left(\frac{1}{2} + \frac{1}{2} \coth \left[\frac{m-1}{2m} \left(x + \frac{1}{a_1} t \right) \right] \right) \right\}^{-1/m-1} \tag{18}$$

The solution given by eq.(18) and that obtained in [2], shows good agreement.
(3) $A = 1, B = 0, C = -1$

Assuming, $a_0 = a_1$ and $h = \frac{m-1}{2m}$ in eq.(14), we get

$$a_0 = a_1, a_{-1} = 0, a_1 = a_1, v = \frac{1}{2a_1} \tag{19}$$

From appendix and eq.(19), we have

$$u_3(x,t) = \left\{ a_1 + a_1 \tanh \left[\frac{m-1}{2m} \left(x + \frac{1}{2a_1} t \right) \right] \right\}^{-1/m-1} \tag{20}$$

Again assuming $a_0 = -a_1$ and $h = -\frac{m-1}{2m}$ in eq.(14), we get

$$a_0 = -a_1, a_{-1} = 0, a_1 = a_1, v = -\frac{1}{2a_1} \tag{21}$$

From appendix and eq.(21), we have

$$u_4(x,t) = \left\{ -a_1 - a_1 \coth \left[\frac{m-1}{2m} \left(x - \frac{1}{2a_1} t \right) \right] \right\}^{-1/m-1} \tag{22}$$

(4) $A = \frac{1}{2}, B = 0, C = -\frac{1}{2}$

Assuming, $a_0 = a_1$ and $h = \frac{m-1}{m}$ in eq.(14), we get

$$a_0 = a_1, a_{-1} = 0, a_1 = a_1, v = \frac{1}{2a_1} \tag{23}$$

From appendix and eq.(23), we have

$$u_5(x,t) = \left\{ a_1 + a_1 \left(\coth\left[\frac{m-1}{m}\left(x + \frac{1}{2a_1}t \right) \right] \pm \csc h\left[\frac{m-1}{m}\left(x + \frac{1}{2a_1}t \right) \right] \right) \right\}^{-\frac{1}{m-1}} \tag{24}$$

$$u_6(x,t) = \left\{ a_1 + a_1 \left(\tanh\left[\frac{m-1}{m}\left(x + \frac{1}{2a_1}t \right) \right] \pm i\sec h\left[\frac{m-1}{m}\left(x + \frac{1}{2a_1}t \right) \right] \right) \right\}^{-\frac{1}{m-1}} \tag{25}$$

Trigonometric function solutions:

(5) $A = \frac{1}{2}, B = 0, C = \frac{1}{2}$

Assuming, $a_0 = -ia_1$ and $h = \frac{m-1}{im}$ in eq.(14), we get

$$a_0 = -ia_1, a_{-1} = 0, a_1 = a_1, v = \frac{i}{2a_1} \tag{26}$$

From appendix and eq.(26), we have

$$u_7(x,t) = \left\{ -ia_1 + a_1 \left(\sec\left[\frac{m-1}{im}\left(x + \frac{i}{2a_1}t \right) \right] + \tan\left[\frac{m-1}{im}\left(x + \frac{i}{2a_1}t \right) \right] \right) \right\}^{-\frac{1}{m-1}} \tag{27}$$

$$u_8(x,t) = \left\{ -ia_1 + a_1 \left(\csc\left[\frac{m-1}{im}\left(x + \frac{i}{2a_1}t \right) \right] - \cot\left[\frac{m-1}{im}\left(x + \frac{i}{2a_1}t \right) \right] \right) \right\}^{-\frac{1}{m-1}} \tag{28}$$

(6) $A = -\frac{1}{2}, B = 0, C = -\frac{1}{2}$

Assuming, $a_0 = -ia_1$ and $h = -\frac{m-1}{im}$ in eq.(14), we get

$$a_0 = -ia_1, a_{-1} = 0, a_1 = a_1, v = \frac{i}{2a_1} \tag{29}$$

From appendix and eq.(29), we have

$$u_9(x,t) = \left\{ -ia_1 - a_1 \left(\sec\left[\frac{m-1}{im}\left(x + \frac{i}{2a_1}t \right) \right] - \tan\left[\frac{m-1}{im}\left(x + \frac{i}{2a_1}t \right) \right] \right) \right\}^{-\frac{1}{m-1}} \tag{30}$$

$$u_{10}(x,t) = \left\{ -ia_1 - a_1 \left(\csc\left[\frac{m-1}{im}\left(x + \frac{i}{2a_1}t \right) \right] + \cot\left[\frac{m-1}{im}\left(x + \frac{i}{2a_1}t \right) \right] \right) \right\}^{-\frac{1}{m-1}} \tag{31}$$

Case [II]: $n = 2m-1, \ m > 1$

We consider $n = 2m-1$ in eq.(1), we get,

$$u_t = \left(u^m \right)_{xx} + \left(u^{2m-1} \right)_x, \ m > 1. \tag{32}$$

Differentiating eq.(32) with respect to x we have following partial differential equation,

$$u_t - m(m-1)u^{m-2}\left(u_x \right)^2 - mu^{m-1}u_{xx} - (2m-1)u^{2m-2}u_x = 0 \tag{33}$$

Suppose the solution of eq.(33) is of the form

$$u(x,t) = u(\xi) \text{ where } \xi = h(x + vt) \tag{34}$$

where $h \neq 0$ and v are constants to be determined. Substituting eq.(34) into eq.(33), we get ODE,

$$vu^{-(m-1)}u' - m(m-1)hu^{-1}\left(u' \right)^2 - mhu'' - (2m-1)u^{m-1}u' = 0 \tag{35}$$

where prime denotes differentiation with respect to ξ. Now, balancing the order of $u^{m-1}u'$ with u'' in eq.(35), we obtained integer $N = \dfrac{1}{m-1}$. Again we use the transformation $u(\xi) = w^{1/m-1}(\xi)$ into the eq.(35), we get following ODE

$$v\,w^{-1}w' - m\left(\frac{1}{m-1}\right)h\,w^{-1}\left(w'\right)^2 - mh\,w'' - (2m-1)w\,w' = 0 \qquad (36)$$

According to homogeneous balance between ww' and w'', we have $N = 1$. So we can write solution of eq.(32) in the following form,

$$u(\xi) = w^{1/m-1}(\xi) \text{ where } w(\xi) = a_0 + a_{-1}F^{-1}(\xi) + a_1 F(\xi) \qquad (37)$$

Substituting eq.(37) into eq.(36) and using eq.(6), the left-hand side of eq.(36) can be converted into a finite series in $F^p(\xi)$, ($p = -4, -3, -2, -1, 0, 1, 2, 3, 4$). Equating each coefficient of $F^p(\xi)$ to zero yields the following set of algebraic equations:

$$F^{-4}(\xi): -2A^2hma_{-1}^2 - \frac{A^2hma_{-1}^2}{m-1} - Aa_{-1}^3 + 2Ama_{-1}^3 = 0$$

$$F^{-3}(\xi): -2A^2hma_0a_{-1} - 3ABhma_{-1}^2 - \frac{2ABhma_{-1}^2}{m-1} - 2Aa_0a_{-1}^2$$
$$+ 4Ama_0a_{-1}^2 - Ba_{-1}^3 + 2Bma_{-1}^3 = 0$$

$$F^{-2}(\xi): -3ABhma_0a_{-1} - Aa_0^2a_{-1} + 2Ama_0^2a_{-1} - B^2hma_{-1}^2 - 2AChma_{-1}^2$$
$$- \frac{B^2hma_{-1}^2}{m-1} - \frac{2AChma_{-1}^2}{m-1} - 2Ba_0a_{-1}^2 + 4Bma_0a_{-1}^2 - Ca_{-1}^3 + 2Cma_{-1}^3$$
$$- 2A^2hma_{-1}a_1 + \frac{2A^2hma_{-1}a_1}{m-1} - Aa_{-1}^2a_1 + 2Ama_{-1}^2a_1 - Aa_{-1}v = 0$$

$$F^{-1}(\xi): -B^2hma_0a_{-1} - 2AChma_0a_{-1} - Ba_0^2a_{-1} + 2Bma_0^2a_{-1} - BChma_{-1}^2$$
$$- \frac{2BChma_{-1}^2}{m-1} - 2Ca_0a_{-1}^2 + 4Cma_0a_{-1}^2 - 4ABhma_{-1}a_1 + \frac{4ABhma_{-1}a_1}{m-1}$$
$$- Ba_{-1}^2a_1 + 2Bma_{-1}^2a_1 - Ba_{-1}v = 0$$

$$F^0(\xi): -BChma_0a_{-1} - Ca_0^2a_{-1} + 2Cma_0^2a_{-1} - \frac{C^2hma_{-1}^2}{m-1} - ABhma_0a_1 + Aa_0^2a_1$$
$$- 2Ama_0^2a_1 - 2B^2hma_{-1}a_1 - 4AChma_{-1}a_1 + \frac{2B^2hma_{-1}a_1}{m-1} + \frac{4AChma_{-1}a_1}{m-1}$$
$$- Ca_{-1}^2a_1 + 2Cma_{-1}^2a_1 - \frac{A^2hma_1^2}{m-1} + Aa_{-1}a_1^2 - 2Ama_{-1}a_1^2 - Ca_{-1}v + Aa_1v = 0$$

$$F^1(\xi): -B^2hma_0a_1 - 2AChma_0a_1 + Ba_0^2a_1 - 2Bma_0^2a_1 - 4BChma_{-1}a_1$$
$$+ \frac{4BChma_{-1}a_1}{m-1} - ABhma_1^2 - \frac{2ABhma_1^2}{m-1} + 2Aa_0a_1^2 - 4Ama_0a_1^2 + Ba_{-1}a_1^2$$
$$- 2Bma_{-1}a_1^2 + Ba_1v = 0$$

$$F^2(\xi): -3BChma_0a_1 + Ca_0^2a_1 - 2Cma_0^2a_1 - 2C^2hma_{-1}a_1 + \frac{2C^2hma_{-1}a_1}{m-1} - B^2hma_1^2$$
$$- 2AChma_1^2 - \frac{B^2hma_1^2}{m-1} - \frac{2AChma_1^2}{m-1} + 2Ba_0a_1^2 - 4Bma_0a_1^2 + Ca_{-1}a_1^2$$
$$- 2Cma_{-1}a_1^2 + Aa_1^3 - 2Ama_1^3 + Ca_1v = 0$$

$$F^3(\xi): -2C^2hma_0a_1 - 3BChma_1^2 - \frac{2BChma_1^2}{m-1} + 2Ca_0a_1^2 - 4Cma_0a_1^2 + Ba_1^3$$
$$- 2Bma_1^3 = 0$$

$$F^4(\xi): -2C^2hma_1^2 - \frac{C^2hma_1^2}{m-1} + Ca_1^3 - 2Cma_1^3 = 0$$

$$\qquad (38)$$

Solving the above algebraic equations by Mathematica, we considered different cases as follows:

Case 1: $A = 0$, we have

$$a_0 = -\frac{Bhm}{2(m-1)}, a_{-1} = 0, a_1 = -\frac{Chm}{m-1}, v = \frac{B^2 h^2 m^2}{4(m-1)^2} \tag{39}$$

Assuming, $h = 2\left(\frac{m-1}{m}\right)$ in eq.(39), we get,

$$a_0 = -B, a_{-1} = 0, a_1 = -2C, v = B^2 \tag{40}$$

Case 2: $B = 0$, we have

$$a_0 = 0, a_{-1} = 0, a_1 = -\frac{Chm}{m-1}, v = -\frac{ACh^2 m^2}{(m-1)^2} \tag{41}$$

Assuming, (1) $h = 2\left(\frac{m-1}{m}\right)$ (2) $h = \frac{m-1}{m}$ and (3) $h = -\frac{m-1}{m}$ respectively in eq.(41), we get,

$$(1)\ a_0 = 0, a_{-1} = 0, a_1 = -2C, v = -4AC \tag{42}$$

$$(2)\ a_0 = 0, a_{-1} = 0, a_1 = -C, v = -AC \tag{43}$$

$$(3)\ a_0 = 0, a_{-1} = 0, a_1 = C, v = -AC \tag{44}$$

Case 3: $A = B = 0$, we have

$$a_0 = 0, a_{-1} = 0, a_1 = -\frac{Chm}{m-1}, v = 0 \tag{45}$$

Using cases 1 to 3 and appendix, we obtained the following exact generalized travelling wave solutions of eq.(32).

Soliton-like solutions:

(1) $A = 0, B = 1, C = -1$, from eq.(40) and appendix, we have

$$u_1(x,t) = \left\{ \tanh\left[\frac{m-1}{m}(x+t)\right]\right\}^{1/m-1} \tag{46}$$

(2) $A = 0, B = -1, C = 1$, from eq.(40) and appendix, we have

$$u_2(x,t) = \left\{ \coth\left[\frac{m-1}{m}(x+t)\right]\right\}^{1/m-1} \tag{47}$$

(3) $A = \frac{1}{2}, B = 0, C = -\frac{1}{2}$, from eq.(42) and appendix, we have

$$u_3(x,t) = \left\{ \coth\left[\frac{2(m-1)}{m}(x+t)\right] \pm \csc h\left[\frac{2(m-1)}{m}(x+t)\right]\right\}^{1/m-1} \tag{48}$$

$$u_4(x,t) = \left\{ \tanh\left[\frac{2(m-1)}{m}(x+t)\right] \pm i\sec h\left[\frac{2(m-1)}{m}(x+t)\right]\right\}^{1/m-1} \tag{49}$$

(4) $A = 1, B = 0, C = -1$, from eq.(43) and appendix, we have same solutions given by eq.(46) and eq.(47).

Trigonometric function solutions :

(5) $A = \frac{1}{2}, B = 0, C = \frac{1}{2}$, from eq.(44) and appendix, we have

$$u_5\left(x,t\right)=\left\{-\frac{1}{2}\left(\sec\left[\frac{m-1}{m}\left(x-\frac{t}{4}\right)\right]+\tan\left[\frac{m-1}{m}\left(x-\frac{t}{4}\right)\right]\right)\right\}^{1/_{m-1}}$$ (50)

$$u_6\left(x,t\right)=\left\{-\frac{1}{2}\left(\csc\left[\frac{m-1}{m}\left(x-\frac{t}{4}\right)\right]-\cot\left[\frac{m-1}{m}\left(x-\frac{t}{4}\right)\right]\right)\right\}^{1/_{m-1}}$$ (51)

(6) $A=-\dfrac{1}{2}, B=0, C=-\dfrac{1}{2}$, from eq.(44) and appendix, we have

$$u_7\left(x,t\right)=\left\{\frac{1}{2}\left(\sec\left[\frac{m-1}{m}\left(x+\frac{t}{4}\right)\right]-\tan\left[\frac{m-1}{m}\left(x+\frac{t}{4}\right)\right]\right)\right\}^{1/_{m-1}}$$ (52)

$$u_8\left(x,t\right)=\left\{\frac{1}{2}\left(\csc\left[\frac{m-1}{m}\left(x+\frac{t}{4}\right)\right]+\cot\left[\frac{m-1}{m}\left(x+\frac{t}{4}\right)\right]\right)\right\}^{1/_{m-1}}$$ (53)

(7) $A=1, B=0, C=1$, from eq.(44) and appendix, we have

$$u_9\left(x,t\right)=\left\{-\tan\left[\frac{m-1}{m}\left(x-t\right)\right]\right\}^{1/_{m-1}}$$ (54)

(8) $A=-1, B=0, C=-1$, from eq.(44) and appendix, we have

$$u_{10}\left(x,t\right)=\left\{\cot\left[\frac{m-1}{m}\left(x-t\right)\right]\right\}^{1/_{m-1}}$$ (55)

Rational solution :
(9) $A=0, B=0, C\neq0$, from eq.(45) and appendix, we have

$$u_{11}\left(x,t\right)=\left\{\frac{C\,h\,m}{m-1}\left(\frac{1}{C\,h\,x+b}\right)\right\}^{1/_{m-1}}$$ (56)

where b is an arbitrary constant.
The solutions given by eq.(46), eq.(47), eq.(54) and eq.(55) obtained by modified F-expansion method and those obtained in [12,15], shows good agreement.

IV. Conclusion

In this paper, the modified F-expansion method is implemented to produce new exact travelling wave solutions of the convection diffusion equation. The used method is straightforward and concise. Moreover, the obtained solutions satisfy given convection diffusion equation and reveal that this method is promising mathematical tool because it can provide a different class of new travelling wave solutions which may be of important significance for the explanation of some relevant physical problems in mathematical physics and engineering.

Appendix: Relations between values of (A, B, C) and corresponding $F\left(\xi\right)$ in Riccati equation

$$F^{'}\left(\xi\right)=A+B\,F\left(\xi\right)+C\,F^2\left(\xi\right)$$

A	B	C	$F\left(\xi\right)$
0	1	−1	$\dfrac{1}{2}+\dfrac{1}{2}\tanh\left(\dfrac{\xi}{2}\right)$
0	−1	1	$\dfrac{1}{2}-\dfrac{1}{2}\coth\left(\dfrac{\xi}{2}\right)$

$\dfrac{1}{2}$	0	$-\dfrac{1}{2}$	$\coth(\xi)\pm\csc h(\xi),\tanh(\xi)\pm i\sec h(\xi)$
1	0	-1	$\tanh(\xi),\coth(\xi)$
$\dfrac{1}{2}$	0	$\dfrac{1}{2}$	$\sec(\xi)+\tan(\xi),\csc(\xi)-\cot(\xi)$
$-\dfrac{1}{2}$	0	$-\dfrac{1}{2}$	$\sec(\xi)-\tan(\xi),\csc(\xi)+\cot(\xi)$
$1(-1)$	0	$1(-1)$	$\tan(\xi),\cot(\xi)$
0	0	$\neq 0$	$-\dfrac{1}{C\xi+b}$ (b is an arbitrary constant)

REFERENCES

[1]. Abassy T. A. et al. (2007). The solution of Burgers and good Boussinesq equations using adm-pade technique, Chaos, Solitons and Fractals 32, 1008-1026.

[2]. Asgari A. et al. (2011). A generalized analytical solution for a nonlinear infiltration equation using the exp-function method, Sci. Irani. A 18, 28-35.

[3]. Aslanov A. (2011). Homotopy perturbation method for solving wave-like nonlinear equations with initial-boundary conditions, Discrete Dyn. in Nature and Soci. 2011, 1-10.

[4]. Bear J. (1972). Dynamics of fluids in porous media, Elsevier, New York.

[5]. Buckmaster J. (1977). Viscous sheets advancing over dry beds, J. Fluid Mech. 81, 735-756.

[6]. Cai G. et al. (2006). A modified F-expansion method for solving braking soliton equation", Int. J. nonlinear Sci. 2, 122-128.

[7]. Cai G., Wang Q. (2007). A modified F-expansion method for solving nonlinear PDEs, J. of Inform. and Comput. Sci. 2, 03-16.

[8]. Darvishi M. T. et al. (2012), Traveling wave solutions for foam drainage equation by modified F-expansion method, Food and Public Health 2, 06-10.

[9]. Ghotbi A. R. et al. (2011). Infiltration in unsaturated soils an analytical approach, Comput. and Geotech. 38, 777-782.

[10]. Grundy R. E. (1983). Asymptotic solution of a model nonlinear convective-diffusion equation, IMA J. Appl. Math. 31, 121-137.

[11]. He J-H. (1999). Variational iteration method a kind of non-linear analytical technique: some examples, Int. J. of Non. Mech. 34, 699-708.

[12]. Hearns J. and Van Gorder R. A. (2012). Classical implicit travelling wave solutions for a quasilinear convection-diffusion equation, New Astro. 17, 705-710.

[13]. Kutluay S. et al. (1999). Numerical solution of one-dimensional Burgers equation: explicit and exact-explicit finite difference methods, J. of Comput. and App. Maths. 103, 251-261.

[14]. Rashidi M. M. et al. (2009). Approximate solutions for the Burger and regularized long wave equations by means of the homotopy analysis method, Non. Sci. and Num. Simul. 14, 708-717.

[15]. Vanaja V. (2009). Exact solutions of a nonlinear diffusion-convection equation, Phy. Scrip. 80,01-07.

[16]. Wazwaz A. M. (2009), Partial differential equations and solitary waves theory, Springer

[17]. Wazwaz A. M. (2005). Travelling wave solutions for generalized forms of Burgers, Burgers-Kdv and Burgers-Huxley equations, App. Math. and Comput. 169,639-656.

[18]. Zhang J L. et al. (2006). The improved F-expansion method and its applications, Phys. Lett. A 350,103-109.

[19]. Zhang J-F. et al. (2005). Variable-coefficient F-expansion method and its application to nonlinear Schrodinger equation, Opt. Commun. 252, 408-421.

[20]. Zhang S. and Xia T. (2006). A generalized F-expansion method and new exact solutions of Konopelchenko-Dubrovsky equations, Appl. Math. Comput. 183,1190-1200.

[21]. Zhao Y-M. (2013). F-expansion method and its application for finding new exact solutions to the Kudryashov-Sinelshchikov equation J. of Appl. Math. 2013,01-07.

Safety Margin of Slope Stability Using Common Deterministic Methods

Mr. Amro Z.Osman[1]

[1](Ms.c in Civil Engineering , School of Civil Engineering, Benghazi university, Benghazi, Libya)

Abstract: *The objective of this research was to develop a model for deterministic slope stability analysis. The study was performed through different methods of analysis and compared with Bishop simplified method, the variation of each input parameter ranged using traditional behavior equations to produce a distribution of the factor of safety verses the variables. A sensitivity analysis is then applied to the output factor of safety with each variable to select the slope design parameters with acceptable effect on factor of safety. To demonstrate the application of the deterministic methods developed during this paper, the methodology was applied to case study to present the effect of each variable on factor of safety, the study of slope failure was assumed to be circular slip surface .*
Keywords: *Safety factor, Sensitivity analysis, Slope stability.*

I. INTRODUCTION

The slope stability problems is difficult to accurately modeled because of variety of factors. one of main problem is that the exact behavior of slopes cannot be exactly predicted. Hence, engineers resort to a factor of safety approach to reduce risk of slope failure. the approach of deterministic methods present systematic way to treat uncertainties of variables, especially slope stability. The stability of a slope has a considerable effect on the surrounding area of the slope, because very often, human lives are in danger or significant material damage results if a slope fails. Thus the slope stability analysis is one of the most important areas of practical use in soil engineering.[10].

 in this paper study a model of embankment dam using different methods of analysis in deterministic behavior. many variables affecting the safety factor value ,these variable are tabled in this paper as ranged values with mean value for each variable to include the effect of variation of variables in sensitivity analysis.

the safety factor is computed for mean value of each variable to make comparison study between different methods of analysis with Bishop method.

II. SLOPE FAILURE MODES

The analytical prediction of the slope failure in a given system requires the location of the slip surface, the determination of acting forces, and the prediction of the available reactive forces on it which acting along the slip surface and the working shear is the sum of the shearing stresses produced by causes (dead load, water, etc.) along the same surface. The stability analysis is largely a trial-and-error process, accomplished by numerical or graphical methods. Because of the cyclic (repetitive) nature, the calculations and the graphical constructions are well suited to computer programming, which reduces the involved labor considerably.[3,6,7] . Classification of gravity induced movements was introduced by Varnes that was based on two variables; type of material and type of movement. The main difference between this classification and the submarine classification, derived by Varnes, is that the material is totally saturated in water, so there is no degree of wetness. Some geologists argue that there is no concrete classification scheme for submarine slides because there is not just one type involved in one event; i.e. sliding results in a turbidity flow as acceleration of the debris increases, they can be summarized as follows:-

Falls occur when rock, mud or sand sized particles break free from the top of a steep or nearly vertical slope and pummels to a lower position. Multiple events in one location accumulate to form talus deposits at the base of the slope.

Slides which the most frequent type of wasting that moves a mass with translational motion down the contour due to failure of its base.

Flows occur when bodies of sediment or rock fragments are set into motion down a slope at a slow rate sometimes experiencing turbulence. There are several types of flows that are dependant on the size of the

particle and the type of motion within the flow. Turbidity flows are events in which denser water forces sand-size and smaller debris to flow turbulently down the slope. Also; slope of failures may be classified according to the type of the failure surface as shown in fig.1 to:

1. Straight lines (particularly so in granular media).
2. Approximate to arcs of circles.
3. Approximate to logarithmic spirals.
4. Combination of straight lines, arcs of circles, and/or
5. Logarithmic spirals.

These types of the slope failure may differ as the material type, and the degree of complexity is function in the variety of the variables in the failure zone. Slopes often appear to fail on circular slip surfaces and it is often reasonable to analyze slope stability using circular slip surfaces. However, there are also many instances when this is not the case. Non-circular slip surfaces may be more critical than circular slip surfaces when:

1-There is a weak layer present in the foundation. The weak layer could be soft clay or liquefiable sand.

2-There is a heavily over consolidated, stiff fissured-clay or clay-shale foundation for an embankment.

3- A dam's core is sloping and is significantly weaker than its shell.[4,9,10]

Slope failure may also take the shape of the following when firm layer existed under the slope:

1. The base failure figure (2.a) in cohesive soils is preceded by the formation of tension cracks above the upper edge of the slope, followed by a shear failure along a slip surface.

2. The slope failure figure (2.b) in cohesive soils is again preceded by the Formation of tension cracks at the top, followed by a critical shear failure along slip surface that intersects certain point of slope.

3. The toe failure Figure (2.c) in soils of $\varphi > 0$ forming steep slopes is a Shear failure along a slip surface that intersects the toe of the slope.

Although this group classification is a convenient descriptive approach, sometimes the actual failures occur in a less distinct form as a combination of two modes. [1, 2, 8]
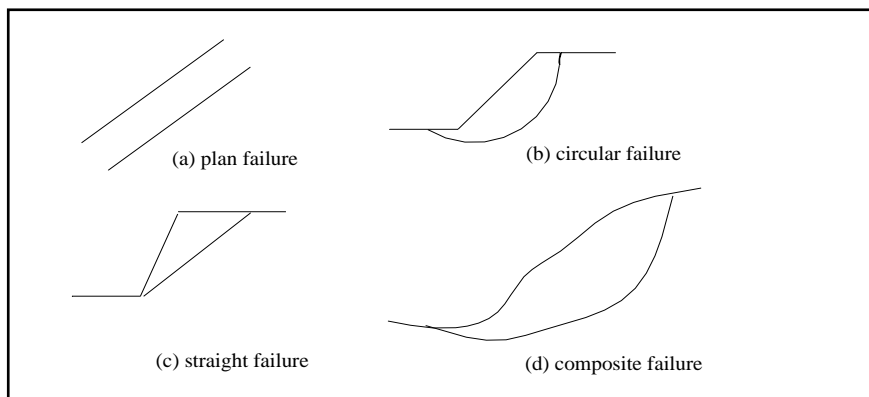

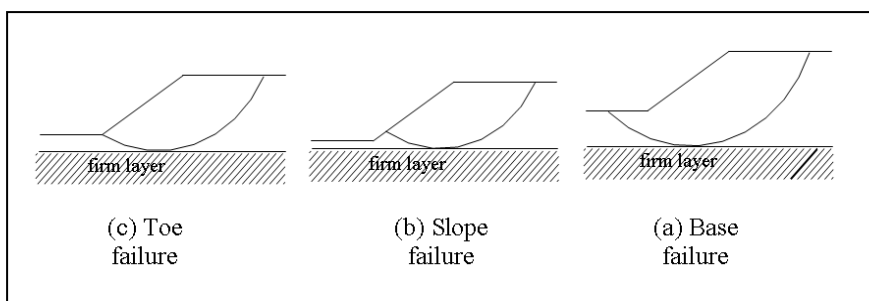Fig.1 General types of the slope failure.

Fig.2 Types of failure of slope contain firm layer. (8)

III. ANALYSIS OF FAILURE AND SAFETY FACTOR
At any surface of slope failure safety factor can be found from the following equation:

$$F_s = \frac{\text{forces opposing slip (ultimate shear)}}{\text{forces causing slip (working shear)}} \qquad (1)$$

Where the ultimate shear is the sum of the critical shearing stresses as the next equation

$$\tau = c + \sigma \tan \varphi \qquad (2)$$

many methods studied the slip surface considering certain number of slices to determine the critical safety factors such as :
1. Karl Edward Peterson method (1915).
2. Bishop's Simplified Method - popular - use for circular failure (1950).
3. Janbu's Simplifies Method - popular - use for noncircular failures.
4. Lowe and Karafiath's Method.
5. Corps of Engineer's Method (1982).
6. Spencer's Method - use for rigorous analysis (1973).
7. Bishop's Rigorous Method.
8. Jambu's Generalized Method.
9. Sarma's Method.
10. Morgenstern - Price Method (1965).

All involve the principle of limit equilibrium of tangential and normal forces on the slip surface as shown in Fig.3
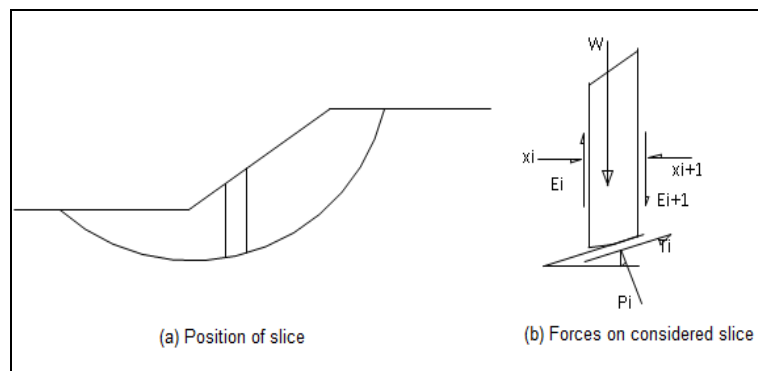

Fig.3 forces on slice from slip surface

IV. SIMULATION RESULTS
Case study is used to compute the safety factor, the dimensions of studied earth dam is as shown in Fig.4
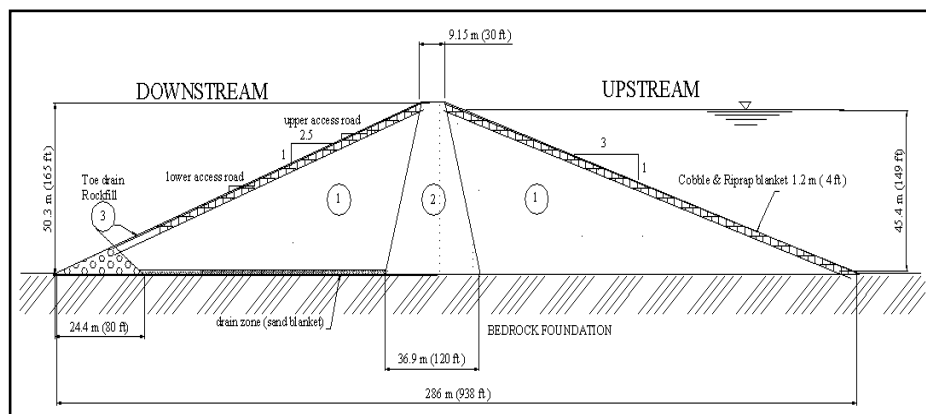

Fig.4 Earth dam considered as case of study (Miramar earth dam)

Input variables for this case of study used with mean values of detailed in table .1 below

Table.1 input variables for case study

	variable	Unit	Mean value
Zone 1		kN/m^3	18.2
	C	kN/m^2	30
	Φ	degree	30.6
Zone 2	Γ	kN/m^3	15.8
	C	kN/m^2	37.2
	Φ	degree	15
	Γ	kN/m^3	18
Zone 3	Φ	degree	25
General variables	γ_w	kN/m^3	9.81
	H	m	50.3
	$h_{capillary}$	m	0
	h_{water}	m	0
	X1	m	29.5
	Y1	m	38.3
	R	m	68.3
	S	dimensionles s	2.5

where

C:Cohesion
H: height of dam above underlying stiff layer
h:height of dam in upstream side
$h_{capillary}$: Capillary rise of water .
h_{water}: water height in upstream side.
R: raduis of the failed surface.
S: slope of upstream side

X1:horizontal distance of center of failure to toe
Y1: vertical distance of center of failure to toe
γ: unit weight
φ: internal friction angle

During the process of the analysis the factor of safety is estimated to the method accepted for solving the problem, the value of the factor of safety in some cases does not converge to certain value with some methods such as Bishop method. thus in such a case we should treat the slope with other method of analysis. Bishop simplified method has some what degree of convergence to the exact solution for the reason that it considered the equations of equilibrium in the force and moment and at the same time omit one of the interslice forces which some what has no great effect to the factor of safety. evaluation and the results as shown in Table. 2

Table (2) The Values of factor of safety with each method.

Method of analysis	Factor of safety F_s	Deviation to Bishop method %
Peterson	1.984	-3.9
Solution of Upper bound	2.449	18.6
Solution of lower bound	2.324	12.5
Bishop simplified	2.065	-
Spencer	2.082	0.8
Morgenstern	1.940	-6.1

the safety factor varies according to value of each variable , Fig.5 through Fig.10 shows these variations
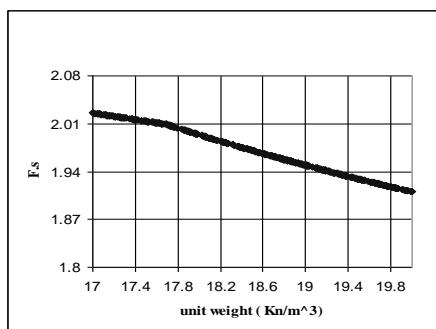
Fig. 5 variation of Fs with γ Fig. 6 variation of Fs with C
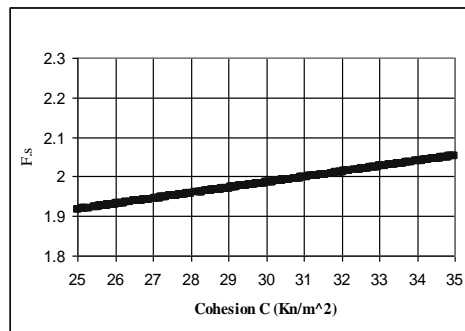
Fig.7 variation of factor of safety with S   Fig.8 variation of Fs with hw
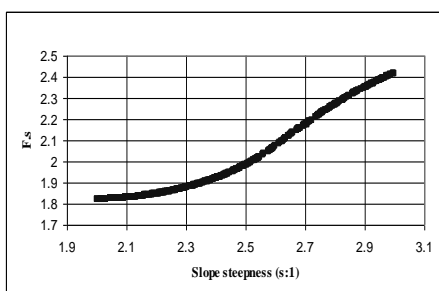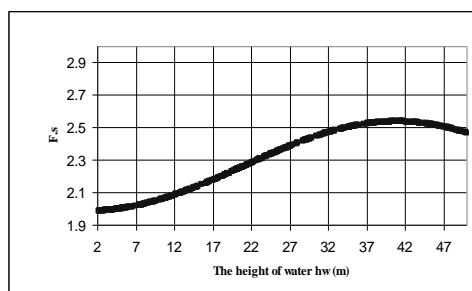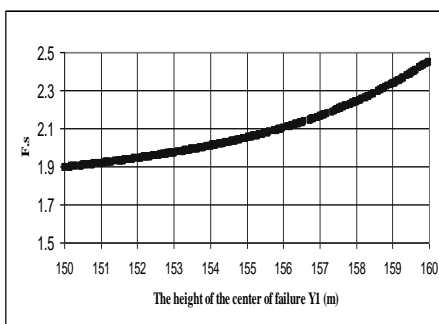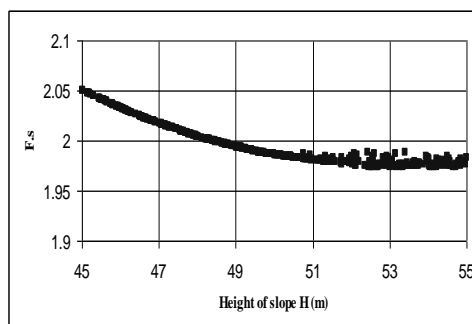

Fig.9 variation of Fs with H   Fig.10 variation of Fs with y1

Sensitivity analysis is then applied using correlation coefficient to present the more effective parameters to the factor of safety lead to results shown in Fig.11
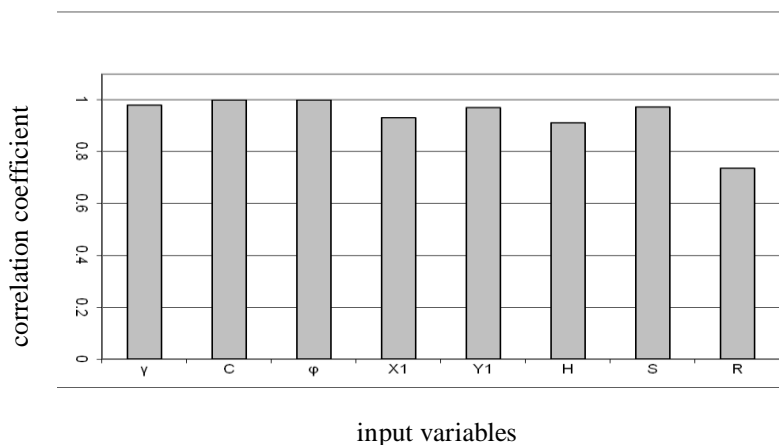

input variables

Fig.11 sensitivity analysis of the input variables with correlation coefficient

V. CONCLUSION

The paper presented herein developed a computer program using different methods of slope stability analysis. Deterministic model for slope analysis were implemented into the SLOPE/SCF program including complete range of traditional slope analysis methods. To demonstrate the capabilities of this methodology, a case study was adopted using circular analysis methods. From the stability analysis of a slope with a circular failure surface and factor of safety for uncorrelated input parameters the following points are concluded.

The sensitivity analysis conducted using a correlation and standard error analysis indicated that the cohesion, internal friction angle, and unit weight were the most critical inputs when analyzing the slope for a circular failure surface. The sensitivity analysis confirms the expected significance of each input parameter.

The mean factor of safety from this analysis was 2.141.This was deviated from the midpoint factor of safety from the modified Bishop's method of slices (2.065) by about 3.7 %. The methods of analysis have same pattern for the variables with percent of variation between them (3 to 20%).

For this model and with comparing the results of the factor of safety from different methods, Morgenstern method appears to have a lower bound of the solution for the factor of safety. The upper bound of solution is the friction circle method, and the Bishop simplified method has a value near to the mean value estimated by the methods.

Acknowledgement

REFERENCES

[1]   Ching – Chuan Huang &Cheng-Chen Tsai , New Method For 3D And Asymmetrical Slope Stability Analysis **,** Journal of Geotechnical and Geoenvironmental Engineering , ASCE ,Vol. 126 No 10 , 2000
[2]   Ellen M.Rathje & Jonathan D.Bray , Non-linear Coupled seismic Sliding Analysis of Earth structures   ,Journal of Geotechnical and Geoenvironmental Engineering , A.S.C.E ,Vol.126 No11, 2000
[3]   Shengxiage Gui , Renduo John P.Turner & Xuzhang , Probabilistic Slope Stability Analysis With Stochastic Soil Hydraulic Conductivity , Journal of Geotechnical and Geoenvironmental Engineering , ASCE ,Vol. 126,2001
[4]   Chandarakant .S .Desai &John T Christian ,Numerical Methods In Geotechnical Engineering (Virginia, 1977)
[5]   C. R. Scott ,Soil Mechanics and Foundations(city university London, 2nd Ed, 1975).
[6]   Darly .L .Logon ,A First Course In Finite Element Method(Hulman institute of technology, 2nd Ed. ,1993)
[7]   G.N.Smith , Elements For Soil Mechanics For Mining Engineering (M .Sc ,M.I.C.E , struct. E M .A .M .Soc .C.E , 3rd edition).
[8]   Irving S.Dunn& Loren R.Anderson, fundamentals of geotechnical analysis (Utah state University ,2nd edition , 1980)
[9]   Jan J.Tuma & M.ABDEL-Hady, Engineering Soil Mechanics (Addison-Wesley 3rd edition ,1973)
[10]   P. Leonard Capper , The Mechanics Of Engineering Soils(John Wiley & Sons 6th Edition, 1976)
[11]   T.William & Robert V.Whitmam , Soil Mehanics (John Wiley & Sons ,2nd edition ,1969).

Implementation of MIL-STD-1553 Data Bus

Elizabeth Sunny[1]

1(Federal Institute of Science and Technology, India)

Abstract: *MIL-tSTD-1553 is a military standard that defines the electrical and protocol characteristics for a data bus. This standard defines requirements for digital and time division multiplexing techniques for a one Megahertz serial data bus and specifies its interface electronics. The effective bandwidth of the systems using this standard can be improved by various data compression techniques. Run-length encoding is one of the lossless data compression techniques suitable for implementation in real-time and mission critical systems. This paper describes the better utilization of the available bandwidth using Run-length encoding algorithm.*

Keywords: *data compression, MIL-STD-1553, run-length encoding, serial data bus, time-division - Multiplexing.*

I. INTRODUCTION

MIL-STD-1553 was developed from the growing complexity of avionics systems and the subsequent increase in the interconnections between terminal devices. In the 1950s and 1960s, the navigation, communications, flight controls, and displays consisted of analog systems. Most of these systems were composed of multiple subsystems, connected to form a single system [1]. Various subsystems were connected with point-to-point wiring. As more and more systems were added, the cockpits became more crowded, and the overall weight of the aircraft increased. As time and technology progressed, a data transmission medium, which would allow all systems and subsystems to share a single and common set of wires, came in to existence. By sharing the use of this interconnects, the various subsystems could send data between themselves and to other systems, one at a time, and in a defined sequence, hence a data bus. The first draft of a standard in 1968, by the Aerospace Branch of the Society of Automotive Engineers laid the foundation for the US Air Force's adoption of MIL-STD-1553 in 1973 [5].

Researches on the standard have shown that a significant amount of the data sent over the MIL-STD-1553 data bus during any time slice carries no new information. In such a case, the effective bandwidth of systems using the MIL-STD-1553 serial data bus can be improved by various data compression techniques. Compression may be implemented through many techniques that result in either lossy or lossless compression. If lossless compression techniques are employed, no information is lost as part of the compression and decompression process. Run-length encoding is one such type which takes advantage of situations where the data contains relatively long runs of consecutive identical numbers [2].

II. BUS ARCHITECTURE

The 1553 data bus is a dual-redundant, bidirectional and Manchester II encoded data bus with a high bit error reliability. The bus architecture consists of remote terminals, bus controllers and bus monitors.Remote terminals are defined within the standard as, all terminals not operating as the bus controller or as a bus monitor. A remote terminal typically consists of a transceiver, an encoder/decoder, a protocol controller, a buffer or memory, and a subsystem interface. The bus controller is the terminal that initiates information transfers on the data bus. All bus communications are controlled and initiated by a bus controller. It sends commands to the remote terminals which reply with a response. The bus will support multiple controllers, but only one may be active at a time. It is the key part of the data bus system, and the sole control of information transmission on the bus shall reside with the bus controller. The bus controller is responsible for directing the flow of data on the data bus. The bus controller is the only one allowed to issue commands onto the data bus [4].
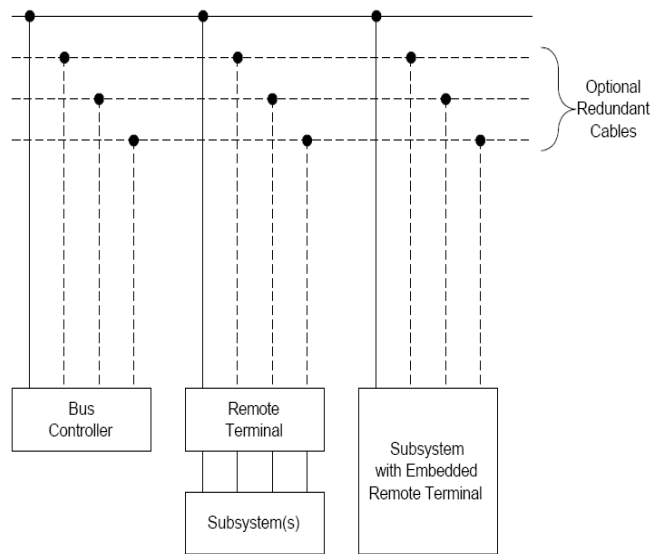
Fig. 1 Bus Architecture

A bus monitor is a terminal that listens to the exchange of information on the data bus. It may collect all the data from the bus or may collect selected data. It is the terminal that has assigned the task of receiving bus traffic and extracting selected information to be used at a later time.

III. WORD TYPES

The control, data flow and management of the bus are provided by the word types .There are three word types, Command word, Data word and Status word. Each word is twenty bits in length. The first three bits are used as a synchronization field. The next sixteen bits are the information field and are different between the three word types. The last bit is the parity bit and is based on odd parity for the single word.
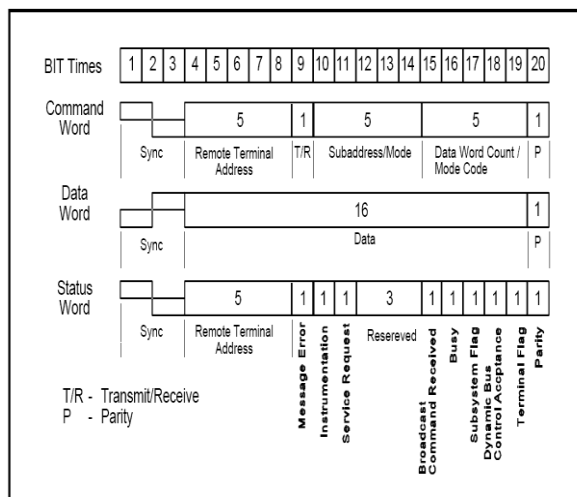
Fig. 2 Word formats

1. Command Word

The Command Word (CW) specifies the function that remote terminal is to perform. Only the active bus controller transmits this word. The word begins with command sync in the first three bit times followed by sixteen-bit information field and a parity bit. The sync field of command word and the status word are identical and the inverse of the data word sync pattern. Therefore, command and status words, can always be distinguished from data word sync patterns.

2. Data Word

The Data Word (DW) contains the actual information that is being transferred within a message. The first three-bit time contains a data sync. This sync pattern is the opposite of that used for command and status words and therefore is unique to the word type. Data words can be transmitted by either a remote terminal (transit command) or a bus controller (receive command).

3. Status Word

A remote terminal in response to a valid message transmits only the status word (SW). The status word is used to convey to the bus controller whether a message was properly received or to convey the state of the remote terminal (i.e., service request, busy, etc.).The optional status bits are, instrumentation, service request, broadcast command received, busy, subsystem flag, dynamic bus control acceptance and terminal flag.

IV. MESSAGE FORMATS

The standard defines ten types of message transmission formats. The message formats have been divided into two groups. These are referred to within the standard as the "information transfer formats" and the "broadcast information transfer formats". The information transfer formats are based on the command/response philosophy in that all error free transmissions received by a remote terminal are followed by the transmission of a status word from the terminal to the bus controller. This handshaking principle validates the receipt of the message by the remote terminal.
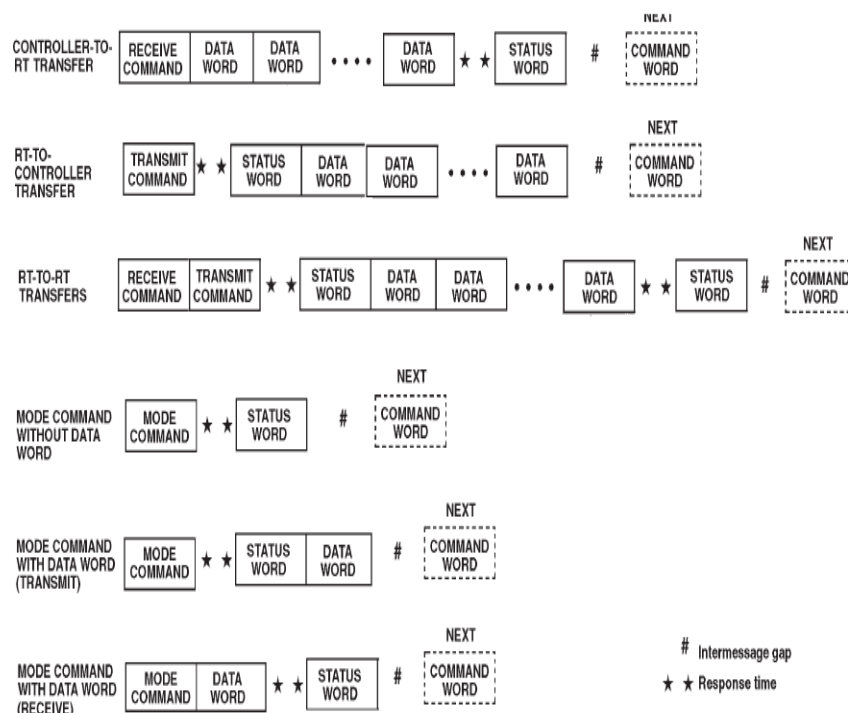
Fig. 3 Information transfer formats

Broadcast messages are transmitted to multiple remote terminals at the same time. The terminals suppress the transmission of their status words. In order for the bus controller to determine if a terminal received the message, a polling sequence to each terminal must be initiated to collect the status words. The broadcast option can be used with the message formats where the remote terminal receives data. Obviously, multiple terminals cannot transmit data at the same time, so the RT-BC transfer format and the transmit mode code with data format cannot be used. The broadcast RT-RT allows the bus controller to instruct all remote terminals to receive and then instructs one terminal to transmit, thereby allowing a single subsystem to transfer its data directly to multiple users.

1. Bus Controller to Remote Terminal

The bus controller to remote terminal (BC-RT) message is referred to as the receive command since the remote terminal is going to receive data. The bus controller outputs a command word to the terminal defining the Sub address of the data and the number of data words it is sending. Immediately (without any gap in the transmission), the number of data words specified in the command word is sent. The remote terminal upon validating the command word and all of the data words issues its status word within the response time requirements .The remote terminal must be capable of processing the next command that the bus controller issues.

2. Remote Terminal to Bus Controller

The remote terminal to bus controller (RT-BC) message is referred to as a transmit command. The bus controller issues only a transmit command word to the remote terminal. The terminal, on validating the command word, transmits its status word followed by the number of data words requested by the command word. The remote terminal doesn't know the sequence of commands to be sent and doesn't normally operate on a command until the command word has been validated.

3. Remote Terminal to Remote Terminal

The remote terminal to remote terminal (RT-RT) command allows a terminal to transfer data directly to another terminal without going through the bus controller. However, the bus controller may also collect the data and use them. The bus controller issues a command word to the receiving terminal immediately followed by a command word to the transmitting terminal. The receiving terminal is expecting data, but instead of data after the command word it sees a command sync (the second command word). The receiving terminal ignores this word and waits for a word with data sync.

4. Mode Command

Three mode command formats are provided. This allows for mode commands with no data words and for the mode commands with one data word (either transmitted or received). The status/data sequencing is the same as the BC-RT or RT-BC messages except that the data word count is either one or zero.

V. DATA COMPRESSION

Data compression has many benefits depending on its various applications. A few of these advantages include reduced time for communication, reduced transmission errors, and increased security. For a serial communication system, data compression allows greater bus utilization by allowing more data to be sent during a given transmission time interval, reducing the transmission time. Compression may be implemented through many techniques which is lossy or lossless compression. Lossy compression reduces the data size by identifying data that carries the least information and removing it away. This means that when the data is uncompressed, the result will not be identical to the original pre-compressed data, resulting in a loss of information. Lossy compressing routines are frequently used for picture and video compression. Examples of lossy compression are JPEG and MPEG compression. Lossless compression reduces redundancy in input data and is reversible resulting in decoded data that is identical to its pre-compressed form. Lossless compression is necessary for critical systems such as avionics.

Run-length encoding is a suitable lossless compression technique [2]. It takes advantage of situations where the data contains relatively long runs of consecutive identical numbers. In this scheme, a position-indicating word is used along with data words. The encoded data consists of the position-indicating word followed by non-zero data words listed in the original order of their appearance. A zero bit in the position-indicating word implies that the value does not repeat. A one indicates that the value repeats. When the position bit with a value of zero is encountered, the data word is read from the data section of the block. After that, if value one is encountered this value is repeated as the consecutive data word. At the decoder if the position bit with a value zero is read , the data words following the position-indicating word are taken in the original order of their appearance. If a bit

One is found, the previous data word is repeated. The TABLE 1 shown below is an example for the above scheme.

Table 1 Run-length encoding scheme

Word count (Hex)	Input Data (Hex)	Position-indicating Word	Encoded Data (Hex)
0	0	0	6BDF
1	0	1	0
2	0	1	FFFF
3	FFFF	0	1204
4	FFFF	1	5342
5	1204	0	
6	1204	1	
7	1204	1	
8	1204	1	
9	1204	1	
A	5342	0	
B	5342	1	
C	5342	1	
D	5342	1	
E	5342	1	
F	5342	1	

VI. RESULTS AND DISCUSSION

The software designing of the data bus is done in VHDL using Xilinx 1SE design suit 14.2 and the simulation is done using Xilinx ISE Simulator. Referring to the example shown in TABLE 1 instead of transmitting the entire 16 data words, we are transmitting 5 Run-length encoded data words .The simulation results shows that the time taken to encode and transmit the data words can be reduced effectively and the effective utilization of the bandwidth during data transmission is improved.

VII. CONCLUSION

MIL-STD-1553 is a military standard which is used as one of the basic tool by the Department of Defense for the integration of weapon systems. The serial data bus has solved the complex scenario of a crowded system and finds application in the areas of military aircrafts, submarines, tanks and launch vehicles. Since the amount of the data sent over the data bus during any time slice carries no new information, the paper describes a data compression technique called Run-length encoding. Comparing the time taken to encode and transmit the data words with compression and without compression shows that the above method is a better option to be used for the effective utilization of the band-width.

REFERENCES

[1.] Duren, Russell W, June 2006, "Options for upgrading legacy avionics systems," Journal of Aerospace Computing, Information, and Communication, vol. 3, pp. 251-259
[2.] Duren, Russell W. and Michael W. Thompson, 1-8 March 2008, Application of Data Compression to the MIL-STD-1553 Data Bus, Proc. of the 2008 IEEE Aerospace Conf., Big Sky, MT.
[3.] Duren, Russell W, Algorithmic and architectural methods for performance enhancement of avionics systems, Proc. of the 28th Digital Avionics Systems Conf., October 25-29, 2009
[4.] Data Device Corporation, " MIL-STD-1553 designer's guide ", sixth edition .
[5.] E. C. Gangl, "Evolution from analog to digital integration in aircraft avionics - a time of transition,"Aerospace and Electronic Systems, IEEE Transactions on, vol. 42, 1163-1170, 2006.

Microcontroller Based Obstacle Detection Device Using Voice Signal for the Visually Impaired

E. Shobhana[1]

[1]*(Department of physics, Kumaraguru College of Technology, India)*

Abstract: *This paper aims in helping the visually impaired people through an electronic aid, which senses any obstacle in the path and alarms the user of the obstacle. The device uses a simple principle of transmitting an ultrasonic signal in the path generated by a wave generator. The signal gets reflected by the obstacle (if any) in the path. The reflected signal is sensed by a sensor and produces a sound signal in the form of voice. This voice signal directs the visually impaired person to identify the obstacles in front of them.*

Keywords: *Navigation, Obstacle detection, Voice signal, visually impaired.*

I. Introduction

The development and application of technology for orientation and mobility has a long history covering the postwar period. Although some early endeavors envisaged systems that might replace the cane or dog guide, more recent efforts have focused on devices and systems designed to supplement and provide a support system for these basic mobility tools. The technological growth in the education of the disabled has two fold objectives namely, Technology for reducing the disabling conditions and Technology for enhancing learning opportunities. While the former deals with the invention of hardware technology the latter pertains to both the hardware and software technologies. Both the approaches become equally important [1]**.**

The most ultrasonic sensorial systems are based on transducers that work as emitters and receivers in the same scanning process. This fact implies that during the emission process the reception stage stays disabled, in order to avoid the emission coupled. This work presents a novel encoding technique, based on Golay complementary pairs, where the dimension of the blind zone is reduced to negligible distances [2].

II. Materials And Methods

Visual impairment is the consequence of a functional loss of vision, rather than the eye disorder itself. Independent travel is a source of anxiety for many blind people and indeed some avoid it altogether. The usage of Light Rapid or Light Rail Transit (LRT) systems by persons with severe visual impairment would resolve many of the difficulties [3]. To remove the anxiety various types of orientation & mobility aids, an Electronic Travel Aid (ETA) which transform visual environmental cues into other sensory modality have been proven to help visually impaired people travel with a greater degree of psychological comfort and independence. In the following we discusses the construction, characteristics of the Microcontroller based Obstacle Detection using voice circuitry for visually impaired.

2.1 Ultrasonic Distance meter

A navigation aid for the blind using echolocation principle and ultrasonic sensors have been developed [4].A commercially available, Ultrasonic Sensor the Sona Switch 1700 (Electronic Design and packing, Livonia, Michigan) was used to expand the environmental detection range of blind individuals [5] .The power supply to this entire circuit is provided by a 12V rechargeable battery to carry out various actions. An ultrasonic distance meter cancels out the effects of temperature and humidity variations by including a measuring unit and a reference unit. This circuit designed as shown in Fig .1 is used to measure the distance of the object with the help of ultrasonic waves. The 12F675 microcontroller is used to generate the 40 KHz frequency signal. This signal is given to level logic converter (MAX232) in order to convert to TTL(Transistor-Transistor Logic) output pulse to +12v and -12v pulse. Then this pulse is transmitted through ultrasonic transmitter.

2.2 Ultrasonic Transmitter

Ultrasonic transmitter produces ultrasonic waves according to its vibration. The 1 level is given to the upper plate and 0 level to the lower plate. The 1 level is nothing but a 40 KHz frequency and 0 level is anything but the delay time. The ultrasonic sensor accepts only 40 KHz frequency as its input. These sensor waves travel

in space, when interruption is made by the obstacle it gets reflected back. The ultrasonic receiver receives the reflected waves [6].

2.3 Ultrasonic Receiver

An ultrasonic wave of 40 KHz frequency is generated by the oscillator .The generated frequency is transmitted through the ultrasonic transmitter sensor which it is subjected back when an obstacle is placed. The reflected back frequency is received in the ultrasonic receiver sensor. Thus with respect to the time the reflection of the noise to the distance that is received. The received output is amplified, which is converted to voltage. This voltage output which is analog is given to ADC which converts the analog to 8 bit Digital output .The 8 bit data is interfaced with microcontroller through its I/O Lines .The data is thus monitored in the Display. The data is nothing but the distance travelled by the ultrasonic sensor. The blind guidance systems use ultrasound because of its immunity to the environmental noise , relatively inexpensive and also ultrasound emitters and detectors are small enough to be carried without the need for complex[7].

2.4 MAX232 (Logic Level Converter)

MAX232 is the voltage level converter. It converts voltage level from CMOS (microcontroller output is CMOS) to TTL (PC output is TTL) and vice versa, but it drives voltage level from one to another voltage, hence it is also called as voltage driver IC. MAX232 has wide applications in Battery-Powered systems, Modems, Computers etc.

2.5 12F675

12F675 is a PIC micro controller that has one analog comparator. The PIC12F675 has four analog inputs, multiplexed into one sample and hold circuit. The output of the sample and hold is connected to the input of the converter. The converter generates a binary result and stores the result in the 10-bit register.

2.6 Data EEPROM Memory

EEPROM stands for Electrically Erasable Programmable Read-Only Memory and is a type of non-volatile memory used in computers and other electronic devices to store small amounts of data that must be saved when power is removed. The PIC12F675 device has 128 Bytes of data EEPROM with an addressing range from 0h to 7h. The EEPROM data memory allows byte read and write.

2.7 APR9600

The APR9600 is a low cost, high performance sound record/replay IC ,incorporating flash analogue storage technique. The device offers true single-chip voice recording, non-volatile storage, and playback capability for 40 to 60 seconds. The IC is non –volatile, recorded sound retained even after the power supply is removed from the module. The voice circuitry designed to record the voice signal. During sound recording, sound is picked up by the microphone. A microphone pre- amplifier amplifies the voltage signal from the microphone. The constructed obstacle device sense the obstacles at every five inches and simultaneously voice signal will be produced.

2.8 Microcontroller

The heart of the micro controller is the CPU core. AT89C51 is the 40 pins, 8 bit Micro controller manufactured by Atmel group. It is the flash type reprogrammable memory. Advantage of this flash memory is we can erase the program within few minutes. It has 4kb on chip ROM and 128 bytes internal RAM and 32 I/O pin as arranged as port 0 to port 3 each has 8 bit bin. It is a low-power, high-performance CMOS 8-bit microcomputer with 4K bytes of Flash Programmable and Erasable Read Only Memory (PEROM). The pin diagram of AT89C51 is shown in Fig.2.

2.9 SMCL - LCD

AT89C51 is the 40 pin, 8 bit Microcontroller manufactured by Atmel group. It is the flash type reprogrammable memory. Advantage of this flash memory is we can erase the program within few minutes. It has 4kb on chip ROM and 128 bytes internal RAM and 32 I/O pin as arranged as port 0 to port 3 each has 8 bit bin .Port 0 contain 8 data line(D_O-D_7) as well as low order address line(A_O-A_7). Port contain higher order address line (A_8-A_{15}). Port 3 contains special purpose register such as serial input receiver register SBUF, interrupt INT0,INT1 and Timers T_0 , T_1 many of the pins have multi functions which can be used as general purpose I/P pins (or) Special purpose function can be decided by the programmer itself. The pin diagram of SMCL-LCD is shown in Fig.3.

2.9.1 Crystal

The heart of the micro controller is the circuitries which generate the clock pulse. Then micro controller provides the two pins XTAL 1, XTAL 2 to correct the external crystal resonator along with capacitor. The crystal frequency is the basic clock frequency of the microcontroller.

2.9.2 Reset

The memory location for 89C51 is 0000H to 0FFFH. Whenever switch on the supply the memory location starts from 0000H.The 89C51 micro controller provide 9th pin for Reset Function .Here the reset circuitry consists of 10Mf capacitor in series with 10K resister. When switch on the supply the capacitor is changed and discharged gives high low pulse to the 9th pin through the 7414 inverter. Here we interface LCD display to microcontroller via port 0 and port 2. LCD control lines are connected in port 2 and Data lines are connected in port 0.

2.9.3 LCD

Liquid Crystal Display has 16 pins in which first three and the 15th pins are used for power supply. 4th pin is RS (Register Selection) if it is low data and if it is high command will be displayed. 5th pin is R/W if it is low it performs write operation. 6th pin act as enable and remaining pins are data lines.

Microcontroller based obstacle detection device for Visually Impaired is shown in the Fig.4.
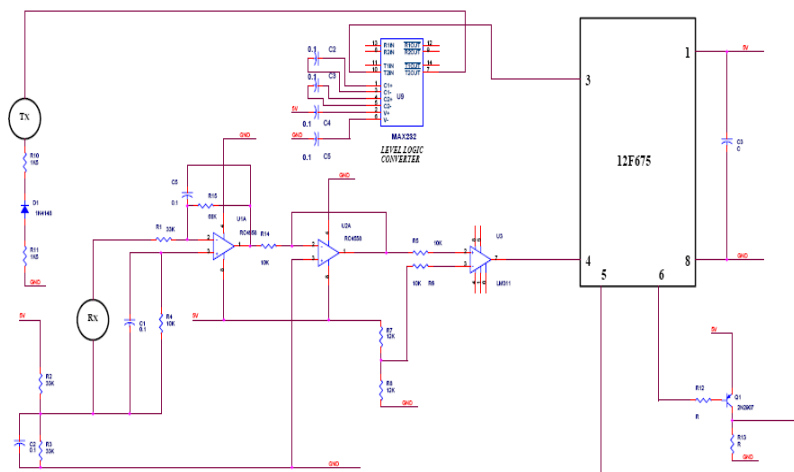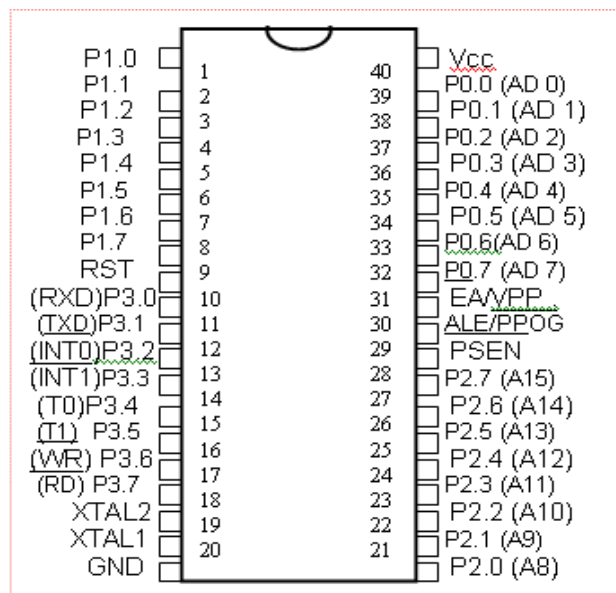

Fig .1 Ultrasonic Distance Measurement

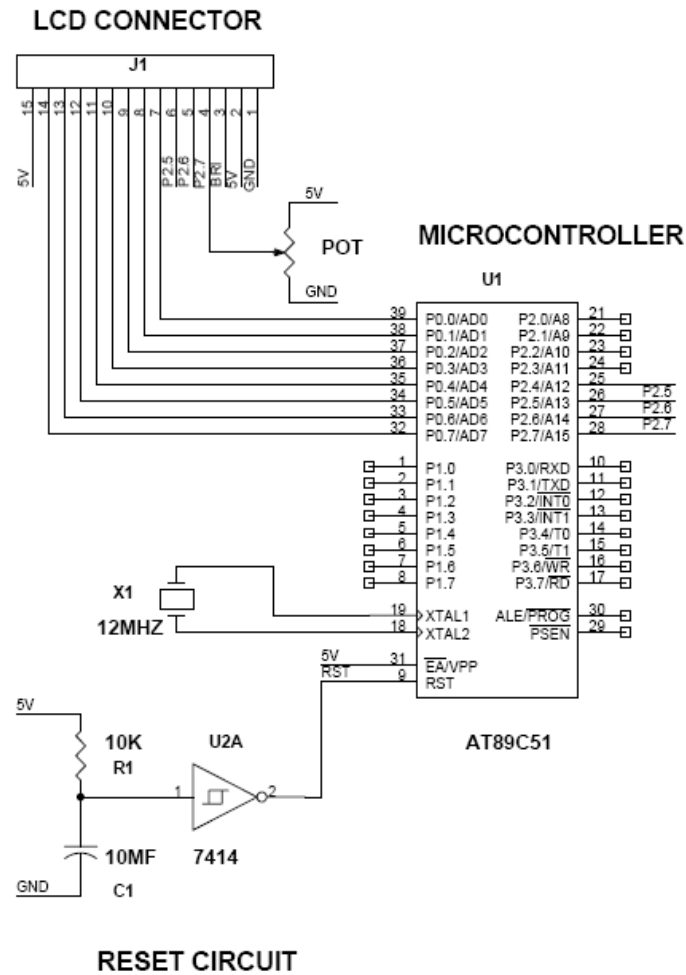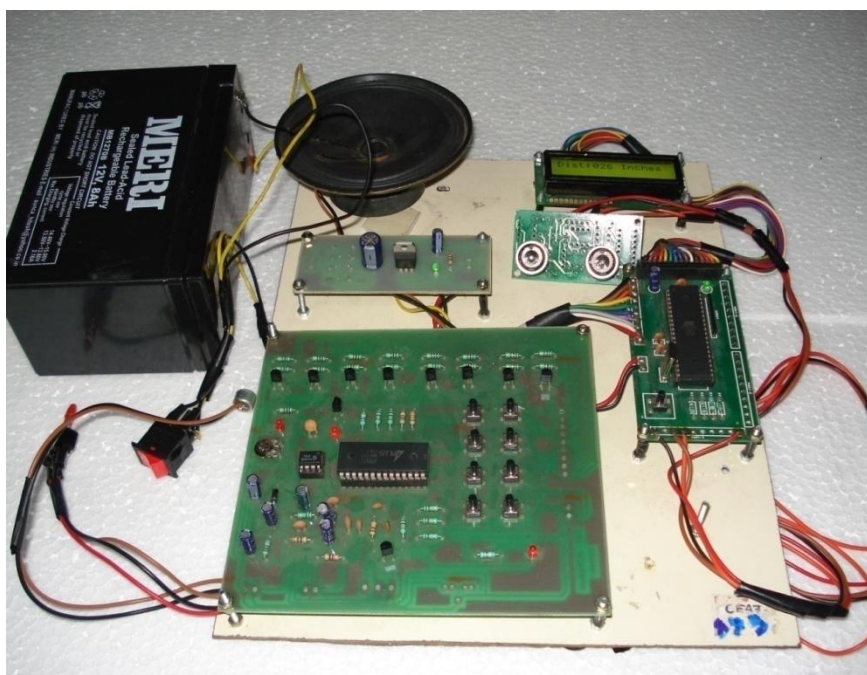Fig. 2 Pin diagram of AT89C51-Microcontroller

Fig. 3 SMCL-LCD

Fig. 4 Microcontroller based obstacle detection device for Visually Impaired

III.   Result and Discussion

To help the visually impaired sense obstacles in the linear path, obstacle detection device using ultrasonic transmitter has been designed. An ultrasonic wave of 40 KHz frequency generated by the oscillator is transmitted through the ultrasonic transmitter which when hits the obstacle reflects back the frequency wave and it is received in the ultrasonic receiver sensor. The received output is amplified and converted as analog voltage. An analog to digital converter converts the analog output to a digital output and is shown in the LCD display. The output seen in the display gives the distance of obstacle in inches and simultaneously sound signal in the form of voice is produced starting from five inches to the maximum of forty inches. This voice signal helps the visually impaired to identify the obstacle in their linear path.

Sound intensity of the voice signal generated by APR9600 was measured using sound level intensity meter (LUTRON, make).The measured sound intensity (dB) for various distance of obstacles, is found to be slightly varying and the sound intensity output lies between 90 and 100 dB. This output intensity is higher than the noise level of normal environment and hence the voice signal will caution the blind in all places except in heavy traffic congested roads and industries with noisy machineries.

IV.   Conclusion

Visually impaired persons encounter serious difficulties in conducting an independent life, which are inherent to the nature of their impairment. In particular, orientation and navigation in unknown environment seems impossible without an external help. The constructed obstacle detection device for the visually impaired using voice signal   found to be highly useful and comfortable for totally blind as they cannot move here and there without the aid of a cane or assistance. The most popular method of obstacle detection is the transmission of ultrasonic waves and the decoding of received reflections to sense the presence of an obstacle in the travel path. Thus the navigational devices are referred as clear path indicators. The constructed obstacle detection device is a light weight system and can be easily worn by visually impaired person.

REFERENCES

[1]   J .P Singh, Technology for the blind concept &   Context (Kanishka,2003).
[2]   Alvaro Hernandez, Jesus Urena, Manuel Mazo, Juan J Garcia, Ana Jimenez and Fernando J Alvarez, Reduction of blind zone in Ultrasonic   transmitter/receiver transducer, Sensor& Actuators-A Physical sensor, 133, 2007,96-103
[3]   K Svendsen, The use of light rail or light rapid transit system by individuals with severe visual impairment, Journal of visual Impairment & Blindness, 88(1), 1994, 69-74.
[4]   Aziz, Izzatdin Abdul Mahamad, Sajee Mehat, Mazlina Samiha, Blind echolocation using Ultrasonic sensors, Information technology, 4 2008, 1-7.
[5]   D .T Batarseh, T .N Burcham, G .M McFadyen, An ultrasonic ranging system for the blind, Biomedical Engineering Conference, 4,1997,411.
[6]   J .Kumar, Moorthy, S. Babu , Vasudevan, Engineering physics ,(vijay Nicole imprints,2006).
[7]   Shruti Dambhare and A. Sakhare,Smart stick for Blind: Obstacle Detection, Artificial vision and Real-time assistance via GPS, Proc. 2nd National Conference on Information and Communication Technology (NCICT),2011, 31.

International Journal of Modern Engineering Research (IJMER)

Contents :

Robust and Radial Image Comparison Using Reverse Image Search

Miss. G. Kavitha[1], Mr. E. Gurumoorthi[2]

[1, 2](MCA Student, Assistant Professor, Dept. of MCA, Sri Manakula Vinayagar Engineering College, Pondicherry-605106)

Abstract: *This paper proposed a robust, radial and effective content-based image retrieval (CBIR) or query by image content (QBIC) or content based visual information retrieval (CBVIR) approach, which is based on colour, texture and shape features. Due to the enormous increase in image database sizes, as well as its vast deployment in various applications, the need for CBIR development arose. In this proposed approach, image attributes like image name, keywords and meta data are not used to compute image similarity and image retrieval. So, concept based image retrieval is not used. If an image is given as an input query and the output is based on the input image query, it is called as reverse image search. So, images can be searched based on their contents (pixels) but not by their keywords. It is difficult to measure image content similarity due to visual changes caused by varying viewpoint and environment. In this paper, a simple and efficient method to effectively measure the content similarity from image measurements is proposed. The proposed approach is based on the three well-known algorithms: colour histogram, texture and moment invariants. It ensures that the proposed image retrieval approach produces results which are highly relevant to the content of an image query, by taking into account the three distinct features of the image and similarity metrics based on Euclidean measure. Colour histogram is used to extract the colour features of an image. Gabor filter is used to extract the texture features and the moment invariant is used to extract the shape features of an image. It also uses fuzzy similarity measures.*

Keywords: *reverse image search, concept based image retrieval, content based image retrieval, Euclidean measure, histogram, Gabor filter, moment invariant.*

I.   Introduction

In recent years, the availability of large, unordered image collections on the Internet has given rise to a need for robust, efficient, effective and scalable image retrieval systems. With the development of digital image processing technology, it has become imperative to find a method for efficient image retrieval. One of the most interesting (comparatively) new methods currently being developed around the web revolves around the idea of using images as a basis for search queries. Using an image as an input query and getting effective results by analyzing its contents is still under research in image processing. Image processing is a method to convert an image into digital form and perform some operations on it, in order to get an enhanced image or to extract some useful information from it. Image processing is also a form of signal processing for which the input is an image, such as a photograph or video frame; the output of image processing may be either an image or a set of characteristics or parameters related to the image.

In the traditional methods, searching, comparing and retrieving of images are based on the text attributes such as keywords, metadata related to that image. In our proposed system, the visual contents of an image such as colour, texture and shape are analysed to produce effective results. Content based image retrieval method is used to analyse the image contents. Content based methods are still under development.

Different researchers proposed various algorithms in order to address the problem of image retrieval using content based approaches. Mostly, those algorithms rely on one algorithm and ignore the existence of others. Approaches based on one specific algorithm (ie) colour, texture and shape can work effectively only on specific types of images. When different types of images are input to these systems their performance is degraded. For example, approaches based on colour histogram take into account only the visual contents relating to colours and ignore shape and texture. Similarly, approaches based on shape perform reasonably well when dealing with the shape of images without taking into account colour histogram and texture but do not produce effective output for all set of images.

The proposed system will take into account all the visual features of an image like color, texture and shape. So, the output produced by the system is efficient and effective. Typically, a large-scale retrieval system focuses on the following: (i) image representation, (ii) image similarity measure and (iii) refinement of retrieval results.

Analyzing the contents of an image is still under development. In Google images, mostly people specify text or keywords to retrieve images from the database. In June 2011, searching and comparing by images contents is permitted. The user can search by an image in Google images. Google images will analyse the contents of an image query and produce the desired results which contains the information about the image and also specify in which websites that image is available. But in Yahoo images, Bing images and Ask images, searching and comparing by images contents is not permitted and the user can specify only the text attributes to retrieve the images. This shows that using the image as an input query is a new emerging method. The following table shows different image retrieval systems and their characteristics.

IMAGE RETRIEVAL SYSTEM	INPUT		OUTPUT
	Text	Image	
Google Images	Allowed	Allowed	A Set of Related Images
Yahoo Images	Allowed	Not Allowed	A Set of Related Images
Bing Images	Allowed	Not Allowed	A Set of Related Images
Ask Images	Allowed	Not Allowed	A Set of Related Images

II. Existing System

In the existing system, the input can be either text or metadata or colour. If the user specifies an input, then the input is compared with the image database. Based on the input, the results are retrieved from the database. The output will contain the image which has attributes similar to the input. Images are not compared by its contents (pixels). The images are compared by its attributes like text. So, the existing system uses Concept based or Description based or Text based image indexing/retrieval. The existing system will not consider the major characteristics of an image like colour, texture and shape. Only the colour is considered.

The existing system can be defined as follows:
- Compare by text
- Compare by colour
- Compare by text and colour

1. Compare by Text:

It is predominantly and traditionally used method to search, compare and retrieve images from the database. In this method, images are searched and compared based on the attributes of the image. The attributes of the image include image name, identifier (ID), keywords related to that image, metadata, title, subject. This method retrieves all the images from the database whose attributes are similar to the input query and those images are displayed to the user. This method works well with any set of image database.

2. Compare by Colour:

In this method, the user can specify only the colour as an input. The results will be produced based on the colour given as an input. If the images contain the specified colour, then it is included in the output. The user cannot specify the image attributes like keywords, metadata as an input.

3. Compare by Text and Colour:

In this method, both text and colour are given as an input query. The output will be produced based on the user's input. There are two approaches.

a) Compare by Text and Single Colour:

In this method, text and colour are given as an input. Multiple colours cannot be specified. Only single color can be specified.

b) Compare by Text and Multiple Colours:
In this method, text and multiple colours are specified as an input. The results will be based on the text and colours specified by the user.

2.1. Problems Related With Existing System

➢ If we don't know any details or description about an image, then we cannot use the existing system since it uses Description based image indexing or retrieval.
➢ Reverse image Search is not used so image cannot be given as an input query. Only the attributes of an image like text or keywords can be given as an input.
➢ Major characteristics of an image like colour, texture and shape are not considered while producing the output.
➢ The pose and expressions of a person in an image are not considered in the existing system.
➢ Similar images cannot be produced.

III. Proposed System

In the proposed system, Reverse by Image Search method is used. In this method, images are searched by its contents (pixels). Since the contents of an image are used for comparison, it can be called as Content based image retrieval (CBIR) or Content based Visual Information Retrieval (CBVIR).

Since the image is given as an input query, CBIR can also be called as Query by Image Content (QBIC). CBIR does not use the attributes of an image like keywords or metadata for comparison and producing the desired results. CBIR system mainly focuses on the major characteristics of an image like colour, texture and shape. A desirable output is produced from the large collection of images stored in the database based on their visual contents.

Image is captured and it is given as an input. If the image is taken in an improper light source which is because of environmental factors like fog or snow or at midnight, the image may not be clear and quality may be reduced and it may obscure the details of an image. In this case, image preprocessing can be done. The brightness of an image can be adjusted. To increase or reduce the brightness of an image, all the values of pixels must be changed. To increase the brightness, add some constant value to each and every pixel. To decrease the brightness. Subtract some constant value from each and every pixel. This will enhance the contents of an image and improve its quality and resolution can be increased.

This enhanced input image is used by the system to extract visual features from the image. The visual features include shape, colour and texture. These features are examined in order to search, compare and retrieve similar images from the image database.

The similarity of visual features between query image and each image in a database is calculated based on their distance by comparing the feature vectors of two images. To calculate the similarity, an image distance measure is used which uses the visual feature of the images, If the image distance measure is 0, an exact match of input image is found in the image database. If the value is greater than 0, an exact match is not found and only similar images are retrieved and displayed. The image retrieval system displays images, as the result of an image query that have the closest similarity and also displays similar images and the details of the image will also be displayed.

If the input image matches exactly with the image stored in the database then that image will be retrieved and displayed to the user. Even though if the input image does not match exactly with the input image, similar images will be displayed.

Fig 1: Overall Representation of the Proposed Approach
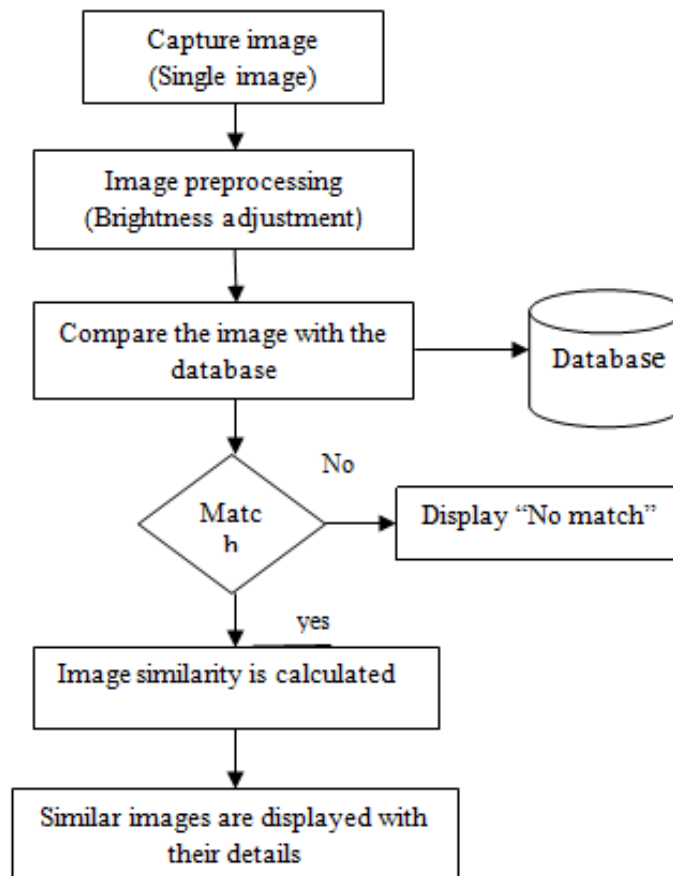
3.1. BUILDING BLOCKS OF THE PROPOSED APPROACH
3.1.1 Colour Features

Colour feature is the most commonly used visual feature for image retrieval. Many colour models are available that can be used to represent images such as HSI, HSV and YCbCr. Colours play a major role in human perception. The most commonly used colour model is RGB, where each component represents red, green and blue and these are primary colours. Several millions of colours can be formed by combining primary colours. RGB colour space is based on RGB colour model. This colour space defines how colours are represented as tuples (ordered list) of numbers. Images displayed on monitor are defined in RGB colour space. There are different ways to use

colour for image retrieval purpose such as colour histogram, colour moment and colour coherence. But the most effective method is colour histogram.

Colour histogram is a representation of the distribution of colours in an image. It describes the proportion of colours in each pixel. The colour histogram provides meaningful information for measuring the similarity between two images, as it is robust against object distortion and scaling of the object. Additionally high effectiveness, computational simplicity and low storage requirements possibility makes it best among others. Due to these characteristics, many researchers have started to use histogram based colour image retrieval method.

Colour histogram is used to extract colour from any kinds of image formats like jpeg, bmp, png. Every pixel in an image is basically represented as a point in RGB colour model. This colour point is represented by three values that hold the colour information. Suppose if the extracted colour is red, the RGB values can be 255,0,0. If the colour is violet, the values are 255,0,255 and for white colour, values are 255,255,255.

3.1.2 Texture Features

Texture is another important feature of an image that can be extracted for the purpose of image retrieval. Image texture refers to surface patterns or visual patterns which show granular details of an image. It also gives information about the spatial arrangement of different colours or intensities in an image.

There exist two main approaches for texture analysis. They include structural and statistical approaches. In structural texture approach, the surface pattern is repeated such as floor design that contains the same pattern. In statistical texture, the surface pattern is not regularly repeated in the same pattern such as different flower objects in a picture that normally contains similar properties but not exactly the same

Texture information can be extracted from an image using co-occurrence matrix. Co-occurrence matrix is a popular representation of texture feature of an image. It is constructed based on the orientation and distance between image pixels. Co-occurrence matrix captures the numerical features of a texture using the spatial relations. Numerical features computed from the matrix can be used to represent, compare and classify the textures.

Gabor filters were found to be very effective in texture analysis. Gabor filter is used in various type of applications due to its effectiveness in the area of texture based image analysis.

3.1.3 Shape Features

Shape feature plays a vital role in object detection and recognition. Object shape features provide robust and efficient information of objects in order to identify and recognize them. Shape features are considered very important in describing and differentiating the objects in an image.

Shape features can be extracted from an image by using two kinds of methods: contour and regions. Contour based methods are normally used to extract the boundary features of an object shape. Such methods completely ignore the important features inside the boundaries.

Region-based methods that rely on shape descriptors are normally able to extract both kinds of features: boundary and region. These provide valuable information to represent the shape of an image for feature extraction. Region-based image retrieval methods firstly apply segmentation to divide an image into different regions/segments, by setting threshold values according to the desirable results. On the other hand the boundary of an image can be obtained by applying any edge detection method to an image.

Retrieval Approach

Fig 2: PROPOSED CONTENT BASED IMAGE RETRIEVAL APPROACH
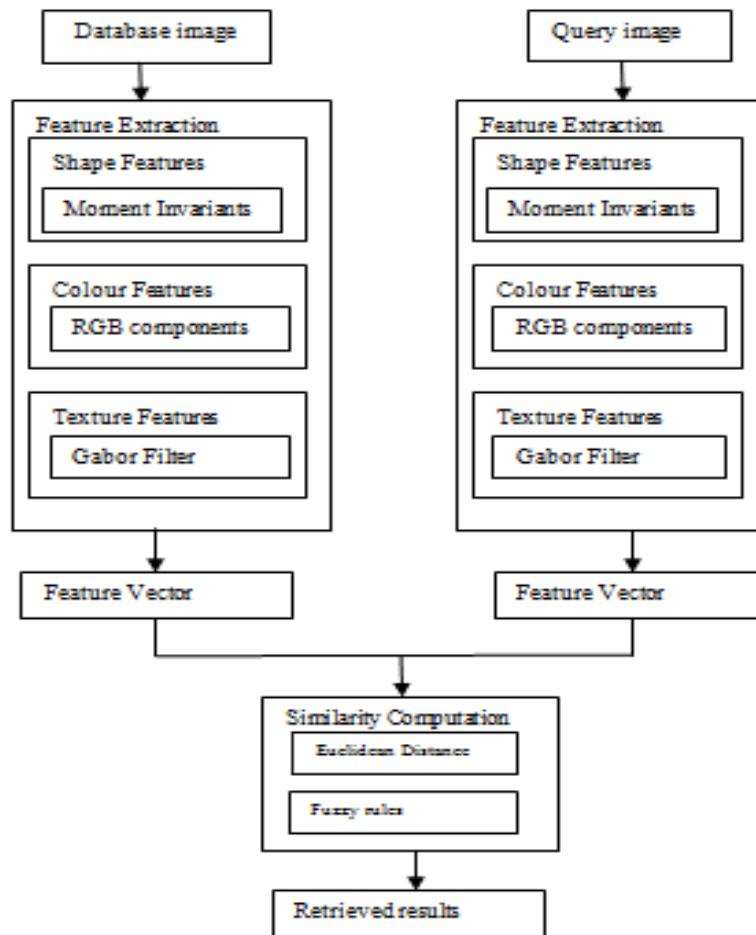
3.2 STEPS INVOLVED IN THE PROPOSED APPROACH

Step 1: An image histogram can be generated as follows:

A digital image is commonly seen as a 2D mapping $I : \mathbf{x} \to v$ from $M \times N$ pixels $\mathbf{x} = [i, j]T$ to values v (where i =1, 2, . . . ,M and j = 1, 2, . . . , N correspond to y-axis and x-axis respectively). Often the values v are discrete intensity values in the range [0–255]. The image histogram is calculated as:

$$h_b = \sum_{i=1}^{M} \sum_{j=1}^{N} \delta_b(i, j), \forall_b = 0, 1, 2 \ldots \quad (1)$$

where $\delta_b(i, j) = 1$ if the v at pixel location [i, j] falls in b, and $\delta_b(i, j) = 0$ otherwise.

Step 2: To extract the texture features:

Step 2(a): A 2D Gabor function consists of a sinusoidal plane wave of some orientation and frequency, modulated by a 2D Gaussian. The Gabor filter in spatial domain is given below:

$$g, \lambda, \theta, \Psi, \sigma, \gamma \, (x, y) = exp\left(-\frac{x'^2 + \gamma^2 y'^2}{2\sigma^2}\right) \cos(2\pi \frac{x'}{\lambda} + \Psi)$$

$$\ldots\ldots (2)$$

where $x' = x \cos(\theta) + y \sin(\theta)$
$y' = y \cos(\theta) - x \sin(\theta)$

In the above equation, wavelength of cosine factor is represented by λ; θ represents the orientation of the normal to parallel stripes of a Gabor function in the degree; the phase offset in degree is represented by Ψ; the spatial aspect ratio which specifies the elliptically of the support of the Gabor function is represented by γ ; and σ is the standard deviation of the Gaussian that determines the linear size of the receptive field.

Step 2(b): When an image is processed by Gabor filter; the output is the convolution of the image $I(x, y)$ with the Gabor function $g(x, y)$ which is
r(x, y) = I(x, y) *g(x, y)   (3)
where * represents the 2D convolution.

Step 2(c): After applying Gabor filters on the image by orientation and scale, we are able to obtain an array of magnitudes
$$E(m, n) = \Sigma_x \Sigma_y \left| G_{mn}(x, y) \right|$$

$$m = 0, 1,...,M - 1; n = 0, 1,...,N - 1 \quad (4)$$

Step 2(d): The following mean μ_{mn} and standard deviation σ_{mn} of the magnitude of the transformed coefficients are used to represent the texture feature of the region:
$$\mu_{mn} = E(m, n)/P \times Q \quad (5)$$

$$\sigma_{mn} = \sqrt{\Sigma_x \Sigma_y (\left| G_{mn}(x, y) \right| - \mu_{MN})^2 / P*Q} \quad (6)$$

where M represents the scale and N represents the orientation.

Step 3: Calculate the descriptions of shape features which are independent of location, orientation and size.

Step 3(a): The 2D moment of order (p +q) of a digital image $f(x, y)$ is defined as

$$m_{p,q} = \Sigma_x \Sigma_y x^p y^q f(x, y) \quad (7)$$
for p, q = 0, 1, 2 where the summations are over the values of the spatial coordinates x and y spanning the image.

Step 3(b): The corresponding central moment is defined as

$$\mu_{pq} = \Sigma_x \Sigma_y (x - \overline{x})^p (y - \overline{y})^q f(x,y) \quad (8)$$

$\overline{x} = m_{10}/ m_{00}, \overline{y} = m_{01}/ m_{00}$
where $\overline{x}, \overline{y}$ are called the centre of the region.

Step 3(c): The normalized central moment of order (p+q) is defined as

$$\eta_{p,q} = \mu_{p,q} \,/\, \mu_{0,0}^{\gamma} \qquad\qquad (9)$$

for p, q = 0, 1, 2,... where $\gamma = [(p+q)/2]+1$.

Step 4: To calculate the similarity, we use Euclidean distance between two feature vectors as follows.

$$ED(M^k, M^t) = \sqrt{\sum_{i=1}^{n}(M_i^k - M_i^t)^2} \qquad\qquad (10)$$

where M^k and M^t are image query and image database respectively, i is a feature range. Closer distance represents the higher similarity between images.

3.2.1 Fuzzy Similarity Measure

We use fuzzy heuristics to measure similarity between the query image and the database images in order to retrieve and display relevant or similar results to the user query. There are three types of preferences that are taken into account while checking the similarity between images. The first priority is given to the shape features, as shape of an image is not easily affected by external factors, and also it is invariant to the rotation, translation and orientation The second priority is given to the colour features, as these features are invariant to the rotation and translation. The third priority is given to the texture features. By defining these criteria along with the fuzzy rules, we assume that better results can be achieved using our proposed approach. The Mamdani fuzzy inference method is used to perform fuzzy rules in our proposed approach.

X, Y and Z are three visual features of images that have been retrieved using Moment Invariants, Histogram of images(Red, Green, Blue and Intensity) and Gabor wavelet. Based on the Euclidean distance algorithm we find the images that have high similarity between query and database image. After obtaining the relevant images to the query image, we need to find common images between X, Y and Z set of images. The common set of images are considered the most relevant images. Commonality is measured using the below criteria.

X = Shape features are used to calculate the distance between query and database image
Y= Colour features are used to calculate the distance between query and database image
Z= Texture features are used to calculate the distance between query and database image
S= Image similarity

Several fuzzy rules can be used: If shape is low and colour is low and texture is low then similarity is high. If shape is low and colour is high and texture is low then similarity is medium. If shape is high and colour is low and texture is high then similarity is low. If shape is high and colour is high and texture is low then similarity is low.

3.3 ADVANTAGES
The advantages of the proposed system are discussed below:

➢ The proposed system can be used if we don't know any details or description about an image since it uses Content based image retrieval. Only the contents of an image are analyzed to produce effective results and the text attributes like metadata, keywords are not used.
➢ An image can be rotated to several angles and it can be given as an input. But still the image database contains the images which are not rotated. The rotated input image is compared with the database and results are produced. Suppose image i1 is stored and it is rotated to 180 degree and given as an input query. Even though input i1 is rotated and it differs from the database image, both are similar according to our system.
➢ Cropped versions of images also work in our proposed system. Suppose an image i2 contains three persons and stored in the database. Now image i2 is cropped and it contains only one person and given as an input. Even though both images differ, our proposed system will identify the uncropped image stored in the database and gives the effective results.
➢ Even though if the background colour of an input image differs from the images stored in the database, our system will produce effective results. Suppose the background colour of an image i2 stored in the database is blue. In the input query, it's background colour is changed to some other colour say white, then also our system will produce better results.

➢ The pose and expressions of a person in an image may vary from time to time but this will not affect the effective output produced by the system. The pose and the expression in the input image may vary from the pose and the expression of the images stored in the database.
➢ Location, orientation and size of the image may not affect the output produced by the system.
➢ This system works well on black and white, colour and grayscale images.
➢ Image can be given as an input query. The output will be produced based on the input query since reverse image search is used.
➢ Images which are similar to input can be produced as an output. If there is an exact match that image will be displayed or similar images will be displayed.
➢ This system accepts all kinds of image formats (jpeg, png, bmp) and dimensions (103*151, 184*274 etc). It works well for some gif images.
➢ This system is fully automatic and does not require any human intervention to extract the visual features of an image and to produce an effective output.
➢ To find information about unidentified products and other objects.

3.4 APPLICATIONS
The Proposed system has several applications. Each of the applications is discussed below:

➢ Crime prevention: Image recognition systems are used by police forces to find the criminals involved in a particular case.
➢ Medical Diagnosis: Using CBIR in a medical database of medical images to aid diagnosis by identifying similar past cases.
➢ Intellectual Property: Trademark image registration, where a new candidate mark is compared with existing marks to ensure no risk of confusing property ownership. It enforces compliance with the copyright regulations.
➢ Military: This system can be used to identify whether a person belongs to Indian army or not. This is also used to find information about the destruction weapons used by the enemy countries.
➢ Architectural and Engineering and Interior design: Reverse image search can be used to find what new technologies are used in those designs
➢ Cultural heritage: We can find information about a snapshot of the famous traditions followed in foreign countries.

IV. Results And Conclusion

In this paper, an effective and efficient image retrieval approach is proposed. CBIR is an active research topic in image processing, pattern recognition and computer vision. This approach is based on the three well known algorithms: colour histogram, texture and moment invariants. The colour histogram is used to extract the colour features. Gabor filter is used to extract the texture features and moment invariant is used to extract the shape features of an image. It ensures that the proposed image retrieval approach produce results which are highly relevant to the content of query image, by taking into account the three distinct features of the image and similarity metrics based on Euclidean measure. Fuzzy similarity measures are used to find the similar images.

V. Future Enhancements

In this proposed system, only one image is captured and it is given as an input. Based on the input query, the desired results are produced. This project can be extended as specified below:

➢ Multiple images of a person can be captured either through laptop camera or digital camera or phone camera.
➢ The quality of those images can be affected by several reasons like environmental factors such as rainfall, fog or snow and movement of objects and usage of low resolution cameras. These factors obscure the image details and create noise in the image. In this case, Image preprocessing can be done to all the images to enhance their resolution.
➢ After image preprocessing, face accuracy is calculated. Face accuracy determines which image has clear and accurate face in a maximum level.
➢ Among the multiple images, we can select an image with maximum face accuracy and it can be given as an input.
➢ Then the input query is compared with all the images in the database and similarity is calculated and similar images are produced as output with their details.

REFERENCES

[1]   Datta Ritendra, Joshi Dhiraj, Li Jia, Wang James Z. Image retrieval: ideas, influences, and trends of the new age. ACM Computing Surveys 2008;40(2):1–60.

[2]   Samuel Rota Bulo, Massimo Rabbi, Marcello Pelillo, Content based image retrieval with relevance feedbacks using random walks, Elsevier Ltd, March 2011, 2109-2122.

[3]   Miguel Arevalillo-Herraez, Francesc J. Ferri, Juan Domingo, A naïve relevance feedback model for content-based image retrieval using multiple similarity measures, Elsevier Ltd, August 2009, 619-629.

[4]   Panagiotis Sidiropoulos, Stefanos Vrochidis, Ioannis Kompatsiaris, Conent based binary image retrieval using the adaptive hierarchical density histogram, Elsevier Ltd, September 2010, 739-750.

[5]   Chung-Lin Huang, Dai-Hwa Huang, A content based image retrieval system, Image and Vision Computing, 149-163.

[6]   Kashif Iqbal, Michael O. Odetayo, Anne James, Content based image retrieval approach for biometric security using colour, texture and shape features controlled by fuzzy heuristics, November 2011, 1258-1277.

[7]   Yohan Dupuis, Xavier Savatier, Jean-Yves Ertaud, Pascal Vasseur, Robust Radial face detection for omnidirectional vision, IEEE Trans on Img Processing, Vol 22, No; 5, May 2013, 1808-1821

[8]   Guoyong Duan, Jing Yang, Yilong Yang, Content based image retrieval research, ICPST 2011, 471- 477.

[9]   K. Arthi, J. Vijayaraghavan, Content Based Image Retrieval Algorithm using Colour Models, IJARCCE, Vol 2, Issue 3, March 2013.

[10] Kobus Barnard, Nikhil V. Shirahatti, A method for comparing content based image retrieval methods

[11] Zu-Chuen Lu, Chang Chin-Chen. Color image retrieval technique based on color features and image bitmap. Information Processing and Management 2007;43(2):461–72.

[12] W.I. Grosky, Image Retrieval-existing Techniques, Content-based (CBIR) Systems, Department of Computer and Information Science, University of Michigan-Dearborn, Dearborn, MI, USA, 2010.

[13] Chuen Horng Lin, Rong-Tai Chen, Yung-Kuan Chan,A smart content-based image retrieval system based on color and texture feature, Image and Vision Computing 27 (2009) 658–665

Simulation of Direct Torque Control of Induction motor using Space Vector Modulation Methodology

Arpit S. Bhugul[1], Dr. Archana G. Thosar[2]

[1, 2] *(ME Student, Associate Professor & Head, Electrical Engineering Department, Government College of Engineering, Aurangabad, India)*

Abstract: *This paper presents simulation of Direct Torque Control (DTC) of Induction Motor using Space Vector Modulation (SVM). Direct Torque Control is a control strategy used for high performance torque control of Induction Motor. This SVM based DTC technique reduces torque ripple and improves torque response. The performance is explained using simulation in MATLAB environment. Result of the simulation done in the paper shows improvement in flux and torque. These results verifies the merits of DTC- SVM over conventional Direct Torque Control technique.*

Keywords: *About DTC, SVM, Stator flux, Flux error, Torque error.*

I. LIST OF SYMBOLS

IM	Induction Motor
DTC	Direct Torque Control
SVM	Space Vector Modulation
Hz	Hertz
kW	kilo-Watt
VSI	Voltage Source Inverter
P	Number of pair poles
T_e	Electromagnetic Torque
R	Resistance
L	Inductance
J	Inertia
T	Torque
Ω	Ohm
ω_s	Stator Angular Speed
ω_r	Rotor Angular Speed
ψ	Flux Linkage
α	Angle between stator flux & Rotor flux
H	Hysteresis Band
IGBT	Insulated Gate Bipolar Transistor

II. INTRODUCTION

Direct Torque control (DTC) for induction motor was introduced about thirty years ago by Japanese and German researchers Takahashi and Noguchi is considered as an alternative to the field oriented control (FOC) or vector control techniques. These two control strategies are different on the operation principle but their objectives are the same.

Direct torque control is receiving wide spread attention in the recent literature [3], [4]. It minimizes the use of machine parameters [5], [6]. Direct Torque Control (DTC) is one of the excellent control strategies of torque control/ speed control in induction machine. This uses the hysteresis band to control the flux and torque of the machine directly. When the stator flux falls outside the hysteresis band, the inverter switching stator changes so that the flux takes an optimal path toward the desired value [5], [6]. The name direct torque control is derived from the fact that on the basis of the errors between the reference and the estimated values of torque and flux it directly controls the inverter states in order to reduce the torque and flux errors within the prefixed band limits [7], [8].

This paper describes simple & effective MATLAB simulation of direct torque control of Induction Motor using Space Vector Modulation. The induction motor model, principal of space vector modulation technique, advantages of DTC SVM are explained. The results of this simulation is explained at the end

III. INDUCTION MOTOR MODEL

The following equations written in terms of space voltage vector in a stationary reference frame describe the dynamic behavior of an induction motor

3.1 Voltage Equation

$$\vec{V_s} = R_s \vec{I_s} + \frac{d}{dt}\vec{\psi_s} \dots\dots\dots\dots\dots\dots \quad (1)$$

$$\vec{V_r} = 0 = R_r \vec{I_r} + \frac{d}{dt}\overline{\psi_r} - j\omega_r \overline{\psi_r} \dots\dots\dots\dots \quad (2)$$

Where

$\vec{V_s} = [V_{ds} \quad V_{qs}]^T$ = Space vector of stator voltage,

$\overline{\psi_s} = [\psi_{ds} \quad \psi_{qs}]^T$ = Stator Flux Vector

$\overline{\psi_r} = [\psi_{dr} \quad \psi_{qr}]^T$ = Rotor Flux Vector

$\vec{I_s} = [I_{ds} \quad I_{qs}]^T$ = Stator Current Vector

$\vec{I_r} = [I_{dr} \quad I_{qr}]^T$ = Rotor Current Vectors

$(R_s R_r)$ and $(L_s L_r)$ are respectively the stator & rotor resistance and inductance , L_m is mutual inductance, ω_r is motor angular speed in electrical rad/sec.

3.2 Torque Equations

The torque equation for induction machine can be represented by in vector form as,

$$T_e = \frac{3}{2}\frac{P}{2}\overline{\psi_s}\,\overline{I_s} \dots\dots\dots\dots\dots\dots\dots\dots \quad (3)$$

In this equation, $\overline{I_s}$ is to be replaced by rotor flux $\overline{\lambda_r}$. In this complex form, $\overline{\lambda_s}$ and $\overline{\lambda_r}$ can be expressed as functions of currents as,

$$\vec{\psi_s} = L_s \vec{I_s} + L_m \vec{I_r} \dots\dots\dots\dots\dots\dots\dots\dots\dots (4)$$

$$\vec{\psi_r} = L_r \vec{I_r} + L_m \vec{I_s} \dots\dots\dots\dots\dots \dots\dots\dots\dots (5)$$

Eliminating $\vec{I_r}$ from equation (5) we get,

$$\vec{\psi_s} = L_m \frac{L_m}{L_r}\vec{\psi_r} + L_s'\vec{I_s} \dots\dots\dots\dots\dots\dots\dots (6)$$

Where,

$$L_s' = L_s L_r - \overline{L_m^2}$$

The corresponding equation of $\vec{I_s}$ is

$$\vec{I_s} = \frac{1}{L_s'}\vec{\psi_s} + \frac{L_m}{L_r L_s'}\vec{\psi_r} \dots\dots\dots\dots\dots\dots\dots(7)$$

Substituting equation (7) in (3) and simplifying yields

$$T_e = \frac{3}{2}\frac{P}{2}\frac{L_m}{L_r L_s'}\overline{\psi_r}\overline{\psi_s} \dots\dots\dots\dots\dots\dots\dots\dots(8)$$

That is magnitude of torque is,

$$T_e = \frac{3}{2}\frac{P}{2}\frac{L_m}{L_r L_s'}|\vec{\psi_r}|\,|\vec{\psi_s}|\sin\propto \dots\dots\dots\dots\dots\dots(9)$$

IV. DIRECT TORQUE CONTROL

DTC provides very fast response with simple control structure and hence this technique is gaining popularity in industries. In DTC, stator flux and torque are directly controlled by selecting the appropriate inverter state. The stator currents and voltages are indirectly controlled hence no current feedback loops are required. Stator fluxes and stator currents enable high dynamic performance even at standstill. The generic DTC scheme for a Voltage source PWM inverter-fed IM drive is shown in Fig.1. The stator flux controller

imposes the time duration of the active voltage vectors, which move the stator flux along the reference trajectory, and the torque controller determinates the duration of the zero voltage vectors which keeps the motor torque in the predefined hysteresis tolerance band. At every sampling time the voltage vector selection block chooses the inverter switching state (SA, SB, SC) which reduces the instantaneous flux and torque errors
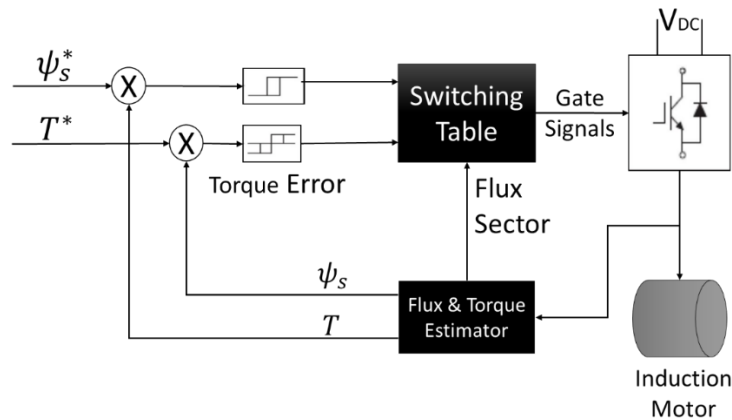

Fig. 1 Basic DTC Scheme

V. DIRECT TORQUE CONTROL OF INDUCTION MOTOR USING SPACE VECTOR MODULATION

Direct Torque control of Induction Motor using Space Vector Modulation is shown in fig2. As shown in this scheme the stator voltage & current parameters are used for calculation or estimation of actual flux & torque. Estimated flux & torque are the compared with reference flux & torque values. Error obtained after comparison is given to the flux & torque controller. The limits of these hysteresis controllers are explained in equations below. Suitable vector is selected from the lookup table as per the values of flux error, torque error & flux sector number. The vector selected is given to the inverter and the converter output is applied to the motor.
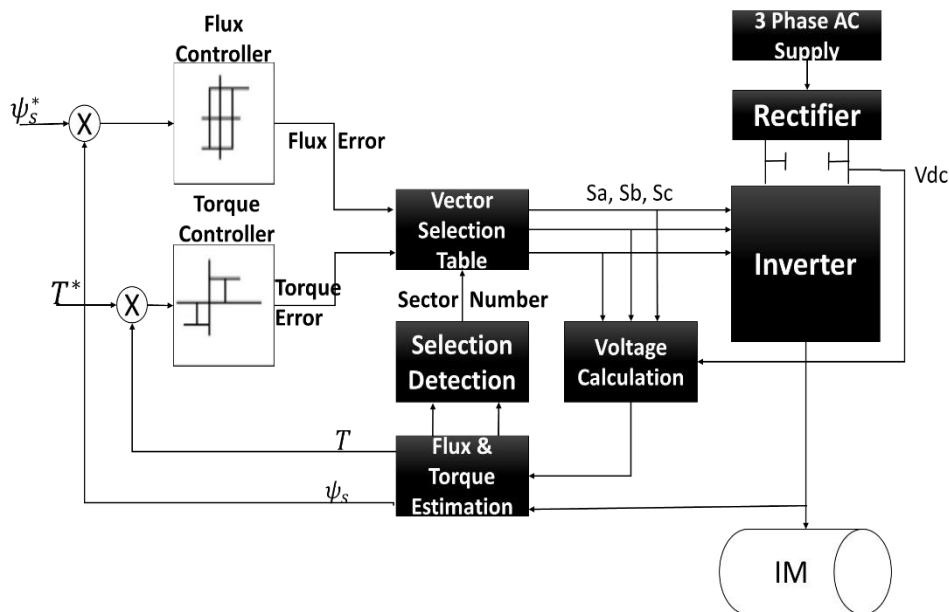

Fig. 2 DTC SVM Scheme

The basic idea of the switching table DTC SVM concept is shown in Fig. 2. The command stator flux Ψ_s^*, and torque T^* values are compared with the actual Ψ_s and T_e values in hysteresis flux and torque controllers, respectively. The flux controller is a two-level comparator while the torque controller is a three level comparator. The digitized output signals of the flux controller are defined as in equation (7) and (8)

$$\psi_{error} = 1, for\ \psi_s < \psi_s^* - H_\psi \ldots\ldots\ldots\ldots(7)$$

$$\psi_{error} = -1, for\ \psi_s < \psi_s^* + H_\psi \ldots\ldots\ldots(8)$$

And those of the torque controller as in equations λλ

$$T_{error} = 1, for\ T < T^* - H_\psi \ldots\ldots\ldots\ldots\ldots(9)$$
$$T_{error} = 0, for\ T = T^* \ldots\ldots\ldots\ldots\ldots(10)$$
$$T_{error} = -1, for\ T < T^* + H_\psi \ldots\ldots\ldots\ldots\ldots(11)$$

where 2HΨ is the flux tolerance band and 2Hm is the torque tolerance band. The digitized variables Ψ, Te and the stator flux section (sector) N, obtained from the angular position
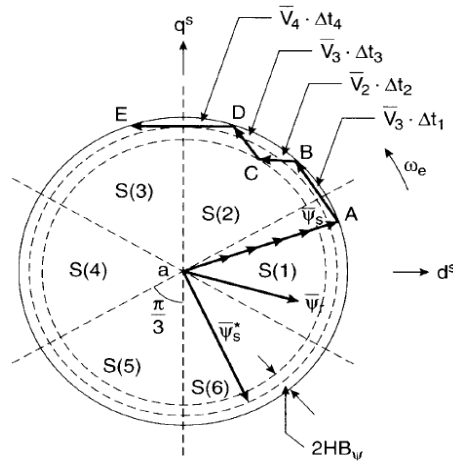

Fig. 3. Trajectory of stator flux vector in DTC Control
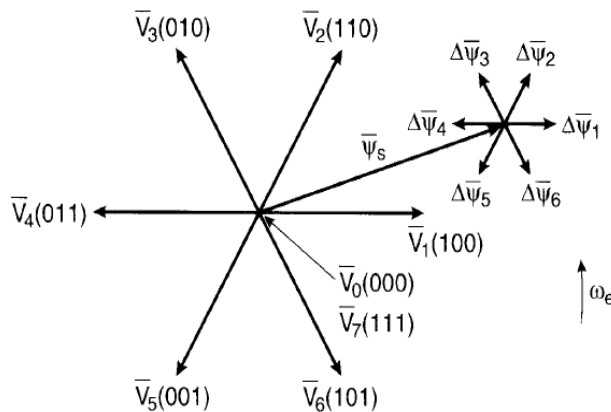
Fig.4. Inverter Voltage vectors and corresponding stator flux variation in time Δt

The angular position flux vector can be calculated using following angle ranges as

- 30< α (1) < 30
30< α (2) < 90
90< α (3) < 150
150< α (4) < 210
210< α (5) < 270
270< α (6) < 330

On the basis of torque and flux hysteresis status and the stator flux switching sector, which is denoted by α, DTC algorithm selects the inverter voltage vector from the table.
The outputs of the switching table are the settings for the switching devices of the inverter. Fig.2 shows the relation of inverter voltage vector and stator flux switching sectors.
Six active switching vectors V1, V2, V3, V4, V5, V6 and two zero switching vectors V0 and V7 determine the switching sequence of the inverter. Depending on inverter switching pulses, PWM is achieved and hence stator voltages and currents are controlled [3]. Therefore to obtain a good dynamic performance, an appropriate inverter voltage vectors Vi (i=1 to 6) has to be selected.

Ψ error	T error	α (1)	α (2)	α (3)	α (4)	α (5)	α (6)
		Sec 1	Sec 2	Sec 3	Sec 4	Sec 5	Sec 6
1	1	V2	V3	V4	V5	V6	V1
	0	V7	V0	V7	V0	V7	V0
	-1	V6	V1	V2	V3	V4	V5
0	1	V3	V4	V5	V6	V1	V2
	0	V0	V7	V0	V7	V0	V7
	-1	V5	V6	V1	V2	V3	V4

VI.   SIMULATION OF DIRECT TORQUE CONTROL OF INDUCTION MOTOR

6.1 FLUX & TORQUE ESTIMATOR
This block is used to calculate values of flux and torque.
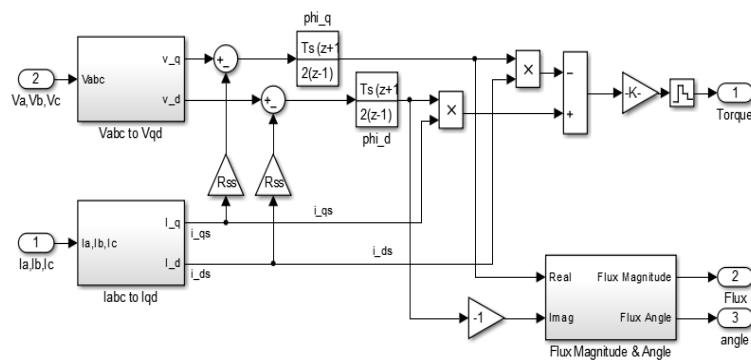
Fig. 5. Flux & Torque estimator

6.2 SPEED CONTROLLER
In this block reference speed & actual speed are calculated. By calculating actual & reference speed, error is given to the PI controller. The PI controller is tuned by setting proper values for proportional and integral constant and these values are found to be $K_P = 1$ and $K_i = 80$. Output of this controller acts as a reference torque.

6.3 FLUX AND TORQUE HYSTERESIS CONTROLLER
After comparison of reference flux & torque with actual flux & torque, errors are calculated in this block. In flux hysteresis controller, two level hysteresis controller is used. The switch ON & OFF limits are 0.02 & -0.02. For calculating torque error, three level hysteresis controller is used.. Outputs of this block are flux & torque error. These errors are given to switching table.
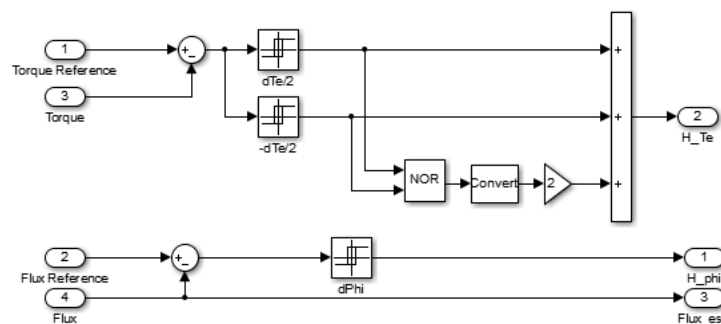

Fig. 6 Flux & Torque Hysteresis Controller

6.4 SWITCHING TABLE

After receiving the error signals from hysteresis controller, suitable voltage vectors from V_0 to V_7 are selected from the look up table shown in section 4. The output of this is given to IGBT inverter. But as IGBT inverter required six pulses such that in each arm both IGBT's should get input inverted from other hence we have inverted the voltage vectors and all six pulses are given to inverter. The delay of 10μs is added between these pulses.

VII. SIMULATION & RESULT

The following model is developed in MATLAB using above mentioned blocks. This model is run for typical conditions of reference speed & applied torque. The flux produced along with reference flux is shown. Switching states of all the IGBT during running are shown. The parameters 3 phase induction motor is shown in following
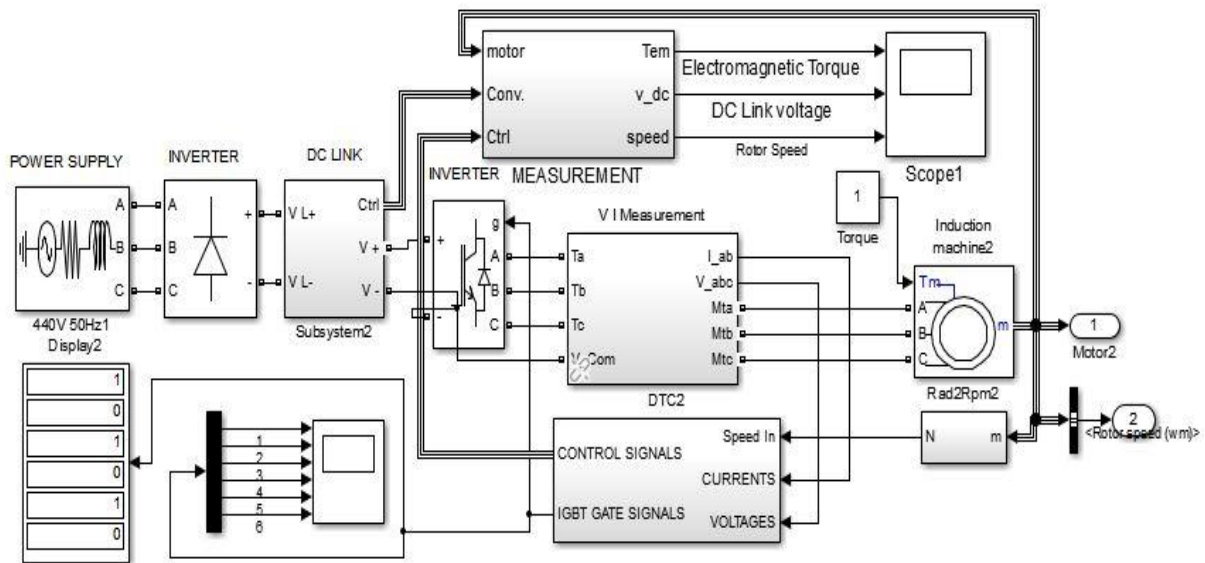

Fig.7. Simulation of DTC -SVM

The same induction motor is also run without any type of torque control strategy. The stator flux pattern is observed and studied. The stator flux with DTC is shown in fig. 8 (a). Another stator flux without any type of control strategy is shown in fig. 8 (b).

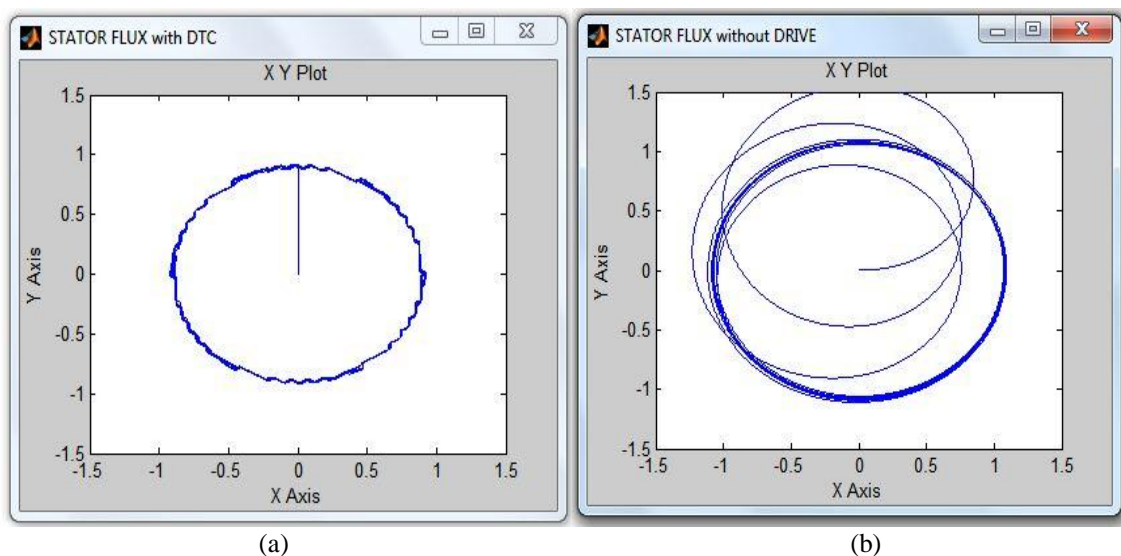
(a)   (b)

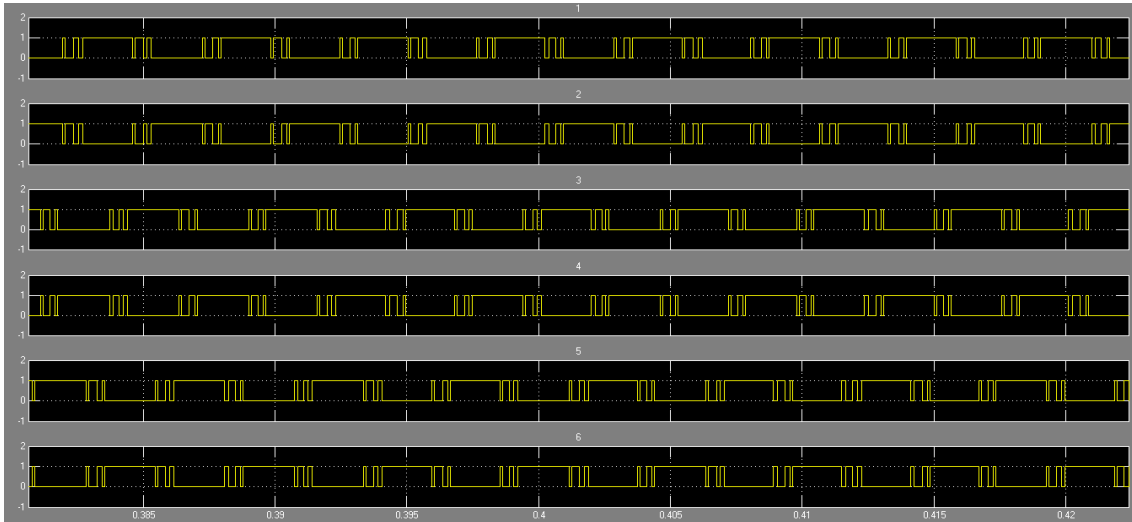Fig. 8 (a) Stator Flux with DTC Drive (b) Stator Flux without DTC Drive

Fig. 9. Switching States of IGBT

The DC Link Voltage is shown below. It is observed that DC link voltage is increase to high value before settling at 580V. The variation is shown in fig.10.
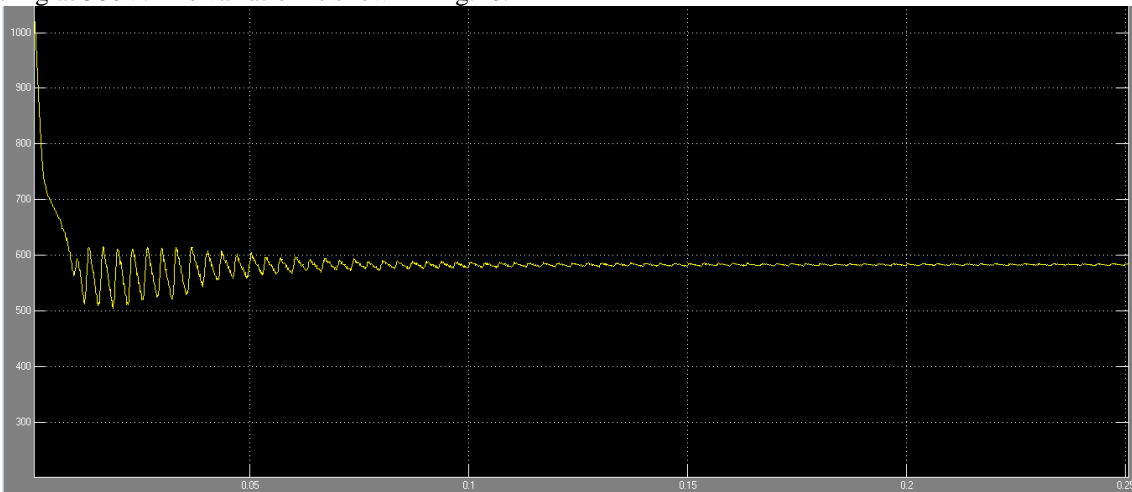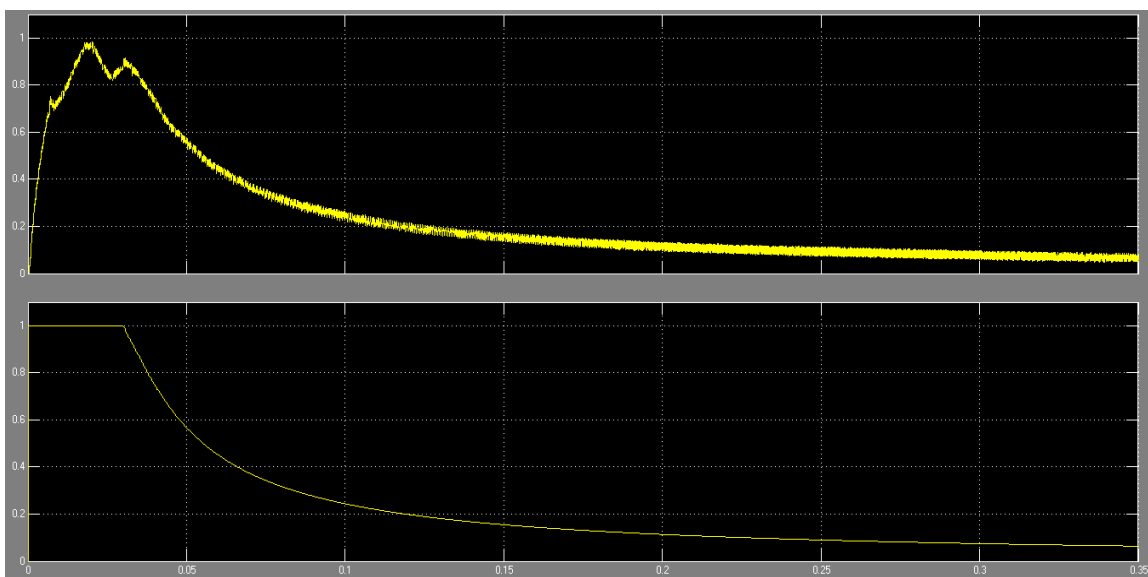

Fig. 10 DC Link Voltage

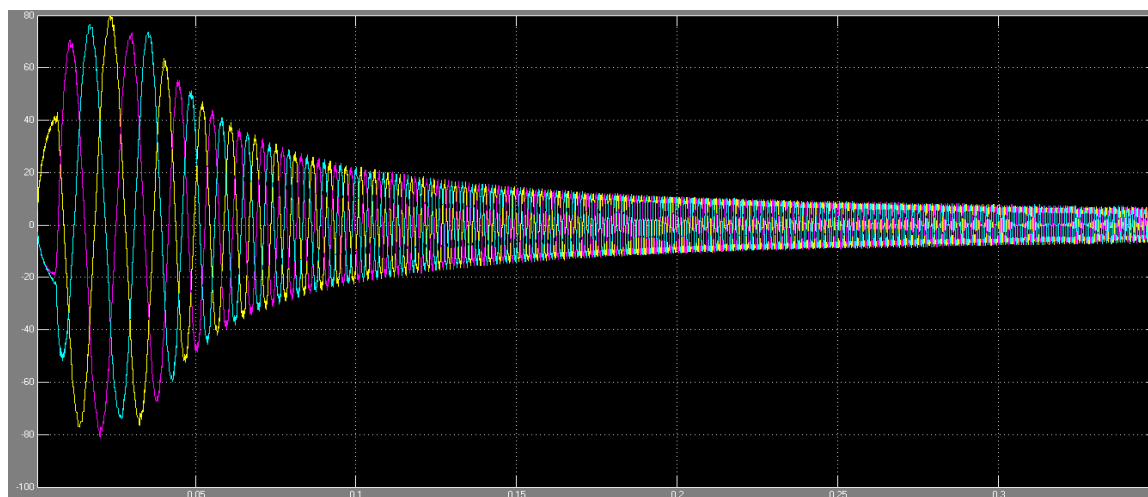Fig.11 Actual & Reference Stator Flux

Fig. 12 Stator Currents

VIII. CONCLUSION

The DTC scheme is analyzed using MATLAB Simulink environment. It is observed that this open loop torque control of Induction motor develops uniform torque with reduction in torque ripples & improvement in torque response. This type of control requires estimation of torque and flux form the stator parameters which is explained in this paper. Implementation of DTC has shown uniform stator flux. The simulation of Induction motor without DTC with comparison of non-uniform flux produced in absence of DTC. Thus the results verifies the merits of the DTC SVM system.

IX. Future Work

Implementation of DTC scheme using high power switching devices like IGBT & IGCT & compare the performance. Implementation of DTC with modified control strategy of 12 voltage sectors can also be done.

REFERENCES

[1]   C. Thanga Raj, Energy Efficient Control of Three-Phase Induction Motor - A Review, International Journal of Computer and Electrical Engineering, Vol. 1, No. 1, April 2009 1793-8198, page no 61-70.
[2]   Hamid A. Toliyat, Emil Levi, Mona Raina, A Review of RFO Induction Motor Parameter Estimation Techniques, IEEE TRANSACTIONS ON ENERGY CONVERSION, VOL. 18, NO. 2, JUNE 2003, page 271-283.
[3]   U. V Patil, H. M. Suryawanshi, and M. M. Renge, Performance Comparison of DTC and FOC Induction Motor Drive in Five Level Diode Clamped Inverter, IEEE-International Conference On Advances In Engineering, Science And Management (ICAESM -2012), March 30, 31, 2012 page no.227-230.
[4]   I. Takahashi and T. Noguchi, A new quick-response and high efficiency control strategy of an induction machine, IEEE Trans. Ind. Application 22, 820–827 (1986).
[5]   S. Allirani1 and V. Jagannathan, High Performance Direct Torque Control of Induction Motor Drives Using Space Vector Modulation, IJCSI International Journal of Computer Science Issues, Vol. 7, Issue 6, November 2010 pp.178-186
[6]   P. Pillay, IEEE, Mathematical models for Induction Machines, 0-7803-3008-0195 0 1995 IEEE
[7]   B. K. Bose, Modern Power Electronics and AC Drives. Englewood Cliffs, NJ: Prentice-Hall, 2002
[8]   Mustafa A. Al-Refai, Matlab/Simulink Simulation Model for Direct Torque Control Based on Space Vector Modulation (DTC-SVM) of Induction Motor Drive, World Academy of Science, Engineering and Technology, 76 2013 pp658-662.
[9]   D. CASADEI, G. SERRA, A. TANI & L. ZARRI, Assessment of direct torque control of induction motor drives, Bulletin of the Polish Academy of Sciences, vol.54., no.3, 2006, pp.237-254
[10] T. G. Habetler, F. Profumo, M. Pastorelli, L. Tolbert, Direct Torque Control of Induction Machines Using Space Vector Modulation, IEEE Transactions on Industry Applications, Vol. 28, no. 5, pp. 1045–1053, September/October 1992
[11] Joachim Holtz, Sensor less control of induction motor drives, Proceeding of IEEE, vol.90, no8, Aug.2002 pp. 1359-1394.
[12] S. Mythili, Dr. K. Thyagarajah, Direct Torque Control (DTC) of Multi-phase Induction Motor using TMS320F2407 Digital Signal Processor, IEEE PEDS, 2005, 0-7803-9296-5/05, pp1024 -102.

Minimization of Shrinkage Porosity in A Sand Casting Process By Simulation In AUTOCAST-X Software with Experimental Validation by Destructive testing

A.K.Gajbhiye[1], C.M.Choudhari[2], D.N.Raut[3], B.E.Narkhede[4], B.M.Bhandarkar[5]

[1](Student, M. Tech., Department of Production Engineering, V.J.T.I. Mumbai, India.)
[2](Professor, Fr. C. Rodrigues Institute of Technology, Vashi, Navi Mumbai, India.)
[3](Professor and Dean Administration, Department of Production Engineering, V.J.T.I., Mumbai, India.)
[4](Professor and Head, Department of Production Engineering, V.J.T.I., Mumbai, India)
[5](Chairman, Indian Institution of Industrial Engineering {IIIE}, Navi Mumbai, India)

Abstract: *There is an increasing demand in manufacturing environment for the best quality of casting products at the right time and quantity. In order to survive in the competitive market and to achieve customer satisfaction trial-and-error method to produce defect free casting products from design to manufacturing is too costly and not effective [1]. Modernization is the only key to improve casting quality and productivity. This paper discusses the simulation process of casting solidification with the AutoCAST-X software of a intricate shape small size casting of LM6 (Al alloy) metal. With the help of simulation study hot spot in the casting has been identified. This has immensely helped in locating the optimum position and size of the feeder required. This paper also shows the application of feeding aids as exothermic sleeve. The simulation study has shown the improvement in feeding yield and quality of the casting.*
Keywords: *AutoCAST-X, Casting, Design, Feeding aid., Hotspot, LM6(Al Alloy), Shrinkage, Simulation Software.*

I. INTRODUCTION

Metal casting is one of the oldest manufacturing processes used to manufacture the complex shape objects. There is an increasing demand in manufacturing environment for the best quality of casting products at the right time and quantity. In order to survive in the competitive market and to achieve customer satisfaction trial-and-error method to produce defect free casting products from design to manufacturing is too costly and not effective[1]. Numerical simulation provides a powerful means of analyzing various physical phenomena occurring during casting processes. It gives an insight into the details of fluid flow, heat transfer and solidification. The goal of such simulations is to help shorten the design process and optimize casting parameters to reduce scrap, use less energy and, of course, make better castings. Shrinkage is a major defect in sand casting and often becomes a cause of casting rejections and rework in casting industry. Shrinkage is a phenomenon concerning the reduction in the size of a casting during its transition from a liquid to a solid state. The volume in both the liquid and solid phases changes under the influence of temperature. The difference in density of the liquid and solid phases, which causes a significant difference in the volume of these phases, should be taken into account. The phenomenon of metal shrinkage has a substantial impact on the quality of castings. The phenomenon of casting shrinkage cannot be avoided. It is however possible to minimize the occurrence of its negative effects on the casting. In order to achieve this computer simulation is inevitably necessary. Various simulation software's based on different numerical techniques such as Finite Element Method (FEM), Vector Element Method (VEM), Finite Difference Method (FDM), Finite Volume Method (FVM), Vector Gradient Method (VGM) etc. are available to find these defects and minimize them. AutoCAST which is based on VGM is providing easy computer interface to deal with these issues for entire method designing of casting. Hence it become customary for a foundry engineer or a product designer to anticipate all issues prevailing to the potential defects in the casting and take a suitable measure in advance to minimize them. Hence one best way is to use the casting solidification simulation practices. The simulations were compared with experimental trials to ensure that the simulation results are in good agreement with the experimental trials.

II. LITERATURE REVIEW

From the existing and recent literature citations it is found that the currently available casting solidification simulation software's have a lot of capabilities to analyse the defects and have received considerable attention from researchers in the past. Various research and their finding related to improvement in casting quality and minimization of shrinkage defects using simulation software has been mentioned in this section. Yeh-Liang Hsu et. al. [2] carried the casting simulation using ProCAST software for aluminium wheels. Here, shrinkage index was used to predict the casting quality of aluminum wheels to find the optimal parameters affecting the casting process. Thoguluva R. V. et. al. [3] studied the role, prospects, and application of computers in foundries to improve casting quality and productivity. Author has mentioned about the different casting simulation softwares available. Prabhakara Rao et. al. [4] has discussed about the simulation process of casting solidification with the aid of an example, which will help the foundry industries to optimize the design parameters, better understand the mould filling and temperature history of the solidifying castings to identify the defects with the aid of obtained time-temperature contours using ProCAST softwares. Author has also mentioned the limitation of the conventional sand casting and gating design. T. Ramu et. al. [5] has developed a solid model of flywheel by using PRO-E and exported it to MAGAMA-5 software to simulate the model and to develop the pattern so as to avoid the foundry defects which will help in reducing the manufacturing cost. A. Kermanpur et. al. [6] studied the metal flow and solidification behaviors in a multi-cavity casting mould of two automotive cast parts using FLOW-3D simulation software and validated the simulation model against the experimental observations showing that the four-cavity mould is more suitable than the three-cavity one, in getting a more uniform casting quality for all cast parts. The simulation model was also able to study the effects of several casting parameters including the melt superheat, pouring time (velocity), mould surface roughness, gating design, and the mould configuration for the quality and soundness of automotive cast parts. T.Nandi et. al. [7] studied plate castings to investigate the solidification behavior of aluminum alloy (LM6) with different sizes of feeders based on conventional methods and computer simulation technique. Author has concluded that the application of casting simulation software in the foundries not only minimizes the wastages of resources but also enhances the quality and yield of castings, which implies higher value addition and lower production cost. In the present work intricate shape small size casting of LM6 (Al alloy) is taken for study. Design calculations using conventional methods has been done. designed calculation has been verified by performing solidification simulation using AutoCAST software.

III. PROBLEM DEFINITION

Fig. 1. below shows the different views of casting pattern with various allowances. The component shown in Fig. 1. has, Volume of casting, $V_c = 201800$ mm3, Surface area of casting, $SA_c = 29000$mm2 and Casting modulus $M_c = 6.9586$ mm. Here, non-pressurized gating ratio as 1:2:2 is used.
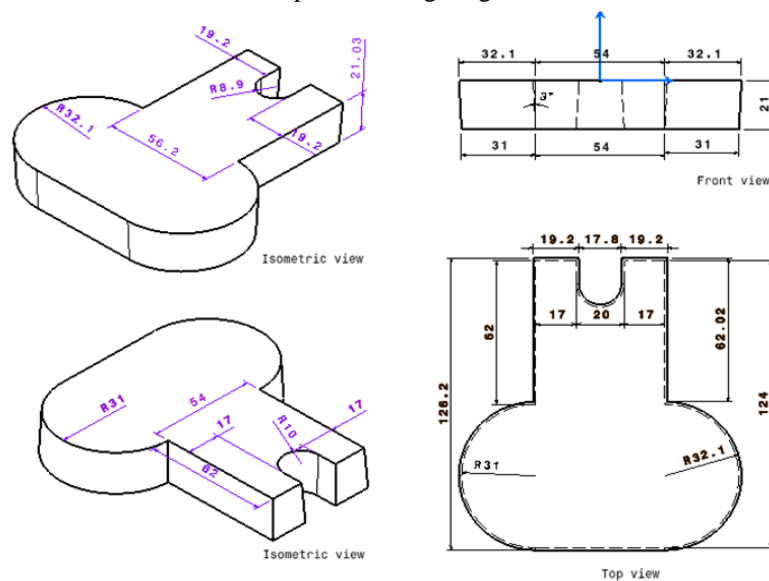

Fig.1. wooden pattern with allowances for casting

Initially design calculations were carried theoretically to find the various dimensions. Design calculations begin with calculation for pattern allowances followed by gating system and finally design of the feeder. Feeder design has been carried out using three different methods such as Caine's method, Modulus method and Naval Research Laboratory (NRL) method and the highest value obtained by Caine's method is taken for analysis. here, Feeder has been design in such a way that it should solidify last. A few important calculation result are mentioned in the Table 1 as given below.

Table 1. Design parameters and their calculated values.

Sr. No.	Designed Part	Values
1.	Mass of the casting (in Kg)	0.547
2.	Pouring Time (in Seconds)	5.472
3.	Diameter of Sprue at Top, Bottom and Sprue Length (in mm)	18, 15, 30
4.	Sprue well: Diameter and Height (in mm)	30, 30
5.	Runner dimensions: Width, Height and Length (in mm)	9, 18
6.	Ingate dimensions: Width, Height and Length (in mm)	9, 18, 44
7.	Feeder dimension based on Caine's method: Diameter of Feeder at Top, Bottom & Height (in mm)	50, 48, 50
8.	Neck: Diameter and height (in mm)	22, 10
9.	Pouring basin: Diameter at Top, Bottom and Height (in mm)	60, 40, 30

IV. SOLIDIFICATION SIMULATION USING AUTOCAST-X SOFTWARE

The software simulates the way casting engineers decide the casting process, parting line, cores, mold box, feeders, gating system and mold layout, and analyzes each decision to suggest how the design could be modified to improve quality as well as reduce tooling and manufacturing costs.

Solidification Simulation has been performed in AutoCAST-X environment according to the design dimensions obtained for Pattern with allowances, gating system and feeder. Simulation study of castings aims at identifying the hot spot locations, solidification time and thereby minimizing the shrinkage porosity etc. Step wise procedure for method design, internal quality assessment and obtaining the yield of the casting using AutoCAST-X software is outlined below:

The START module allows creating or opening a casting project, importing a part model, setting the materials and process, selecting the mold size, and saving a layout. These inputs are required for all other modules.
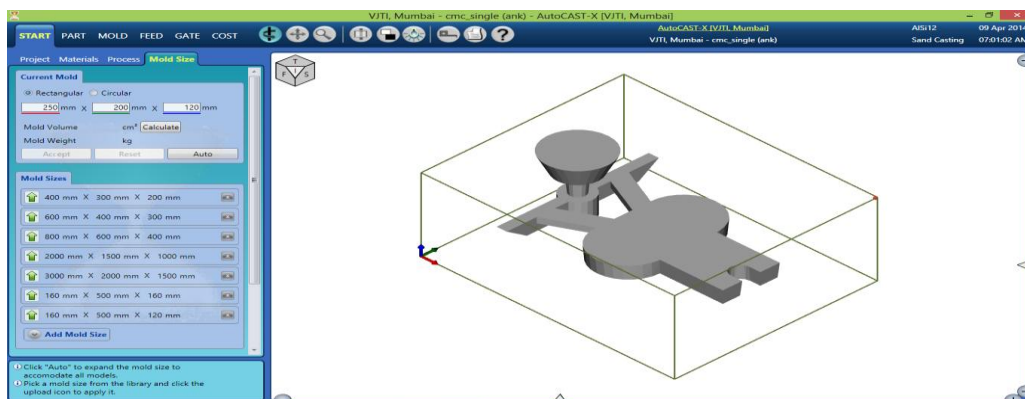

Fig. 2. imported part model of casting with mould shape and size

- Imported a 3D part model created in any CAD software as standard .STL file as shown in Fig. 2. A fitting mould will be automatically created and displayed.
- The rectangular mould box was chosen and dimensions have been taken as 250×200×120 mm.

- The entire mould containing the casting was automatically sub-divided into cubic elements for internal computations such as thickness, solidification and mould filling. The element size was defined as 2.01 mm
- Material selected was LM6 Grade Al alloy and sand casting was used as process.

The PART module is meant for computing the geometric and mass properties, analyzing the thickness (including reference radiograph), and identifying cored holes if any. These results are needed for methods design as well as for checking part-process compatibility. Part process compatibility has been checked using the optimize function. Here three parameters are checked for part-process compatibility viz. part weight, part size and minimum thickness as shown in Fig. 3.

Compatibility index = Σi importance of parameter i × compatibility of parameter i = 100%. A high compatibility index indicates an optimal process-friendly part design. The index is zero if even one parameter is incompatible (located in red zone).
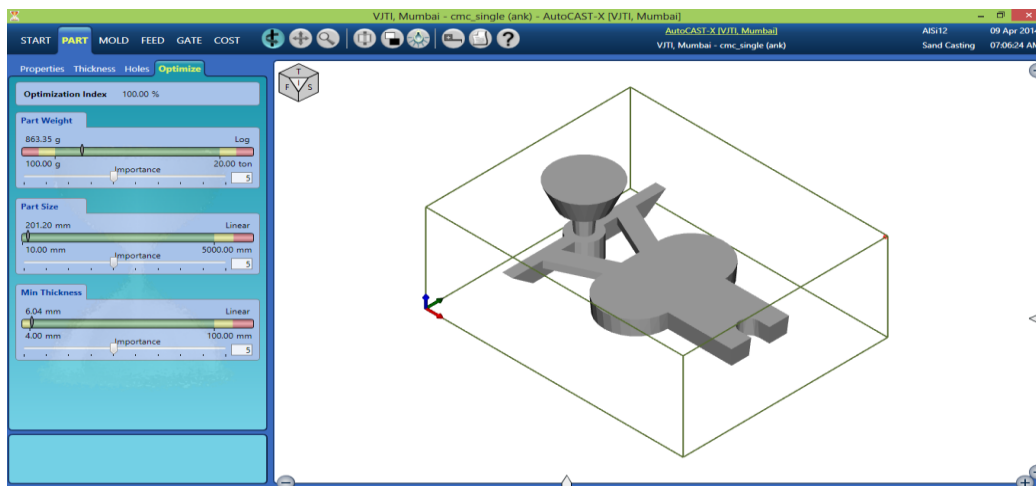

Fig. 3. part-process compatibility evaluation

The MOLD module contains functions for orienting the part in mold, setting the parting line (flat or stepped), designing cores (prints), deciding the number of cavities and their layout in mold. The mold size and cavities can be optimized considering the ratio of cast metal to mold material. Part orientation as well as parting plane placement is done in mold module as shown in Fig. 4.
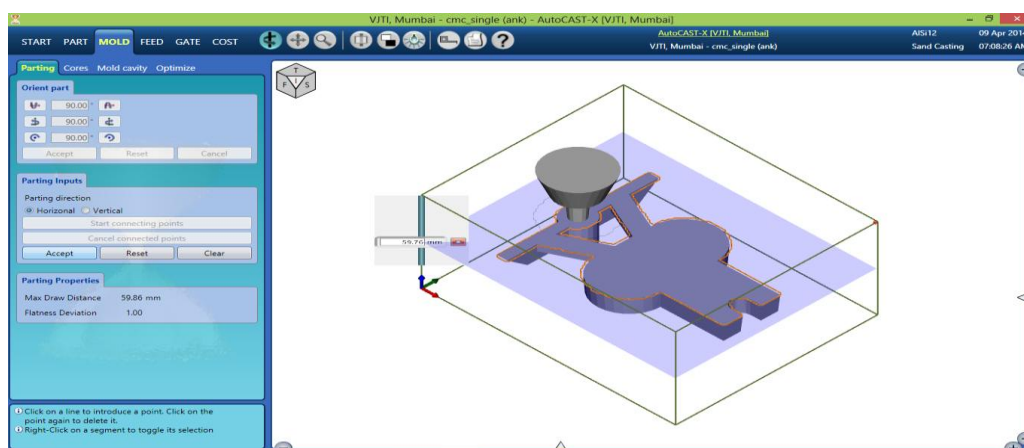

Fig. 4. placement of horizontal parting plane

The parting line is created using the volumetric mesh elements. Parting direction is selected as horizontal. Moldability index is 100% which is computed on the basis of metal to mold volume ratio, and number of mold elements as shown in Fig. 5.
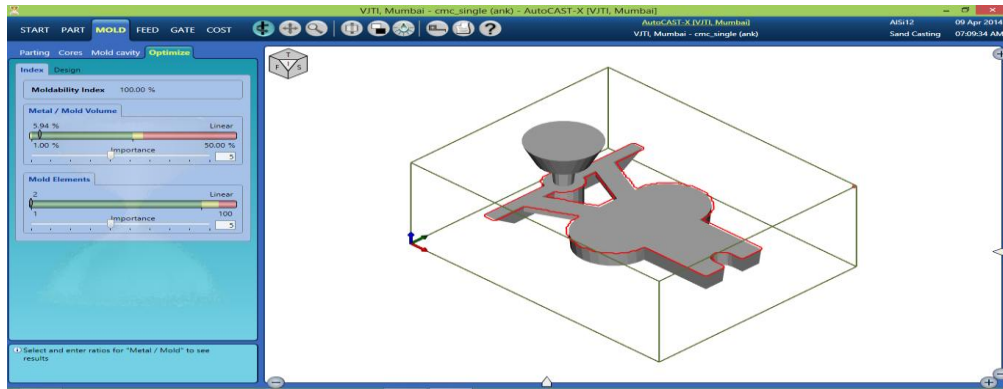
Fig. 5. moldability index

The FEED module enables designing and optimizing the feeders (feeders) with or without the feedaids to obtain the desired quality with high yield. Casting solidification is simulated and the results are shown as cooling animation and feed metal paths. The feeder design can be automatically optimized, driven by user constraints. Here, the last solidifying region of the casting has been identified as shown in Fig. 6. Green colored dot in the Fig. 8. indicates the location of the feeder.
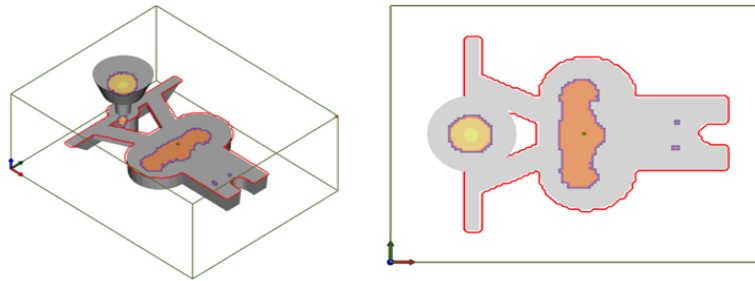

Fig. 6. hotspot indicating the last solidifying region

Now the feeder has been model according to the design dimensions and has been placed exactly on the top of the hotspot as shown in Fig. 7. to allow feed metal transfer during volumetric contraction that accompanies solidification shrinkage.
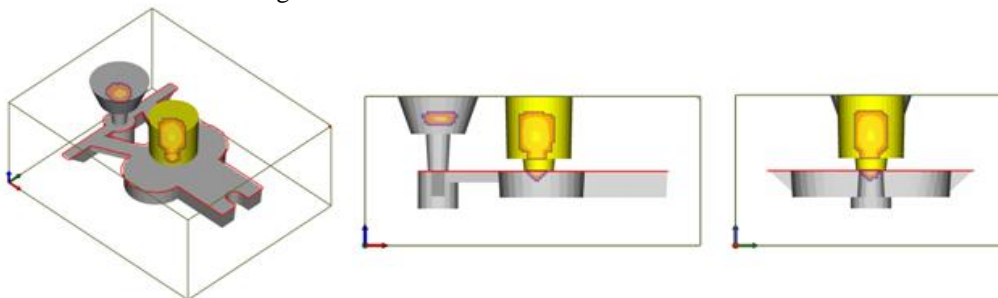

Fig. 7. partial shifted position of hotspot with the application of feeder

When insulating sleeve (exothermic) of 10mm thickness was incorporated and simulation was run. The hotspot got completely shifted in the feeder as shown in Fig. 8.
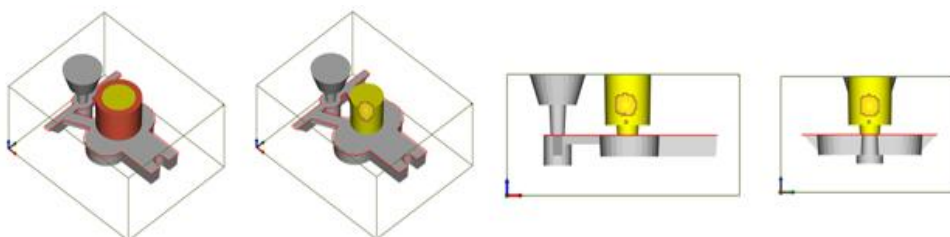

Fig. 8. completely shifted position of hotspot with the application of feeder along with sleeve

Two main results are produced in Solidification function:
- Cooling animation: progressive solidification as shown in Fig. 9.
- Feed metal paths: directional solidification as shown in Fig. 10.

Shrinkage porosity can be predicted by interpreting the above two results. This is expected in regions of high temperature and low gradient. Ideally, feedpaths should end inside a feeder. Long and hot feedpaths converging inside the casting imply a local hotspot that can result in a shrinkage porosity defect. Short and cold feedpaths are usually harmless. Good (directional) feeding is characterized by:
- Absence of isolated hot spots inside the casting
- Feedpaths converging and leading inside the feeders
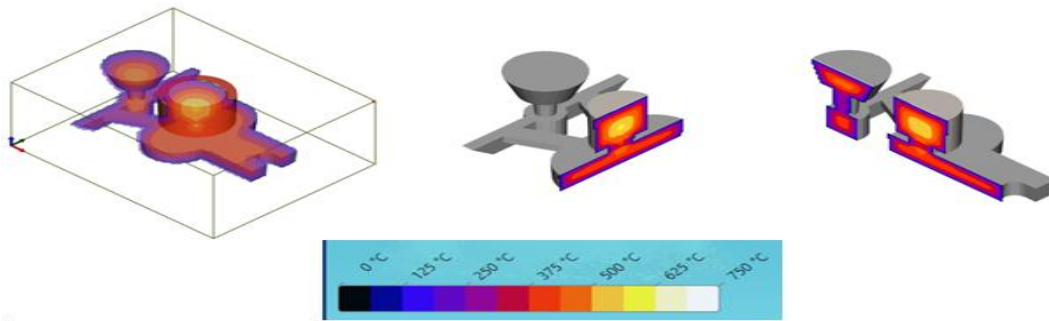

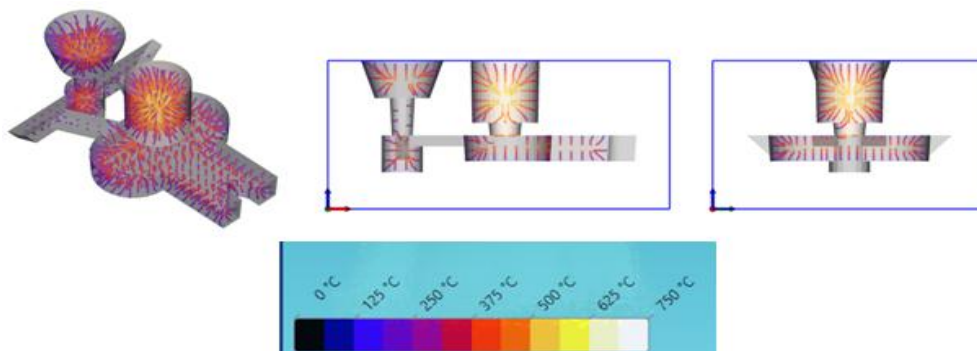Fig. 9. cooling simulation of casting in 3D

Fig. 10. feed metal paths in 3d and in cross section

Shrinkage porosity was computed from the temperature and gradients using metal-specific process characteristics. The shrinkage porosity is displayed as dots inside the casting red for macro and orange for micro as shown in Fig.11. The simulation gives the value of macro porosity and micro porosity as 3.12 cm3.
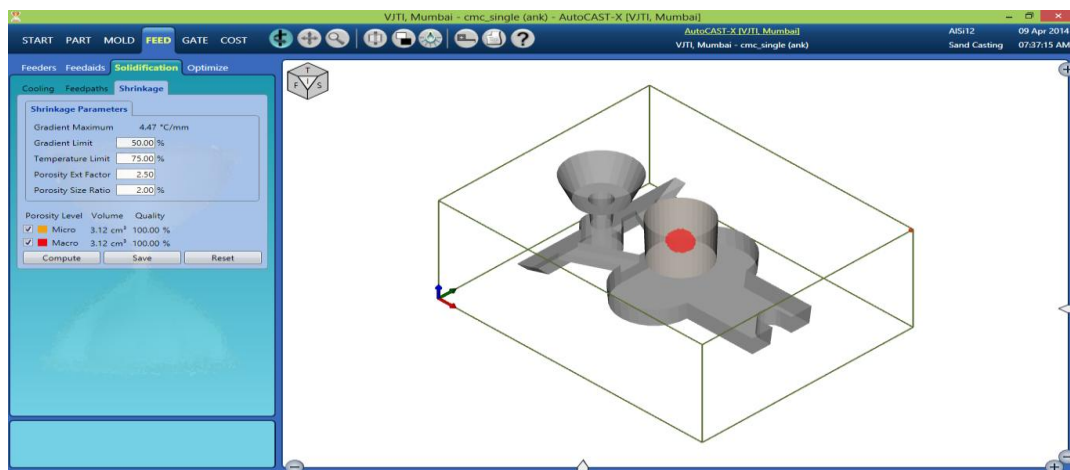

Fig. 11. shrinkage porosity as seen in 3d, side view and front view (macro-red, micro-orange)

The feeding design is evaluated (in terms of feedability index), and automatically optimized in this function. A composite weighted feedability index is computed using the above criteria and their importance (1-10 scale). The index is 100% if all criteria are in the green zone, and 0% if even one criterion is in the red zone.
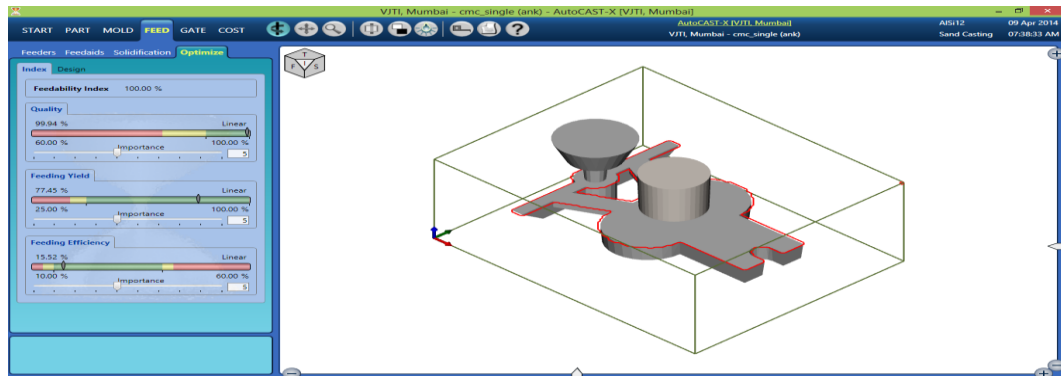
Fig. 12. feedability index

V. EXPERIMENTAL VALIDATION

After making wooden patterns as per design calculations for aluminium casting as shown in Fig. 13. A mould box of size 250 x 200 x 120 was rammed using silica sand and the mould cavity was prepared in two parts, Cope and Drag as shown in Fig. 14.

Pouring basin, Sprue, Sprue well

Pattern

Runners, Ingates, Sprue well

Riser

Fig. 13. wooden rigging system with pattern

Cope

Drag

Fig. 14.cope and drag with pattern embedded in mould box

VI. RESULT

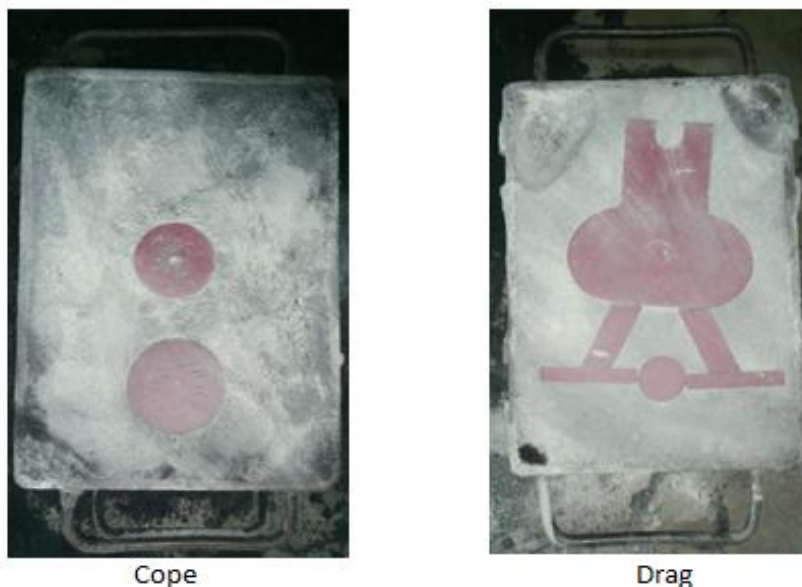Casting trials were carried out without feeder, with feeder and feeder with exothermic sleeve. It can be seen that casting without feeder directly shows shrinkage defect at the centre as shown in Fig.15., when the feeder of 50mm diameter was placed no surface defects were present but when the component was machined shrinkage porosity was found as shown in Fig. 16. but when same feeder was placed with an exothermic sleeve of 10mm thickness no shrinkage related defects were found in the casting after machining as shown in Fig.17.
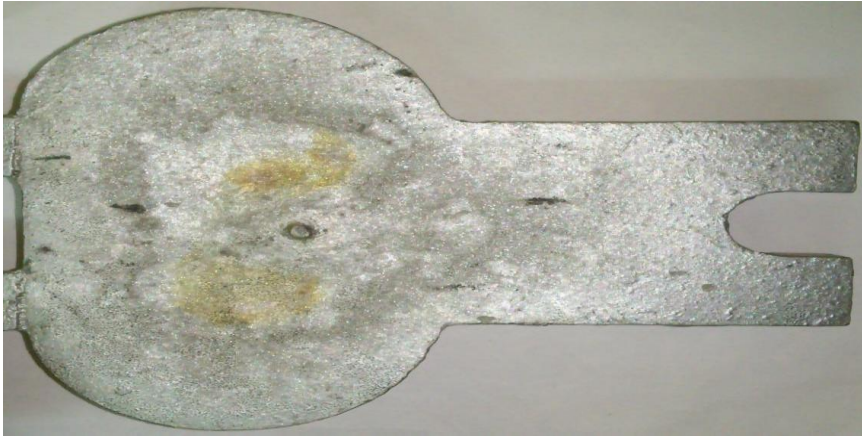

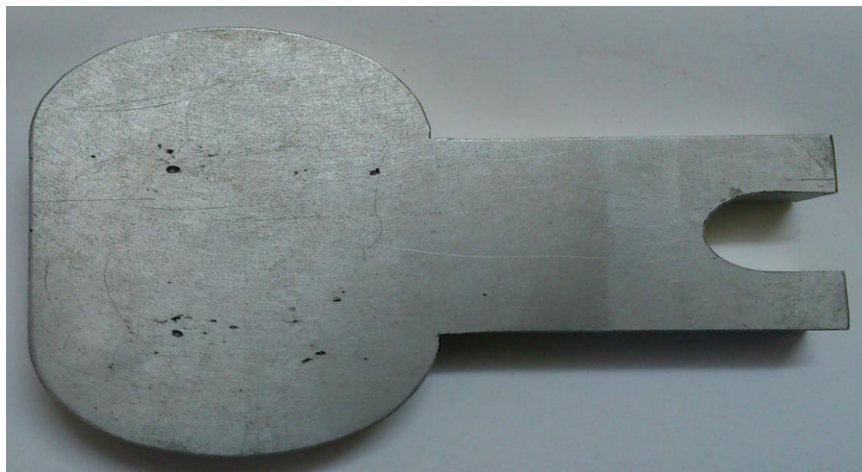Fig. 15. casting without feeder shows defect

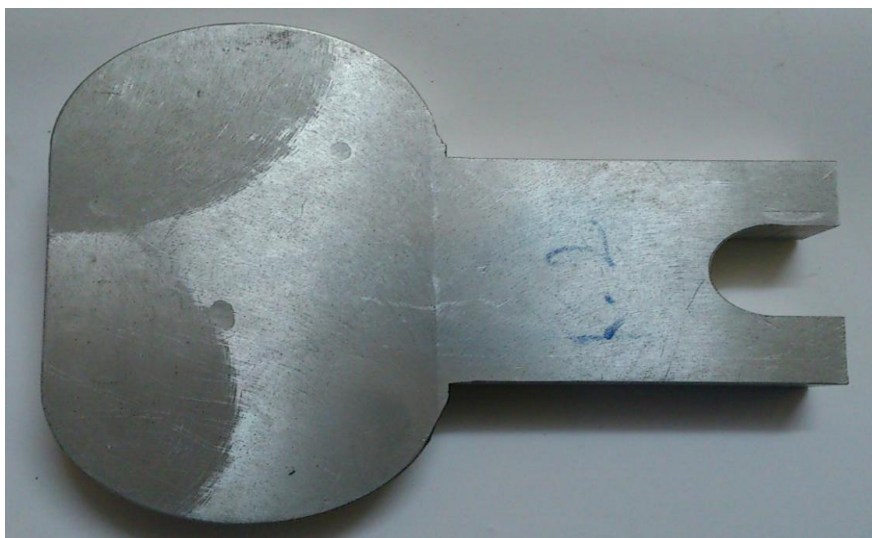Fig. 16. casting with feeder of diameter 50mm shows defect after machining

Fig. 16. casting with feeder of diameter 50mm and sleeve thickness 10mm shows no defects after machining

Fig. 17. section cut of casting with feeder of diameter 50mm and sleeve thickness 10mm shows no defects

VII. CONCLUSION

Solidification simulation has been performed in AutoCAST-X environment according to the design dimensions obtained for pattern with allowances, gating system and feeder. Simulation study of castings has provided the temperature contours which has helped in identifying the hot spot locations, solidification time etc. Step wise procedure for method design, internal quality assessment and obtaining the yield of the casting using AutoCAST-X software is outlined in this study.

When insulating sleeve(exothermic) of 10mm thickness was incorporated with the design dimensions of the feeder and simulation was run. The hotspot has got completely shifted in the feeder.

Shrinkage porosity was computed from the temperature and gradients using metal-specific process characteristics. The simulation gives the value of macro porosity and micro porosity as 3.12 cm3. This study has shown that entire shrinkage porosity has been shifted in the feeder when it was designed properly. Therefore more emphasise should be given on design phase of the casting by anticipating the probable occurrence of the defects rather than controlling the process parameters. It save time to develop new casting, wastage of material in carrying number of trials, to develop sound casting, energy and most important is money.

Casting with feeder of diameter 48mm along with the sleeve of thickness 10mm has been validated by performing actual trials in a foundry. Using sleeve as a feed aid helped in increasing casting yield.

REFERENCES

Journal Papers:
[1]   Shamsuddin Sulaiman, Lim Ying Pio, Validation Of MAGMAsoft Simulation Of The Sand Casting Process, The Institution of Engineers, Malaysia, September/December 2004, Vol. 65, No. 3/4, 55-64.
[2]   Yeh-Liang Hsu, Chia-Chieh Yu, Computer Simulation Of Casting Process Of Aluminium Wheels – A Case Study, J. Engineering Manufacture, 2006, Vol. 220, Part B, 203-211.
[3]   Thoguluva Raghavan Vijayaram, Paolo Piccardo, Computers in Foundries, Metallurgical Science and Technology, 2012, Vol. 30-2, 28-38.
[4]   P. Prabhakara Rao, G. Chakraverthi, A. C. S. Kumar, G. Srinivasa Rao, Modeling and Simulation of Solidification in Alloy Steel Sand Castings, International Journal of Thermal Technologies, Dec. 2011, Vol.1, No.1, 110-116.

[5]   T. Ramu, M. L. S. Deva Kumar, B. K. C. Ganesh, Modeling, Simulation And Analysis In Manufacturing Of A Flywheel Casting By S.G.Iron, International Journal of Materials and Biomaterials Applications, 2012; 2(4): 25-28.

[6]   A. Kermanpur, Sh. Mahmoudi, A. Hajipour, Numerical Simulation Of Metal Flow And Solidification In The Multi-Cavity Casting Moulds Of Automotive Components, Journal Of Materials Processing Technology, 2008, 1-7.

[7]   T. Nandi, R. Behera, S. Kayal, A. Chanda, G.Sutradhar, Optimization Of Feeder Size Of Aluminium Alloy (LM6) Castings By Using Conventional Method And Computer Simulation Technique, Nov. 2011, International Journal Of Scientific & Engineering Research, Volume 2, Issue 11, 1-6.

[8]   El Hassan E. M. Khalafalla, Hashim A. A. El Hashimi, Simulation Of Heat Flow In Aluminum Sand Casting, Shendi University Journal, January 2010, Issue No. 8, 15-48.

[9]   AutoCAST information and case studies, Advanced Reasoning Technologies Pvt. Ltd., http://www.adva-reason.com.

Books:

[10]   P. N. Rao, Manufacturing Technology (TATA Mc Graw-Hill Education, New Delhi, 2008).

[11]   B. Ravi, Metal Casting: Computer Aided Design and Analysis (PHI Learning Pvt. Ltd.2011).

About the 2-Banach Spaces

Risto Malčeski[1], Katerina Anevska[2]

[1, 2] *(Faculty of informatics/ FON University, Skopje, Macedonia)*

Abstract: *In this paper are proved a few properties about convergent sequences into a real 2-normed space* $(L, \|\cdot, \cdot\|)$ *and into a 2-pre-Hilbert space* $(L, (\cdot, \cdot | \cdot))$, *which are actually generalization of appropriate properties of convergent sequences into a pre-Hilbert space. Also, are given two characterization of a 2-Banach spaces. These characterization in fact are generalization of appropriate results in Banach spaces.*

2010 *Mathematics Subject Classification:* *Primary* 46B20; *Secondary* 46C05.

Keywords: *convergent sequence, Cauchy sequence, 2-Banach space, weakly convergent sequence, absolutely summable series.*

I. INTRODUCTION

Let L be a real vector space with dimension greater than 1 and, $\|\cdot, \cdot\|$ be a real function defined on $L \times L$ which satisfies the following:

a) $\|x, y\| \geq 0$, for each $x, y \in L$ и $\|x, y\| = 0$ if and only if the set $\{x, y\}$ is linearly dependent,

b) $\|x, y\| = \|y, x\|$, for each $x, y \in L$,

c) $\|\alpha x, y\| = |\alpha| \cdot \|x, y\|$, for each $x, y \in L$ and for each $\alpha \in \mathbf{R}$,

d) $\|x + y, z\| \leq \|x, z\| + \|y, z\|$, for each $x, y, z \in L$.

Function $\|\cdot, \cdot\|$ is called as 2-*norm of L*, and $(L, \|\cdot, \cdot\|)$ is called as *vector 2-normed space* ([1]).

Let $n > 1$ be a natural number, L be a real vector space, $\dim L \geq n$ and $(\cdot, \cdot | \cdot)$ be real function on $L \times L \times L$ such that:

i) $(x, x | y) \geq 0$, for each $x, y \in L$ и $(x, x | y) = 0$ if and only if a and b are linearly dependent,

ii) $(x, y | z) = (y, x | z)$, for each $x, y, z \in L$,

iii) $(x, x | y) = (y, y | x)$, for each $x, y \in L$,

iv) $(\alpha x, y | z) = \alpha(x, y | z)$, for each $x, y, z \in L$ and for each $\alpha \in \mathbf{R}$, and

v) $(x + x_1, y | z) = (x, y | z) + (x_1, y | z)$, for each $x_1, x, y, z \in L$.

Function $(\cdot, \cdot | \cdot)$ is called as 2-*inner product*, and $(L, (\cdot, \cdot | \cdot))$ is called as 2-*pre-Hilbert space* ([2]).

Concepts of a 2-norm and a 2-inner product are two dimensional analogies of concepts of a norm and an inner product. R. Ehret ([3]) proved that, if $(L, (\cdot, \cdot | \cdot))$ be 2-pre-Hilbert space, than

$$\|x, y\| = (x, x | y)^{1/2}, \text{ for each } x, y \in L \quad (1)$$

defines 2-norm. So, we get 2-normed vector space $(L, \|\cdot, \cdot\|)$.

II. CONVERGENT AND CAUCHY SEQUENCES IN 2-PRE-HILBERT SPACE

The term convergent sequence in 2-normed space is given by A. White, and he also proved a few properties according to this term. The sequence $\{x_n\}_{n=1}^{\infty}$ into vector 2-normed space is called as *convergent* if there exists $x \in L$ such that $\lim_{n \to \infty} \|x_n - x, y\| = 0$, for every $y \in L$. Vector $x \in L$ is called as *bound* of the sequence $\{x_n\}_{n=1}^{\infty}$ and we note $\lim_{n \to \infty} x_n = x$ or $x_n \to x$, $n \to \infty$, ([4]).

Theorem 1 ([4]). Let $(L, \|\cdot, \cdot\|)$ be a 2-normed space over L.

a) If $\lim_{n \to \infty} x_n = x$, $\lim_{n \to \infty} y_n = y$, $\lim_{n \to \infty} \alpha_n = \alpha$ and $\lim_{n \to \infty} \beta_n = \beta$, then

$$\lim_{n\to\infty}(\alpha_n x_n + \beta_n y_n) = \alpha x + \beta y.$$

б) If $\lim\limits_{n\to\infty} x_n = x$ and $\lim\limits_{n\to\infty} x_n = y$, then $x = y$. ∎

Theorem 2 ([4]). a) Let L be a vector 2-normed space, $\{x_n\}_{n=1}^{\infty}$ be the sequence in L and $y \in L$ is such that $\lim\limits_{n\to\infty} \| x_n - x_m, y \| = 0$. Then the real sequence $\{\| x_n - x, y \|\}_{n=1}^{\infty}$ is convergent for every $x \in L$.

b) Let L be a vector 2-normed space, $\{x_n\}_{n=1}^{\infty}$ be a sequence in L and $y \in L$ is such that $\lim\limits_{n\to\infty} \| x_n - x, y \| = 0$. Then $\lim\limits_{n\to\infty} \| x_n, y \| = \| x, y \|$. ∎

In [7] H. Gunawan was focused on convergent sequences in 2-pre-Hilbert space $(L,(\cdot,\cdot|\cdot))$, and he gave the term weakly convergent sequence in 2-pre-Hilbert space. According to this he proved a few corollaries.

Definition 1 ([5]). The sequence $\{x_n\}_{n=1}^{\infty}$ in the 2-pre-Hilbert space $(L,(\cdot,\cdot|\cdot))$ is called as *weakly convergent* if there exists $x \in L$ such that $\lim\limits_{n\to\infty}(x_n - x, y | z) = 0$, for every $y, z \in L$. The vector $x \in L$ is called as *weak limit* of the sequence $\{x_n\}_{n=1}^{\infty}$ and is denoted as $x_n \xrightarrow{w} x$, $n \to \infty$.

Theorem 3. Let $(L,(\cdot,\cdot|\cdot))$ be a 2-pre-Hilbert space. If $x_n \xrightarrow{w} x$, $y_n \xrightarrow{w} y$, $\alpha_n \to \alpha$ and $\beta_n \to \beta$, for $n \to \infty$, then $\alpha_n x_n + \beta_n y_n \xrightarrow{w} \alpha x + \beta y$, for $n \to \infty$.

Proof. The validity of this theorem is as a direct implication of Definition 1, the fact that every convergent real sequence is bounded and the following equalities:

$$\lim_{n\to\infty}(\alpha_n x_n + \beta_n y_n - \alpha x - \beta y, u | v) = \lim_{n\to\infty}(\alpha_n x_n - \alpha x, u | v) + \lim_{n\to\infty}(\beta_n y_n - \beta y, u | v)$$
$$= \lim_{n\to\infty}\alpha_n(x_n - x, u | v) + \lim_{n\to\infty}(\alpha_n - \alpha)(x, u | v) +$$
$$+ \lim_{n\to\infty}\beta_n(y_n - y, u | v) + \lim_{n\to\infty}(\beta_n - \beta)(y, u | v). \ \blacksquare$$

Corollary 1 ([5]). Let $(L,(\cdot,\cdot|\cdot))$ be a 2-pre-Hilbert space. If $x_n \xrightarrow{w} x$, $y_n \xrightarrow{w} y$, for $n \to \infty$ and $\alpha, \beta \in \mathbf{R}$, then $\alpha x_n + \beta y_n \xrightarrow{w} \alpha x + \beta y$, for $n \to \infty$.

Proof. The validity of this Corollary is as a direct implication of Theorem 3 for $\alpha_n = \alpha, \beta_n = \beta, n \geq 1$. ∎

Lemma 1 ([5]). Let $(L,(\cdot,\cdot|\cdot))$ be a 2-pre-Hilbert space.

a) If $x_n \to x$, $n \to \infty$, then $x_n \xrightarrow{w} x$, $n \to \infty$.

б) If $x_n \xrightarrow{w} x$ and $x_n \xrightarrow{w} x'$, $n \to \infty$, then $x = x'$. ∎

Theorem 4. Let $(L,(\cdot,\cdot|\cdot))$ be a real 2-pre-Hilbert space. If $x_n \to x$, $y_n \to y$, $\alpha_n \to \alpha$ and $\beta_n \to \beta$, for $n \to \infty$, then

$$\lim_{n\to\infty}(\alpha_n x_n, \beta_n y_n | z) = (\alpha x, \beta y | z), \text{ for every } z \in L. \tag{2}$$

Proof. Let $x_n \to x$, $y_n \to y$, $\alpha_n \to \alpha$ and $\beta_n \to \beta$, for $n \to \infty$. Then, Theorem 1 a) implies

$$\lim_{n\to\infty}\| \alpha_n x_n - \alpha x, z \| = 0, \quad \lim_{n\to\infty}\| \beta_n y_n - \beta y, z \| = 0, \text{ for every } z \in L. \tag{3}$$

Properties of 2-inner product and the Cauchy-Buniakowsky-Schwarz inequality imply

$$0 \leq |(\alpha_n x_n, \beta_n y_n | z) - (\alpha x, \beta y | z)|$$
$$= |(\alpha_n x_n, \beta_n y_n | z) - (\alpha_n x_n, \beta y | z) + (\alpha_n x_n, \beta y | z) - (\alpha x, \beta y | z)|$$
$$\leq |(\alpha_n x_n, \beta_n y_n | z) - (\alpha_n x_n, \beta y | z)| + |(\alpha_n x_n, \beta y | z) - (\alpha x, \beta y | z)|$$
$$= |(\alpha_n x_n, \beta_n y_n - \beta y | z)| + |(\alpha_n x_n - \alpha x, \beta y | z)|$$
$$\leq \| \alpha_n x_n, z \| \cdot \| \beta_n y_n - \beta y, z \| + \| \alpha_n x_n - \alpha x, z \| \cdot \| \beta y, z \|.$$

Finally, letting $n \to \infty$, in the last inequality, by Theorem 2 b) and equality (3) follows the equality (2). ∎

Corollary 2 ([5]). Let $(L,(\cdot,\cdot|\cdot))$ be a real 2-pre-Hilbert space. If $x_n \to x$ and $y_n \to y$, for $n \to \infty$, then $\lim_{n \to \infty}(x_n, y_n | z) = (x, y | z)$, for every $z \in L$.

Proof. The validity of this Corollary is as a direct implication of Theorem 4, $\alpha_n = \beta_n = 1, n \geq 1$. ∎

Theorem 5. Let $\{x_n\}_{n=1}^{\infty}$ be a sequence in 2-pre-Hilbert space L. If

$$\lim_{n \to \infty} \|x_n, y\| = \|x, y\| \text{ and } \lim_{n \to \infty}(x_n, x | y) = (x, x | y), \text{ for every } y \in L,$$

then $\lim_{n \to \infty} x_n = x$.

Proof. Let $y \in L$. Then

$$\|x_n - x, y\|^2 = (x_n - x, x_n - x | y)$$
$$= (x_n, x_n | y) - 2(x_n, x | y) + (x, x | y)$$
$$= \|x_n, y\|^2 - 2(x_n, x | y) + \|x, y\|^2,$$

So,

$$\lim_{n \to \infty} \|x_n - x, y\|^2 = \lim_{n \to \infty} \|x_n, y\|^2 - 2 \lim_{n \to \infty}(x_n, x | y) + \|x, y\|^2$$
$$= 2\|x, y\|^2 - 2(x, x | y) = 0.$$

Finally, arbitrariness of y implies $x_n \to x$, $n \to \infty$. ∎

A. White in [4] gave the term Cauchy sequence in a vector 2-normed space L of linearly independent vectors $y, z \in L$, i.e. the sequence $\{x_n\}_{n=1}^{\infty}$ in a vector 2-normed space L is Cauchy sequence, if there exist $y, z \in L$ such that y and z are linearly independent and

$$\lim_{m,n \to \infty} \|x_n - x_m, y\| = 0 \text{ and } \lim_{m,n \to \infty} \|x_n - x_m, z\| = 0. \tag{4}$$

Further, White defines 2-Banach space, as a vector 2-normed space in which every Cauchy sequence is convergent and have proved that each 2-normed space with dimension 2 is 2-Banach space, if it is defined over complete field. The main point in this state is linearly independent of the vectors y and z, and by equalities (4) are sufficient for getting the proof. Later, this definition about Cauchy sequence into 2-normed space is reviewed, and the new definition is not contradictory with the state that 2-normed space with dimension 2 is 2-Banach space.

Definition 2 ([6]). The sequence $\{x_n\}_{n=1}^{\infty}$ in a vector 2-normed space L is *Cauchy sequence* if

$$\lim_{m,n \to \infty} \|x_n - x_m, y\| = 0, \text{ for every } y \in L. \tag{4}$$

Theorem 6. Let L be a vector 2-normed space.

i) If $\{x_n\}_{n=1}^{\infty}$ is a Cauchy sequence in L, then for every $y \in L$ the real sequence $\{\|x_n, y\|\}_{n=1}^{\infty}$ is convergent.

ii) If $\{x_n\}_{n=1}^{\infty}$ and $\{y_n\}_{n=1}^{\infty}$ are Cauchy sequences in L and $\{\alpha_n\}_{n=1}^{\infty}$ is Cauchy sequence in $\mathbf{R}$, then $\{x_n + y_n\}_{n=1}^{\infty}$ and $\{\alpha_n x_n\}_{n=1}^{\infty}$ are Cauchy sequences in L.

Proof. The proof is analogous to the proof of Theorem 1.1, [4]. ∎

Theorem 7. Let L be a vector 2-normed space, $\{x_n\}_{n=1}^{\infty}$ be a Cauchy sequence in L and $\{x_{m_k}\}_{k=1}^{\infty}$ be a subsequence of $\{x_n\}_{n=1}^{\infty}$. If $\lim_{k \to \infty} x_{m_k} = x$, then $\lim_{n \to \infty} x_n = x$.

Proof. Let $y \in L$ and $\varepsilon > 0$ is given. The sequence $\{x_n\}_{n=1}^{\infty}$ is Cauchy, and thus exist $n_1 \in \mathbf{N}$ such that $\|x_n - x_p, y\| < \frac{\varepsilon}{2}$, for $n, p > n_1$. Further, $\lim_{k \to \infty} x_{m_k} = x$, so exist $n_2 \in \mathbf{N}$ such that $\|x_{m_k} - x, y\| < \frac{\varepsilon}{2}$, for $m_k > n_2$. Letting $n_0 = \max\{n_1, n_2\}$ we get that for $n, m_k > n_0$ is true that

$$\|x_n - x, y\| \leq \|x_n - x_{m_k}, y\| + \|x_{m_k} - x, y\| < \frac{\varepsilon}{2} + \frac{\varepsilon}{2} = \varepsilon,$$

The arbitrariness of $y \in L$ implies $\lim\limits_{n\to\infty} x_n = x$. ∎

Theorem 8. Let L be a 2-pre-Hilbert space. If $\{x_n\}_{n=1}^{\infty}$ and $\{y_n\}_{n=1}^{\infty}$ are Cauchy sequences in L, then for every $z \in L$ the sequence $\{(x_n, y_n \mid z)\}_{n=1}^{\infty}$ is Cauchy in $\mathbf{R}$.

Proof. Let $z \in L$. The properties of inner product and Cauchy-Buniakovski-Swartz inequality imply

$$|(x_n, y_n \mid z) - (x_m, y_m \mid z)| \leq |(x_n, y_n \mid z) - (x_m, y_n \mid z)| + |(x_m, y_n \mid z) - (x_m, y_m \mid z)|$$

$$= |(x_n - x_m, y_n \mid z)| + |(x_m, y_n - y_m \mid z)|$$

$$\leq \| x_n - x_m, z \| \cdot \| y_n, z \| + \| x_m, z \| \cdot \| y_n - y_m, z \|.$$

Finally, by the last inequality, equality (4) and Theorem 6 *i)* is true that for given $z \in L$ the sequence $\{(x_n, y_n \mid z)\}_{n=1}^{\infty}$ is Cauchy sequence. ∎

III. CHARACTERIZATION OF 2-BANACH SPACES

Theorem 9. Each 2-normed space L with finite dimension is 2-Banach space.

Proof. Let L be a 2-normed space with finite dimension, $\{x_n\}_{n=1}^{\infty}$ be a Cauchy sequence in L and $a \in L$. By $\dim L > 1$, exist $b \in L$ such that the set $\{a, b\}$ is linearly independent. By Theorem 1, [7],

$$\| x \|_{a,b,2} = (\| x, a \|^2 + \| x, b \|^2)^{1/2}, \ x \in L \tag{5}$$

defines norm in L, and by Theorem 6, [7] the sequence $\{x_n\}_{n=1}^{\infty}$ is Cauchy into the space $(L, \| \cdot \|_{a,b,2})$. But normed space L with finite dimension is Banach, so exist $x \in L$ such that $\lim\limits_{n\to\infty} \| x_n - x \|_{a,b,2} = 0$. So, by (5) we get

$$\lim_{n\to\infty} \| x_n - x, a \| = \lim_{n\to\infty} \| x_n - x, b \| = 0. \tag{6}$$

We'll prove that for every $y \in L$,

$$\lim_{n\to\infty} \| x_n - x, y \| = 0. \tag{7}$$

Clearly, if $y = \alpha a$, then (6) and the properties of 2-norm imply (7). Let the set $\{y, a\}$ be linearly independent. Then $(L, \| \cdot \|_{y,a,2})$ is a Banach space, and moreover because of the sequence $\{x_n\}_{n=1}^{\infty}$ is Cauchy sequence in $(L, \| \cdot \|_{y,a,2})$, exist $x' \in L$ such that

$$\lim_{n\to\infty} \| x_n - x' \|_{y,a,2} = 0. \tag{8}$$

But in space with finite dimension each two norms are equivalent (Theorem 2, [8], pp. 29), and thus exist $m, M > 0$ such that

$$m \| x_n - x' \|_{y,a,2} \leq \| x_n - x' \|_{a,b,2} \leq M \| x_n - x' \|_{y,a,2},$$

This implies $\lim\limits_{n\to\infty} \| x_n - x' \|_{a,b,2} = 0$ and moreover $\lim\limits_{n\to\infty} \| x_n - x \|_{a,b,2} = 0$. So, we may conclude $x' = x$. By (8), $\lim\limits_{n\to\infty} \| x_n - x \|_{y,a,2} = 0$, and thus (7) holds. Finally the arbitrariness of y implies the validity of the theorem i.e. the proof of the theorem is completed. ∎

Definition 3. Let L be a 2-normed space and $\{x_n\}_{n=1}^{\infty}$ be a sequence in L. The series $\sum\limits_{n=1}^{\infty} x_n$ is called as *summable* in L if the sequence of its partial sums $\{s_m\}_{m=1}^{\infty}$, $s_m = \sum\limits_{n=1}^{m} x_n$ converges in L. If $\{s_m\}_{m=1}^{\infty}$ converges to s, then s is called as a sum of the series $\sum\limits_{n=1}^{\infty} x_n$, and is noted as $s = \sum\limits_{n=1}^{\infty} x_n$

The series $\sum\limits_{n=1}^{\infty} x_n$ is called as *absolutely summable* in L if for each $y \in L$ holds $\sum\limits_{n=1}^{\infty} \| x_n, y \| < \infty$.

Theorem 10. The 2-normed space L is 2-Banach if and only if each absolutely summable series of elements in L is summable in L.

Proof. Let L be a 2-Banach space, $\{x_n\}_{n=1}^{\infty}$ be a sequence in L and for each $y \in L$ holds $\sum_{n=1}^{\infty} \| x_n, y \| < \infty$. Then the sequence $\{s_m\}_{m=1}^{\infty}$ of partial sums of the series $\sum_{n=1}^{\infty} x_n$ is Cauchy in L, because of

$$\| s_{m+k} - s_m, y \| = \| x_{m+1} + x_{m+2} + ... + x_{m+k}, y \| \leq \| x_{m+1}, y \| + \| x_{m+2}, y \| + ... + \| x_{m+k}, y \|,$$

for every $y \in L$ and for every $m, k \geq 1$. But, L is a 2-Banach space, and thus the sequence $\{s_m\}_{m=1}^{\infty}$ converge in L. That means, the series $\sum_{n=1}^{\infty} x_n$ is summable in L.

Conversely, let each absolutely summable series be summable in L. Let $\{z_n\}_{n=1}^{\infty}$ is a Cauchy sequence in L and $y \in L$. Let $m_1 \in \mathbf{N}$ is such that $\| z_m - z_{m_1}, y \| < 1$, for $m \geq m_1$. By induction we determine $m_2, m_3, ...$ such that $m_k < m_{k+1}$ and for each $m \geq m_k$ holds $\| z_m - z_{m_k}, y \| \leq \frac{1}{k^2}$. Letting $x_k = z_{m_{k+1}} - z_{m_k}$, $k = 1, 2, ...$, we get $\sum_{k=1}^{\infty} \| x_k, y \| \leq \sum_{k=1}^{\infty} \frac{1}{k^2} < \infty$. The arbitrarily of $y \in L$ implies the series $\sum_{k=1}^{\infty} x_k$ is absolutely summable. Thus, by assumption, the series $\sum_{k=1}^{\infty} x_k$ is summable in L. But, $z_{m_k} = z_{m_1} + \sum_{i=1}^{k-1} x_i$. Hence, the subsequence $\{z_{m_k}\}_{k=1}^{\infty}$ of the Cauchy sequence $\{z_n\}_{n=1}^{\infty}$ converge in L. Finally, by Theorem 7, the sequence $\{z_n\}_{n=1}^{\infty}$ converge in L. It means L is 2-Banach space. ∎

REFERENCES

[1]   S. Gähler, Lineare 2-normierte Räume, Math. Nachr. 28, 1965, 1-42
[2]   C. Diminnie, S. Gähler, and A. White, 2-Inner Product Spaces, Demonstratio Mathematica, Vol. VI, 1973, 169-188
[3]   R. Ehret, Linear 2-Normed Spaces, doctoral diss., Saint Louis Univ., 1969
[4]   A. White, 2-Banach Spaces, Math. Nachr. 1969, 42, 43-60
[5]   H. Gunawan, On Convergence in n-Inner Product Spaces, Bull. Malaysian Math. Sc. Soc. (Second Series) 25, 2002, 11-16
[6]   H. Dutta, On some 2-Banach spaces, General Mathematics, Vol. 18, No. 4, 2010, 71-84
[7]   R. Malčeski, K. Anevska, Families of norms generated by 2-norm, American Journal of Engineering Research (AJER), e-ISSN 2320-0847 p-ISSN 2320-0936, Volume-03, Issue-05, pp-315-320
[8]   S. Kurepa, Functional analysis, (Školska knjiga, Zagreb, 1981)
[9]   A. Malčeski, R. Malčeski, Convergent sequences in the n-normed spaces, Matematički bilten, 24 (L), 2000, 47-56 (in macedonian)
[10]   A. Malčeski, R. Malčeski, n-Banach Spaces, Zbornik trudovi od vtor kongres na SMIM, 2000, 77-82, (in macedonian)
[11]   C. Diminnie, S. Gähler, and A. White, 2-Inner Product Spaces II, Demonstratio Mathematica, Vol. X, No 1, 1977, 525-536
[12]   R. Malčeski, Remarks on n-normed spaces, Matematički bilten, Tome 20 (XLVI), 1996, 33-50, (in macedonian)
[13]   R. Malčeski, A. Malčeski, A. n-seminormed space, Godišen zbornik na PMF, Tome 38, 1997, 31-40, (in macedonian)
[14]   S. Gähler, and Misiak, A. Remarks on 2-Inner Product, Demonstratio Mathematica, Vol. XVII, No 3, 1984, 655-670
[15]   W. Rudin, Functional Analysis, (2nd ed. McGraw-Hill, Inc. New York, 1991)

Single User Eigenvalue Based Detection For Spectrum Sensing In Cognitive Radio Network

Sheetal Jain[1], Madhukar Deshmukh[2]

[1, 2] *(Assoc. Professor, Department of electronics and telecommunication, Trinity College of Engg. and Research University of Pune, Pune)*

Abstract: *Scarcity of spectrum is the issue that wireless communication technology has to deal with. Primary user is the licensed user of the spectrum. When primary user is idle or not using the spectrum secondary user can utilize the spectrum. This sharing of spectrum can be enabled by cognitive radio (CR) technology. The heart of enabling this technology is spectrum sensing. Spectrum sensing involves detection of primary signal at very low SNR (in the range of -20 dB), under noise and interference uncertainty. This requirement makes spectrum sensing, a hard nut to crack. Another major issue in detection is hidden node problem wherein the node in vicinity of primary transmitter also indicates absence of the primary signal since it is hidden behind the large object. There are various algorithms for detection viz. energy detection, matched filter detection, feature detection (cyclostationary detection, eigen-value based detection etc.) These algorithms have limitations of complexity, requirement of signal knowledge and detection performance. In this paper the performance of eigenvalue based detection (EBD) method in presence of noise and low SNR of the received signal has been evaluated for a single user.*

Keywords-: *Cognitive radio, eigenvalue based detection, energy detector, spectrum sensing.*

I. INTRODUCTION

With new technologies and services in wireless communication, demand for spectrum has been evolved as major issue to deal with. Spectrum should be efficiently used and spectrum allocation should be dynamic to meet growing demand. A way out is to sense the spectrum and act as secondary user when primary user is not in picture. Figure (1) below demonstrates concept of opportunistic sharing. First image shows primary user is using the resource (laptop) while second one show when primary user is not utilizing the resource (laptop) secondary user can temporarily use it. This management is done by special system. In the same way to reduce and utilize unused spectrum a special system is been designed which can intelligently manage sharing of spectrum. Cognitive radio is one way to handle this issue. Cognitive radio is a transceiver having spectrum sensing capability to find temporarily holes in the spectrum and accordingly changes its transmission or reception parameters so that spectrum is never vacant and meets our demand for spectrum usage. This process is what called as dynamic spectrum management. Spectrum sensing is the main functionality in cognitive radio. [4]Cognitive radio is responsible for quality of service to primary user. Sensing the spectrum has many challenges first is finding exact noise model which is very difficult, secondly low signal to noise ratio and lastly to avoid hidden node problem. The hidden terminal issue occurs when a node is in coverage area of primary transmitter, but hidden by larger object so that it cannot receive the signal from primary transmitter or receiver. In this study it is assumed that the primary system is a broadcast system and primary receivers are passive (unable to transmit). Main challenge in spectrum sensing lies in low SNR. In the figure (2) shown below is the primary and secondary network. PU is the primary user and CR1 and CR2 are the cognitive radio 1 and 2 in coverage area of PU. Thus CR1 and CR2 can sense the spectrum used by primary user PU and if it is not active then cognitive radio 1 or 2 in secondary network can opportunistically use the spectrum. Once the primary user occupies the spectrum then secondary user discontinues its use and searches for another vacant space. Main issue to discuss with is if say cognitive radio 3 (CR3) is not in coverage area of primary user PU, CR3 may be behind big buildings or topologically crowded places then CR3 may erroneously decide that channel is vacant and use the channel causing interference in the primary user. [6][10]This particular situation is called as hidden node terminal and can be avoided by cooperative sensing. Thus decision whether channel is used by primary user or not is made by cooperation of cognitive radios. In the above eg CR1 and CR2 will inform CR3 that spectrum is occupied or not thereby avoiding interference with primary user. Taking all these into consideration we have to find a robust way of spectrum sensing wherein noise uncertainty makes no difference on the performance. Various detection methods include [1][9] i) Matched filter ii) Energy detection iii) Feature

detection iv) Eigenvalue detection. Disadvantages of first three methods are given: The most important feature of matched filter is low execution time but knowledge of signal properties is needed which is not possible in cognitive radio case. Here receiver should agree with the source channel conditions and signal nature must be known.

Energy detection method has low computational and execution complexity. An energy detector sets a threshold according to the noise level and compares it with the energy of the data stream in input. This detector only requires minimal information, such as the signal bandwidth and carrier frequency Moreover the threshold depends of the noise level so it's very difficult to fix it in changing conditions but its performance depends upon number of samples the time required for sensing is larger which is undesired in cognitive radio.

In feature detection statistical properties that vary periodically with time, which are called cyclostationary features of the primary signal are detected to find out spectrum hole but this method leads to high computational efficiency hence sensing time is again large. Also, knowledge of some signal parameters such as carrier frequency is necessary. This method needs a great complexity computational and the knowledge of some signal parameters of the signal under test like the carrier frequency should also be known.

In this backdrop spectrum sensing techniques based on the eigenvalues of the received sample covariance matrix has recently been emerged as a promising solution, as they do not require a priori assumptions on the signal to be detected, and typically outperform the popular energy detection method.
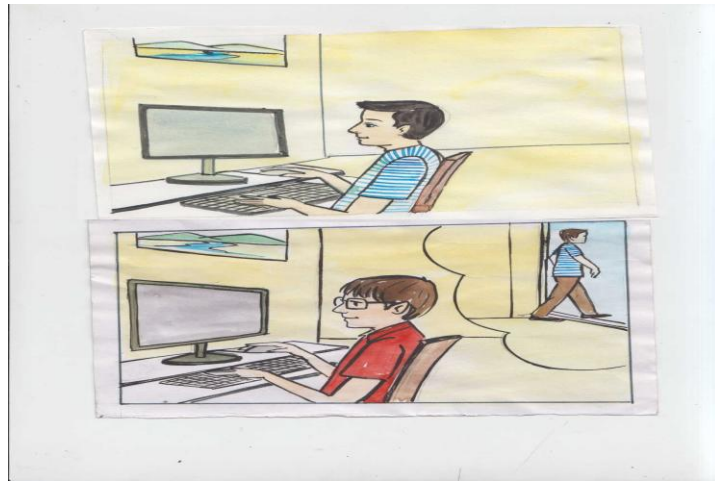
Fig(1) Primary and secondary user
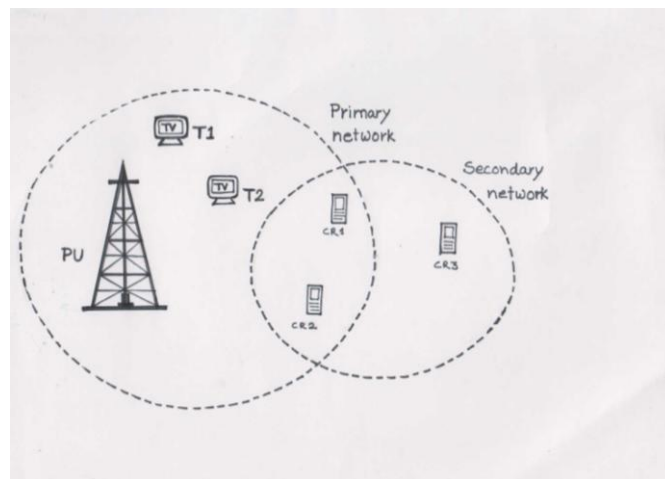
Fig(2) Primary and secondary network

II. System Model

Let s(n) = Primary users signal, x(n) = Received signal samples η(n) = received white noise , The detection problem can be formulated with two hypothesis no signal and only noise; signal with additive white noise [2]. First case signal is present is denoted as hypothesis H1 and second case signal is not present is denoted by hypothesis H0

$$H_0 : x(n) = \eta(n) \quad \text{------------------------- (1)}$$

$$H_1 : x(n) = s(n) + \eta(n) \quad \text{-------------- (2)}$$

Let N_s be the number of collected samples. Eigenvalue based detection is based on sample covariance matrix of received signal.

In practice number of samples are limited so sample covariance matrix is been considered. Following is the equation for sample covariance matrix of received signal.

$$R_x(N_s) = (1/N_s) \sum_{n=L-1}^{L-2+N_s} \hat{x}(n)\hat{x}^\dagger(n)$$

Where xˆ(n) is estimated received signal sample. And xˆ†(n) is transpose conjugate of estimated received signal sample. L being the number of consecutive outputs also called smoothing factor. Maximum and minimum eigenvalue of sample covariance matrix is obtained.

λ_{max} is maximum eigenvalue of sample covariance matrix and λ_{min} is minimum eigenvalue.

Maximum to minimum eigenvalue ratio is compared with threshold (γ). If ratio is greater than threshold signal is present otherwise signal is not present.

$$\frac{\lambda_{max}}{\lambda_{min}} > \gamma \quad \text{---------- signal exists}$$

$$\frac{\lambda_{max}}{\lambda_{min}} < \gamma \quad \text{--------- signal does not exist}$$

III. Flowchart

Eigenvalue based detection (EBD) schemes can be divided into two categories: methods that assume knowledge of noise level (referred to as semi-blind), and methods that do not assume this knowledge (blind)[8][9]. Methods belonging to the first class provide better performance when the noise variance is known exactly; on the other hand blind methods are more robust to uncertain or varying noise level. Spectrum sensing techniques based on the eigenvalues of the received sample covariance matrix provides efficient detection, as they do not require any information of the primary signal to be detected, and proves better than the popular energy detection method. EBD methods are based on eigenvalue calculation of received signal's sample covariance matrix. Maximum and minimum eigenvalue is found out from sample covariance matrix, thereafter ratio of maximum to minimum eigenvalue ratio is been compared with threshold. If the ratio is greater than threshold signal is detected means primary user is using the spectrum. If the ratio is less than threshold signal is not detected means primary user is not using the spectrum so secondary user can opportunistically use the spectrum.
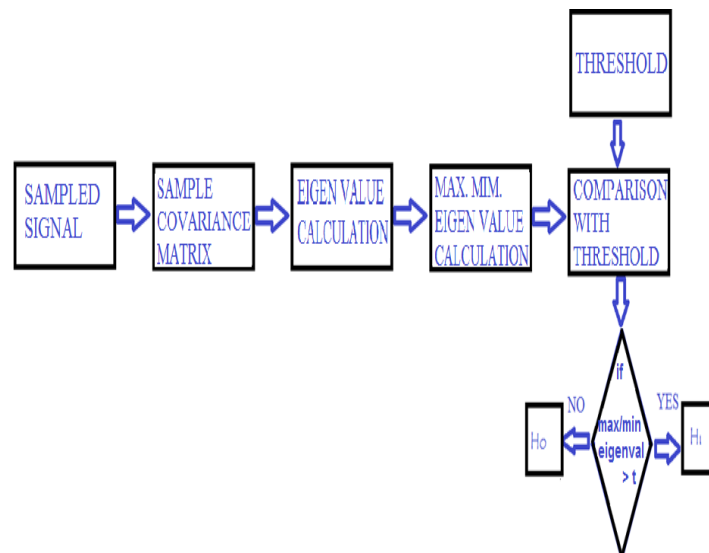

Fig. (3) Flowchart of EBD

IV. RESULTS

The results have been implemented using Matlab R2013a. Modulation for the input signal used is PSK. PSK   modulated signal with noise added is shown in the results below.
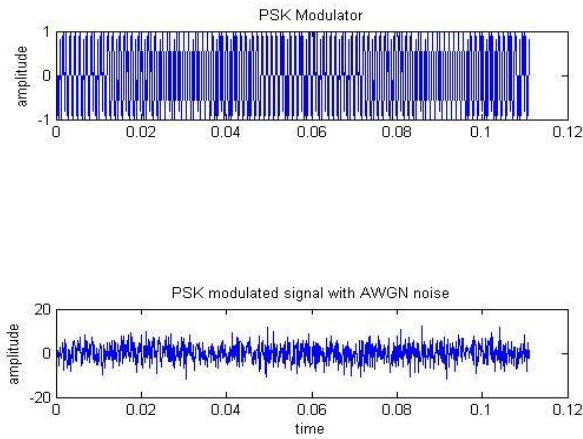

Fig. (4) Modulated output and modulated output with   noise added

Plot of probability of detection vs SNR is been shown in results below in fig.(5). Plot represents the probability of detection versus SNR for probability of false alarm of 0.1. Graph shows that at low SNR with high probability of false alarm probability of detection is poor.
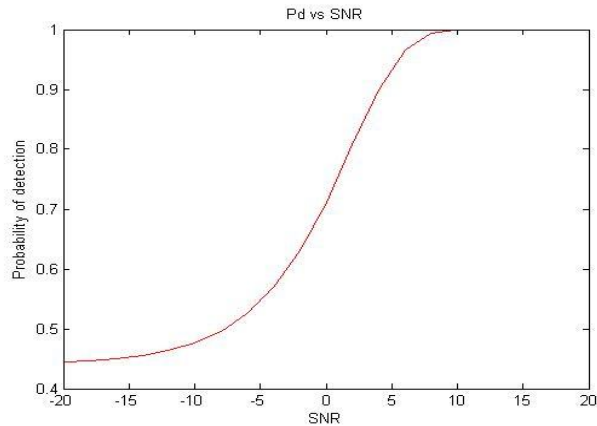

Fig. (5) P_d vs. SNR

Fig.(6) represents plot of probability of detection versus SNR for probability of false alarm of 0.04,0.2,0.3. Graph shows that at low SNR with high probability of false alarm probability of detection is poor.
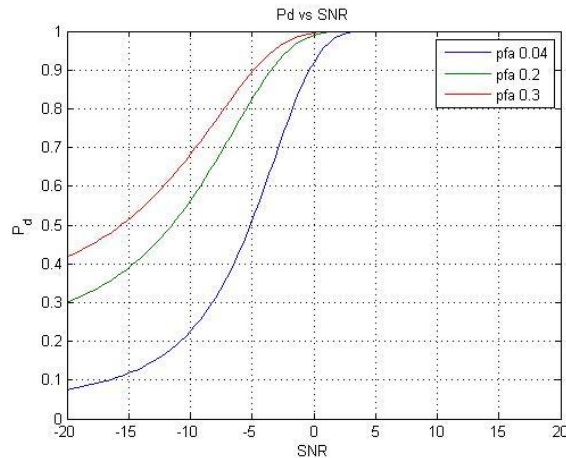

Fig. (6) P_d vs. SNR for different P_{fa}

V. Future Work

Eigenvalue based detection is done for a single user and single cognitive radio. Detection can be improved by taking into consideration more than one cognitive radio and avoid hidden node problem. More than one cognitive radio is been considered and with the cooperation of all the sensors hidden node issue is handled. Cooperative Eigenvalue based detection (CEBD) methods considers low SNR to avoid hidden node problem thereby protects primary user.

VI. CONCLUSION

Eigen value based detection methods use the received signal sample for detection and require no information on the transmitted signal, channel and noise power. EBD method overcomes the noise uncertainty difficulty

ACKNOWLEDGEMENT

REFERENCES

[1] Mourad Barkat - Signal detection and estimation.
[2] Yonghong Zeng, Senior Member, IEEE, and Ying-Chang Liang, Senior Member, IEEE: Eigen value based spectrum sensing algorithm for cognitive radio.
[3] Antonia M. Tulino - Random matrix theory and wireless communication.
[4] Aldo Buccardo - A signal detector for cognitive radio System.
[5] Khaled Ben Letaief and Wei Zhang - cooperative spectrum sensing.
[6] Yonghong Zeng, Ying-Chang Liang, Edward C. Y. Peh and Anh Tuan Hoang -IEEE "GLOBECOM" - Cooperative covariance and eigenvalue based detections for robust sensing.
[7] Alan Edelman Department of Electrical Engg. Computer Science Massachusetts Institute of Technology - Random matrix theory.
[8] Boaz Nadler, Federico Penna and Roberto Garello Performance of eigenvalue-based signal detectors with known and unknown noise level.
[9] Pedro Alvarez, Nuno Pratas, Ant´onio Rodrigues, Neeli Rashmi Prasad, Ramjee Prasad, Center for TeleInFrastruktur Aalborg University,Denmark - Energy detection and eigenvalue based detection: An experimental study using GNU radio.
[10] Yonghong Zeng, Ying-Chang Liang, Edward C. Y. Peh and Anh Tuan Hoang Institute for Infocomm Research, A*STAR, Singapore - Cooperative covariance and eigenvalue based detections for robust sensing.

Secure File Sharing In Cloud Using Encryption with Digital Signature

Miss. N. Kanchana[1], Mr. S. Balamurugan[2]

[1,2] *(PG Student, Assistant Professor, Sri Manakula Vinayagar Engineering College, Pondicherry-605106)*

Abstract: *This paper we discuss about the data sharing in a cloud with multiple owner by generating keys and digital signature. The proposed methodology suggests the encryption of the files to be uploaded on the cloud. To ensure the security of data, we proposed a method by implementing AES algorithm. The integrity and confidentiality of the data is achieved by not only encrypting it but also providing Digital Signature for successful authentication. It provides two way security for data sharing.*

Keywords: *Cloud, Encryption, Integrity, Confidentiality, Digital Signature.*

I. Introduction

Cloud computing is a type of computing that relies on sharing computing resources rather than having local servers or personal devices to handle applications. It comes into focus only when you think about what IT always needs: a way to increase capacity or add capabilities on the fly without investing in new infrastructure, training new personnel, or licensing new software. "the cloud" is essentially a metaphor for the Internet. Marketers have further popularized the phrase "in the cloud" to refer to software, platforms and infrastructure that are sold "as a service", i.e. remotely through the Internet. Typically, the seller has actual energy-consuming servers which host products and services from a remote location, so end-users don't have to; they can simply log on to the network without installing anything. Cloud computing providers offer their services according to several fundamental models: infrastructure as a service (IaaS), platform as a service (PaaS), and software as a service (SaaS).

(A) Software as a Service

Delivery of software applications over the internet. The software is frequently delivered using a one-to-may approach and is not customized. Hence on the supply-side, the provider is managing one application from one or more dedicated locations, whilst on the demand-side; customers are not required to make any hardware (such as servers) or software investments. For example: Gmail, hotmail, yahoo.

(B) Platform as a service

Delivery of a computing platform for the development of services and applications from a cloud. This category of service tends to be not as mainstream as the other "-aaS" options. Since it is used almost exclusively by programmers. For example: Google App Engine, Amazon EC2, Microsoft Azure Platform.

(C) Infrastructure as a Service

Delivery and remote management of computer and networking hardware, as well as processing power, as a service over the internet. Customers can purchase storage, processing power, networking capability etc, as and when needed, and commensurate with their actual needs. For Example: Storage-Dropbox, icloud, Adrive, mozy, amazon web service. Web hosting- Go daddy, bluehost, fatcow. Virtual Servers-IBM, Rimu Hosting.

II. Advanced Encryption Standard (AES)

AES is a symmetric-key algorithm, meaning the same key is used for both encrypting and decrypting the data.

Block length: 128 bits (P = C = $\{0,1\}^{128}$)

Key lengths: 128, 192, 256 bits (K = $\{0,1\}^{128}$, ...)

The key size used for an AES cipher specifies the number of repetitions of transformation rounds that convert the input, called the plaintext, into the final output, called the ciphertext. The number of cycles of repetition are as follows:

* 10 cycles of repetition for 128-bit keys.
* 12 cycles of repetition for 192-bit keys.
* 14 cycles of repetition for 256-bit keys.
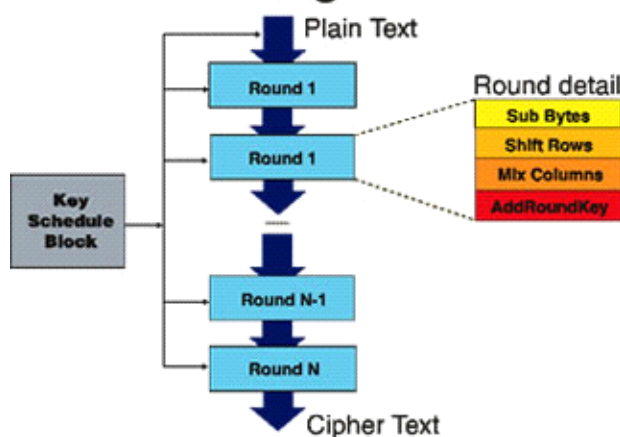
(i) KeyExpansion: round keys are derived from the cipher key using Rijndael's key schedule. AES requires a separate 128-bit round key block for each round plus one more.
(ii) InitialRound:
AddRoundKey—each byte of the state is combined with a block of the round key using bitwise xor.
**(iii) Rounds:**
1.SubBytes—a non-linear substitution step where each byte is replaced with another according to a lookup table.
2.ShiftRows—a transposition step where the last three rows of the state are shifted cyclically a certain number of steps.
3.MixColumns—a mixing operation which operates on the columns of the state, combining the four bytes in each column.
4.AddRoundKey
(iv) Final Round (no Mix Columns):
1.SubBytes
2.ShiftRows
3.AddRoundKey.

III. Key Generation

If owner needs to send a file to the user then the unique key will be generated for each user by the owner. Suppose owner would like to send the same file to the different users then the owner can just share the unique key to different users and the owner need not to send the same file again and again. So it eliminates the redundancy in database. If user deletes the file then it won't affect the other users to access that file its because only the key will be deleted not the file. In case if we don't use the key management then it definitely affects the other users to access the files.
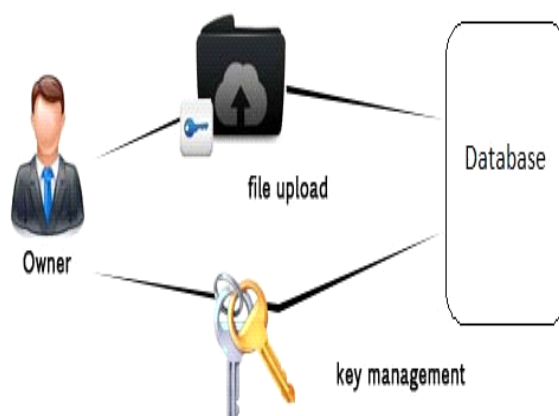

IV. Digital Signature

A digital signature is a mathematical scheme for demonstrating the authenticity of a digital message or document. Digital signatures are commonly used for software distribution, financial transactions, and in other cases where it is important to detect forgery or tampering. It is basically a way to ensure that an electronic

document (e-mail, spreadsheet, text file, etc.) is authentic. Authentic means that you know who created the document and you know that it has not been altered in any way since that person created it.

Digital signatures rely on certain types of encryption to ensure authentication. Encryption is the process of taking all the data that one computer is sending to another and encoding it into a form that only the other computer will be able to decode. Authentication is the process of verifying that information is coming from a trusted source. Once file is uploaded based on the owner name, user name, key, file name, file type then the digital signature will be created and it is send to the user.
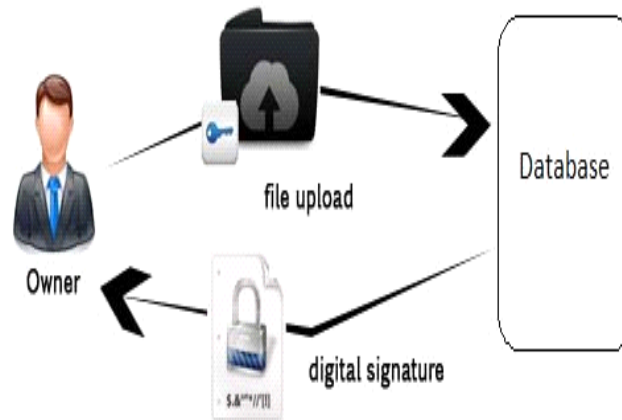
V. File Upload

Steps involved in file upload process are explained below:

Step 1: Accept owner id and password from the owner.
*   If owner is authorized,
        then allow to connect with the cloud
*   Else,
        show authentication error and don't allow

Step 2: Ask owner to select a file to be uploaded onto the cloud
Step 3: Ask the owner to select a user
Step 4: Ask the owner to enter a unique key for user
Step 5: Apply the encryption algorithm
Step 6: Upload the file on to the cloud
Step 7: The user gets the key through SMS and the Digital Signature file will be generated automatically by the system and it is send to the user through Email once the file is uploaded.
Step 8: Disconnect from the cloud.

VI. File Download

Steps involved in file download process are explained below:

Step 1: Accept user id and password from the user
*   If user is authorized,
        then allow to connect with the cloud
*   Else,
        show authentication error and don't allow

Step 2: Ask user to select a file to be download which is sent by the owner
Step 3: Ask the user to enter a key which is received through SMS
Step 4: Ask the user to download the Digital Signature file from Email
Step 5: Ask the user to upload the Digital Signature file
Step 6: Check the validity
*   If the key and the digital signature is matched,
        then Apply the decryption algorithm for download the file from the cloud
*   Else,
        show an error message and reject the download process
Step 7: Disconnect from the cloud

VII. Conclusion

In this paper we mainly focused on data confidentiality and integrity so we used an encryption algorithm and we also designed a digital signature scheme to invoke high secured data transaction in the cloud. It also eliminates the redundancy it's because of key management. Here, anyone could be a owner if they are registered in the cloud. The user of a particular organization can be able to access the particular information which is available in the file. It is more reliable to the cloud for better security.

REFERENCES

[1]   S. Kamara and K. Lauter, "Cryptographic Cloud Storage," Proc. Int'l Conf. Financial Cryptography and Data Security (FC), pp. 136-149, Jan. 2010.

[2]   S. Yu, C. Wang, K. Ren, and W. Lou, "Achieving Secure, Scalable and Fine-Grained Data Access Control in Cloud Computing," Proc. IEEE INFOCOM,pp. 534-542,2010

[3]   Minqi Zhou, Rong Zhang, Wei Xie, Weining Qian and Aoying Zhou, "Security and Privacy in Cloud Computing: A Survey", In Sixth International Conference on Semantics, Knowledge and Grids, 2010.

[4]   Farhan Bashir Shaikh and Sajjad Haider, "Security Threats in Cloud Computing", In 6th International Conference on Internet Technology and Secured Transactions, 2011.

[5]   Balachandra Reddy Kandukuri, Ramakrishna Paturi V and Dr. Atanu Rakshit, "Cloud Security Issues", In IEEE International Conference on Services Computing, 2009.

[6]   D. Boneh, X. Boyen, and H. Shacham, "Short Group Signature," Proc. Int'l Cryptology Conf. Advances in Cryptology (CRYPTO),pp. 41-55, 2004.

[7]   D. Boneh and M. Franklin, "Identity-Based Encryption from the Weil Pairing," Proc. Int'l Cryptology Conf. Advances in Cryptology (CRYPTO), pp. 213-229, 2001.

[8]   M. Kallahalla, E. Riedel, R. Swaminathan, Q. Wang, and K. Fu "Plutus: Scalable Secure File Sharing on Untrusted Storage," Pro USENIX Conf. File and Storage Technologies, pp. 29-42, 2003.

[9]   D. Pointcheval and J. Stern, "Security Arguments for Digital Signatures and Blind Signatures," J. Cryptology, vol. 13, no. 3, pp. 361-396, 2000.

Making Trust Relationship For Peer To Peer System With Secure Protocol

Miss. I. Jancy[1], Mr. S. Balamurugan[2]

[1,2] *(PG Student, Assistant Professor, Sri ManakulaVinayagar Engineering College, Pondicherry-605106)*

Abstract: *In the peer-to-peer systems exposes them to malicious activity. Building trust relationships among peers can mitigate attacks of malicious peers. This paper presents distributed algorithms that enable a peer to reason about trust worthiness of other peers based on past interactions and recommendations. Peers create their own trust network in their proximity by using local information available and do not try to learn global trust information. Two contexts of trust, service, and recommendation contexts are defined to measure trustworthiness in providing services and giving recommendations. So, neighbouring node will give the recommendation to peer. Based on the recommendation only Peer decides whether the node is good (or) malicious. Find the node is malicious node means peer will not interact with malicious node. Isolate the malicious node from the network. Find the node is good means peer interact with good peer. Peer stores a separate history of interactions for each Acquaintance. This paper also discuss the malicious threats, privacy concerns, and security risks of three commonpeer-to-peer network systems that are gaining popularity today. The malicious threats discussed willinclude how malicious threats can harness existing peer-to-peer networks, and how peer-to-peernetworking provides an additional (potentially unprotected) vector of delivery for malicious code.*

Index Terms: *Peer-to-peer systems, trust management, reputation, security.*

I. Introduction

Open nature of peer-to-peer systems exposes them to malicious activity. Building trust relationships among peers can mitigate attacks of malicious peers. This paper presents distributed algorithms that enable a peer to reason about trust worthiness of other peers based on past interactions and recommendations. Peers create their own trust network in their proximity by using local information available and do not try to learn global trust information. Two contexts of trust, service, and recommendation contexts are defined to measure trustworthiness in providing services and giving recommendations. Interactions and recommendations are evaluated based on importance, recentness, and peer satisfaction parameters. Additionally, recommender"s trustworthiness and confidence about a recommendation are considered while evaluating recommendations. Simulation experiments on a file sharing application show that the proposed model can mitigate attacks on 16 different malicious behavior models. In the experiments, good peers were able to form trust relationships in their proximity and isolate malicious peers. Peer to Peer (P2P) systems rely on collaboration of peers to accomplish tasks. Ease of performing malicious activity is a threat for security of P2P systems. Creating long-term trust relationships among peers can provide a more secure environment by reducing risk and uncertainty in future P2P interactions.

And Therefore, classic peer-to-peer unaware viruses could inadvertently be transmitted via a peer-to-peer network. Viruses could also take advantage of the regular use of a peer-to-peer network. For example, viruses could specifically attempt to copy themselves to or infect files within the shared peer-to-peer space.

A peer sharing files is called an uploader. A peer downloading a file is called a downloader. The set of peers who downloaded a file from a peer are called downloaders of the peer. An ongoing download/ upload operation is called a session. Simulation parameters aregenerated based on results of several empirical studies [6], [7] to make observations realistic. A file search request reaches up to 40 percent of the network and returns online uploaders only. A file is downloaded from one uploader to simplify integrity checking. All peers are assumed to have antivirus software so they can detect infected files Four different cases are studied to understand effects of trust calculation methods under attack conditions:

No trust. Trust information is not used for uploader selection. An uploader is selected according to its bandwidth. This method is the base case to understand if trust is helpful to mitigate attacks.

No reputation query. An uploader is selected based on trust information but peers do not request recommendations from other peers. Trust calculation is done based on SORT equations but reputation (r) value is always zero for a peer. This method will help us to assess if recommendations are helpful.

SORT. In SORT, peers are assumed to be strangers to each other at the beginning. A peer becomes an acquaintance of another peer after providing a service, e.g., uploading a file. If a peer has no acquaintance, it chooses to trust strangers.

Flood reputation query.SORT equations are used but a reputation query is flooded to the whole network. This method will help us to understand if getting more recommendations is helpful to mitigate attacks.

In SORT, to evaluate interactions and recommendations better, importance, recentness, and peer satisfaction parameters are considered. Recommender"s trustworthiness and confidence about recommendation are considered when evaluating recommendations. Additionally, service and recommendation contexts are separated. This enabled us to measure trustworthiness in a wide variety of attack scenarios. Most trust models do not consider how interactions are rated and assume that a rating mechanism exists. In this study, we suggest an interaction rating mechanism on a file sharing application and consider many real-life parameters to make simulations more realistic. A good peer uploads authentic files and gives fair recommendations. A malicious peer (attacker) performs both service and recommendation-based attacks. Four different attack behaviors are studied for malicious peers: naive, discriminatory, hypocritical, and oscillatory behaviours. A non-malicious network consists of only good peers. A malicious network contains both good and malicious peers.

***And Therefore, classic peer-to-peer unaware viruses could inadvertently be transmitted via a peer-to-peer network. Viruses could also take advantage of the regular use of a peer-to-peer network. For example, viruses could specifically attempt to copy themselves to or infect files within the shared peer-to-peer space.

The systems discussed include the Napster, Gnutella, and Freenet protocols. These protocols will be examined due to their popularity and different methods of achieving peer-to-peer networking.

Many other peer-to-peer networking systems exist (for example, Microsoft Networking), and while not explicitly discussed, conclusions can be applied to these systems as well.

II. Virus Protection

Viruses could actually harness the existing peer-to-peer network infrastructure to propagate themselves. For example, a worm could set up a servent on an infected system. The user with the infected system does not have to initially be part of the peer-to-peer network. Then, this servent could return the exact matches for incoming search queries, and those downloading and executing the file will in turn become infected. An example of such a worm is W32.Gnuman.

Since peer-to-peer malicious threats still need to reside on the system's current desktop, a scanninginfrastructure can provide protection against infection. However, desktop protection may not proveto be the best method in the future.

Should peer-to-peer networking become standard in home and corporate computing infrastructures,network scanning may become more desirable. Such scanning is not trivial since, by design,peer-to-peer transfer of data does not pass through a centralized server, such as an email server.

Systems such as network-based IDS may prove useful, as well as gateway/proxy scanning to preventmalicious threats from using peer-to-peer connections that pass inside and outside of organizations.

However, peer-to-peer networking models such as Freenet will render networking scanning uselesssince all data is encrypted. You will not be able to scan data that resides in the DataStore on a system.

Detection of threats passed via Freenet type models will only be scanned on the unencrypted file atthe desktop just prior to execution. The issue of encryption reinforces the necessity fordesktop-based, antivirus scanning.

III. The Computational Model Of Sort

We make the following assumptions. Peers are equal in computational power and responsibility. There are no privileged, centralized, or trusted peers to manage trust relationships. Peers occasionally leave and join the network.

A peer provides services and uses services of others. For simplicity of discussion, one type of interaction is considered in the service context, i.e., file download.

3.1 Preliminary Notations

pi denotes the ith peer. When pi uses a service of another peer, it is an interaction for pi. Interactions are unidirectional. For example, if pi downloads a file from pj, it is an interaction for pi and no information is stored on pj. If pi had at least one interaction with pj, pj is an acquaintance of pi. Otherwise, pj is a stranger to pi. Ai denotes pi's set of acquaintances. A peer stores a separate history of interactions for each acquaintance. SHij denotes pi's service history with pj where shij denotes the current size of the history. shmax denotes the

upper bound for service history size. Since new interactions are appended to the history, SHij is a time ordered list.

Parameters of an interaction. After finishing an interaction, pi evaluates quality of service and assigns a satisfaction value for the interaction. Let 0 _ skij _ 1 denote pi's satisfaction about kth interaction with pj. If an interaction is not completed, skij ¼ 0. An interaction's importance is measured with a weight value. Let 0 _ wkij _ 1 denote the weight of kth interaction of pi with pj. Semantics to calculate skij and wkij values depend on the application. In a file sharing application, authenticity of a 16 IEEE TRANSACTIONS ON DEPENDABLE AND SECURE COMPUTING, VOL. 10, NO. 1, JANUARY/FEBRUARY 2013 file, average download speed, average delay, retransmission

Background Protocols

- **GNUTELLA**

Gnutella does not utilize a centralized server. Each computer is a client as well as a server, hereinafter called a servent. Such a true peer-to-peer networking model decreases reliability, speed, and search capabilities, and increases network traffic. Figure 1 illustrates the standard communication process involved in obtaining a file.
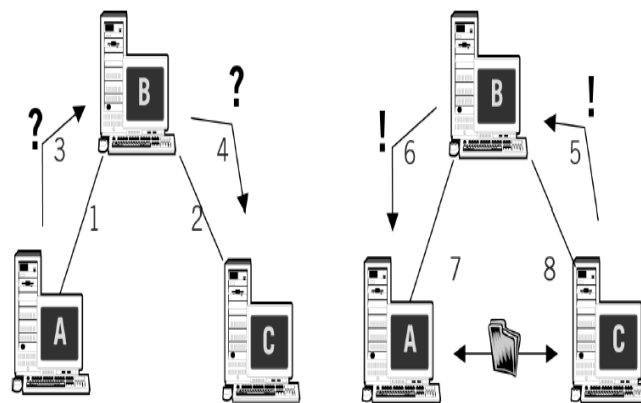

Fig.1 Standard Communication Process: Obtaining a File

- **NAPSTER**

The Napster peer-to-peer networking model involves a centralized directory server. Clients primarily communicate with a directory server that passes messages among, and maintains particular states of, clients. Figure 2 illustrates the standard communication process involved in downloading a file in the Napster protocol.Figure 2 illustrates the standard communication process involved in downloading a file in the Napster protocol.
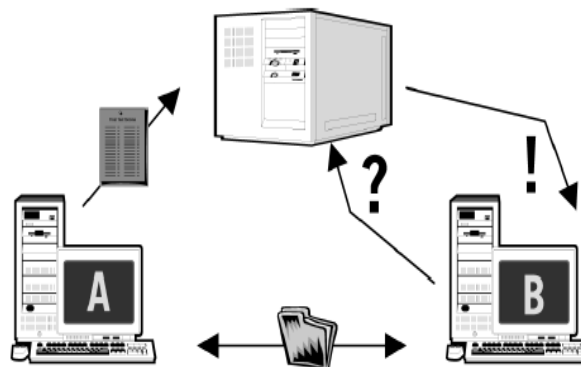

Fig.2 Standard Communication Process: Downloading a File in Napster Protocol

- **FREENET**

The Freenet model of exchange is similar to Gnutella, being a true peer-to-peer model. However, users do not have control over what content is held in their shared space, known as a DataStore. A user inserts a file into the Freenet network, where it is encrypted and propagated along the network to an appropriate node determined by a unique key, which identifies the file.

This allows data with close keys to be sorted to the same nodes on the network, which causes the clustering of close key data. This allows a fast response to search queries. Since all data is encrypted, users only have control of the amount of space they wish to make available on their systems, not the content that resides on their systems. Figure 3 illustrates the standard communication process involved in obtaining a file in the Freenet protocol.
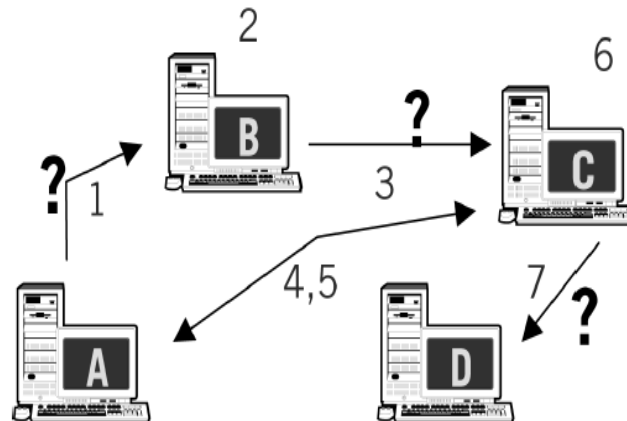

Fig.3 Standard Communication Process: Downloading a File in GNUTELLA Protocol

3.2 Service Trust Metric*(stij)*

This section describes the calculation of service trust metric. A peer first calculates competence and integrity belief values using the information about service interactions. *Competence belief* is based on how well an acquaintance satisfied the needs of interactions .*cbij*denotes the competence belief of *pi* about *pj* in the service context. Average behavior in the past interactions can be a measure of competence belief.

$$cbij = \overline{cb}(eijk \; ¢ \; wijk \; ¢ \; fijk) \qquad (2)$$

$$1shij$$

$$=1$$

$$Xk$$

IV. PerformanceAnalysis&Design

Downloading a file is an interaction. A peer sharing files is called an uploader. A peer downloading a file is called adownloader. The set of peers who downloaded a file from a peer are called ownloaders of the peer. An ongoingdownload/ upload operation is called a session.
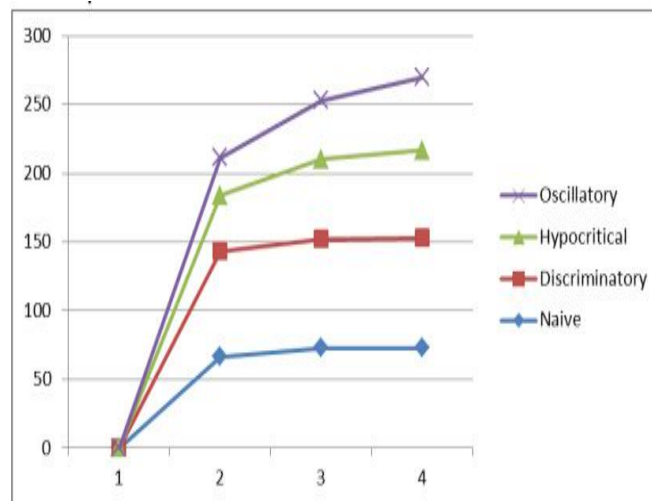
4.1 (a) Existing System

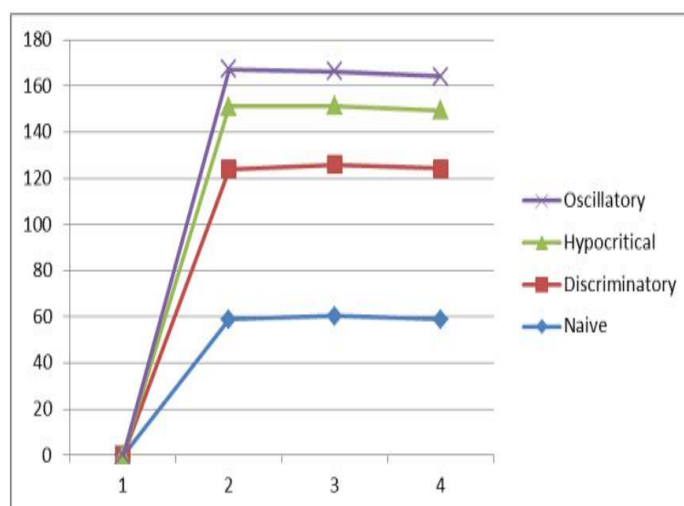Fig.4Existing System (15% malicious)

(b) Proposed System

Fig.5Proposed System (50% malicious)

V. Conclusion

Peer-to-peer networks obviously pose a danger as an additional vector of delivery. Their impact on security will depend on the adoption of peer-to-peer networks in standard computing environments. If systems use peer-to-peer networks as email is used today, then they will be significant methods of delivery of malicious code. The use of two-way network communication also exposes the system to potential remote control.

More importantly, the usage of a peer-to-peer network creates a hole in a firewall and can lead to the exporting of private and confidential information. Therefore, administrators should begin analyzing their networks for peer-to-peer network usage and configure firewalls and systems accordingly to limit or prevent their usage.

REFERENCES

[1]   AhmetBurakCan and Bharat(2013),"A Self-Organizing Trust Model for Peer-to-Peer Systems"IEEETrans. Dependable and Secure Computing,vol 10,No.1.
[2]   Aberer.K and Despotovic.Z(2001), „Managing Trust in a Peer-2-Peer Information System" Proc. 10th Intl Conf. Information and Knowledge Management (CIKM).
[3]   Kamvar.S, Schlosser.M, and Garcia-Molina.H,(2003) „The (Eigentrust) Algorithm for Reputation Management in P2P Networks" Proc. 12th World Wide Web Conf. (WWW).
[4]   SelcukA.A ,Uzun.E, and Pariente.M.R(2004), „A Reputation-Based Trust Management System for P2P Networks" Proc. IEEE/ACM Fourth Int"lSymp. Cluster Computing and the Grid (CCGRID).
[5]   Zhou. R, Hwang. K, and Cai. M(2008), „Gossiptrust for Fast Reputation Aggregation in Peer-to-Peer Networks" IEEE Trans. Knowledge and Data Eng., vol. 20, no. 9.
[6]   Abdul-Rahman. A and Hailes.S(2008), „Supporting Trust in Virtual Communities" Proc. 33rd Hawaii Int"l Conf. System Sciences (HICSS).

Fatigue Performance in Grinding and Turning: An Overview

Jose Cherian[1], Dr Jeoju M Issac[2]

[1](Jose Cherian ,Research scholar, Department of Mechanical engineering, Karpagam University, Tamil Nadu, India)

[2](Dr Jeoju M Issac, Professor, Department of Mechanical engineering, MA college of Engineering, India)

Abstract: *This paper analysis the influence of Abrasive Flow Machining (AFM), Turning and Grinding on fatigue performance of Fe250. Surface condition has a strong effect on fatigue life, and that most surfaces produced by conventional manufacturing operations such as machining and forging have poor fatigue behavior than polished surfaces commonly used for laboratory specimens. It is found that the surfaces produced with different machining process and having the same surface roughness having different fatigue performances. High –cycle fatigue data was obtained for Fe 250 using three types of machining process viz, AFM, Turning and Grinding .S-N curve is plotted for the samples obtained with all the three process. It was found that the samples produced with AFM having the highest fatigue life.*

Keywords: *Abrasive flow machining, Fatigue life, Surface roughness, Turning, Grinding.*

I. Introduction

The achievement of high quality, in terms of work piece dimensional accuracy, fatigue strength, surface finish, less wear on the cutting tools, economy of machining are the main and effective challenges of modern metal cutting and machining industries. Fatigue performance of materials will be reducing when they are subjected to various machining process. Fatigue cracks in these components usually may be initiated in geometrical features, which cause local stress concentrations, in most cases at the surface. It is well known that the fatigue life of a machine component depends strongly on its surface layer condition. Fatigue crack nucleation and propagation, in most cases, can be attributed to surface integrity, which includes surface roughness, structure and stress conditions of the surface layer. The importance of surface integrity increases with increasing loads, temperature and frequency. This becomes critical for high strength steels, which are more sensitive to stress concentration.

The surface roughness and surface texture of a machine component is decided mainly by finishing operations. Machining can be used to produce a wide range of mechanical components such as gears, cams, shafts, axles and others, which are continuously subjected to cyclic loads. During the process of turning the surface generated is influenced by several variables: steel properties (elastic and plastic deformations), tool material and geometry, vibration of cutting tool, cutting speed, feed, depth of cut, lubricant, etc. During machining, the surface layer is subjected to elastic-plastic deformation and heating, which result in structural changes, strain hardening and residual stresses, while irregularities may appear, creating surface roughness. All these factors will lead to reduce fatigue life in Turning operations. Whereas girding is a micromachining process and it results in (i) increased hardness of the surface layer, (ii) more compressive residual stresses (iii) Changes in material property at the surface. In grinding due to work hardening the initiation of crack and crack propagation is little delayed. This will result in increase in fatigue life. However work hardening will reduce the fatigue life. As a result of these factors the fatigue will not have much improvement during the grinding process.

In AFM any surface defects present in the surface of the work piece will be removed. It will also remove residual stresses present in the work piece. During AFM no thermal stresses or work hardening effects will be developed within the material. Present study is to assess the fatigue performance during AFM and compare Fatigue performance in AFM with the turning and grinding operations.

II. PREVIOUS RESEARCH

A damaged region is produced on the surface of metal which is different from the inner surface of the material as a result of machining [1]. During machining, the surface layer is subjected to elastic-plastic deformation and heating, which result in structural changes, strain hardening and residual stresses, while irregularities may appear, creating surface roughness. The influence of cutting parameters (cutting speed, feed rate and depth of cut) on surface quality, and consequently on roughness surface, is well studied. A large number of analytical and experimental studies have been conducted on surface roughness of steels in machining operations. These research developments have been performed with the objective of optimizing the cutting

conditions to obtain surface finish [2]. Davim [3] studied the influence of cutting conditions on the surface finishing obtained by turning. According to this paper, the cutting speed had the greatest influence on the roughness followed by the feed rate. The depth of cut had no significant influence on the roughness. Similar results were found by Feng (2001) that also observed that in addition to feed rate, nose radius, work material and speeds, the rake angle has a significant influence on the surface roughness [4].

The fatigue strengths of machined and as-cast surfaces of ferritic SG iron have been compared by Starkey and Irving [5]. They found endurance of machined specimens was found to be higher than that of as-cast surfaces. Micro pores initiated failure in the machined specimens, whereas surface irregularities or dross defects initiated cracks from the as-cast surface.

Taylor and Clancy have compared the fatigue limit of AISI 4140 using four types of machined surfaces produced by polishing, grinding, milling and shaping[6]. The residual stress was eliminated by heat treatment. They found that fatigue limit of ground surfaces decreased when compared to polished specimens, that is, the fatigue limit decreased with increasing surface roughness. However, a comparison of the fatigue limits of the specimens with ground surfaces with those of milled surface specimens showed an opposite tendency, that is, an increasing of fatigue limit with increasing surface roughness. Besides, there was not observed difference between fatigue limits of the polished and fine milled specimens, even though surface roughness values were quite different.

The effects of surface roughness on cracking initiation and S-N curves of a Ni-Cr-Mo steel were studied by Itoga et al. [7]. Surface roughness was the most important influencing factor in short life regime, and the fatigue life was found to decrease with increasing surface roughness. On the contrary, in long life regime, surface roughness exerted no influence on fatigue life, because cracks nucleated at inclusions and grew inside the specimens. Arola and Williams (2002) found that the high-cycle fatigue life of machined specimens of AISI 4130 steel is surface-texture dependent, and that the fatigue strength decreased with an increase in surface roughness from 2 to 6 μm. On the other hand, an increase in fatigue life occurred with increasing surface roughness under low-cycle fatigue. It was also found that the notch sensitivity of these machined specimens did not change significantly with surface roughness. The effects of surface roughness, work-hardened layer and humidity on S-N curves of high strength AISI 4340 steel was studied by Nakajima et al. [8]. Buff-finished and electro-polished specimens with two different surface conditions were prepared. Fatigue lives were longer in the buff-finished than in the electro-polished specimens, due to the presence of a work-hardened layer.

Becker studied the deformation of polycrystals and showed that the surface roughness increases with plastic strain [9]. Under fatigue loading, it was found that the surface roughness increased with fatigue life, and the deformation is localized in some specific places, where micro-cracks are nucleated .As shown, the importance of both surface roughness and integrity is well recognized, with many experimental and analytical models relating these characteristics with fatigue life. However, there are only few results in literature that show the influence of machining cutting parameters on fatigue life of commercial steels. In general more attention is given on the influence of grinding on fatigue strength. However, in these days materials can be machined and finished with newly developed tools, eliminating the need for other finishing operations. Thus, it is necessary to know the relationship between fatigue parameters and cutting operations. In the present study, the influence of cutting speed, depth of cut and feed rate on the fatigue endurance of turned specimens of commercial AISI 4140 steel is analyzed.

III.   EXPERIMENTAL PROCEDURE

In this investigation the AISI4140 steel was used as the work material. Whose chemical. This material was supplied in the form of cylindrical bars. This bar is turned into the dimensions as shown in fig (1)
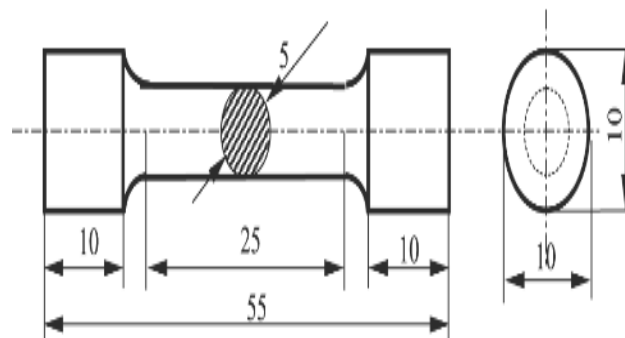

Fig 1 1.1. Fatigue analysis in Turning

The specimens received, after heat treatment, turned to the configuration shown in Fig. 1.The cutting parameters selected is shown in table 1. All these conditions are used in finishing turning operations. They were chosen in order to have specimens with three different feed rates (group 2, conditions 2.1 to 2.3), three different depths of cut (group 1, conditions 1.1, 1.2 and 2.1), and three different cutting speeds (group 3, conditions 3.1, 3.2 and 2.1). Thus, each group has two constants and only one variable cutting parameter. These specimens will be designated according to their condition number hereafter (Ex.: condition 1.1, etc). The turning process was carried out using a CNC lathe.

Table 1

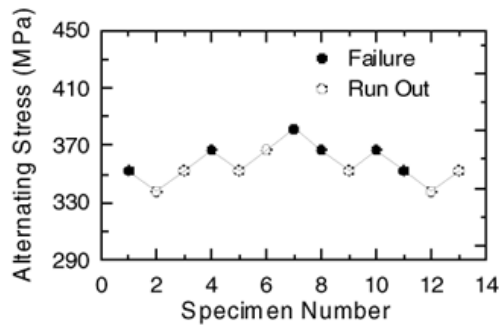| Group 1		Group 2			Group 3	
$v_c = 60$ m/min		$v_c = 60$ m/min			$f = 0.12$ mm/rev	
$f = 0.12$ mm/rev		$a_p = 1.2$ mm			$a_p = 1.2$ mm	
Condition 1.1	Condition 1.2	Condition 2.1	Condition 2.2	Condition 2.3	Condition 3.1	Condition 3.2
$a_p = 0.4$ mm	$a_p = 2.0$ mm	$f = 0.12$ mm/rev	$f = 0.18$ mm/rev	$f = 0.25$ mm/rev	$v_c = 15$ m/min	$v_c = 100$ m/min

Fig 2 .Stair case fatigue test - Condition 1.1

The experimental tests of the specimens machined according to condition 1.1 were performed with alternating stress varying from 323.15 to 381.09 MPa fig (2)The fatigue limit of this condition was found to be equal to 287.96 ± 21.54MPa.

The stair case test of the specimens of the condition 2.1 with alternating stress varying from 395.97 to 424.54 MPa is showed in fig (3). The fatigue limit for this condition 2.1 was found to be equal to 366.84 ± 16.32 MPa.
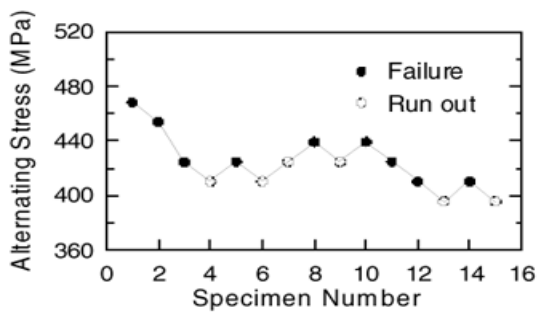

Figure 6. Stair case fatigue test - Condition 2.1.

Fig 3.Stair case fatigue test - Condition 2.1
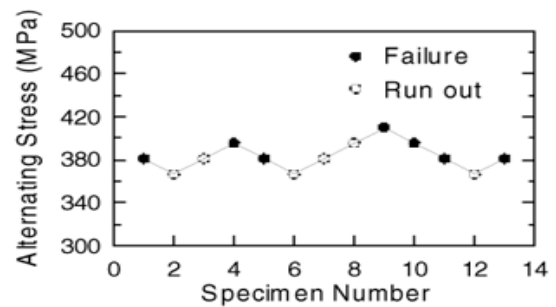

Figure 7. Stair case fatigue test - Condition 3.1.

Fig 4 .Stair case fatigue test - Condition 3.1

The stair case test of the specimens of the condition 3.1 was performed using alternating stresses from 366.66 vto 410.06MPa, as shown in fig (4) The fatigue limit of this condition 3.1 was equal to 341.10 ± 13.72 MPa. The influence of depth of cut (ap) on fatigue limit is shown in fig (5)The fatigue limit of AISI 4140 steel increases almost 18% with increasing depth of cut from 0.4 to 1.2 mm. Further increase in depth of cut to 2.0

mm has no pronounced influence on the average fatigue limit of this steel. However, the dispersion of the fatigue limit increases with increasing depth of cut. The influence of depth of cut on fatigue limit is similar to those observed in Fig. 2.
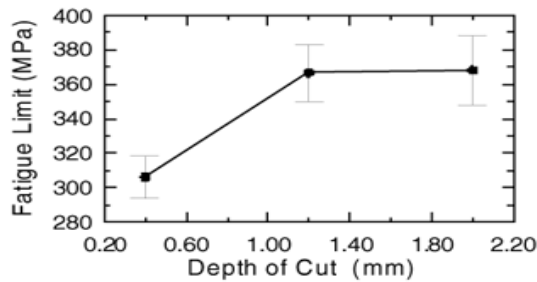

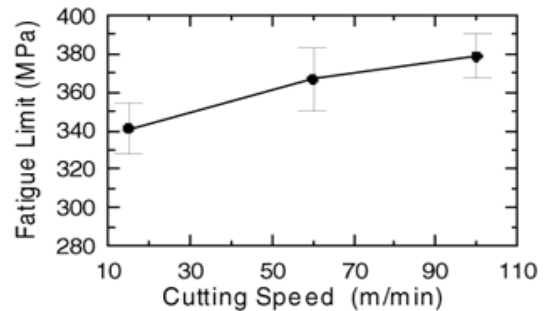**Fig 5 .Influence of depth of cut on fatigue limit**

Fig 6 .Influence of cutting speed on fatigue limit

The fatigue limit of AISI 4140 steel increases almost linear with increasing cutting speed (vc), as shown in the Fig(6) This result was expected, since increasing cutting speed leads to smaller roughness values. Besides, the cutting speed had no influence on the dispersion of the fatigue limit.

The fatigue limit of the AISI 4140 steel is only slightly influenced when the feed rate (f) is increased from 0.12 to 0.18 mm/rev, as shown in fig (7). A sharp decrease in fatigue limit is observed when the feed rate is further increased to 0.25 mm/rev. It was previously shown that surface roughness increased almost linear with increasing feed rate. Thus, it was expected a similar behavior between fatigue limit and feed rate. It becomes evident that fatigue limit is determined not only by roughness values. Residual stresses originated by machining are also important.
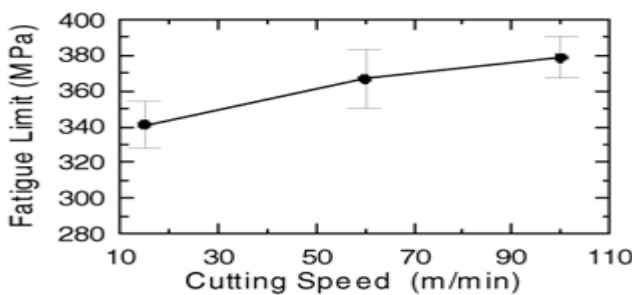

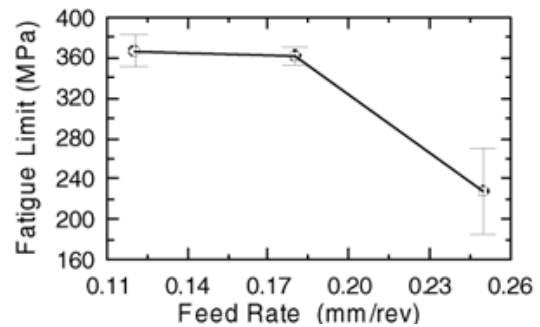**Fig 7 .Influence of cutting speed on fatigue limit**

Fig 8 .Influence of feed rate on fatigue limit

The variation of all measured fatigue limits with cutting parameters is summarized in Table(5)The most influent parameter on fatigue limit is the feed rate. This is in accordance with the surface roughness results (Table4) However, the changes of fatigue limits with cutting parameters are quite lower than that observed previously by the roughness parameters. Thus, only the roughness parameters can not explain the changes of fatigue limits of this steel. The fatigue endurance of machined component depends strongly on its surface layer condition. During the machining, the surface layer is subjected to several phenomena, which result in structural changes, strain hardening and residual stresses, while irregularities may appear, creating surface roughness. The fatigue limit is determined by all these parameters.

Table 3.Changing fatigue limit with cutting parameters

	Changing of surface roughness parameters (%)		
	R_a	R_q	R_t
Feed rate (f)	66	65	52
Cutting speed (v_c)	-41	-45	-56
Depth of cut (a_p)	-38	-40	-50

Table 4.Changing fatigue limit with cutting parameters

	Changing of fatigue limit (%)
Feed rate (f)	-38
Cutting speed (v_c)	12
Depth of cut (a_p)	18

The influence of roughness surface on fatigue limits of all machined and polished specimens is summarized in fig(8)The fatigue limit decreases almost linear with increasing roughness surface. This tendency is not obeyed when the specimens without residual stress (heat treated) is included. Besides, the highest value of fatigue limit was reached in the polished specimens, without relief stress. However, relief stress heat treatment in machined specimens can substantially raise their fatigue endurances. If machined specimens with better initial fatigue limit than that previous utilized would stress relief heat treated, a higher fatigue limit could be reached. Thus, it could be cheaper to produce components using only commercial machining parameters and stress relief heat treatment, than polished specimens.
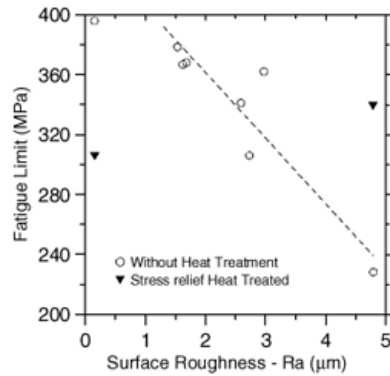

Fig 9 .Summary of fatigue limits of all analyzed

Condition	Hardness (HV)		Change (%)
	Without Relief Stress	After Heat treatment	
Machined (2.3)	256.7 ± 33.9	196.5 ± 19.5	-23
Polished	213.2 ± 8.5	207.7 ± 8.9	-3

Table 4. Hardness (HV) of specimens of AISI 4140 steel

This paper presents the influence of commercial cutting parameters during machining on fatigue limits of AISI 4140 steel. Fatigue rotating bending tests were performed on steel specimens with zero mean stress at room temperature. The fatigue limit decreases with increasing roughness parameters. The influence of cutting parameters on fatigue limits is lower than that on surface roughness. The relation between residual stresses, strain hardening and roughness surface plays a dominant role. Stress relief heat treatment causes an increase of fatigue limit of machined specimens with high roughness parameters and a decrease in polished specimens. The softening of both specimen types (polished and machined) caused by the heat treatment is not similar. The sharp increase of fatigue limit of machined specimens is due to elimination of residual stress, which overcome the effect of surface layer softening.

1.2. Fatigue analysis in Grinding

In order to study the fatigue damage of AISI 4140, rotating bending fatigue tests of EP-0, EP-3 and EP-15 specimens were carried out. Here, EP-0 means the specimen finished by the grinding, EP-3 and EP-15 are the specimens whose 3 and 15 Pm surface layer were electropolishedafter the grinding, respectively. The main conclusions from analysis of fatigue data may be summarized as follows.

(1) The fatigue strength of EP-0 exhibited large scatter and it tended to drop again in the long-life field in excess of 107 cycles. The fracture origin in such a long life field was principally inner defects. At around the fatigue limit stress at 107 cycles, two different fracture modes, surface fracture and inclusion governed inside fracture, were mixed together.

(2) Fatigue strength of EP-15 was dramatically decreased and the scatter in S-N plots is very small when compared to the EP-0. All the cracks of EP-15 were initiated from the surface even at the stress below the fatigue limit at 107 for EP-0.

(3) S-N plots for EP-3 exhibited large scatter, but the range of scatter is smaller than EP-0. This may come from the decreased scatter in geometric shape of the surface by electro polishing. On the other hand, the difference in the mean value of S-N plots between EP-0 and EP-3 is not large. removing 3 Pm surface layer ,the drop in fatigue strength due to the reduced hardened layer and the increase in fatigue strength derived from the decreased surface roughness may balance.

(4) Considering above experimental results synthetically, it can be concluded that the peculiar S-Characteristics observed in ground specimen results from the surface strengthened layer (work hardening and residual stresses) due to grinding. Those experimental facts indicates that the re-drop in fatigue strength in super long-life field frequently reported in high-strength material is not necessary the proper characteristics of material itself.

IV. CONCLUSION

From the above results it can be concluded that the fatigue strength generally depends on the surface finish.But the surface finish alone does not improve the fatigue strength. This paper presents the influence of commercial cutting parameters during machining on fatigue limits of AISI 4140 steel. Fatigue rotating bending tests were performed on steel specimens with zero mean stress at room temperature. The fatigue limit decreases with increasing roughness parameters. The influence of cutting parameters on fatigue limits is lower than that on surface roughness. The relation between residual stresses, strain hardening and roughness surface plays a dominant role. Stress relief heat treatment causes an increase of fatigue limit of machined specimens with high roughness parameters and a decrease in polished specimens. The softening of both specimen types (polished and machined) caused by the heat treatment is not similar. The sharp increase of fatigue limit of machined specimens is due to elimination of residual stress, which overcome the effect of surface layer softening.

REFERENCES

[1]   Benardos, P. G. and Vosniakos, G. –C., 2003, "Predicting Surface Roughness in Machining: A review", Int. J. of Mach. Tools & Manufacture, Vol. 43, No. 8, pp. 833-844.
[2]   Trent, E. M. and Wright, P. K., 2000, "Metal Cutting", Ed. Butteworths-Heinemann Ltd., London, England, 446p.
[3]   Davim, J. P., 2001, "A Note on the Determination of Optimal Cutting. Conditions for Surface Finish obtained in Turning using Design of Experiments", J. of Mater. Process. Techn. Vol. 116, pp. 305-308.
[4]   Feng, C-X., 2001, "An Experimental Study of the Impact of Turning Parameters on Surface Roughness", Proc. of the 2001 Industrial Engineering Research Conference, Institute of Industrial Engineers, Paper No. 2036, pp. 1-6.
[5]   Starkey, M. S. and Irving, P. E., 1982, "A Comparison of the Fatigue Strength of Machined and as-cast Surfaces of SG Iron", Int. J. of Fatigue, Vol. 4, No. 3, pp. 129-136.
[6]   Taylor, D. and Clancy, O. M., 1991, "The Fatigue Performance of Machined Surfaces", Fatigue Fract Engng Mater Struct, Vol. 14, pp. 329-336.
[7]   Itoga, H., Tokaji, K., Nakajima, M. and Ko, H. –H., 2003, "Effect of Surface Roughness on Step-Wise S-N Characteristic in High Strength Steel", Int. J. of Fatigue, Vol. 25, No. 5, pp. 379-385.
[8]   Nakajima, M., Tokaji, K., and Ko, H. –N., 2003, "Morphology of Step-wise S-N curves depending on Work-hardened layer and humidity in a High-strength Steel", Fatigue Fract Engng Mater Struct, Vol.26, No. 12, pp. 1113-1118.
[9]   Becker, R., 1998, "Effects of Strain localization on Surface Roughening during Sheet Forming", Acta Mater., Vol. 46, pp. 1385-1401.
[10]   Matsumoto, Y., Magda, D., Hoeppner, D. W. and Kim T. Y. 1991, "Effect of Machining Processes on the Fatigue Strength of hardened AISI Steel", J. Eng. Ind., Vol. 13, pp.154-159.